doi: 10.3289/geomar_rep-094_1999

FS SONNE
FAHRTBERICHT SO144/1&2
CRUISE REPORT SO144/1&2

PAGANINI

PANAMA BASIN AND GALAPAGOS "PLUME"
NEW INVESTIGATIONS OF INTRAPLATE MAGMATISM

SAN DIEGO - CALDERA
SEPTEMBER 7 - NOVEMBER 7, 1999

Edited by
Jörg Bialas, Ernst R. Flueh, and Gerhard Bohrmann
with contributions of cruise participants

GEOMAR
Forschungszentrum
für marine Geowissenschaften
der Christian-Albrechts-Universität
zu Kiel

KIEL 1999

GEOMAR REPORT 94

GEOMAR
Research Center
for Marine Geosciences
Christian Albrechts University
in Kiel

Redaktion dieses Reports:
Jörg Bialas, Ernst R. Flueh, Gerhard Bohrmann
und Gerhard Haass

GEOMAR REPORT
ISSN 0936 - 5788

GEOMAR
Forschungszentrum
für marine Geowissenschaften
Wischhofstr. 1-3
D - 24148 Kiel
Tel. (0431) 600-2555, 600-2505

Editors of this issue:
Jörg Bialas, Ernst R. Flueh, Gerhard Bohrmann,
and Gerhard Haass

GEOMAR REPORT
ISSN 0936 - 5788

GEOMAR
Research Center
for Marine Geosciences
Wischhofstr. 1-3
D - 24148 Kiel
Tel. (49) 431 / 600-2555, 600-2505

TABLE OF CONTENTS SO144-1 & 2

1.1 ZUSAMMENFASSUNG

Die SONNE - Fahrt SO144 – 1&2 im Rahmen des Projektes PAGANINI (PAnama basin and GAlápagos plume - New INvestigations of Intraplate magmatism) fand in der Zeit vom 07. September bis zum 07. November 1999 statt. Ausgangshafen war San Diego, USA. Für zwei Unterbrechungen und als Endhafen wurde Caldera, Costa Rica, angelaufen. Auf den beiden ersten Fahrtabschnitten (SO144 1a&b) standen nach dem Transit ins Arbeitsgebiet vornehmlich seismische Messungen im Vordergrund. Während der gesamten Fahrt wurden kontinuierlich hydroakustische Daten aufgezeichnet und, soweit möglich, magnetische Messungen durchgeführt. Diese sind zur Ergänzung und Erweiterung der Datenbasis früherer Sonne - Fahrten (SO76, SO81, SO107) und anderer Expeditionen für die plattentektonische Rekonstruktion und die morphotektonische Entwicklung des Untersuchungsgebietes von großer Bedeutung. Nach Möglichkeit wurden Transitprofile so gewählt, daß bislang nicht vermessene Gebiete erstmals überdeckt wurden. Die ersten Auswertungen zeigen deutliche Unterschiede in der Kontinentalhangmorphologie zwischen Nicaragua und Costa Rica, die zum Teil von den Unterschieden der abtauchenden Platte herrühren, aber auch den variablen Aufbau des Kontinentalrandes reflektieren.

Nach Erreichen des Untersuchungsgebietes und ersten Arbeiten am Kontinentalrand von Nicaragua wurde nordwestlich der Osa - Halbinsel ein seismologisches Netzwerk aus 14 Stationen vom SCRIPPS Institute of Oceanology ausgebracht. Diese Stationen decken die Region des starken Bebens vom 20. August 1999 (Mw 6.7) ab und sollen die Grundlage für eine Detailuntersuchung der Prozesse in der seismogenen Zone liefern. Die Stationen sind zusätzlich mit einem Flowmeter ausgestattet, und zusätzliche 7 Flowmeter einer anderen Konfiguration wurden in der unmittelbaren Umgebung ausgesetzt. Alle Geräte sollen im Dezember 1999 auf dem Fahrtabschnitt SO144-3b geborgen werden. Zusätzliche Landstationen sowie Sprengungen an Land zur Kalibrierung der Stationen runden das Meßprogramm ab. Die Positionierung der Geräte um die geplante ODP-Bohrung ermöglicht einen wichtigen Beitrag für den Pre-Site Survey.

Für die aktiven seismischen Untersuchungen standen 21 Ozeanbodenhydrophone (OBH) bzw. –Seismometer (OBS) des GEOMAR sowie 13 OBS des IRD und ein OBH vom IFREMER zur Verfügung. Insgesamt wurden mit diesen Geräten 162 Positionen besetzt. Die Anregung der seismischen Signale erfolgte mit bis zu drei BOLT 800 c - PAR 800 CT Airguns, jede mit einem Kammervolumen von 32 Litern. Lediglich für die hochfrequenten seismischen Untersuchungen der BSR-Strukturen am Kontinentalrand vor Costa Rica wurde ein kleinvolumiges Airgunarray, bestehend aus bis zu vier Airguns, eingesetzt.

Am Kontinentalrand von Nicaragua wurden in Erweiterung der Messungen der Fahrt SO107 zwei küstenparallele Profile auf dem Schelf aufgenommen, die Datenqualität ist aber durch den hohen Störpegel nachhaltig beeinflußt. Dennoch läßt sich im Profilverlauf die Vertiefung des Sandino-Beckens sehr gut verfolgen, die Beckentiefe nimmt von 5 km im Südosten auf über 10 km im Nordwesten zu. Unter den Beckensedimenten zeichnet sich durch einen starken Geschwindigkeitssprung von 5.0 auf 6.3 m/s das Basement ab. Die hohen Geschwindigkeiten von 6.3 bis 6.6 km/s in dieser Schicht legen in einer ersten Interpretation die Annahme von ozeanischer Unterkruste (Ophiolithe) für das Basement nahe.

Alle übrigen Profile hatten die Untersuchung der ozeanischen Kruste und ihrer untermeerischen Strukturen, wie auflagernde Rücken, Plateaus und Seamounts, zum Ziel. Dabei zeigte sich, daß sowohl der Cocos - Rücken (auf drei Profilen vermessen) als auch der Malpelo - Rücken (ein Profil) eine ganz ähnliche interne Krustenstruktur und mit einer Mohotiefe von 21 km eine ähnliche Krustengesamtdicke haben. Interessant ist, daß bei beiden Rücken an der nordwestlichen Flanke der Übergang von normaler ozeanischer Kruste mit einer Mächtigkeit von ca. 9 km zum Rücken hin über eine sehr kurze Entfernung stattfindet, während nach Südosten der Übergang in einer sehr breiten Zone verläuft.

Im Bereich der Osa - Halbinsel wurde eine dreidimensionale Untersuchung des Kontinentalrandes angestrebt.. Dazu wurden die Airgunschüsse um die Halbinsel herum bis in den Golfo Dulce hinein abgefeuert. Die Schüsse wurden sowohl von Geräten auf einem Profil im Streichen des Cocos -Rückens als auch von Stationen, die senkrecht zum Rücken ausgelegt waren, als auch von den Stationen des seismologischen Netzes aufgezeichnet. Ein abschließendes Profil

verlief auf der ebenen ozeanischen Kruste vor der Nicoya - Halbinsel an der Stelle, wo wir aufgrund der magnetischen Anomalien den Übergang von der am Galápagos Spreading Zentrum gebildeten Kruste zu der am ostpazifischen Rücken gebildeten Kruste vermuten. Eine erste visuelle Inspektion der qualitativ hochwertigen Seismogramme deutet tatsächlich auf Unterschiede zwischen beiden Krustenprovinzen hin.

Im Rahmen der Ausfahrt wurden zudem neue Systeme getestet. Dabei hat nicht nur das IFREMER - OBH, basierend auf der Aufzeichnungselektronik des GEOMAR - OBH, seine Bewährungsprobe bestanden, auch das am GEOMAR entwickelte Breitbandozeanbodenseismometer mit dem neuen GEOLON - MLS-Recorder haben zu unserer Zufriedenheit gearbeitet und lassen für die Zukunft langfristige marine seismologische Untersuchungen machbar erscheinen.

Im Rahmen von SO144-2 vom 19.10 bis 08.11.1999 wurde erstmals auf FS SONNE das tiefgeschleppte Multifunktionssystem TOBI vom Southampton Oceanography Centre eingesetzt. Während 4 Einsätzen wurden 950 Profilkilometer vermessen, die südlich des Golfes von Nicoya den unteren Kontinentalhang bis zur Tiefseerinne mit einer Gesamtfläche von 4950 km^2 überdecken. Hochauflösende Side-Scan-Sonar-Aufzeichnungen von TOBI geben Einblicke in Detailstrukturen am Meeresboden, mit denen die Subduktionspuren der Seamounts und die Vorgänge der Rutschungsereignisse rekonstruiert werden können. Verschiedene Vertikalbewegungen haben deutlich ihre Spuren hinterlassen. Weiterhin treten an unterschiedlichen Stellen Bereiche mit hoher Reflektivität auf, die nicht durch die Morphologie zu erklären sind. Sehr wahrscheinlich stellen diese Bereiche Gebiete dar, in denen es zu einer verstärkten Zementation durch aufsteigende und zirkulierende Fluide kommt.

Wie in anderen Subduktionszonen kommt es auch in dem Untersuchungsgebiet zu einem Fluid- und Gastransport, der an das Kompressionsgeschehen des aktiven Plattenrandes gebunden ist. Gashydrate wirken dabei als ein Speicher für Gas, Wasser und andere Spurenstoffe. Im Rahmen von 10 Untersuchungsprofilen mit dem Videoschlitten OFOS und 9 gemessenen Methanprofilen in der Wassersäule wurden zahlreiche Fluidaustrittsstellen nachgewiesen. Während die Methanprofile im Bereich von Fluidaustrittsstellen durch deutlich erhöhte Werte, meist am Boden, gekennzeichnet sind, dokumentieren die Beobachtungen mit dem Videoschlitten die Austrittsstellen direkt, durch die Existenz von chemosynthetischen Organismengemeinschaften und Präzipitaten. Solche Austrittsstellen wurden vor allem in aktiven oder recht jungen Rutschungsgebieten wie dem Jaco Scar oder Parrita Scar gefunden. An einer kleinen Rutschung im Osten wurden große zusammenhängende Felder von Bakterienmatten gefunden und an einem aktiven Schlammvulkan im Westen eine spektakuläre Ventfauna nachgewiesen, die sehr differenziert sein Zentrum besiedelt.

1.2 SUMMARY

SONNE cruise SO144-1&2 started on 7 September 1999 in San Diego, California, and ended on 8 November 1999 in Caldera, Costa Rica. Two visits were paid to the port of Caldera for exchange of personnel and equipment. The cruises, together with the follow-up cruise SO144-3, constitute the PAGANINI (PAnama basin and GAlápagos plume - New INvestigations of Intraplate magmatism) project. After transit to the working area, the first two legs (SO144 1a&b) were mainly dedicated to seismic data acquisition. During the entire cruise, hydroacoustic data were collected and magnetic measurements were made whenever possible. The data sets will extend the existing database, mainly collected on previous SONNE cruises (SO76, SO81, SO107), but also by other ships. They provide an essential element for the morphotectonic development of the survey area and plate tectonic reconstruction. Where possible, transit profiles were placed so that unsurveyed areas were covered. First results of the newly acquired hydroacoustics indicate profound differences in the morphology of the continental slope between Nicaragua and Costa Rica, which can partly be related to differences of the incoming plate, but partly also document the variability of the upper plate structure and composition.

Having reached the survey area and after some investigations off Nicaragua had been performed, 14 ocean bottom stations from SCRIPPS Institute of Oceanology were installed northwest of Osa peninsula. They cover the region of the 20 August 1999 (Mw:6.7) earthquake and will be used for detailed studies of the processes in the seismogenic zone. The stations are also equipped with a flow meter, 7 additional flow meters were deployed in the immediate vicinity. All instruments are to be recovered in December 1999 during leg SO144-3b. Additional land stations and explosive charges on land for the calibration of the marine stations are an integral part of this investigation. They will also be a valuable contribution to the proposed ODP drilling into the seismogenic zone.

For the active seismic experiments, 21 GEOMAR Ocean Bottom Hydrophones (OBH) and Ocean Bottom Seismometers (OBS), 13 IRD OBS and one IFREMER OBH were available and used at a total of 162 positions. Seismic waves were generated using up to three BOLT 800 c - PAR 800 CTairguns, each with a volume of 32 liters. In addition, for high resolution investigation of BSR structures on the Costa Rican margin, a small-volume array was used consisting of up to 4 airguns.

Two seismic wide angle profiles were shot along the continental margin of Nicaragua, adding on to the existing profiles of SO107. However, the signal-to-noise ratio is rather poor due to the high noise level at the shelf. Still, the depth of Sandino basin can be interpreted, increasing from 5 km in the southwest to more than 10 km in the northeast. The basement is seen with rather high velocities of 6.3-6.6 m/s, which indicate an ophiolitic nature of the basement.

All other profiles concentrated on the oceanic crust and anomalous structures such as ridges, plateaus and seamounts. Cocos Ridge (investigated along three profiles) and Malpelo Ridge show a rather similar structure with a Moho depth of 21 km. It is interesting to note that on both ridges the northeastern flank is marked by a sharp transition to the 9-km-thick neighboring oceanic crust, while to the southwest the transition extends over a very broad zone.

Near Osa peninsula we tried a quasi-3-D investigation of the continental margin. Airgun shots were fired around the peninsula, extending into Golfo Dulce. These shots were recorded by instruments deployed along strike of Cocos Ridge as well as stations perpendicular to the ridge. In addition, they were close to the seismological net. The final profile was located off Nicoya peninsula, where, based on magnetic anomalies, the transition of crustal provinces is expected to occur. Here, crust generated at the East Pacific Rise should be in contact to crust

generated at the Galápagos Spreading Center. A first visual inspection of the data indicates differences between the two provinces.

We also tested new instrumentation. The IFREMER OBH, based on GEOMAR OBH electronics, worked satisfactorily. The new GEOLON recorder and the broadband seismometer attached to a GEOMAR OBS worked rather well, and thus long-time marine recordings for seismological application seem feasible in the future.

During SONNE cruise SO142-2 (19 October to 8 November) the TOBI deep tow system from the Southampton Oceanography Centre was used for the first time on RV SONNE. In 4 deployments, 950 km of trackline were surveyed, mainly covering the lower margin south of the Golfo de Nicoya, extending over an area of 4950 km^2. High resolution side scan sonar images from TOBI provide insight into details of seafloor morphology, which enable us to study the subduction of seamounts and accompanying slope failure. Differential vertical movements are easily deciphered. Regions of high reflectivity are identified which cannot be explained by morphology alone. These are interpreted as areas where precipitation takes place, caused by circulating fluids.

As in other subduction zones, off Costa Rica we find fluid and gas transport due to compression along the active margin. Gas hydrates store gas, water and other trace elements. 10 profiles were run with the OFOS video sled and 9 for sampling methane. Numerous seeps were encountered. While methane concentrations are high in the bottom water near seeps, the video pictures documented the seeps by the appearance of chemosynthetic vent organisms. Such vents were concentrated near slide scars such as the Jaco or Parrita scars. Next to smaller scars, large fields of bacteria mats and active mud volcanoes were seen, with a spectacular fauna near the center of the mud volcanoe.

2. INTRODUCTION TO THE PAGANINI PROJECT

(R. von Huene, C. Ranero, E. Flueh, J. Bialas, P. Charvis, K. McIntosh)

2.1 THE OBJECTIVES OF PAGANINI

Previous PACOMAR and TICOSECT program investigations since 1992, and the Alvin dives followed by ODP Leg 170, formed the basis for an expanded multidisciplinary project called Paganini (**Pa**nama Basin and **Ga**lapagos Plume **n**ew **in**vestigations of **I**nterplate Magmatism). It involves a large international group of investigators from Germany, France, Costa Rica, Ecuador, Colombia, and the US. The project is internationally funded and involves several institutions within the participating nations. Scientific studies extend geographically over the deep ocean areas and continental margins between Nicaragua and Ecuador, and include the Cocos, Carnegie, Malpelo, and Coiba ridges (Figure 2.1). The broad objectives of the Paganini project can be summarized as follows:

1. Reconstruct mantle plumes, hotspot magmatism, and development of "large igneous provinces (LIPS)" for a more complete understanding of the Galapagos Plume system.
2. Refine understanding of the "Galapagos volcanic system (GVS)" by constraining a plate tectonic history of the Panama Basin region.
3. Characterize the relationship between the subduction of normal GVS and thick Cocos Ridge crust and seismicity, arc volcanism, and rapid coastal uplift to aid in assessments of natural hazards. How is seismogenic rupture affected by the character of the subducting plate?
4. Record earthquakes with an array of ocean bottom instruments and a network on land to define the seismogenic zone configuration. Particular emphasis is given to the updip end of the seismogenic zone which is poorly resolved when only using land-based networks.
5. Investigate destabilization of gas hydrates as they are uplifted over subducting seamounts at the continental margin off Costa Rica. The active collision process elevates gas hydrated sediment which is then exposed at the seafloor in slump scars and may vent gas. Does gas hydrate tend to stabilize slopes or form a slip surface for gravity failure?

US participation is under the MARGINS program of the National Science Foundation and is directed toward goals of both the SEIZE (Seismogenic Zone Experiment) and Subduction Factory initiatives. SEIZE is focussed on understanding the three-dimensional distribution and nature of the seismogenic zone and specifically the processes which generate destructive tsunamis. The techniques include GPS, optical leveling, seismographs on land, and Ocean Bottom Seismographs and MCS data offshore. The Subduction Factory is directed toward understanding and quantifying mass and chemical fluxes through the subduction system. Characterizing thickness and compositional variation of the subducting Cocos plate is a key to this process. French participation is under the SISTEUR program of IRD and CNRS and is part of the International Margins Program. It is concentrated off the coasts of Colombia and Ecuador where the principal objectives are to image the seismogenic zone with controlled source seismic techniques and test models for the generation of large thrust earthquakes.

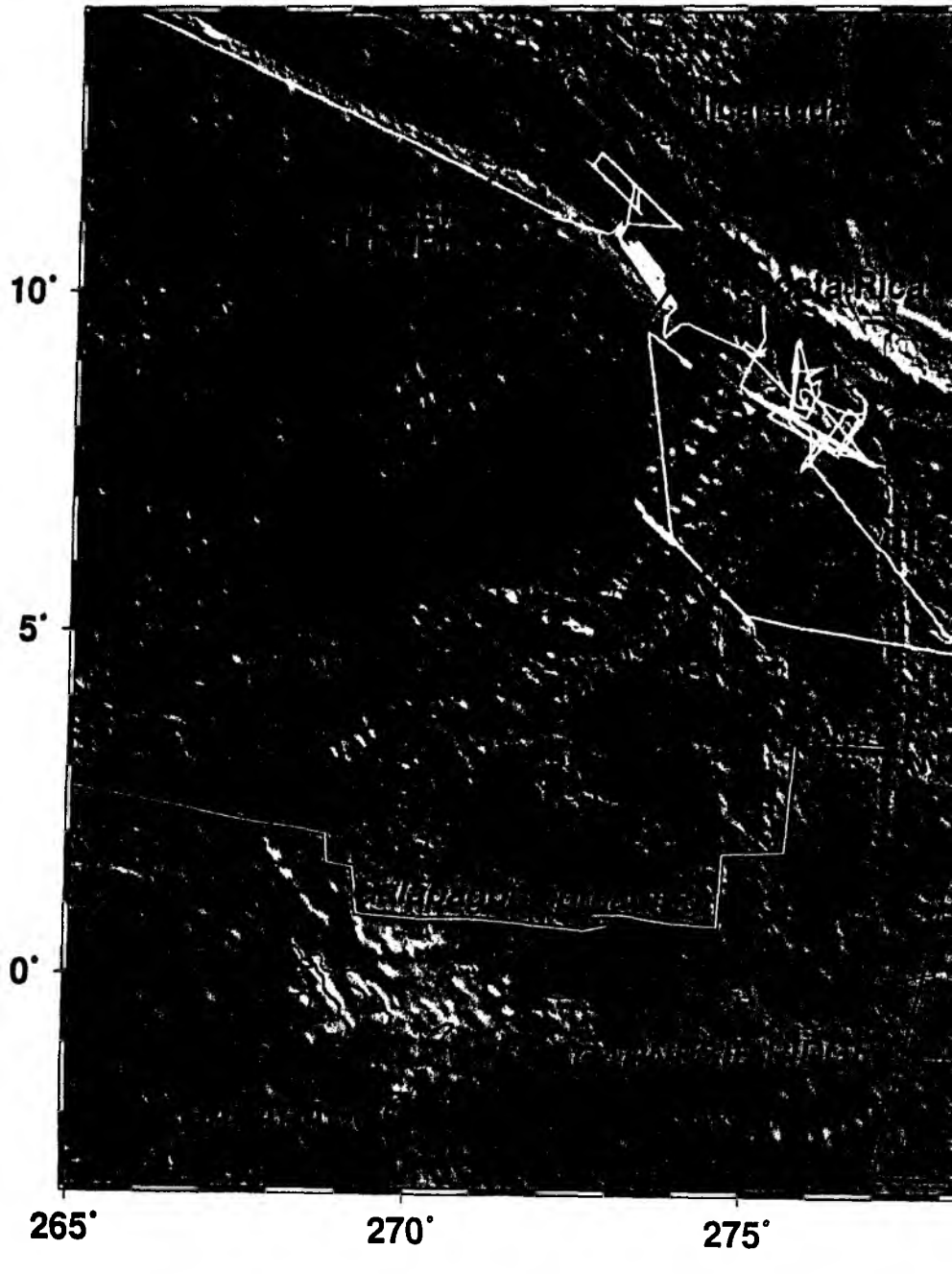
10°
5°
0°
265°
270°
275°

Figure 2.1: Tracks of the PAGANINI Cruise (SO144-1) and location of related international projects.

2.2 RESULTS OF PREVIOUS INVESTIGATIONS AND REGIONAL GEOLOGIC SETTING

Along convergent margins, upper plate tectonism is closely allied with the character and relief of the subducted lower plate. This concept is generally accepted but a question is how much tectonism is controlled in this way? The upper-lower plate interaction is often underappreciated without high resolution geophysical data. On the oceanic plate many physical features significant to the upper-lower plate relation are not apparent without swathmapping. This is shown off Costa Rica where previous Sonne swathmapping revealed uncharted 1.5 - 2.5 km high seamounts on the subducting ocean floor and the adjacent continental slope has muted domes and locally the trailing flanks of seamounts (von Huene et al., 1995). In a few instances the seamounts on the lower plate beneath these domes are imaged in seismic reflection lines (von Huene et al., submitted 1999). Tracks of subducted seamounts are seen up to the shelf edge even where the upper plate is 10 km thick. It is further inferred that along a projection of linear seamount chains clusters of earthquakes beneath the shelf and uplifted coastal terraces are a continuation of this expression. The significance of these observations toward understanding nucleation of great earthquakes is that lower plate character and relief may be retained at distances >100 km from the trench rather than being obliterated in the first 50-100 km of the megashear between the converging upper and lower plates. If lower plate character can be projected into the seismogenic zone it may help understand the nucleation process and differences in frictional behavior in rupture planes. Thus characterization of the oceanic plate relates to understanding dynamics of the continents.

Previous work in the Costa Rica area has shown that if swathmapping data are well edited, the gridded density of soundings can be increased up to 5 times thereby increasing resolution and sharpening the morphological image. Using such high resolution bathymetry and other geophysical data three types of ocean crust entering the Costa Rican subduction zone become obvious: (1) the Cocos Ridge has thicker than normal crust which stands 2 km above the surrounding seafloor, (2) the ridge is flanked by crust of normal thickness covered 40% by seamounts, (3) the adjacent ocean crust is the oldest Cocos-Nazca spreading center crust with a smooth morphology near the trench (von Huene et al., submitted 1999). Off Costa Rica the segment boundaries are marked by aligned seamounts and ridges. This geology provides an opportunity to investigate the significance of lower plate character on frictional behavior in a subduction zone. Here plate convergence and sedimentation are essentially uniform, and the variable is lower plate character. Thus upper plate structure and seismicity in adjacent areas of the subduction zone can be compared.

The continental slope off Nicaragua and Costa Rica begins with a 3- to 10-km-wide frontal prism whose form appears independent of lower plate morphology. In the Ocean Drilling Program Leg 170 transect this prism was found to be composed of material of the slope sediments rather than accreted sediments (Kimura et al., 1997). This may be generally the case for this area although it has not been drilled elsewhere. Where the prism is locally eroded by subducting seamounts, it is quickly (0.1-0.2 My) restored to its original width once they pass. The short healing time from local collision with seamounts provides it with only a short geologic memory of lower plate perturbations. The upper plate retains a longer history of the subducted lower plate character in the upper and middle slopes. This is shown by the

similar character displayed in oceanic and continental segments across from each other. Where Cocos Ridge has subducted beneath the Osa platform erosion is pronounced. Opposite the adjacent seamount segment broad embayments indicate an eroded upper slope, and thinning along the underside of the upper plate is observed in seismic images over the peaks of seamounts (Ranero et al., submitted 1999). Where only a smooth lower plate has subducted, the middle and upper slopes are more uniform and relatively stable. Each oceanic morphology is overlain by an upper plate morphologically different from its neighbor and is bounded by linearly aligned seafloor relief.

Morphological interpretation is complemented by seismic and magnetic data. Magnetic anomalies recorded along closely spaced swathmap tracks define the field sharply. Seismic reflection data processed with pre-stack depth migration software systems image a distinctive plate boundary reflective sequence. OBH/S wide-angle seismic data constrain the position of this boundary at greater depths. Wide-angle seismic velocity models show rock masses with mantle velocities underneath the Nicaragua seismogenic zone, which are not observed off Costa Rica (Walther et al., in review). The morphological differences between the Costa Rica margin and the Nicaraguan margins are expressions of upper plate structural differences which locally correspond with major features in the lower plate.

Segmentation boundaries on the ocean plate continue transversely across the lower slope to the coast. They coincide in varying degrees with physical and geochemical segmentation of the arc and perhaps seismogenic rupture zones. It is not clear that the geochemical slab signal in arc lavas of Costa Rica and Nicaragua correlates with subducted sediment or erosional flux, so other sources for that geochemical signal may be important. A first order effect that could provide the slab signal may be the fluid held by fractures in the subducted ocean crust. Faulting associated with ocean crust flexure into the trench axis is most severe off Nicaragua where the slab signal is greatest. Thus segmentation of the subducting lower plate may offer a guiding framework for investigating processes in the seismogenic zone and along the volcanic arc.

The Nicoya and Osa Peninsulas, by their seaward projection toward the trench, are particularly well suited for GPS measurements because critical parts of the seismogenic zone are above water. The deformation of the earth above the seismogenic interface can be observed with geodetic techniques. Where the interface is locked, the signal is likely to be greatest, but locked areas are commonly under water. The program of geodetic measurements on the peninsulas will be combined with data from the OBS array offshore to outline the active slipping part of the seismogenic zone.

Two related projects are now planned for the Paganini area that seek to build on the success of Paganini. The NICSEIS project, planned for June, 2000, is a joint project between University of Texas, University of California, GEOMAR, and Nicaraguan institutions INE and INETER. This project will extend MCS coverage along much of the Nicaraguan margin and also include three wide-angle seismic profiles. This survey will cover the transition in the Cocos plate from relatively smooth to heavily faulted from northern Costa Rica to northwest Nicaragua (Figure 2.1). Onshore, this segment features an offset in the volcanic arc and dramatic gradients in geochemical tracers.

The SISTEUR project is to be conducted by the UMR Geosciences Azur (IRD, CNRS, University of Paris, and University of Nice) along the Ecuador-Colombia active margin (Figure

2.1) in cooperation with GEOMAR (Kiel), the Escuela Politecnica Nacional (EPN) of Ecuador, Ingeominas, and the Universidad de los Andes of Colombia. The cruise is part of the International Margins Program and PNRN (Natural Hazards National Program) and is scheduled in 2000 on board the R.V. Nadir (seismic sources and streamer) and R.V. Antea (OBS-OBH).

The main goal of the project is to image the inter-plate seismogenic zone and to test occurrence models of large thrust-type subduction earthquakes and their implication on coastal tectonics. The Ecuador-Colombian margin encompasses two seismically and tectonically contrasting segments: a northern segment (3.5°N-0.5°S) that is globally subsident and underwent four great (7.8<M<8.7) historical earthquakes, and a southern segment (0.5°S-3°S) that is uplifting and has no record of great earthquakes. The SISTEUR project will characterize and compare the geometry of the subduction channel within these two segments of the margin, and document deformation, sedimentary accretion, and underplating. Approximately 2200 miles of 360-channel seismic reflection data using a tuned, 40-litre airgun array and 2000 miles of wide-angle seismic profiling using a low-frequency 128-litre airgun array and recorded by 50 OBSs and 35 land stations will document the shallow and deep structures of the margin.

2.3 SEAFLOOR SPREADING HISTORY OF THE COCOS-NAZCA SPREADING SYSTEM

(M. Meschede)

The evolution of the large tectonic units in the Eastern Pacific is still not very well known. During the Mesozoic and Early Cenozoic the East Pacific Rise separated the Pacific plate in the west from the Farallon plate in the east. During the Oligocene a triple point was created when the Farallon plate was split into the northern Cocos and the southern Nazca plate. The main difficulty is that oceanic crust which was formed by seafloor spreading at the E-W trending spreading center between Cocos and Nazca plates has been overprinted by the Galapagos hotspot. Two major ridges in the Eastern Panama Basin, the Cocos and Carnegie ridges, were formed at the Galapagos hotspot during the last ca. 22 Mio. years (Hey, 1977; Lonsdale and Klitgord, 1978). Two minor ridges, the Malpelo and Coiba ridges, are assumed to have formed at the Galapagos hotspot as well. According to Hey's model (Hey 1977) the oceanic crust of the Cocos plate was formed by highly asymmetric seafloor spreading along the boundary of the Nazca and Cocos plates, with spreading at the Cocos-Nazca spreading center active since 25 to 28 Ma. The oldest identified seafloor spreading anomalies formed at the Cocos-Nazca spreading center exist in the northeasternmost part of the Panama Basin and are correlated to anomaly 6C (Lonsdale and Klitgord, 1978). This corresponds to an age of 23.6 Ma according to the geomagnetic polarity time scale of Cande and Kent (1995).

Hey (1977) noted the tectonic history of the Galapagos area is difficult to reconstruct because the older magnetic anomalies are extremely difficult to correlate despite a good data base. Anomalies younger than anomaly 4A, however, are easily correlated. Another explanation of the spreading history was provided by Wilson and Hey (1995) who presented a detailed map of the younger part of the Cocos-Nazca spreading center including anomalies 1 through 4A.

Based on magnetic, gravimetric and bathymetric data from earlier Sonne cruises (SO-76, von Huene et al., 1995, SO-107, Mrazek et al., 1996) and on data from other sources (e.g., Smith and Sandwell, 1997; Sandwell and Smith, 1997; Lonsdale and Klitgord, 1978; National Geophysical Data Center, 1996), Meschede et al. (1998) presented a three-stage model for the tectonic evolution of the Cocos-Nazca spreading center.

Barckhausen et al. (1997, 1998) pointed out that magnetic anomalies obtained during the Sonne cruises cannot be related to the East-Pacific Rise nor to the present Cocos-Nazca spreading center, because seafloor spreading anomalies formed at the East-Pacific Rise are oriented N15°W to N45°W, while those formed at the present Cocos-Nazca spreading center are oriented N90°E. The anomalies indentified offshore Nicoya peninsula are, however, oriented N50°E and N70°E and are in discordant contact. This precludes a rotation from an early ENE-WSW orientation into its present E-W orientation as it has been suggested by Hey (1977).

Reviewing all available ship track data and bathymetric information covering the Cocos and Malpelo ridge areas, the magnetic data indicate a NE-SW and ENE-WSW oriented linear magnetic anomaly pattern on both ridges which are in discordant contact to and different from the E-W oriented pattern of the present Cocos-Nazca spreading center and from the NW-SE oriented pattern of the East Pacific Rise generated crust.

Meschede et al. (1998) identified two sets of anomaly patterns on magnetic profiles crossing the Cocos and Malpelo ridges, (1) an older one striking N50°E, and (2) a younger one oriented N70°E (Fig. 1). Symmetric anomalies indicate the center of the younger abandoned spreading system at the northwestern flank of the Cocos ridge and on top of the Malpelo ridge, the center of the older system is suggested to be south of the Carnegie ridge. According to this model, two precursors (CNS-1 and CNS-2) of the presently active Cocos-Nazca spreading center (CNS-3) existed. The identification of the seafloor spreading anomalies correlated to a synthetic profile (Cande and Kent, 1995; Fig. 2) attributes anomalies 6Bn.1n through 6An.2r to the older spreading system (CNS-1) which was active from 22.8 to 19.5 Ma. Anomalies 6 through 5ADr are attibuted to the younger spreading system (CNS-2) which was active from 19.5 to 14.7 Ma. Spreading rates have been determined as 50 mm/y for CNS-1 and 40 mm/y for CNS-2.

Strong E-W trending and symmetric linear anomalies west of Cocos Island indicate a second small E-W trending spreading axis parallel to the presently active Cocos-Nazca spreading center which has been active from 3.0 to 1.8 Ma (anomalies 2A to 2; Fig. 2). This abandoned spreading system is probably related to another failed rift of the Cocos-Nazca spreading system identified by Anderson et al. (1976) and Batiza (1986).

The oldest preserved anomaly of the CNS-1 spreading system (6B, Fig. 1) intersects the same anomaly on crust of the East Pacific Rise, located 80 km southwest of ODP Sites 1039/1040 (Kimura et al., 1997). Anomalies associated with the southeasternmost part of the CNS-1 spreading system are suggested to be displaced towards the south by the active CNS-3 spreading and today located on the Nazca plate north of the Grijalva Scarp where anomalies are also determined as anomalies 6 through 6B (Lonsdale and Klitgord 1978).

The boundary between oceanic crust formed at the East-Pacific Rise and that formed at the Cocos-Nazca spreading center (Barckhausen et al., in prep.) has been termed the "rough-smooth boundary" (Hey, 1977). It has two prominent kinks: One in the north at about 5°N, 89.5°W where the boundary changes from an ENE-WSW trend to a NE-SW trend, and another one in the south at 4.5°S, 84.5°W, with a change from E-W to NE-SW. An elegant way to explain this

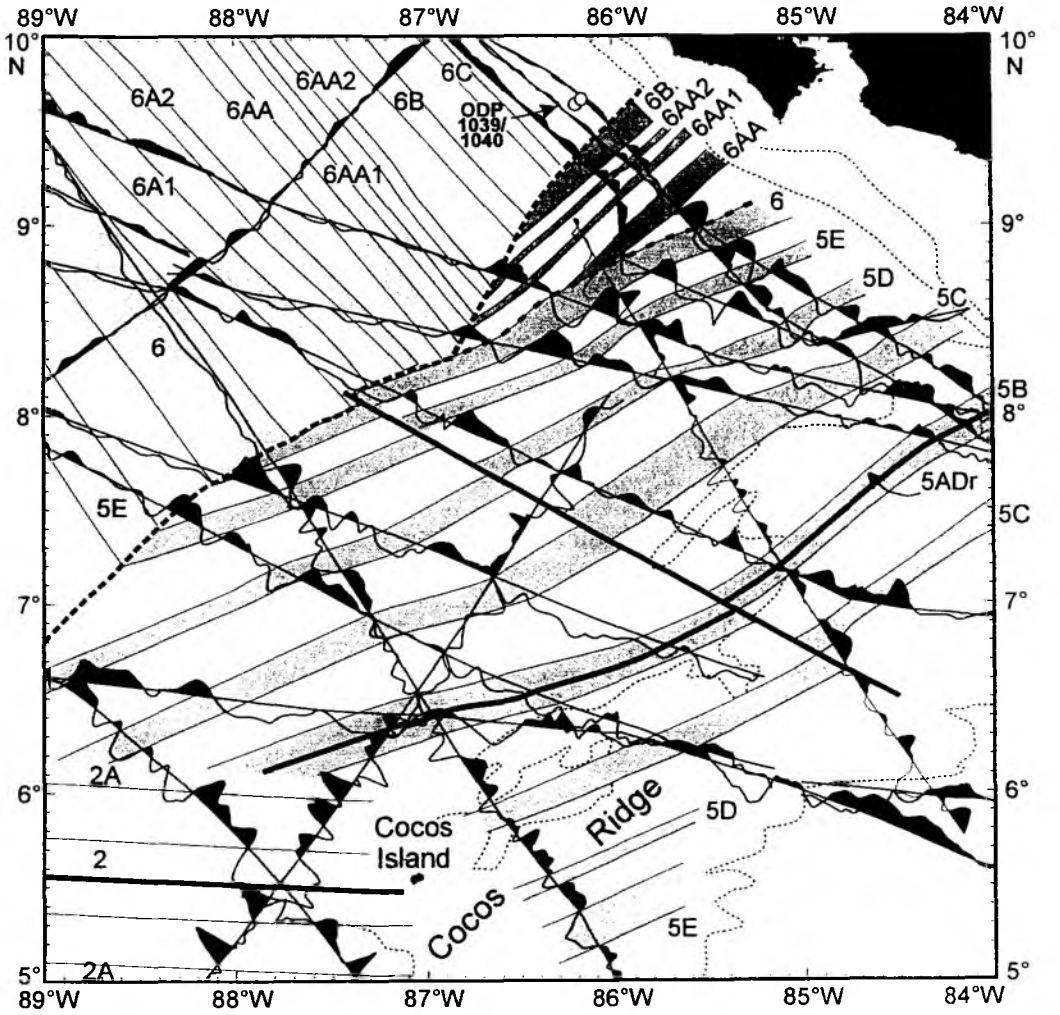

Figure 2.3.1: Magnetic anomalies in the Cocos ridge area. Correlation of representative ship tracks and chron identification refers to Fig. 2.3.2. Ship tracks are from National Geophysical Data Center (1996), von Huene et al. (1995) and Mrazek et al., (1996). Anomalies 6 and 6A at East-Pacific Rise generated oceanic crust (upper left) according to Wilson (1996).

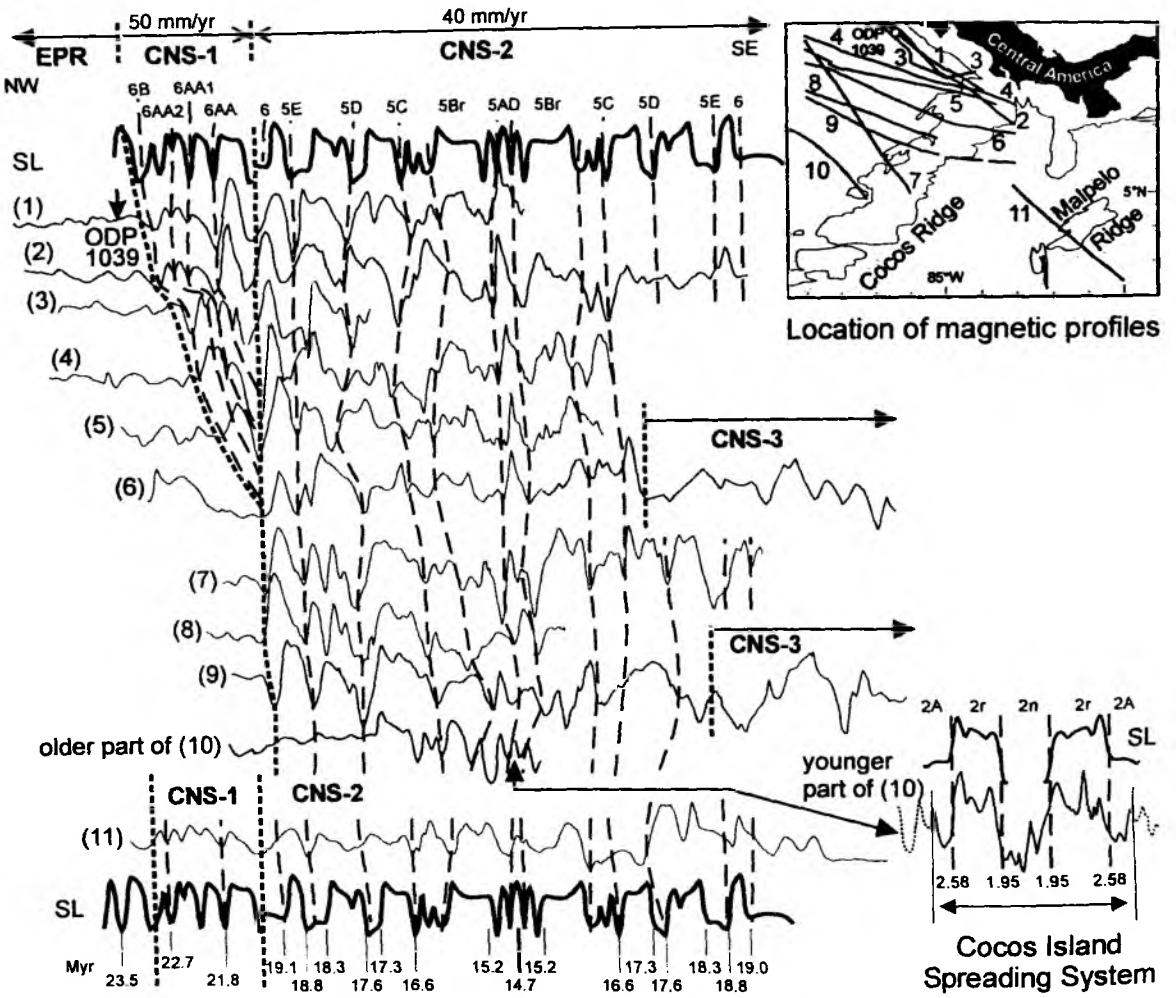

Figure 2.3.2: Correlation of magnetic profiles at the Cocos and Malpelo ridges, line 1 crossing ODP Site 1039, line 7 as an example for a symmetric magnetic profile crossing the extinct spreading center of the precursor 2 of the Cocos-Nazca spreading system (5ADr). SL: Synthetic line of magnetic anomalies. EPR: East Pacific Rise generated crust. CNS-1: Generated at the precursor 1 of the Cocos-Nazca spreading Center (22.8 - 19.5 Ma); CNS-2: Generated at the precursor 2 of the Cocos-Nazca spreading Center, 19.5 - 14.7 Ma); CNS-3: Generated at the Present Cocos-Nazca spreading Center (since 14.7 Ma). Chron identification refers to the geomagnetic polarity time scale (Cande and Kent, 1995). Inset shows location of the ship tracks.

irregular geometry is the three-stage model of Meschede et al. (1998) who suggest jumping spreading axes with different spreading directions and more or less symmetric spreading.

A palinspastic restoration of the CNS-2 at 14.7 Ma juxtaposes the Malpelo and Cocos ridge (Hey, 1977; Lonsdale & Klitgord, 1978). The missing 200-250 km of the Cocos-Malpelo ridge system has been subducted beneath the Central American volcanic arc and is responsible for the uplifted Cordillera de Talamanca in Central and Southern Costa Rica. There, plutonic rocks of Miocene age are exposed more than 3500 m above sea level (Drummond et al., 1995, De Boer et al., 1995 , Graefe 1998). Assuming a constant subduction rate of 81 mm per year (DeMets et al., 1990) the onset of the Cocos ridge subduction began about 3-4 Ma ago. This is supported by geological data from Costa Rica which document a change from marine to mainly continental sedimentation (Sprechmann et al., 1994), a shallowing from bathyal to near-shore conditions in the back-arc of Costa Rica and western Panama (Collins, 1993; Collins et al., 1995), and the absence of strato-volcanoes in the southeastern part of Costa Rica since the Pliocene (De Boer et al., 1995).

Additional magnetic profiles to be collected during Paganini will hopefully contribute to a better defined anomaly pattern and thus can be used for better confirmed interpretation.

2.4 GAS HYDRATE RESEARCH OFF CENTRAL AMERICA

(G. Bohrmann and E. Flüh)

Gas hydrates are crystalline compounds consisting of gas and water that form at high pressure and low temperatures when the low molecular weight gas is present in excess of solubility. Methane hydrates are stable under the temperature and pressure conditions generally found in the Arctic and near the seafloor at water depths greater than 500 m (Kvenvolden, 1993). They are quite common beneath the continental slope of both active and passive margins as well as in sedimentary sequences of marginal basins (Kvenvolden, 1993). Typically, hydrates occur tens to hundreds of meters below the seafloor, depending on methane availability, temperature and pressure.

Gas hydrates have recently become a major focus of international research because of increasing recognition that large volumes of gas are stored in hydrates. These deposits represent a significant fraction of the global methane budget and may therefore be a potential energy resource for the future (Kvenvolden 1988). Several authors have also suggested that decomposition of hydrates in subseafloor sediments in response to changing environmental conditions can have a significant effect on past climate (Dickens et al. 1997; Paull et al. 1991). Hydrates have been mapped based on the distribution of the bottom simulating reflector (BSR) - a characteristic reflection caused by a strong impedance contrast between hydrate-bearing sediment above and gas-filled pore space below (Trehu et al. 1999; Pecher et al. 1998). Current research is focused on quantifying the relationship between BSR characteristics, the free gas volume (Rempel and Buffet, 1997), solid hydrate volume (Hyndman et al. 1992), fluid flow rates (Suess et al. 1999), the stability regime (Zapsepina et al. 1997) and past gas hydrate manifestations like gas hydrate carbonates (Bohrmann et al. 1998). In particular, at the Costa Rican continental margin, the relationship between land slides and gas hydrates is interesting because huge areas of land sliding (von Huene et al. in press), are present as well as large volumes of gas hydrates (Kimura et al. 1998).

The first recovery of gas hydrate in the Pacific consisted of a small piece in a DSDP Leg 66 core. More pieces were found on DSDP Leg 67 - the discovery causing the GLOMAR CHALLENGER to be directed to other objectives because of the safety rules at that time. Later, on DSDP Leg 84 off Guatemala, a full core section of gas hydrate was recovered and preserved in cooled pressure vessels, thus allowing the first in-depth chemical studies on shore. The first drill site off Costa Rica during the same leg was terminated above its target depth with recovery of hydrate in a volcanic ash. Considerable amounts of hydrate were also recovered during Leg 170 (Kimura et al. 1998). It is notable, no BSR was observed in seismic records of 1970 or in those later collected off the central Nicoya Peninsula by the University of Texas - even with 3D processing (Shipley et al. 1992). In these cases, BSR absence may be due to the abnormally low temperatures in that area (Langseth and Silver, 1996). Nevertheless, with careful processing of records from SO81 off central Costa Rica, many BSRs were observed (Ranero et al. 1996).

The distribution of BSRs in the SO81 data is ubiquitous between 100-400 mbsf off central and southern Costa Rica (Pecher et al. 1998; Fig. 2.4.1.). BSRs start at the décollement and

extend almost across the entire slope in some seismic lines, but are absent in areas affected by slumping. An exception was observed in lines 15 and 21 on the Nicoya slide mass. Along line 15, where slumping was greater, no BSR can be identified. However, a BSR present through much of the slump structure along line 21 (Pecher et al. 1998) can be attributed to the coherence of the slumped mass maintaining the sediment column intact.

The gas hydrate recovered on Legs 84 and 170 came from a relatively stable area underthrust by smooth ocean crust. Most of the well developed BSRs occur where rough ocean crust subducts and tectonic activity is relatively vigorous. Tectonic BSRs can form in areas of uplift (von Huene and Pecher 1999). A full wave inversion study indicates moderate concentrations of hydrate over a small amount of free gas (Pecher et al. 1998).

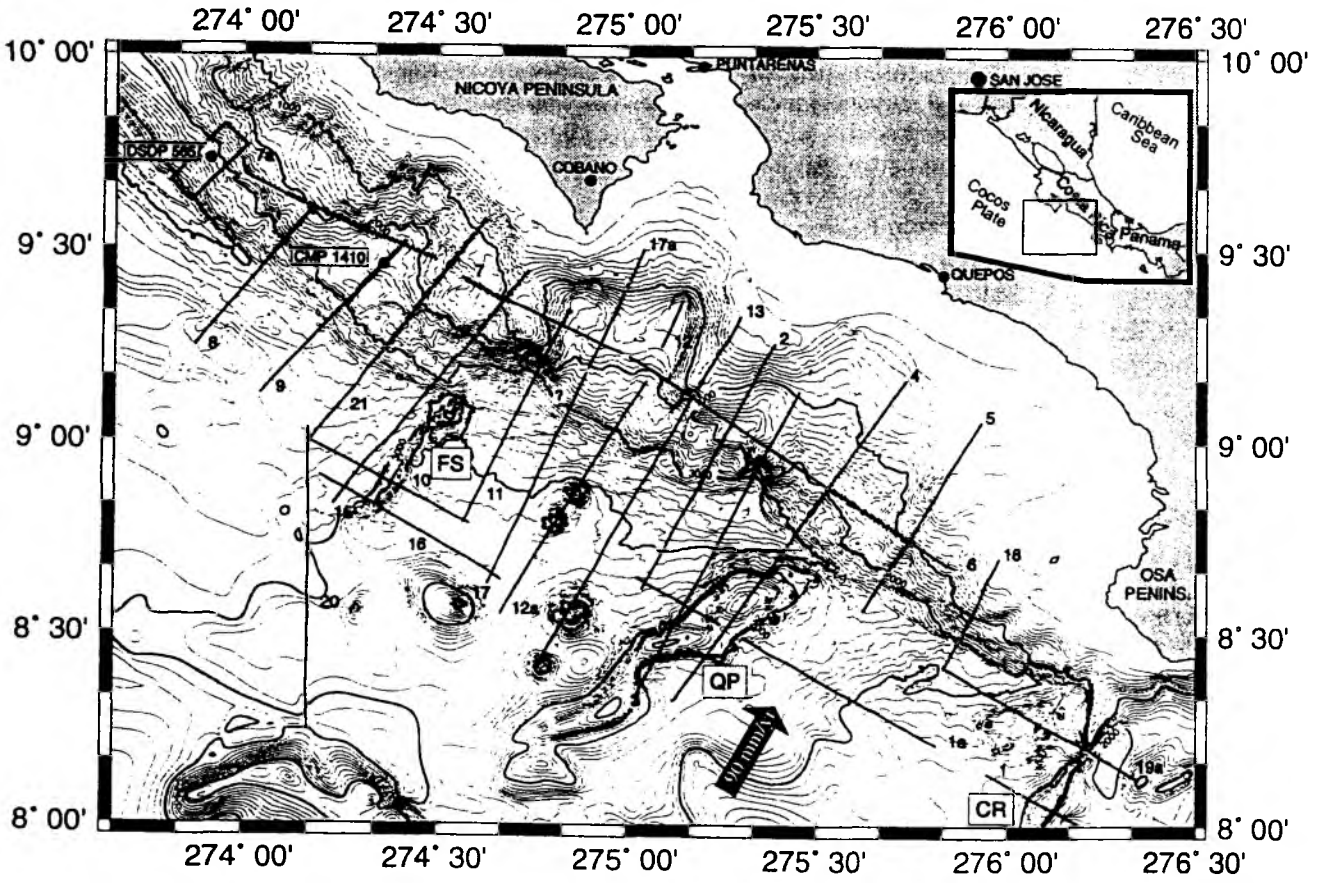

Figure 2.4.1. BSR occurrence in seismic lines along the Costa Rica margin (from Pecher et al. 1998).

2.5 THE SEISMICITY IN COSTA RICA

(I. Arroyo)

Costa Rica is located on the western margin of the Caribbean plate, where Cocos plate subduction is taking place along the Middle America Trench (MAT). To the southeast, the trench is shallowed by the Cocos Ridge. The MAT ends at a triple point located on the Pacific side of the Costa Rica-Panama border, where it joins the northern Panama Fracture Zone – a dextral transform fault defining the boundary between the Nazca and Cocos Plates.

The zone of seismic interaction between the Cocos and Caribbean plates and the intermediate depth of the Wadati-Benioff zone exhibit variation along the Pacific border of Costa Rica (Burbach *et al.*, 1984; Montero, 1986; Protti *et al.*, 1994; Montero, 1994). To the northwest, the terminal part dips about 60° with maximum focal depths of about 200 km. The central Pacific region is transitional, with the maximum depth of earthquakes shallowing to 100-120 km (Montero, 1994). In the southeast, the Benioff zone is very shallow and maximum hypocenters do not exceed 50 km. These changes are related to the subduction of the Cocos Ridge or the different lithospheric ages of the Cocos plate (Protti *et al.*, 1994).

The seismicity recorded for Costa Rica by the National Seismological Network (RSN) between January 1995 and August 1999 is shown in Figure 2.5.1. In that period, about 70% of the recorded seismicity corresponds to depths less than 30 km and 85% less than 50 km (Figure 2.5.1). It can also be seen that the low seismicity of the north contrasts with the central land and the central Pacific coastal areas which exhibit large seismic activity. Montero (1994), in his compilation regarding neotectonics of Costa Rica, describes the related stress distribution for the morphotectonic provinces of the country as follows:

Forearc

The interplate Cocos-Caribbean (or Panama microplate) earthquakes with magnitudes larger than 6,75 (Ms < 8,0) have shown underthrusting-type focal mechanisms, with a maximum horizontal compressive stress trending N30°E.

There are some areas with different focal mechanisms, the principal one being southward of Quepos. Here, some intermediate-magnitude earthquakes have strike-slip mechanisms, but they show different slip senses along similar-trending nodal planes. Broadly however, the maximum horizontal compressive stress is trending N30°E for these strike-slip mechanisms.

Inner Arc

The inner arc is divided into four morphostructural units: the Guanacaste Quaternary Volcanic Cordillera, the Aguacate Range (Tertiary to Early Quaternary intrusive and volcanic cordillera), the Central Quaternary Volcanic Cordillera and the Talamanca Cordillera (Tertiary to Quaternary intrusive-volcanic-sedimentary cordillera).

From the forearc to the inner arc region, the compressive stress varies in direction. A number of different focal mechanisms exist in the area of the Guanacaste Cordillera, but a reliable maximum horizontal compressional stress can not be defined. This is probably because the seismic sources are related to complex tectono-volcanic processes. An 0° trend is presumed. The maximum compressive stress rotates from N30°E to the north in the central inner arc and central Talamanca Cordillera, but in the eastern Talamanca area, the stress trends

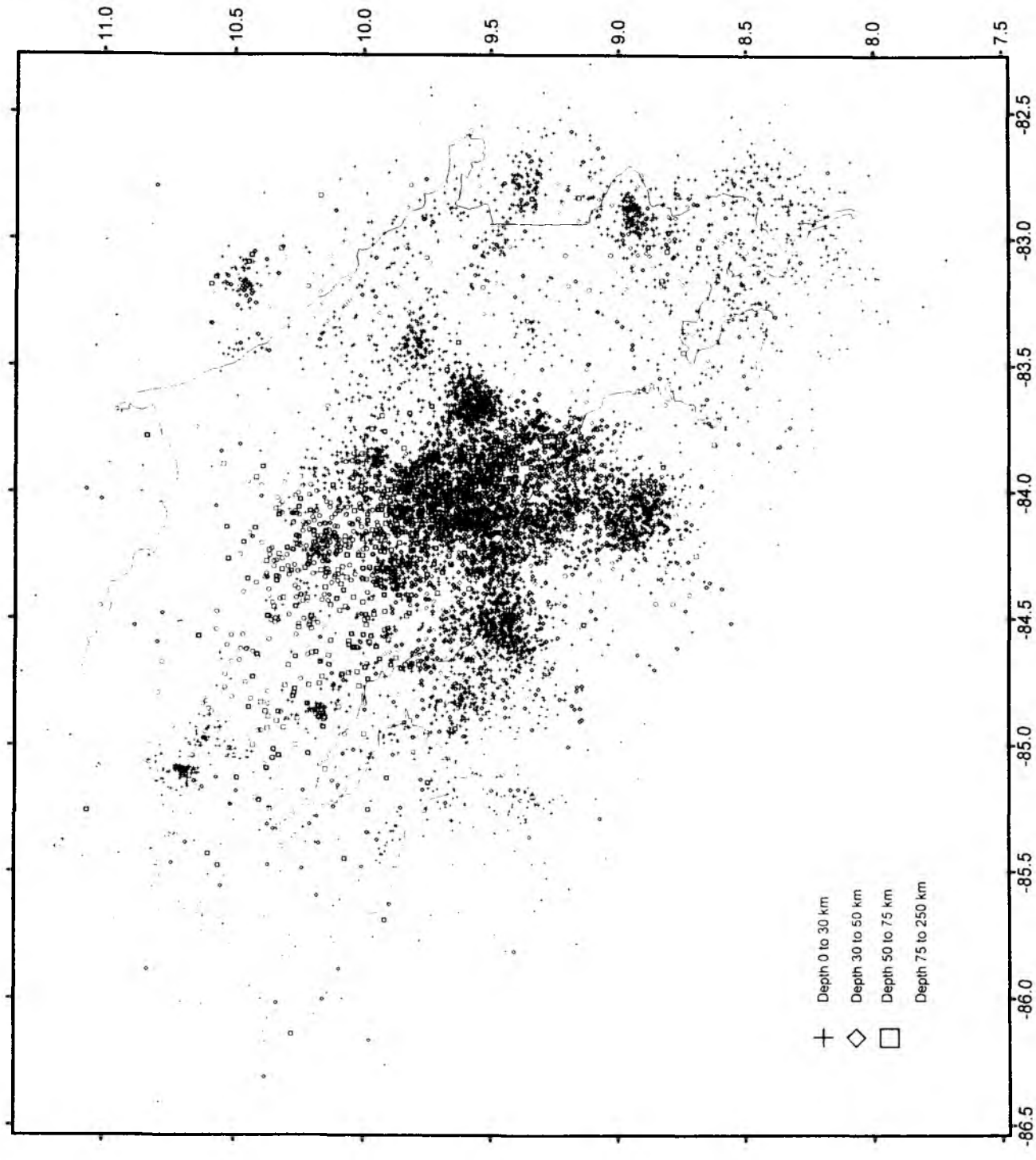

Figure 2.5.1: Seismicity recorded for Costa Rica between January 1995 and August 1999 by the National Seismological Network (RSN).

again N30°E . These changes are attributable to the interaction of the Cocos Ridge with the subduction zone.

In the Aguacate Range, historical or recent damaging shallow earthquakes are not known, except at the boundaries with other cordilleras. Few neotectonic data are known for this region.

Backarc

There are no reports of strong earthquakes with focus along the northwestern backarc area. The data are limited to the Caribbean side of the Talamanca Cordillera, where the destructive Limon earthquake (1991) occurred, and support a N30°E trend for the maximum compressive stress.

Montero (1994) also proposes that the Cocos Ridge behaves as a rigid indenter and central and eastern Costa Rica resemble a collisional tectonic environment.

In a more general study, Güendel & Protti (1998) reviewed seismic information recorded on a world-wide basis and analyzed the information using a rose diagram and the triangular representation of Frohlich and Apperson (1992) for classifying focal mechanisms. They divided the seismicity in Costa Rica in two zones: shallow seismic zone (0-50 km) and intermediate seismic zone (50-300 km):

Shallow Seismic Zone (0-50 km):

For this zone, the compressive stress is oriented N30°-40°E. The triangular projection shows that the earthquakes associated with the volcanic cordilleras have a dominant strike-slip mechanism, whereas, along the southeastern Caribbean coast, the inverse mechanisms dominate owing to the thrusting environment in the North Panama Deformed Belt. The inverse mechanisms are also preferential along the Coastal Range in the south Pacific zone and are related to the subduction of a young lithosphere (Protti *et al.*, 1994) and to the presence of the Cocos Ridge.

The shallow seismicity of the subduction plane off the Pacific coast shows a noteworthy inverse focal mechanism incidence. The compressive stress resulting from these typical subduction mechanisms has a N30°E trend.

Intermediate Seismic Zone (50-300 km):

The intermediate zone begins at a depth of 50 km, where the Cocos plate reaches the upper mantle after its abrupt collision against the Caribbean plate.

Güendel & Protti (1998) subdivide this zone into three depth ranges: 50 to 75 km, 75 to 100 km and 100 to 300 km.

Between 50 and 75 km, the compressive stress is oriented N30°-40°E; the focal mechanisms are mainly inverse. Conditions are similar for the 75-100 km ambit, with the compressive stress oriented N30°E. However, the reported events are few if compared with the other depth ranges. Finally, the compressive stress trend of the deepest intermediate zone shows a minor difference: N50°-60°E, but the focal mechanisms are still mainly inverse.

Protti & McNally (1989) have found the existence of at least two zones of stress distribution for the intermediate seismicity zone under Costa Rica. For earthquakes deeper than 75 km, the extensional stress is oriented parallel to the subduction direction. However, for events between 50 and 75 km they found a change from vertical extension to vertical compression in the zone northeastward and southeastward of 9°45' N - 84°15' W. This

change could be related to the Cocos Ridge subduction under the central and southern regions of Costa Rica.

The Boruca Seismological Network

At present, there are two seismological networks in Costa Rica, covering the whole country:

- The Seismology and Vulcanology Office of the Costa Rican Institute of Electricity (Instituto Costarricense de Electricidad, ICE) and the Section of Seismology, Vulcanology and Geophysics at the University of Costa Rica (UCR) constitute the National Seismological Network (Red Sismológica Nacional, **RSN**). It was officially opened in 1983.
- The other seismological network belongs to the National University (Universidad Nacional, UNA), which is named "Vulcanological and Seismological Observatory of Costa Rica" (Observatorio Vulcanológico y Sismológico de Costa Rica, **OVSICORI**). It started in 1984.

Nevertheless, as Suárez *et al.* (1995) point out, these two seismological networks mainly cover the plate boundary along the Pacific and the active faults in the Central Valley – the country's two areas most frequently affected by seismic phenomena.

In this way, until May 1998 the R.S.N. had only two seismological stations located on the southernmost zone of the country: ACR and BAR (Figure 2.5.2). For that reason, most of the earthquake location and hypocentral estimation had carried a substantial error (Boschini, 1996). Also, the low-magnitude earthquakes ($M < \sim 3,5$) were not locatable because of an insufficient number of stations.

Consequently, a temporary – 3-year – network was installed in May 1998. Some technical problems delayed the full operation until September 1998. Now, there are seven stations (ACR and BAR included), but one more is expected at the end of 1999 (Figure 2.5.2 and Table 2.5.1). The goal is to achieve a more accurate understanding of the seismicity in the southern area, not only because of scientific purposes (UCR), but also to obtain better knowledge of the seismogenic sources for the Boruca hydroelectric project seismic hazard studies (ICE). This project is designed to be the largest of the Central America region (capacity: ~1400 MW).

Three of the seismic stations (ACR, BAR, SAB) and the one that is going to be mounted (CHO) are vertical-component type and manufactured by Mark Products. The remaining four are three-component instruments fabricated by Mark-Rand. All of them have short period seismometers.

The three-component seismometers allow fault rupture propagation analysis, the seismic energy directivity and the amplification factors produced by different soil types (Boschini, 1996).

RIC1 and PRG are telemetric stations: the rest transmit by telephone communication. The recorder centre is located near the town of Maíz de Boruca, over the Coastal Range (Fila Costeña), on the same site as the station FMA (Figure 2.5.2). This locality is 5-km northwest from the future dam site of the Boruca Project, which is located on the margins of the Grande de Térraba River.

The earthquakes are detected and recorded by the SEISLOG software (University of Bergen, Norway) installed on a PC with a QNX operating system. Signals are transmitted to San José via modem and saved on a SUN computer. The locating process is performed with

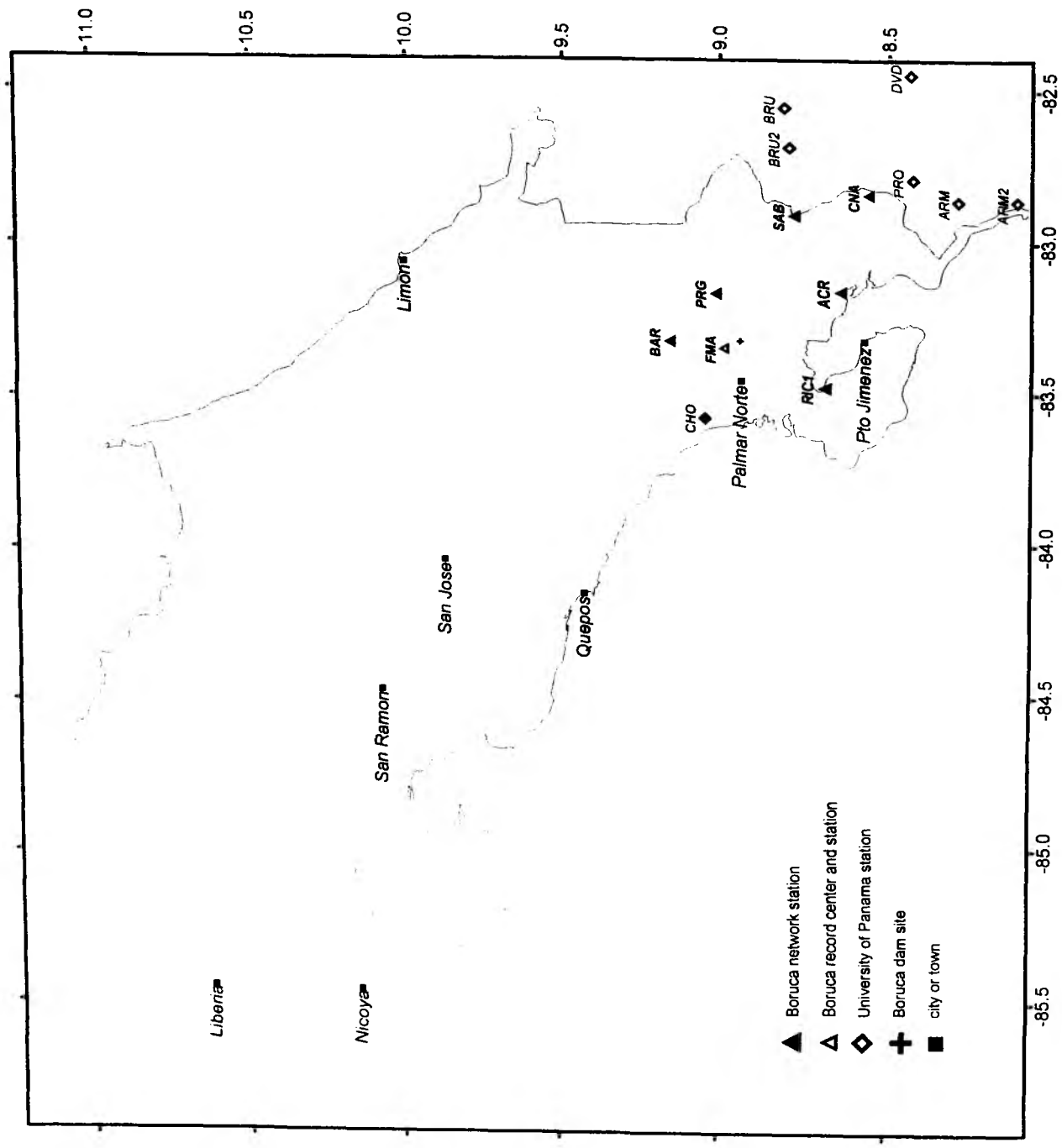

Figure 2.5.2: Stations of the Boruca seismological network. Also, the stations of the University of Panama are shown.

Table 2.5.1: Boruca Seismological Network stations

Station	*Code*	*Latitude, N*	*Longitude, W*	*Elevation (m)*
Fila de Mora	FMA	08°59,45'	83°21,20'	1 100
Potrero Grande	PRG	09°01,15'	83°10,57	200
Rincon	RIC1	08°41,69'	83° 29.00'	10
Canoas	CNA	08°34,95'	82°50,85'	220
Sabalito	SAB	08°46,80'	82°54,90'	1 120
Buenos Aires	BAR	09°09,80'	83°20,15'	375
Adams	ACR	08°39,18'	83°10,08'	500

the SEISAN software (Havskov, 1997), which is a set of programs (mostly written in Fortran, a few in C) and a database for analyzing earthquake data from analog and digital data.

The location program used for locating earthquakes is a modified version of Hypocenter (Lienert *et al.*, 1986), and plane parallel layers are assumed for local events. Station input and crustal structure is given in near standard HYPO71 format. The crustal model used for location is based on the work of Matumoto *et al.* (1977).

Presently, the location process has been completed for the data until May 1999. There are 1 145 earthquakes recorded, 626 of them are located in the southeastern zone of the country (Figure 2.5.3), where the interest of the network resides.

A process of relocating some events using University of Panama (Universidad de Panamá, UPA) stations (Figure 2.5.1) and an independent private station (BRU2) will be attempted. Also, a new site for station PRG, northeastward its current position, is being planned. This will provide a better coverage of the relatively high seismic activity recorded in the Coto Brus region.

The main activity during recording is located at the easternmost part of the Osa Peninsula (seismic swarm of March 1999), the Dulce Gulf, Coto Brus zone and the Burica Peninsula (Figure 2.5.3). During the March 1999 seismic swarm on the Osa Peninsula, 165 locatable events were recorded. This is attributed to subduction because of its dispersed epicentral distribution. However, the idea of some reactivation of the local faulting is also possible as indicated by the hypocenter range (3-30 km).

At the Dulce Gulf, the activity is generated by a strike-slip fault system (Berrangé & Thorpe, 1988). The Coto Brus seismicity is mainly shallow (< 30 km) suggesting faulting hitherto unrecognised in the literature. The high seismic activity of the Burica Peninsula is attributed to a dextral strike-slip faulting, which accommodates the Middle-America Trench deflection along the Cocos plate's eastern border (Corrigan *et al.*, 1990; Montero *et al.*, 1998).

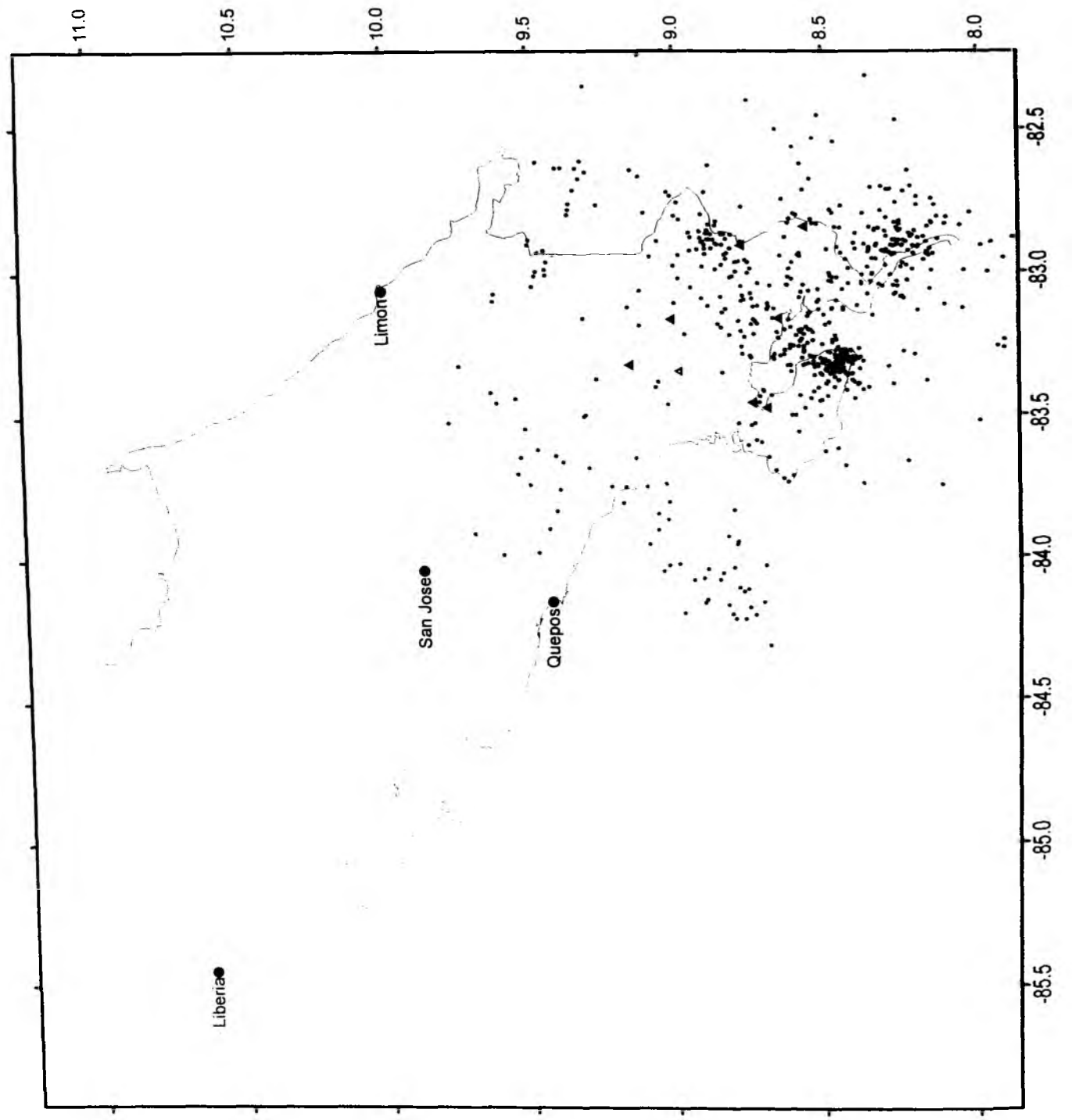

Figure 2.5.3: Stations of the Boruca seismological network. Also, the stations of the University of Panama are shown.

3. PARTICIPANTS

3.1 SCIENTISTS

3.1.1 SCIENTISTS – Leg SO144-1a

Jörg M. Bialas	GEOMAR, chief scientist
Philippe Charvis	GéoAzur
Heather R. Deshon	UCSC
LeRoy M. Dorman	SIO
Sharon Escher	SIO
Bettina Finkenberger	GEOMAR
Yann M. Hello	GéoAzur
Petra Liersch	GEOMAR
C. Jörg Petersen	GEOMAR
David S. Portugal	IGP/GéoAzur
Cesar I. Ranero	GEOMAR
Allan W. Sauter	SIO
Irmgard Schaffer	GEOMAR
Klaus-Peter Steffen	KUM
Harald W. Steiner	GEOMAR
Hans R. Thomas	ZAM
Michael D. Tryon	SIO
Roland E. von Huene	GEOMAR
Christian H. Walther	GEOMAR

3.1.2 SCIENTISTS – Leg SO144-1b

Ernst R. Flüh	GEOMAR, chief scientist
Ivonne Arroyo	ICE
Yves Auffret	IFREMER
Hajnal Borús	GEOMAR
Béatrice Cailleau	GEOMAR
Philippe Charvis	GéoAzur
Bettina Finkenberger	GEOMAR
Louis Geli	IFREMER
Yann M. Hello	GéoAzur
Richard Heath	GEOMAR
Dirk Kläschen	GEOMAR
Thomas Leythäuser	GEOMAR
Martin Meschede	IGPUT
Kirk McIntosh	UTIG
C. Jörg Petersen	GEOMAR
David S. Portugal	IGP/GéoAzur
Irmgard Schaffer	GEOMAR
Arne Schwenk	KUM
Klaus-Peter Steffen	KUM
Harald W. Steiner	GEOMAR
Christian H. Walther	GEOMAR

3.1.3 SCIENTISTS – Leg SO144-2

Gerhard Bohrmann	GEOMAR, chief scientist
Boris Baranov	IORAS
Mavin Camacho	INRECOSMAR
Béatrice Cailleau	GEOMAR
Hana Florianova	GEOMAR
Richard Heath	GEOMAR
Katja Heeschen	GEOMAR
Veit Hühnerbach	SOC
Matthias Hort	GEOMAR
Carmen Jung	GEOMAR
Thomas Kath	IfM
Douglas Masson	SOC
Duncan Matthew	SOC
Matthias Müller	GEOMAR
Christine Röckmann	GEOMAR
Omar Rodriguez	INTRECOSMAR
Ian Rouse	SOC
Irmgard Schaffer	GEOMAR
Robert Wallace	SOC
Reimer Weinrebe	GEOMAR

3.2 CREW

3.2.1 CREW – Leg SO144-1a

Henning Papenhagen	Master
Leszek T. Szymanski	Chief Officer
Walter Baschek	1st Officer
Peter Rost	Radio Officer
Ingo Naeve	Surgeon
Uwe Thaysen	Chief Engineer
Eberhard G. Bochnik	2nd Engineer
Rolf Konrath	Electrician
Rudolf Angermann	Chief Electronic Engineer
Helmut Vöhrs	Electronic Engineer
Kurt Stammer	System Operator
Andreas Klein	System Operator
Rudolf Tscharntke	Fitter
Volker Blohm	Motorman
Helmut Meyer	Motorman
Werner Sosnowski	Motorman
Holger Zeitz	Motorman
Wilhelm Wieden	Chief Cook
Willy Braatz	2nd Cook
Werner Slotta	Chief Steward
Hans-Jürgen Prechtl	2nd Steward
Werner Scheller	2nd Steward
Harald Boldt	Boatswain

Norbert M. Bosselmann	A. B.
Werner M. Hoffmann	A. B.
Erhard Kähler	A. B.
Hermann H. Röpti	A. B.
Andreas M. Schrapel	A. B.
Günter M. Stängl	A. B.

3.2.2 CREW – Leg SO144-1b

Henning Papenhagen	Master
Lutz Mallon	Chief Officer
Walter Baschek	1st Officer
Wolfgang Sturm	Radio Officer
Anke Walter	Surgeon
Uwe Thaysen	Chief Engineer
Eberhard G. Bochnik	2nd Engineer
Helge Beyer	Electrician
Rolf Konrath	Chief Electronic Engineer
Helmut Vöhrs	Electronic Engineer
Jens Grigel	System Operator
Andreas Klein	System Operator
Rudolf Tscharntke	Fitter
Volker Blohm	Motorman
Helmut Meyer	Motorman
Werner Sosnowski	Motorman
Holger Zeitz	Motorman
Wilhelm Wieden	Chief Cook
Willy Braatz	2nd Cook
Werner Slotta	Chief Steward
Hans-Jürgen Prechtl	2nd Steward
Werner Scheller	2nd Steward
Harald Boldt	Boatswain
Norbert M. Bosselmann	A. B.
Werner M. Hoffmann	A. B.
Erhard Kähler	A. B.
Hermann H. Röpti	A. B.
Andreas M. Schrapel	A. B.
Günter M. Stängl	A. B.

3.2.3 CREW – Leg SO144-2

Henning Papenhagen	Master
Lutz Mallon	Chief Officer
Walter Baschek	1st Officer
Wolfgang Sturm	Radio Officer
Anke Walter	Surgeon
Peter Neumann	Chief Engineer
Eberhard Boschnik	2nd Engineer
Helge Beyer	Electrician

Rolf Konrath	Electrician
Hilmar Hoffmann	Chief Electronic Engineer
Volkmar Gebhard	System Operator
Jens Grigel	System Operator
Volker Blohm	Motorman
Helmut Meyer	Motorman
Werner Sosnowski	Motorman
Holger Zeitz	Motorman
Wilhelm Wieden	Chief Cook
Willy Braatz	2nd Cook
Werner Slotta	Chief Steward
Hans-Jürgen Prechtl	2nd Steward
Werner Scheller	2nd Steward
Harald Boldt	Boatswain
Norbert M. Bosselmann	A. B.
Werner M. Hoffmann	A. B.
Erhard Kähler	A. B.
Werner Hoedl	A. B.
Andreas M. Schrapel	A. B.
Günter M. Stängl	A. B.

3.3 ADDRESSES OF PARTICIPATING INSTITUTIONS

GEOMAR: GEOMAR Forschungszentrum für marine Geowissenschaften
der Christian-Albrechts-Universität zu Kiel
Wischhofstraße 1-3
24148 Kiel, Germany
Tel.: 0049 - 431 - 600 - 2972
Fax: 0049 - 431 - 600 - 2922
e-mail: nn@geomar.de

GéoAzur: UMR Géosciences Azur IRD
2 Quai de la Darse
06235 Villefranche- sur-mer, France
Tel.: 0033-49376-3883
Fax: 0033-49376-3768
e-mail: charvis@ccrv.obs-vlfr.fr

ICE: Instituto Costaricense de Elektricidad
C.S. Exploratió Subterránea, Sabona Norte
Apartado 10032 San José, Costa Rica
Tel.: 00506-220-6394
00506-695-6522
Fax: 00506-220-8212
e-mail: igarroyo@cariari.ucr.ac.cr

IfM: Institut für Meereskunde
Düsternbrokerweg
24148 Kiel, Germany
Tel: 0049 – 431 – 597 - 3855
e-mail: tkath@ifm.uni-kiel.de

IFREMER: Département Géosciences Marines
Ifremer Center de Brest
BP 70 – 29280 Plouzané, France
Tel.: 0033-298-224-613 (Y. Auffret)
0033-298-224-227 (L. Geli)
Fax: 0033-298-224-549
e-mail: yauffret@ifremer.fr
geli@ifremer.fr

IGP: Instituto Geofisico del Perú
Calle Morquez de Calatrava 216
Urb. Camino Real – La Molina
Lima 12, Perú
Tel.: 00511-4361992
Fax: 00511-4379923
e-mail: david@geo.igp.gob.pe

IGPUT: Institut für Geologie und Paläontologie
Universität Tübingen
Sigwartstr. 10
72076 Tübingen, Germany
Tel.: 0049-7071-2972494
Fax: 0049-7071-5059
e-mail: meschede@uni-tuebingen.de

INRECOSMAR: Institute for Coastal and Marine Resources
P.O. Box: 108-2015
San José, Costa Rica
Tel.: 00506 - 280 - 8215
Fax: 00506 – 224 - 9557
e-mail: proambie@sol.racsa.co.cr

IORAS: Institute of Oceanology, Russian Academy of Sciences
Nakhimovsky Pz., 38
Moscow 117851, Russia
Tel.: 7 – 095 – 124 - 7942
Fax: 7 – 095 – 124 - 5983
e-mail: baranov@sio.rssi.ru

KUM: K.U.M. Umwelt- und Meerestechnik Kiel Gmbh
Wischhofstr. 1-3, Geb. D5
24148 Kiel, Germany
Tel.: 0049 – 431 – 7209 – 220
Fax: 0049 – 431 – 7209 – 244
e-mail: KUM.Umweltmeerestechnik@t-online.de

SIO: Scripps Intitution of Oceanography
IGPP, MC 0225
La Jolla, CA 92093-0225, USA
Tel.: 001 – 619 – 534 – 2406
Fax: 001 – 619 – 534 – 6849
e-mail: ldorman@ucsd.edu

SOC: Southampton Oceanography Centre,
Empress Dock
Dock Gate 4
Southampton, SO14 3ZH, United Kingdom
Tel.: 0 – 1703 – 596568
Fax: 0 – 1703 – 596554
e-mail: d.masson@soc.soton.ac.uk

UCSC: University of California Santa Cruz
Earth Sciences Department UC Santa Cruz
1156 High Street
Santa Cruz, California 95064, USA
Tel.: 001-831-459-4426
Fax: 001-831-459-3074
e-mail: hdeshon@earthsci.ucsc.edu

UTIG: University of Texas
Institute for Geophysics
4412 Spicewood Spring Rd., Building 600
Austin, Texas 78759-8500, USA
Tel.: 001-512-471-0480
Fax: 001-512-471-8844
e-mail: kirk@utig.ig.utexas.edu

ZAM: Zentrum für angewandte Meerestechnik
Wischhofstr. 1-3, Geb. C4
24148 Kiel, Germany
Tel.: 0049-431-600-2808
Fax: 0049-431-600-2945
e-mail: thomas@zam.uni-kiel.de

4. CRUISE NARRATIVE

4.1 SONNE CRUISE SO144-1a, 07.09 – 27.09, SAN DIEGO-CALDERA

(J. Bialas)

RV SONNE cruise SO144-1a commenced on 7 September at the port of San Diego, USA, when 19 scientists of 6 nationalities and of 4 different research institutions arrived on board. Under the leadership of GEOMAR, Germany, researchers from GÉO AZUR, France and SCRIPPS Institution of Oceanography and University of California Santa Cruz, USA participated in the first three-week leg of the PAGANINI (**Pa**nama Basin and **Ga**lápagos "Plume" – **N**ew **In**vestigations of **I**ntraplate Magmatism) research programme.

The reality of the undertaking became apparent as four containers of freight for the Ocean-Bottom Seismometers (OBS) and Ocean-Bottom Hydrophones (OBH) from GEOMAR and GÉO AZUR, as well as the 14 instruments from SCRIPPS, were brought on board. A total of 56 instruments were planned for deployment during the next 2 legs. They were stowed in all available laboratories and occupied most of the afterdeck.

RV SONNE left the port of San Diego on 8 September at 10:00 to start the 2200-mile-long transit south for dredging off the coast of Nicaragua. During the eight days of transit, all groups set up their equipment and prepared for the first deployment. Arriving at the Nicaraguan border on 15 September, 16:00 local time, Hydrosweep swath mapping was intiated and continued throughout the entire cruise. Digital data processing started immediately, with the results, apart from their scientific value, also contributing to further cruise planning.

More research activities continued a few hours later when SONNE arrived at the "Five-Fault" Seamount (11°05″ N - 87°51.7″ W). The steep flanks were probed with a dredge and the three and a half-hour track succeeded in its goal of filling a bag of edged rocks, which were stored on board for later study by geologists attending following legs of the cruise. Geochemical analyses and age dating of these specimens from the fast-spreading centre of the East Pacific Rise will be compared to those sampled on the slow-spreading crust of Galapagos Plume origin.

During the transit above the shelf of Nicaragua, three Hydrosweep profiles were collected covering the area of multi-channel seismic line "NIC239", which will be integrated in the interpretation of the active seismic experiment undertaken during the cruise.

Seismic wide-angle work started on 16 September with the deployment of 18 OBH and 2 OBS from GEOMAR, as well as 7 IRD-OBS from GÉO AZUR, along two parallel profiles (SO144-61 and SO144-62) on the shelf of Nicaragua. Profile 61 (58 nm) was positioned on top of line A, collected during SO107 in 1996 and Profile 62 (105 nm) was situated 13 nm further landward. The OBH/S were deployed as close as 10 nm towards the coast of Nicoya, whereas the airgun shooting terminated 5 nm off the coast where the water depth was less than 80 m. During 48 hours of airgun shooting, up to three 32 l (1000 cu. in) airguns were fired simultaneously. Unfortunately, two of the guns failed during the final night and could not be replaced in operation until the end of the line. All OBH/S were recovered by 11:30 on 20 September,.

Before leaving the Nicaraguan coast, swath mapping and magnetic recording was attained across the continental margin to fill a gap in the previous recordings of SONNE. Slide scars were found that may have contributed to the 1992 tsunamogenic earthquake. Magnetic profiling was added to enlarge the existing database, particularly in the area of the proposed triple junction off Nicoya.

Profiles 9 to 11 were shot with a small airgun array on top of a subducted seamount. The shots were observed by three IRD and 2 GEOMAR OBS, which were deployed along two crossing lines. For reference, a short profile was shot 20 nm apart in an undisturbed area. In addition, both experiments were recorded with a three-channel streamer.

During 24 September, 7 SCRIPPS OBS and 7 Flux Meters were deployed west of Osa Peninsula as the first part of a seismological network comprising 14 OBS. These instruments are to record local seismicity in order to better locate hypocenters. Because of the Mw 6.9 earthquake on 20 August, records of aftershocks are expected. The network is centred around a proposed ODP drill hole and will support pre-site surveys.

In preparation for leg SO144-1b, 13 IRD instruments were deployed along profile 1 during the afternoon of 24 September. The line crosses the Cocos Ridge following the MCS lines 1 and 1a of the SO081 cruise. They will remain until 4 October and, with permanent recording, contribute to the collection of local earthquake records.

While Yann Hello was transferred to the port of Quepos, we deployed the GEOMAR MLS prototype in shallow water. This test verified that the system's buoyancy is strong enough to pull the seismometer sphere's anchor out of the seafloor mud. After several test runs of the ship's W5 winch, deployment of the seismology network was continued. On 25September, 23:00, the last OBS was deployed.

Night hours and the morning of 26 September were used to collect Hydrosweep and magnetic data across the Cocos Ridge. These lines extend the older SONNE surveys seaward and contributed magnetic intensity values of a previously unsampled area.

Deployment of 20 GEOMAR OBH/S terminated the scientific work during leg SO144-1a at midnight on 27 September and prepared a 121 nm wide-angle transect for leg SO144-1b. After 8 hours of transit, SONNE arrived at the port of Caldera, Costa Rica, in the morning of the 27 September for partial exchange of scientific crew and equipment.

The cruise track of this leg is shown in Figure 4.1.1.

4.2 SONNE CRUISE SO144-1b 28.09 – 18.10, CALDERA-CALDERA

(E. Flueh)

SONNE cruise SO144-1b started on 28 September in Caldera, Costa Rica, after a less than 24-hour-long port stop, during which personnel was exchanged and equipment as well as ships supplies were loaded. Sonne left the pier at 10:00 and headed southward to the first seismic profile, for which an array of 33 instruments had been deployed during the last days of the previous cruise. Since all laboratories were already equipped, the scientific work started immediately with the deployment of the magnetometer (Profile 101) once the water depth was in excess of 200 meters. Airgun deployment was at 16:30 local time, and all three guns were in operation one hour later. Profile 01 was 140nm long and the ship sailed at 3.5 knots, firing the guns every 60 s. The profile was finished on 30 September at 09:00, and throughout most of the line at least two guns had been in operation. Problems on the trigger lines and the firing unit stopped the third gun from operating during the second half of the profile.

The set of 20 GEOMAR instruments were picked up between 16:00 on 01.October and 11:00 on 02 October. Before recovery a track parallel profile was run with magnetics. Immediately afterwards these 20 instruments were deployed on profile 02 along the crest of Cocos Ridge. Deployment was finished in the evening of 02.10. Another magnetic profile including hydroacoustics, was run before Sonne reached Quepos at 14:00 the following day, for transfer of a scientist.

Seismic profile 2A started at 20:25 in the evening with a circular line around Osa Peninsula into Gulfo Dulce. This line was intended to provide some 3D constraints on the plate boundary. The shots were recorded by onshore stations and offshore by the SCRIPPS passive network, the 13 IRD instruments remaining on line 1 and the 20 GEOMAR instruments placed along the crest of Cocos Ridge along profile 02. In perfectly calm weather this line was terminated at 16:00 03.10, and a transit profile out of Gulfo Dulce with

hydroacoustics and magnetics was run until midnight when recovery of the 13 IRD instruments from line 1 started.

The IRD recovery was finished by 15:00 on 04 October, with all instruments safely recovered at the predicted time. Sonne headed to the southwest to start shooting the line along the crest of Cocos Ridge. This profile (SO144-2B) was shot with the usual acquisition parameters (60 s interval, 3.5 kn, magnetometer deployed) from 18:00 on 04 October to 15:00 on 05 October. Recovery of the 20 GEOMAR instruments was started immediately and had been finished by 03:00 the following night.

Since the research permit for Colombian waters had just arrived, the 30-hour transit to the Malpelo ridge was started immediately, and interrupted only by a short OBH test at 3000 m water depth on 06 October between 16:00 and 18:00. The 33-element linear array across Malpelo ridge was deployed on 07 October between 07:00 and 22:00. Shooting started shortly after midnight with two airguns, and the third airgun was added on 08 October around 14:00. The end of the 135-nm-long profile was reached at 14:00 on 09.10., and recovery of the instruments started immediately. Again, the magnetometer was deployed during shooting. Recovery of the 33 instruments (OBH/S 90 to 122) was completed without any delay by 20:00 on 10.10, with an additional 4 hours spent for magnetics and hydroacoustics on the top of the ridge (profile 120).

Seismic line 04 is a cross profile of Cocos ridge, sampling a portion of the ridge southwest of profile 01. A total of 27 instruments (OBH/S 123 to 149) was deployed after transit between 14:00 on 11 October and 05:00 on 12 October. Among these instruments were 6 IRD OBS, the IFREMER OBH and the maiden voyage of the new GEOMAR broadband seismometer. Only two airguns were available for shooting along this profile, and the magnetometer was also deployed. Because of time constraints, the speed during shooting was increased to 4.3 knots. Shooting was interrupted for two minutes on 12 October at 18:00 to listen (instrumentally) for an explosion fired on land near Osa peninsula. A second large explosion was fired the following evening, just after the shooting was terminated. Instrument recovery started immediately, and 18 of the 21 GEOMAR/IFREMER instruments were picked up before Sonne had to go ahead to arrive in time for the scheduled popup of the six IRD OBS, all of which reached the surface at the expected time. Afterwards, the remaining three GEOMAR instruments were recovered on 14.10 until 22:00 and SONNE headed north to the last profile (Profile 05). Along the 180-nm-long transit line the magnetometer was deployed (profile 125).

Here, due to time constraints, only 13 GEOMAR OBH (OBH 150 to 162) were deployed in the afternoon of 15 October, and shooting along the 60 nm long line began at 20:00 with two airguns in operation. The magnetometer was also launched, and shooting was done at 3.8 kn with a shot interval of 60 s. The profile and was finished on 16 October at 12:00. The OBH were all safely recovered by 21:30, and the last hours were used to fill gaps in the magnetic and bathymetric grid (profile 127).

Between 09:00 and 10:00 an attempt was made to recover an OBH lost several years ago, but again no release command was acknowledged, and the transit to Caldera continued. At 12:00 water depths of less than 100 m were encountered and the magnetometer was retrieved, thus terminating the scientific programme of SO144-1b. SONNE met the pilot at 14:00 and docked at 14:50 in Caldera after 20 days at sea cruising for 3190 nm. The cruise track of this leg is shown in Figure 4.2.1.

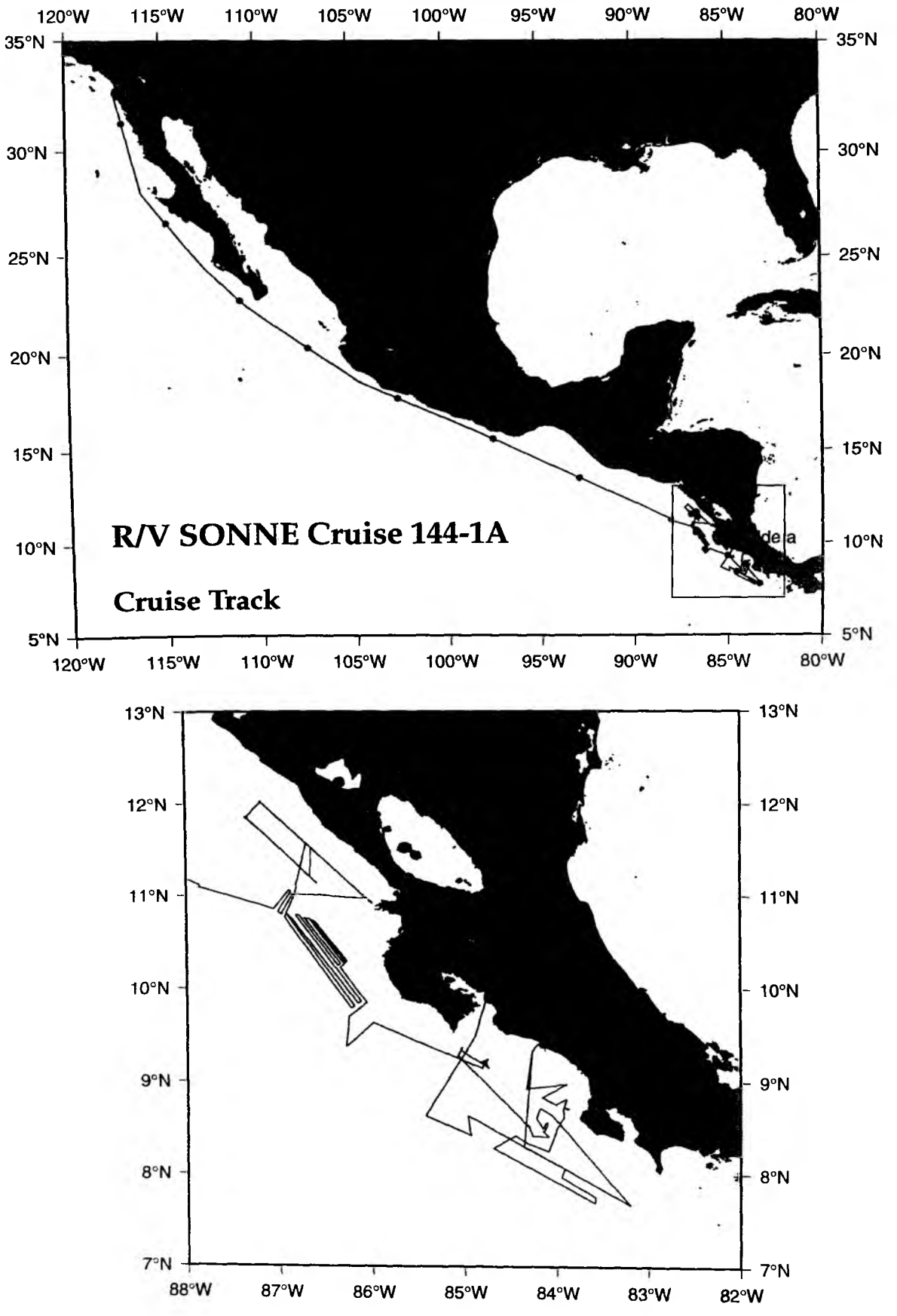

Figure 4.1.1: R/V Sonne cruise SO144-1A total track.

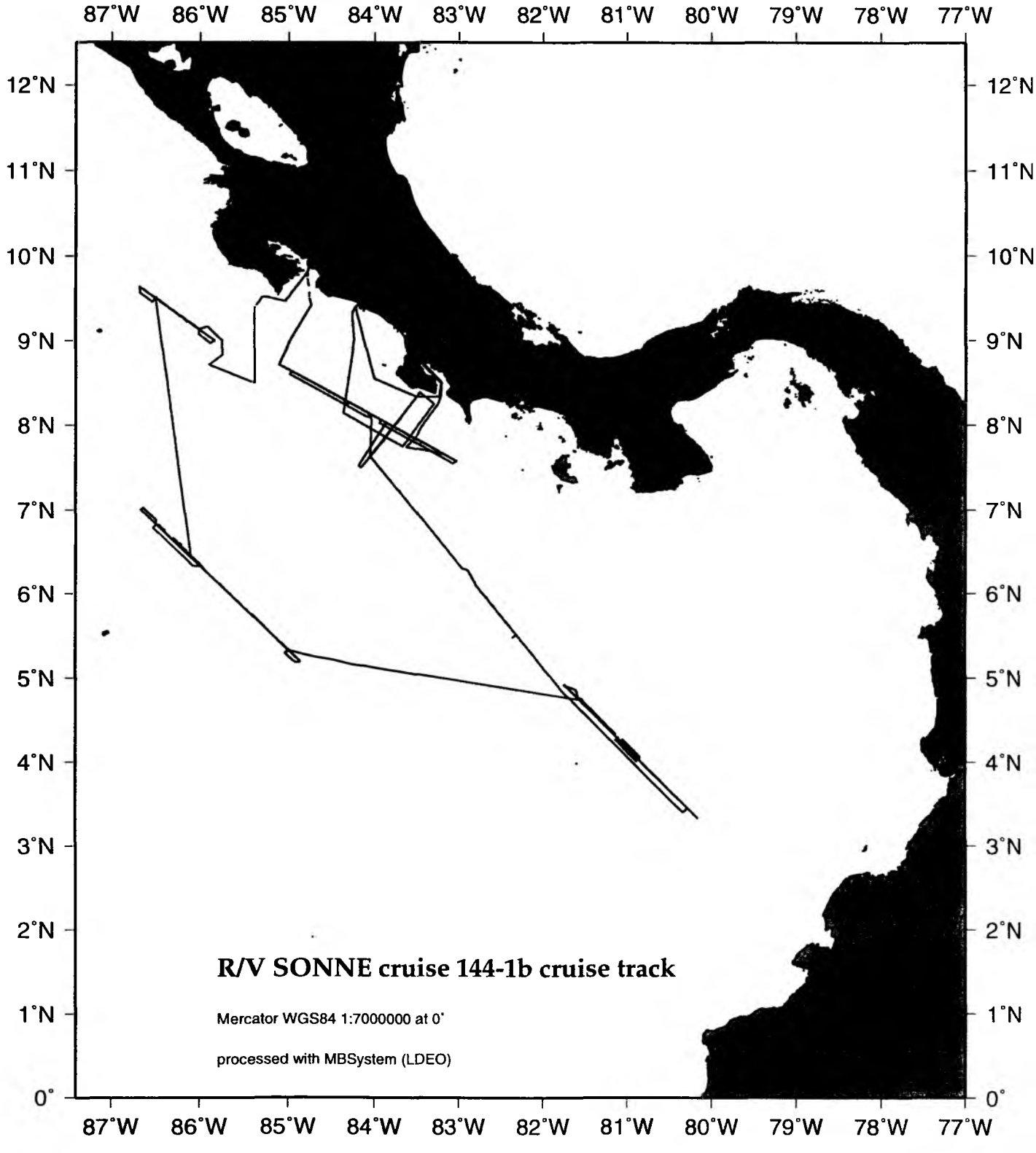

Figure 4.2.1: Cruise track of SO144-1b

4.3 SONNE CRUISE SO144-2: 19 OCT. – 7 NOV., CALDERA-CALDERA

(G. Bohrmann)

The research vessel SONNE left Puerto Caldera, Costa Rica, in the evening of 19 October to start the second leg of Sonne cruise 144, which focused on geochemical, geological and geophysical investigations in the framework of the Paganini research program. The 20 scientists on board of SONNE were from Costa Rica, Australia, Austria, France, Great Britain, Germany, Russia and the Czech Republic.

The research area was located on the continental margin of Costa Rica south of the Gulf of Nicoya (Fig. 4.3.1). Continuous subduction of the rough plate creates a distinctive continental slope morphology characterised by deep erosional scars. The bathymetric map of this area, created during several earlier cruises of RV SONNE, shows at least 7 or 8 of such scars, each indicating the subduction of a seamount or ridge. Since research was focused on the land slide scars, these distinct morphological features were, for the first time given names (Fig. 4.3.1.). Seismic surveys of the continental slope off Costa Rica, as well as drill cores from ODP Leg 170 southwest of the Nicoya Peninsula, indicate a widespread occurrence of gas hydrates in the slope sediments. Gas hydrates are a very efficient way of storing methane and are often related to fluid venting in a compressive continental margin environment. During this cruise, a variety of techniques were used to locate fluid venting associated with gas hydrates. In addition to measuring methane concentrations in the water column, the video sled (OFOS) was used to survey the seafloor (Fig.4.3.2). Furthermore, for the first time on RV SONNE, the TOBI system of the Southampton Oceanographic Center in the UK was used for high resolution mapping of the ocean floor (Fig.4.3.3).

During the first day of the cruise, repairs were carried out on the two hydraulic winches. A first CTD profile (CTD-1) was then taken down to a depth of 3500 m, for calibration of the HYDROSWEEP system. The first OFOS profile had to be cancelled after 1.5 hours due to technical problems. Swath mapping continued through the rest of the night. On the morning of the 21st, we returned to Puerto Caldera to pick up missing air freight and to disembark the winch expert. On the return to the next OFOS profile, some gaps in the bathymetric map were filled. During the night of the 21st, OFOS Profile 2 of 7 nm was recorded through the Jakó Scar, which is the most spectacular scar on the continental margin (Fig. 4.3.2). Above this structure, at 800-900 m depth, the first signs of fluid venting were indicated by the occurrence of pogonophora and mineral preciptates. These cold vents are related to tectonic faults which are well known from seismic profiles and are clearly visible in the morphology of the seafloor as imaged by the OFOS camera. Immediately below the headwall of the scar the observation of occasional bacterial mats suggests the existence of gas hydrates. Further down the slope, a few scattered clams were seen. Between 1800-1950 m, extended areas of chemosynthetic clams are good indicators of seafloor fluid and gas venting. This area was chosen for CTD/hydrocast profile 2 which revealed methane enrichment of up to 300 nM up to 100 m above the sea floor and background values of 2 nM in the water column above.

Following this first. very successful survey we started TOBI mapping on 22 October. Four NW-SE profiles, spaced 5 km apart, were planned to map a 20 km wide and 120 km long area in the middle of the Costa Rican continental slope at a very high resolution. TOBI deployment began at 08:00 and was complete ast 10:45. The complicated launch procedure was handled smoothly by the ship's crew. The survey then continued without problems until 22:00 on the 25th, when TOBI's CTD unit failed. At this point, we decided that we would

complete the third of the four planned survey lines, but that the fourth would be postponed until the repairs were completed. TOBI was recovered on the 26th between 06:00 and 07:30.

In the eastern part of the survey, the first TOBI data revealed spectacular images of two landslide scars – subsequently named the Parrita and Jacó Scars (Fig. 4.3.1) - related to seamount subduction. The scars consist of deep horseshoe-shaped depressions characterised by steep walls and a general high level of backscatter from the scar walls and floors, indicating rough chaotic terrain. The uplifted area upslope from the headwall and areas adjacent to the lateral walls of the scar are highly fractured. Complex cross-cutting fracture patterns are characteristic, with many faults downthrown in an upslope direction. It appears that these faults may have formed in an extensional regime because of uplift from seamount subduction, and that the area affected by uplift and extension is wider than that later affected by collapse over the trailing flank of the seamount. Patches of higher-than-expected backscatter in one of the headwall scars are tentatively interpreted as possible signs of fluid venting. In the western part of the survey area, we imaged the headwall of a large slump which represents the Puerto Coyote Scar and the Rio Bongo Scar (Fig. 4.3.1). Again, complex fault patterns are seen in the headwall region. Within the body of the slump, a northward decrease in surface roughness, apparently related to increasing thickness of undeformed sediment cover, may suggest that the slump is a compound feature, younging towards the south.

During the time before the next TOBI survey two days later, four OFOS and four CTD casts were made. Different locations with regard to geology and possible fluid venting sites were chosen based on TOBI results. We ran a long OFOS (Profile 3) from the landward flank of the Parrita scar at 1400 m depth, via the distinctly cracked summit at approximately 1250 m, to the seaward flank of the seamount scar at 2600 m. Indicators of cold vents (e.g., clam fields or single clams, sometimes also smaller bacterial mats and rarely large pogonophora) were detected at different water depths. At 1600 m, we found definite manifestations of fluid venting: larger clam fields and increased methane concentrations of 30 nmol/l. Higher concentrations of up to 75 nmol/l were measured within 50 m above the seafloor at a submarine landslide south of Quepos. Here, between 269-850 m, OFOS-4 (Fig. 4.3.2) showed bacterial mats of amazing thickness below a 150-m-deep wall, assumed to be the landslide's scar. Along a section of 220 m, more than 70% of the seafloor has a massive or net-like covering of the snowy white, but sometimes orange, wiry material. In the uncovered interfaces, a monospecific fauna of gastropods was found. Several cold vents were seen further downslope. Another highlight was the discovery of chemohermcarbonate - a distinct sign of fossil vent activity. The examination of the Cabo Blanco scar (OFSO-6; Fig. 4.3.2.) at the southern tip of Nicoya Peninsula did not show any signs of fluid venting. Similar results were gained from OFOS-7 (Fig. 4.3.2.), except for some clam fields in a crater-like depression, which, with the help of the sidescan image from TOBI, was identified as a mud volcano.

After two days of searching for vents, the TOBI CTD unit had been replaced by a simpler pressure (depth) sensor and was ready for redeployment. On Oct. 28th at 16:00, TOBI was launched again to complete three survey lines across the lower continental slope. The covered area includes the deformation front at the foot of the slope and the subducting oceanic plate immediately adjacent. Unfortunately, the survey had to be interrupted because of electric problems with the swivel that connects the deep sea wire with TOBI – which came out of the water on the 30th at 22:00. The break was used to run CTD-06 and a OFOS-7 in the area of the Puerto Coyote Scar down to the Nicoya slide (Figs. 4.3.1 and 4.3.2). Several indications of

fossil fluid venting (e.g., carbonates) were found above the scar and no recent fluid venting could be observed along the track.

A third TOBI survey was run between the 1 and 3 of November. This survey consisted of two 150-km-long lines parallel to the foot of the continental slope and the trench, extending the area previously imaged in a downslope direction. Spectacular images of the deformation front, showing a distinct, lobate boundary between undeformed trench sediments to the south and a narrow band of intensely folded sediments to the north, were obtained. The area where the Fisher Ridge intersects the margin showed particularly complex deformation. A huge blocky debris deposit covers the oceanic crust for a least 40 km north of Fisher Ridge. However, it appears to be covered by a considerable thickness of sediment, suggesting it is relatively old. At the end of the third survey, TOBI was recovered and a short passage to the upper slope area was completed. Here, the final TOBI survey - a one-day survey across old landslide scars (Tarcoles and Cabo Blanko Scar) on the upper slope - was begun on 4 November and ended 5 November at 8:00.

We used the last two days to deploy CTD and OFOS stations in the western part of the research area. OFOS-8 was run north of the Rio Bongo Scar between 500-900 m, which is the critical depth for potential gas hydrate formation at the seafloor. Cold vents were revealed by the occurrence of clam fields and a few isolated patches of bacterial mats on the sediment surface. OFOS-9 on the 6th November covered a large area from over the scar slope above the Nicoya Slide to the lower slide area. On the last day we investigated a mud volcano that showed quite a lot of activity. Chemosynthetic organisms like Calyptogena, pogonophera etc. as well as carbonate precipitates were found. After a short Hydrosweep survey in the night R/V SONNE reached the harbour of Caldera in the morning of 7 November.

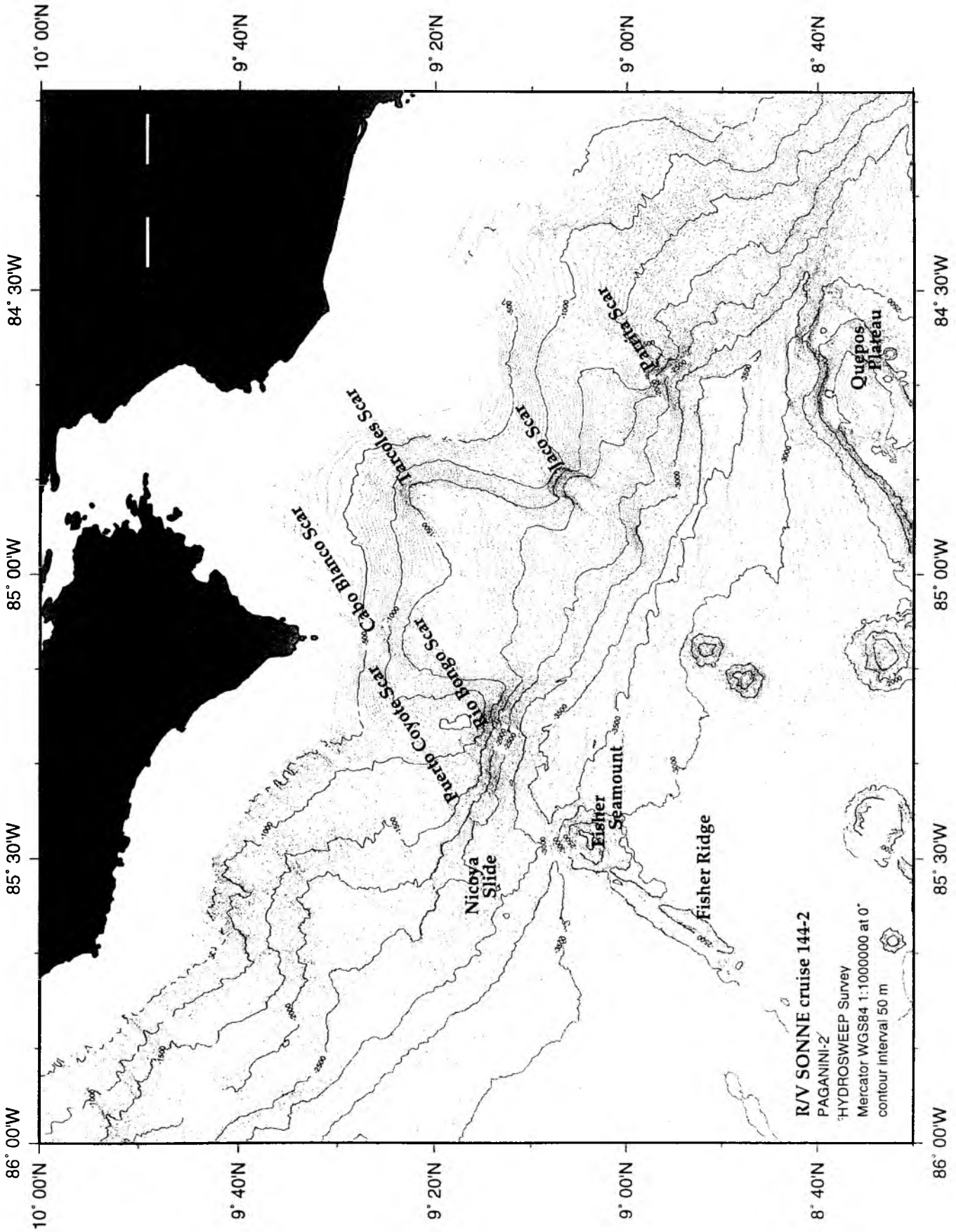

Figure 4.3.1 Area of research during RV SONNE cruise SO144-2. Some new names for the landslide scars were used for the first time and are introduced within this cruise report

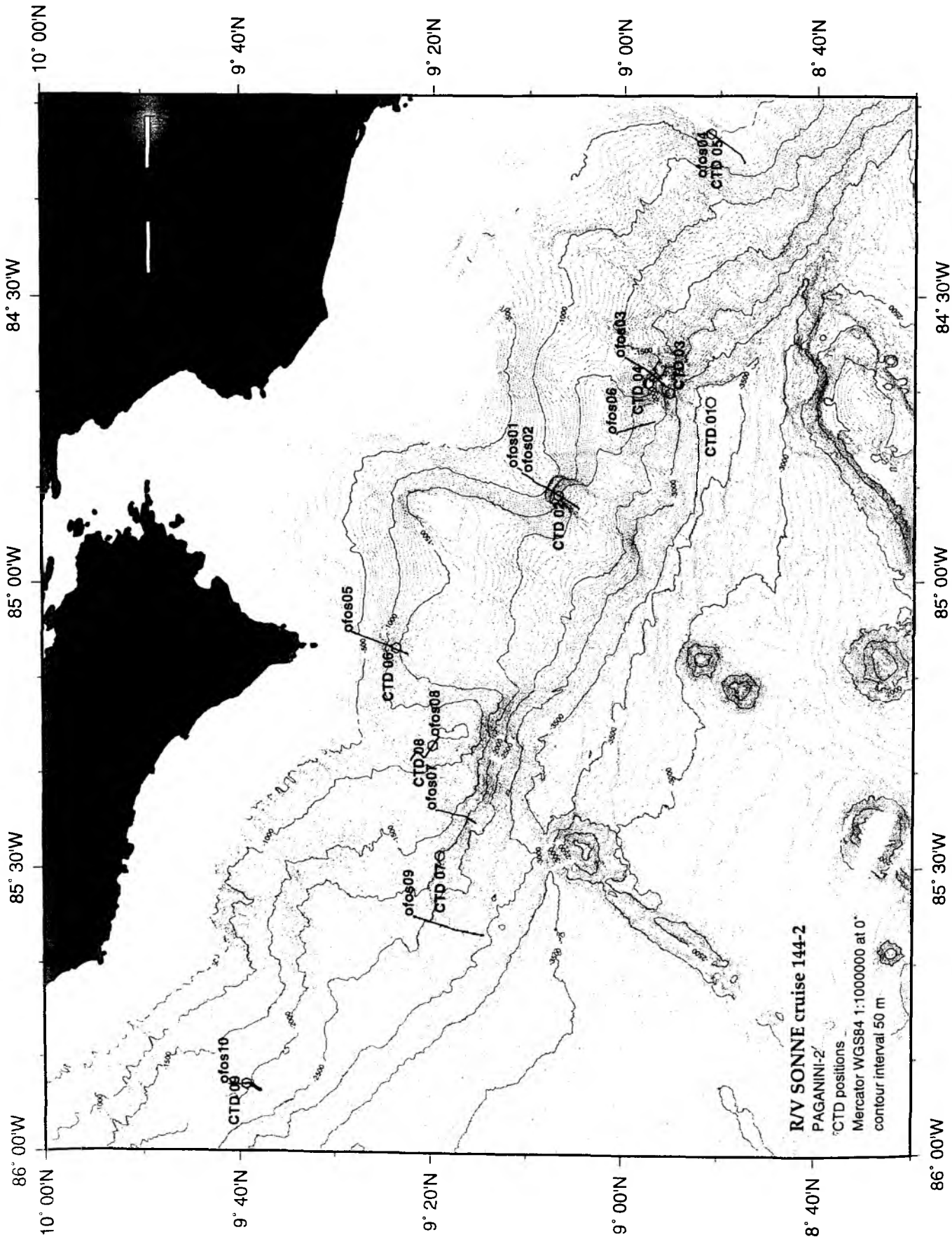

Figure 4.3.2 OFOS track chart including CTD stations of SO144-2

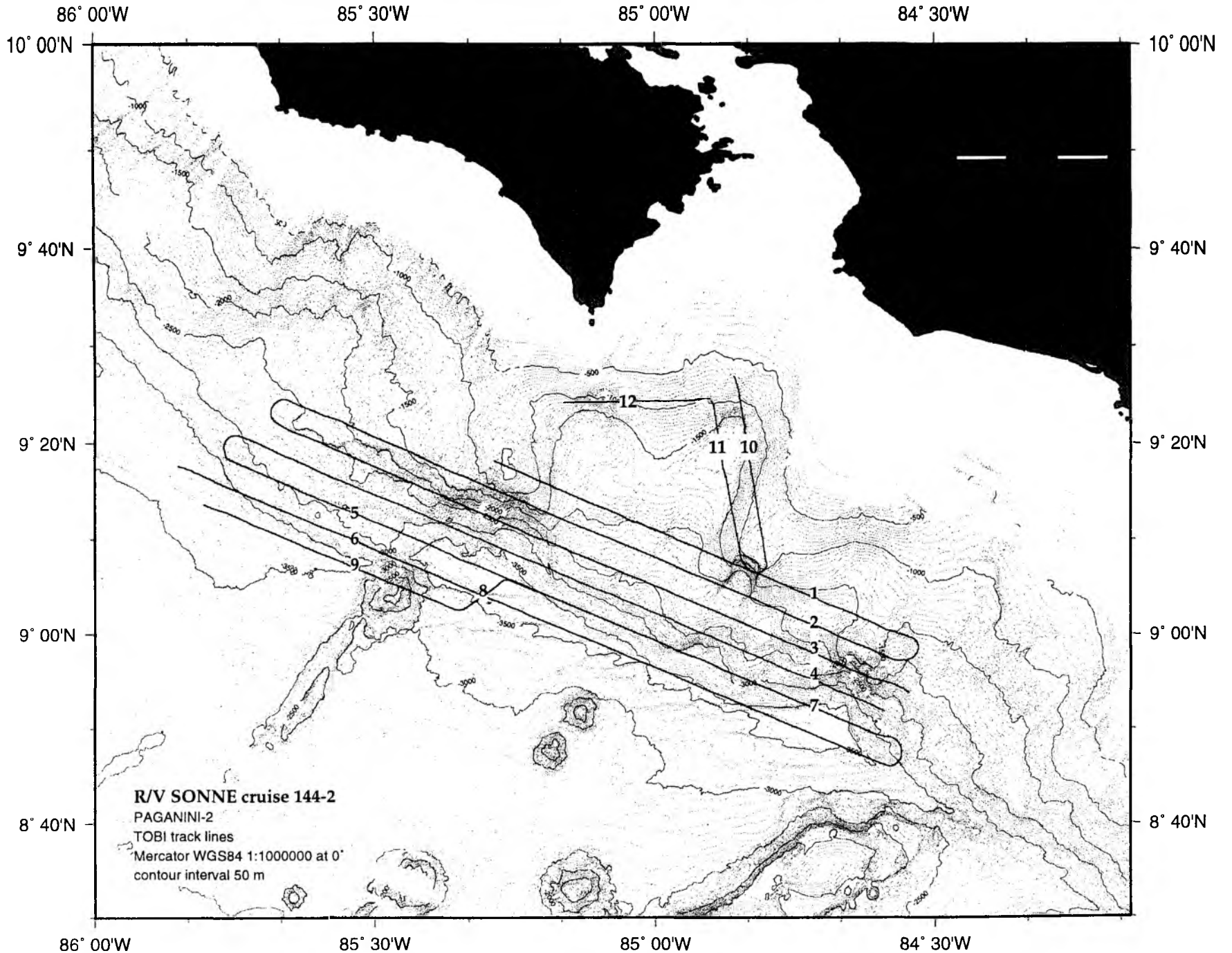

Figure 4.3.3 Profiles of TOBI deployments taken during SONNE cruise SO144-2

5. SCIENTIFIC EQUIPMENT
5.1 COMPUTER FACILITIES

The experiments and investigations performed during SO144 required special computing facilities in addition to the existing shipboard systems. For programming of ocean bottom stations, processing of seismic data and analysis of HYDROSWEEP recordings several workstations were installed by the groups.

Computing facilities (UMR Géosciences Azur, IRD)		
1 Apple Powerbook 170	• 8 Mbytes RAM • 100 Mbytes HD • Standalone	• OBS programming and testing • Clock drift measurements
2 Apple Powerbooks G3	• 32 Mbytes RAM • 16 Gbytes HD (external) • Exabyte 8500 tape drive • connected to ship's network	• Data transfer • Quality control
Sun SPARC 10	• 128 Mbytes RAM • 36 Gbytes HD (external) • Exabyte 8500 tape drive • connected to ship's network	• Data processing OBS relocation clock correction merging with navigation data generating Seg-Y files • Data modelling
PC Pentium II (Linux)	• 64 Mbytes RAM • 4 Gbytes HD	• Data processing (under development)

Géo Azur OBSs are programmed before being deployed using an Apple Powerbook 170 through a RS232 serial port. It is also used for clock drift measurements and predeployment tests. The data stored on a 1.2 Gbytes SCSI hard disk are transferred after the recovery of the OBS on a 16 Gbyte hard disk using a Powerbook G3 for quality control and then to the Sun Sparc workstation, through FTP, for further data processing and modelling.

Computing facilities (University of Texas Institute for Geophysics)		
Sun SPARC 20	• 256 Mbytes RAM • 8 Gbytes HD (external) • DDS3 4 mm tape drive • connected to ship's network	• Data processing OBS relocation clock correction merging with navigation data generating Seg-Y files • Data modelling

Data processing of the Géo Azur OBSs was also performed by University of Texas (UTIG) personnel. The two institutions share a pool of OBSs and have cooperated to develop software used to make the clock corrections, locate instruments, and produce final data sets in SEG-Y data format. Data transfer to and from the Géo Azur computers was done with FTP over the ship's network, and data were archived with the DDS3 tape drive.

Due to the large amount of data transfer GEOMAR installed a workstation cluster onboard comprising the following systems:

1	"neolithikum"	SUN Sparc 20	2 CPU, 256 MB memory	14 GB disks, DAT, Exabyte, CD	Sun Solaris 2.5
2	"devonia"	SUN Ultra 60	2 CPU 1 GB memory	112 GB disks, 2.3 GB MO, 2x DAT, 2x Exabyte	Sun Solaris 2.6
3	"avalonia"	SUN Sparc 5	1 CPU, 64 MB memory	13 GB disks, DAT, CD, Methusalem	Sun Solaris 2.5
4	"galicia"	SUN Sparc 10	1 CPU, 96 MB memory	12 GB disks, DAT, Methusalem	SunOS 4.1.4
5	"OBH"	Pentium II 350 MHz	1 CPU, 128 MB memory	9 GB disk, 3x PCMCIA	Windows95
6	"MBS"	Pentium II 350 MHz	1 CPU, 128 MB memory	9 GB disks, 3x PCMCIA	Windows95
7	"andean"	Pentium 133	1 CPU, 64 MB memory	5 GB disks, DAT, CD	Windows95

For seismic modelling four desktop Macintosh computers were installed:

1 PowerMacintosh G3/300 MHz

2 PowerMacintosh G3/233 MHz

3 PowerMacintosh 8200/120

4 PowerMacintosh 7100/66

In addition to these computers, one X-Windows-Terminal NCD-15r and several laptops/powerbooks were used.

For plotting and printing two HP Postscript Laserprinters (papersize A3 and A4), one OYO-11"-thermoplotter, as well as the shipboard color plotters were available.

The workstation cluster and the Macintosh desktops were placed in the magnetic/gravity lab and the Reinlabor.

The workstation cluster was set up according to a "client-server" model, with "neolithikum" being the server. All important file systems from the main server at GEOMAR were duplicated onto the "neolithikum"-disks. Using NFS-, NIS-, and automounter services the computing environment was identical to that at GEOMAR so every user found his/her familiar user interface.

The convenience of network mounted file systems has to be paid for with a heavy network load, particularly during playback of OBH-data from tape to disk (c.f. SO123 cruise report, Flueh et al., 1997). This required a high-performance network, which was accomplished by a switched twisted-pair ethernet. A 12-port ethernet switching-hub (3COM-SuperstackII 1000) with an uplink connection of 100 Mbps to the server "neolithikum" and dedicated 10 Mbps ports for the client workstations maintained the necessary network performance. In order to keep the shipboard network undisturbed by the workstation cluster, but to allow for communication between them, the server "neolithikum" was equipped with two network interfaces and served as a router. This provided the additional benefit of a simplified network configuration. Considerable setup work was dedicated to "neolithikum", while the other workstations used the same IP-addresses and network configuration as at GEOMAR.

This network setup showed a reliable and stable performance, and no breakdowns or bottlenecks were observed. The reconfigured shipboard network using twisted-pair technology and "star-"topology instead of BNC-cables along a linear "bus" with hubs in the main labs improved the flexibility to easily hook up systems to the network.

5.2 THE GEOMAR OCEAN BOTTOM HYDROPHONE / SEISMOMETER (OBH/S)

(The Seismic Wide-Angle Group, GEOMAR)

The Ocean Bottom Hydrophone

The first GEOMAR Ocean Bottom Hydrophone was built in 1991 and tested at sea in January 1992. A total of 16 OBH and 5 OBS instruments were available for SO144. This type of instrument has proved to have a high reliability; in fact during cruise SO142 (Flueh et al., 1999) the 1000th successful deployment was achieved. 118 sites altogether were occupied during cruise SO144-1.

The principle design of the instrument is shown in Figure 5.2.1, and a photograph showing the instrument upon recovery can be seen in Figure 5.2.2. The design is described in detail by Flueh and Bialas (1996).

The system components are mounted on a steel pipe which holds the buoyancy body on its top. The buoyancy is made of syntactic foam and is rated for a water depth of 6000 m, as are all other components of the system, except for the pressure cylinders holding the recording electronics. Here, various models for variable depths (2500 m, 3000 m, and 6000 m) are available. Attached to the buoyant body are a radio beacon, a flash light, a flag and a swimming line for retrieving from aboard the vessel. The hydrophone for the acoustic release is also mounted here. The release transponder is a model *RT661CE* made by *MORS Technology*. Communication with the instrument is possible through the ship's transducer system, and even at maximum speed and ranges of 4 to 5 miles release and range commands are successful. For anchors, we use pieces of railway tracks weighing about 40 kg each. The anchors are suspended 2 to 3 m below the instrument. The sensor is an *E-2PD* hydrophone from *OAS Inc.*, and the recording device is a *Methusalem* recorder of *DELTA t*, which is contained in its own pressure tube and mounted below the buoyant body opposite the release transponder (see Figures 5.2.1 and 5.2.2). Alternatively, the more advanced *MBS recorder of SEND GmbH* is used.

The Ocean Bottom Seismometer

The Ocean Bottom Seismometer (OBS) construction (Fig. 5.2.3) is based on the experiences with the GEOMAR OBH. It was built by GTG, Kiel, Germany. For system compatibility the acoustic release, the pressure tubes, and the hydrophone are identical to those used for the OBH. Syntactic foam was used as floatation again but of larger diameter due to the increased payload. Other than the OBH the OBS has three legs around its center post to which the anchor weight is attached. While the OBH floats about 1 m above the sea bottom, the OBS touches the sea bottom to avoid collision of the seismometer cable with the anchor. The sensitive seismometer is deployed about 1 m to the side of the system once the sea floor is touched. During diving of the system the footplate of this seismometer release lever is about one meter below the base of the anchor and will therefore hit the seafloor first. At touchdown the base plate forces an upward movement of the lever which will lay out the seismometer hook until the seismometer anchor is about 0.5 m above the seafloor. At about 45 degrees to the vertical the seismometer is released from its hook and falls to the sea floor from about 1 m height. Thus, a coupling of the seismometer to the sea floor is ensured. At this time the only connection from the seismometer to the instrument is a cable and an attached wire which will take the pull load while rising to the sea surface later. A movement or current on the instrument is thus not transmitted mechanically to the seismometer. All three channels are preamplified within the seismometer housing and

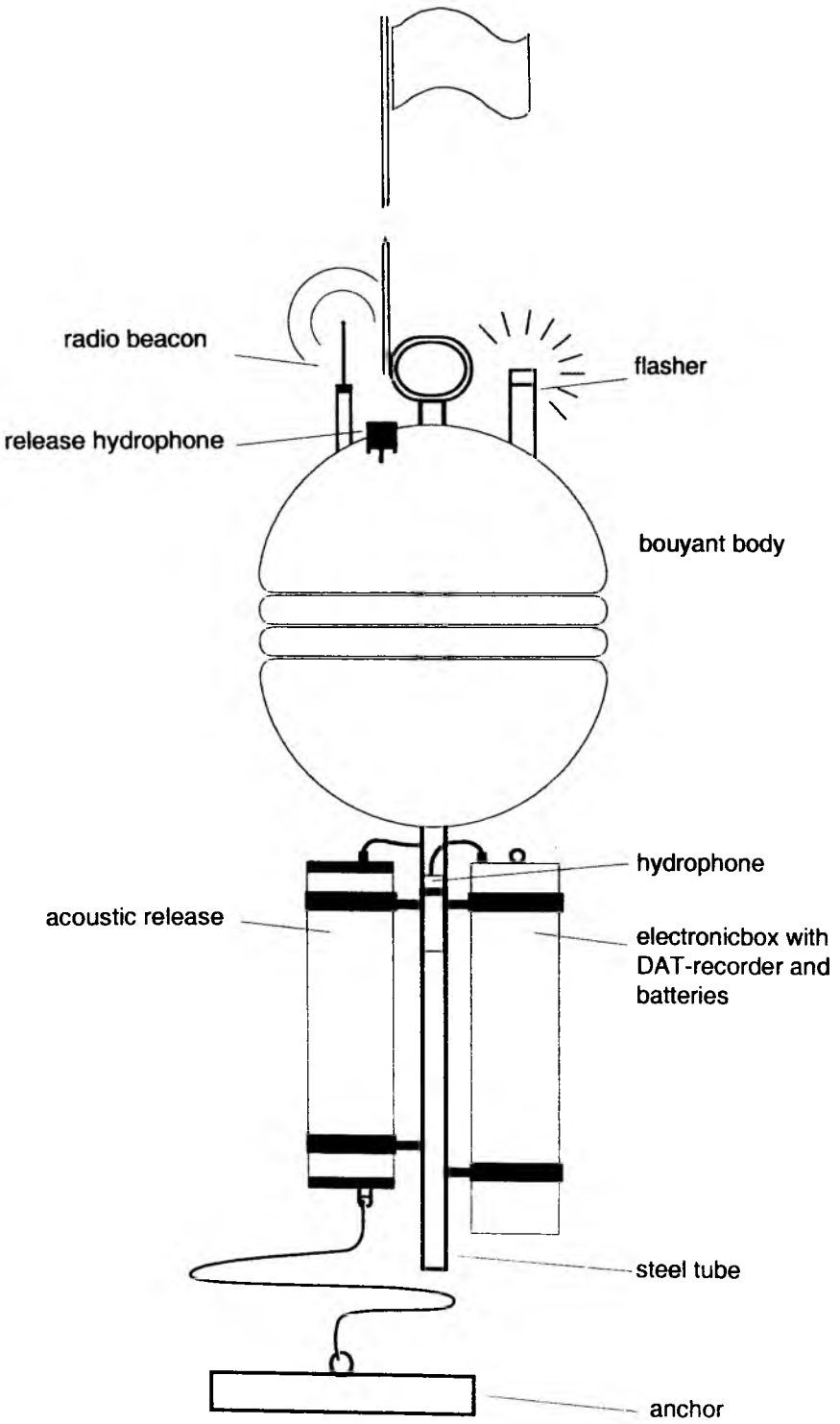

Figure 5.2.1: Principle design of the GEOMAR OBH

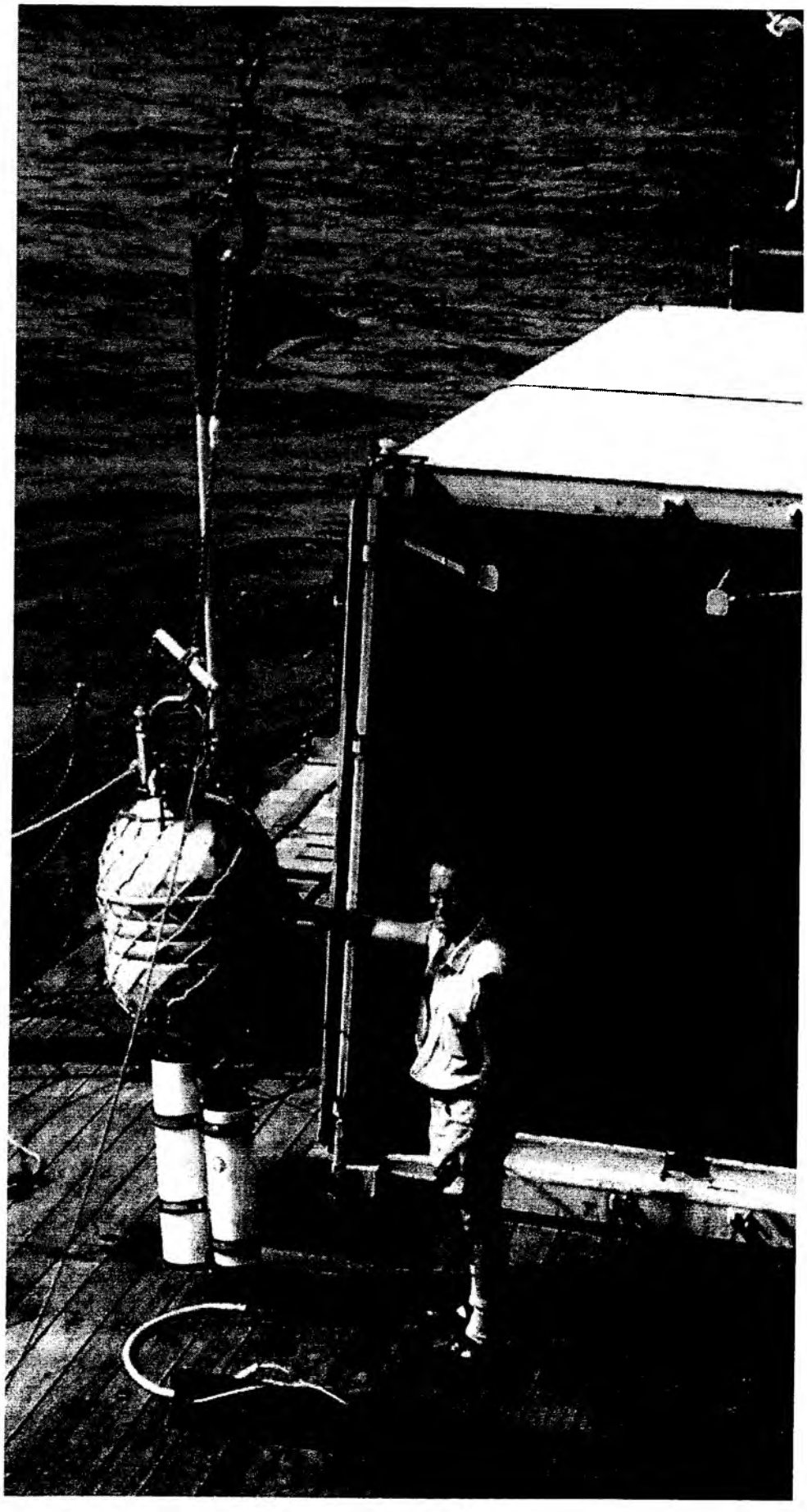

Figure 5.2.2: The GEOMAR OBH before deployment

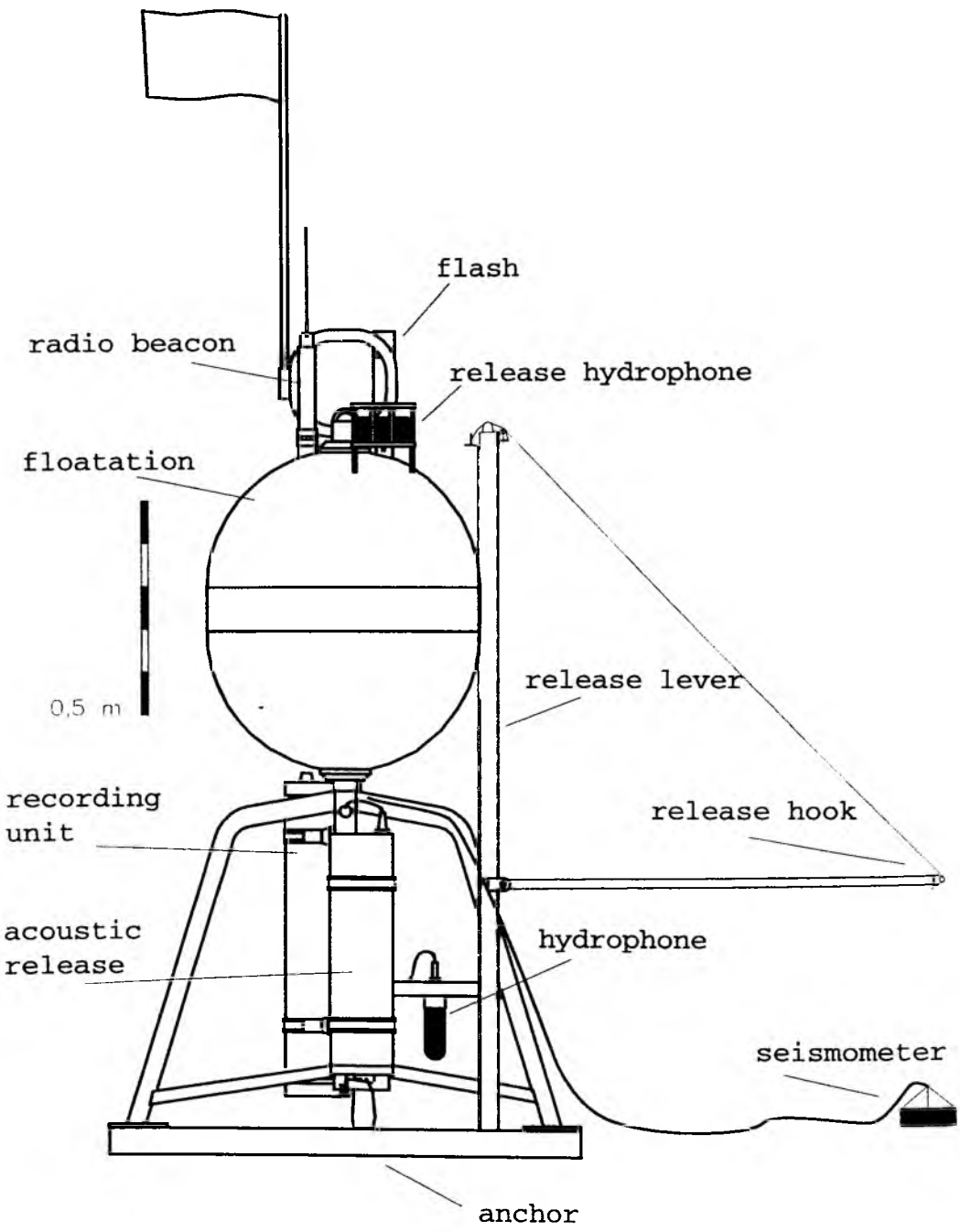

Figure 5.2.3 The GEOMAR Ocean Bottom Seismometer

recorded by the standard Methusalem recorder as used in the OBH units. Parallel to these three channels the standard hydrophone is recorded on the fourth channel.

The Methusalem Dat Recorder

The *Methusalem* consists of a preamplifier (26 dB), a highpass and antialias filter, a 13 bit A/D converter and a core memory of 0.768 MB. Signals are sampled at 800 Hz, and after FIR-decimation filtering, a resolution of 14 to 15 bits is achieved. Data are stored as 16 bit integers on a DAT cassette, which is run in audio-mode to save power consumption and which can store about 1.1 GB of data. The power supply is from alkaline batteries for long term deployments or from rechargeable lead batteries for short term deployments (up to 3.5 days). The instrument can be programmed before deployment through an RS232 interface. Up to 4 channels with different amplifications and sampling rates can be recorded. A DTCXO (0.05 ppm accuracy) is checked against GPS time before and after deployment. The DAT cassettes are read from a playback system, which simulates a SCSI interface, to a workstation for data reduction and analysis (see Chapter 6.2.2).

Marine Broadband Seismic Recorder (MBS)

Apart from the older DAT recording units a new generation of digital seismic recorders was used. The so-called *Marine Broadband Seismic recorder (MBS;* Bialas and Flueh, 1999*)*, manufactured by *SEND GmbH*, was developed based upon experience with the DAT based recording unit Methusalem (Flueh and Bialas, 1996) over the last years. This new recorder avoids mechanically driven recording media, and the PCMCIA technology enables static flash memory cards to be used as unpowered storage media. Read/write errors due to failure in tape handling operations should not occur any more. In addition, a data compression algorithm is implemented to increase the data capacity. Redesign of the electronic layout enables a decreased power consumption (1.5 W) of about 25% compared to the *Methusalem* system. Depending on the sampling rate the data output could be 16 to 18 bit signed data. Based on digital decimation filtering the system was developed to serve a variety of seismic recording requirements. Therefore, the bandwidth reaches from 0.1 Hz for seismological observations to the 50 Hz range for refraction seismic experiments and up to 10 kHz for high resolution seismic surveys. The basic system is adapted to the required frequency range by setting up the appropriate analogue front module. Alternatively, 1, 2, 3 or 4 analogue input channels may be processed. Operational handling of the recording unit is similar to the *Methusalem* system or by loading a file via command or automatically after power-on. The time base is based on a DTCXO with a 0.05 ppm accuracy over temperature. Setting and synchronizing the time as well as monitoring the drift is carried out automatically by synchronization signals (DCF77 format) from a GPS-based coded time signal generator. Clock synchronization and drift are checked after recovery and compared with the original GPS units. After software preamplification the signals are low-pass filtered using a 5-pole Bessel filter with a -3 dB corner frequency of 10 kHz. Then each channel is digitized using a sigma-delta A/D converter at a resolution of 22 bits producing 32-bit signed digital data. After delta modulation and Huffman coding the samples are saved on PCMCIA storage cards together with timing information. Up to 4 storage cards may be used. Currently, up to 440 MB per card are available. Data compression allows more than 2 GB data capacity. Recently technical specifications of flashdisks (disk drives of PCMCIA technology) have been modified to operate below 10 °C, therefore 1 GB drives are now available for data storage. After

recording the flashcards need to be copied to a PC workstation. During this transcription the data are decompressed and data files from a maximum of four flash memory are combined into one data set and formatted according to the PASSCAL data scheme used by the *Methusalem* system. This enables full compatibility with the established processing system. While the *Methusalem* system did provide 16 bit integer data, the 18 bit data resolution of the *MBS* can be fully utilized using a 32 bit data format.

The Marine Longtime Seismograph

Although power consumption could be reduced with the MBS data logger long term deployments of about one year time which would be useful for seismological observations could not be achieved. For this purpose the prototype of a new data logger, the Marine Longtime Seismograph (MLS) was developed by *SEND GmbH* under the direction of GEOMAR.

The MLS is again a four-channel data logger whose input channels have been optimized for 3-component seismometers and one hydrophone channel. The modular design of the analogue front end allows to adapt for different seismometers and hydrophones or pressure sensors. Front ends for the Spahr Webb seismometer and differential pressure gauge (DPG), the Guralp seismometer and the OAS hydrophone have been developed so far. With these sensors we are able to record events between 50 Hz and 120 s. The very low power consumption of 250 mW during recording together with a high precision internal clock (0.05 ppm drift) allows data acquisition for one year. The data are stored on up to 12 PCMCIA type II flashcards. The instrument can be parameterized and programmed via a RS232 interface. After low pass filtering the signals of the input channels are digitized using Sigma-Delta A/D converters. A final decimating sharp digital low-pass filter is realized in software by a Digital Signal Processor. The effective signal resolution depends on the sample rate and varies between 18.5 bit at 20 ms and 22 bits at 1 s. The playback of the data adheres to the same scheme as described for the MBS above. After playback and decompression the data is provided in PASSCAL format from which it should be easily transformed into standard seismological data formats. Since the recording of data through this prototype uses a sample rate of 200.32 Hz, a correct transformation into SEGY-format is not yet possible. A picture of the GEOMAR OBS equipped with a Spahr Webb 3-component sensor is shown in Figure 5.2.4.

The Spahr Webb 3-component sensor was deployed along profile SO144-04 (BOBS 136). Parts of the record sections are shown in Figure 5.2.5 to 5.2.8. The DPG was deployed along profile SO144-05 (OBH152b). A part of the record section can be seen in Figure 5.2.9.

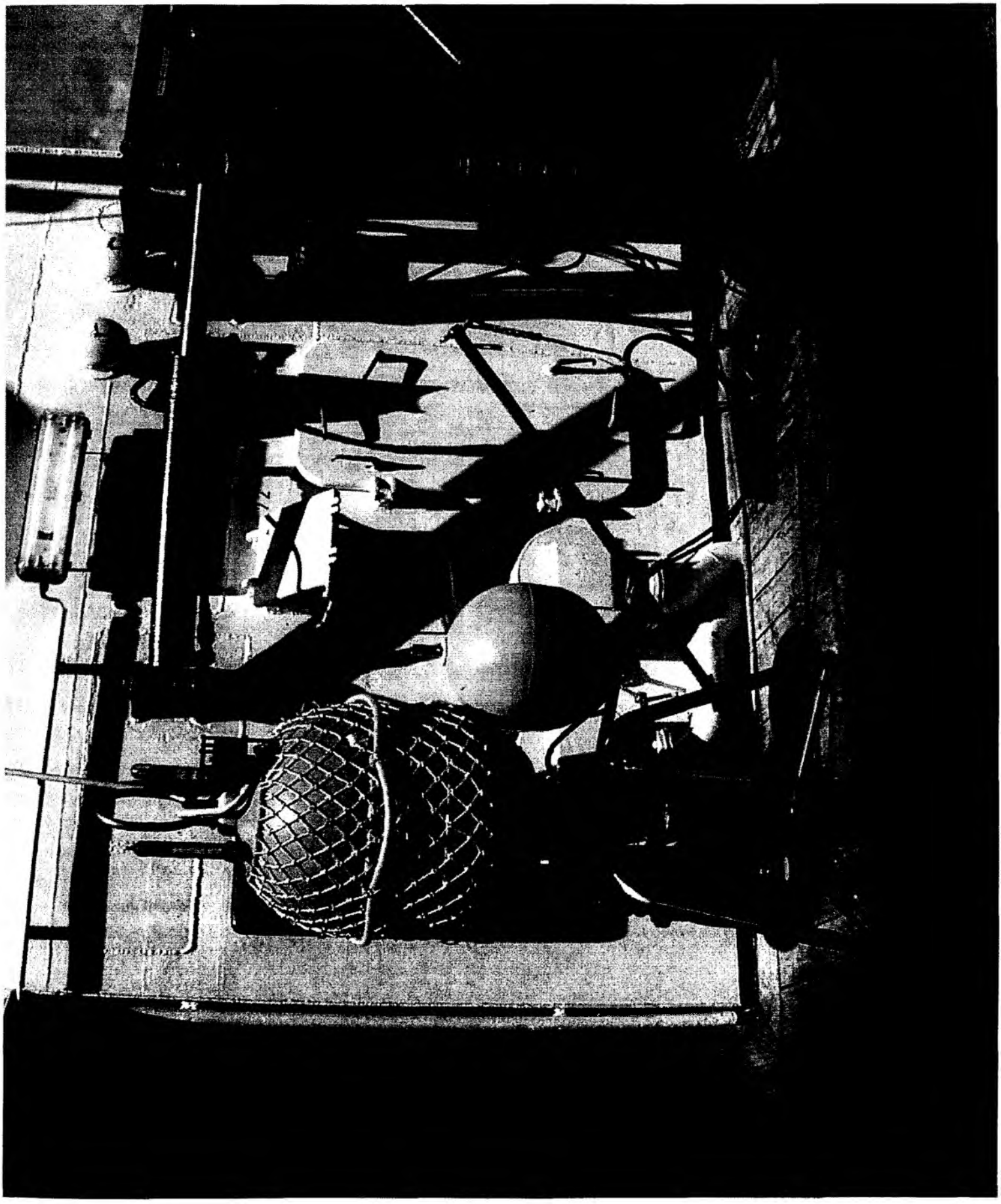

Figure 5.2.4.: The GEOMAR Broadband OBS with the Spahr Webb sensor

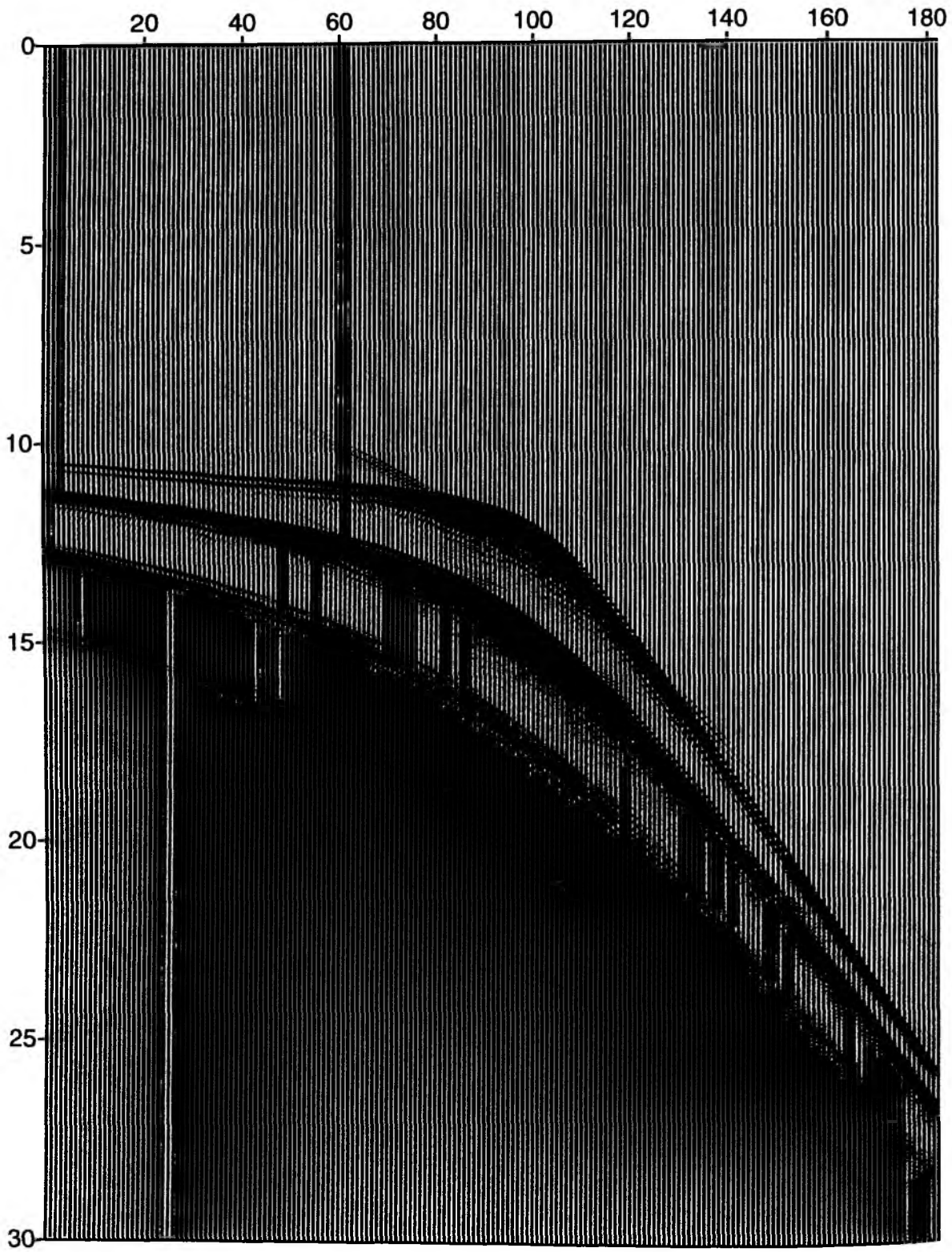

Figure 5.2.5: Part of record section from bobs 136 hydrophone, Profile 04

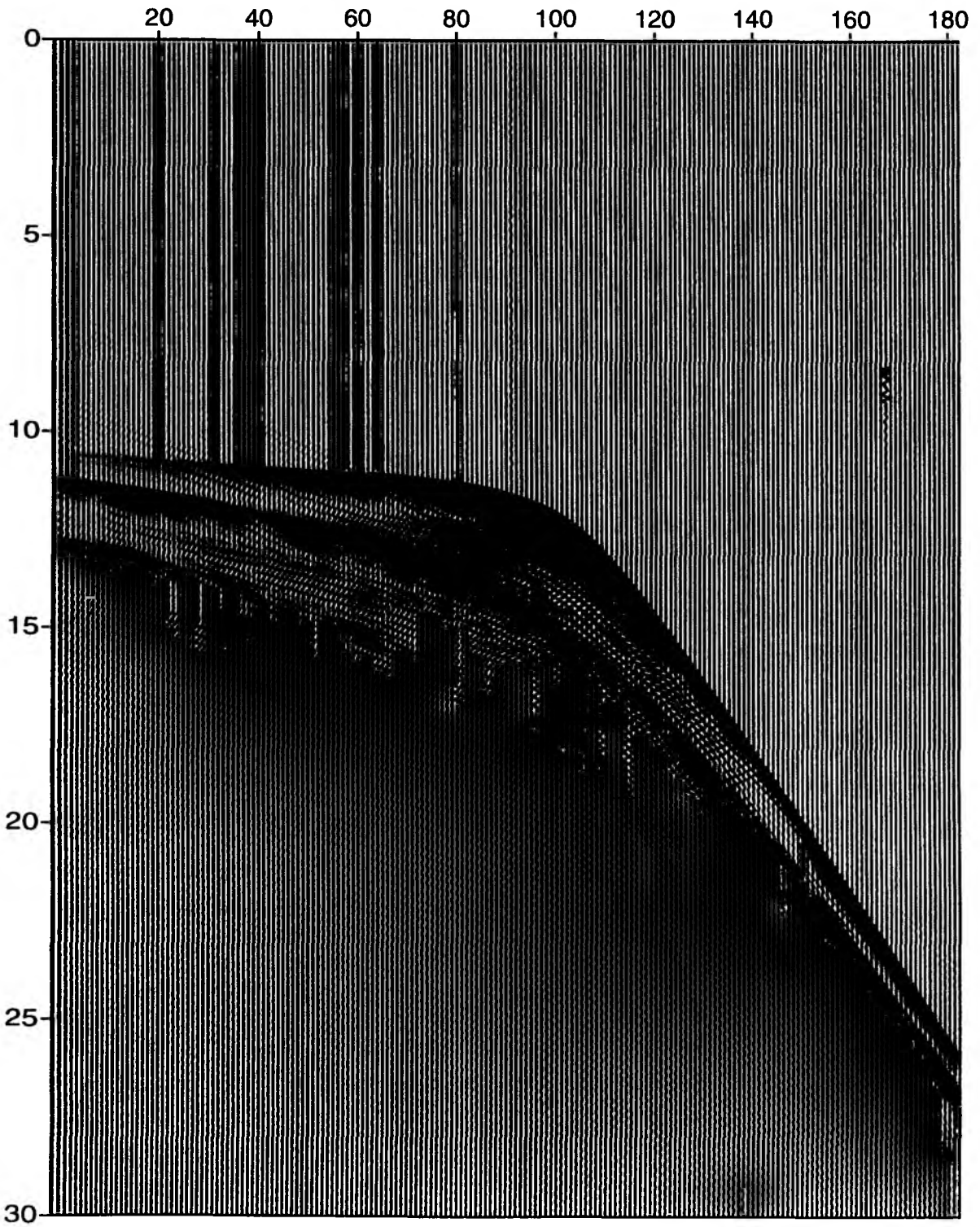

Figure 5.2.6: Part of record section from bobs 136 vertical component , Profile 04

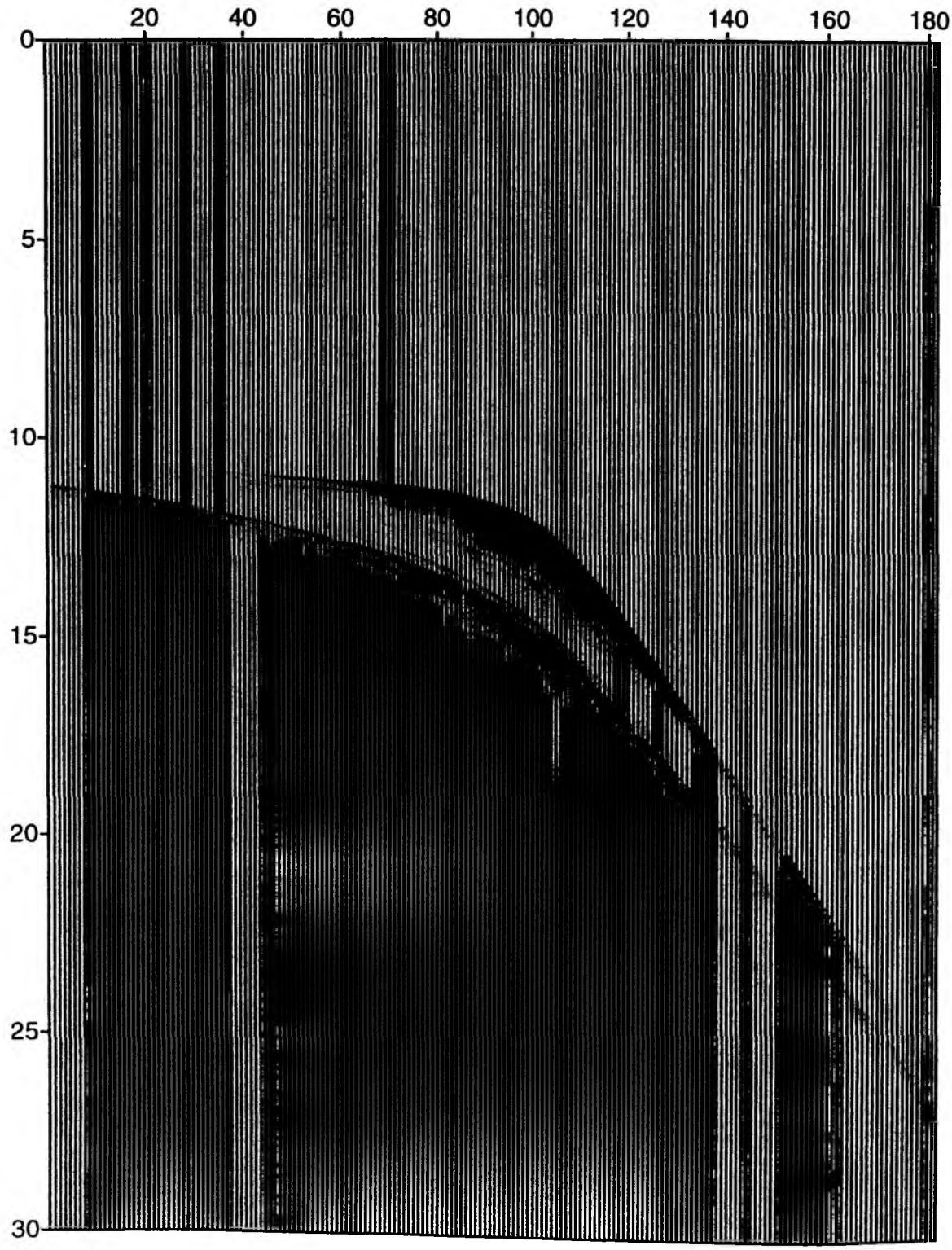

Figure 5.2.7: Part of record section from bobs 136 horizontal component 1, Profile 04

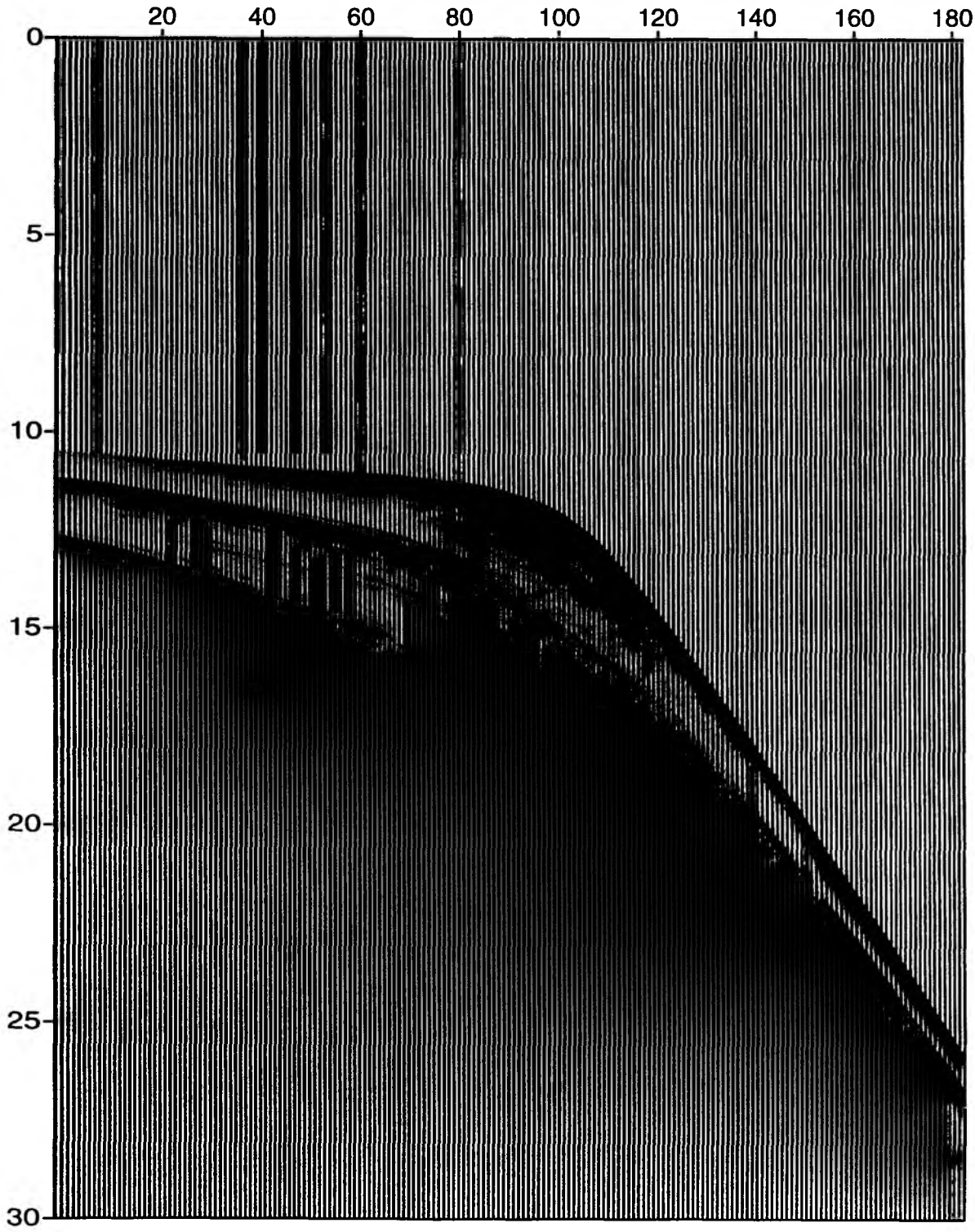

Figure 5.2.8: Part of record section from bobs 136 horizontal component 2, Profile 04

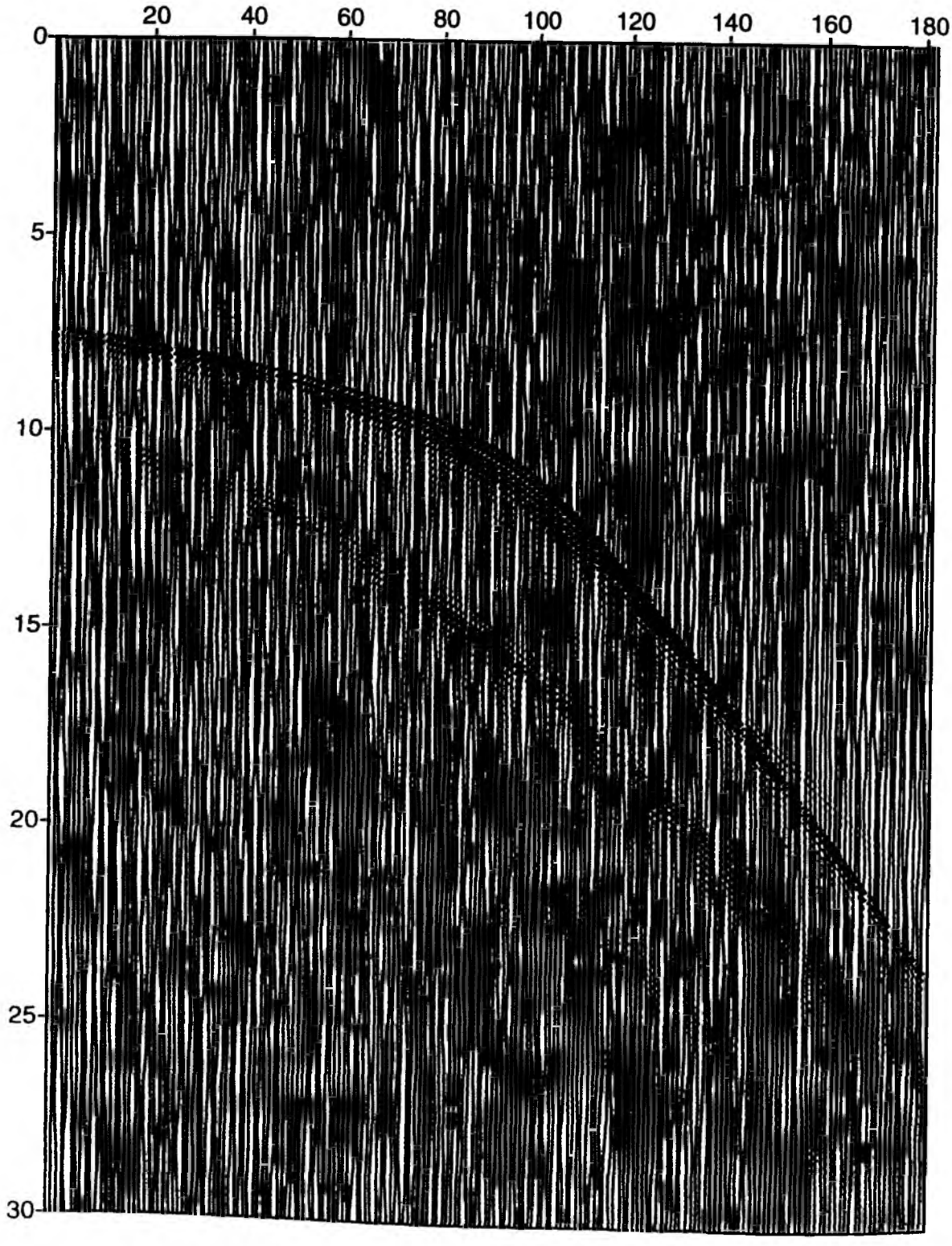

Figure 5.2.9: Part of record section from obh 152b hydrophone , Profile 05

5.3 THE IRD - GÉOSCIENCES AZUR OCEAN BOTTOM SEISMOMETERS

(Ph. Charvis and Y. Hello)

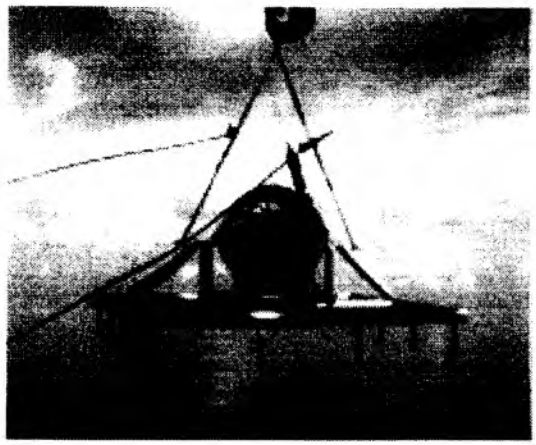

Figure 5.3.1: OBS just before deployment: the glass sphere containing 3 geophones and the data acquisition system is fixed on the anchor frame

Our laboratory: the "Unité Mixte de Recherche (UMR) Géosciences Azur" uses 15 Ocean Bottom Seismometers (OBS) developed and built in the framework of a long-term cooperation between IRD (Institut de Recherche pour le Développement) and UTIG (University of Texas, Institute for Geophysics).

These instruments are small and light so that they can be deployed easily from small research vessels. They consist of a single glass sphere used as flotation and pressure case which contains the acquisition system and three gimballed geophones. A radio beacon, used for recovery, and an optional hydrophone are fixed outside the glass sphere (Figures 5.3.1 and 5.3.2). This unit fastened to an anchor frame for deployment, is released from the anchor at the end of the recording phase. During the cruise SO144-1 (PAGANINI) a total of 42 deployments were sucessfully made.

Acquisition system

Developed at UTIG (Nakamura and Garmany, 1991) the acquisition system is based on a C44 Bus, and controlled by a low power CPU-80C88 microprocessor. A 4 channel preamplifier also ensures filtering of the analog data. The cut-off frequency of anti-alias filter is selectable by replacing plug-in resistor blocks. The data are stored temporarily in the 512 Kbytes RAM and then transferred to the SCSI 1.2 Gbytes hard disk. The real-time clock (TCXO) is compensated for temperature ranging from 0 to 30°C with a precision of 0.3×10^{-6}. For more details see Table 5.3.1.

Sensors

A set of 3 gimballed 4.5 Hz geophones is installed in the inner part of the bottom half sphere. An optional hydrophone is fixed outside the sphere for wide-angle seismic profiling. The OBS is fastened to the anchor frame using bungy cords connected to a stainless steel wire triangle on the top of the sphere. The bungy cords are tightened to their limit of elasticity to ensure a proper coupling of the OBS to the anchor frame.

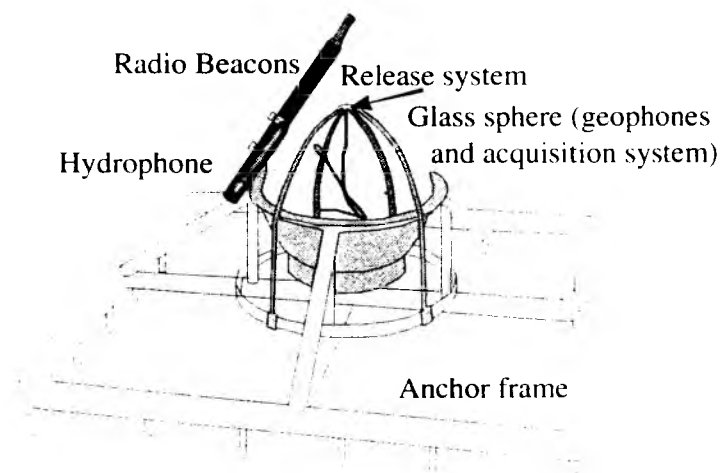

Figure 5.3.2: sketch of an OBS before deployment

Release

The OBS is released from the anchor by the rupture of a stainless steel wire triggered by the main clock and the back-up clock. Electrolytical phenomena of current in salt water will break the steel wire after approximately 5 minutes and liberate the bungy cords which fasten the glass sphere to its anchor frame allowing the OBS to rise up to the surface at ~1m/s.

Table 5.3.1: main characteristics of the IRD-UTIG Ocean Bottom Seismometers

CHARACTERISTICS OF IRD - UTIG OCEAN BOTTOM SEISMOMETERS	
Sensors	3-component gimballed geophones and a hydrophone
Pass Band	4.5 - 100 Hz
Alias filter	selectable with plug-in resistor blocks
Filter roll-off	-24 dB/oct
Sensitivity	1.2 nm/s Mark Products L-15B geophones
Dynamic range	126 dB theoretical, 112 dB re rms electronic noise
Analog/Digital converter	14 bits plus dynamic gain ranging
Sample interval	1 to 255 ms at 1 ms steps
Number of channel	1, 2, 3 or 4
Timing accuracy	0.3 ppm with a temperature compensated crystal (TCXO)
Instrument location accuracy	10 m, from post-recovery analysis of water-wave arrival data
Instrument orientation accuracy	5° from post-recovery analysis of water-wave arrival data
CPU	80C88
Temporary data memory	RAM 512 Kbytes standard, 4 Mbytes optional
Acquisition	Continuous record length 675 s (4 channels @ 10 ms sampling rate)
Transfer rate to recorder	90 Kbytes/s
Data gap	22 s for 512 Kbytes transfer to 1.2 Go IBM hard disk
Recording capacity	1.2 Gbytes on IBM 2.5'' hard disk
Autonomy	6 months dormant; 50 days recording (3 channels @ 20 ms samp. r.)
Batteries	24 to 37 lithium or alkaline D cells
Pressure case	43 cm diameter glass sphere
Weight at deployment	85 kg
Weight at recovery	35 kg
Overall dimension at deployment	128 x 128 x 145 cm
Maximum depth of deployment	8 km
Method of instrument recovery	Timed release from anchor controlled by two independent clocks

Operation at sea

Operations at sea are described in Nakamura et al. (1987) and Hello et al. (1992), and summarised in (Figure 5.3.3) they consist mainly in:

- preparation and programming of acquisition system
- closing the glass sphere
- tests and clock drift measurements using GPS time
- deployment of the OBSs fastened to the anchor
- shooting of seismic lines over the network of recording OBSs
- recovery of OBS at surface after release from anchor
- post-recovery clock drift measurement
- opening the glass sphere
- data transfer and back-up

Data processing

The initial data processing is done on-board using OBSTOOL, a software developed as part of the collaboration between IRD and UTIG (Christeson, 1998).

OBS CLOCK CORRECTION

Pre-deployment and post-recovery clock drift measurements allow to correct for clock drift during data acquisition phase.

RELOCATION AND ORIENTATION OF THE INSTRUMENT ON THE BOTTOM

Using the arrival time of the water wave recorded either on the hydrophone or on the vertical geophone, and the polarity of horizontal components it is possible to calculate, from a least-square fitting:

- the actual location of the instrument on the bottom relative to shot locations
- the actual orientation of horizontal components
- the residual clock correction when passing over the OBS

Table 5.3.2: Seg-Y Trace Header Fields (Barry et al., 1975). Major fields in bold.

Field	Description	Offset (bytes)	Field	Description	Offset (bytes)
1	trace sequence number within line	[1-4]	37	mute time--start	[111-112]
2	trace sequence number within reel	[5-8]	38	mute time--end	[113-114]
3	field record number	[9-12]	**39**	number of samples in this trace	[115-116]
4	trace # within field record (channel)	[13-16]	**40**	sample interval in micro-seconds	[117-118]
5	energy source point number	[17-20]	41	gain type of field instruments code	[119-120]
6	CDP ensemble number	[21-24]	42	instrument gain constant	[121-122]
7	trace number within CDP ensemble	[25-28]	43	instrument early or initial gain	[123-124]
8	trace identification code	[29-30]	44	correlated	[125-126]
9	number of vertically summed traces	[31-32]	45	sweep frequency at start	[127-128]
10	# of horizontally summed traces	[33-34]	46	sweep frequency at end	[129-130]
11	data use	[35-36]	47	sweep length in ms	[131-132]
12	distance from source to receiver (m)	[37-40]	48	sweep type code	[133-134]
13	receiver group elevation from sea	[41-44]	49	sweep trace length at start in ms	[135-136]
14	source elevation from sea	[45-48]	50	sweep trace length at end in ms	[137-138]
15	source depth (positive)	[49-53]	51	taper type: 1=linear, 2=cos^2, 3=other	[139-140]
16	datum elevation at receiver group	[53-56]	52	alias filter frequency if used	[141-142]
17	datum elevation at source	[57-60]	53	alias filter slope	[143-144]
18	water depth at source (m)	[61-64]	54	notch filter frequency if used	[145-146]
19	water depth at receiver group (m)	[65-68]	55	notch filter slope	[147-148]
20	scale factor for previous 7 fields	[69-70]	56	low cut frequency if used	[149-150]
21	scale factor for next 4 coordinates	[71-72]	57	high cut frequency if used	[151-152]
22	X source coordinate	[73-76]	58	low cut slope	[153-154]
23	Y source coordinate	[77-80]	59	high cut slope	[155-156]
24	X group coordinate	[81-84]	60	year data recorded	[157-158]
25	Y source coordinate	[85-88]	61	day of year	[159-160]
26	coordinate units	[89-90]	62	hour of day (24 hour clock)	[161-162]
27	weathering velocity	[91-92]	63	minute of hour	[163-164]
28	subweathering velocity	[93-94]	64	second of minute	[165-166]
29	uphole time at source	[95-96]	65	time basis	[167-168]
30	uphole time at receiver group	[97-98]	66	trace weighting factor	[169-170]
31	source static correction	[99-100]	67	GPN* of roll switch position one	[171-172]
32	group static correction	[101-102]	68	GPN of first trace	[173-174]
33	total static applied	[103-104]	69	GPN of last trace within original field record	[175-176]
34	lag time A in ms	[105-106]			
35	lag time B in ms	[107-108]	70	gap size (total nb of groups dropped)	[177-178]
36	delay recording time in ms	[109-110]	71	overtravel taper	[179-180]

* GPN = geophone group number.; # = number

SEG-Y FILE GENERATION

It consists in merging the navigation file, i.e. time, location and water depth at each shot, with the seismic data. In the Paganini project, for each shot a window of 20 s is stored, for each component of the OBS, with a shift with distance of 6 km/s. The shot number, the component number (1= vertical; 2 and 3 = horizontal; 4 = hydrophone), the distance between source and receiver, the delay recording time (delay in ms between the shot and the first sample of the trace), the number of samples per trace and the sampling interval are the main parameters stored in the trace header (see table 5.3.2 and Barry et al., 1978).

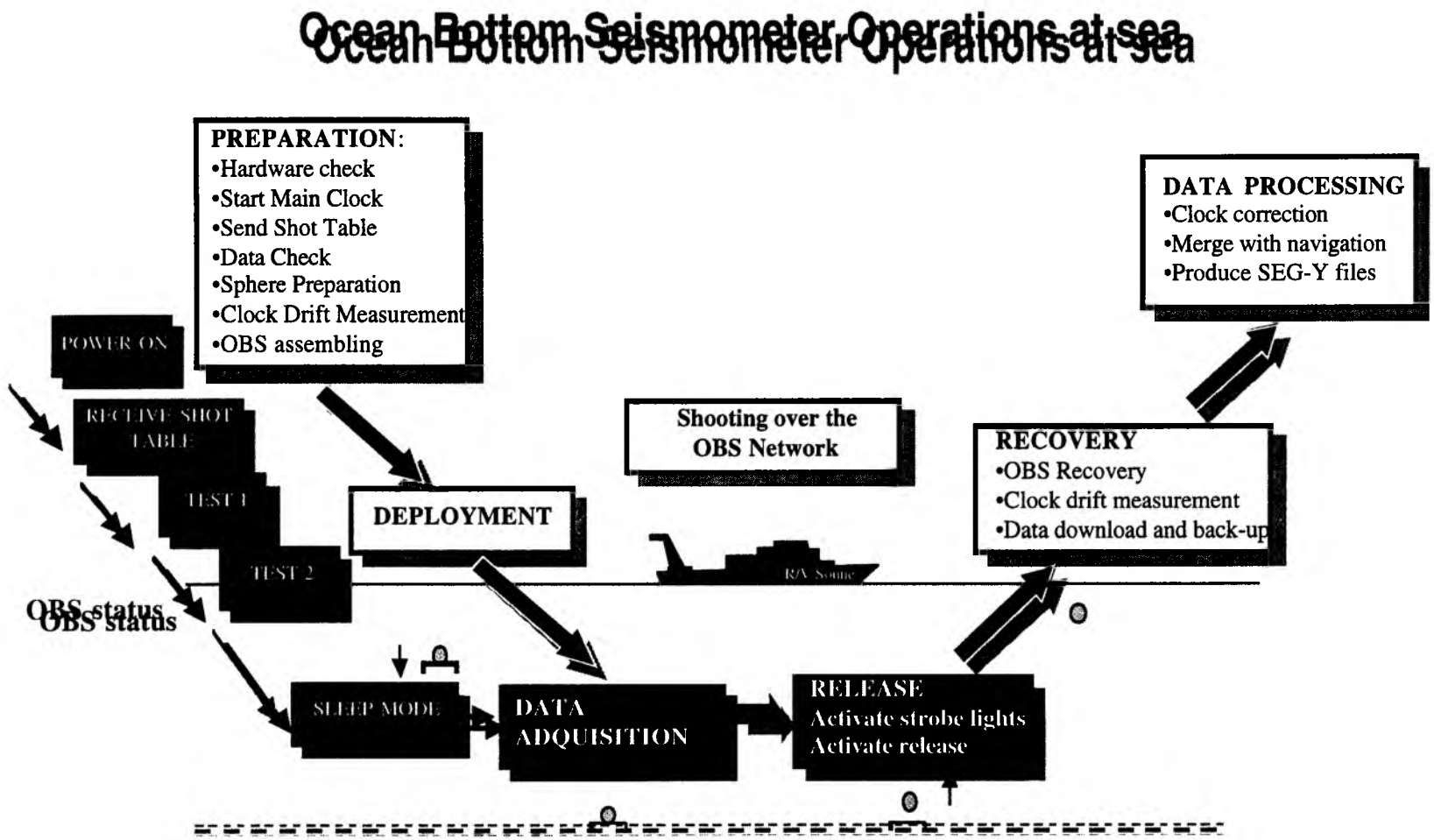

Figure 5.3.3: sketch showing the different phases of an OBS experiment

5.4 THE IFREMER OCEAN BOTTOM HYDROPHONE

(L. Geli and Y. Auffret)

In May 1999, IFREMER signed with Geomar an agreement for scientific and technical collaboration in marine geophysics. Following this agreement, Ifremer bought 11 recording packages for OBH/OBS, including each: one pressure resistant titanium cylinder, a *SEND* MBS acquisition system equipped with PCMCIA memory cards and one OAS hydrophone ; and GEOMAR adviced with software problems.

Using these packages, the marine geosciences department of IFREMER built a series of 11 instruments designed to be used either as OBHs, either as OBSs. The electronics (produced by *SEND*) and the hydrophone are exactly the same as those used in GEOMAR OBHs. The differences are in the mechanical concept, which was tested in the Mediterranean Sea in August 1999.

In order to reduce costs, cylindrical floats out of syntactic foam already existing at IFREMER were used. This conditioned the mechanical design, as shown in Figure 5.4.1. A photograph showing the instrument ready for deployment is given in Figure 5.4.2.

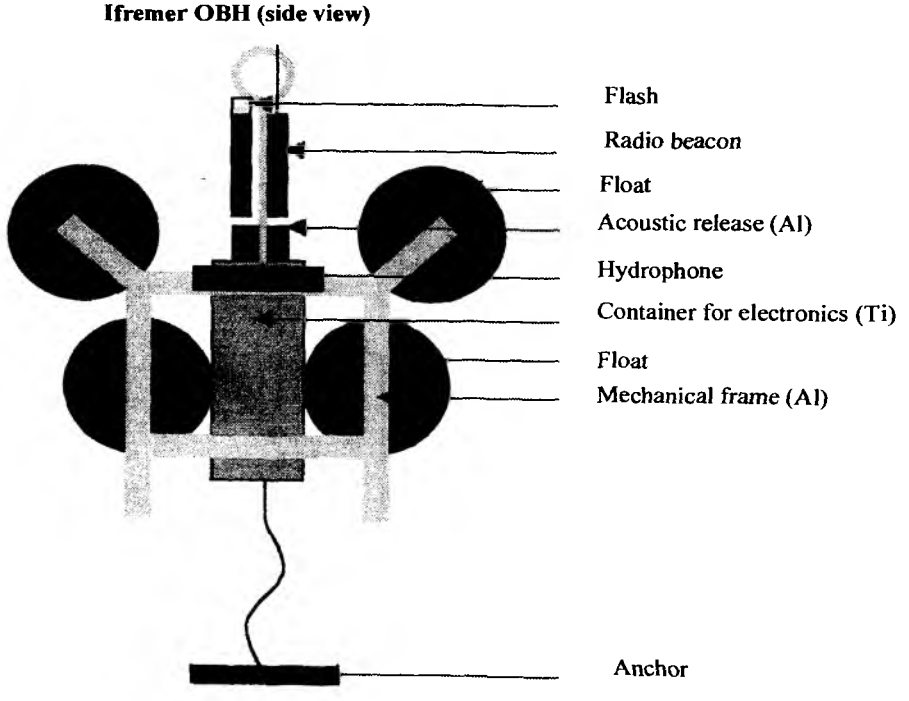

Figure 5.4.1 : Sketch of the Ifremer OBH.

The total weight in air is about 230 kg. When used as OBHs, the instruments include :

- one aluminium mechanical frame, equipped with a prehension mast. In the OBS version, this frame is stiffly attached to an anchor weight, specifically designed to ensure coupling with the sea floor.

- a titanium cylinder, containing the *SEND* MBS acquisition system and the energy source (alkaline batteries or accumulators)
- a hydrophone attached to the frame and built by *Ocean Acoustic Systems*
- an acoustic release, built by *MORS*
- 4 floats made of syntactic foam, providing each 16 kilograms of floatability
- 1 releasable anchor weight

During the Paganini cruise, one IFREMER OBH was fully tested for the first time in operational conditions. In total, the instrument was launched three times. The tests were globally satisfying. Besides the important weight of both the accumulator and the titanium cylinder, the ascent speed of the instruments is 0.8 m/s.

The tests suggested some necessary improvements to operate the instruments. Mainly, the time for mounting and dismounting the cylinder from the mechanical frame before launching and after recovery must be reduced. Additional floatation is needed to speed up the ascent of the OBH from the bottom to the surface.

Figure 5.4.2 : The Ifremer OBH ready for deployment.

5.5 SEISMIC SOURCES

(K. P. Steffen, J. Bialas)

32 l BOLT Airguns

The seismic signals were generated by three Model 800 CT *BOLT* airguns (one on loan from UTIG); a photo of one of the guns is shown in Figure 5.5.1. Each gun has a volume of 32 liters (2000 inch^3), and generates a signal with a main frequency centered around 6 to 8 Hz and including higher harmonics (see also 6.2.2). Two guns were towed attached to blocks on the outer side of the A-frame, with two pier winches controlling the towing. The third gun was towed through the center block of the A-frame using the W6 deep sea cable. Trigger cables and airhoses were deployed manually. Each gun was suspended on two floats with an additional float attached to the supply lines to prevent contact between the gun and the towing wire. A sketch of the towing configuration is shown in Figure 5.5.2. The guns were towed 60 m behind the vessel and operated at 133 bar in 7 to 8 m depth. Onboard, the guns were stored inside the A-frame from where the outer guns were launched using an additional winch on the inside of the A-frame. The recent modifications on the deck (closing the slip) provided an easier launch and recovery operation compared to earlier cruises (e.g. SO103; Flueh, 1995). Due to the large distance needed for safety reasons between guns and the rear of the vessel the outer guns tend to drift to the center, leaving no space to have the third gun in between. Unfortunately no boom was available to take the force of the towing cable and provide a larger distance between port and starbord gun. However the small boom used to lower the core carrier on the starbord side and the magnetic boom on the port side were used to hold pressure hoses and trigger cables farther to the side which helps prevent them from being damaged by the towing cable. The center gun was towed about 50 m behind the vessel to keep clear of the other two guns. This configuration is probably not appropriate during weather conditions with high sea state. Booms at the aft are necessary to further hold the guns away from each other. By the end of profile SO144-03 the piston of the center gun was severely damaged, and the gun was not available for the last two profiles.

During cruise SO144 PAGANINI, the guns were used along six seismic profiles. During the first profile two guns failed after one day of shooting and required major repair as internal sealings need to be replaced. The total operation time was close to 220 hours, with more than 13000 shots being fired, always at a 60 s shot interval. This was well within the capability of the ship's compressor system, which worked smoothly and caused no delays or interruptions.

Seven element Airgun Array

Besides the large sources used for wide angle seismic profiling a small size airgun array was set up on the port airgun slide of RV SONNE. The seven guns include one 2 l, one 1.2 l, two 0.65 l and three 0.33 l Prakla Seismos guns, some of them are on loan from the Institute of Geosciences, Kiel. Their configuration is shown in figure 5.5.3. For gun control a *LongShot Seismic Source Controller* from *Real Time System* was available. This unit was specially adapted to the Prakla Seismos type valves and sensors, and it is equipped with two power circuits (four guns each) to control the array. During onboard testing it turned out that the control unit failed to serve the power units for gun five to eight and therefore only half of the array could be used at once. This was the first time the guns had been operated using sensor signal output which was used for automatic gun synchronization up to 1 msec resolution. The array was operated on three

short range experiments dedicated to BSR observations above the structure of a subducted seamount (s. ch. 6.2.4).

External Trigger

The trigger signal was supplied from the ship's *Ashtech* GG24 GPS/Glonass receiver, and was available in the Geology Lab and the Seismic Lab. The receiver can provide a one-millisecond-long 5 V-TTL pulse at intervals between 0.2 and 999 s. The impulse should be stable to within the accuracy of the GPS Time, which is 70 nanoseconds. The impulse was delivered to the *BOLT* Par Airgun Firing Circuit FC300 and the *Real Time Systems* LongShot Seismic Source Controller. The shotbreaks, necessary for subsequent data processing and instrument location, were stored on a MBS recorder and displayed in real time to double check. For this process the same time basis was used as for the OBH (see chapter 5.2) and the trigger signal was converted into a 5 V TTL pulse of 250 ms length by a circuit provided from the ship's technical support staff (WTD). Exact position calculation for the shot time should be done by later post-processing using shot time and UTC time values stored with DGPS coordinates in the ship's data base. During preliminary discussion, it was discovered that the coordinates stored within the data base were provided by the *Atlas ANP 2000* system, which does not copy the exact GPS time values but adds time stamps of its internal uncontrolled clock to the high precision coordinates of the DGPS system. The accuracy of the time values mainly depends on the operator's skills in manually setting the ANP clock to GPS time. This is clearly a somewhat conservative method compared to the efforts of precise positioning.

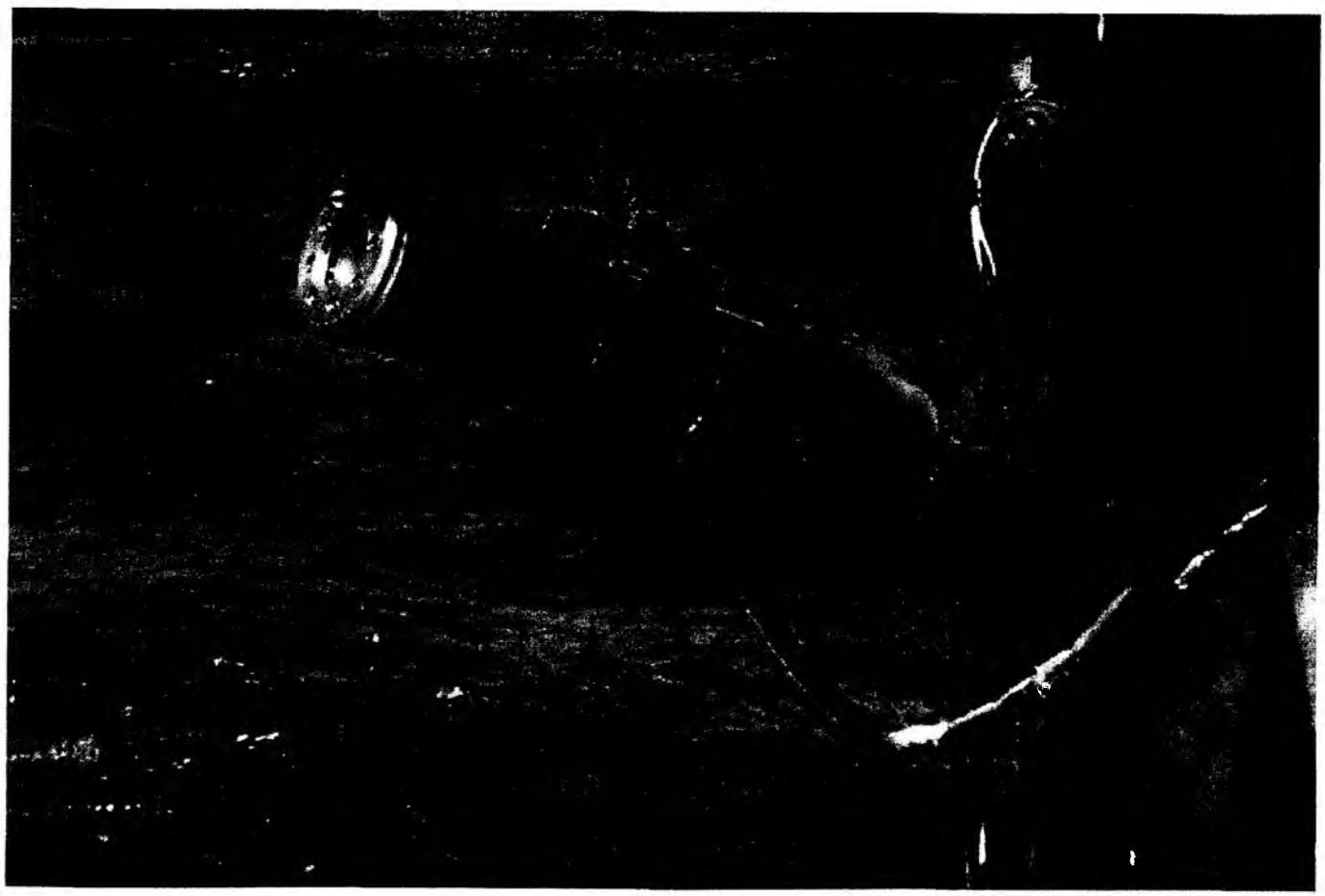

Figure 5.5.1: A CT800 BOLT airgun upon deployment.

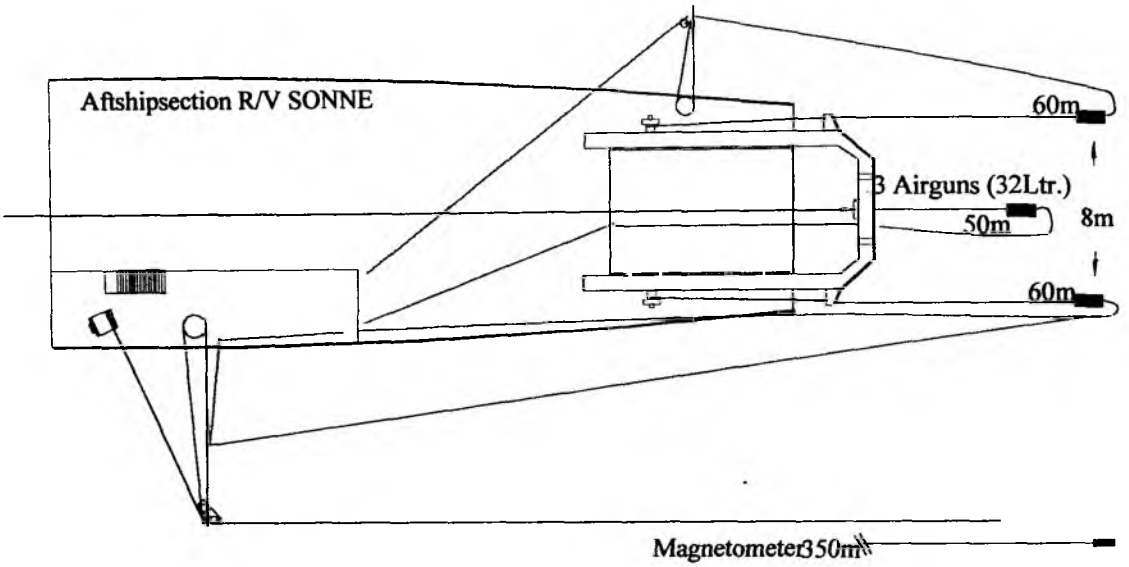

Figure 5.5.2 Configuration of three 32 l airguns towed behind RV SONNE.

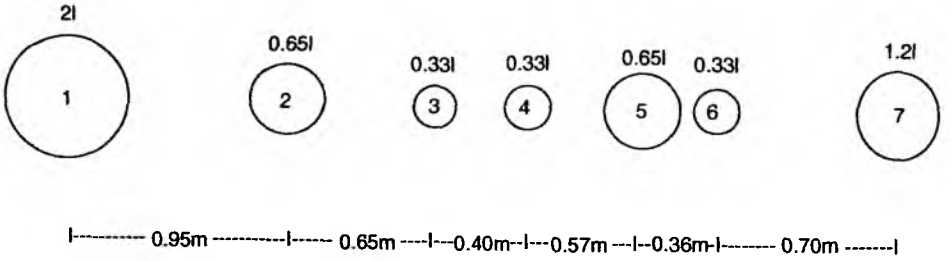

Figure 5.5.3 Gun configuration for seven element array.

5.6 THE MAGNETOMETER

(J. Bialas, C. Ranero)

During cruise SO144 we used a GeoMetrics G801/3 Marine Proton Magnetometer. This unit uses a gasoline-filled sensor with a 350 m marine cable and a control unit. During a polarisation cycle an electric current generates a strong magnetic field in the coil and forces the magnetic moments of the protons to be aligned for a short time parallel to the excited field. During the following measuring cycle, i.e. when the electric current is turned off, the previously excited field is removed and the protons "try" to realign themselves with the Earth's magnetic field. According to the moment preservation law, this happens by precession of the protons with a certain frequency which is directly proportional to the intensity of the Earth's magnetic field. Basically, this frequency is measured as AC electric current created by magnetic induction in the coil, amplified, counted and transformed to magnetic field intensity values (measuring unit: 10^{-9} Tesla = 1 nT), which are recorded.

In order to minimise the influence of the ship's hull, the sensor is towed at three times the ship's length behind the ship for a resolution of about 1 nT. In our experiment, the sensor was towed at 300 m from the ship (the length of R/V SONNE is 95m.). Therefore, the sensor was towed at a distance outside the ship's magnetic field.

On board of RV SONNE, the winch was placed on the port back deck and the sensor was towed to the port side of the vessel. A boom leads the cable about 7 m to the side of the ship in order to prevent it from being tangled with the ship. The system worked well throughout the cruise.

The measured values of the total intensity magnetic field were displayed on a console and written as digital output coded in BCD values. The system was set to deliver one data value every 3 seconds via a digital multiport interface to a PC, where a special software was used to store the data together with UTC-time in ASCII tables.

After data backup the files were transferred to a SUN workstation. GPS coordinates and time were taken from the ship's navigation system and assigned to each magnetic stamp on the basis of the recorded time. The magnetic and the navigation data were resampled to 10 s interval. After optional median filtering they were displayed using GMT plot routines (Wessel and Smith, 1995).

5.7 THE SCRIPPS OCEAN BOTTOM SEISMOMETER

(LeRoy Dorman, Sharon Asher, Heather Deshon, Allen Sauter, Michael Tryon)

History

The general specifications for the ONR OBSs were established by a broadly based ad hoc committee named the Seafloor Noise Advisory Group (SNAG), in response to a navy need to understand more about the seismo-acoustic noise on the sea floor. The design of the instruments was, however, made sufficiently flexible that they are useful for a wide variety of marine or lacustrine seismic experiments, both passive and active.

The design and manufacture of the instrument was undertaken by a consortium consisting of the Scripps Institution of Oceanography, the Woods Hole Oceanographic Institution, the Massachusetts Institute of Technology, and the University of Washington. The SIO group provided the analog systems and control computer, the WHOI group undertook the mechanical systems design and recording module, the MIT group the mechanical design of the sensor package. The UW group designed the analog-to-digital converter (ADC) board.

Thirty-one of the instruments were constructed and divided between the West Coast (SIO) and East Coast (WHOI) operating bases and the instruments have been in frequent use since about 1990, on projects supported by the Office of Naval Research and by the National Science Foundation. Two have been lost.

Since the original design, the SIO instruments have been upgraded to (i) reduce the power consumption, (ii) increase storage capacity, and (iii) upgrade to a broadband sensor. The power conservation was accomplished by using a analog-to-digital converter (ADC) of more recent design, and by programming the computer CPU to sleep between samples, interrupting from a halt state. These changes reduced the power requirements from the original 1.2 Watts to about 350 mWatts, enabling longer deployments. The recording system was designed to use the SCSI interface to enable easy incorporation of technical advancements in computer hardware. The original units used WORM (Write Once Read Many) disks of 380 Mbytes capacity. These were supplanted by Digital Audio Tape (DAT) storage, using up to 3 two-Gbyte units, and now we are using 9.1 Gbyte disk drives. These two changes allow us to make 1-year deployments, although the longest we have actually carried out is six months. Half of the SIO instruments have been fitted with PMD broadband seismic sensors, replacing the 1 Hz geophones, allowing greatly improved recording of surface waves and opening a new range of studies of seismic sources.

General Description

The instruments are described in Sauter and others, 1990. The analog electronics are based on a series of earlier systems operated at SIO (Prothero, 1976), (Moore and others, 1981) all of which used seismometers of 1 Hz frequency.

The orthogonal 3-component set of seismometers (Mark Products L4-3D or PMD Broadband sensors) are mounted in gravity-leveled gimbals damped in a high-viscosity fluid (polydimethylsiloxane, 980 Pa-s viscosity). The gimbals are suspended in a pressure case of 0.35 m diameter. The properties of this sensor package have been extensively studied (Barash and others, 1994) and are well known. In use the pressure case is deployed on a pivoting arm which drops it to the seafloor about a meter away from the instrument frame (Figure 5.7.1). This provides some isolation from mechanical noises generated by the recording devices and

from vortex shedding from seafloor current acting on the mechanical frame (Trehu and others, 1994).

The external sensor package contains the preamplifier, which is controlled by the acquisition computer to provide gains ranging from unity to 512 (0 to 54 dB), and the circuits which generate a pseudo-random telegraph code for calibration (Berger, Agnew, Parker and Farrell, 1979; Sauter and Dorman, 1986). The analog amplifiers utilize shaping filters which reduce the dynamic range required to cope with the background noise on the seafloor (which has steeper spectrum than that encountered on land). The OBS uses a 16-bit ADC which provides a dynamic range of 90 dB. Immediately before the digitizer is a fast gain-ranging circuit which allows reduction of gain by a factor of 4, 16, or 64 (36 dB) to avoid clipping on very large signals. Thus the aggregate dynamic range is 120+ dB.

The system operates on batteries and writes the digital seismic and timing information to a SCSI storage device. We are using IBM disk recorders with 9.1 gbyte capacity. The disks allow recording of 4 channels at 128 Hz for 100 days.

An external computer (either a DOS or Unix) is used to program and operate the OBS. Once data is recorded, the raw data tape is read and converted to ROSE (Latraille and Dorman, 1979), SAC or SEG-Y format. We are now committed to provide the SEED format.

Typical operation configurations:

Sample Rate	Input Channels	Recording Time
128 Hz	4	100 days
64 Hz	4	200 days
32 Hz	4	400 days

Table 5.7.1 Sample rates and recording times available with 9.1 gbyte disks.

Broadband Sensors

Work accomplished thus far:

We chose to adapt the Precision Measurement Devices (PMD) 2123 seismic transducers to the seafloor. The choice of these sensors was made based on the their ruggedness, robust leveling requirements, and cost. The horizontal sensors are inherently self-leveling, up to a tilt of 5°. This applies to the vertical sensor as well, but there will be be an error since the translation measured will not be truly vertical. The sensors are electrochemical in nature, and are related to the Solion sensors used in early versions of the Sacks-Evertson dilatometer. The power requirements are low, around 42 mW. This is excellent compared to the 300 mW of the Guralp low-power sensors. The development of these sensors was supported, in art, by the National Science Foundation. The price of the sensor is just over $6,000, about twice that of the Mark Products L4-3D, but considerably lower than the price of the Guralp sensor. Although the noise floor of these sensors is above the continental low-noise model, so is the noise on the sea floor. The particular model we are using is flat in response to velocity and has a low-frequency corner at 0.03 Hz (33 second period). We now have seven of these sensors in use.

The PMD sensor is shown in Figure 5.7.2, which shows the PMD device next to the L4-3D sensor package presently in use.

Because the initial proposal was supported at a reduced level, we adapted the existing sensor packages Barash and others (1994) for use with the PMD sensor. This package has undergone extensive testing (Trehu and Sutton, 1994) .

Land tests:

We have tested the sensor in the laboratory as part of the MELT sensor intercomparison (Sauter and Dorman, 1997, see http://www-mpl.ucsd.edu/obs/reports/tn061/comparison/comparison.html) and found that it provided about 30 dB improvement in low-frequency noise level over the Mark Products L-4. This allow access to many more earthquakes.

Sea tests:

Figure 5.7.3 shows spectra from the first large-scale use of the new sensors. Spectra of seismic noise are shown for three components for the same time segment from nearby instruments. The difference in noise below the microseism peak is significant. The broadband instruments can see signals from earthquakes two magnitude units smaller than the smallest quakes seen on the 1 Hz seismometers.

Figure 5.7.4 shows seismograms from a distant earthquake. The traces have been offset for clarity so the distances are approximate. The upper two traces are from 1 Hz sensors and the lower 3 are from the broadband sensors.

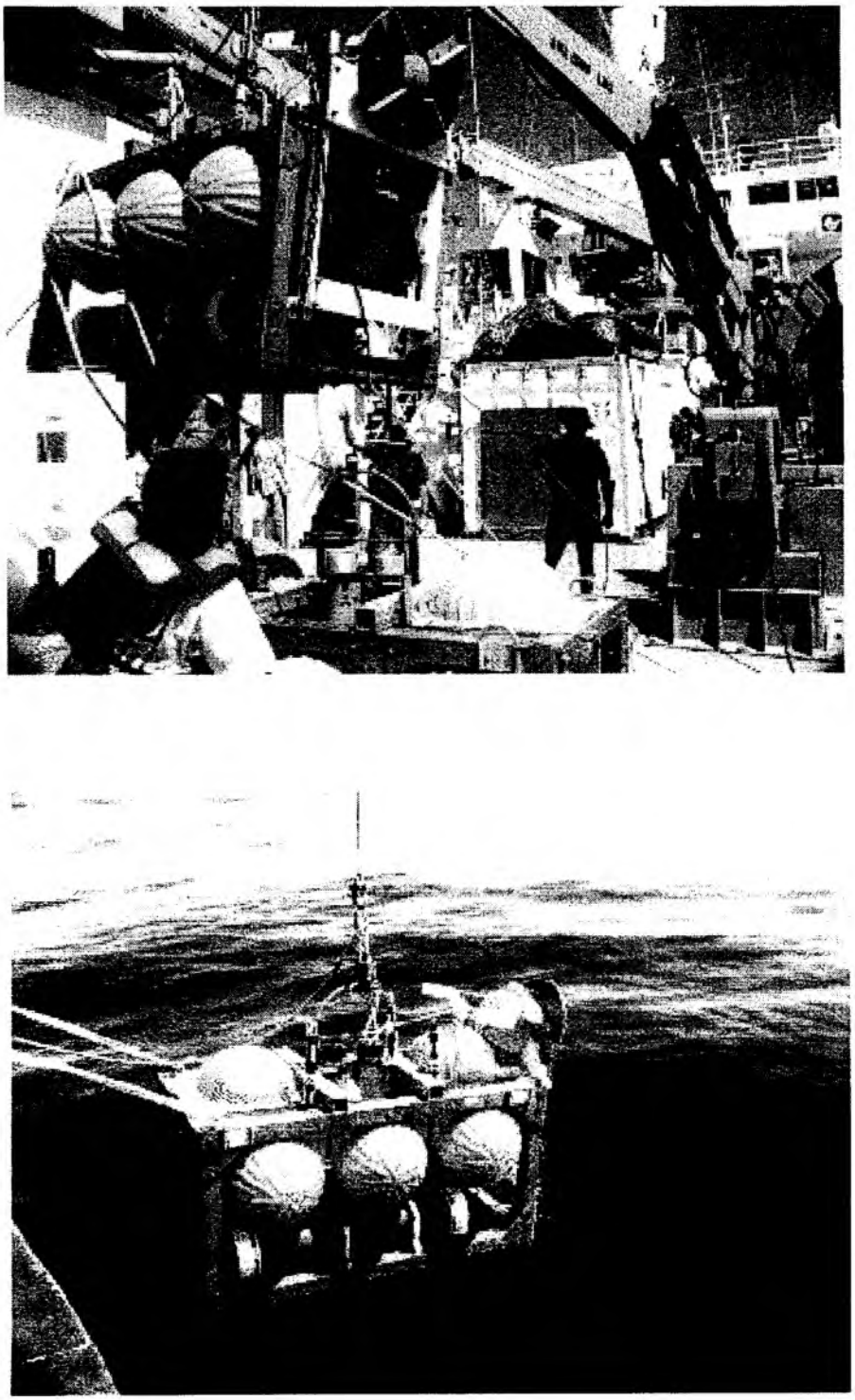

Figure 5.7.1 SCRIPPS Ocean Bottom Seismometer during launch

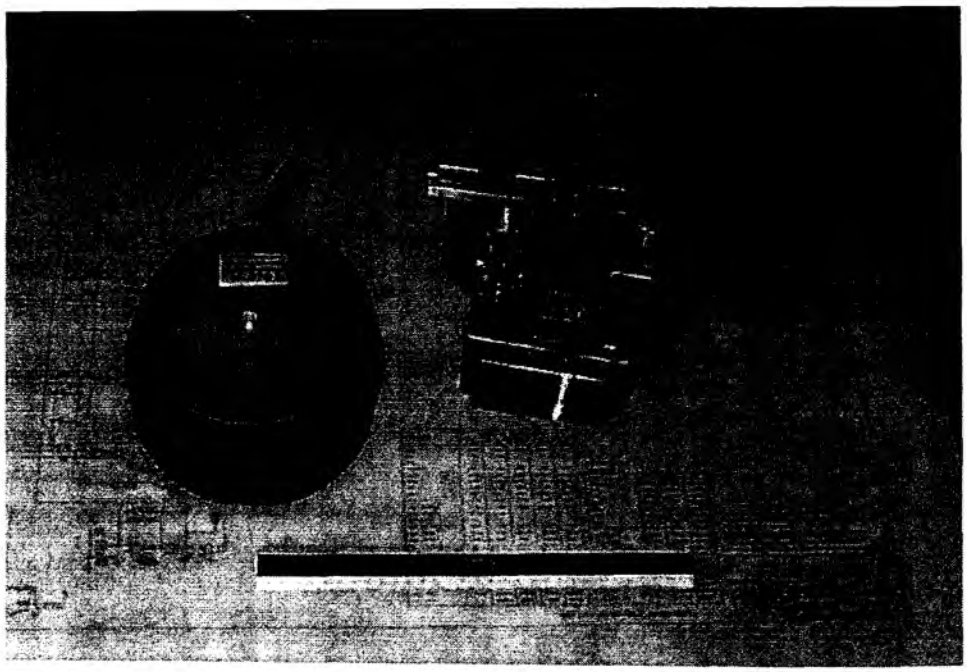

Figure 5.7.2 Photograph of PMD (left) and L4-3D (right) sensors

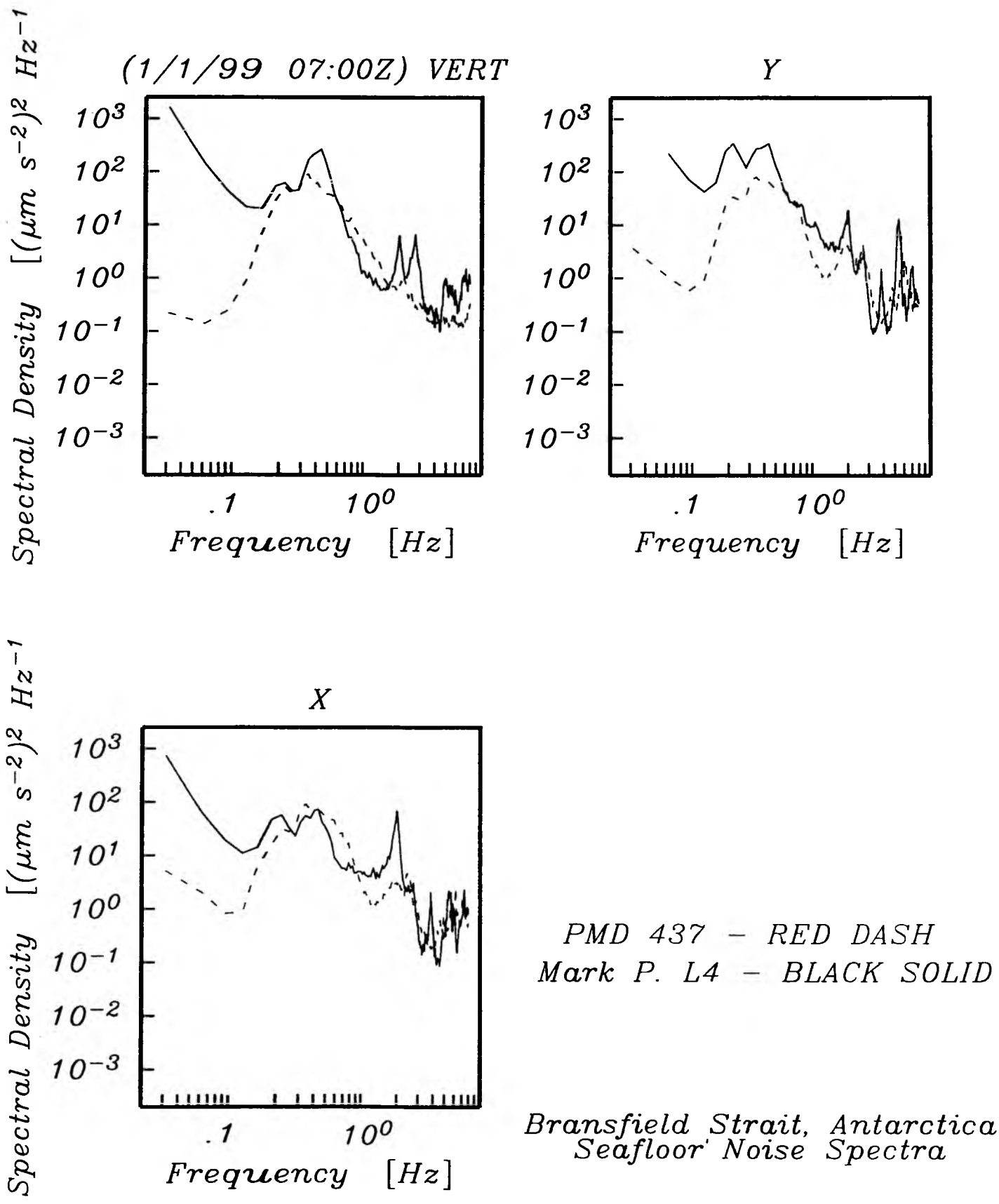

Figure 5.7.3 Spectra from the first large-scale use of the PMD sensor

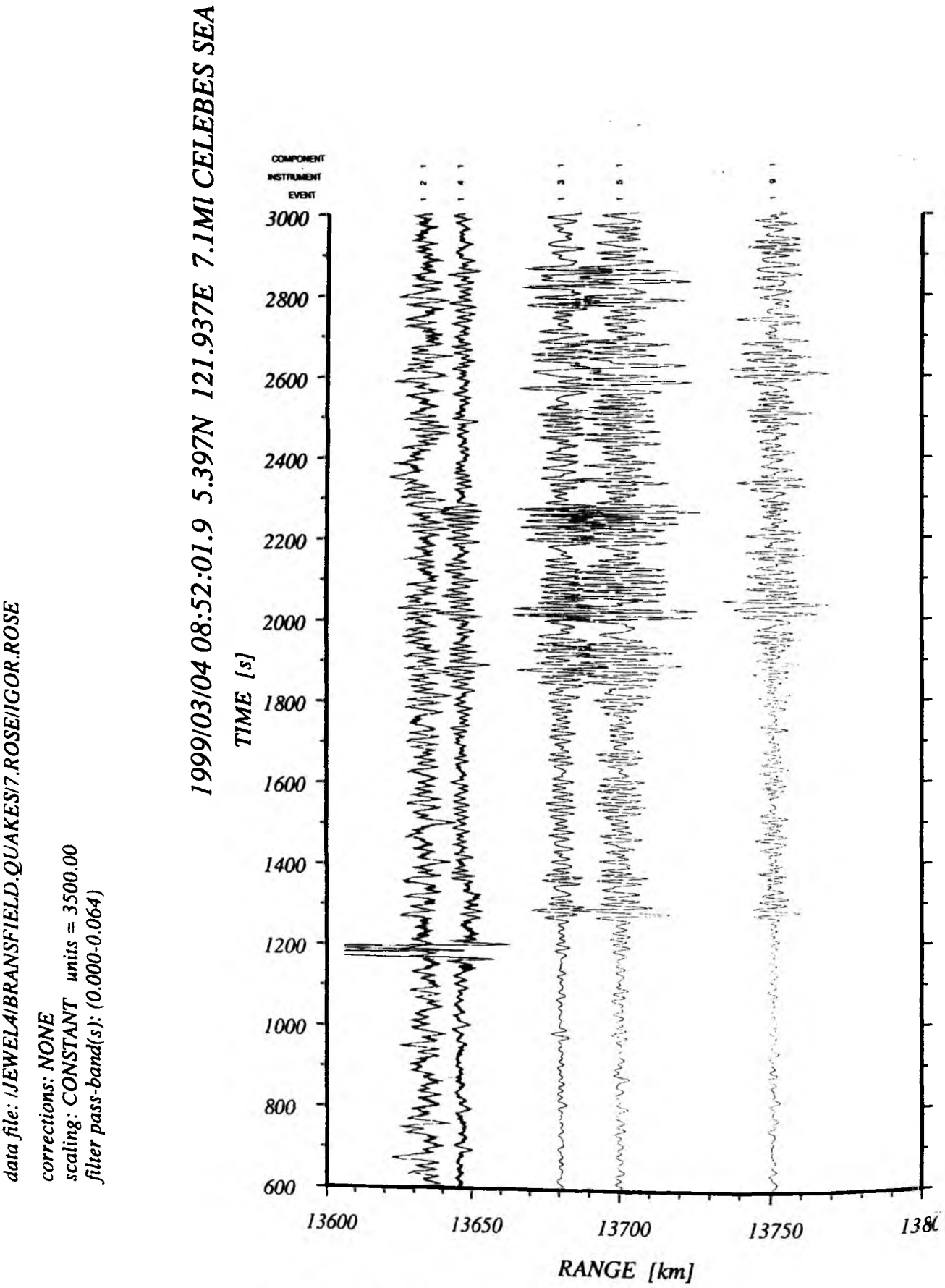

Figure 5.7.4 Seismograms from a distant earthquake

5.8 SIO BENTHIC FLUX METER

(Michael Tryon)

The Costa Rica flux meter study consists of the deployment of 14 OBS/flux meter combinations and another 7 autonomous benthic flux meters (Fig. 5.8.1, 5.8.2) across the Costa Rica margin northwest of the Osa Peninsula for a period of about 75 days. This will be followed up by a second deployment of the 14 combination instruments across the margin off the Nicoya Peninsula for approximately 6 months. These measurements will provide information about the regional changes in diffuse fluid expulsion patterns across this convergent margin. This is the largest attempt to date to obtain a transect of direct measurements of diffuse surface fluid expulsion patterns across a subduction system. This large number of measurements is necessary because lateral changes and variability in fluid expulsion patterns is to be expected. This study is of particular relevance to the associated studies of forearc deformation and seismicity patterns because the general deep suspicion is that they are all somehow coupled processes.

The SIO Benthic Flux Meter design is similar to others in that it has an open ended collecting chamber inserted into the sediment but differs principally in the way it measures the fluid flux through the chamber. The meter uses the dilution of a chemical tracer to measure flow through the outlet tubing at the top of the chamber. A tracer solution of similar density but different composition than the seep fluid is injected at a constant rate by two osmotic pumps into the water stream as it moves through the outlet tubing. These same pumps withdraw a sample of the seep fluid/tracer mixture from downstream of the tracer injection port giving a serial record of the tracer dilution. The osmotic pump contains an osmotic membrane that separates chambers containing pure water on one side and a saline side that is held at saturation levels by an excess of NaCl. Due to the constant gradient, distilled water is drawn from the fresh water chamber through the osmotic membrane into the saline chamber at a rate that is constant for a given temperature. The saline output side of the pump system is rigged to inject the tracer while the distilled input side of the two pumps are connected to separate sample coils into which they draw fluid from either side of the tracer injection point. Each sample coil is initially filled with deionized water. A portion of the fluids moving out of the top of the chamber are collected in the coils, displacing the deionized water, and recording a unique pattern of chemical tracer distribution. The two sample coils allow both positive and negative flow to be measured and give a serial record of the flow rates. After recovery the sample coils are subsampled and the Rb+ tracer is analyzed by optical emission spectrometry. A flux rate range of 0.1 mm/yr to 15 m/yr can be measured. The temporal resolution of the meter for the experiment discussed here is approximately 1-2 days.

The Costa Rica margin can be broadly subdivided into the following four tectono-hydrogeologic provinces for the purposes of the flux meter survey:

Province 1 - The margin wedge or basement complex region (arcward from ~8 km from the toe). Pore fluid profiles from Leg 170 indicate freshening of fluids from below in this region. These may be complicated by the presence of gas hydrates. Our flux meter measurements will constrain the diffuse fluid input levels without the concerns of separating out the hydrate freshening artifact.

Province 2 - The region of out-of-sequence-thrusts (~3-7 km from the toe). Alvin observations in the Leg 170 region indicate that cold seeps and a small mud volcano are present in this region. We expect this region to be strongly heterogeneous, with

predominantly low to moderate levels of flow. While high flow rate seeps are present, it is unlikely that we will sample these with this type of deployment.

Province 3 - The sedimentary wedge (0-3 km from the toe). The region is comprised predominantly of deformed slope sediments. Leg 170 results and Alvin observations suggest this region may be dominated by elevated levels of diffuse porous fluid flow without significant focusing at cold seeps.

Province 4 - The incoming sedimentary section. Pore water profiles from Site 1039 do not appear to suggest any significant lateral or upward fluid advection.

Combination OBS/flux meter instruments were deployed on a large scale array with ~20 km spacing. Eight of these are in province 1, two near the province 1-2 boundary, one near the province 2-3 boundary, and three in province 4. Autonomous instruments were deployed in a small array (~3 km spacing) nested within the lower portion of the larger array extending from the province 1-2 boundary to the toe of the prism.

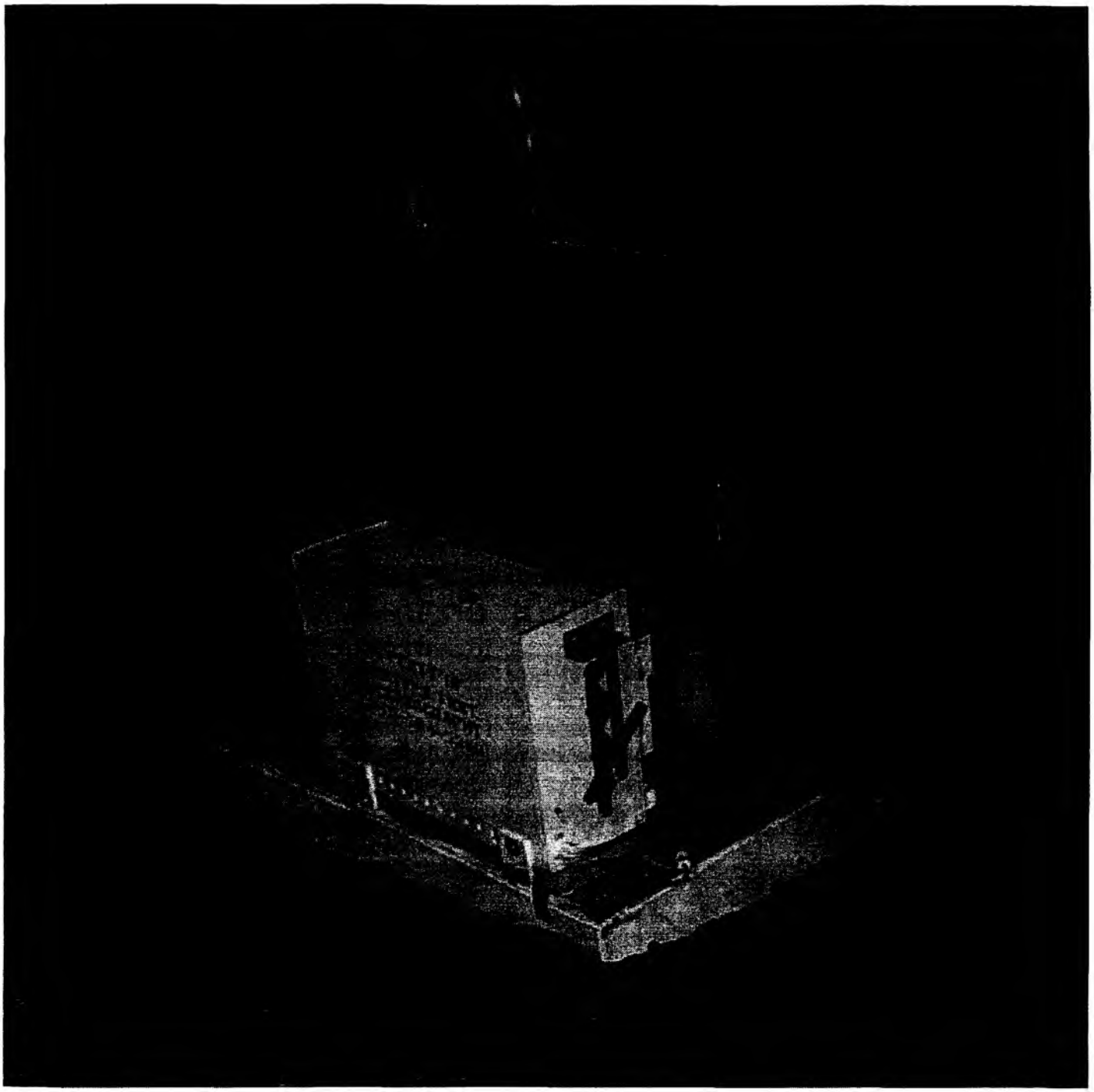

Figure 5.8.2 Photograph of SCRIPPS Flux Meter at the seafloor

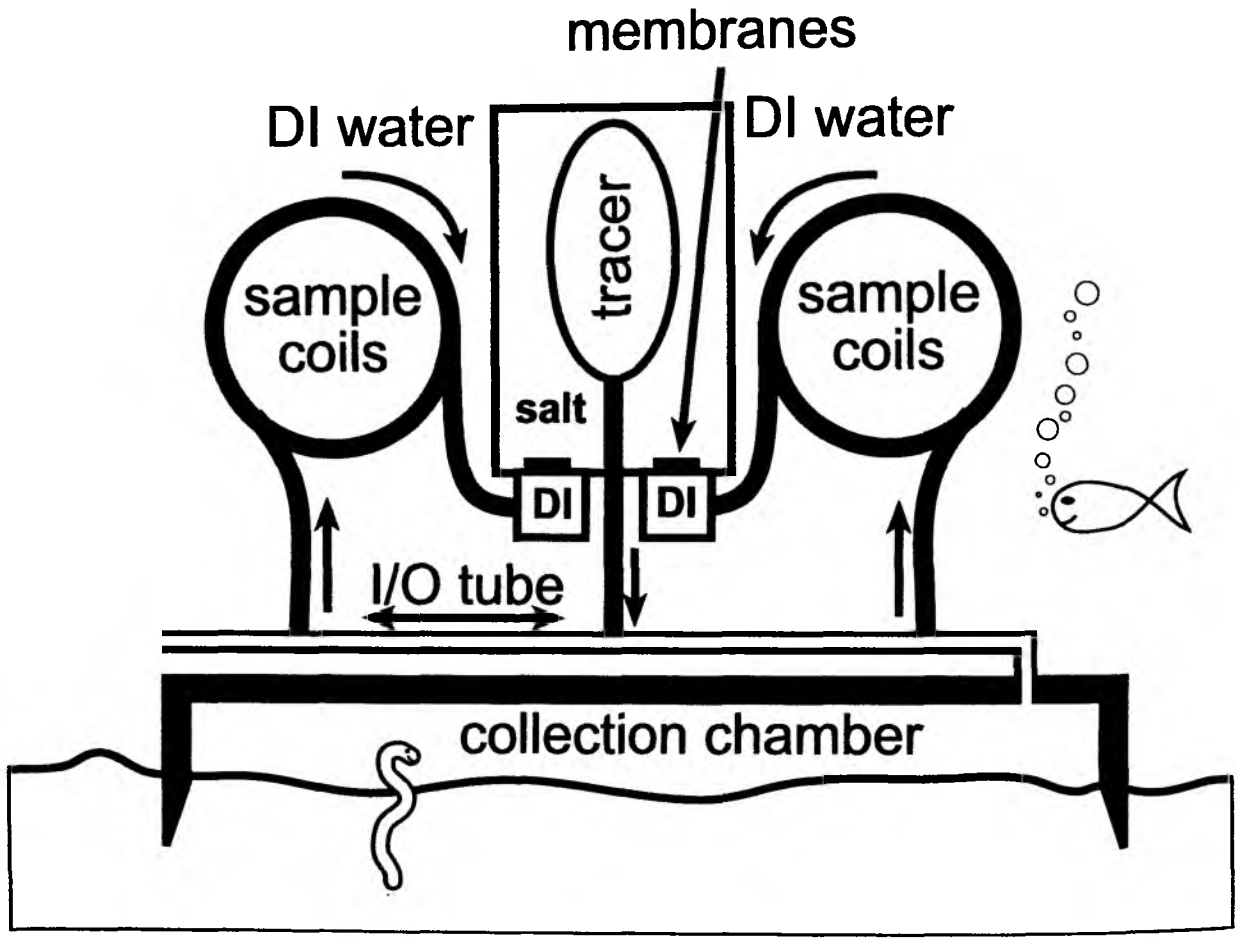

Figure 5.8.1: Schematic display of SCRIPPS Flux Meter

5.9 THE MINI STREAMER

(J. Bialas)

For the case of profiles being shot with the small 7 gun array a short streamer was onboard to record reflection seismic events. It is a three-channel unit originally build by Prakla-Seismos, Hannover, Germany for the Deutsches Hydrographisches Institut in 1979.

The system comprises three parts, a 50 m long active length, a 50 m long stretch length and a 150 m long towing cable. The active length is separated into three groups of 16 HHOC type hydrophones. The first and third group are designed identically while the middle one has a smaller hydrophone separation. Within group one and three the hydrophones are 1.2 m apart building a 18 m long unit. This selection results in an antenna directivity which is sensitive to high frequency wavefronts impinging from the near vertical. The -3 dB point is found to be at 48 Hz for wavefronts traveling at 90° (measured from the vertical), 66 Hz / 30°, 190 Hz / 11.5° and 380 Hz / 5.7°. The central group is only 6 m long with 16 hydrophones each 0.4 m apart. The -3 dB point is found at 110 Hz / 90°, 220 Hz / 30 °, 550 Hz / 11.5° and 1.1 kHz / 5.7°. Adding all three groups together the total directivity is (-3 dB) 18 Hz / 90°, 36 Hz / 30°, 90 Hz / 11.5°, 180 Hz / 5.7°. At the tail a depth sensor is installed which indicates the actual depth modulated as frequency changes. With a base frequency of 990 Hz at the surface it increases by 100 Hz per bar (100 Hz per 10 m). The typical towing depth for the streamer is 15 m. The whole unit is stored and operated from a hydraulic winch at the stern of RV SONNE.

For data recording one of the four channel Marine Broadband Seismic recorders (MBS; see 5.2.2) was available. This unit was chosen to record the streamer signals with 1 kHz sampling interval resulting in a Nyquist frequency of 400 Hz, which is well above the expected maximum energy of 100 Hz. In order to suppress the wave state induced low frequency noise (up to 5 Hz) the input impedance of the channel separator set to 15 Hz. Together with the use of the standard OBH preamplifiers a suitable signal recording was achieved.

5.10 TOBI – DESCRIPTION AND TECHNICAL SPECIFICATION

(D. Masson)

OVERVIEW

TOBI - Towed Ocean Bottom Instrument - is Southampton Oceanography Centre's deep towed vehicle. It is capable of operating in 6000 m of water, although the maximum depth encountered during the cruise was approximately 3700 m. The TOBI vehicle itself measures 4.5 m long by 1.5 m high by 1.1 m wide and weighs between 2 and 2.5 tonnes in air depending on payload. When deployed the TOBI system uses a two bodied tow system. This makes for a very stable towing platform for the onboard sonars but has the disadvantage of being more complicated to deploy and recover. The vehicle weighs two and a half tonnes in air but is made neutrally buoyant in water by using syntactic foam blocks. A neutrally buoyant umbilical connects the vehicle to the 600kg depressor weight. This in turn is connected via a conducting swivel to the main armoured coaxial tow cable (on the Sonne, the ships main winch carrying 10 km of conducting tow cable was used as the tow winch). All signals and power pass through this single conductor. Since its first scientific cruise TOBI has been used on 10 different ships.

Although TOBI is primarily a sidescan sonar vehicle a number of other instruments are fitted to make use of the stable platform TOBI provides. For this cruise the instrument complement was:

1. 30kHz sidescan sonar (Built by SOC) with swath bathymetry capability
2. 7.5kHz profiler sonar (Built by SOC)
3. Three axis fluxgate magnetometer. (Ultra Electronics Magnetics Division MB5L)
4. CTD (Falmouth Scientific Instruments Micro-CTD); replaced with a AML Pressure Smart Sensor during the cruise
5. Gyrocompass (S.G.Brown SGB 1000U)
6. Pitch & Roll sensor (G + G Technics ag SSY0091)

An AutoHelm ST50 GPS receiver provides the TOBI logging system with navigational and time data.

BRIEF TECHNICAL SPECIFICATION.

Mechanical

Towing method: Two bodied tow system using neutrally buoyant vehicle and 600kg depressor weight.

Size	4.5 m length x 1.5 m height x 1.1 m width.
Weight	2200kg in air.
Tow cable	Up to 10km armoured coax.
Umbilical	200m long x 50mm diameter, slightly buoyant.
Tow speed	1.5 to 3 knots (dependent on tow length).

Sonar Systems

Sidescan Sonar

Frequency	30.37kHz (starboard) 32.15kHz (port).
Pulse Length	2.8ms.
Output Power	600W each side.
Range	3000m each side.
Beam Pattern	0.8 x 45 degree fan.

Bathymetry Sonar

Transmitter	Uses sidescan sonar.
Receiver	6 hydrophone arrays in 2 housings for each side.
Detection	Single and multi-phase.
Range	Up to 3000m each side.

Profiler Sonar

Frequency	7.5kHz.
Pulse Length	0.26ms.
Output Power	500W.
Range	Up to 70m penetration over soft sediment.
Resolution	< 1m.
Beam Pattern	25 degree cone.

Magnetometer Ultra Electronics Magnetics Division MB5L.

Range	+/- 100,000nT on each axis.
Resolution	0.2nT.
Noise	+/- 0.4nT.

CTD Falmouth Scientific Instruments, Micro CTD.

Conductivity

Range	0 to 65 mmho/cm.
Resolution	0.0002 mmho/cm.
Accuracy	+/- 0.005 mmho/cm.

Temperature

Range	-2 to 32° Celsius.
Resolution	0.0001° C.
Accuracy	+/- 0.005° C.

Depth

Range	0 to 7000 dbar.
Resolution	0.02 dbar.
Accuracy	+/-0.12% F.S.

Alternative depth sensor AML Pressure Smart Sensor

Range	0-6000 dbar
Resolution	0.02 dbar.
Accuracy	+/-0.05% F.S.

Heading	S.G. Brown SGB 1000U gyrocompass.
Resolution	0.1 degrees.
Accuracy	Better than 1°, latitude < 70°.

Pitch/Roll	Dual Axis Electrolytic Inclinometer.
Range	+/- 20 degrees.
Resolution	0.2 degrees.

Altitude	Taken from profiler sonar.
Range	1000m.
Resolution	1m.

Deck Equipment

Deck equipment required for TOBI operations ideally consists of the following:
Moving 'A' frame with 3m height and ideally >4.5m width.
5 tonne launch winch.
Umbilical winch.
Two capstains, one either side of the 'A' frame.
Double block with launch and tow sheaves mounted centrally on the 'A' frame or separate sheaves mounted close together.
3 tonne deck crane for manoeuvring the vehicle.

The launch winch is mounted in line with the launch sheave a suitable distance from the 'A' frame. The umbilical winch can be mounted off centre but ideally between the line of the 'A' frame legs.

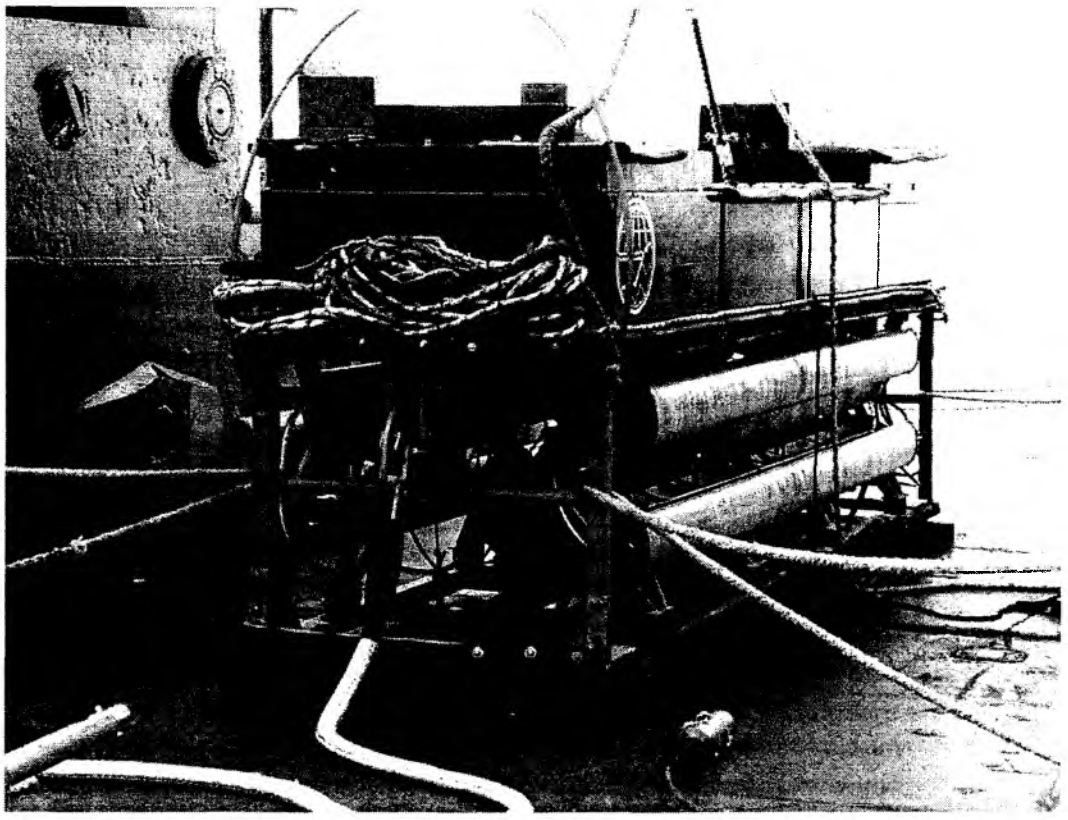

Figure 5.10.1 The Towed Ocean Bottom Instrument (TOBI) of Southampton Oceanography Centre.

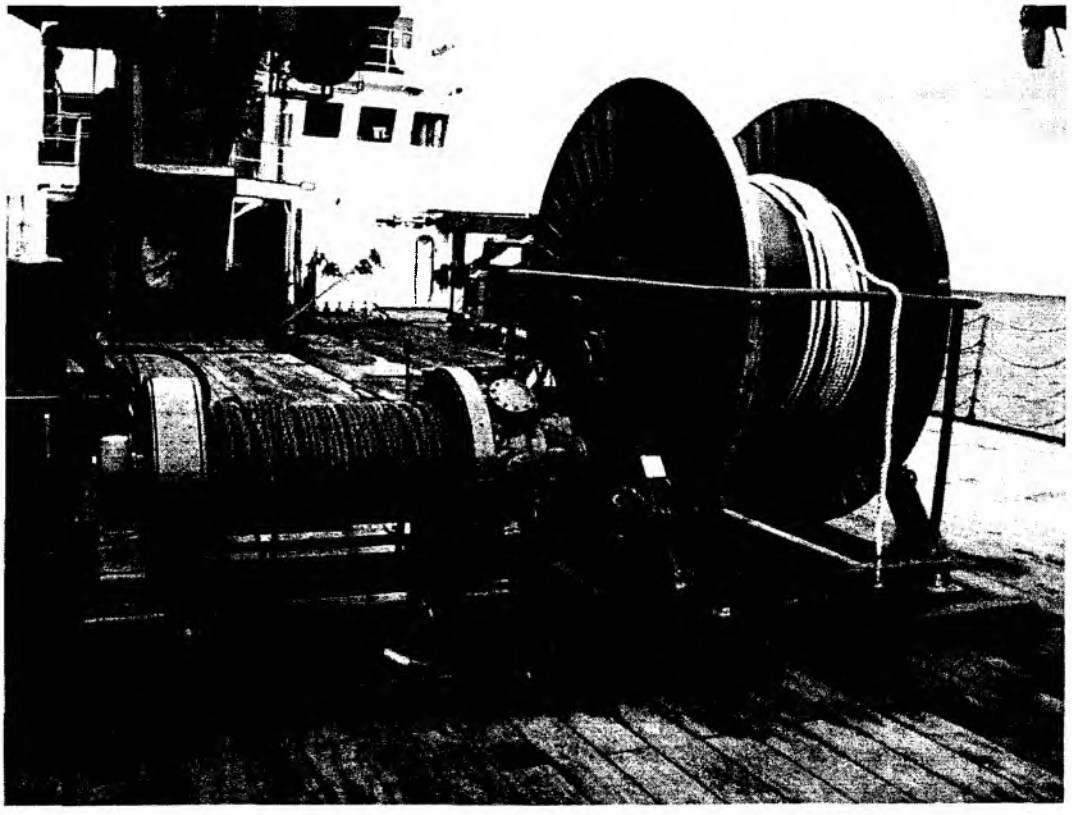

Figure 5.10.2 TOBI launch winch (left) and umbilical winch (right) on deck of RV SONNE

5.11 SHIPBOARD EQUIPMENT

5.11.1 HYDROSWEEP

For continuous bathymetric profiling, the HYDROSWEEP multibeam system by *STN ATLAS-ELEKTRONIK* is available onboard RV SONNE. Using a frequency of 15.5 kHz and 59 beams in a swath of 90°, it can map the seafloor with a scanline width of up to twice the water depth. The range of the central beam is up to 10,000 m with an error of 1% and for the outer beams it is up to 7,000 m with a precision of about 1% if the roll is less than 10° and the pitch is less than 5°. Corrections for roll, pitch, and heave are automatically applied. Due to the fixed angle between the beams, resolution depends upon the water depth and varies from about 170 m to 200 m in depths of 5,000 m to 6,000 m.

To calculate depths from echo time delays the velocity of sound in the different water layers is required. HYDROSWEEP uses a second set of transducers and a calibration scheme with soundings along track to determine an average water sound velocity profile (Schreiber und Schencke, 1990). However in certain areas this algorithm fails (c.f. Flueh and von Huene, 1994), so for better results, direct measurement of sound velocity at different depths using a CTD is required.

The postprocessing of HYDROSWEEP data is comprised of a merging of navigational data, a calculation of depth and positions of the footprints of the beams, removing artifacts and erroneous datapoints, and generation of a digital terrain model (DTM). The *ATLAS* HYDROMAP software, based on the CARIS software package, is available on board for that purpose. However, for several reasons outlined in Flueh and von Huene (1994) and Weinrebe (1997), the academic software MB-System (Caress and Chayes, 1996) from Lamont-Doherty Earth Observatory is used for HYDROSWEEP data processing.

5.11.2 PARASOUND

For geological mapping of the uppermost sedimentary layer as well as high resolution horizontal mapping of the seafloor topography the PARAmetric survey echoSOUNDer PARASOUND from *ATLAS ELEKTRONIK* is available onboard R/V SONNE. This system can be run in two modes: 1. The NBS mode (Narrow Beam Sounder) and 2. The PAR mode (PARametric profiler).

The NBS mode utilizes either a frequency of 18 or 33 KHz where the beam angle in direction of the ship can be varied between 2,4, and 20° (18 KHz) and between 2.5 and 12° (33 KHz). Perpendicular to the ship, the beam openings are 4.2° (18 KHz) and 2.5° (33 KHz), respectively. Due to the non-perfect adaption of the transducers at 33 KHz the transmitted energy is reduced compared to 18 KHz and therefore mainly the 18 KHz frequency is used when the system is run in the NBS-mode.

The PAR-mode uses a parametric signal generated by superposition of two slightly offset, high frequencies to gain deeper penetration and higher resolution than that of ordinary echosounders. One signal is generated with a fixed frequency of 18 kHz, the other can be set to values between 20.5 kHz and 23.5 kHz (at 0.5 kHz increments), thus yielding a parametric signal of 2.5 kHz to 5.5 kHz with a (narrow) beam angle of about 4°. Therefore a clearer and more differentiated image of multi layer sediment structues down to 200 m below the seafloor can be recorded. The footprint of the beam acoustically illuminates an area of approximately 7% of the

water depth. Due to the narrow beam, no echoes from the ocean floor or from sedimentary layers will reach the receiver if the seafloor is inclined more than 2°, thus restricting the application of PARASOUND to relatively flat areas.

5.11.3 NAVIGATION
(J. Bialas)

A crucial prerequisite for all kinds of marine surveys is a precise knowledge of position information (latitude, longitude, altitude above/below a reference level). Since 1993 the global positioning system (GPS) has commercially available and widely used for marine surveys. It operates 24 satellites in synchronous orbits, thus at least 3 satellites are visible anywhere at any moment (Seeber, 1996). The full precision of this originally military service yields positioning accuracies of a few meters, yet this is restricted to military forces and usually unaccessible to commercial users (Blondel and Murton, 1997). For civilian purposes the precision is in the order of 100 meters.

The resolution of GPS can be enhanced with the Differential GPS (D-GPS) scheme (Blondel and Murton, 1997, Knickmeyer, 1996). Using several reference stations the determination of the ship's position can be corrected in real time and enhanced to a 1 m to 5 m accuracy. D-GPS service has been available onboard R/V SONNE since cruise SO-109 (1996). The ship's ASHTEC system provides a validated accuracy of approximately 5 m in the area of the PAGANINI investigations.

D-GPS values were available from the ship's navigation data base and could be extracted by a PC based end user interface program. Out of all ships sensor values the user could select the wanted variables and specify the output in various formats. The amount of data could be controlled by the desired interval of extracted values which could be as short as one second. Stored on the "wiss-data" directory the extracted ASCII file was accessable from every workstation connected to the shipboard network via ftp or volume access. Surprizingly the output data format writes decimal values separated by a colon instead of the standard American dot notation. Therefore a reformating program must be written prior to further computational use of the values.
During preparing the discussion it turned out that the coordinates stored within the data base were provided by the *Atlas ANP 2000* system which does not copy the exact GPS time values but adds time stamps of its internal uncontrolled clock to the high precision coordinates of the DGPS system. the accuracy of the time values mainly depends on the operator's skills in manually setting the ANP clock to GPS time. A somewhat conservative method compared to the efforts of precise positioning.

5.11.4 OFOS – OCEAN FLOOR OBSERVATION SYSTEM
(C. Jung)

The objective of the OFOS program was to map geological, morphological and biological features of the Costa Rican continental margin in support of future investigations at this site, including cold vents and gas hydrate areas, as well as new chemoautotrophic organisms in order to verify previous results. The aims are to investigate the destabilisation of gas hydrates as they are uplifted over subducting seamounts. Optical observation with a video/camera sled provides information on the distribution and extension of potential vent sites.

The OFOS is a video-controlled deep-towed device which sends video signals and data signals simultanously. During the surveys data signals were sent every second. The observations are recorded continuously on video tapes and slides with a stereo photo system.
The OFOS is equipped with a SIMRAD SSBL (Super Short Base Line System) responder for online navigation, allowing exact positioning of the video sled.
Two video cameras are installed, a colour video camera (DEEP SEA POWER AND LIGHT) and a black and white video camera (SIMRAD OSPREY). Two xenon lights and two halogene lights (DEEP SEA POWER AND LIGHT) provide optimal brightness. The stereo photo system (PHOTOSEA) allows for 800 color slides to be taken with each camera, by operator remote control or automatically every 7 to 60 seconds. To control the photographic quality, some films were developed during the cruise, whereas the rest of the slides will be developed in a professional laboratory.
The OFOS is equipped with a sensor for correcting pitch and roll, an altimeter (BENTHOS) and a temperature sensor (RTB), which is housed in the bottom-contact weight. The attached CTD (SEABIRD) allows simultaneous online data aquisition of conductivity, temperature and depth. The fibre optic controls data transfer and the coaxial cable controls the electric power supply. Data and slide management can be controlled manually by the operator.
The sled is also manually adjusted by a winch operator and, at ca. 0.8 kn ship speed, is towed 1.50 m to 2 m above the seafloor. A bottom contact alert for determining the OFOS's distance from the bottom is provided by a weight (20 cm length) on a rope of 1.50 m or 2 m visible by camera.
For scaling the picture, three laser beams are installed 20 cm apart. The slides show an area of 2,20 m^2 (1,80 X 1,20 m) and the date and time of exposure are printed on each. All data are registered and synchronised by time (UTC).

5.11.5 CTD/HYDROCAST

(K. Heeschen)

Water column measurements of depth, salinity, and temperature, as well as water sampling were carried out on cruise SO144-2. The CTD/rosette aboard SONNE (Fig. 5.11.2) consists of a deck unit (SBE 11*plus*), which supports the underwater unit of the CTD (SBE 9*plus*) and the SBE 32 carousel water sampler equipped with 24 *10 l Niskin bottles. The used CTD system (Seabird 911 *plus*) supplies a modular temperature sensor (model SBE 3*plus*), a conductivity sensor (model SBE 4) for salinity measurements, a Digiquartz® pressure sensor, and an oxygen sensor (SBE 13). An external pump (SBE 5) maintains an optimum and constant water flushing speed for temperature, conductivity and oxygen sensors via a TC Duct, thus guaranteeing that all sensors measure the same water.

The deck unit provides DC power to the sea cable, decodes the serial data stream arriving from the underwater unit and passes the data to a companion computer. Binary data from the sensors are transmitted serially 24 times a second. The deck unit has a separate communication channel for controlling the Sea-Bird Carousel and an audible bottom contact alarm. Acquired data are placed on the computer where postprocessing is achieved with software provided by Sea-Bird. The data were averaged and bottle files were produced.

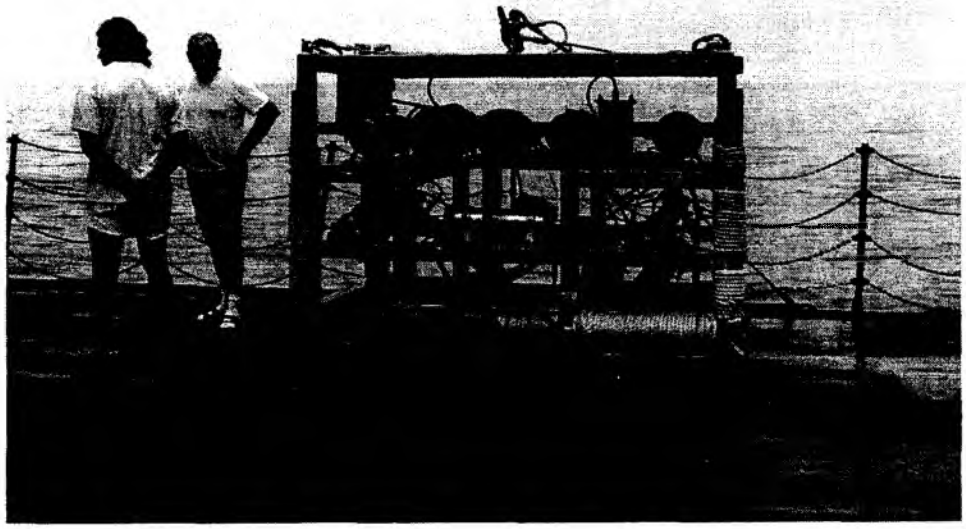

Figure 5.11.4.1 The Ocean Floor Observation System - OFOS

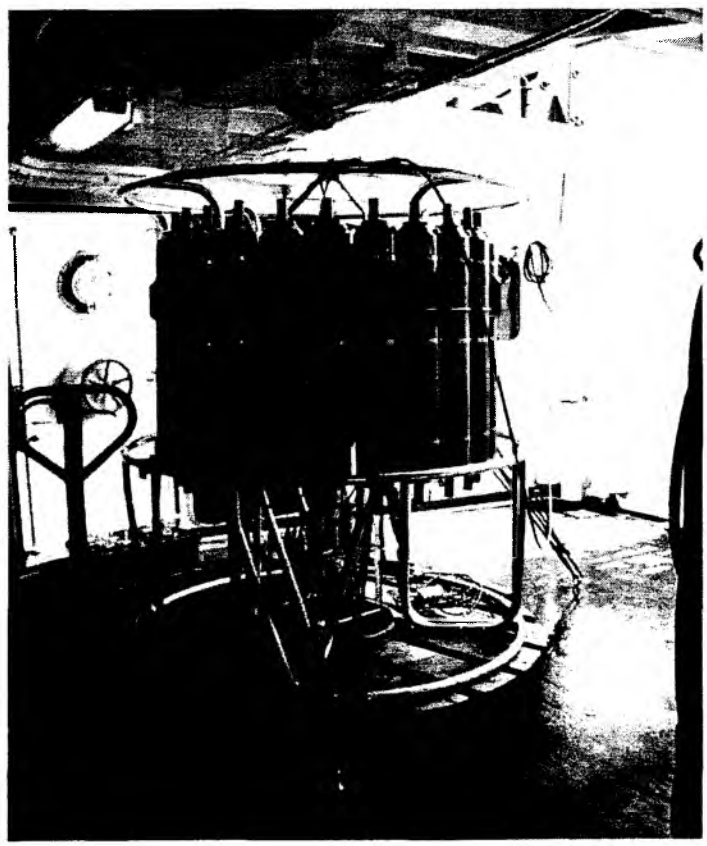

Figure 5.11.5.1 The CTD/rosette onboard RV SONNE

6 .WORK COMPLETED AND FIRST RESULTS

6.1 HYDROACOUSTIC INVESTIGATIONS

6.1.1 MULTIBEAM SWATH MAPPING

6.1.1.1. DATA ACQUISITION

Multibeam bathymetry was continuously recorded over the whole length of legs 1 and 2 after entering Nicaraguan waters. Off Nicaragua, 2 days and 8 hours were devoted to the acquisition of multibeam bathymetry data, which were used to fill the gap between existing Costa Rica and Nicaragua datasets. Off Osa Peninsula, 15 hours where devoted to extending the coverage southward along the crest and flank of the Cocos Ridge.

The multibeam system on board of RV/SONNE is a HYDROSWEEP continuous bathymetric mapping system from *STN ATLAS-ELEKTRONIK*. With a frequency of 15.5 kHz , it uses 59 beams in a swath of 90° and can thus map the seafloor with a scanline width of up to twice the water depth. The range of the central beam and outer beams is up to 10,000 m and 7,000 m respectively, both with an error of about 1%. Precision in the depth soundings requires a roll of less than 10° and a pitch of less than 5°. Corrections for roll, pitch and heave are automatically applied during data acquisition. Due to the fixed angle between the beams, resolution depends upon water depth, and varies from about 10 m in 200 m water depth to 200 m in depths of 5000 m to 6000 m.

Using a two-component gyro system, roll and pitch correction data were also collected by an Ashtech 3DF Attitude Determination System based on the Global Positioning System (GPS). A comparison between the HYDROSWEEP gyro and Attitude Determination Unit (ADU) will show whether the quality of the bathymetric data can be improved.

6.1.1.2 DATA PROCESSING

Calculating depths from echo time delays requires recording sound velocity in the ocean's different water layers. To determine an average water sound velocity profile, HYDROSWEEP uses a second set of transducers and a calibration scheme with soundings along-track (Schreiber und Schencke, 1990). However, in slope areas, this feature introduces error in calculations of depth and decreases sampling.

The postprocessing of HYDROSWEEP data includes a merging of navigation data, a calculation of water depth and positions of the beam's footprints, removing artifacts and erroneous datapoints and the generation of a digital terrain model (DTM). The ATLAS HYDROMAP software, which is based on the CARIS software package, is available on board for that purpose. However, the academic software MB-System (Caress and Chayes, 1996) from Lamont-Doherty Earth Observatory offers better facilities for quality control and editing of individual beams and was therefore the choice for data processing on board.

The MB-System's module 'MB-Clean' was used to broadly filter the data acquired from HYDROSWEEP, the results of which were viewed with the 'MB-Edit' window (Figure 6.1.1.2.1). Data perusal and manual editing could then follow where necessary using this data editor's interactive capabilities.

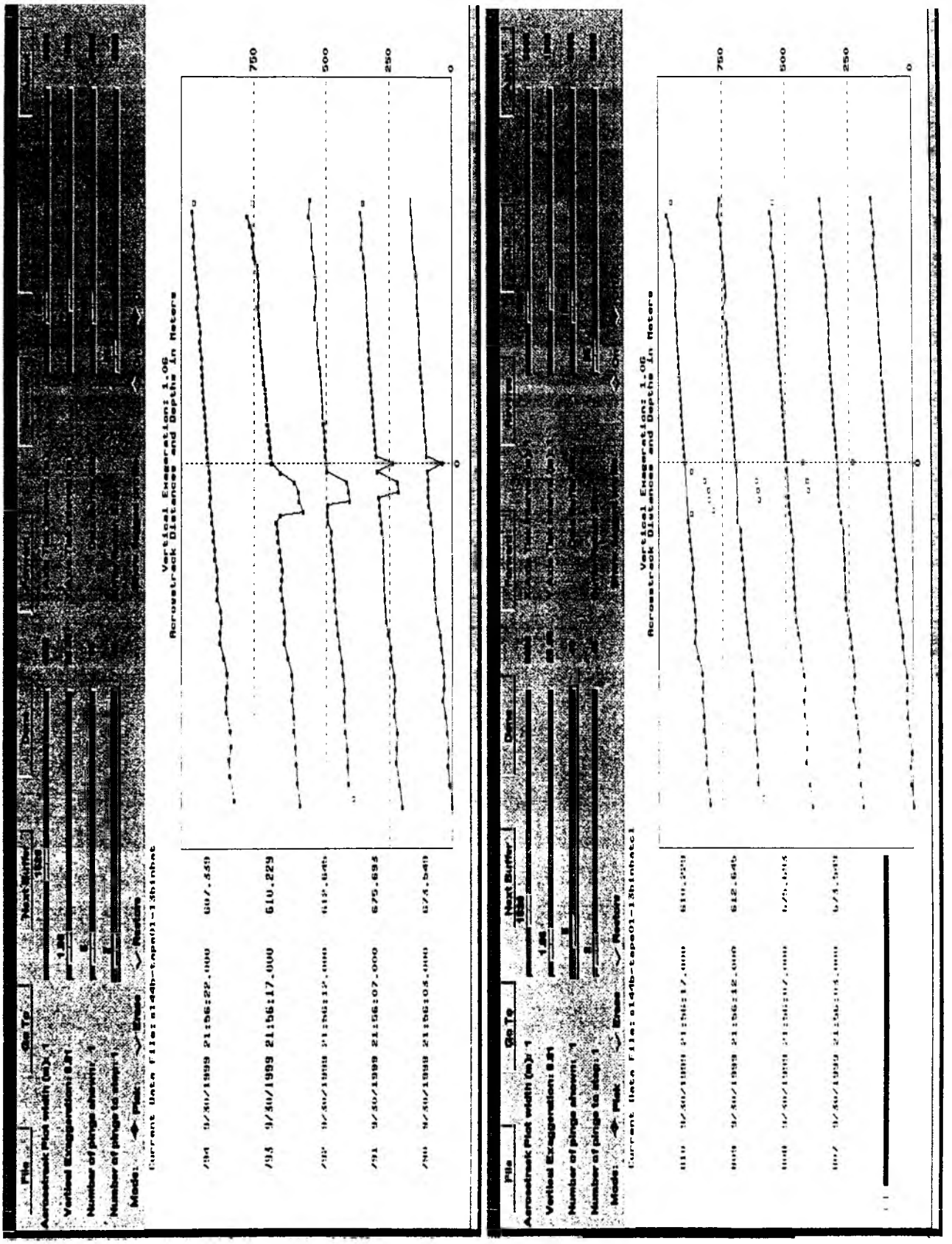

Figure 6.1.1.2.1: The results after automatically cleaning the HYDROSWEEP data as shown on the MB-System's interactive editor

Using an appropiate velocity function for the surveyed area, raw HYDROSWEEP echo time data were converted to depth by complete ray tracing through the different water layers. Sweeps including all 59 beams were then displayed in profile on a screen and edited to eliminate erratic datapoints. Edited sweeps were assembled, gridded and contoured with the GMT software (Wessel and Smith, 1995). No filtering was applied to gridded data in order to view the fine tectonic grain. The low amplitude artifacts observed across individual tracks, particularly clear in flat areas, give a qualitative estimate of the noise level in the maps.

In order to optimize aquisition we overlaid the existing swath bathymetry collected during SO76, SO81 and SO107 on the bathymetry predicted from satellite altimeter data (Sandwell and Smith 1991). Off Nicaragua, we designed tracks parallel to the slope based on this predicted bathymetry, so that the time in ship turns and overlap between adjacent tracks was minimized. The conventional design of short tracks perpendicular to the slope would have required an extra few hours. We also collected two tracks of swath mapping across the ocean plate - one parallel and one slighly oblique to a low scarp shown at the right-hand side of Figure 6.1.1.3.2. Based on data collected during SO107 and data from Scripps Institution of Oceanography, this scarp is presumed to be the fossil trace of the boundary between the East Pacific Rise and the Galapagos Spreading Center (see Magnetics, Section 6.3). The collected data fill the gap in the lower and middle slope between the data collected off Costa Rica and Nicaragua (von Huene et al., in press) (Figure 6.1.1.3.1). Due to time constraints, only the lower part of the slope could be surveyed across the survey area and up to the middle slope in the central section (Figure 6.1.1.3.2).

6.1.1.3 RESULTS OF CRUISE 144-1

(C. R. Ranero, R. von Huene, H. Steiner, and watchkeepers)

Although the new dataset does not cover the entire slope, we located it in an area of major importance for understanding the lateral variation in subduction processes along the margin and, in particular, the influence of ocean plate relief on those processes. The front of the continental margin facing the Middle American Trench has a similar basic structure from Costa Rica to Guatemala (Ranero et al., in press; Stavenhagen et al., 1998; von Huene and Aubouin, 1985; Walther et al., in revision; Ye et al., 1996). It is composed of a margin wedge much of which is a high velocity rock that is probably the seaward extension of oceanic igneous rocks cropping out along the Pacific coast of Costa Rica - the Nicoya Complex - and drilled onshore in Nicaragua (Ranero et al., in press). The margin wedge is covered by about 1-2 km of slope sediment and fronted by a small sediment prism - about 10 km wide - which stores little of the incoming pelagic and hemipelagic ocean plate sediment (Hinz et al., 1996; Kimura et al., 1997; von Huene et al., in press). Although a basic crustal structure for the upper plate applies along the entire mapped segment of the margin, the seafloor morphology of the continental slope changes markedly along strike. The change in upper plate morphology corresponds to the variation in lower plate morphology (Figure 6.1.1.3.1). This correlation (e.g., von Huene et al., in press) indicates a variability in tectonic processes controlled to a large degree by lower plate structure.

At large scale, the continental slope from off Nicaragua to off NW Nicoya Peninsula is approximately linear, corresponding to a subducting ocean plate with topographic features of relatively low relief (Figure 6.1.1.3.1). Further southeastward, from off central Nicoya Peninsula to Osa Peninsula, the continental slope is

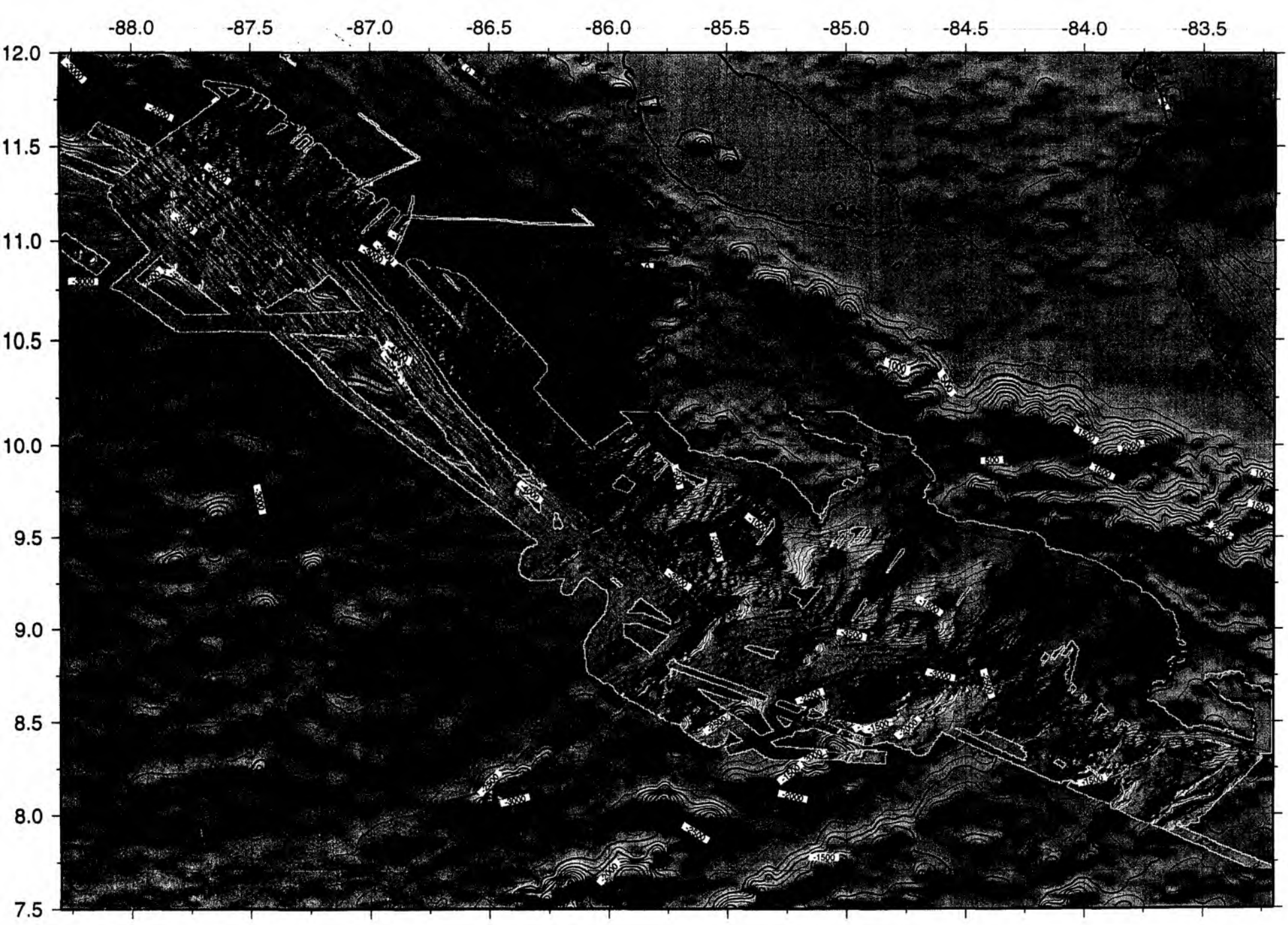

Figure 6.1.1.3.1: Hydrosweep Bathymetry superimposed on satellite derived bathymetry

characterized by a series of large reentrants and protruding headlands and by a general retreat of the margin that increases towards Osa peninsula. This rugged continental morphology is the result of the tectonic erosion from the subduction of the buoyant Cocos Ridge and its associated seamounts, ridges and guyots (von Huene et al.,in press.).

However, at smaller scale, there are also noticable changes along the linear segment of the margin off northern Costa Rica and Nicaragua. At the southern edge of the area surveyed during SO144, is the slope off NW Nicoya Peninsula surveyed during SO76 and 81 (Figure 6.1.1.3.2). There, the data cover the slope from the trench to depths of less than 500 m and show an upper slope with a well developed and relatively stable canyon system, a gentler middle slope, where most canyons stop and a lower slope characterized by the frontal sediment prism. A contrasting topography is observed off Nicaragua in the segment mapped during SO107 and at the NW part of the area mapped during SO144. There, swath mapping covers the seafloor on both sides of the trench to water depths of about 1000 m and shows a steeper upper, middle and lower continental slope when compared to that off Nicoya Peninsula (Figure 6.1.1.3.2). The upper slope is transected by similar canyons off Nicoya Peninsula. There is a sudden increase in dip from upper to middle slope, which is roughly coincident with the heads of a series of scars left by landslides. The lower slope is gentler and shows a series of en echelon ridges, oblique to the strike of the slope, but roughly parallel to the tectonic grain of the subducting ocean plate (von Huene et al., in press). The transition from the gentler slope off Nicoya Peninsula to the steeper slope of Nicaragua occurs in the area mapped during SO144. The relatively gentle and featureless slope off Nicoya Peninsula extends to about the middle of the segment mapped during SO144. Here a broad bowl in the upper slope contains canyons that converge downslope and merge at the upslope extension of a sharp transverse linear scarp reaching the trench (Figures 6.1.1.3.1 and 6.1.1.3.2) and perhaps indicating a tectonic feature in the upper plate. This morphology is located approximately at the seaward projection of the Santa Elena Peninsula. Northwestward, the middle slope becomes markedly rougher and the first of a series of large landslide scars occurs at about 20 km from the morphological break. This slide is about 30 km wide and the scar has a rough seafloor morphology. The head is marked by a hump on the seafloor (Figure 6.1.1.3.2) which might indicate that the slide was triggered by subducting lower plate relief. However, there is no track in the middle/lower slope morphology like those observed behind subducting seamounts off Costa Rica (Figure 6.1.1.3.1). A plausible explanation for the absence of a track in the lower slope is that tectonism from the subducting horst and graben on the ocean plate has obliterated it. Perhaps the slide itself covered a track. Alternatively, the hump upslope of the slump might represent a protruding headland were the slope material was at a critical threshold of stability and unusually prone to slope failure. The lack of sharpness in the morphology indicates that the slide is probably not very recent and thus not related to the 1992 Nicaragua tsunamigenic earthquake (Ihmlé, 1996).

The along-margin variation in morphology from the gentler slope off Nicoya Peninsula to the steeper slope off Nicaragua might be associated with the lateral change in the intensity of ocean plate faulting (Figure 6.1.1.3.3). Opposite the steep continental slope of Nicaragua, closely spaced faults cut the ocean plate and displacement is commonly 500 m (Ranero et al., in press; von Huene et al., in press). Fault spacing increases and displacement decreases southeastwards. Off NW Nicoya Peninsula, fault displacement is only about 100-150 m (Figure 6.1.1.3.3) (McIntosh et

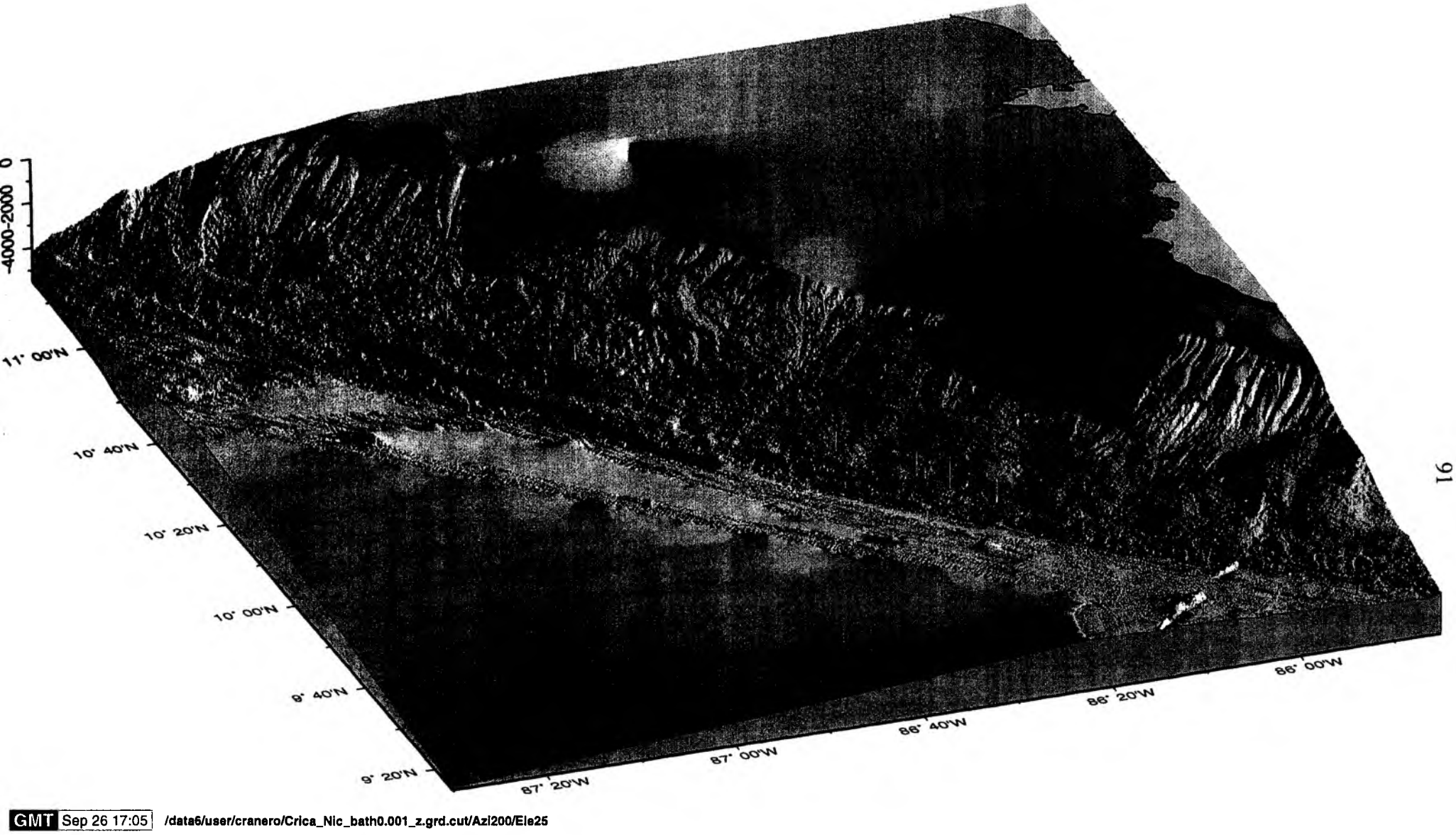

Figure 6.1.1.3.2: Perspective view from the SW of the area surveyed off NW Nicoya Peninsula during SO 144. Data sets covering from the ocean plate to the upper slope were collected during SO76 and SO107 off Nicoya Peninsula and off Nicaragua respectively

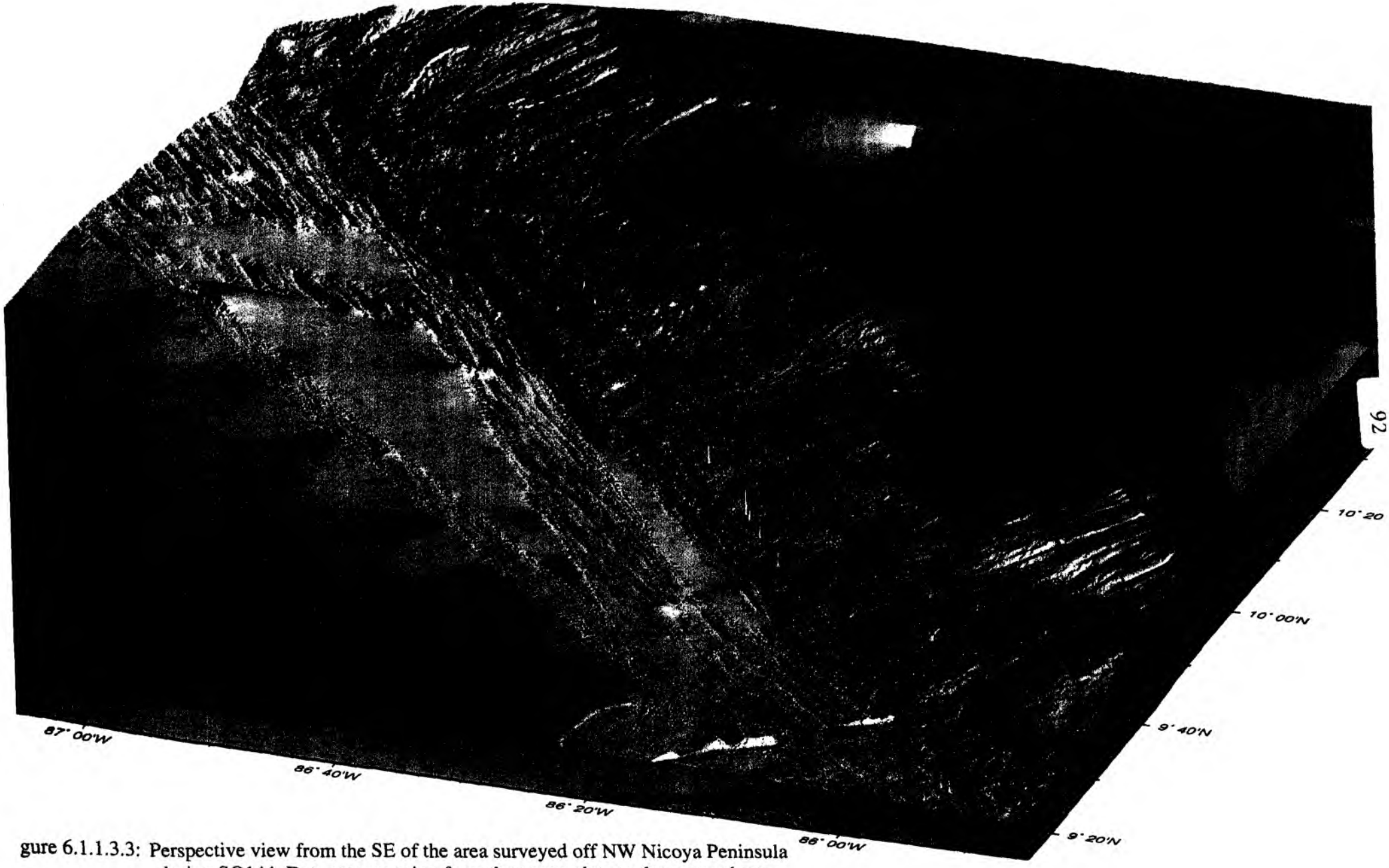

gure 6.1.1.3.3: Perspective view from the SE of the area surveyed off NW Nicoya Peninsula during SO144. Data sets covering from the ocean plate to the upper slope were collected durging SO76 and SO107 off Nicoya Peninsula and off

al., 1993; Shipley et al., 1992). Similarly, the en echelon ridges trending diagonally across the lower continental slope off Nicaragua, which are continuations of subducting horst on the ocean plate, decrease in amplitude and affect a narrower portion of the lower slope from NW to SE (Figure 6.1.1.3.3). Although a gap interrupts coverage of the detail change in lower slope morphology, it seems that the lower plate relief decreases off NW Nicoya Peninsula to where its effects on the continental slope are no longer significant.

The change from a relatively gentle to a steep slope might then be explained by the effectiveness of tectonic erosion from subducting lower plate relief. Off Nicaragua in the area where the ocean plate relief is greatest, the prism that is involved in partitioning subducted from accreted material is widest - perhaps as much as 15 km as indicated by morphology - whereas off Nicoya, the same feature is 5 to 10 km wide. One can hypothesize various mechanisms that could operate here, as have been suggested in the literature. Basal erosion by the "chin saw" model is probably not a sufficient explanation because the ocean plate topography has been filled with upper plate material. We are of diverse opinion as to the nature of the transition between Nicaragua and northern Costa Rica. One of us (CRR) views the change as a rapid transition across a morphological break where the lower plate relief is small enough to allow high pore pressure, caused by sediment dewatering beneath the frontal sediment prism, to facilitate subduction with little or no material transfer between plates at the front of the margin. The steep slope and landslides in the NW of the study area can then be explained as a response of the upper plate to the frontal tectonic erosion. Erosion at the base of the slope promotes steepening of the slope and then landsliding to stabilize the slope profile. The other author (RvH), also views the pronounced difference in character of the continental slope as a process steered by the character of the subducting plate, but possibly influenced by proposed differences in upper plate character across the Chortis and Choretega terrane boundary mapped near the Santa Elena Peninsula. He was expecting to find indications of a clear boundary in both lower and upper plates before the SO144 survey because of the sharp physical offset in the current volcanic chain and contrasting geochemistry of its youngest lavas. RvH suggests that if the slide is removed, both upper and lower plate morphology transitions gradually over ~100 km between the contrasting morphologies found across the international boundary. The break in volcanism would argue for an equally sharp break in subducted crust during the Quaternary and an offset in the Benioff Zone. Clearly, it is still early for a considered, comprehensive analysis of a problem more complex than envisioned before the SO144 morphological data were collected. Additional data and filling of gaps could help clarify and constrain our thinking.

6.1.1.4 RESULTS OF CRUISE 144-2

(W. Weinrebe, M. Müller, I. Schaffer and watchkeepers)

Multibeam bathymetry was continuously recorded with the HYDROSWEEP system during the whole cruise SO144-2. As the area of investigation had already been mapped nearly totally during cruises SO76, SO81, SO107 and SO144-1, only minor extensions could be achieved. However, many of the old HYDROSWEEP tracks, in particular those of SO76, were impaired by unstable navigation. Therefore the new SO144-2 data was also used to fill gaps and to improve the old map. As a result, a nearly complete coverage of the whole Costa Rican continental margin from the shelf's

edge across the Middle America Trench and between 50 km to 90 km of the oceanic plate was attained (Fig. 6.1.1.4.1, Fig. 6.1.1.4.2). A perspective image (Fig. 6.1.1.4.3) of the entire area gives an idea of the enhanced resolution of the bathymetry, which varies from around 8 m at 200 m depth, to around 40 m at 1000 m and approximately 140 m in the deepest part of the area at 3700 m.

The morphology of the area and the tectonic implications are discussed in detail in 6.1.1.4.2. To illustrate the quality of the new combined dataset, three smaller regions are shown in Figs. 6.1.1.4.4 to 6.1.1.4.6.

Fig. 6.1.1.4.4 illustrates the massive mass transport of the Nicoya Slide down the continental margin slope, originating in the Puerto Coyote Scar (foreground) and the Rio Bongo Scar (background). The oceanic plate (right), with Fisher Seamount adjacent to the Nicoya Slide, bends down into the Middle America Trench (center) accomodated by several faults in a characteristic staircase pattern.

To the east of the Nicoya Peninsula, the continental margin is characterized by several pronounced land slide scars. As the oceanic plate opposite this part of the margin is characterized by numerous seamounts of different sizes, these scars may have originated from the subduction of similar seamounts. The local uplift of the area obviously resulted in frontal slope failure, land slides and deeply incised scars. This is clearly visible in Figs. 6.1.1.4.5 and 6.1.1.4.6, showing the Jaco Scar and the Parrita Scar respectively. Numerous small faults on top of the structures demonstrate the ongoing uplift, as is also expressed by the deviation of a prominent canyon around Parrita Scar (Fig. 6.1.1.4.6).

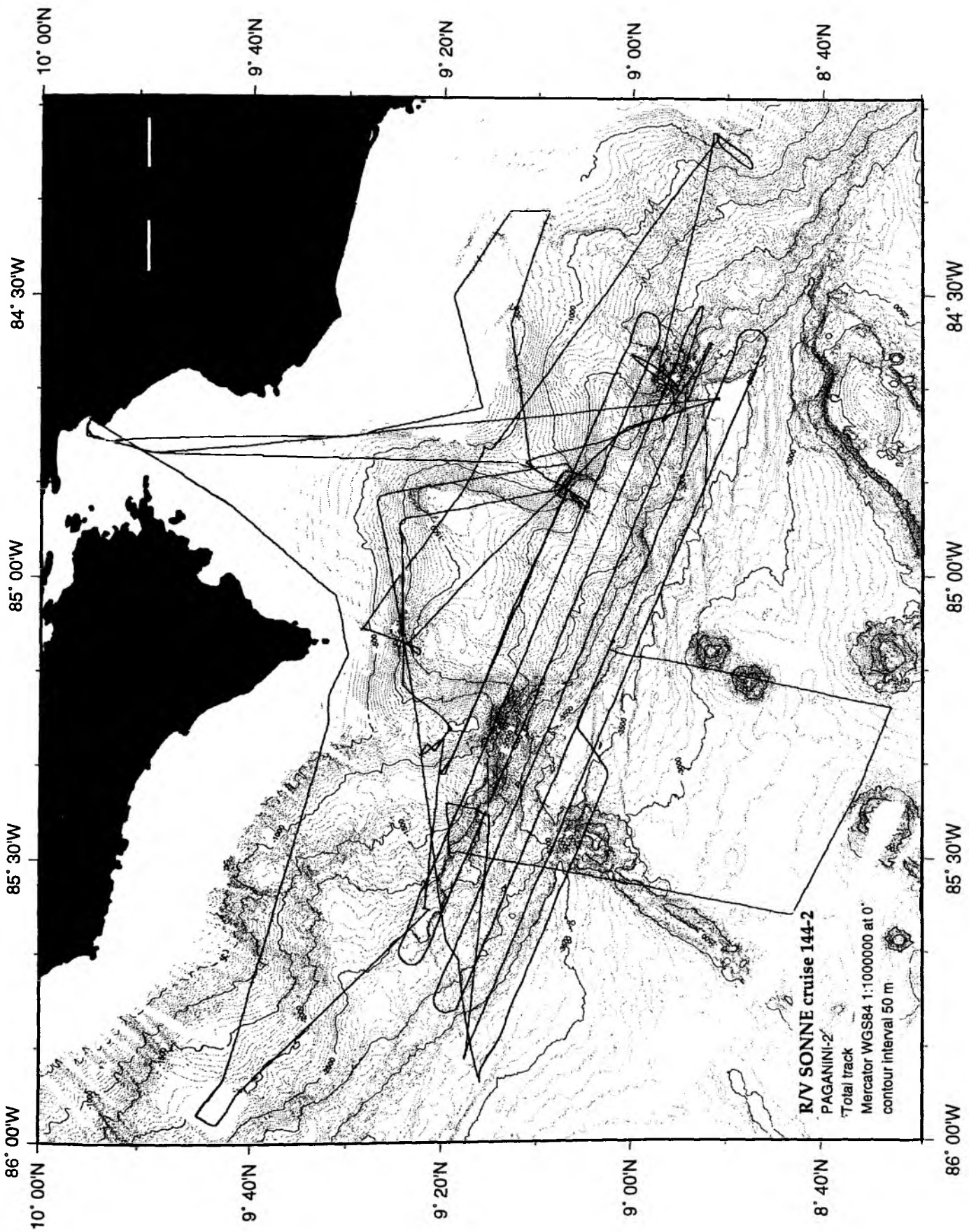

Figure 6.1.1.4.1: Bathymetry of the SO144-2 survey area with the cruise track of RV SONNE.

Figure 6.1.1.4.2: Shaded HYDROSWEEP Bathymetry of the SO144-2 survey area.

85° 00'W
84° 30'W
10° 00'N
9° 40'N
9° 20'N
9° 00'N
8° 40'N
85° 00'W
84° 30'W

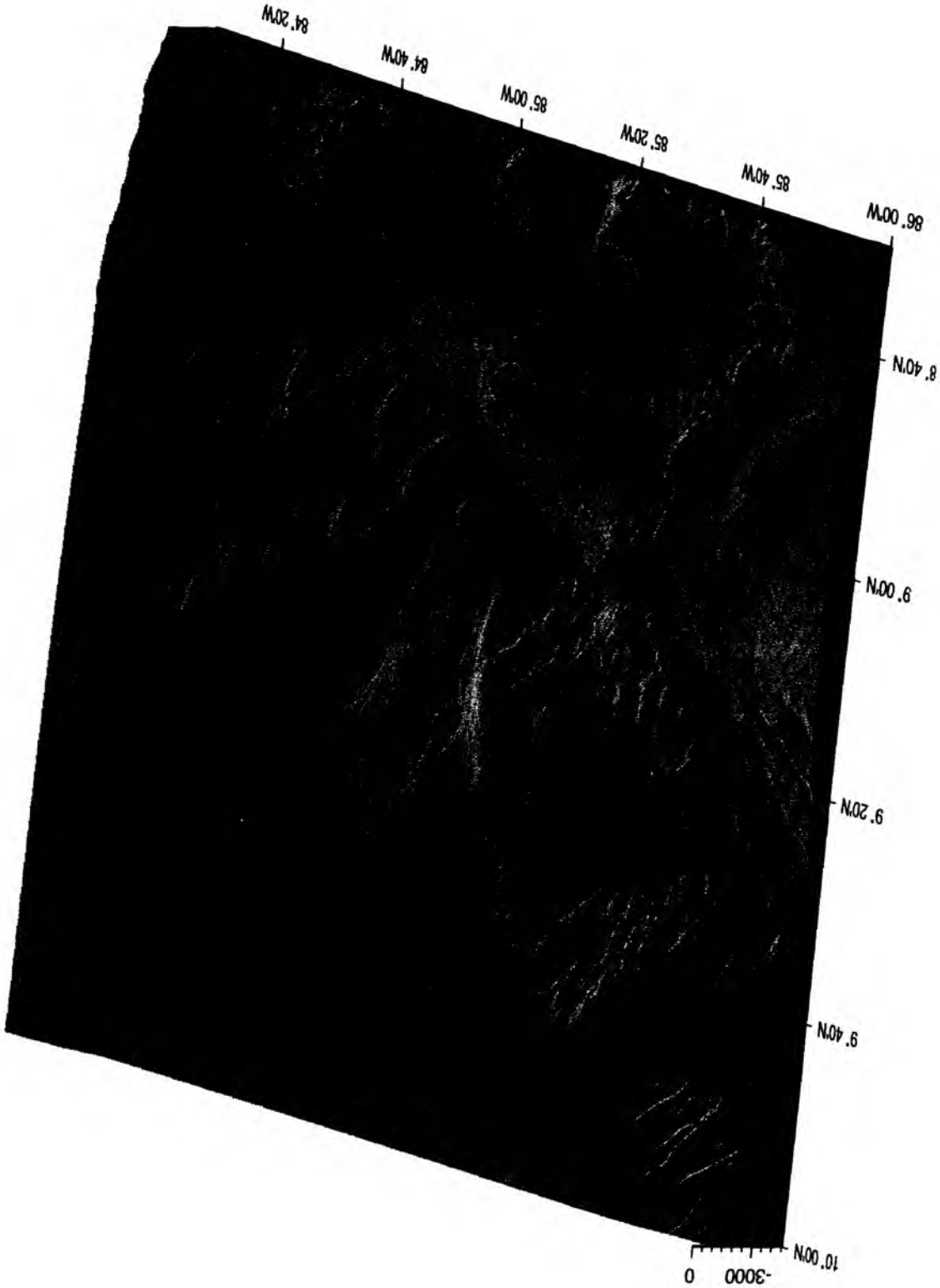

Figure 6.1.1.4.3: Perspective view from WSW of the SO144-2 survey area.

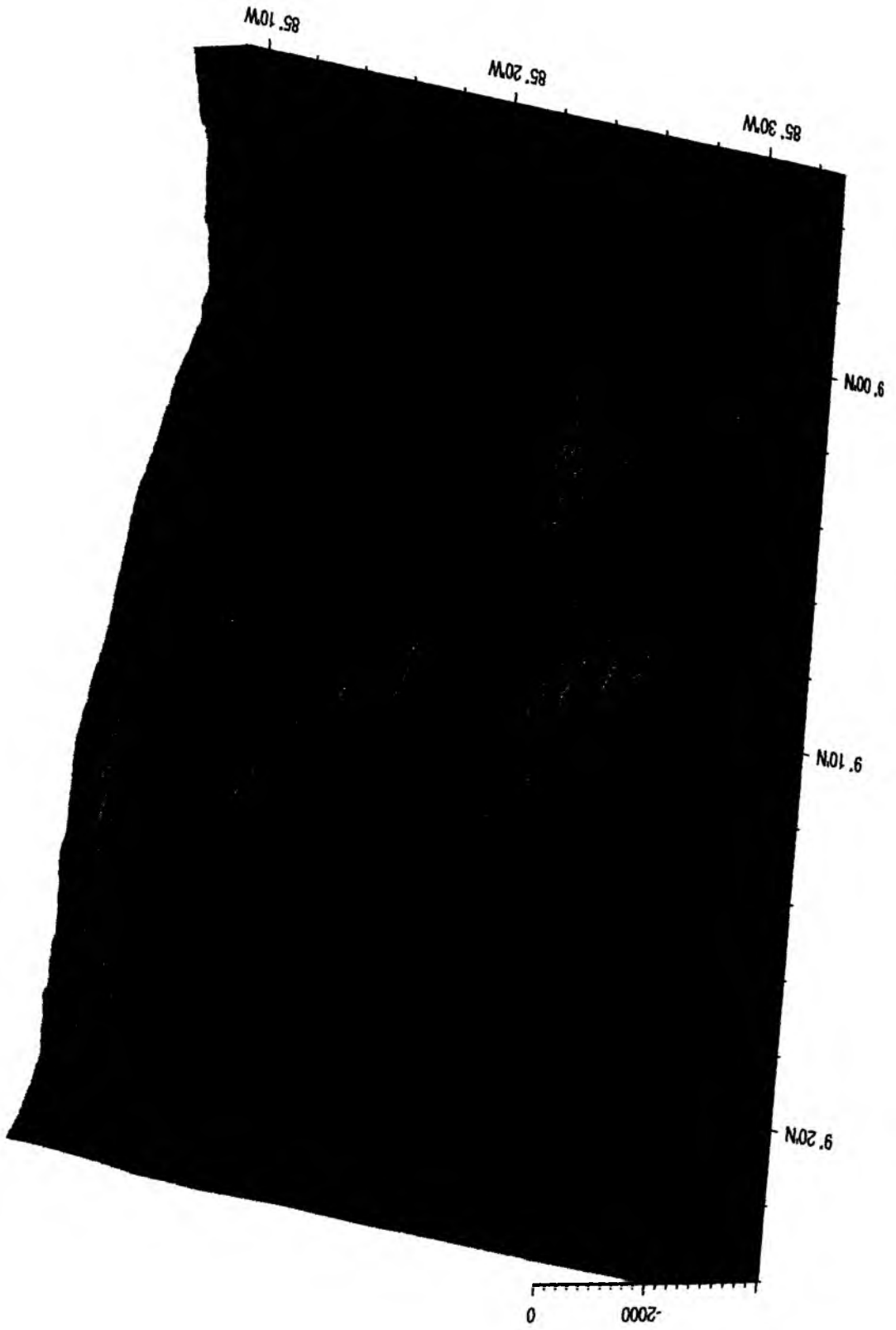

Figure 6.1.1.4.4: Perspective view from WSW of Nicoya Slide and Fisher Seamount.

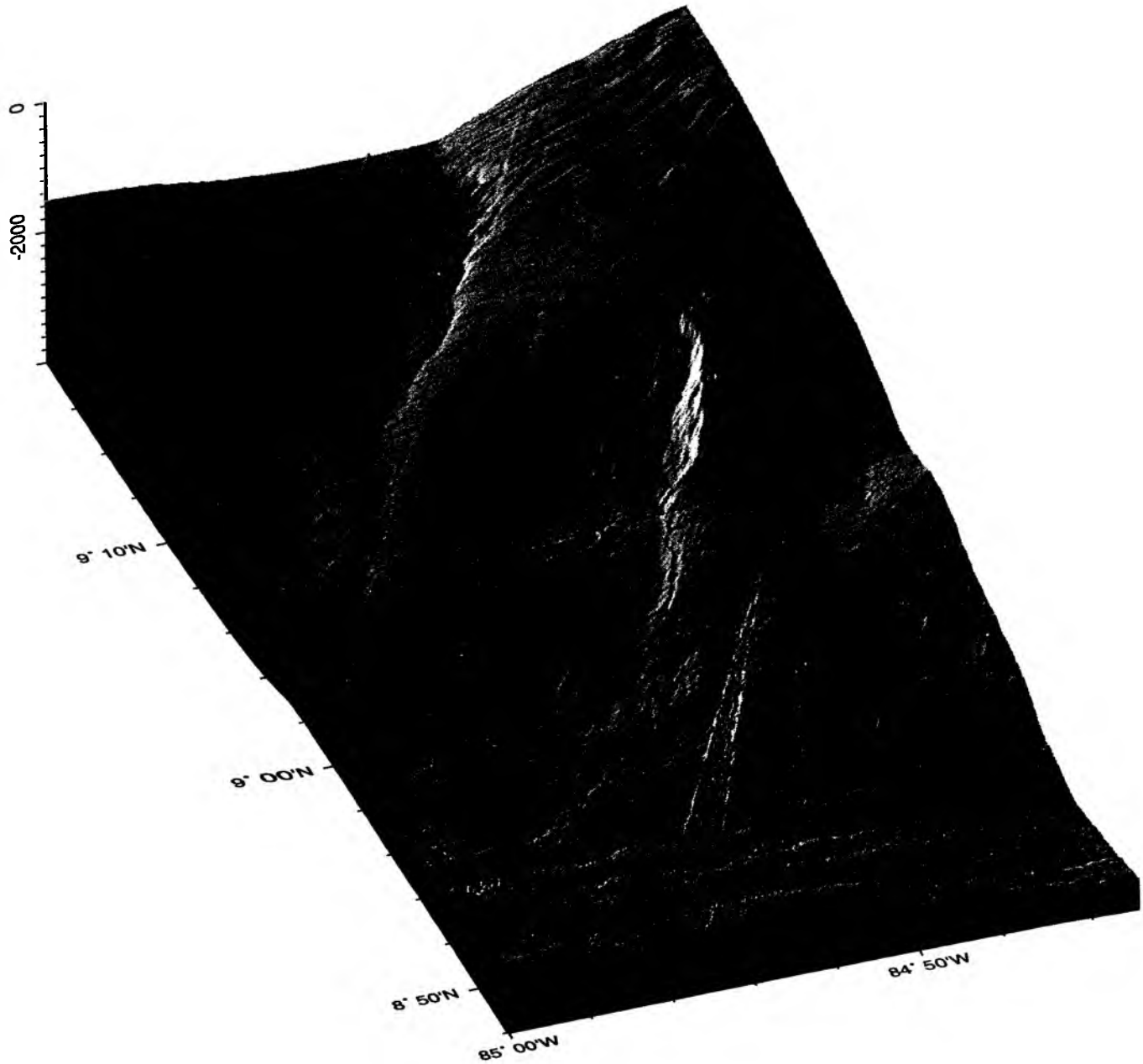

Figure 6.1.1.4.5: Perspective view from S of Jaco Scar.

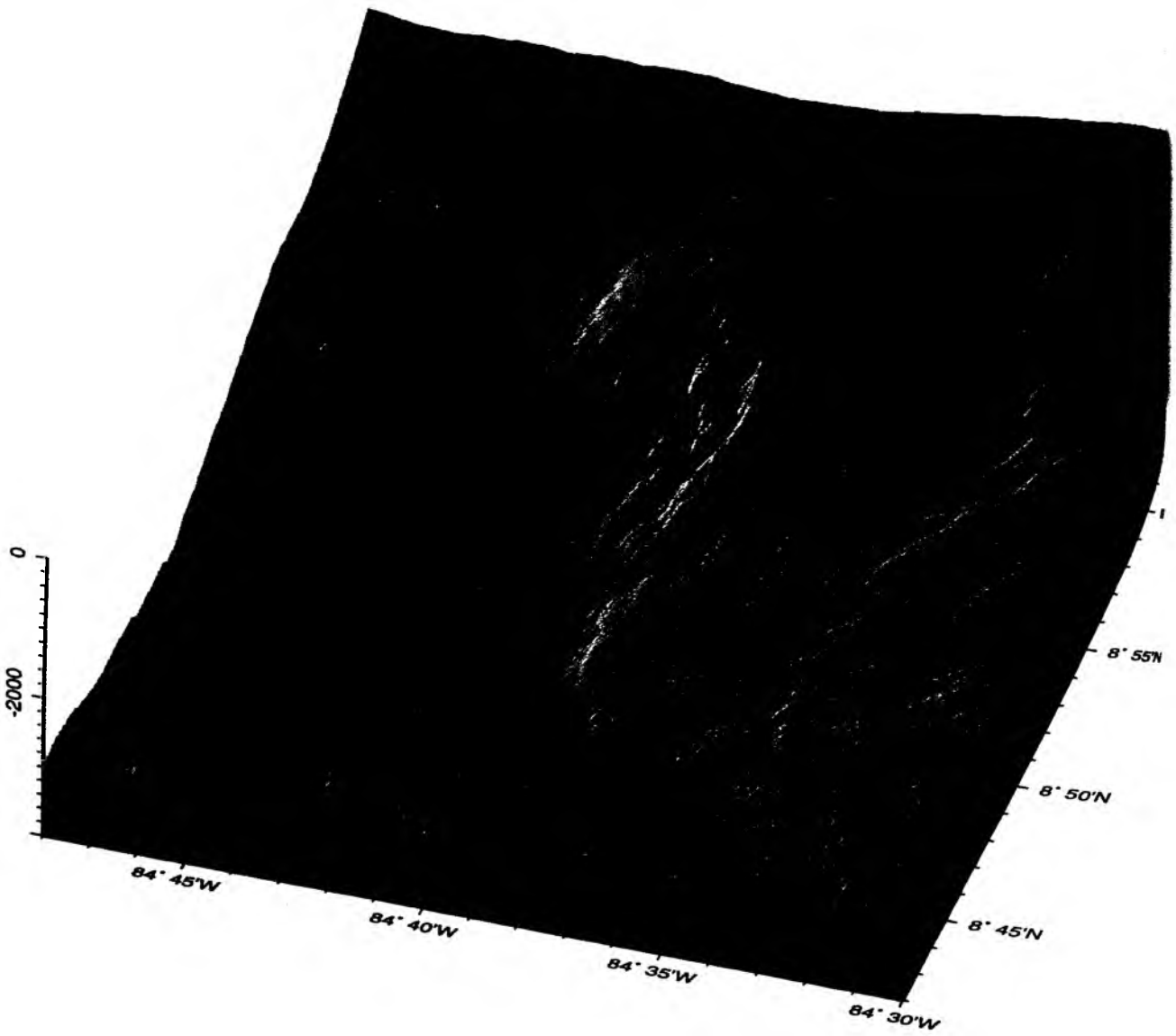

Figure 6.1.1.4.6: Perspective view from S of Parrita Scar.

6.1.2 PARASOUND

6.1.2.1 RESULTS FROM SONNE CRUISE SO144-1

(M. Meschede and watchkeepers)

The parametric echosounder PARASOUND from *ATLAS ELEKTRONIK*, which is available on board R/V SONNE was continuously collecting data from the ocean floor during the PAGANINI cruises. Since the narrow beam angle of 4° only allows observation of slopes of less than 2° inclination, the survey was mostly restricted to areas out of the Cocos and Malpelo ridges. The ridges are characterized by high topographic relief and rapid changes of water depth indicating steep submarine slopes.

From the flat ocean floor area off the Nicoya peninsula (profile SO 144-05), good Parasound images were obtained. Penetration of the parasound signals reached 50-70 m. Figures 6.1.2.1 and 6.1.2.2 are located between 9° 5'N, 85° 55'W and 9° 29'N, 86° 29'W crossing the trace of a suggested paleo - triple junction of the Pacific, Cocos and Nazca plates (Barckhausen et al., in prep.). The triple junction trace is marked by a very narrow, NE-SW striking, slightly elevated structure. Oceanic crust northwest of this feature was formed at the East-Pacific Rise (EPR; Figure 6.1.2.2a) and the crust in the southeast was formed at a precursor of the presently active Cocos-Nazca spreading center (CNS-2; Figure 6.1.2.2b; Meschede et al., 1998; see chapter 2.3). Parasound images are different for EPR and CNS crust. Sediments on EPR crust display a uniformly undisturbed sedimentary section with uniform layering. In contrast, sedimentary layers are strongly disturbed at small scale on CNS crust suggesting more recent tectonic movements of the basement.

Images in the area of the Panama Fracture Zone are of high resolution. Figures 6.1.2.3a and 6.1.4.3b are located at 7° 47'N, 83° 25'W and 7° 36'N, 83° 5'W, about 50-60 km south of the southernmost tip of the Burica peninsula. Sedimentary layers are clearly visible and indicate variations in their thickness. Small basins with thick sedimentary filling (> 60 m) are located between structural highs crested with only thin sedimentary layers (< 10-20 m; Figures 6.1.2.3a and b). The flanks of the structural highs may be interpreted as normal faults indicating active tectonic movement. The vertical exaggeration of the parasound images is, however, extreme, thus precluding a further tectonic interpretation.

A good example of fault structures on the PARASOUND images was observed at the entrance into the Golfo Dulce at the southeastern end of the Osa peninsula (8° 25'N, 83° 13'W; Figure 6.1.2.4). The entrance is marked by a topographic high of less than 100 m water depth, whereas the deepest part of the Golfo Dulce reaches a water depth of more than 250 m. Penetration depth is low and varies from less than 5 m to slightly more than 20 m. The lowest penetration depth is in the middle of the topographic high, where a remarkably irregular surface is observed. Based on observations of coastal outcrops on both sides of the passage into the gulf (Meschede et al., 1999 in press), this is interpreted to reflect the lithologic composition of the Osa basement, which is mainly composed of a mélange dominated by basaltic material. Fault scarps of normal faults, small sedimentary basins and a generally thin sedimentary cover downslope indicate active tectonism.

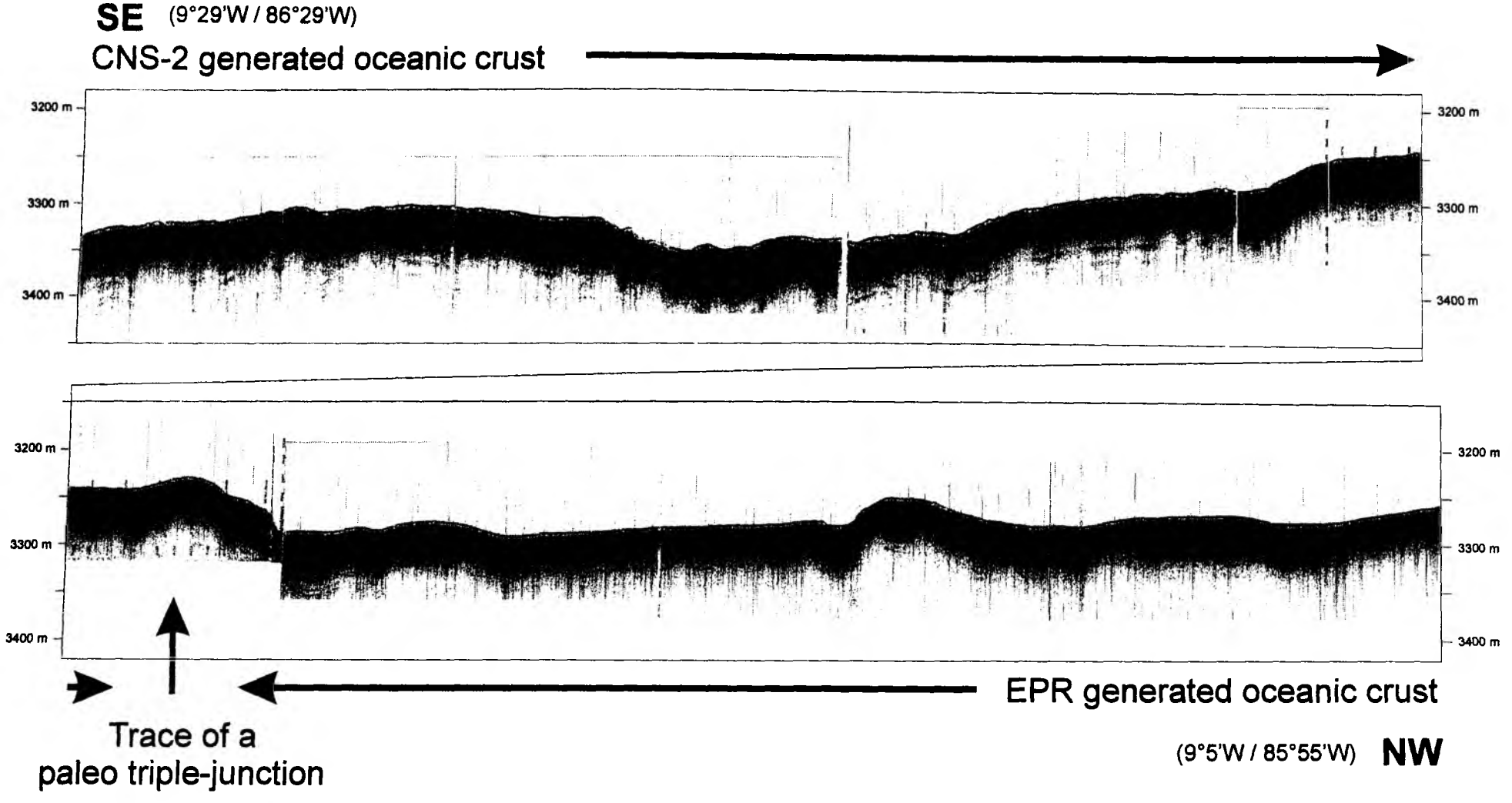

Figure 6.1.2.1: Composite profile from Parasound images obtained at profile SO 144-05 crossing the suggested trace of the paleo-triple junction between Pacific, Cocos and Nazca plates.

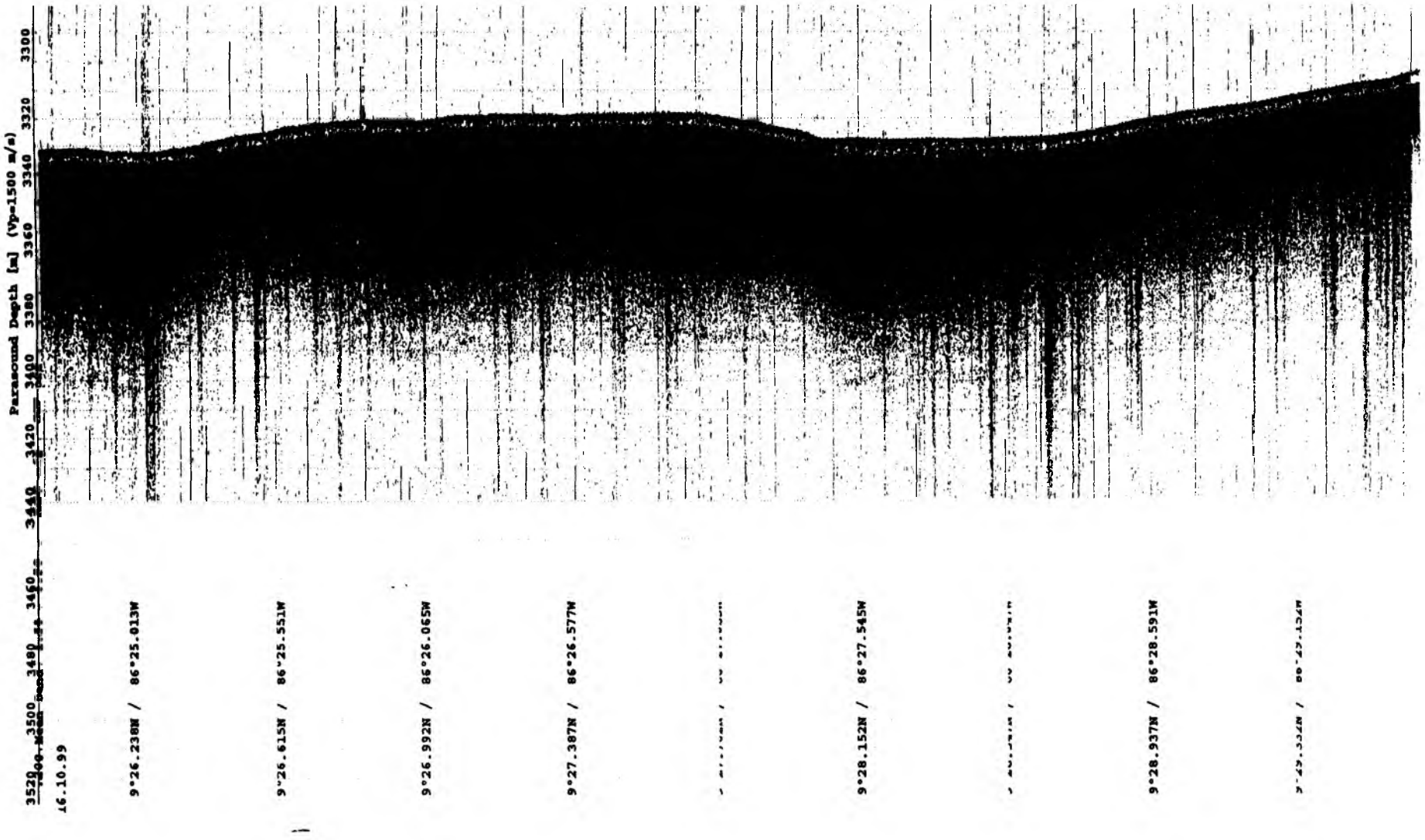

Figure 6.1.2.2a: Parasound images of a) EPR-generated oceanic crust and b) CNS-2 generated oceanic crust. See figure 6.1.4.1 for location. The seafloor of EPR-generated crust has an extremely large reflectance value which causes the poor definition of the other layers. The cause for this high reflectivity is, however, unknown.

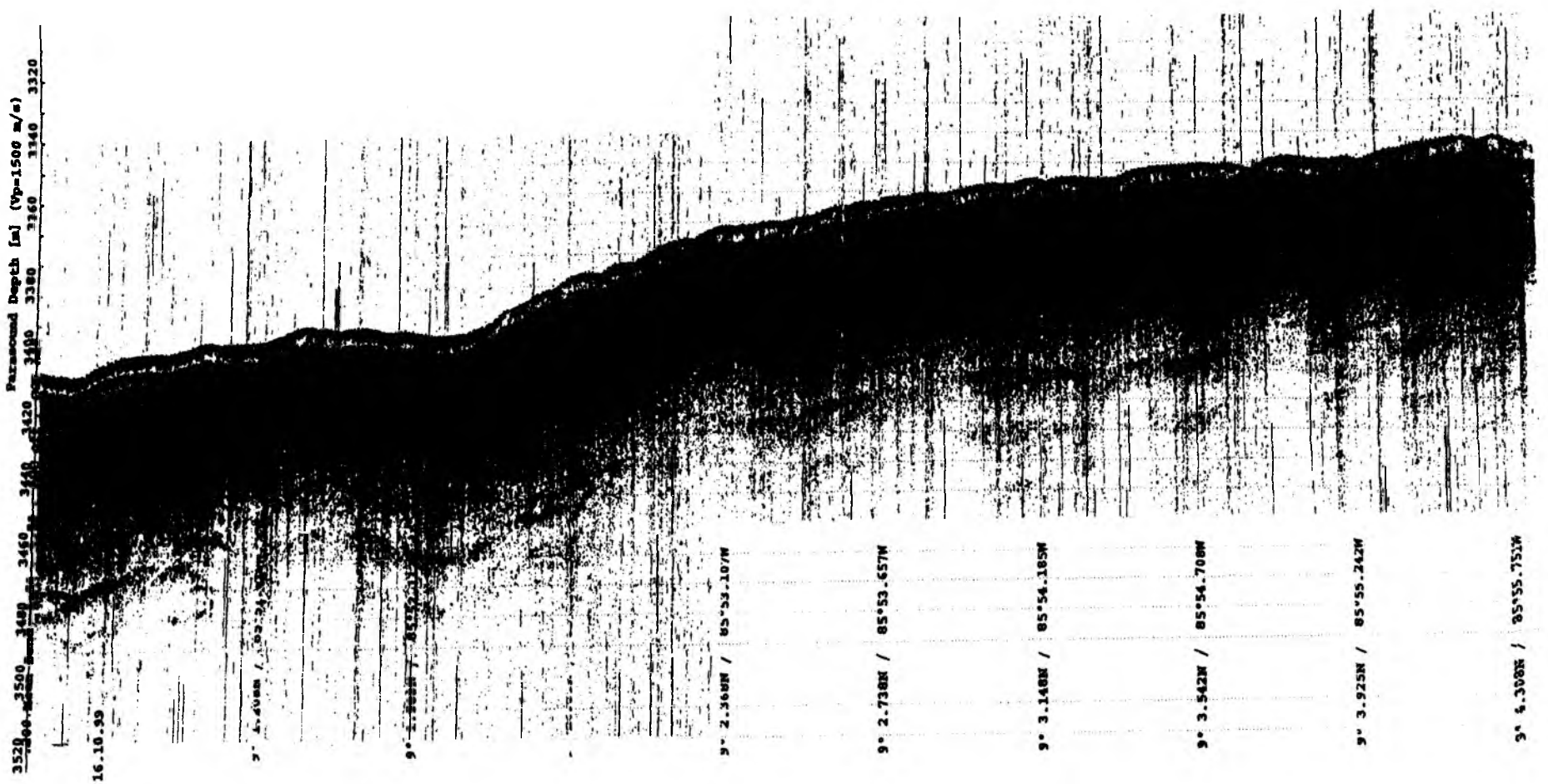

Figure 6.1.2.2b: Parasound images of a) EPR-generated oceanic crust and b) CNS-2 generated oceanic crust. See figure 6.1.4.1 for location. The seafloor of EPR-generated crust has an extremely large reflectance value which causes the poor definition of the other layers. The cause for this high reflectivity is, however, unknown.

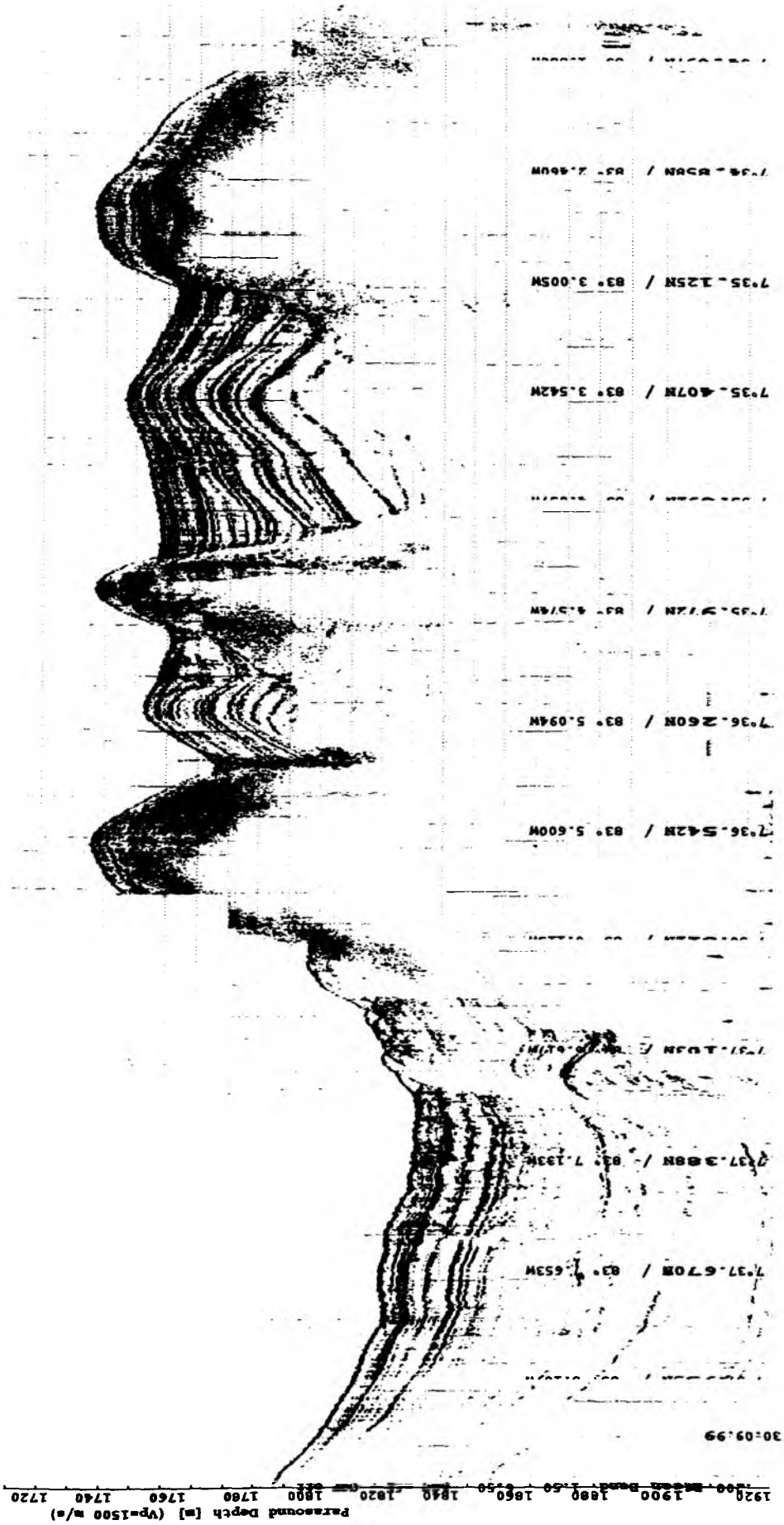

Figure 6.1.2.3a: Parasound images of faulted blocks with small sedimentary basins in between.

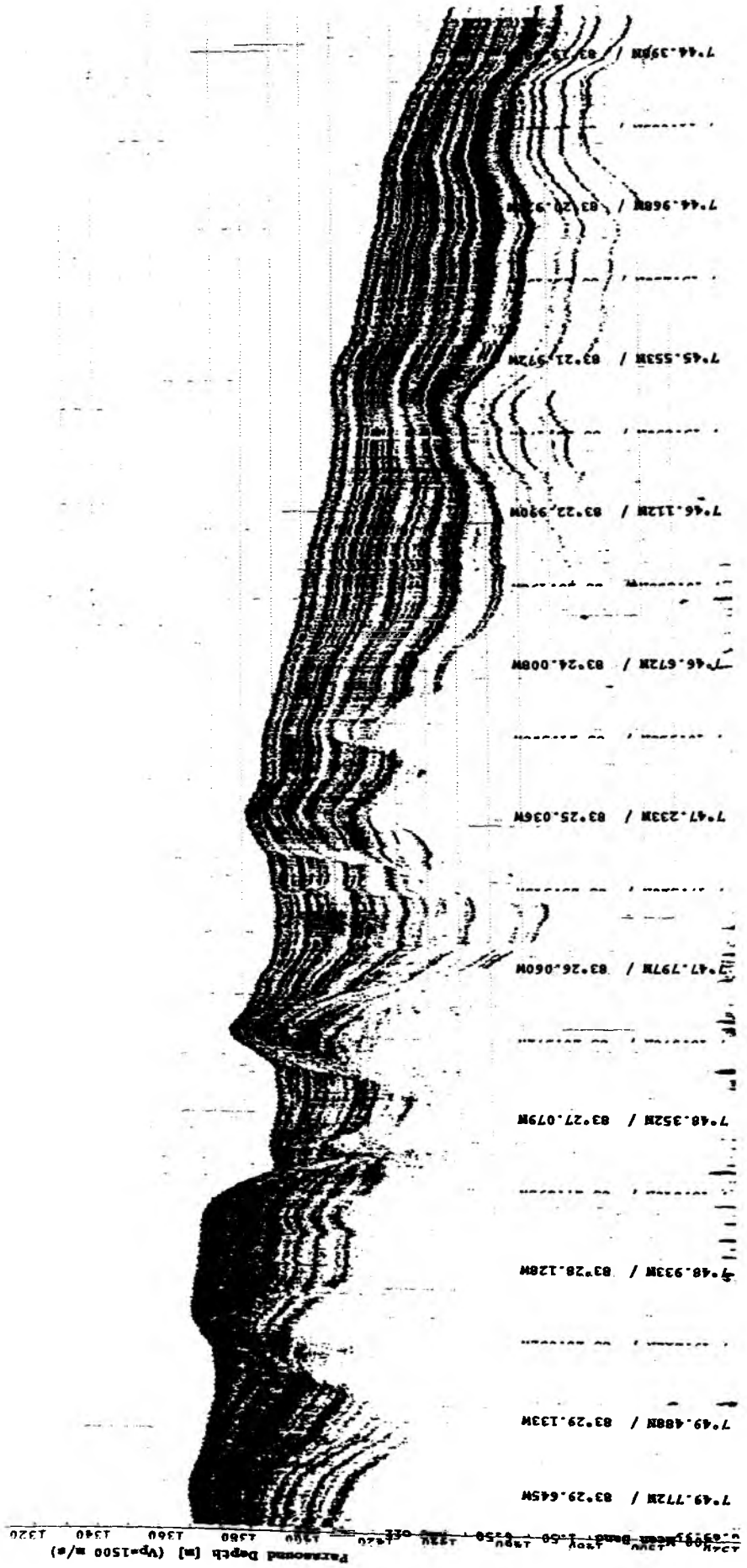

Figure 6.1.2.3b: Parasound images of faulted blocks with small sedimentary basins in between.

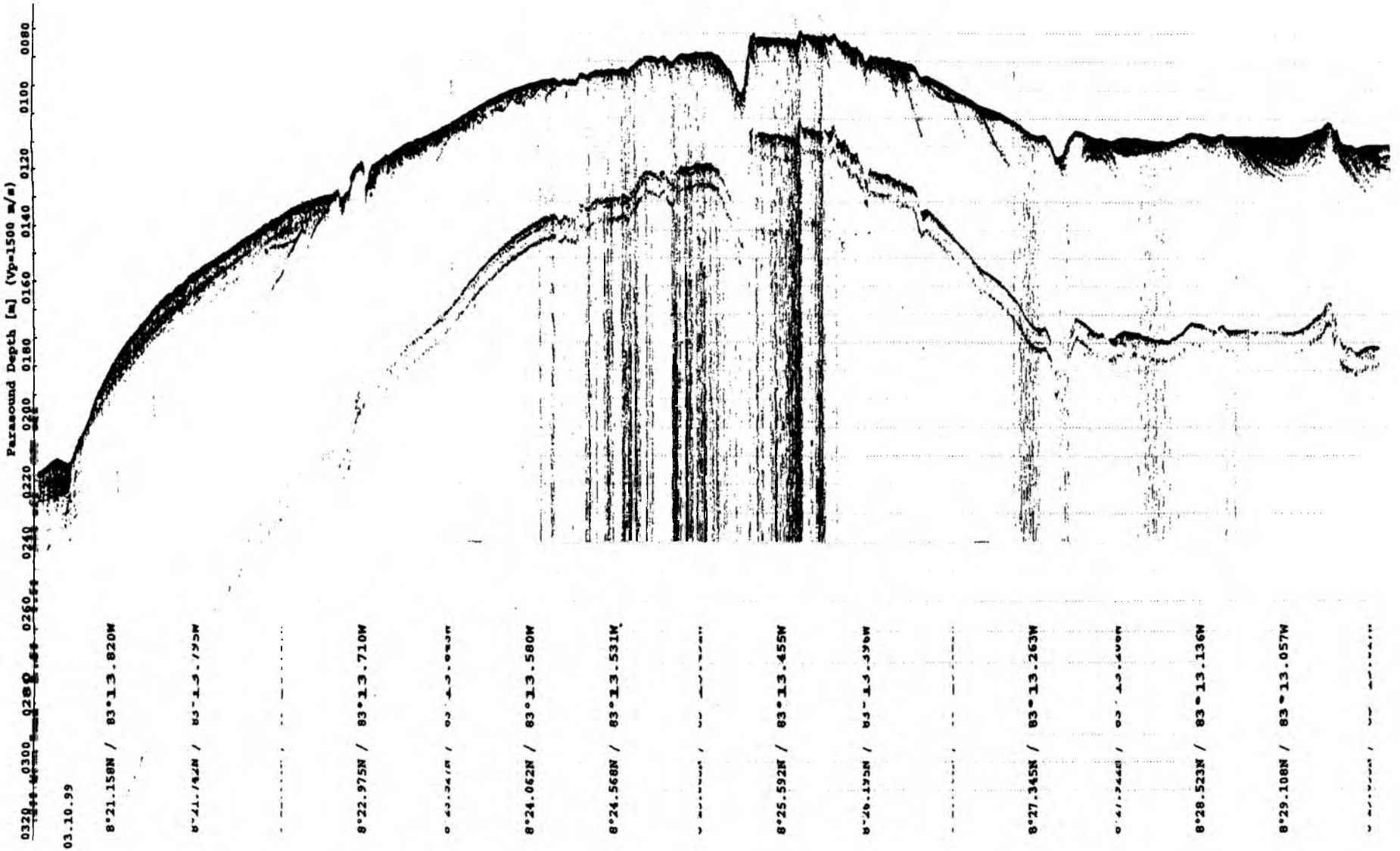

Figure 6.1.2.4: Parasound image of the coastal passage into the Golfo Dulce. The unsual low penetration depth indicates the occurence of basement rocks at a shallow depth.

6.1.2.2 RESULTS FROM SONNE CRUISE SO144-2

(B. Baranov, M. Hort, B. Cailleau, H. Florinova, R. Heath, T. Kath, C. Röckmann, I. Schaffer, and W. Weinrebe)

Most of the time PARASOUND was used in PAR mode to profile the uppermost sediment layers. In addition to the PARASOUND signal recorded with the onboard equipment we also used the SubBottomProfiler records of the TOBI system for a first data interpretation. Figure 6.1.2.5 shows a map of all PARASOUND profiles recorded. The numbers on the map refer to the online profile printouts which were continuously plotted. They are stored at GEOMAR together with the digital data recorded on DAT-Tapes. During the OFOS and CTD profiles and one part of a TOBI profile (TOBI 1), however, PARASOUND was run in NBS mode for the detection of gas plumes in the water column. In the following we first briefly describe the results of the NBS surveys and then turn to a summary of the sediment profiling recorded in PAR-mode.

The detection of plumes in the water column was not as successful as on other cruises with R/V SONNE across hydrate ridges off the coast of Oregon and of R/V PROF. GAGARINSKY in the Okhotsk sea. Due to the highly variable topography of the seafloor during profiling in this area, the beam angle was mostly set to either 2° or 4° to receive a relatively clear signal. However, this also reduces the volume covered in the water column quite a bit compared to a beam angle of 20° and therefore greatly reduces the chance of detecting a plume. During the descent of OFOS at profile OFOS-05 (9°28.5N 85°05.4W, northwest of Cabo Blanco Scar) a strong reflection in the water column was recorded (Fig. 6.1.2.6). Early on it was believed that a plume was detected, but plotting the descent of the OFOS lander into the NBS recording clearly revealed that the recorded signal is due to the descent of OFOS.

On 28.10.1999 between 20:31 and 20:34 UTC (8°56.26'N 84°42,13 W to 8°55.94' N 84°41.65' W, west of Parrita Scar) a plume-like feature was observed in the water column (Fig. 6.1.2.7). One can clearly see the topography with the crest at 2350 m water depth above which a vertically rising diffuse reflector is visible. Plotting the ship track onto the bathymetry map shows that at this point the ship crossed the crest of a sloping ridge. The crest height increased further uphill on the port side of the ship and decreased on the starboard side. A first look at the TOBI profiles also indicated a small hump in the topography on the starboard side of the ship, which is not visible in the bathymetry. Therefore, apart from being a plume, the recorded signal could also be due to side reflections either from the crest on the board side of the ship or from the hump on the starboard side of the ship. An additional question at this point is what gas overpressures are required in the sediment to create gas bubbles in the water at that depth.

The PARASOUND recordings as well as the recordings of the Sub Bottom Profiler mounted on the TOBI system were used to characterize the complex structural elements of the Middle American Trench off the coast of Costa Rica. The recorded profiles display a wide variety of different reflectors, from weak reflections in the sediments of the accretionary prism to the distinct reflectors of the oceanic crust. For our preliminary interpretation, we mainly use the PARASOUND recordings, which show penetration depths of up to 70 m into the sediments. Only in case of sea floor slopes inclining more than 2 - 4 or in areas of rough relief Sub Bottom Profiles records are used.

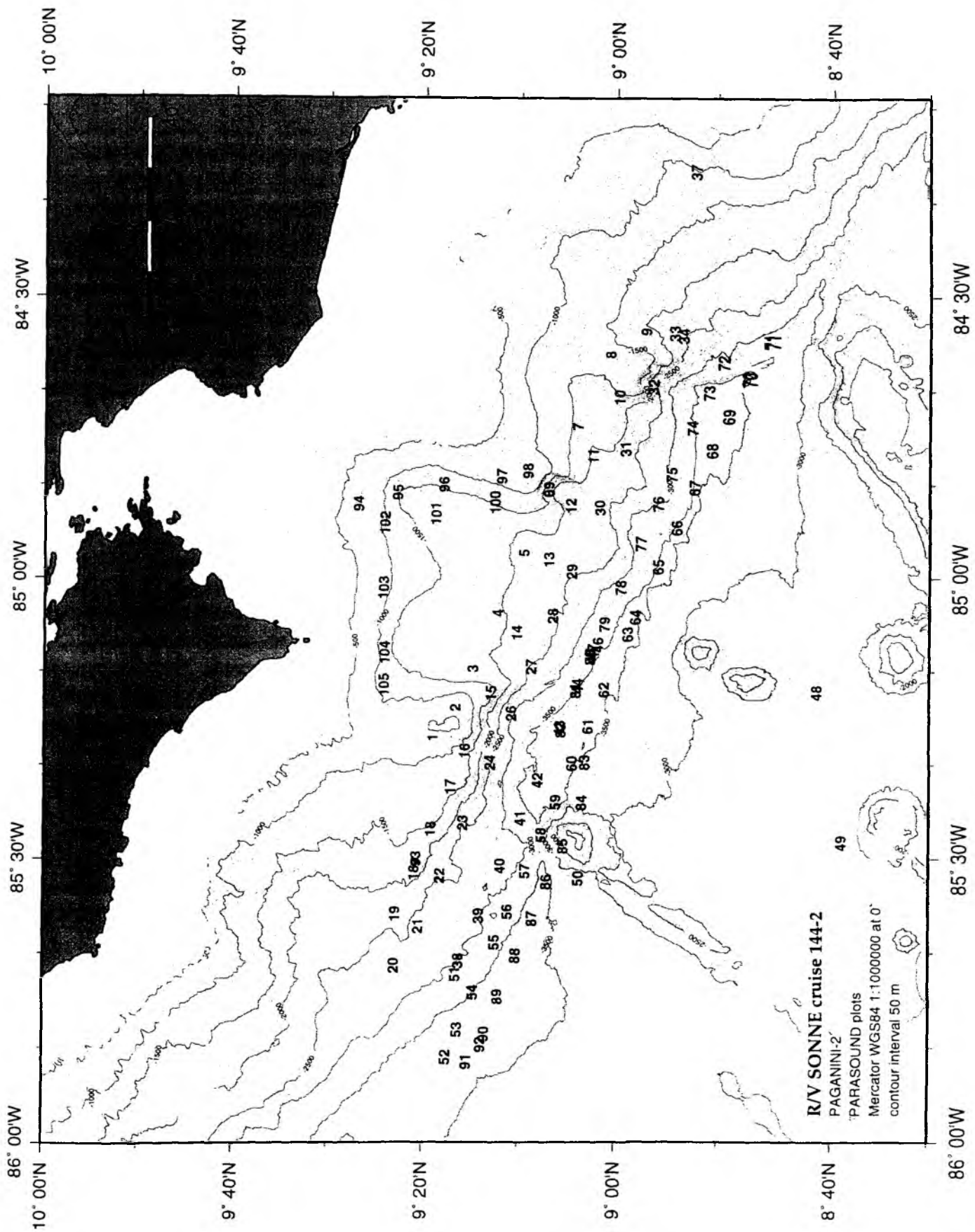

Figure 6.1.2.5: Location of the PARASOUND paper records and digital recordings stored at GEOMAR. The numbers indicate the center of each paper record.

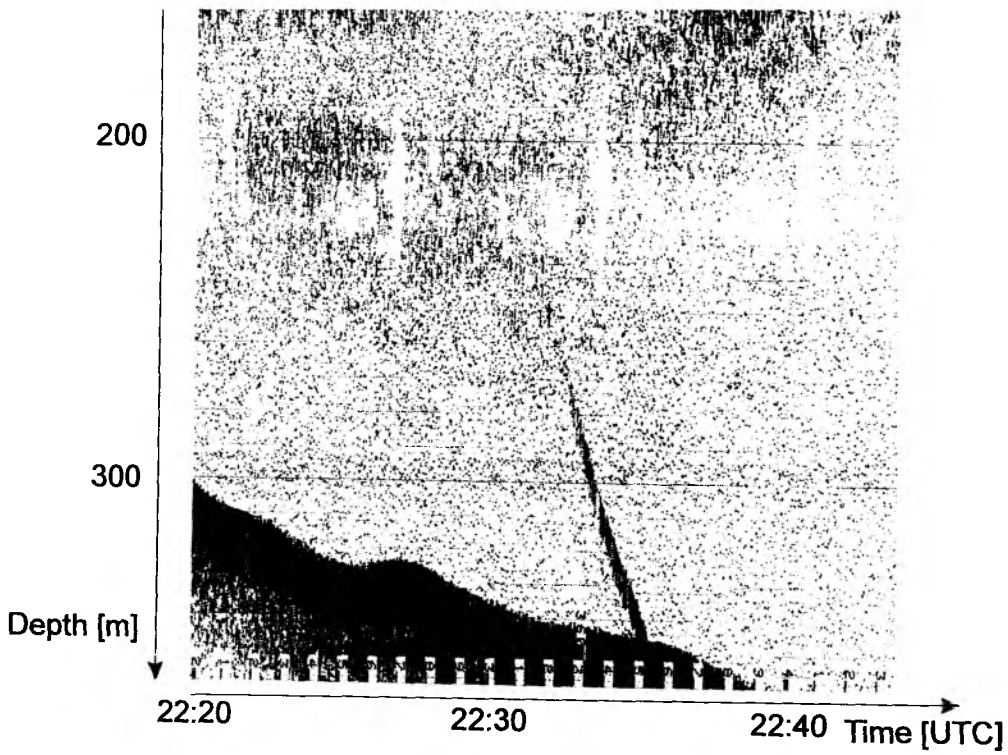

Figure 6.1.2.6: NBS-recording during OFOS descent on 27.10.99

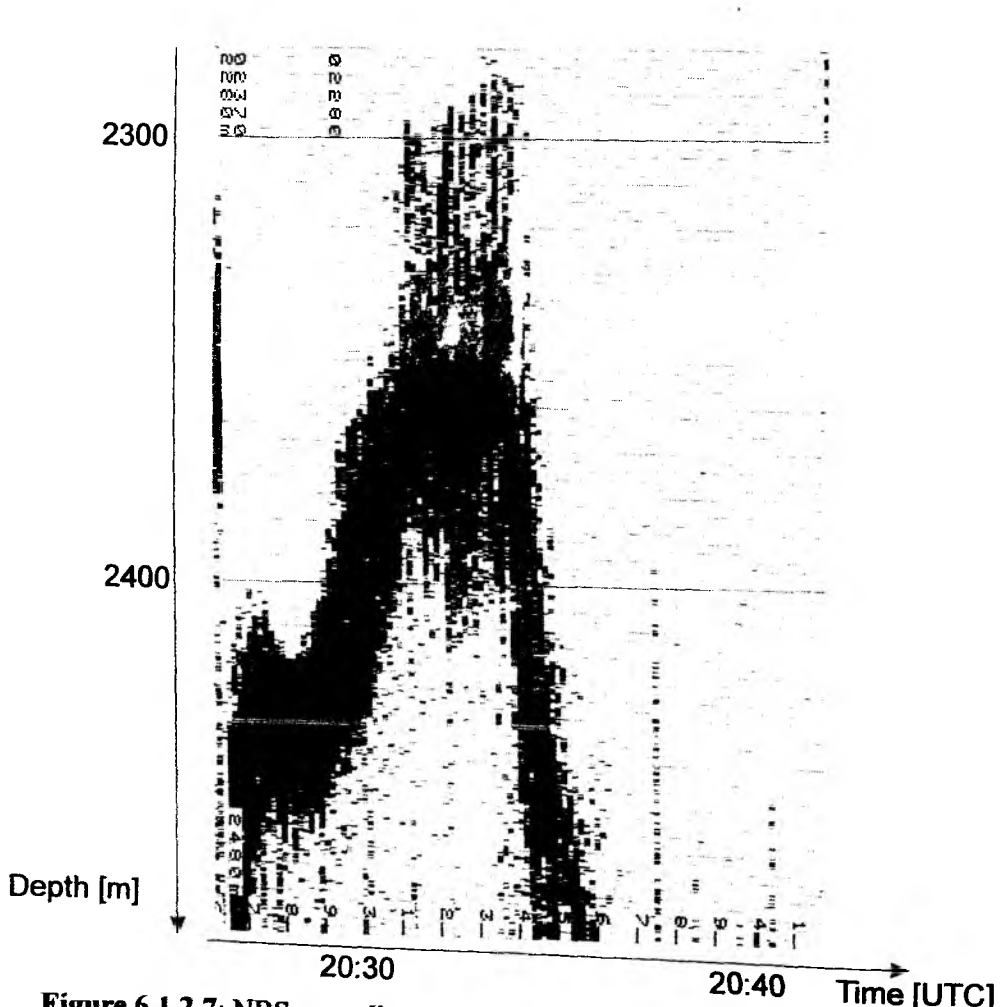

Figure 6.1.2.7: NBS-recording across a ridge on 28.10.99

Several types of reflectors can be distinguished. Each of them corresponds to structural or morphological elements, which are clearly visible in the bathymetry map (Fig. 6.1.2.8) aiding the tectonic interpretation. Strong reflectors from the sea bottom with minimum penetration were observed along isolated bulges inside the continental slope (Fig. 6.1.2.9). These bulges are found to coincide with subducted seamounts, an observation already made by von Huene et al. (1995). Several reasons can explain the nature of these strong reflectors: 1. abundance of sandy material, 2. outcrops of bed rock, and 3. pavement by carbonates as suggested by observations during OFOS surveys along the top of the Rio Bingo and Jaco Scar. The tops of these two scars are intensively fractured and are characterized by a typical saw shape relief. We interpret the features indicated by the errors in Fig. 6.1.2.9 as normal faults, a typical example of which from a similar tectonic environment is shown in Fig. 6.1.2.10. This normal faulting appears to be due to uplift in response to the subduction of seamounts (von Huene et al., 1995). The sides of the scars exhibit a system of thrusts or single thrusts (Fig. 6.1.2.11a,b), and they are most abundant west of Jaco Scar (see Fig. 6.1.2.8). The origin of these thrusts can again be interpreted as a reaction of the accretionary wedge to the subduction of seamounts.

In addition to the thrust faults concentrated near the base of the bulges there is a broad folded zone located in the embayment between Rio Bango and Jaco Scar (see Fig. 6.1.2.8). This zone is more pronounced in the central embayment where the sediments can be resolved up to 70 m below the seafloor (Fig. 6.1.2.12) and disappears toward the trench. Using the contour maps generated from the Hydrosweep data the fold axes can be reconstructed and are oriented in northeastern direction. Embayments are areas of erosion. The erosion is indicated by truncated reflectors and contourite sequences in the canyons cutting the continental slope (Fig. 6.1.2.13). The eroded material was transported and deposited downslope giving rise to unconformities (Fig. 6.1.2.14) or debris flow deposit (Fig. 6.1.2.15).

Areas with stratified reflectors are distributed inside the embayment, where in some places signal penetration reaches 70 m. Changes in seismic reflection sequences are found to occur during transition: 1. Up the slope of bulges with progressively decreasing penetration depth and disappearence of stratification; 2. to frontal prisms (taken from von Huene et al., in press, instead of accretionary prism) with progressively decreasing thickness of the stratification layer and appearance of irregular reflectors. However, the second transition is difficult to determine eastward from the Rio Bongo Scar based on the PARASOUND and Sub Bottom Profiler data.

There are three land slides on the continental slope in the area covered by survey tracks (see Fig. 6.1.2.8). The biggest one – the Nicoya slide – is located in the west. The sedimentary sequences start to disintegrate into land slides and show up on the seismic records as rough relief with chaotic reflectors (Fig. 6.1.2.16). The slides extend downslope to the frontal prism and further into the trench (Fig. 6.1.2.17) overlapping the prism. Our results support the ideas of von Huene et al. (1995, in press) that slide development occurs on very large scales. During our surveys it was found that debris flow deposits cover the oceanic plate seaward of the Nicoya Slide (see Fig. 6.5.6). The thickness of the layered sediments, which cover the debris deposit and postdate the emplacement of the slide, are of the order of 20 m. Rough estimates of sedimentation rates using data of ODP Site 1039 give an approximate age of 250-400 ka for the slide.

We found a difference between the western and eastern Nicoya Slide located opposite to the Puerto Coyote and Rio Bongo Scar. The eastern part shows a rough surface with a strong sea bottom reflector and many scattered reflectors (see Figs. 6.1.2.16, 6.1.2.17). In contrast to

the debris material, the western part is covered by thin, up to 10 m thick layers of transparent sediments (Fig. 6.1.2.18) that indicate an older age of this part, therefore postdating the emplacement. There is no way to determine the sedimentation rate using data from ODP Site 1041, but assuming that the rate is more or less the same as observed on Site 1039, the age of this part of slide should be two times less and equal to approximately 125-200 ka. Therefore, the frontal prism located opposite to the smooth domain can be restored during this period. A closing age of 140 ka for the restoration of the frontal prism opposing the seamount domain was obtained by von Huene et al. (in press).

The uppermost sediment sequence of the oceanic plate in the seamount domain is characterized by stratified reflectors (Fig. 6.1.2.19). Here the penetration depth is about 60 m. Normal faults cut the outer slope of the trench forming step or horst/graben structures. The shift along fault planes increases toward the deformation front (Figs. 6.1.2.19 and 6.1.2.20). There are two systems of lineations on the outer slopes striking east/west and north/west, as suggested by the bathymetry map. The first one corresponds to normal faulting due to bending of the plate (von Huene et al., 1995, in press), the second one can be related to the former structural grain and evidence of thrusting starts to appear along this direction (Fig. 6.1.2.21).

The transition from the oceanic plate to the frontal prism is clearly visible in Fig. 6.1.2.22 (left to right). The oceanic crust is characterized by stratified reflections whereas the frontal prism shows chaotic ones, which occur on all cross sections through the deformation front. The tectonic situation northeast of the Fisher Seamount towards the trench is unclear. Here the deformation front has a complex structure due to mass wasting from the Rio Bongo Scar and the reentrance of host and graben structures into the frontal prism (see Figs. 6.1.2.8 and 6.1.2.20).

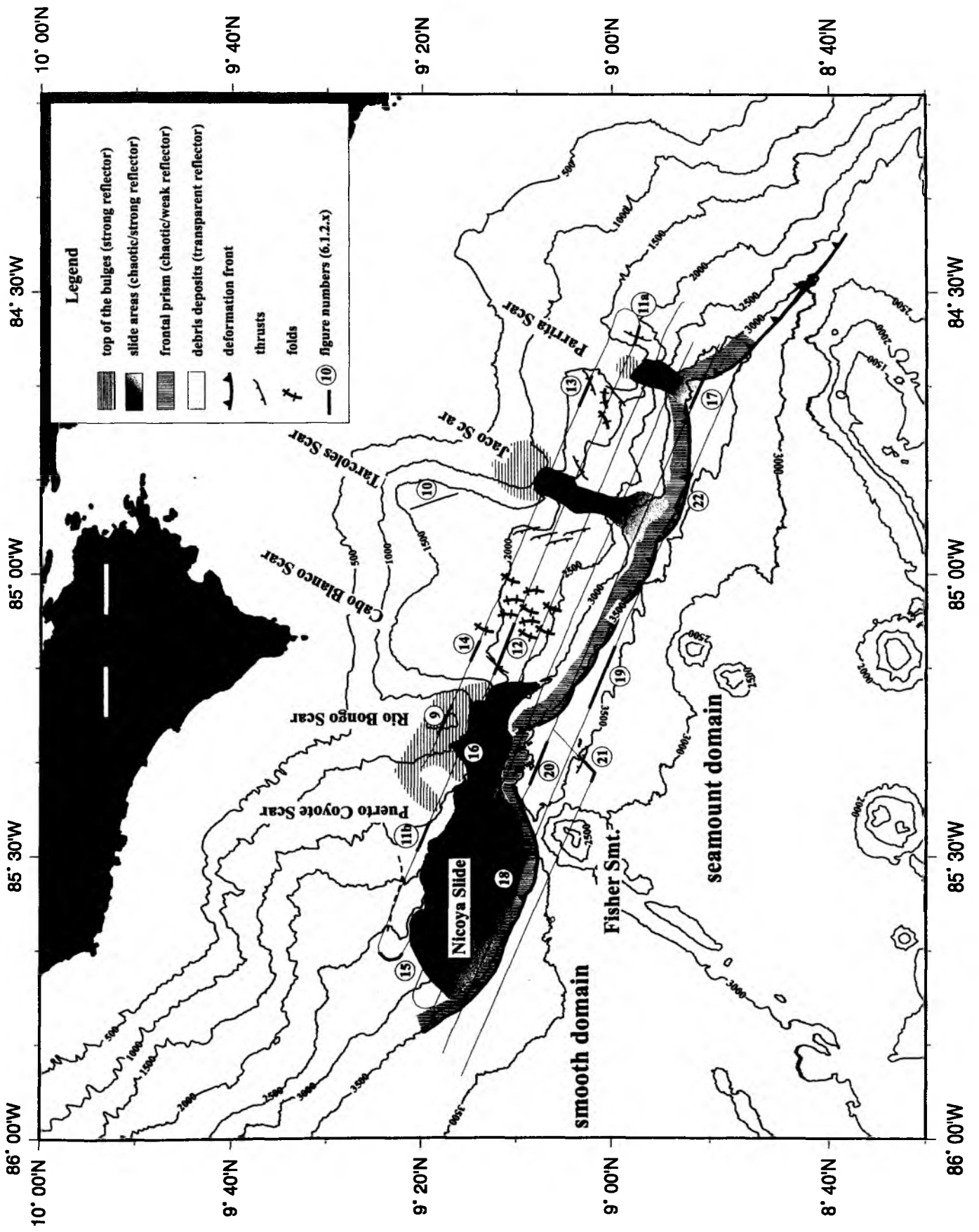

Fig.6.1.2.8: Distribution of areas with different reflectors related to changes in the uppermost sedimentary layers on continental slope off Costa Rica. Some tectonic features are shown as well.

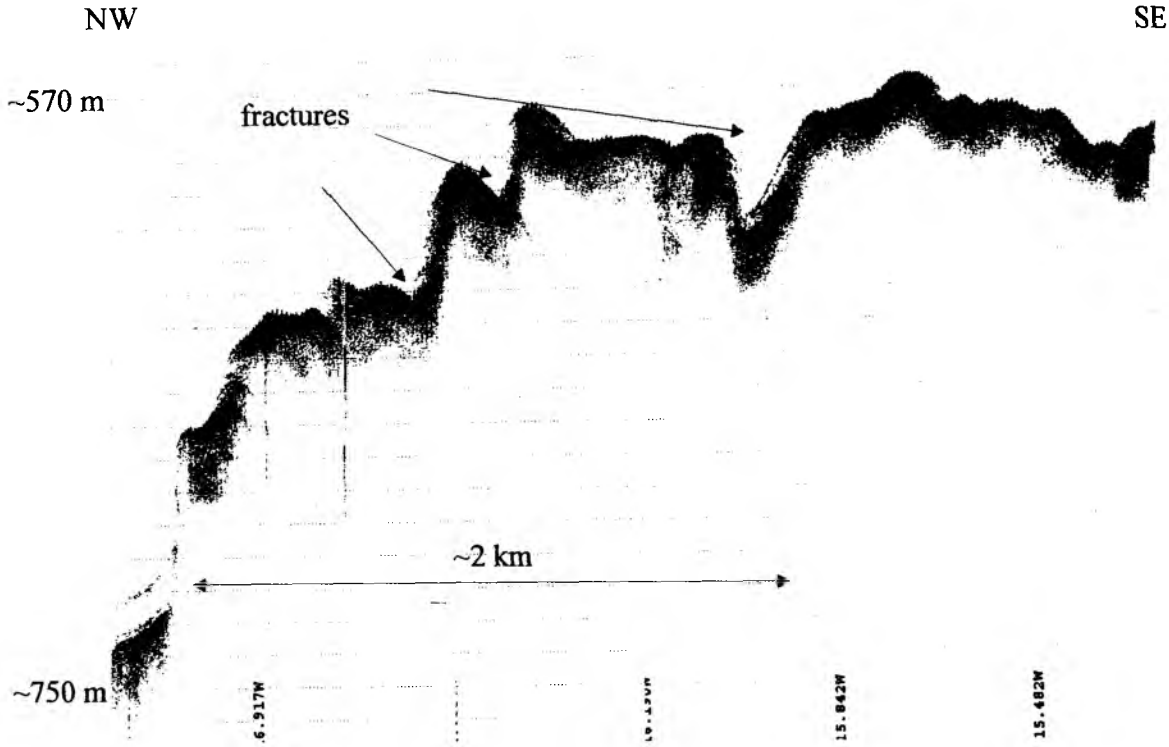

Figure 6.1.2.9: Strong bottom reflector characterize the height tops. Fractures are abundant. Location shown on Fig. 6.1.2.8.

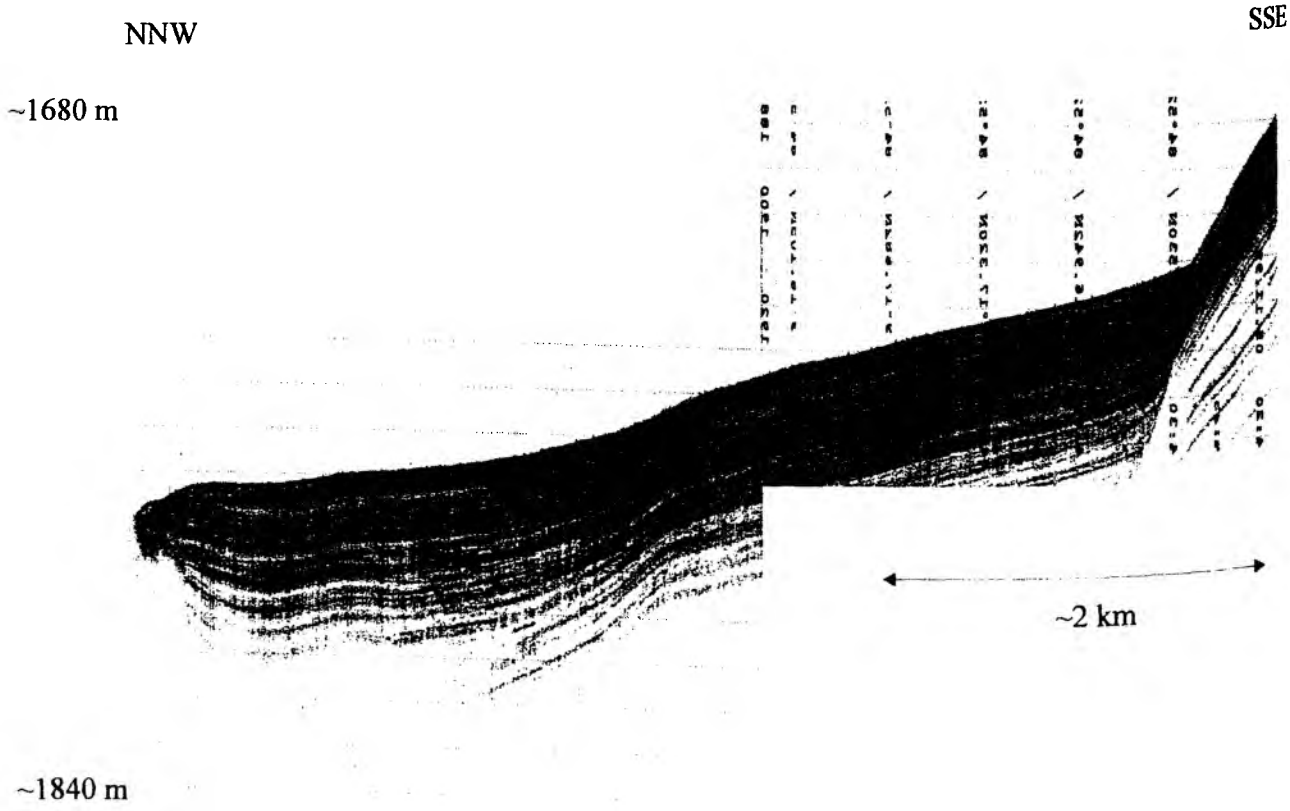

Figure 6.1.2.10: Example of the growth fault, which occurs on the slope base as well as northwards of the main area under investigation. Location shown on Fig. 6.1.2.8.

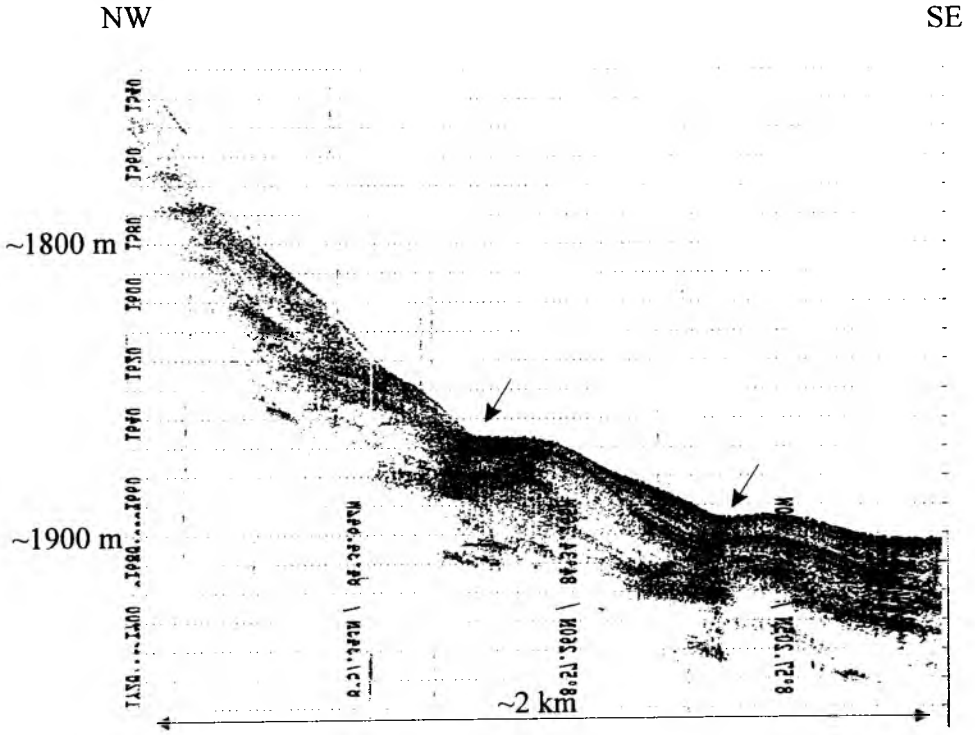

Figure 6.1.2.11a: Two examples of thrusts on the slope base. Location shown on Fig. 6.1.2.8.

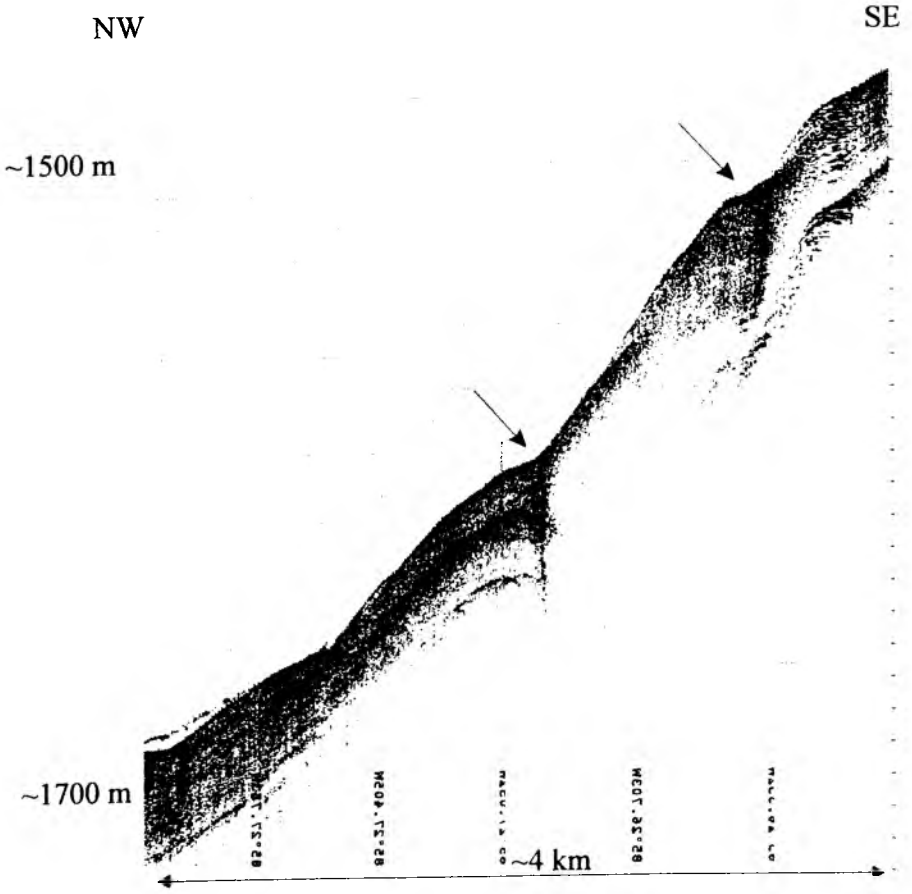

Figure 6.1.2.11b: Two examples of thrusts on the slope base. Location shown on Fig. 6.1.2.8.

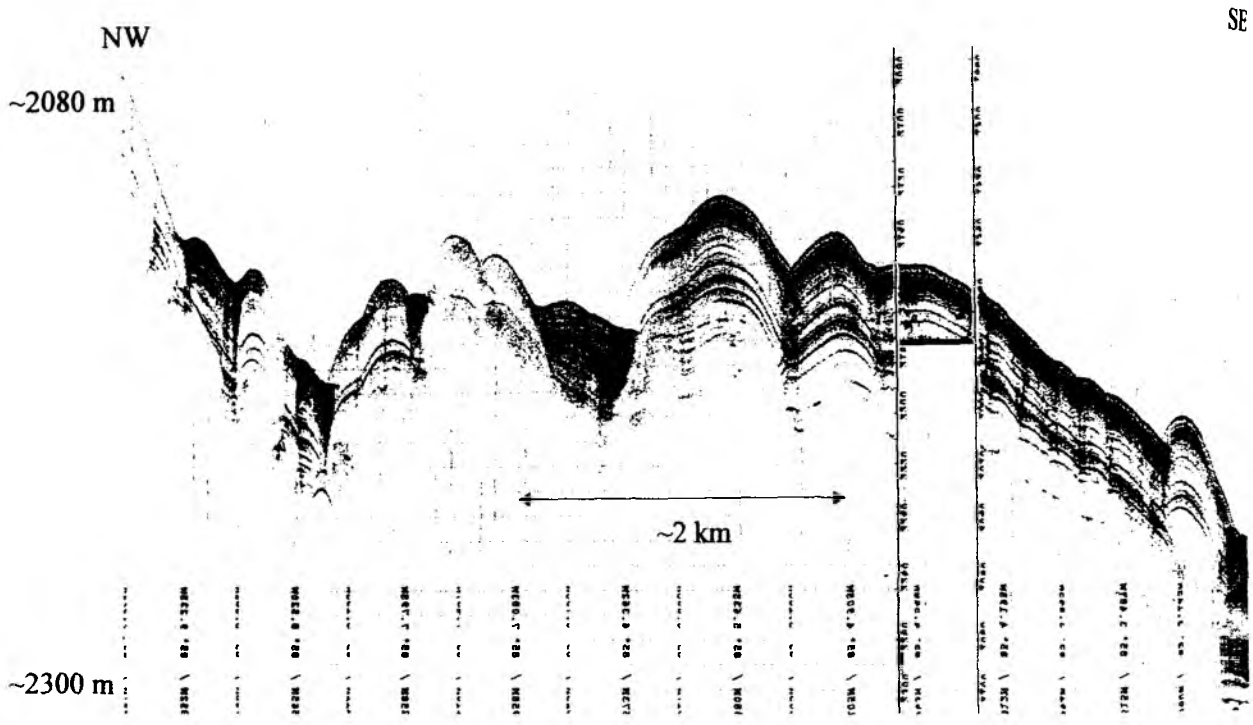

Figure 6.1.2.12: Shallow folding in the embayment between Rio Bingo and Jaco Scars. Location shown in Fig. 6.1.2.8.

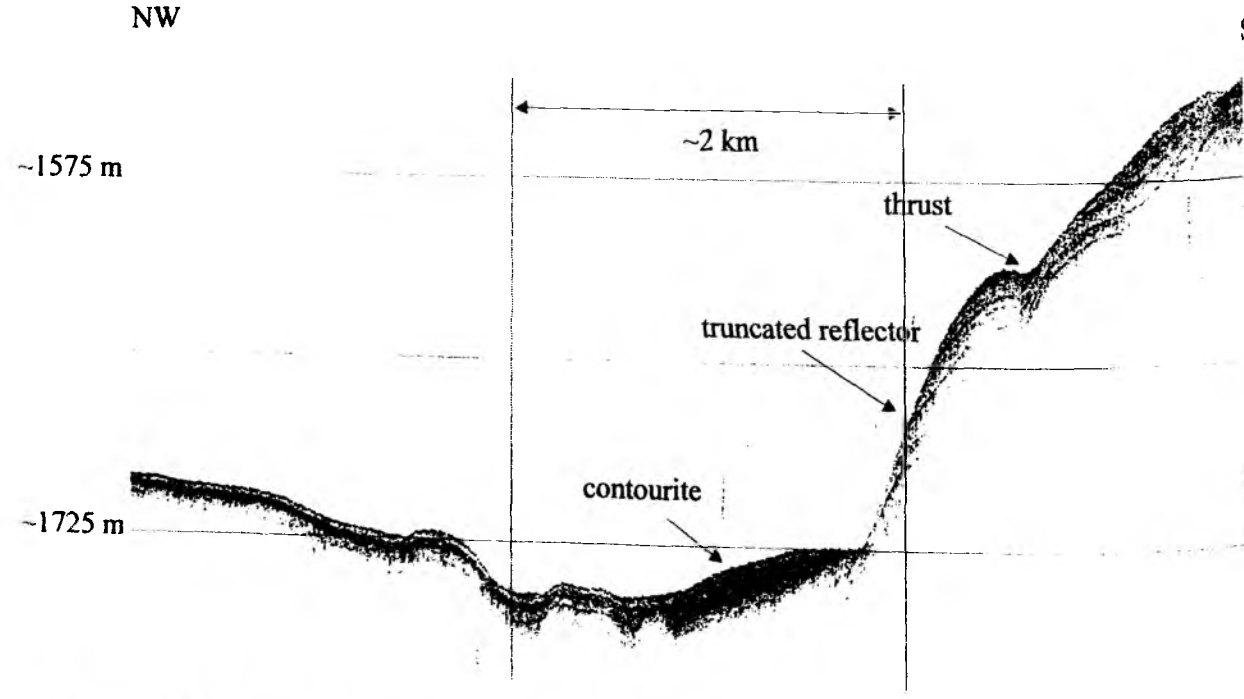

Figure 6.1.2.13: Evidences of erosion on continental slope as indicated by truncated reflectors and contourite sequence. A minor thrust occurs on the base of the slope (Sub Bottom Profiler record). Location shown on Fig. 6.1.2.8.

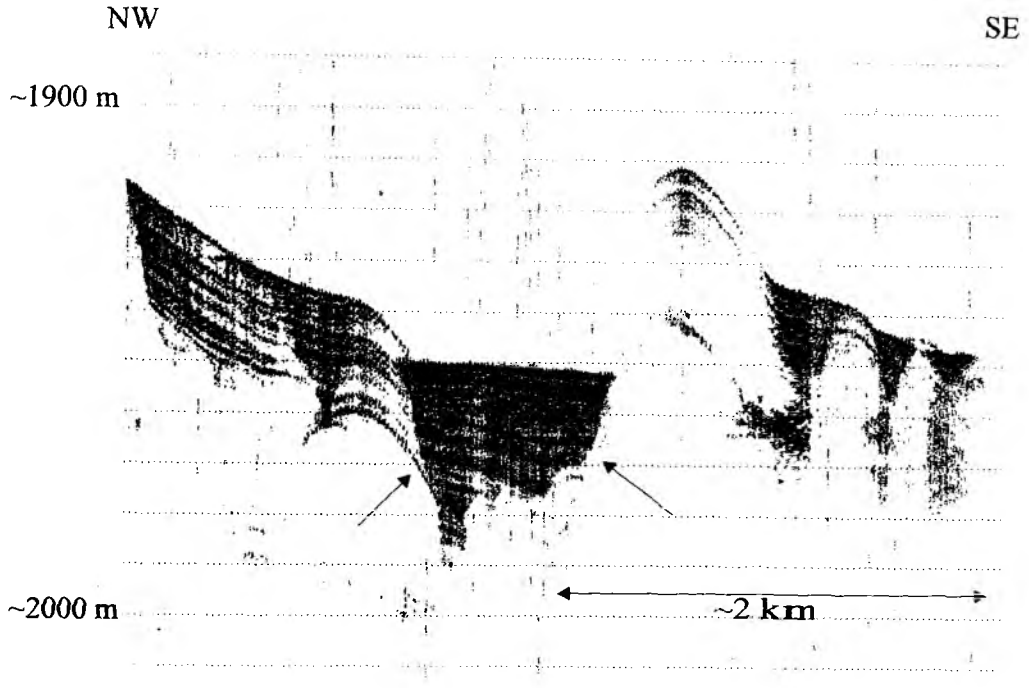

Figure 6.1.2.14: Unconformity between canyonfill and sedimentary sequence on the slope indicated by arrows. Location is shown on Fig. 6.1.2.8.

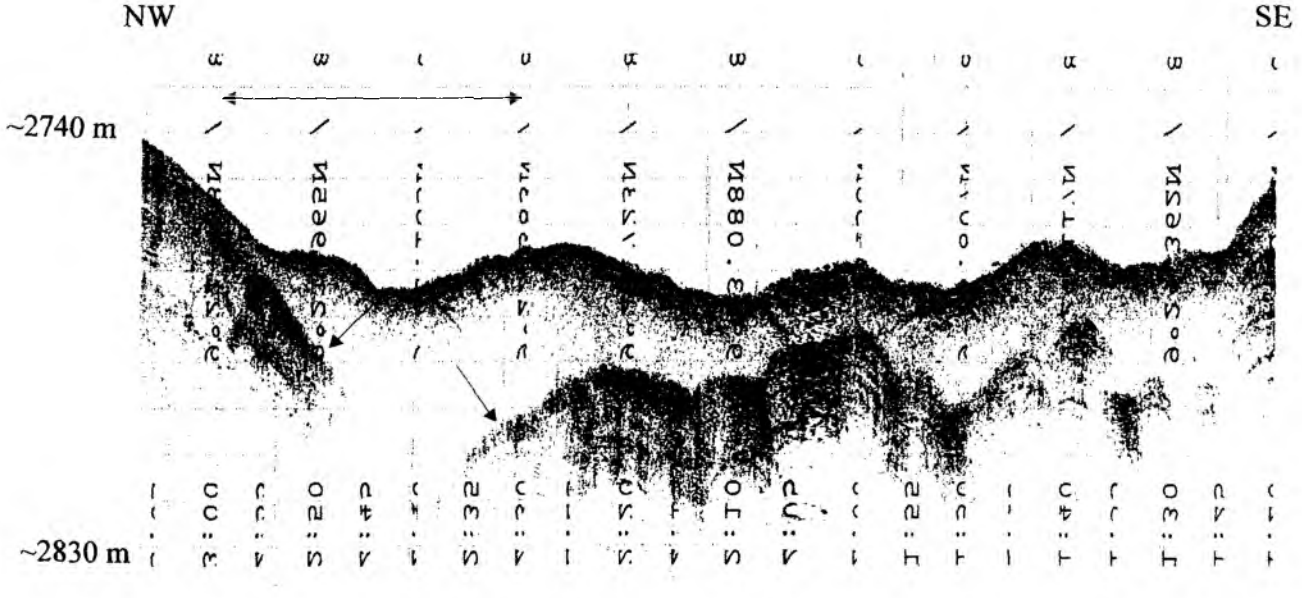

Figure 6.1.2.15: Transparent layer with strong bottom reflector (debris flow deposit) overlapping a stratified sedimentary sequence. Location is shown on Fig. 6.1.2.8.

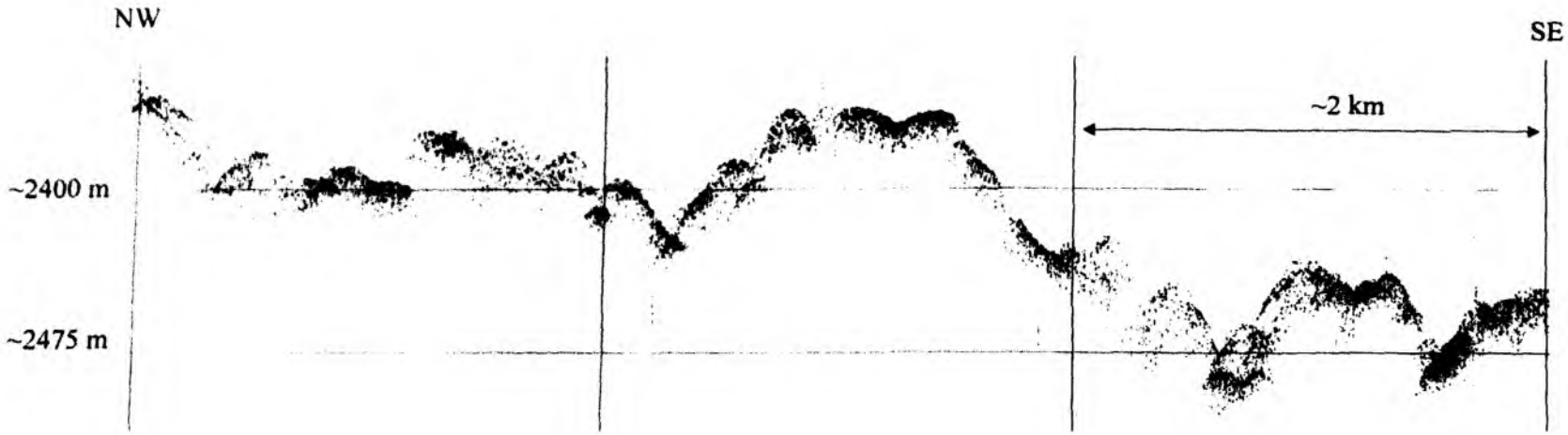

Figure 6.1.2.16: Cross section through the slide of Rio Bango Scar showing the character of the reflectors of recent slides. Sub Bottom Profiler record. Location is shown in Fig. 6.1.2.8

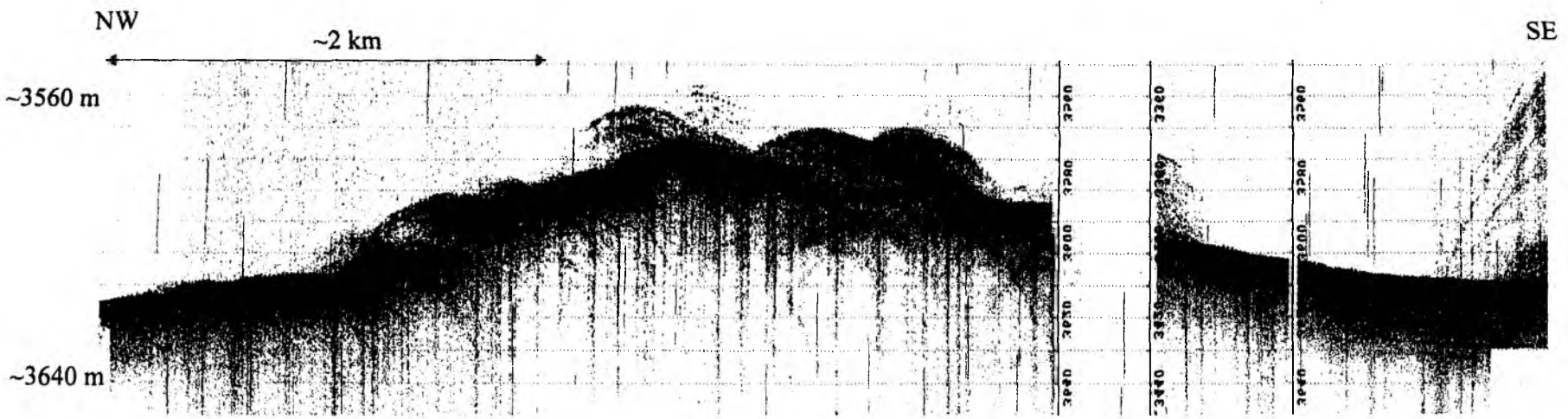

Figure 6.1.2.17: Chaotic reflectors in the trench indicate debris flow deposit. Location is shown on Fig. 6.1.2.8.

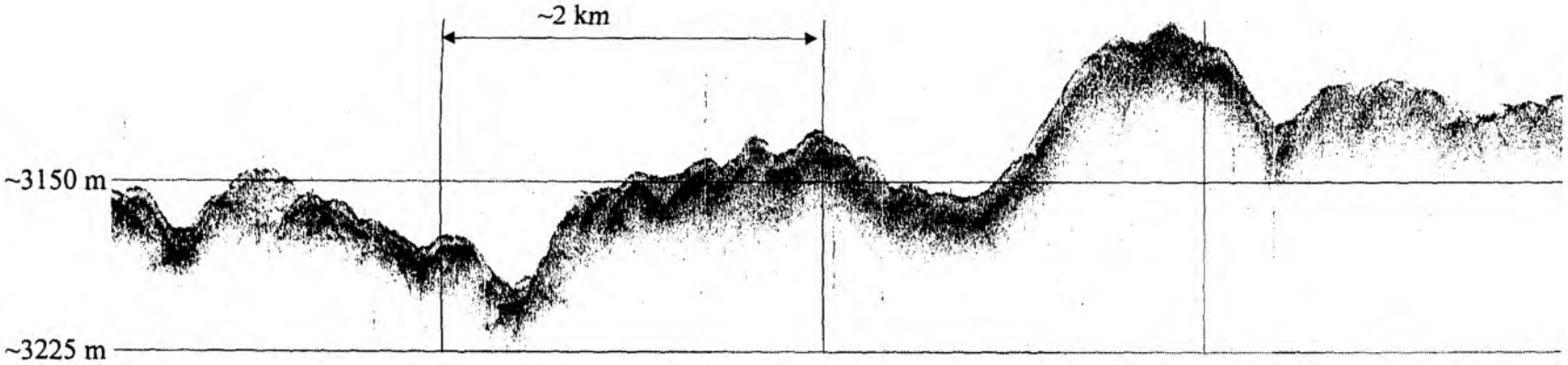

Figure 6.1.2.18: Transparent sediments up to 10 m in thickness cover the western Nicoya slide indicating its older age compared to the eastern part. There is a distinguished transition from the slide domain to the frontal prism domain in right part of the cross section. Sub Bottom Profiler record.Location is shown on Fig. 6.1.2.8.

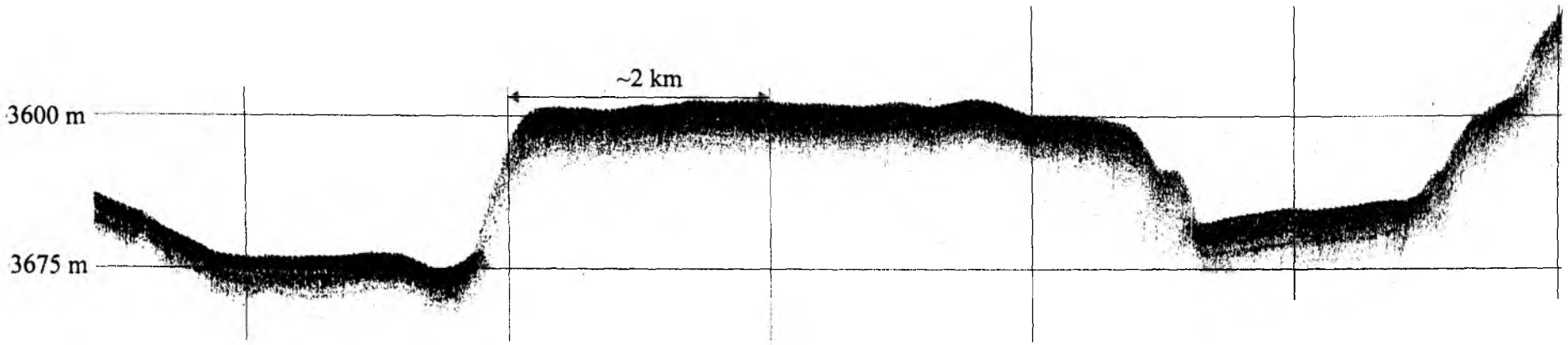

Figure 6.1.2.19: Stratified reflectors cover the oceanic plate. Horst and graben structures are developed due to plate bending (Sub Bottom Profile record). Location is shown on Fig. 6.1.2.8.

Figure 6.1.2.20: Example of horst and graben structure located near the deformation front. The visible shift on the fault planes reaches 100 m. Profile length appr. 7 km. Location is shown in Fig. 6.1.2.8.

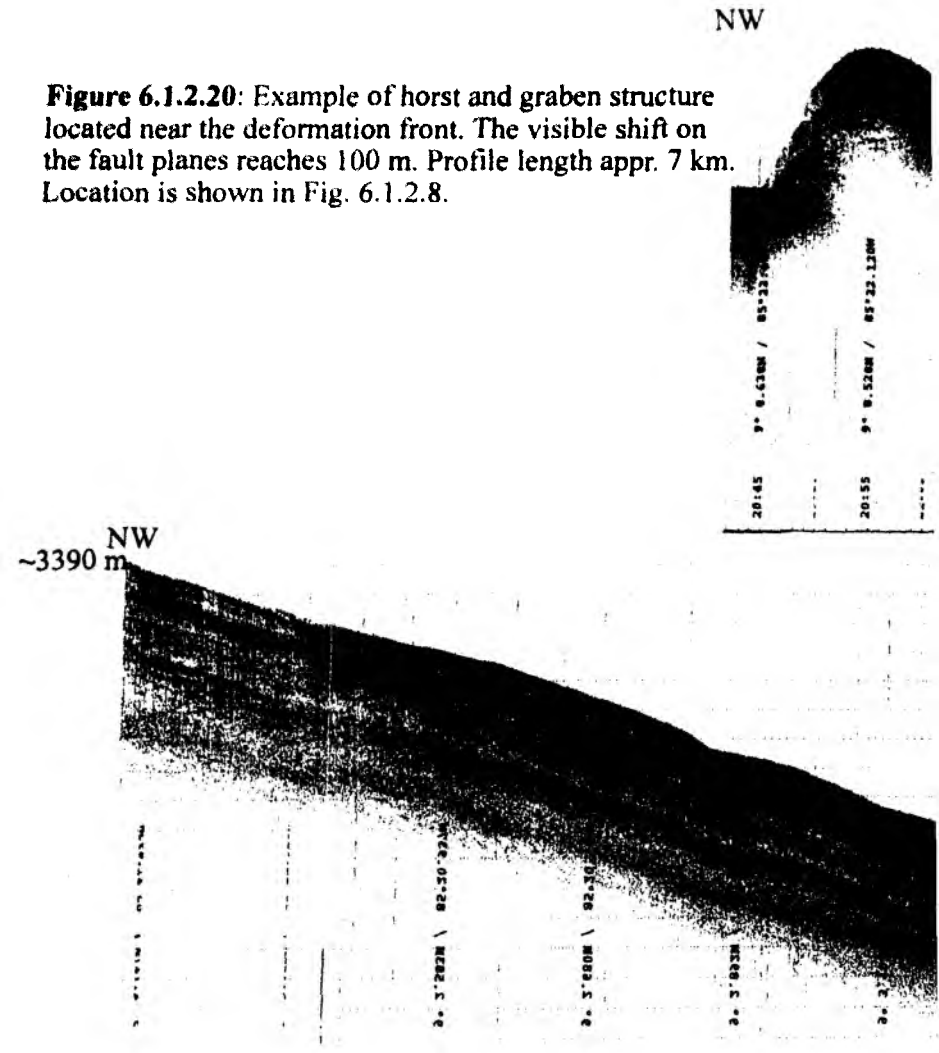

Figure 6.1.2.21: Minor thrusts starts to appear (arrow) on outer trench slope. The suggested strikes are parallel to the direction of the deformation front. Length of profile is approximately 6 km. Location is shown on Fig. 6.1.2.8.

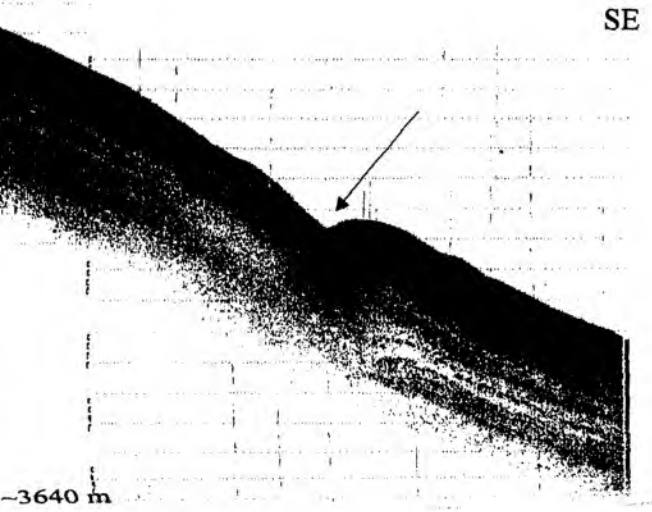

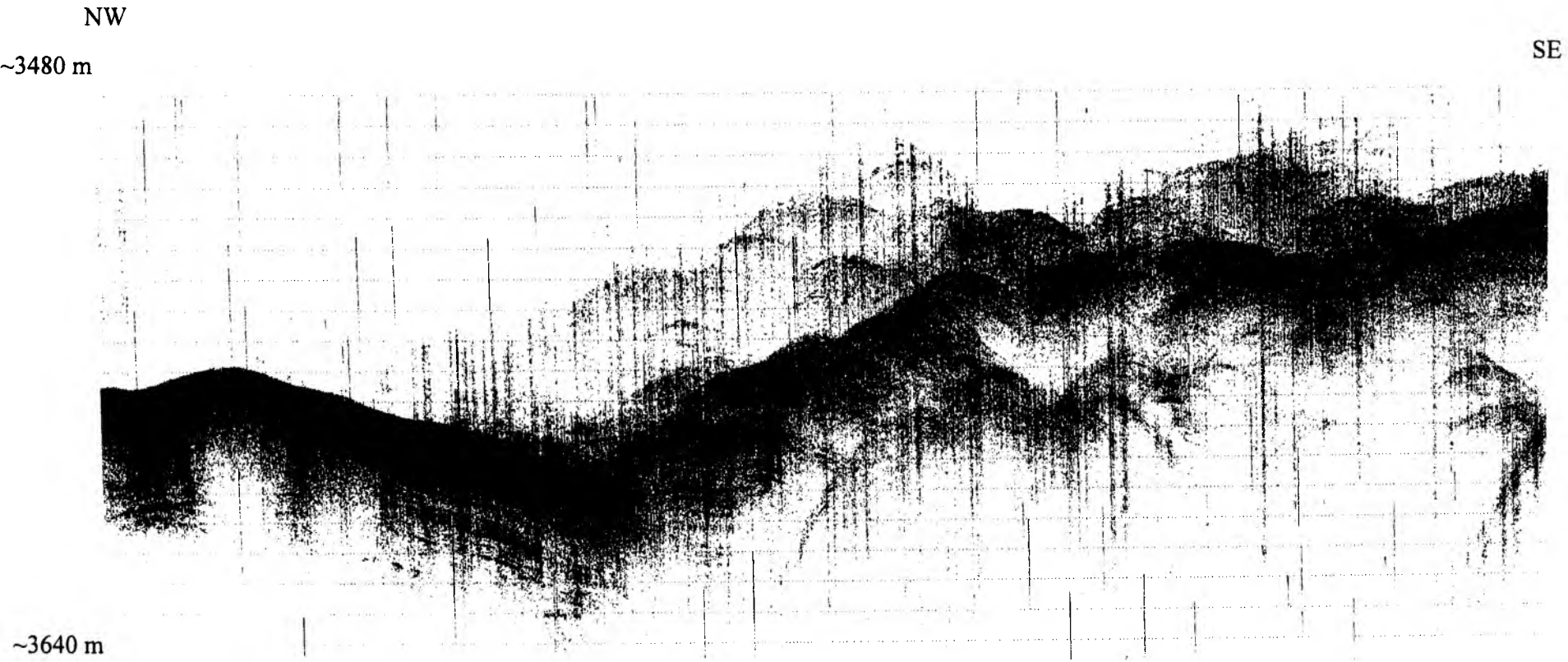

Figure 6.1.2.22: Distinct contact (deformation front) between stratified reflectors of oceanic plate (left) and chaotic reflectors of frontal prism (right). Length of profile is approximately 6 km. Location is shown in Fig. 6.1.2.8

6.2 SEISMIC WIDE-ANGLE WORK

6.2.1 INTRODUCTION

(The Geophysicists of SO144 and Watchstanders)

Most of the work during SO144-1 PAGANINI was devoted to the collection of seismic wide-angle data. A total of 162 OBH and OBS deployments were made along 6 major profiles and four lines in a special high-resolution experiment. All instruments were safely recovered, with none of them causing any delay and problems during recovery. It soon became evident that the acoustic release of the GEOMAR and IFREMER instruments allows a much more flexible operation than the time release of the IRD instruments. This deficit was partially compensated by a 100 % data recovery from the IRD instruments, while numerous problems with GEOMAR instruments caused data loss or problems with tape reading, which could not be resolved on board due to time constraints. Several of the unreadable datasets will be processed in-house at GEOMAR, but some instruments with power failure (often caused by human errors) did not record any data. In Figure 6.2.1.1, a summary of all deployment sites and profiles is shown and details of the instrumentation are given in Appendices 9.1. The data quality is generally very good. However, on the shallow shelf of Nicaragua (profile 6) and along the crest of Cocos Ridge, which has considerable sediment thickness, the data quality deteriorates. In contrast, record sections obtained from the Colombias Basin across Malpelo Ridge are of outstanding quality, with arrivals seen beyond 220 km and a very clear detection of S-waves.

The seismic source array used for the wide-angle work included up to three 2000 cubic inch airguns, but most of the time only two guns were in operation. Because of the model 800 BOLT airgun's design, they are notorious for damaging their airhoses and trigger lines. A severely damaged piston rendered one of the guns non-operational for the last two lines. Details of the profiles with a total number of more than 13000 shots along the profiles, with a total length of ca. 1400 km, are given in Appendix 9.2.

All collected seismic data were played out, processed and plotted during the cruise. They are stored in standard SEG-Y format and copies were made for all participating institutions. This created a heavy load on workstation space and time. The excellent cooperation between the scientific parties on board and the ship's crew enabled a very smooth operation. Preliminary interpretations were made for most of the profiles, especially those collected early during the cruise. In the following chapters the applied processing (chapter 6.3.2) and modelling techniques (chapter 6.3.3) are described first. This is followed by a description of each profile, which includes the chronology of the experiment (all times given correspond to local times), the most important data and some initial results. Obviously, data archiving and quality control, as much as instrument preparation and repair, was the focus of the scientists' effort during the cruise. More detailed and thorough interpretations of the dataset will follow later.

During the cruise, we also tested new equipment designed for future long-time deployments intended to study natural seismicity. Titanium pressure tubes were found to be easy to handle due to their reduced weight and superior corrosion resistance. The GEOLON MLS recorder worked well, although software for correct data playback was not available on board. Also, since the odd sampling rate (250.38 samples/s) of the prototype will be changed by the manufacturer for future instruments, no attempt was made to treat these data with more care. Both new sensors, the DPG (differential pressure gauge) and the self-gimbling, three-component seismometer worked well - although handling of the latter requires improved procedures. The IFREMER OBH, using the same recording technology

as the GEOMAR instrument, worked well, although the ascent speed might be improved by adding additional flotation. We also found that when instruments are deployed at spacing within range of the acoustic release, one instrument can be released while the one before it is being recovered, such that the total time required for pickup can be extremely short (30 minutes per instrument in ideal situations).

Most Important Results

4 seismic lines with a total of 93 instruments (OBH or OBS) were shot on the Cocos and Malpelo volcanic ridges providing a unique set of data on the deep structure of these features. These volcanic ridges are generally interpreted as the result of the interaction between the Galapagos hotspot and the Galapagos spreading centre.

Preliminary modelling of the seismic data shows that the Moho is located at depths ranging from 19 to 24 km (Figures , 6.2.4.3.37, 6.2.4.4.18, 6.2.4.5.36 and 6.2.4.6.25). Beneath the Cocos Ridge the crust is mainly divided in three units: the uppermost unit with velocities of 3.8 to 5.0 km/s could be interpreted either as interlayered volcanic flows and sediments or as altered volcanic flows; the intermediate unit with seismic velocities of 5.0 to 5.8 km/s is consistent with a layer of volcanic origin; the lower unit is very thick (from 12 to 15 km thick) with a velocity increasing gently from 6.4 to 7.5 km/s. This lower layer with high seismic velocities (> 7.0 km/s) is characteristic of oceanic volcanic plateaus.

The transition from the ridge crust to the oceanic basin crust is quite narrow along profile 4 where the crust thins from approximately 18 km to 8 km within less than 30 km.

Line 3 shot on the Malpelo Ridge exhibits a 20 km thick crust with a discontinuity in the lower crust which possibly denotes an underplated layer (Figure 6.2.4.5.36). The structure is highly asymmetric with a very smooth transition from the ridge crust to the basin crust to the south-east whereas it is very steep to the north-west. This asymmetry also exists in the topography and could evidence that the northern flank of the ridge is a rifted flank.

The seismic structure of the Cocos and Malpelo volcanic ridges is very similar to the one of the northern Kerguelen Plateau or to Iceland and supports the hypothesis that these ridges are related to the activity of the Galapagos hotspot near an active spreading centre. The seismic data support the hypothesis that the Malpelo ridge was rifted away from the Cocos and/or Coiba ridge to the north despite the fact that the deep structure is slightly different from the structure of the Cocos Ridge.

This new set of high quality seismic data will provide a new insight in the understanding of Large Igneous Provinces and of the geodynamics of the Cocos plate.

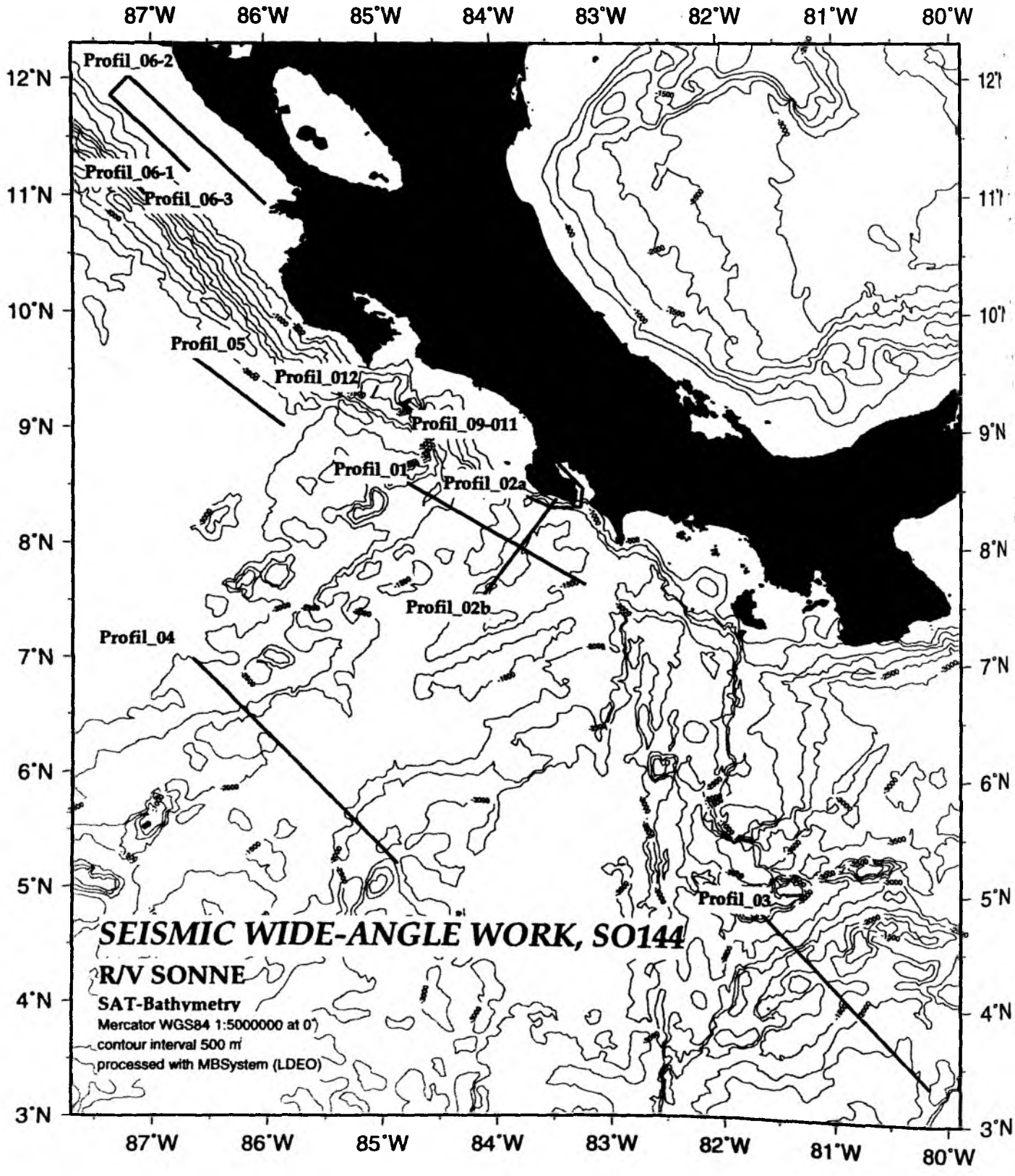

Figure 6.2.1.1: SEISMIC WIDE-ANGLE WORK, Location map

6.2.2 SEISMIC PROCESSING AND DATA ARCHIVING

Data Processing

The OBH/S data recorded on the *Methusalem* and the *MBS* have to be converted into standard SEG-Y format for further processing. The necessary program structure was mainly taken from the existing REFTEK routines and modified for the OBH requirements and GEOMAR's hardware platforms. Because the GEOMAR OBH works in a continuous mode, most of the modifications on the existing program package had to be done in the program parts handling continuous data streams.

A flow chart shown in Figure 6.2.2.1 illustrates the processing scheme applied to the raw data. A detailed description of the main programs follows below:

• mbs2pass

For the PC cards used with the MBS recorder data expansion and format conversion into PASSCAL data format is performed with a DOS based PC. The program mbs2pass reads the data from the set of up to four flashcards used during recording. Decompressed data are written onto the PC's hard disk using the PASSCAL data format, either 16 or 32 bit storage is available. This enables compatibility with the DAT recordings (s.b.). After ftp transmission to a sun workstation ref2segy and all other software can be used to handle and process the data files and store them as SEG-Y traces.

• ref2segy

Downloading the raw data from DAT tape onto a hard disk of a SUN workstation is done by the program ref2segy. It will produce a pseudo SEG-Y trace consisting of one header and a continuous data trace containing all samples. For each channel (different amplifications) one file will be created. The name of this file contains the start time, the serial number of the *Methusalem* and the channel number. In addition a log and an error file will track the download process. In a second mode PASSCAL disk files written by *mbs2pass* in either 16 or 32 bit format can be read in and included into the standard processing scheme. The file size of the data is directly related to the recording time. For example, a recording time of one hour sampled with 200 Hz will produce a file size of 1.44 MB per channel. A record with two channels and a recording time of two days will get a total data volume of 70 MB.

• merge

If a tape error has occurred during the download process, the ref2segy program has to be restarted. This will lead to several data files with different starting times. Merging these files into a single file is done by the merge program. The gap between the last sample and the first sample of the consecutive data trace will be filled up with zeros. Overlapping parts will be cut out.

• segy2trig

The trigger signal, which is provided by the airgun control system, is recorded simultaneously on an additional *Methusalem* during the shooting period. This tape is treated as a regular data tape and downloaded to the hard disk via the ref2segy program. The segy2trig program detects the shot times in the data stream. It determines the shot times by detecting the trigger signal through a given slope steepness. duration and threshold of the trigger pulse. The output is an ASCII table consisting of the shot number and the shot time. The accuracy of the

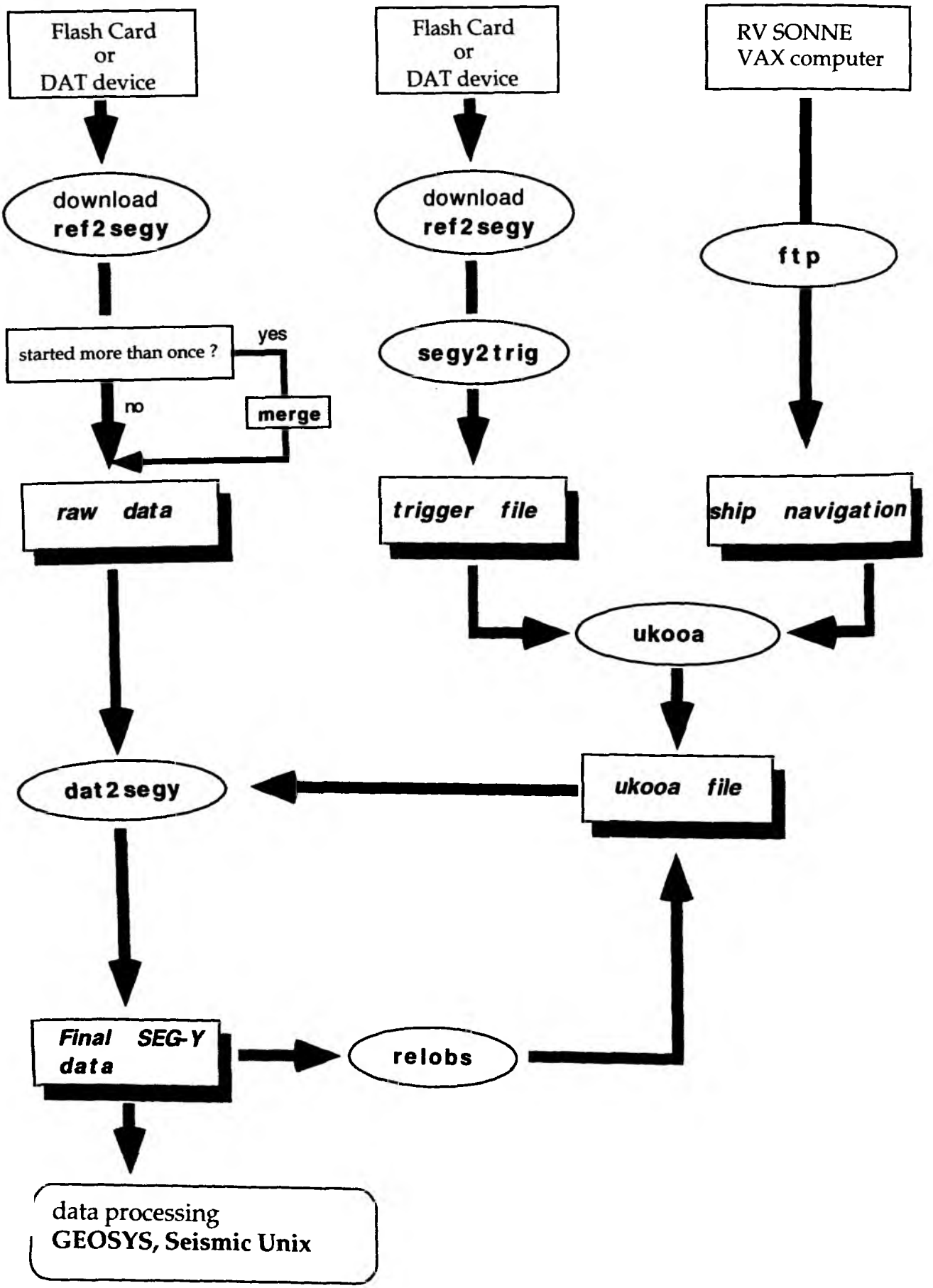

Figure 6.2.2.1 Processing for GEOMAR OBH/OBS data

shot time is one of the most crucial matters in seismic wide-angle work. It has to be reproduced with a precision of 5 ms. Due to this demand the shot times have to be corrected with the shift of the internal recorder clock. As additional information the trigger file contains the profile number and the start/end time of the profile and the trigger recording. The shot times are part of the UKOOA file which links the coordinates of the source and the hydrophones with the shot times.

• **ukooa**

The ukooa program is used to establish the geometric data base. It requires the trigger file containing the shot times, the ship's navigation and the position of each OBH for input. The ship's navigation is stored in a database about every two seconds (see Chapter 5.11.3). The program calculates the coordinates of each shot and creates a file in the UKOOA-P84/1 format as output. Corrections for offsets between antenna and airguns as well as consistency checks are included. This file will be used when creating a SEG-Y section via the dat2segy program.

• **dat2segy**

The dat2segy program produces standard SEG-Y records either in a 16 or 32 bit integer format by cutting one single SEG-Y trace (from the merged ref2segy file) into traces with a certain time length. It reads both the ukooa file with the geometry information and the downloaded raw data as produced with the ref2segy program. In addition, the user can use several parameters for controlling the output. These parameters are information about the profile and the receiver station, number of shots to be used, trace length, time offset of the trace and reduction velocity (to determine the time of the first sample within a record). The clock drift of the recorder is also taken into account and corrected for. The final SEG-Y format consists of the file header followed by the traces. Each trace is built up by a trace header followed by the data samples. The output of the dat2segy program can be used as input for further processing with GEOSYS or Seismic Unix (SU).

Besides these main programs for the regular processing sometimes additional features are needed for special handling of the raw data:

• **divide**

The program divide cuts the raw data stream into traces with a given length without offset and time information. The output is stored in SEG-Y format. The routine is useful for a quick scan at the raw data or if a timing error has occured.

• **segyhdr**

The routine segyhdr prints all the header values of the raw data on the screen.

• **segyshift**

The program segyshift modifies the time of the first sample, which means that the whole raw data trace can be shifted by a given value. This is very useful when shifting the time base from Middle European Time to Greenwich Mean Time or any local time. Because of recording problems, the data sometimes show a constant time shift, which can be corrected with segyshift as well.

• **castout**
The program castout allows you to cut out a specified time window from the raw data stream. When the shooting window is much smaller than the recording time, one can reduce the data volume by cutting out only the useful information. This will reduce the demand on disk space.

• **relobs**

Due to a drift of the OBH during deployment and errors of the ship's GPS navigation system the OBH positioning may be mislocated by up to several 100 m. As this error leads to an asymmetry and wrong traveltime information in the record section it has to be corrected, which is done with the program relobs.
Ahe assumed OBH location, shot locations and the picked traveltimes of the direct wave near to its apex are needed as input. By shifting the OBH position, relobs minimizes the deviation between computed and real traveltimes using a least mean square fitting algorithm assuming a constant water velocity.

• **OBH/OBS-data analysis and processing**

Raw data: As a data example, the OBH record section 49 for profile 1 is shown in Figure 6.2.2.2. For the analysis offset ranges between 5-10 km northwest and 50-55 km southeast are presented in detail.

Frequency filter test: To determine the frequencies of the seismic energy, filter panels for the offset ranges 5-10 km and 50-55 km respectively are shown in Figures 6.2.2.3 and 6.2.2.4. In the last second of the data window the autorrelation function is appended. The amplitude spectra of the Ormsby frequency filter operators are characterised by linear slopes. The filter is described by four corner frequencies:

Lower stop/pass band boundary and upper pass/stop band boundary. The frequencies on the filter panels correspond to the lower and upper pass frequencies. The main energy for the phase between 1.7 and 3.0 s in the offset range from 5-10 km is between 5-17 Hz and for the direct wave more than 30 Hz. The main energy of the phase between 1.0 and 2.0 s in the offset range from 50-55 km is between 3-12 Hz. As a broad frequency range is contained in the data a time and offset dependent filtering was applied (see below).

Deconvolution test: To improve the temporal resolution of the seismic data a deconvolution is applied to compress the basic seismic wavelet. The recorded wavelet has many components, including the source signature, recording filter, and hydrophone/geophone response. Ideally, deconvolution should compress the wavelet components and leave only the earth's reflectivity in the seismic trace. The deconvolution algorithm which was applied is the Wiener deconvolution in sucessive trace segments which is based on the following assumptions:

1. The earth's reflectivity is 'white'.
2. The wavelet shows the minimum-delay phase behavior.

As in wide-angle data the amplitude spectra of the seismic traces vary with time and offset, the deconvolution must be able to follow these time and offset variations. Each trace is therefore devided into 2 s data gates with 1 s overlap, in which time invariant deconvolution operators are computed from the autocorrelation function of the data segment and applied. The overall deconvolved trace results from a weighted merging of the independently deconvolved gates.

The input for the deconvolution process is raw data, 5 Hz lowcut filtered with 48 db slope. As several recordings were influenced by a DC shift, a median filter was applied prior to deconvolution in order to center the amplitudes around zero. The deconvolution test panels are shown in Figures 6.2.2.5 and 6.2.2.6 for the offset ranges 5-10 km and 50-55 km respectively. In the last second of the data window the autorrelation function is appended. A constant operator length of 480 ms and a variation of the predictive length from 0 (spike) to 320 ms is displayed.

On the undeconvolved data in Figure 6.2.2.5 and 6.2.2.6 strong energy of up to 500 ms behind the zero lag is clearly visible in the autocorrelation function. The best resolution is obtained for a predictive length of 0 ms but with a reduction of signal-to-noise ratio especially on the far offset traces. A predictive length of 160 ms was chosen for this data set which is a compromise between temporal resolution and signal-to-noise ratio.

After deconvolution an offset- and time-variant Ormsby filter was applied. As the seafloor depth changes rapidly along the seismic lines, each trace was statically corrected to a fixed seafloor travel time of 6 s based on the water depth. This information is available in the trace headers. The time- and offset-variant filter depends on the reduction velocity. After this filter was applied, the data were shifted back to their original travel times.

Processed data: A comparison of the pre-processed data in Figure 6.2.2.7 to the un-processed data in Figure 6.2.2.2 shows a clear reduction of the low frequency noise on the near and far offset traces and a moderate compression of the wavelet signal. For the picking of events and model building by ray tracing both sections were used to keep all the available seismic information.

- **Final processing sequence**
  - Input: SEGY-data, 5 ms (DAT recorder) or 4 ms (MBS recorder) sampling rate with complete geometry information. Trace length: 20 s, reduction velocity profile 6 km/s, time off first sample -3s or -5 s.
  - Median filter (debias).
  - Low cut frequency filter 5Hz with 48 db slope.
  - Gated Wiener deconvolution: gate length 2 s, overlap 1 s, operator length 480 ms, prediction interval 160 ms.
  - Static correction to a fixed seafloor travel time of 6 s.
  - Time and offset-dependent Ormsby frequency filter.

On time-shifted traces with a reduced time scale of 6 km/s the following filter parameters were used:

offset (km)	100%-time (s)	lower stop/pass	upper pass/stop (Hz)
0	7	3/5	28/48
	8	3/5	18/28
	11	3/5	13/18
30	-6	5/5	28/48
	-1	3/5	18/28
	3	3/5	13/18
40 - max	-6	5/9	28/48
	-6	3/5	18/28
	-6	3/5	13/18

• **Data archiving**

Data recorded with the MBS recorder on flash discs were transferred via a PC to a Sun workstation. On the workstation they were transformed into a so-called PSEUDO-SEGY format. Data from Methusalem DAT devices were played back using a SCSI compatible playback device which provides the data in the same PASSCAL data format as the MBS data on a Sun disk. Both the raw data from the flash discs and the PSEUDO-SEGY data were archived on DAT or Exabyte tapes.

After the navigation data had been merged in and SEGY formatted traces of 20 sec length with the appropriate header words had been created, the data were also archived. Finally, a third set was stored and archived after the shipboard processing, as described above, had been applied. All final processed SEGY data were archived on a single tape. For safty reasons, we did every backup twice.

• **Data exchange**

For the exchange of the OBH/OBS data the SEGY-format on disk in a Sun tar-format was chosen. The trace length for the raw and processed data is 20 s, where the time of the first sample is –3 or –5s at a reduction velocity of 6 km/s. The complete geometry information is positioned in the standard SEGY-trace headers, e.g.:

Information	Receiver No.	Shot No	Offset	reduction velocity
Byte:	13-16	21-24	37-40	93-94

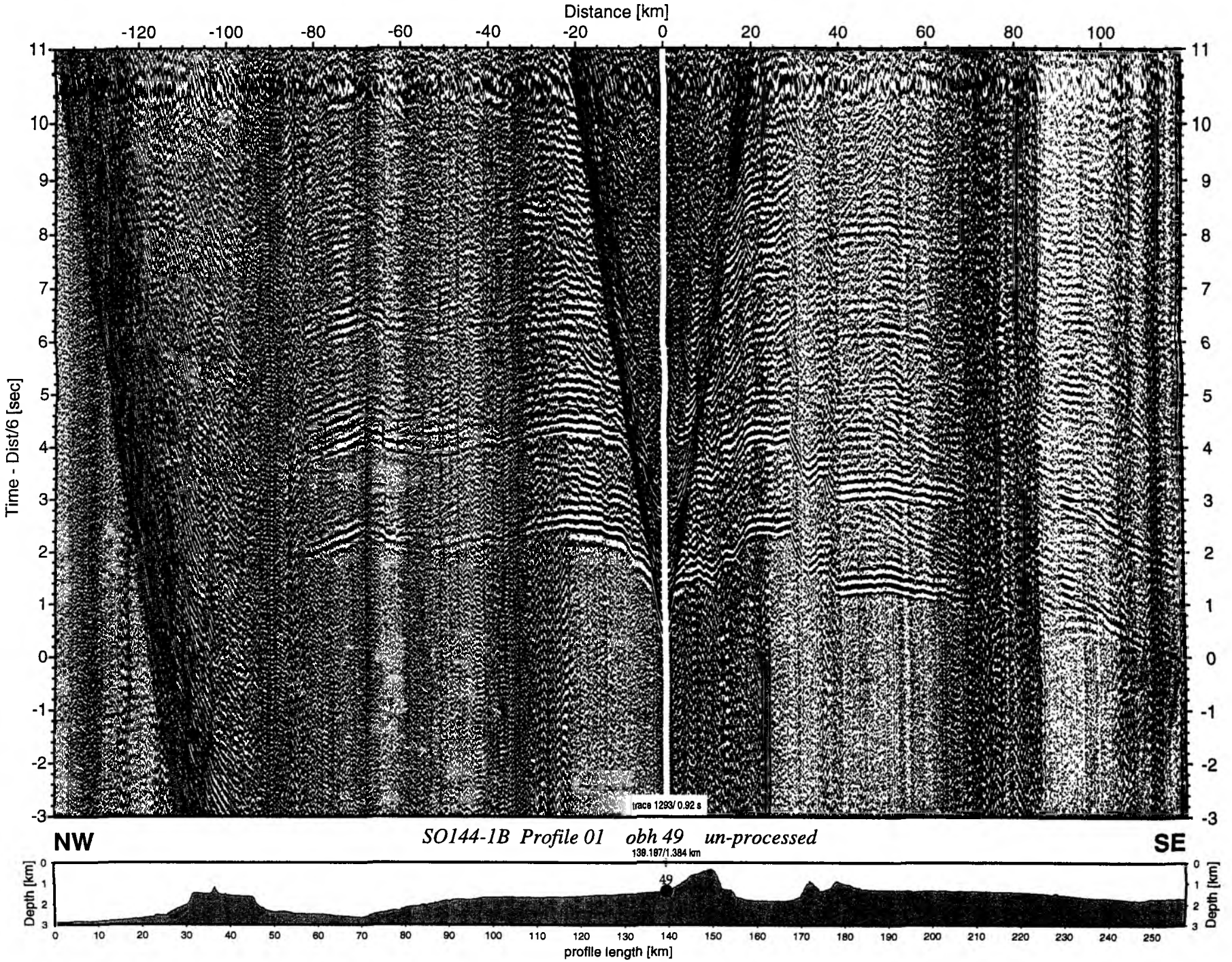

Figure 6.2.2.2: Record section from obh 49 , Profile 01 un-processed.

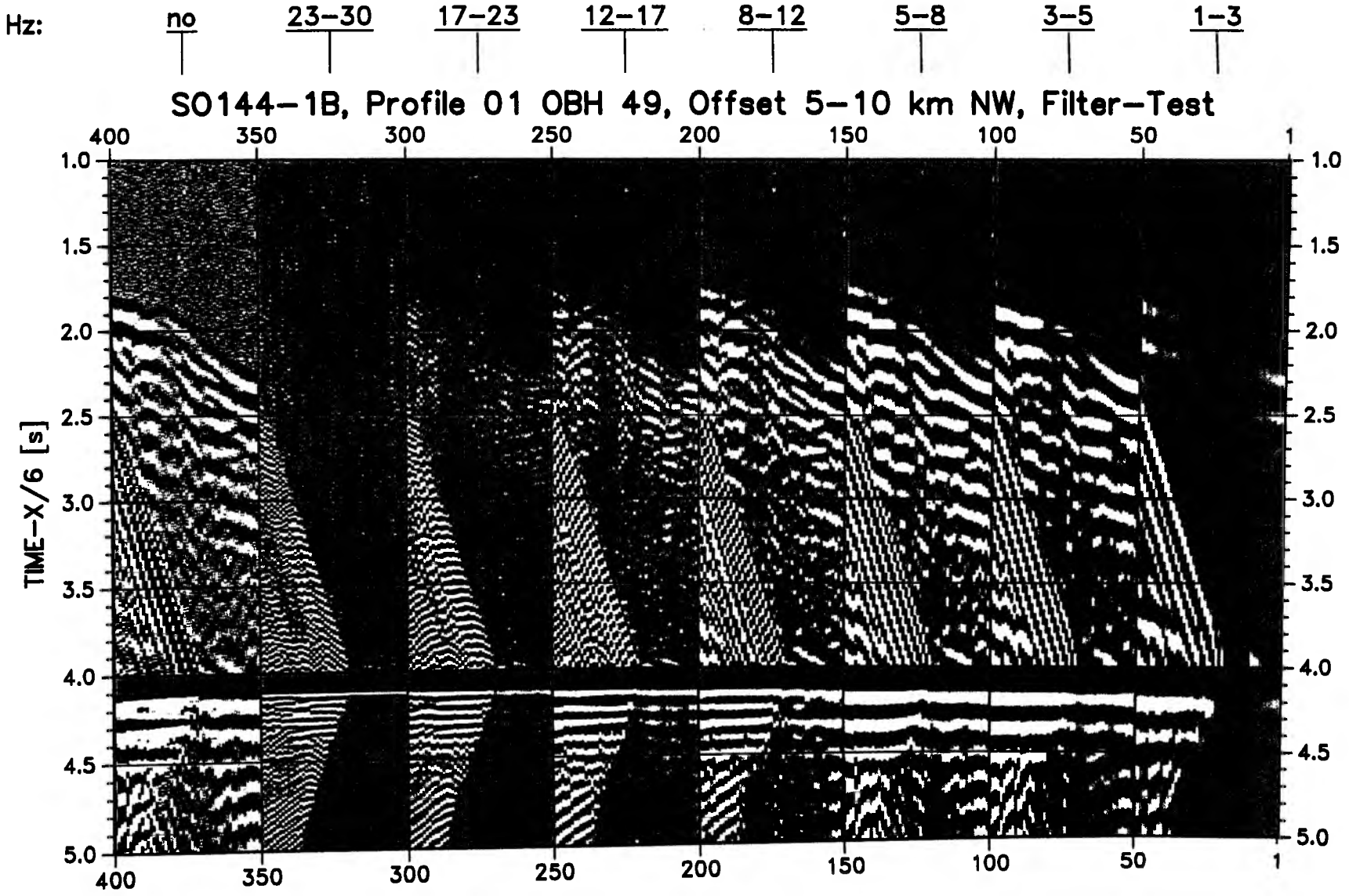

Figure 6.2.2.3: Filter test panels in the offset range 5-10 km northwest.

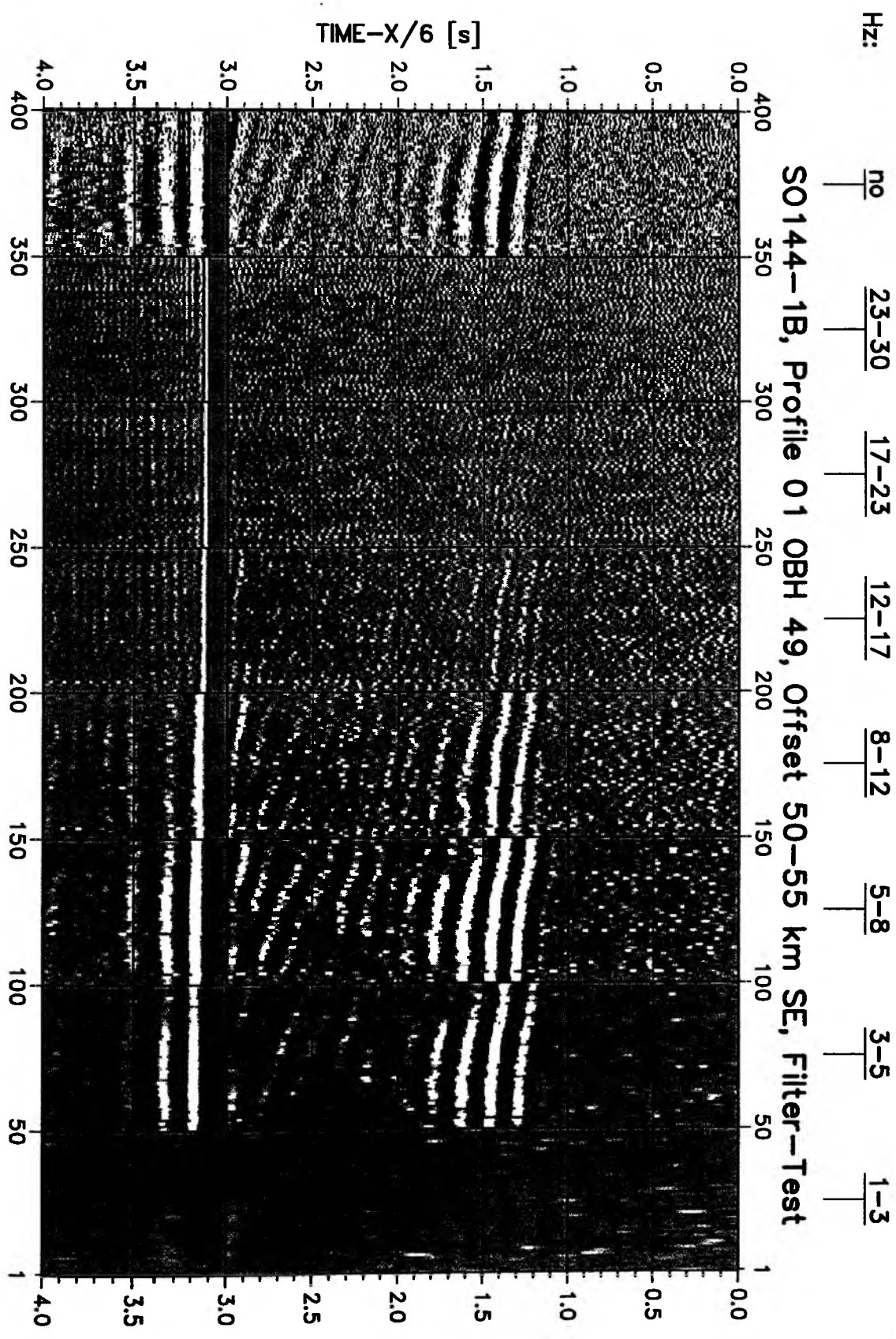

Figure 6.2.2.4: Filter test panels in the offset range 50-55 km southeast.

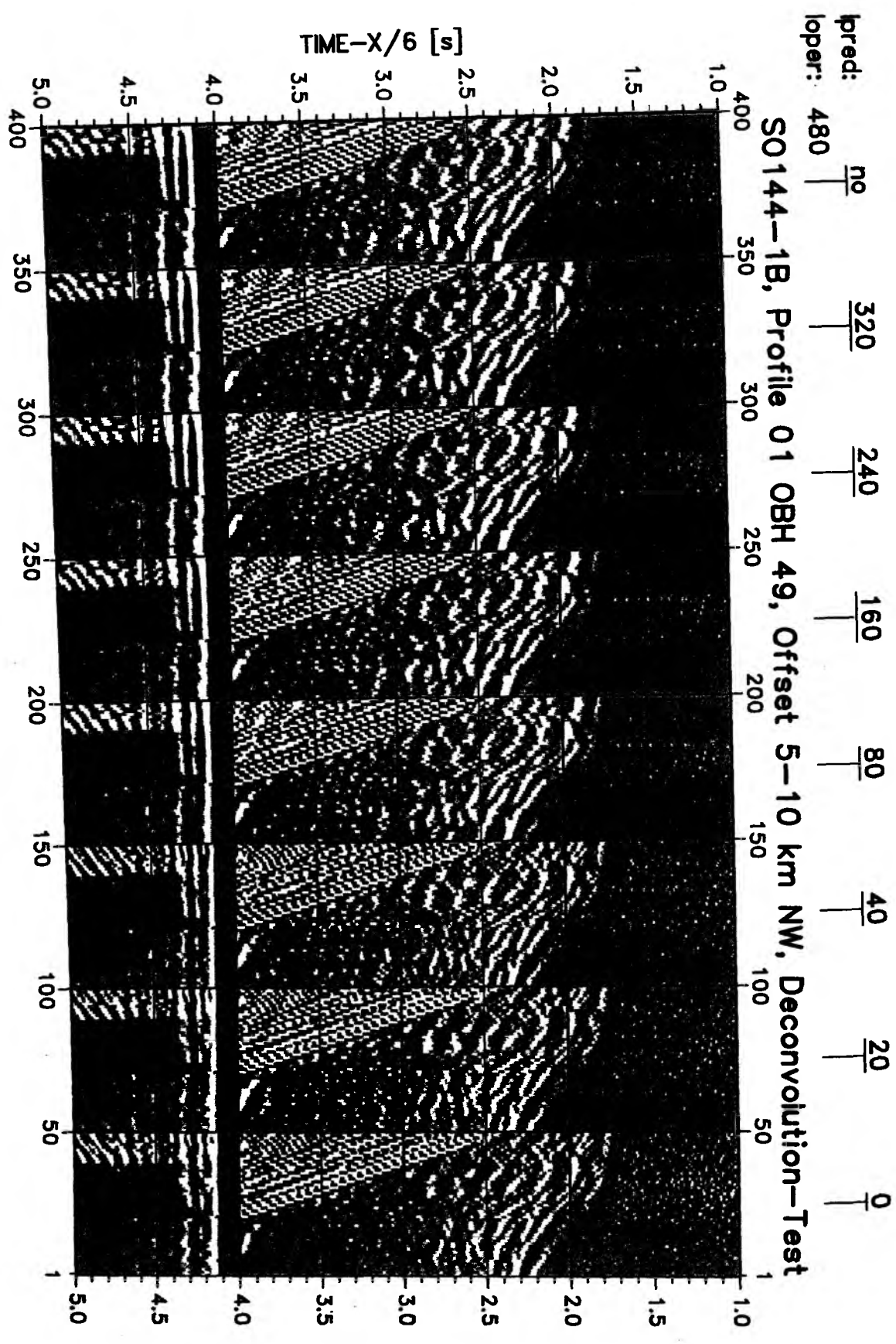

Figure 6.2.2.5: Deconvolution test panels in the offset range 5-10 km northwest.

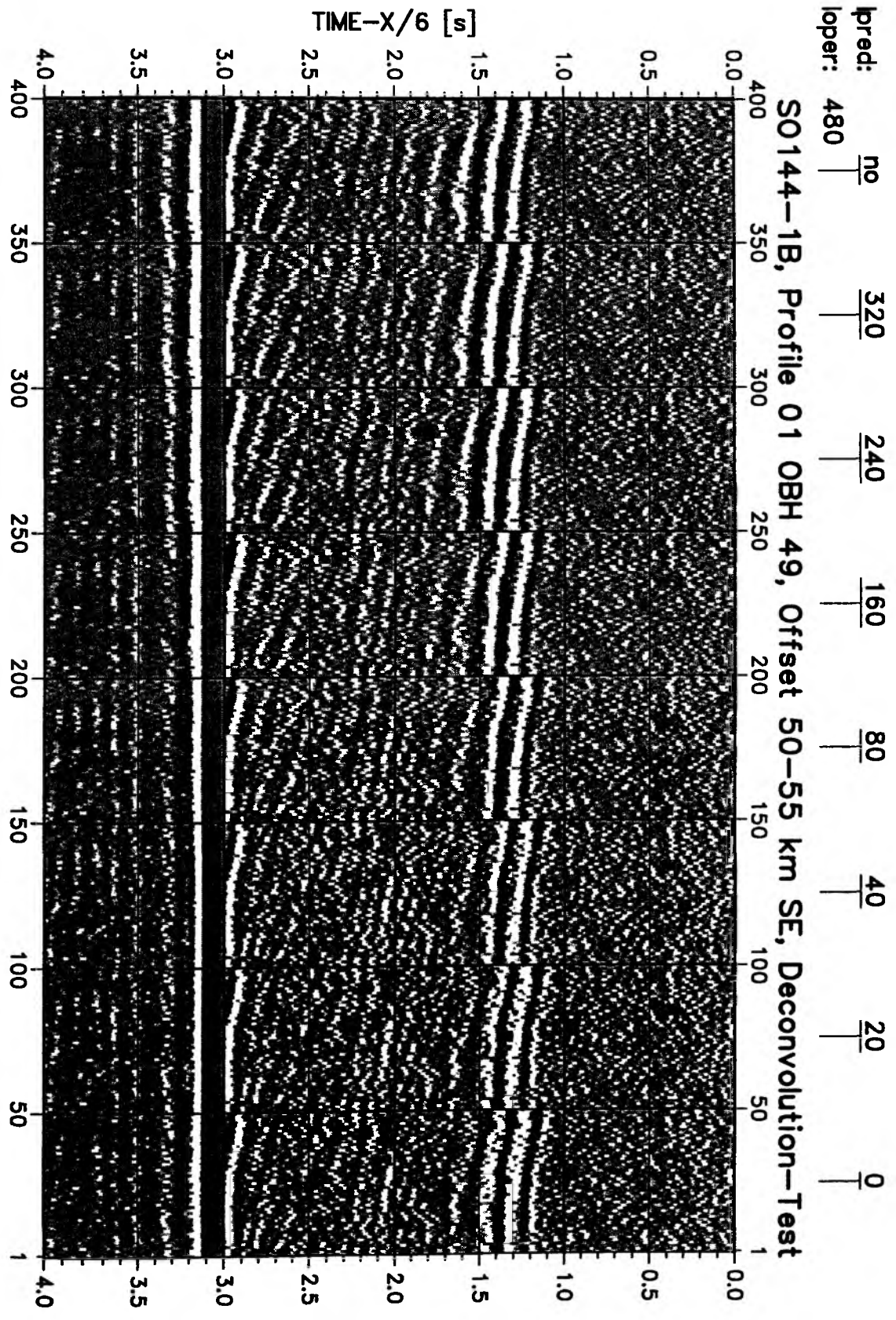

Figure 6.2.2.6: Deconvolution test panels in the offset range 50-55 km southeast.

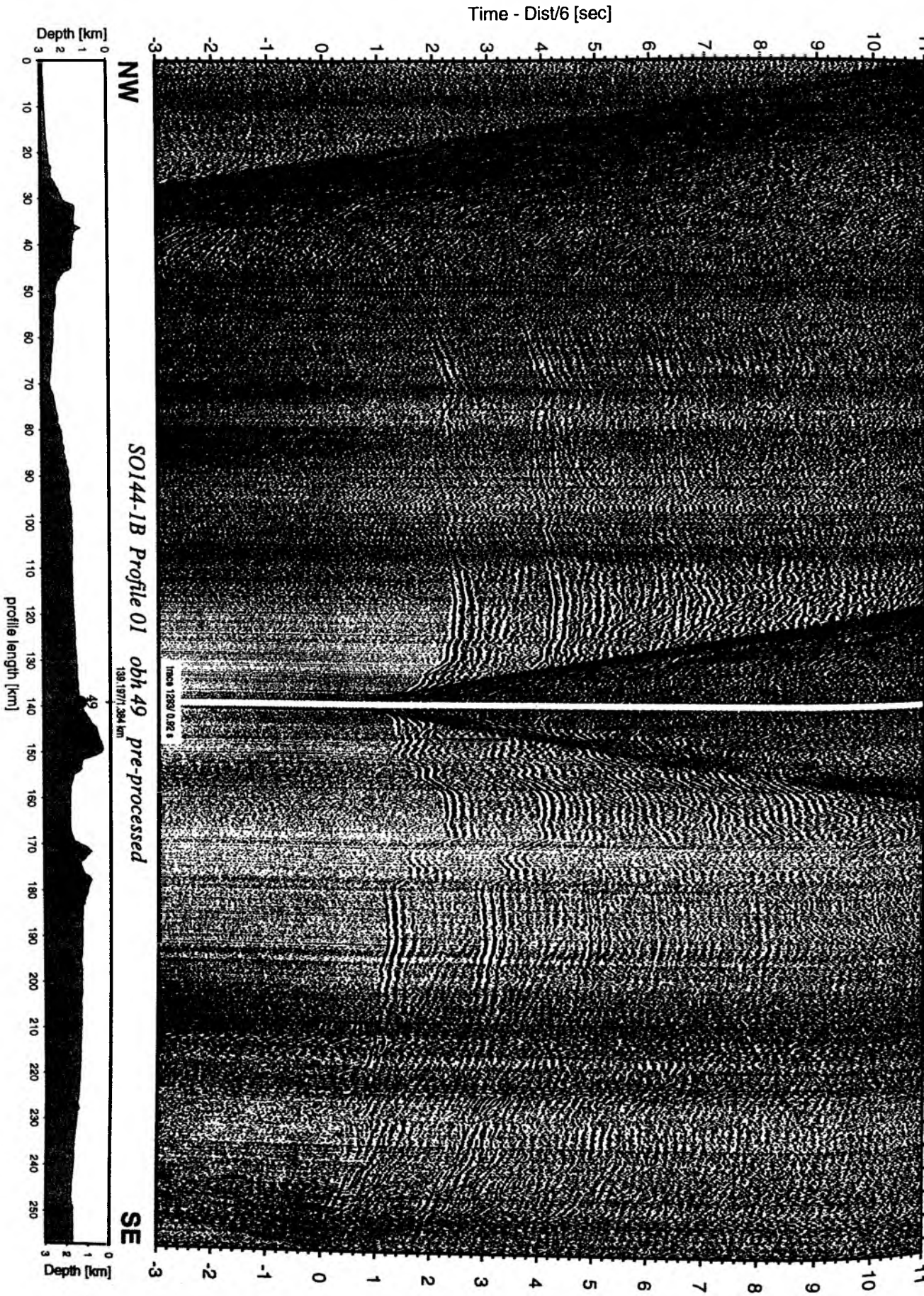

Figure 6.2.2.7: Record section from obh 49 , Profile 01 pre-processed.

6.2.3 WIDE-ANGLE DATA MODELLING

The OBH/OBS data have been analyzed for crust and upper mantle velocity structure. The modelling sequence of the wide-angle data involves three different steps:

A) Picking: The traveltimes of the observed phases are picked interactively on the workstation's screen using Seismic Unix Software. This provides ASCII files, containing offsets and traveltimes of phases for each record, which will be used for the modelling.

B) 1-D modelling: 1-D velocity-depth modelling has been performed on some of the record sections. This first approach to determine the velocity structure along the different lines allows to define preliminary velocity-depth models, which are used as the starting point during the 2-D modelling.

The software used for this purpose is an interactive program "MacR1D" (J. Luetgert, 1992) for calculating travel-time curves from 1-D velocity-depth functions. I allows to quickly manipulate velocity-depth functions and immediately see the resulting travel-times, which gives useful insights into the effects of changing gradients, low-velocity zones, etc.

C) 2-D modelling: Models have been created for some of the lines. For the modelling water depths are taken from UKOOA-files. The models are capable of predicting the correct offset/time of as many of the observed phases as possible. Two different programs have been used to trace rays in 2-D media: "MacRay" and "Rayinvr". Another method for inversion ("Raytomorf") was also applied to find a starting model for detailed forward modelling.

-- "MacRay" (J. Luetgert, 1992) is an interactive application for calculating travel-time curves from 2-D velocity models. It is based upon the RAY84 and RAY86 seismic ray tracing programs written for a DEC VAX/VMS environment and adapted to the Apple Macintosh graphical interface for display and manipulation of velocity models.

Velocity models are defined by two or more interfaces extending across the model. Any pair of successive interfaces describes a layer, within which velocity may be defined in terms of the velocity at the top and bottom of the layer. Within any layer the velocity may be inhomogeneous but continuous. First or second order discontinuities in velocity may occur at interfaces. A ray tracing algorithm is used that calculates the propagation of rays within a layer by the stepwise integration of a system of first order differential equations (Cerveny et al., 1977). Lithologic interfaces are represented in the model as first or second order velocity discontinuities. When an interface is encountered in the calculation of a ray, Snell's law is applied and the calculation is continued. "MacRay" is very useful for quickly manipulating velocity models.

-- "Rayinvr" is a program to trace rays for rapid forward modelling and inversion of refraction and reflection travel times (Zelt and Smith, 1992; Zelt and Forsyth, 1994).

The program assumes a 2-D (x,z) isotropic medium and the velocity model is composed of a sequence of layers separated by boundaries consisting of linked linear segments of arbitrary dip. The velocity within a layer is defined by velocity values specified at arbitrary x-coordinates along the top and bottom of the layer. For the purposes of ray tracing, the model is automatically broken up into an irregular network of trapezoids, each with dipping upper and lower boundaries and vertical left and right sides. The velocities at the four corners of each trapezoid are used to interpolate a velocity field between the trapezoid so that the velocity varies linearly along its four sides. Therefore, horizontal as well as vertical velocity gradients may exist within a trapezoid. Ray tracing is performed by numerically solving the ray tracing equations for 2-D media using a Runge Kutta method. The partial derivates of travel time with

respect to those model parameters selected for adjustment are calculated analytically during ray tracing; these parameters include velocities and the vertical position of boundary nodes. The traveltime residuals with respect to the observed data are also calculated. They are used later to update the model parameters by applying the method of damped least-squares to the linearized inverse problem. The algorithm can include any type of arrival, including multiples and/or converted shear waves.

As a first approach, we have performed velocity-depth modelling through classical forward analysis of arrival times. Finally, an iterative damped least-squares inversion procedure is applied to optimize the velocity and depth values.

-- "Raytomorf" is a two-dimensional inversion routine based on a finite-difference solution for inversion of the velocity field. The finite-difference algorithm is based on equations developed by Vidale (1988). Based on a gridded velocity field the travel time field is calculated with the use of an expanding square. Starting from a point source, fd equations are used to calculate travel times to the neighbouring grid nodes. The nodes are selected according to the scheme of an expanding square where the nodes located on the sides of the square are used. Ammon and Vidale (1993) modified the set of fd equations in order to handle media with strong velocity variations. After determination of the travel time field, rays are traced through and ray length segments are computed for each cell of the velocity model. Then the ray length matrix is inverted for a set of slowness correction values. The inversion of the slowness correction vector can be performed using Singular Value Truncation, Damped Least Squares or Conjugate Gradients (LSQR). Due to the large number of observations the LSQR method was chosen. The code enables to vary the weighting factor for minimization of the Laplacian smoothness of the slowness correction vector as well as the number of iterations in the LSQR matrix inversion. The program was applied within a recursive loop using the last inverted model as the input to the next run.

6.2.4 SEISMIC PROFILES

6.2.4.1 PROFILE SO144-6-1, 6-2 & 6-3

During cruise SO107 one wide-angle seismic line was shot along-dip of the Nicaragua margin and two strike lines on top of the shelf (Walther et al., submitted). Interpretation of the dip line reveals a mantle sliver rising to 12 km depth and coinciding with the down-dip limit of the seismogenic zone. The strike lines were laid out with instruments 15 nm apart. Owing to the high noise level in the shallow water (100 –130 m), low-energy penetration and side-lopes interpretation of these lines was not continued.

During the same cruise, OBH instruments were also deployed some 15 miles along strike line A. During cruise SO144, 7 GÉO AZUR OBS (Fig. 6.2.4.6.1) were deployed to fill the gaps between the earlier SO107 OBH positions giving a total instrument spacing of 7.5 nm (Fig. 6.2.4.6.1). Two OBS elongated line SO144-6-1 SE towards the Nicoya peninsula with 58 nm total length. The position of the second strike line SO144-6-3 was chosen slightly landward of the mantle sliver crest but seaward of the highly-faulted area interpreted from the ST8910-215 MCS line (Ranero et al., in press) around the Corvina-2 drill hole. 18 GEOMAR OBH and 2 GEOMAR OBS were deployed over a distance of 105 nm. Position OBH01 was as close as 10 nm to the coast of Nicoya peninsula. All positions were at relatively shallow water depths between 85 m and 170 m. Therefore, a high noise level could be expected. See Appendix 9.1.1 for details.

For the active wide-angle experiment, three 32 l (2000 cu. in) *BOLT* airguns were available - two from GEOMAR and one on loan from the Institute for Geophysics at the University of Texas, Austin. Although all airguns were tested before deployment, several bursts of the pressure hoses allowed operation of only two guns for the first part of the experiment. Airgun shooting started on the 17 September at 15:40 UTC time at the SE end of line SO144-61 with two airguns in operation. SONNE sailed at 3.5 kn speed over ground and shots were fired every 60 s resulting in a shot spacing of 108 m. The starboard airgun failed at 19:06 UTC on 17 September and was taken into operation again on the 18th at 02:46 UTC. As the third airgun could not be repaired quickly the magnetometer was deployed on the 18th at 05:38 UTC with a cable length of 100 m because of shallow water. On 18 September at 19:11 UTC the third airgun was deployed. Due to continuous auto triggers the port gun had to be turned in on 19 September at 03:45 UTC as well as the center gun on 19 September at 11:11 UTC. Both airguns needed to be opened for repair of internal sealings, which could not be accomplished before the end of the line. Airgun shooting terminated at 19th Sept. 16:40 hrs UTC time. For further details see Appendix 9.2.1.

Soon after airgun recovery, the first GEOMAR OBH were released. The operation was continued until 17:00 hrs local time when SONNE had to return to the location of the GÉO AZUR instruments released on preprogrammed clock. Because they were only marked by flashlight and radio beacon, it was decided to recover them during the night hours. All of them appeared at the surface on schedule and could be picked up within 10 minutes by the use of a Zodiac. The remaining GEOMAR OBH were recovered during daylight on 20 September. All units had been recovered safely by 11:30 UTC.

Preliminary modelling of Profile 6-1

The data quality along Profile 6-1 is variable along the line, as can be seen in the record sections (Figures 6.2.4.1.2 to 6.2.4.26), but tends to be better toward the southeast. The seven IRD seismographs all recorded four components of data, vertical, two horizontal, and hydrophone channels. Interestingly, the hydrophone channel was clearer and less noisy on all records, so it has been used for all interpretations of this profile. All instruments recorded

good near-offset reflections from within the sedimentary section and at its base , and excellent refracted arrivals through this section. OBSs 21 and 22 recorded clear arrivals only to offsets of 25-30 km, although additional signal processing may bring out some interpretable arrivals at larger offsets. OBSs 23 and 24 are generally better, with clear arrivals to 45-55 km, however the first arrival is not continuous because of noise, structural complications, or just low amplitude. OBSs 25, 26, and 27 recorded the best data sets of the profile with coherent arrivals of up to 100 km offset. Even with generally better data quality the records are complicated and the first arrivals are not continuous across each section. Perhaps the most outstanding feature of these records are the deep secondary arrivals, presumably reflections. These arrivals most likely mark the base of the upper plate and possibly the top of the subducting Cocos plate mantle.

The main purposes of this profile are to determine the velocity structure of the upper plate and identify structural or velocity variations along strike. This will suggest the crustal lithology and allow comparison with neighboring Costa Rica. A specific goal is to determine whether the mantle slab interpreted by Walther et al. (submitted) is present in this part of the forearc. Another primary aim is to locate the depth of the Cocos/Caribbean plate boundary at this position approximately 70 km from the Middle America Trench.

As noted above, the records along profile 6-1 are rather complicated, so the shipboard interpretation must be considered quite preliminary. The starting model for travel time modelling was derived from intersecting dipline L that had previously been interpreted by Walther et al. (submitted). The velocity at the intersection was extended as a 1-D model and travel time modelling was performed using Rayinvr (Zelt and Smith, 1992), using over 4300 travel time picks to constrain the model. The sedimentary section was easily modelled using reflections from the base of the section and refractions from within the sedimentary layer and through the higher velocity material (basement?) below (Figure 6.2.4.1.27). The velocities in this layer range from about 1.7-3.7 km/s, and show a strong gradient with depth. The velocity variation coincides with the thickness variation of the section, which is a minimum of 2.8 km but reaches 6.1 km near the SE end of the profile. The next layer, tentatively interpreted as the top of basement, has intermediate velocities of 4.1-4.7 km/s, and is determined by an arrival that is present to offsets of < 20 km. This unit is relatively thin, especially near the NW end of the line, and appears to have a maximum thickness of < 3 km. The next deeper layer appears to be the middle crust of the upper plate (Figure 6.2.4.1.27). It has velocities of about 5.6-6.0 km/s and the thickness is roughly estimated at 6-8 km. At this time the base of this layer is poorly determined because of difficulties in correlating arrivals from instrument to instrument in detail and the variation in apparent velocity caused by the morphology of the basement surface. Deeper layers are not well defined because on most sections the first arrivals are not clear to offsets greater than about 40 km. However, several sections show apparent secondary arrivals, interpreted to be reflections, at intermediate to far offsets (Figure 6.2.4.1.2-7). Assuming a velocity of 6.8 km/s for the fourth layer, deeper arrivals on several of the record sections appear to mark a boundary at 20-22 km. In a first interpretation, if this layer is assumed to extend to the base of the upper plate and the underlying layer is given velocities corresponding to subducted oceanic crust of 5.8-6.8 km/s at its top and bottom, then some additional deep arrivals appear to mark a boundary still deeper at roughly 30 km. Thus, in a preliminary interpretation, the plate boundary may be marked by reflections at about 20-22 km depth, with the top of oceanic mantle near 30 km. This interpretation should be significantly refined with a more detailed correlation of events from station to station and a better definition of the basement surface using coincident seismic reflection data. This interpretation is generally consistent with the model of Walther et al. (submitted), but the presence or absence of a body of mantle material in the upper plate has not been clearly indicated along this section so far.

Preliminary 2-D Modelling of Profile 6-3

The record sections of Profile 6-3 are shown among Figures 6.2.4.1.2 to 6.2.4.26. Most show a high noise level because of the shallow water depth. This is also the reason for the up to 1-sec-long reverberations that could be slightly reduced by deconvolution. The varying number of firing airguns does not show an obvious effect in the seismograms. Range 0 – 39.5 km was shot with 2 airguns, range 39.5 – 94.8 km with 3, range 94.8 — 143.2 again with 2 and from 143.2 to the end of Profile 63 only one airgun was fired.

The first arrivals in the near offset range show low velocities and represent layers of the upper part of the sedimentary Sandino Basin. Apparent velocities range from values slightly above the water velocity up to 3 km/s. A first remarkable phase change appears at about 10 – 15 km offset, where velocities increase to 4 – 5 km/s. This phase is followed by an almost horizontal event in the time-reduced seismograms (Vred=6 km/s). This phase shows very clearly in the SE of the profile, but gets weak and hardly detectable in the northwest part. Beyond that phase, some weak and isolated energy can be traced in a short offset range, but not for all OBHs. In general ,clearly detectable phases in the seismograms are restricted to a maximum offset of 40 – 60 km. They reflect the shallowing Sandino Basin from NW to SE and mark its lower boundary.

The picking accuracy was better than 50 ms for first arrivals in the near offset range, with apparent velocities of < 6 km/s, deteriorating to 50 - 100 ms for phases around 6 km/s apparent velocity. Events beyond 40 km offset had only weak energy and low frequencies of about 5 Hz. Picking these events could be achieved only in a small range of 10 – 15 km and the inaccuracy could increase to 200 ms by picking wrong wavelets. The high noise level and long reverberations prevented the determination of near-vertical reflections. When completed, 2650 picks were extracted from the 15 available seismograms of Profile 6-3 (Fig. 6.2.4.1.28 a).

A preliminary 2-D model for Profile 6-3 has been developed on board of RV SONNE (Fig. 6.2.4.1.28 b). The starting model was the 1-D velocity-depth function at the intersection of Profile 6-3 with the dipline L. The intersection is near to OBH 16, at 36.1 km on Profile 6-3 and at 181.4 km on Profile L. Borehole Corvina-2 is 2.7 km away to the NE. The model orientation is from NW to SE. Modelling was done from top to bottom.

The prelimiary model shows the following results:

- The upper sedimentary unit of the Sandino Basin has velocities increasing from 1.6 km/s at the top to 3 km/s at the bottom and a high velocity gradient of 0.15 – 0.3 s^{-1}.
- The upper sedimentary unit is 4 km thick in the northwestern half of the profile but thins out to less than 1 km at the southeastern end. towards the Nicoya Peninsula.
- The lower sedimentary unit is remarkably higher in velocity and takes mean values from 5.0 km/s in the NW, to 4.5 in the SE.
- In the NW of the profile, an intermediate layer had to be introduced with velocities from 3.8 – 4.2 km/s. When the top of this layer is transformed to two-way-traveltime and compared to MCS line ST8910-215, it coincides with a prominent reflector within the Brito formation marking a Middle to Late Eocene boundary.
- The depth of the Sandino sedimentary basin could be well imaged because of the pronounced refraction from the underlying basement. In the NE the basin reaches 11 km thickness. To the SE the basin shallows to 5 km depth.
- The underlying basement shows an almost constant velocity of 6.3 – 6.6 km/s, with a very low or even non-existing gradient. This velocity value could

be either interpreted as lower continental or lower oceanic crust. The relatively shallow depth of the top of this layer, 5 km in the SE and 11 km in the NW, and the geoevolutionary background which assumes an attached oceanic plateau (Walther et al., submitted), point to lower oceanic crust.

- Another discontinuity is seen at about 20 km depth. It matches the isolated wide-angle reflections occuring in the 40 to 60 km offset range. The velocity below remains presently unresolved.

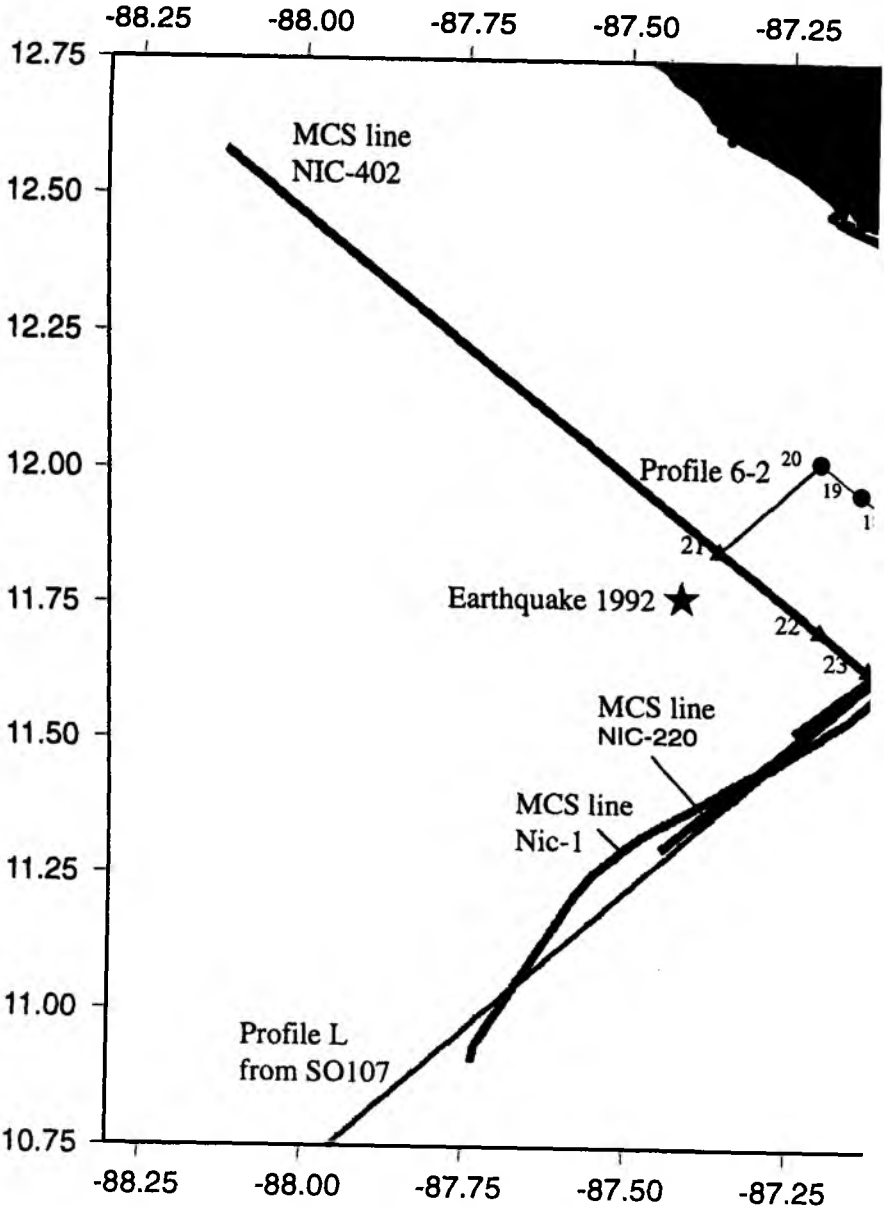

Figure 6.2.4.1.1: Location map for the seismic wide angle investigation during SO144-1a and nearby MCS lines.

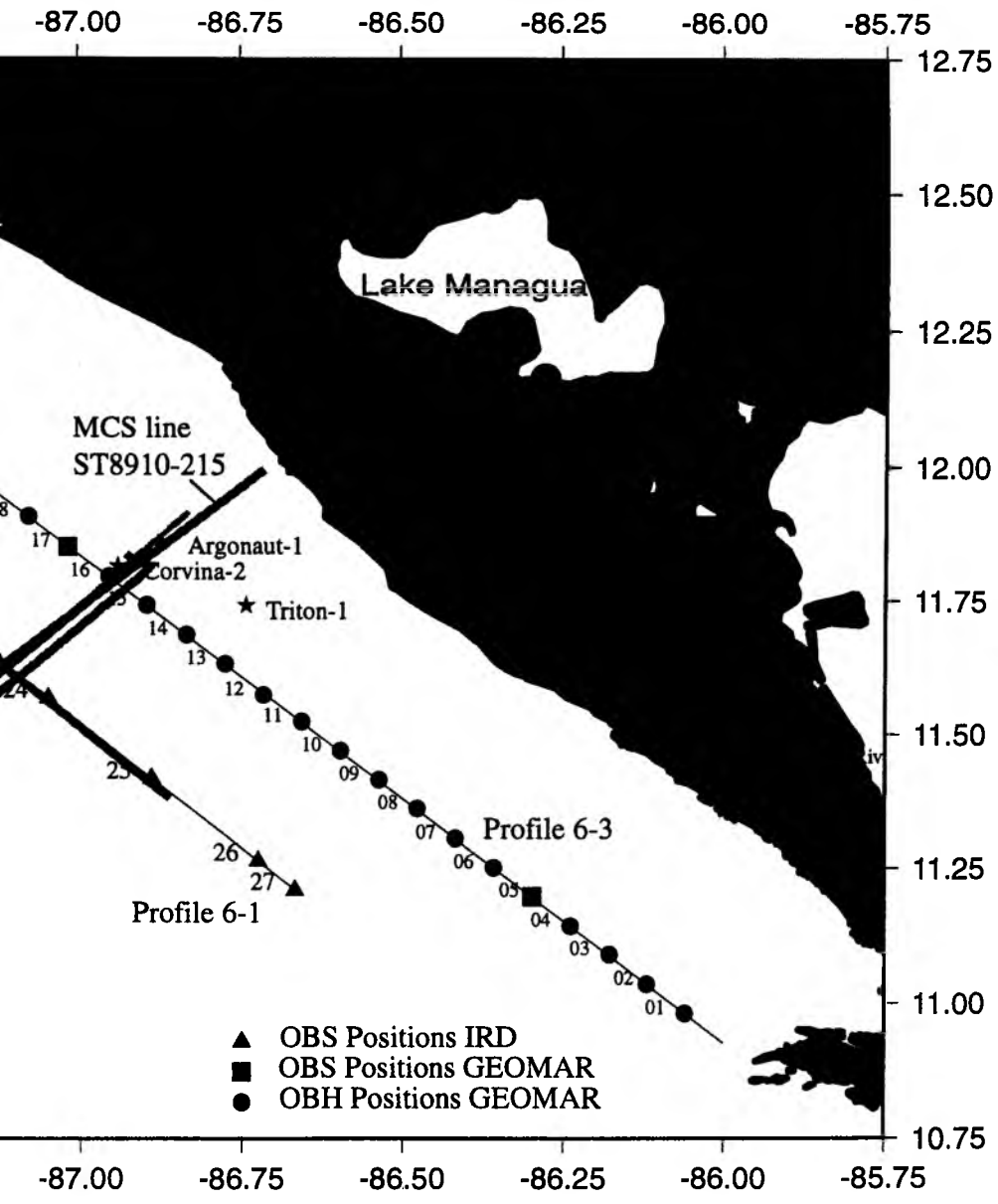
-87.00
-86.75
-86.50
-86.25
-86.00
-85.75
12.75
12.50
12.25
12.00
11.75
11.50
11.25
11.00
10.75
Lake Managua
MCS line
ST8910-215
Argonaut-1
Corvina-2
Triton-1
Profile 6-3
Profile 6-1
OBS Positions IRD
OBS Positions GEOMAR
OBH Positions GEOMAR

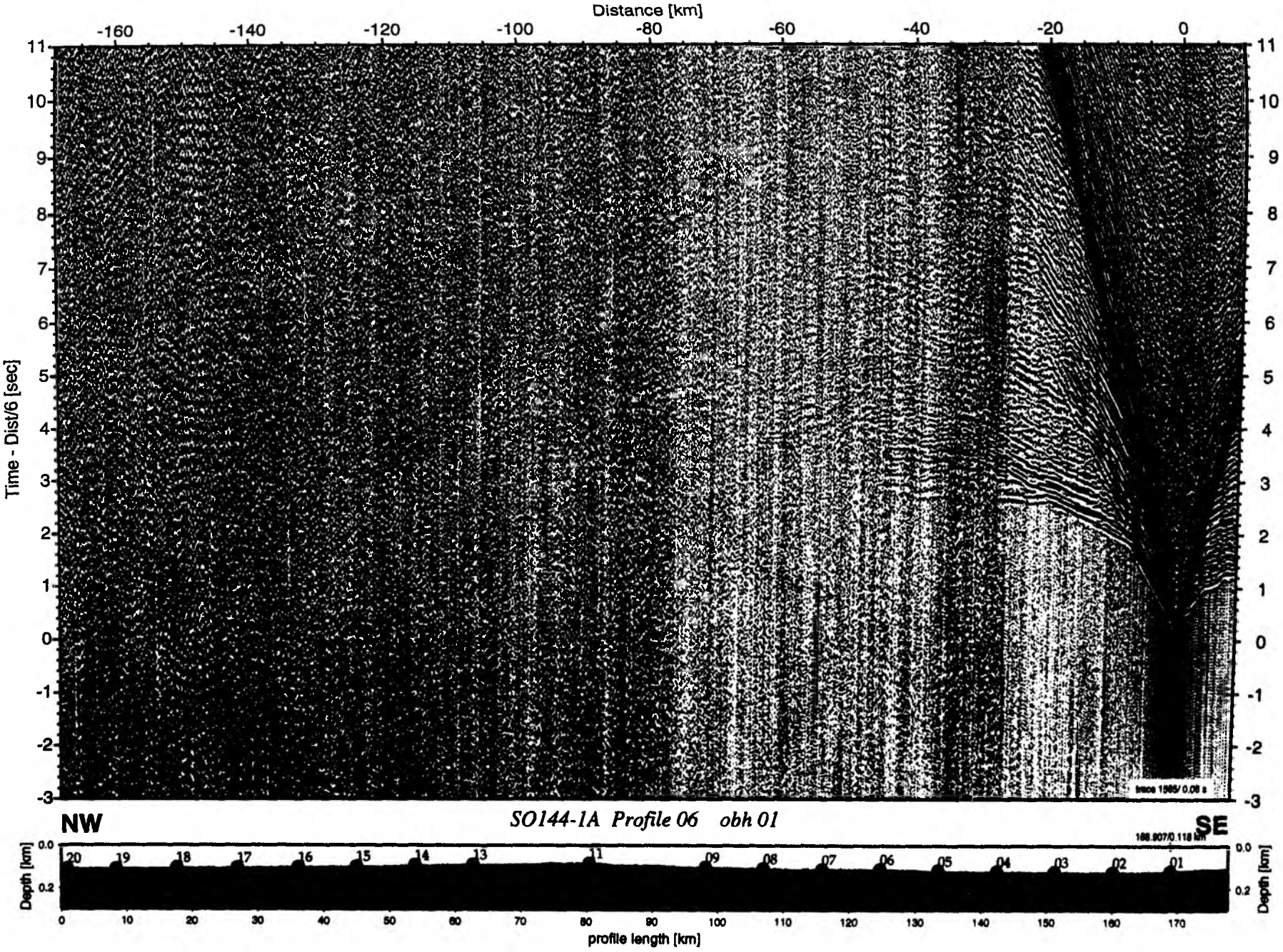

Figure 6.2.4.1.2: Record section from obh 01 , Profile 06.

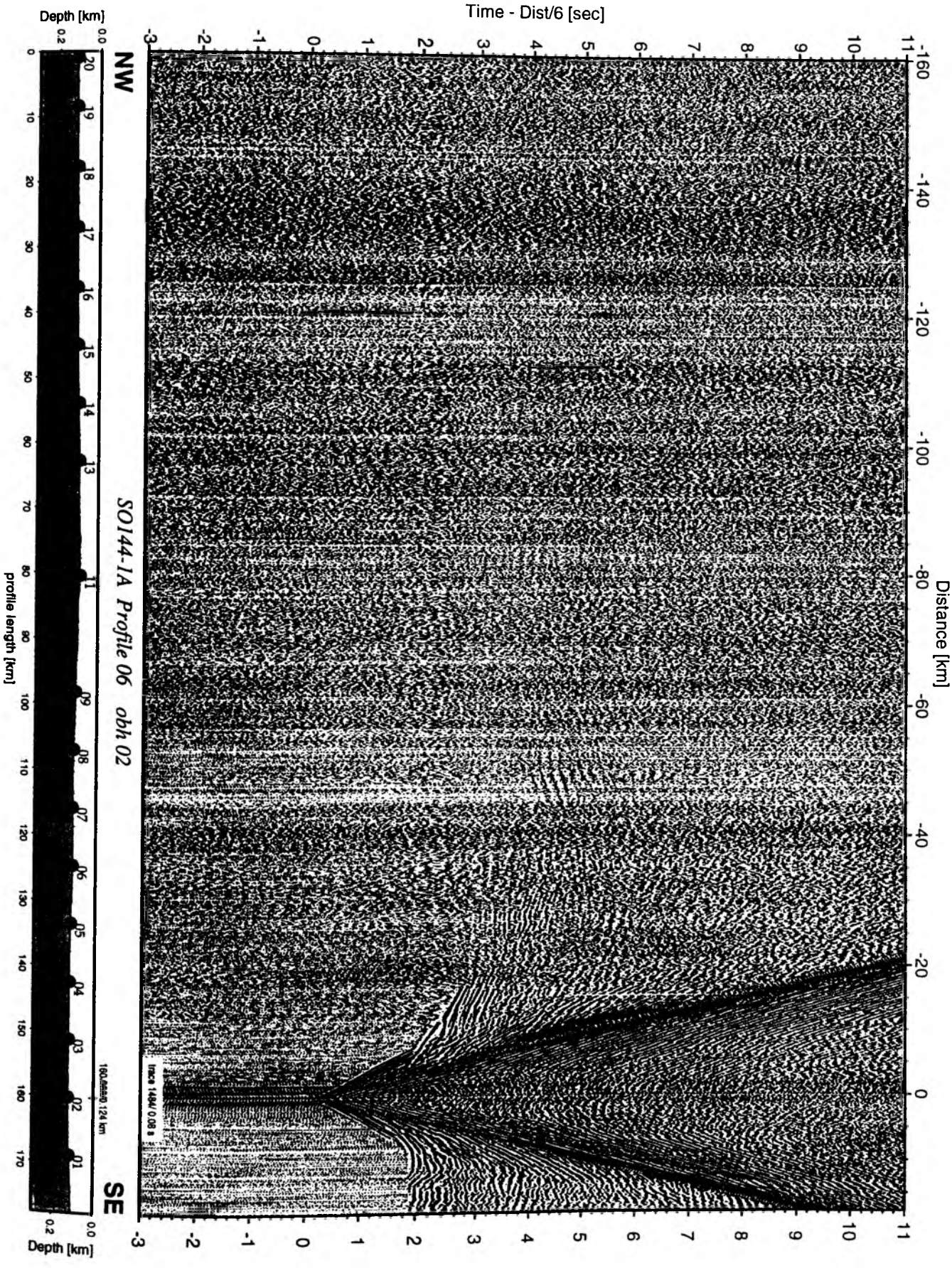

Figure 6.2.4.1.3: Record section from obh 02 , Profile 06.

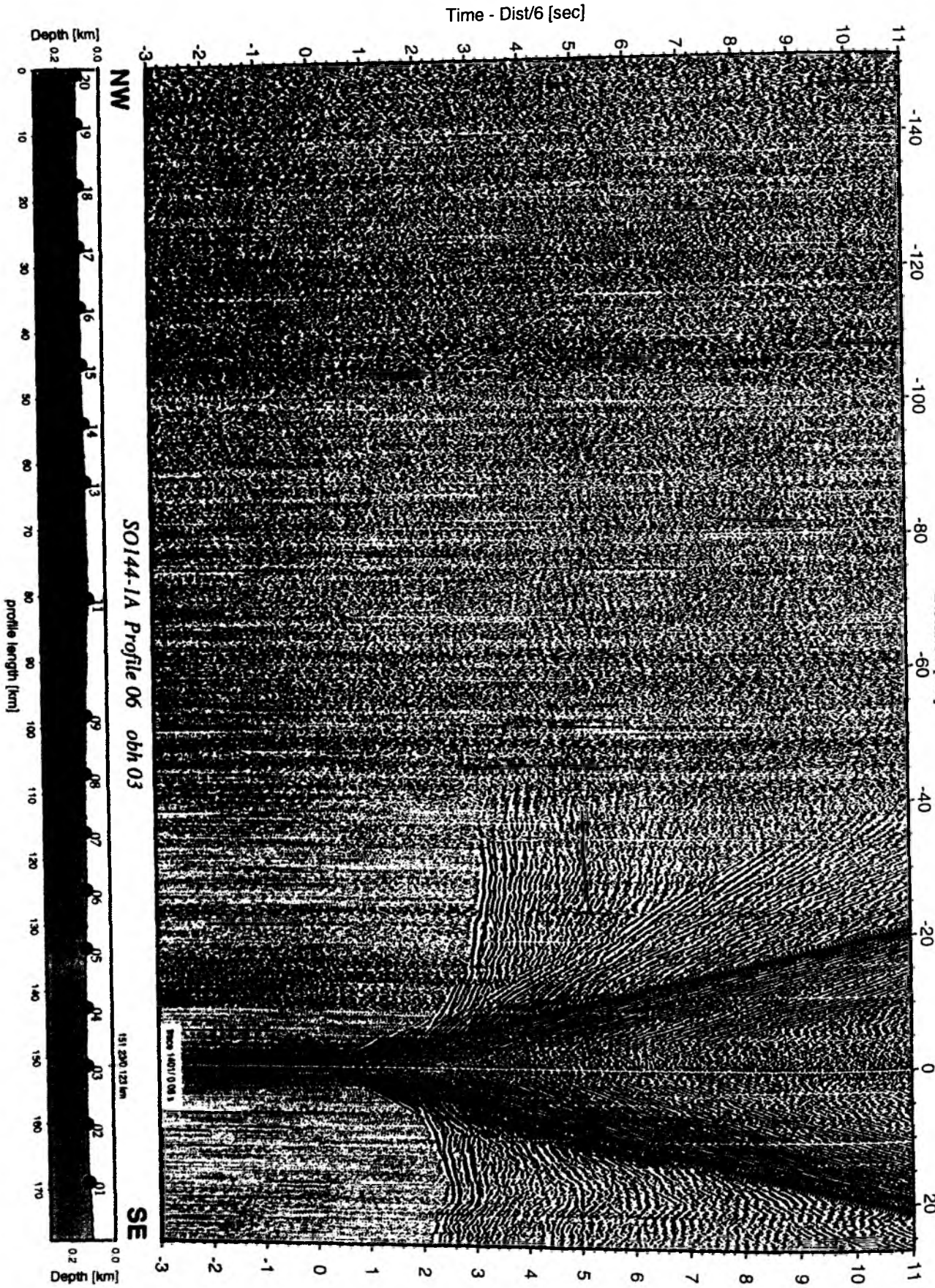

Figure 6.2.4.1.4: Record section from obh 03 , Profile 06.

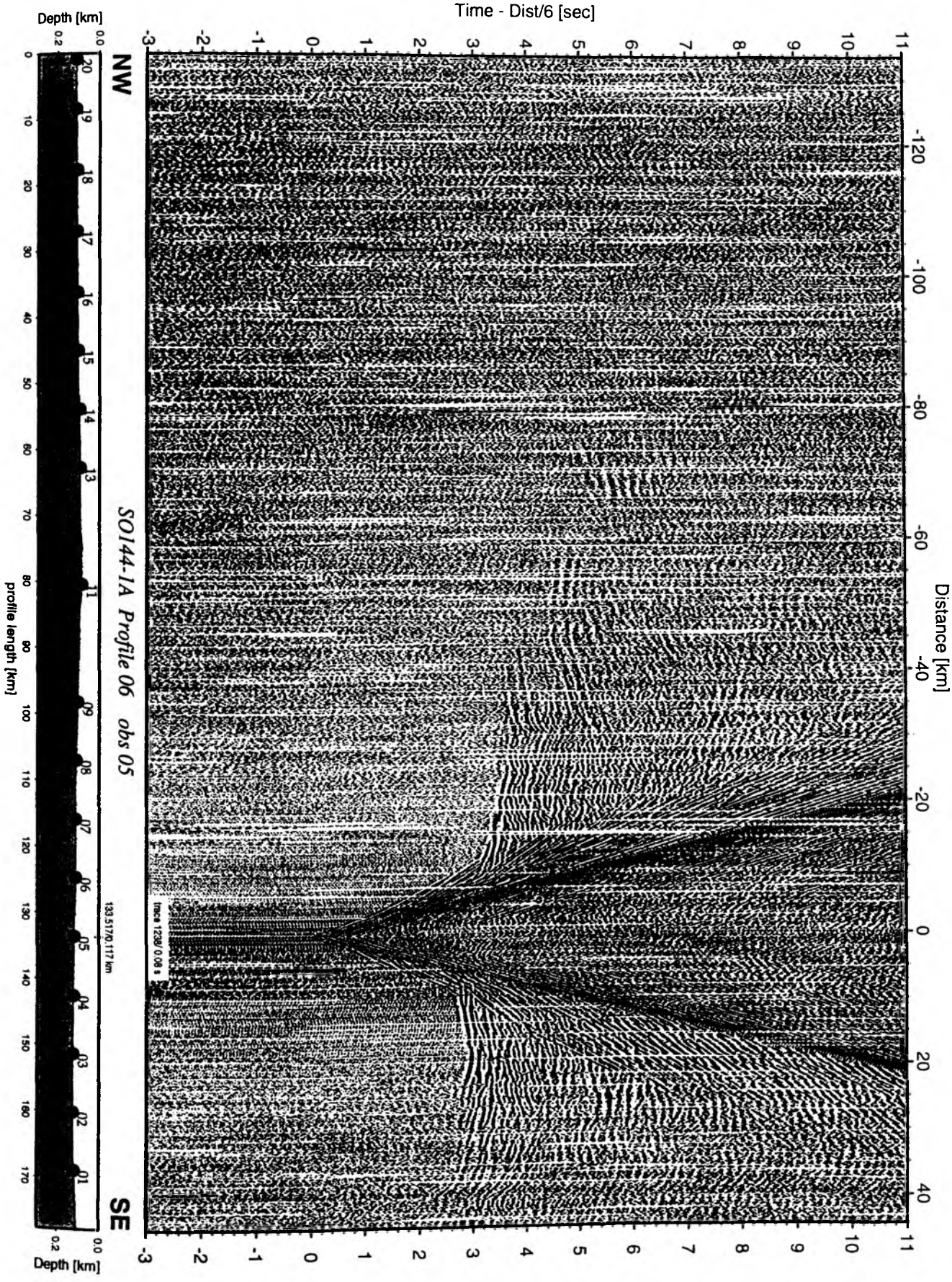

Figure 6.2.4.1.5: Record section from obs 05 hydrophone, Profile 06.

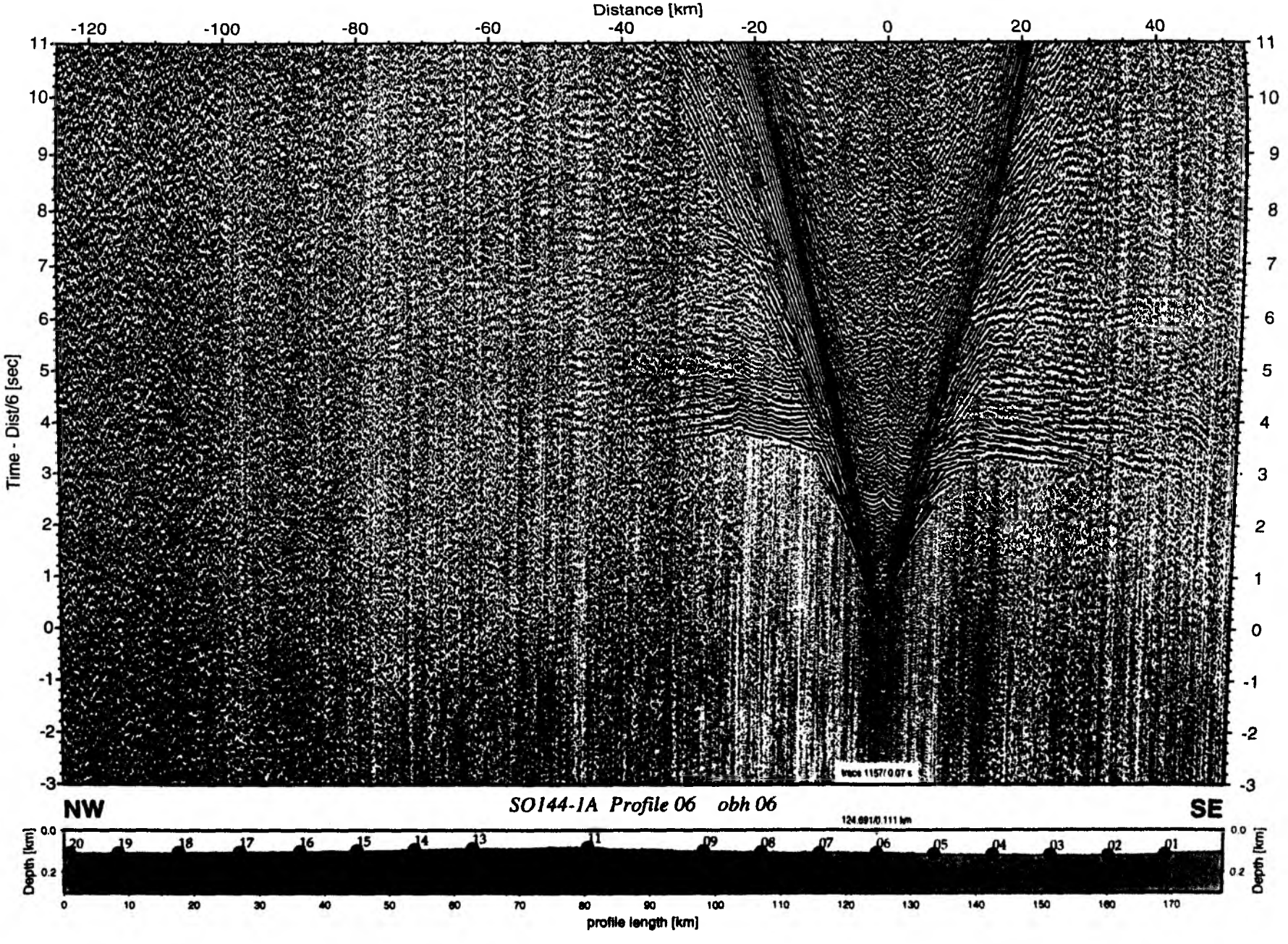

Figure 6.2.4.1.6: Record section from obh 06 , Profile 06.

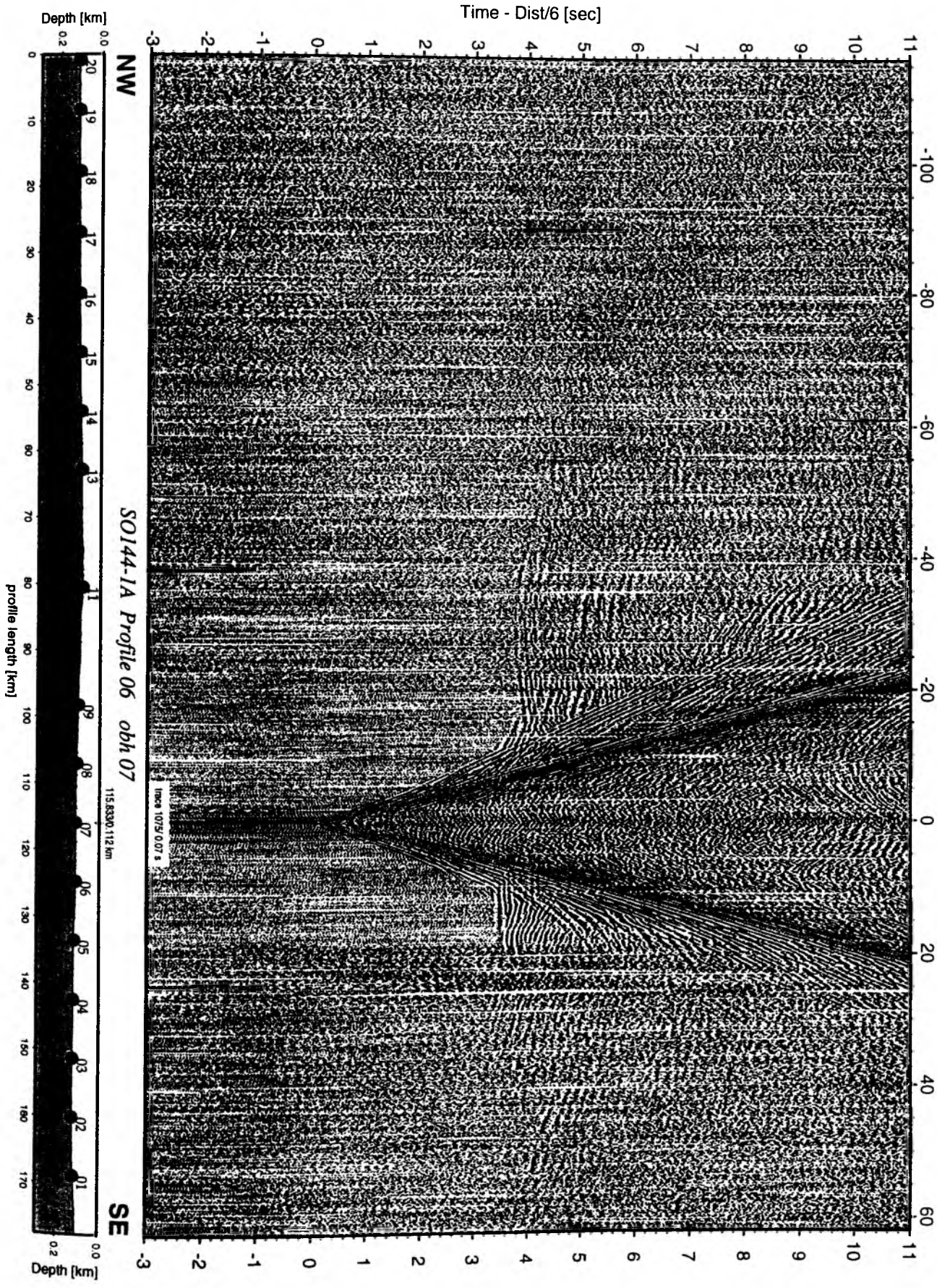

Figure 6.2.4.1.7: Record section from obh 07 , Profile 06.

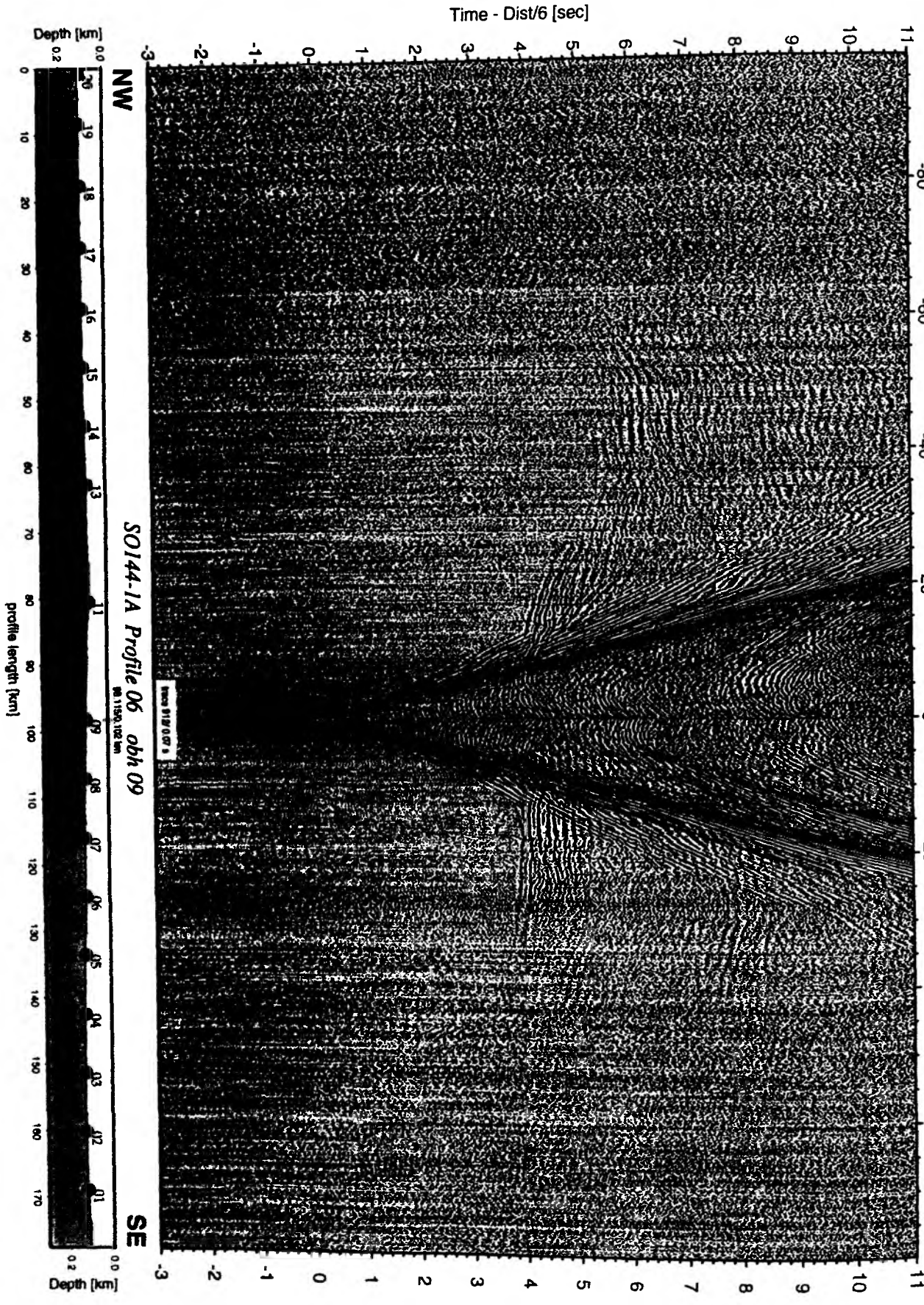

Figure 6.2.4.1.8: Record section from obh 09 , Profile 06.

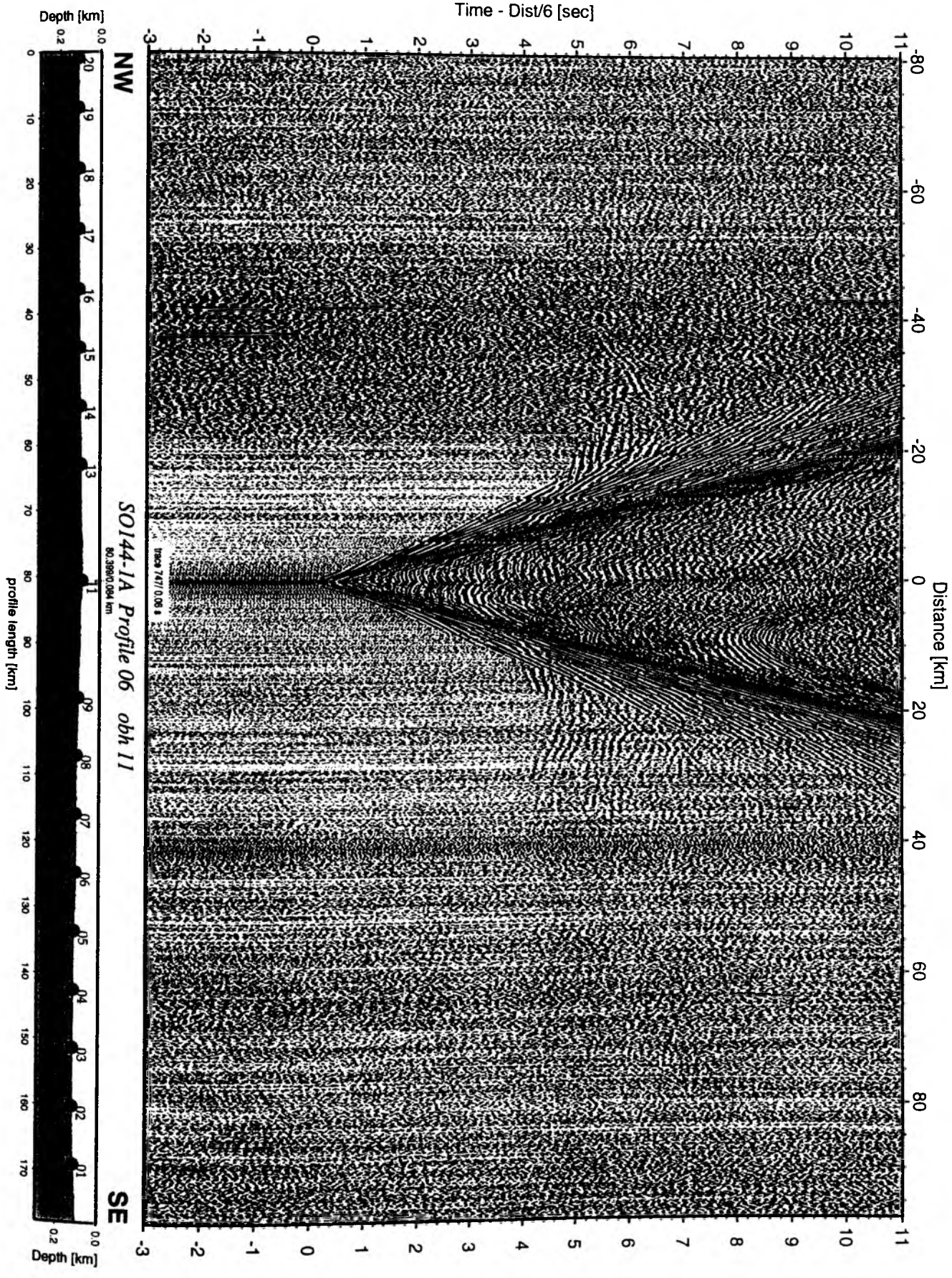

Figure 6.2.4.1.9: Record section from obh 11 , Profile 06.

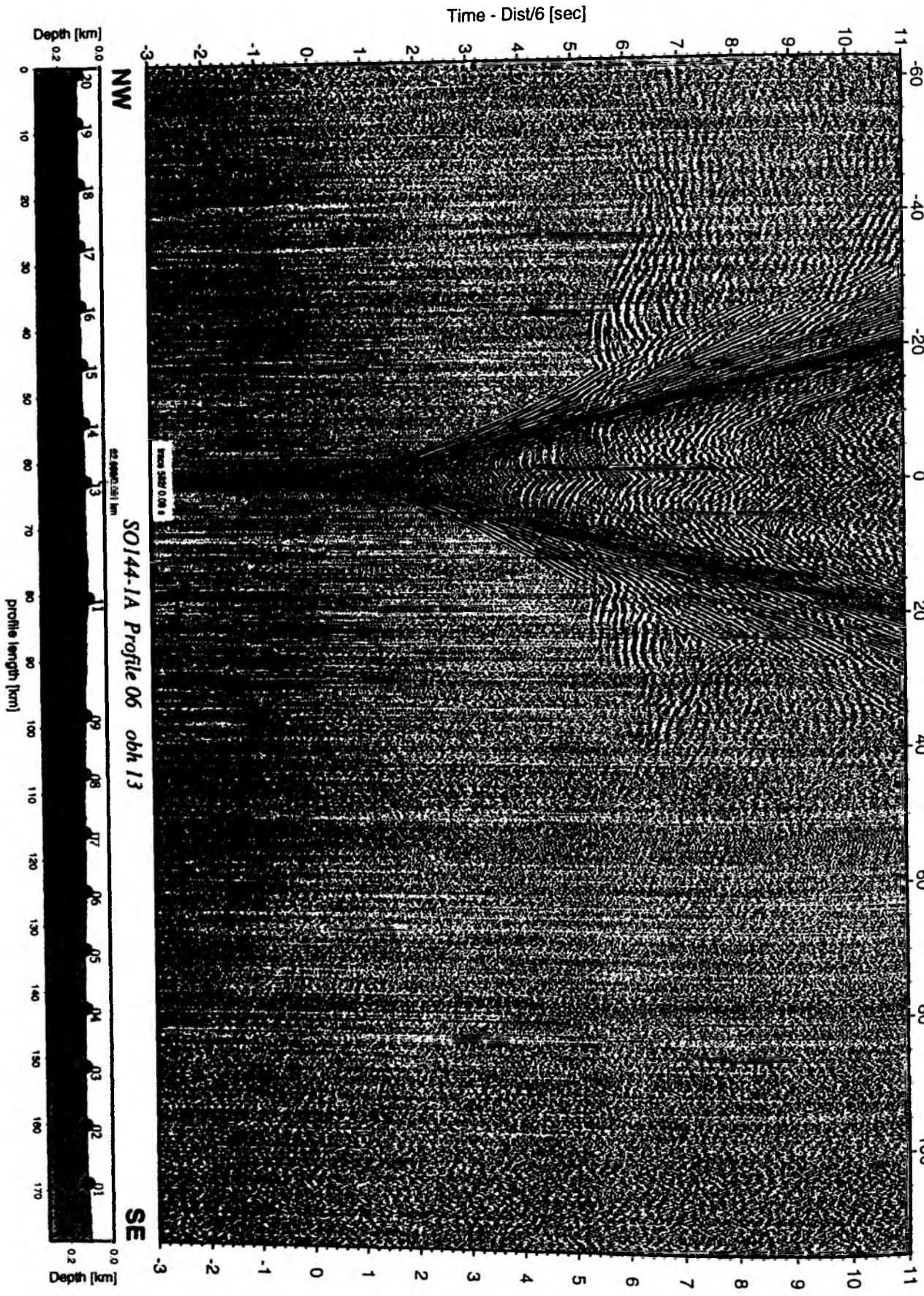

Figure 6.2.4.1.10: Record section from obh 13 , Profile 06.

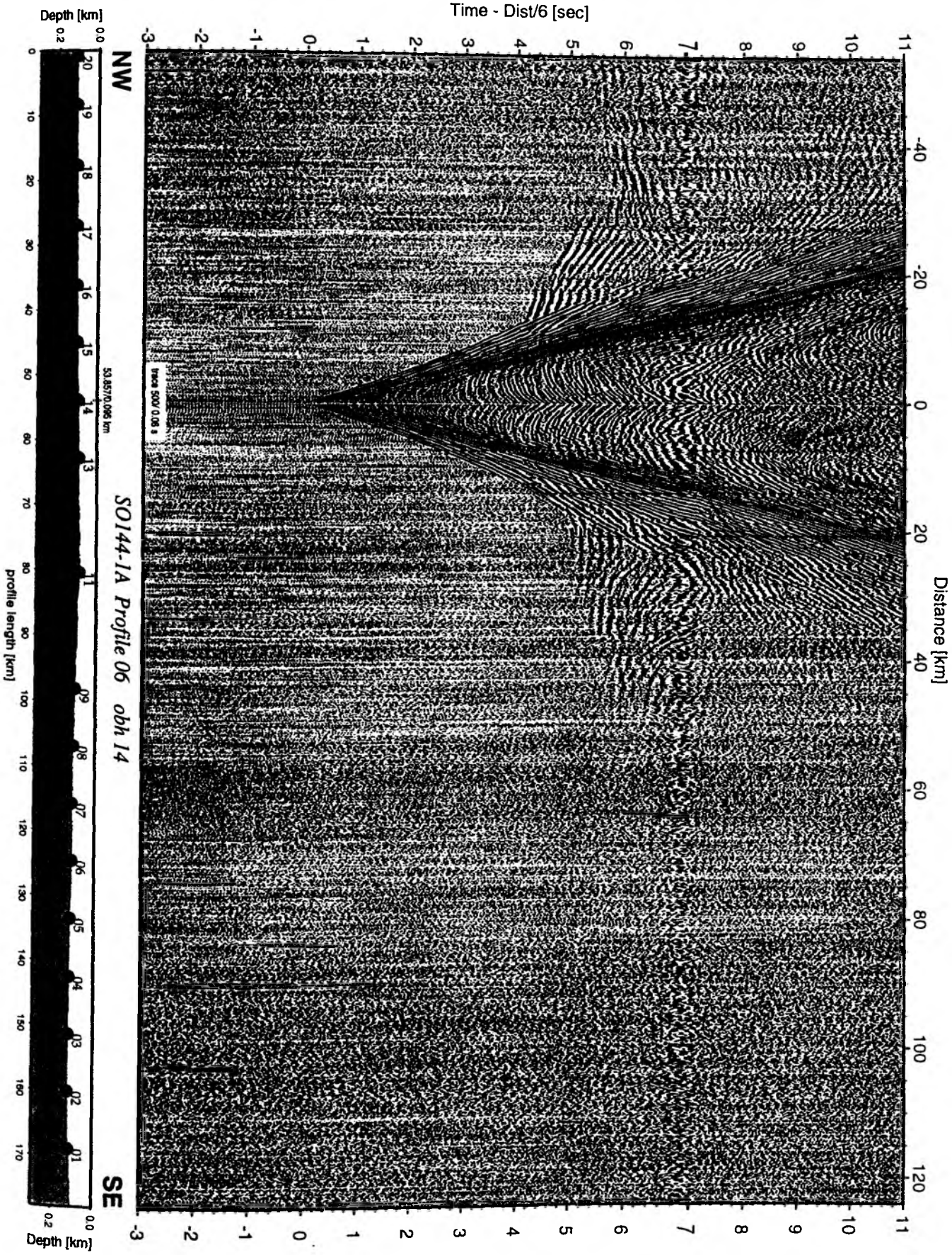

Figure 6.2.4.1.11: Record section from obh 14 , Profile 06.

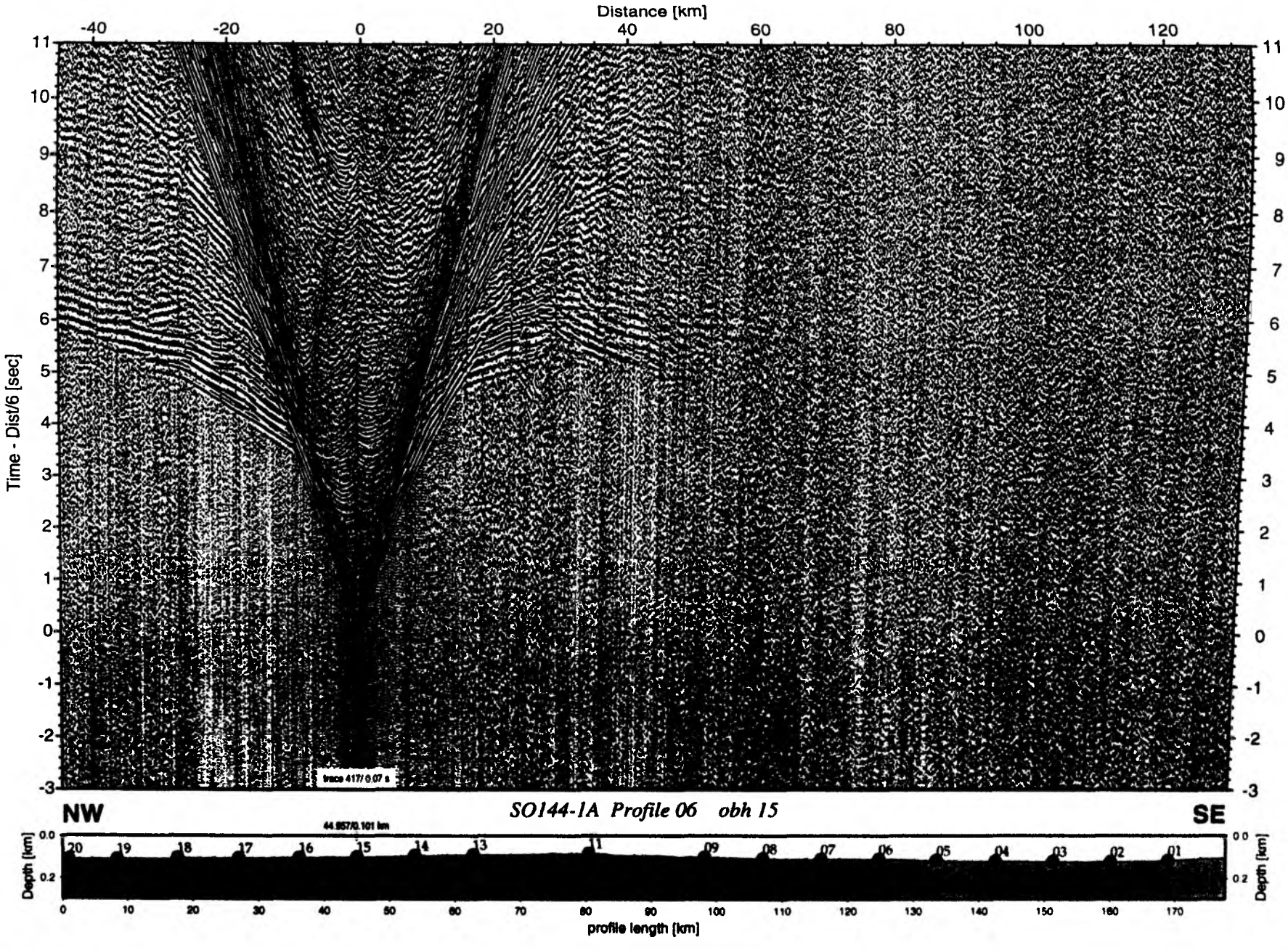

Figure 6.2.4.1.12: Record section from obh 15 , Profile 06.

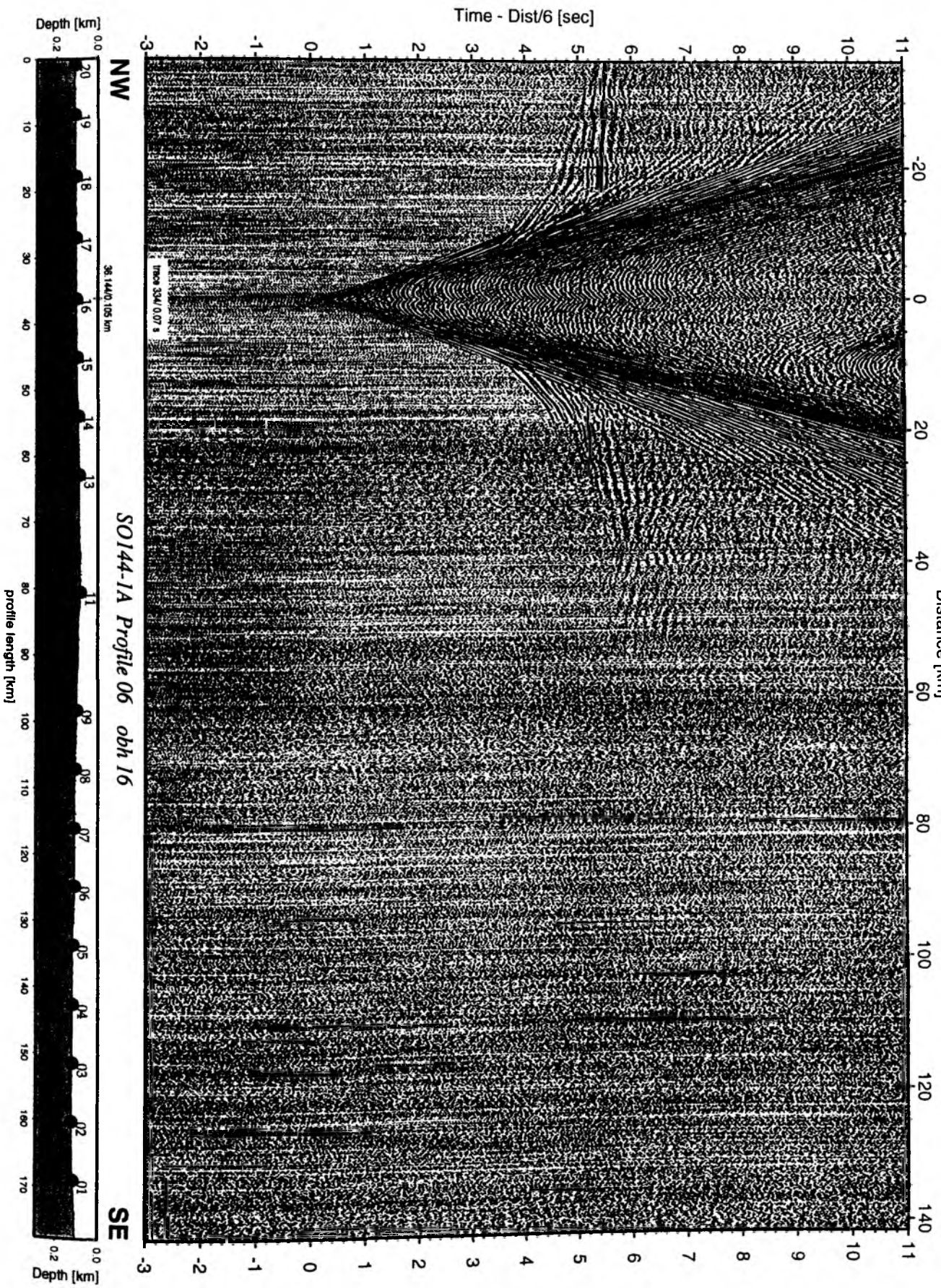

Figure 6.2.4.1.13: Record section from obh 16 , Profile 06.

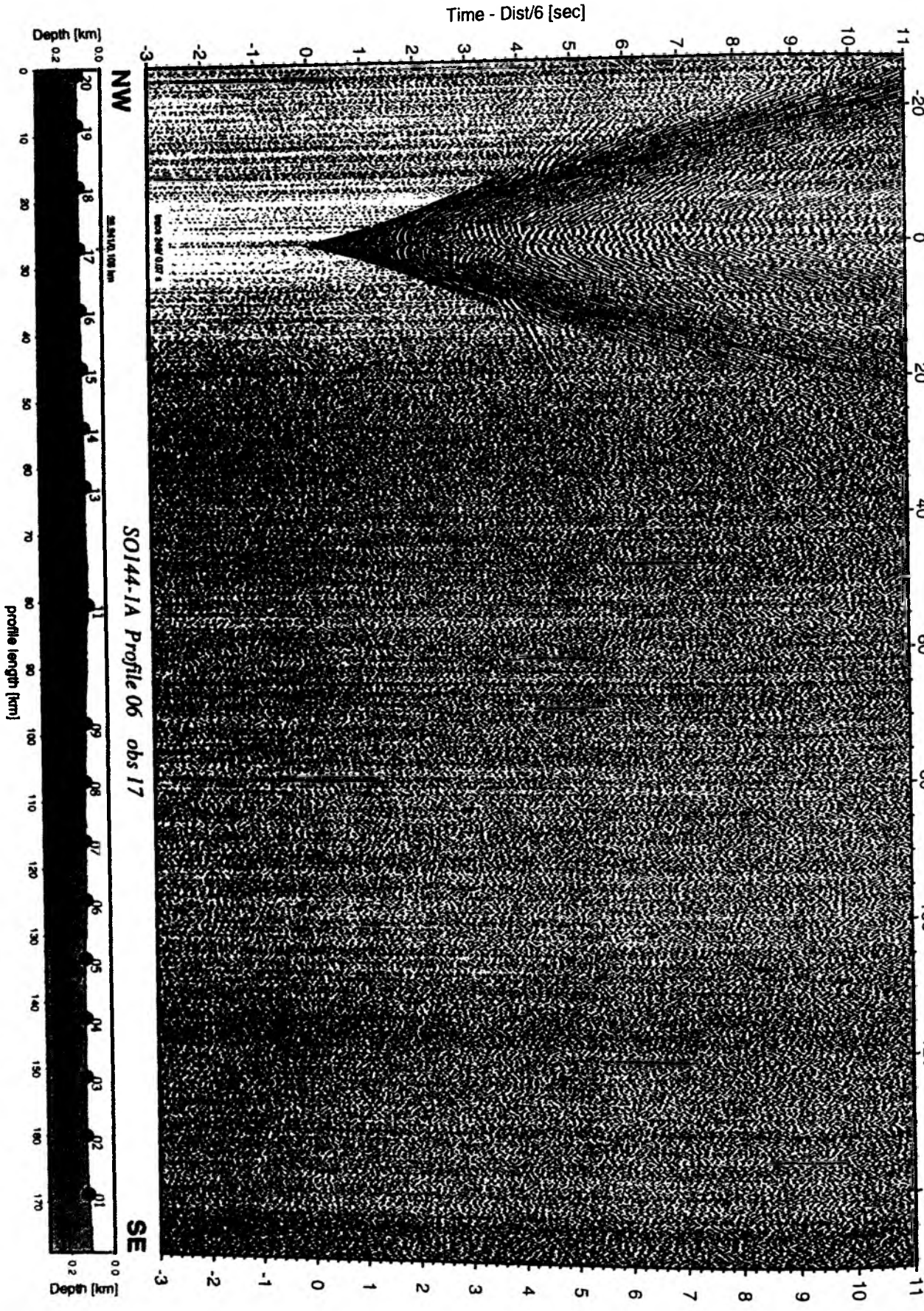

Figure 6.2.4.1.14: Record section from obs 17 vertical component, Profile 06.

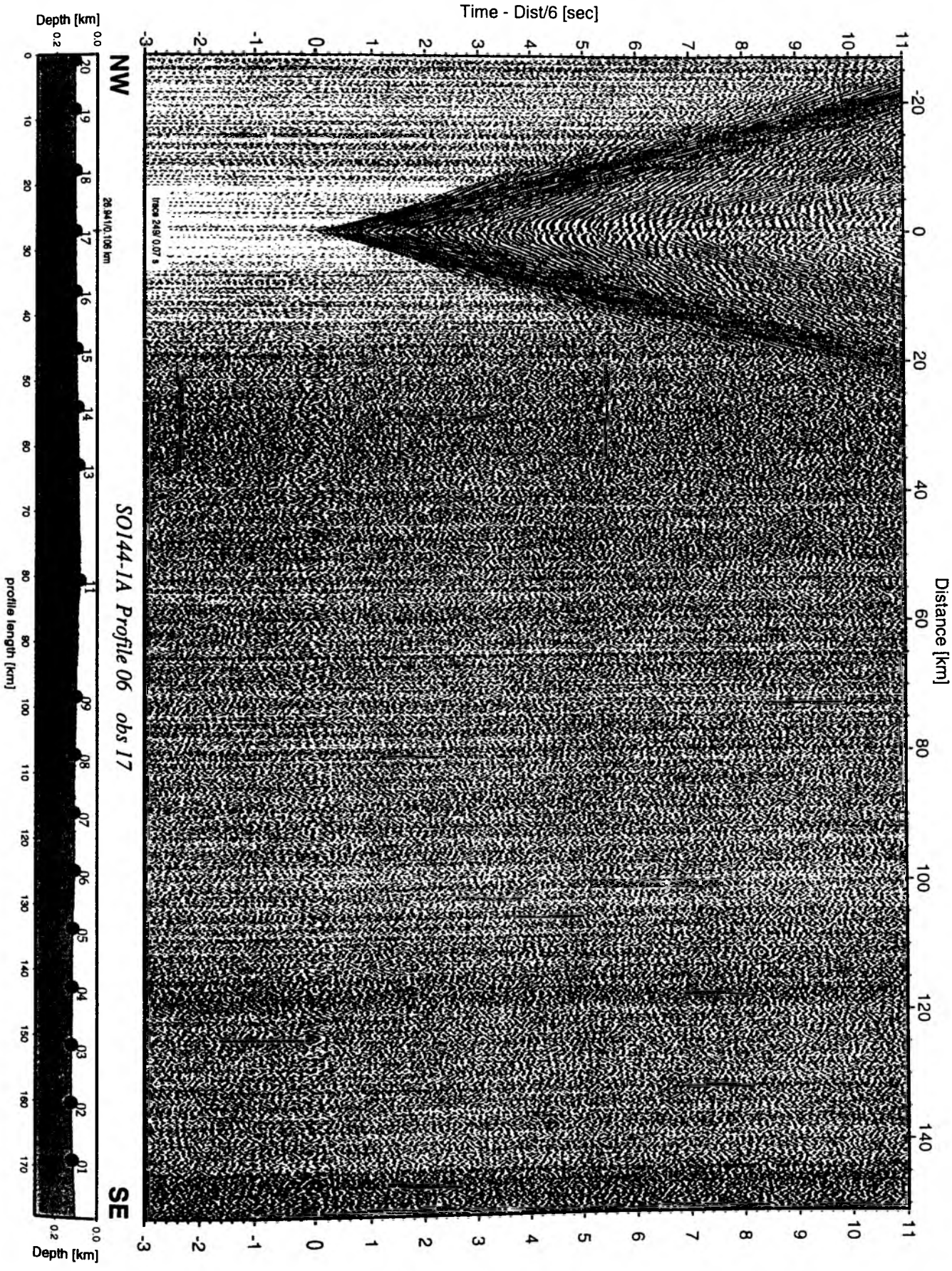

Figure 6.2.4.1.15: Record section from obs 17 horizontal component 1, Profile 06.

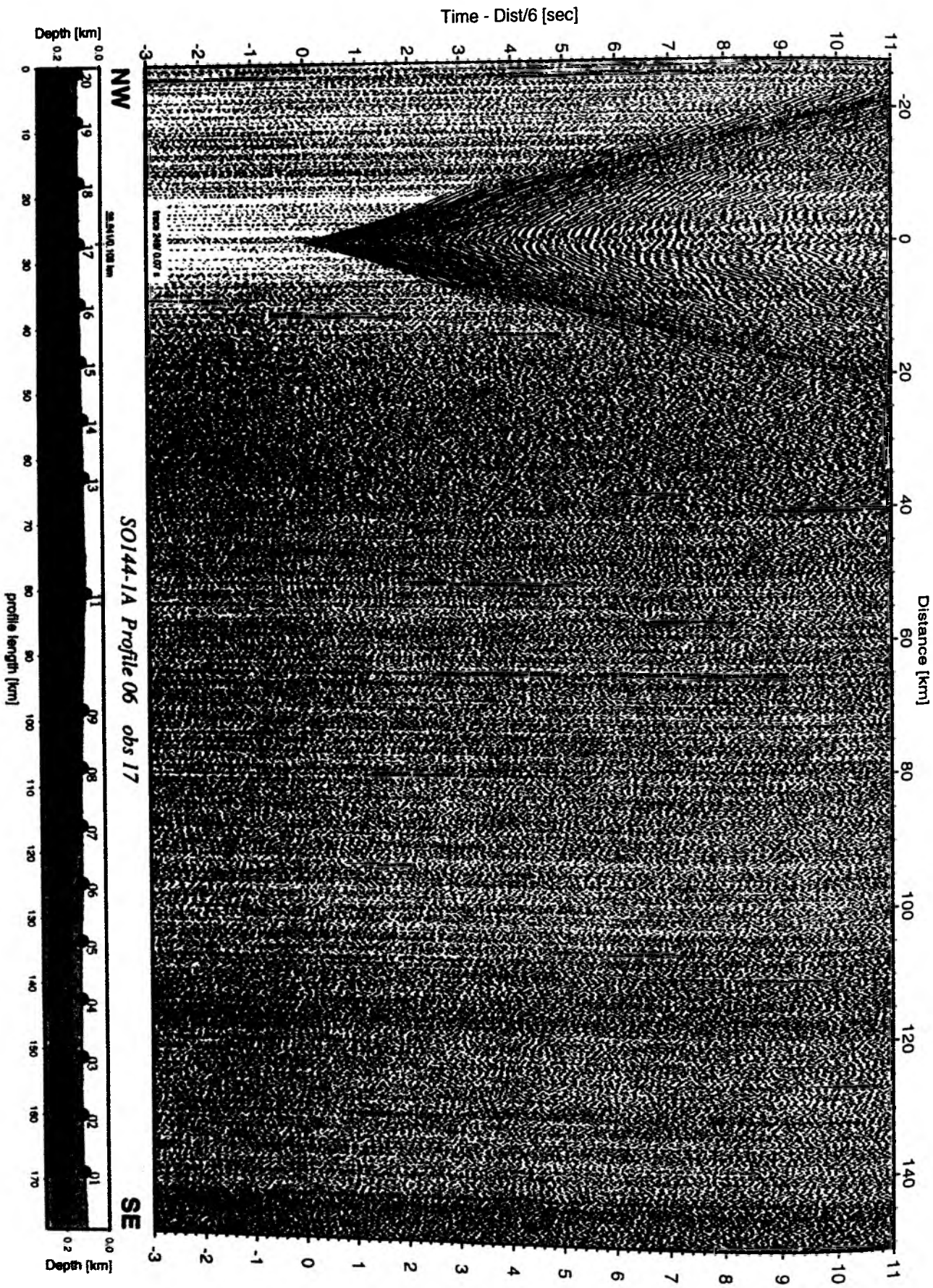

Figure 6.2.4.1.16: Record section from obs 17 horizontal component 2, Profile 06.

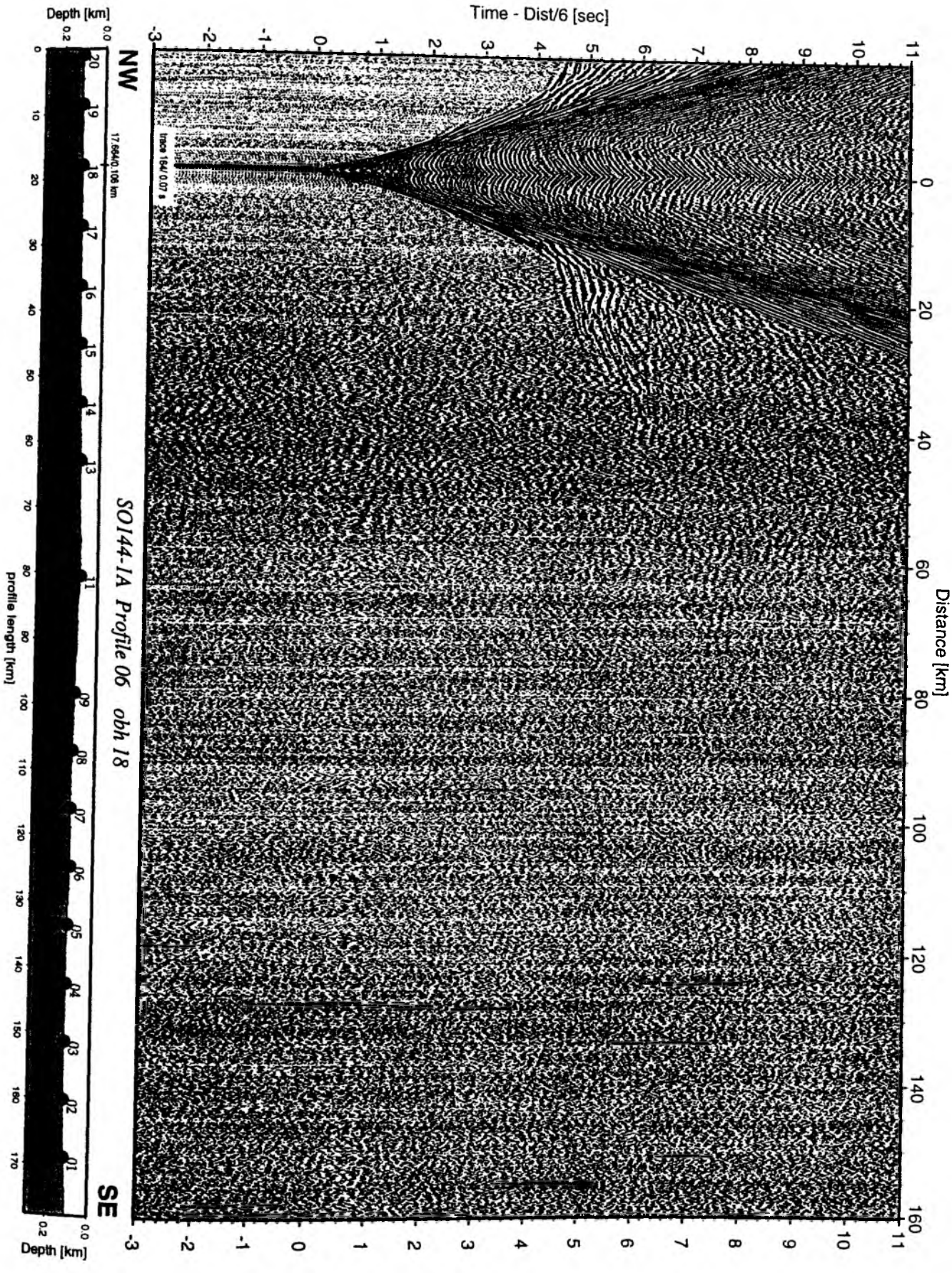

Figure 6.2.4.1.17: Record section from obh 18 , Profile 06.

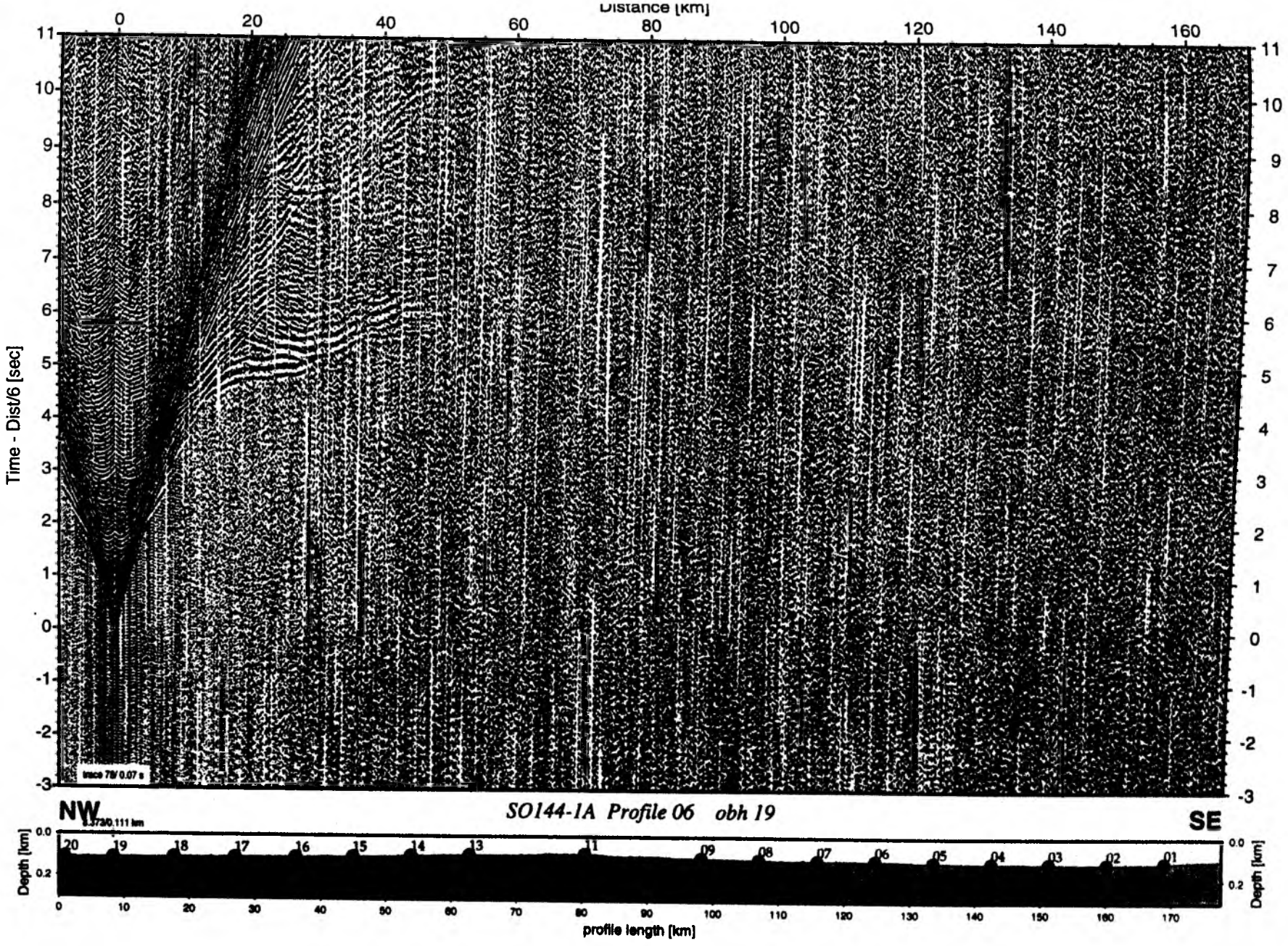

Figure 6.2.4.1.18: Record section from obh 19 , Profile 06.

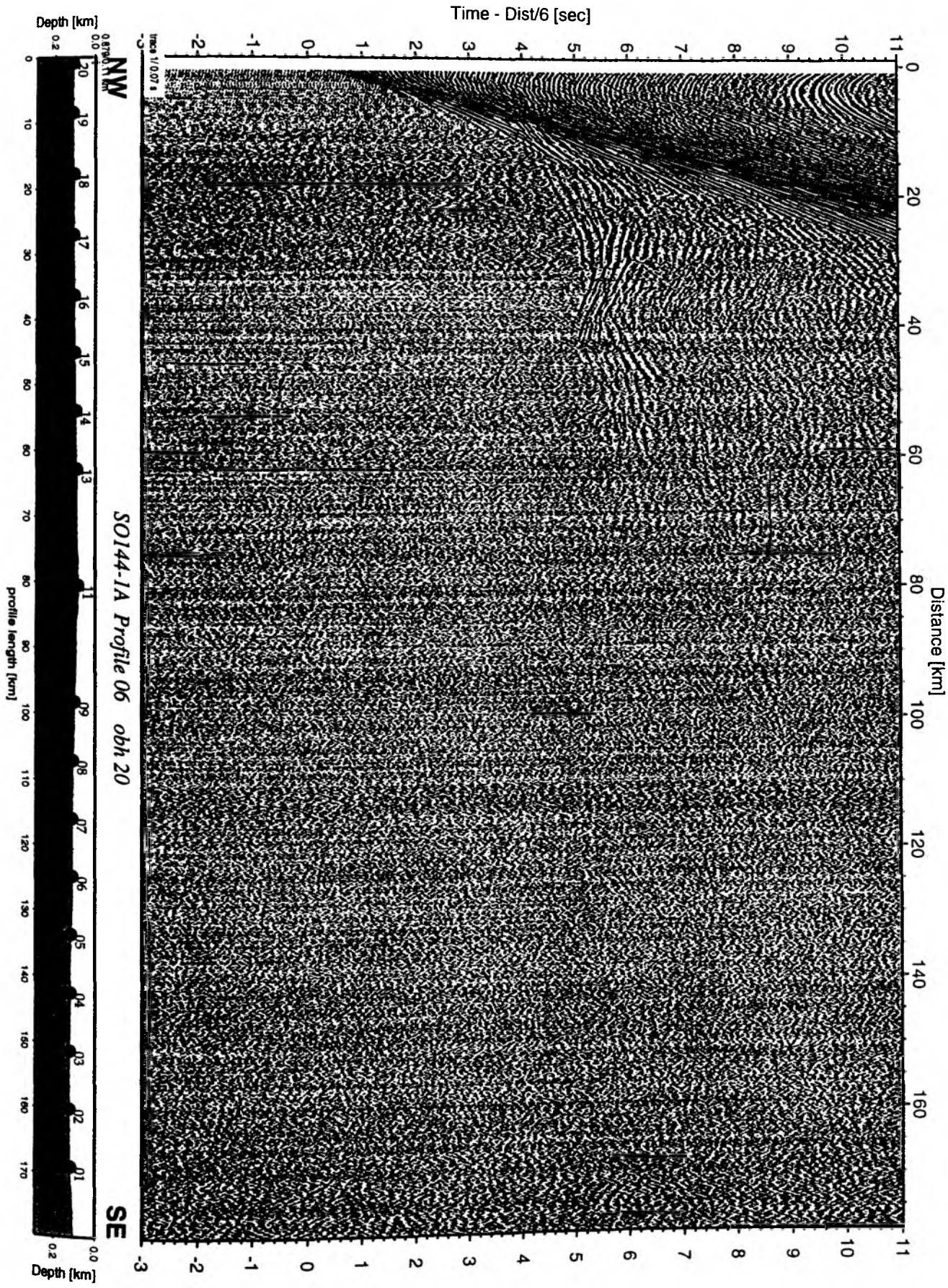

Figure 6.2.4.1.19: Record section from obh 20 , Profile 06.

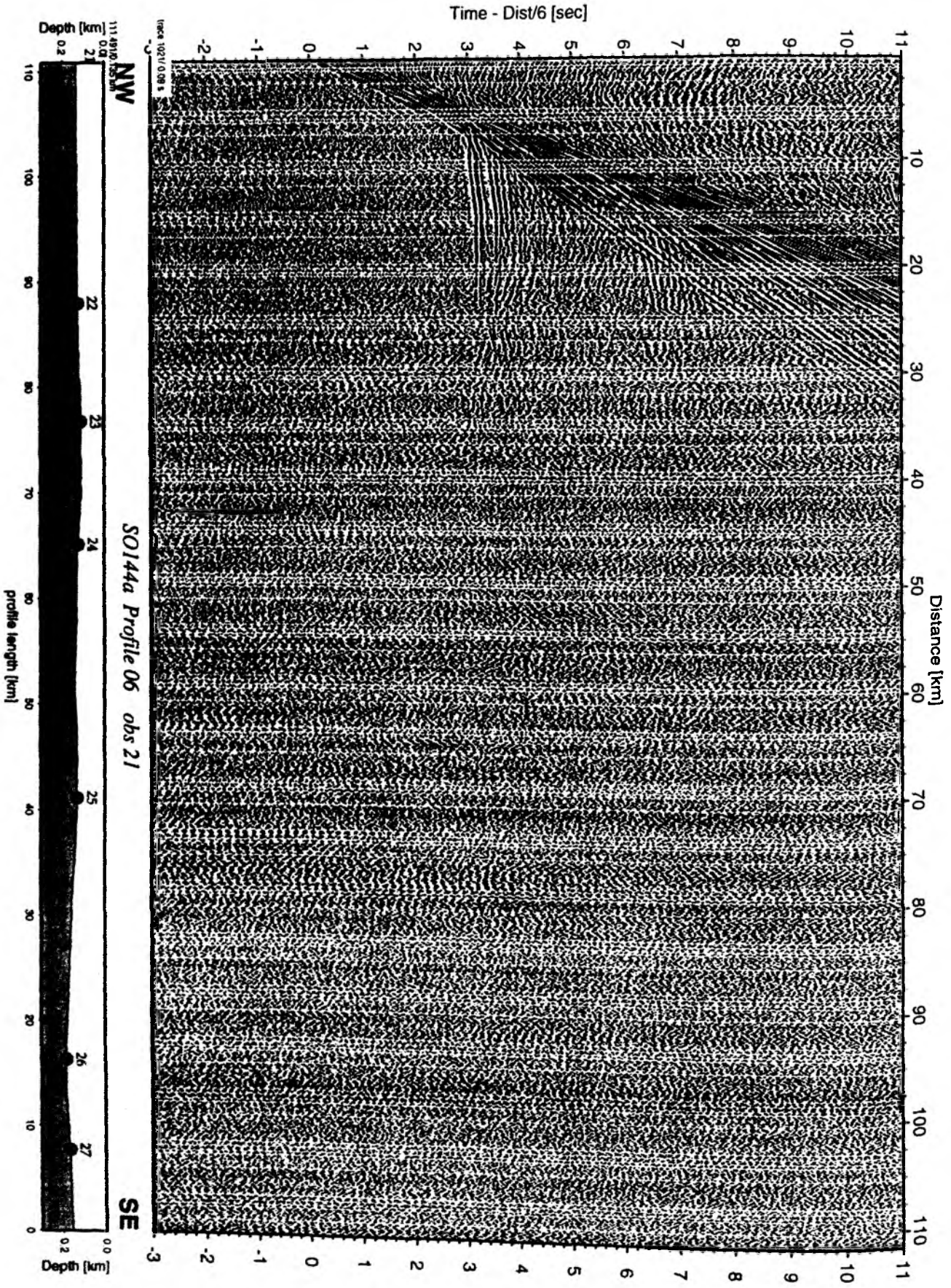

Figure 6.2.4.1.20: Record section from obs 21 hydrophone, Profile 06.

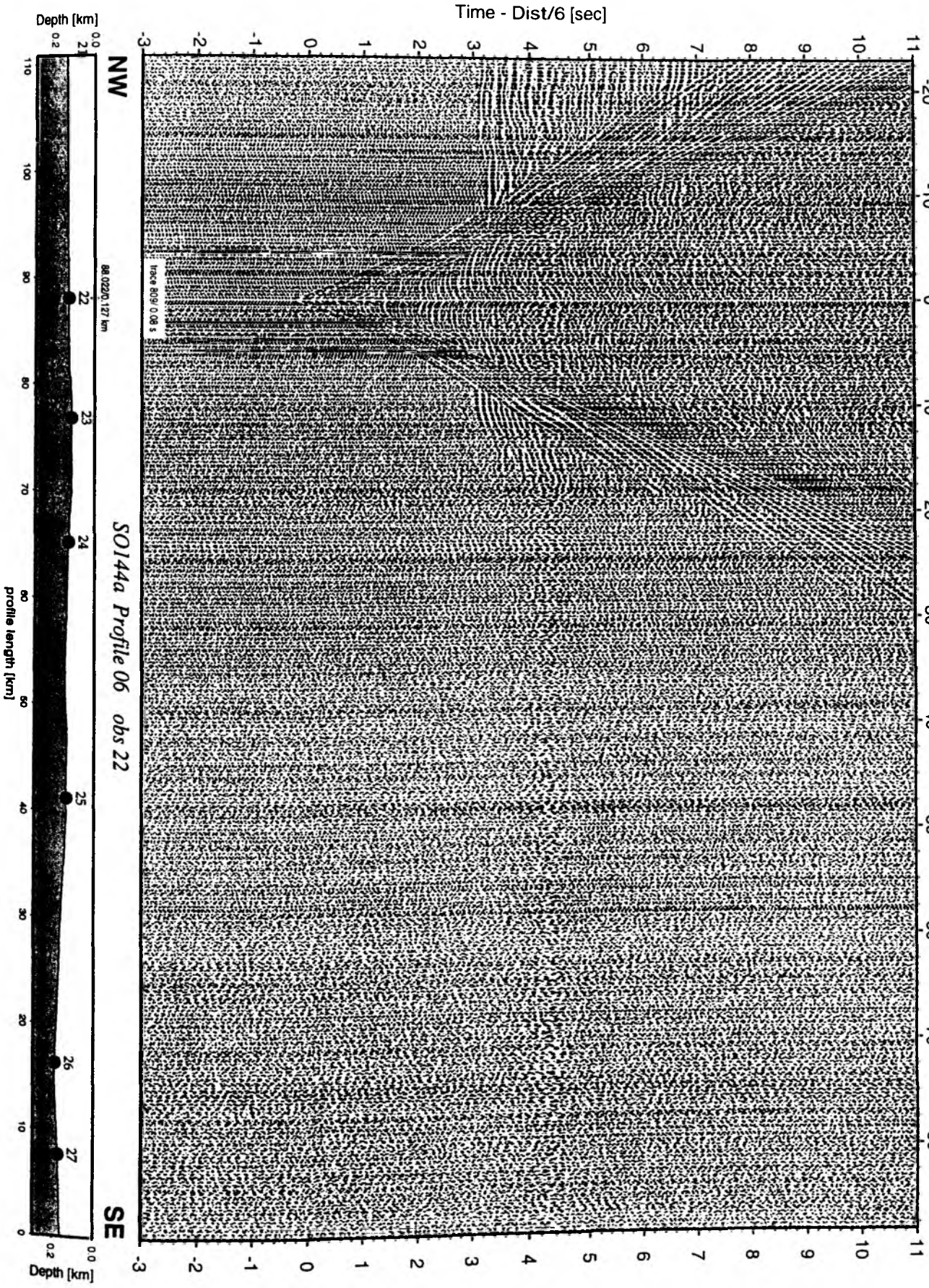

Figure 6.2.4.1.21: Record section from obs 22 hydrophone, Profile 06.

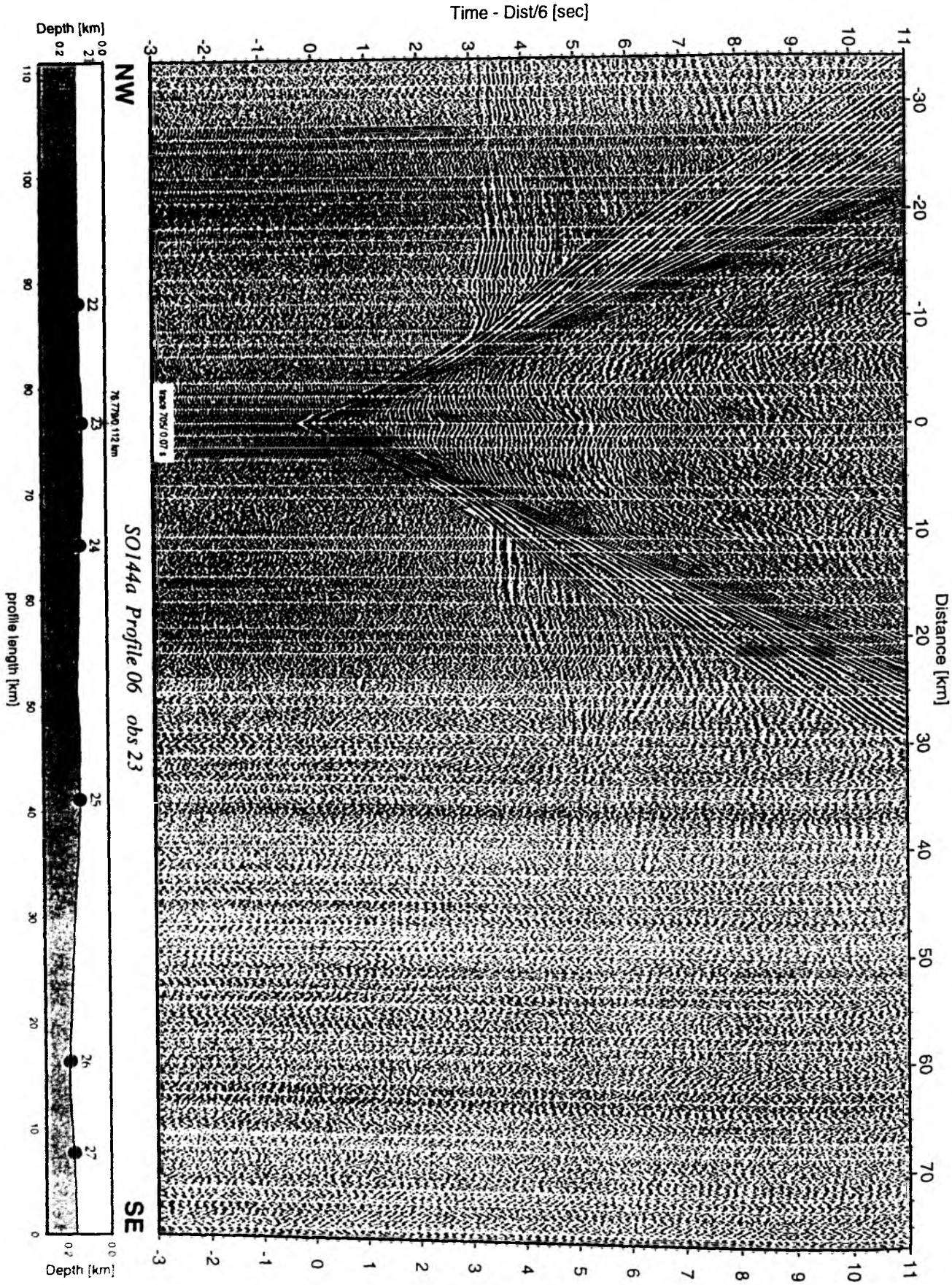

Figure 6.2.4.1.22: Record section from obs 23 hydrophone, Profile 06.

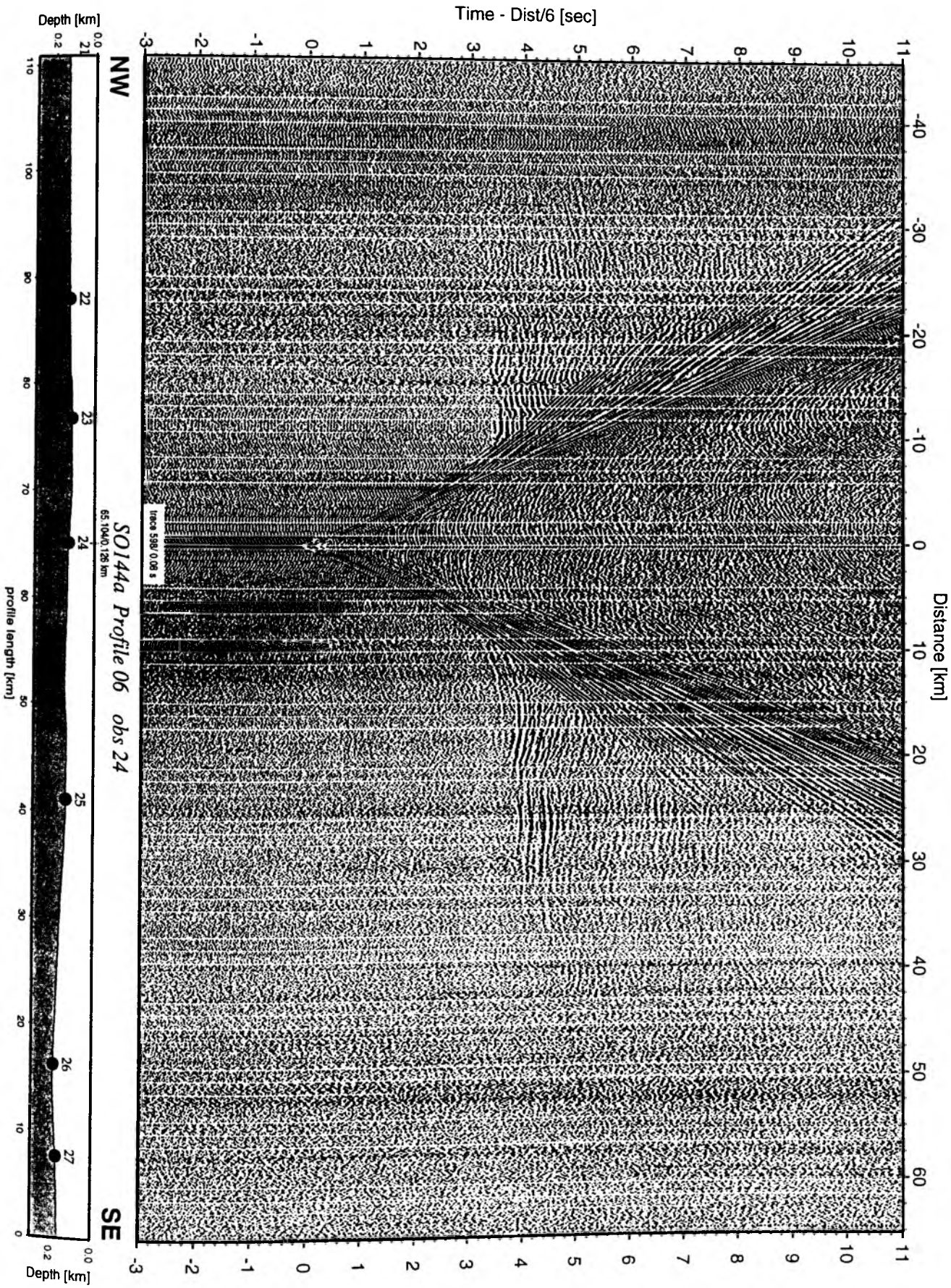

Figure 6.2.4.1.23: Record section from obs 24 hydrophone, Profile 06.

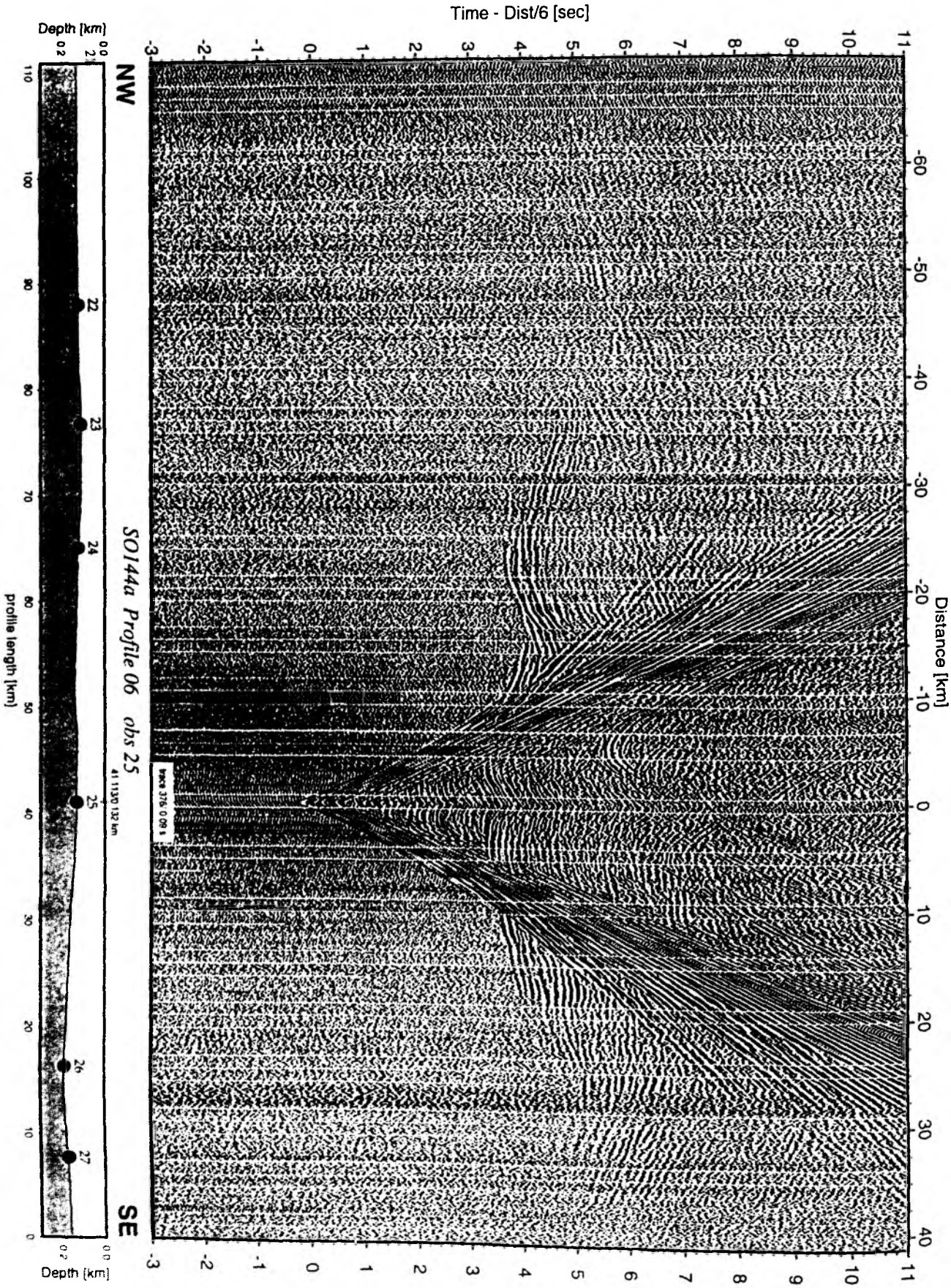

Figure 6.2.4.1.24: Record section from obs 25 hydrophone, Profile 06.

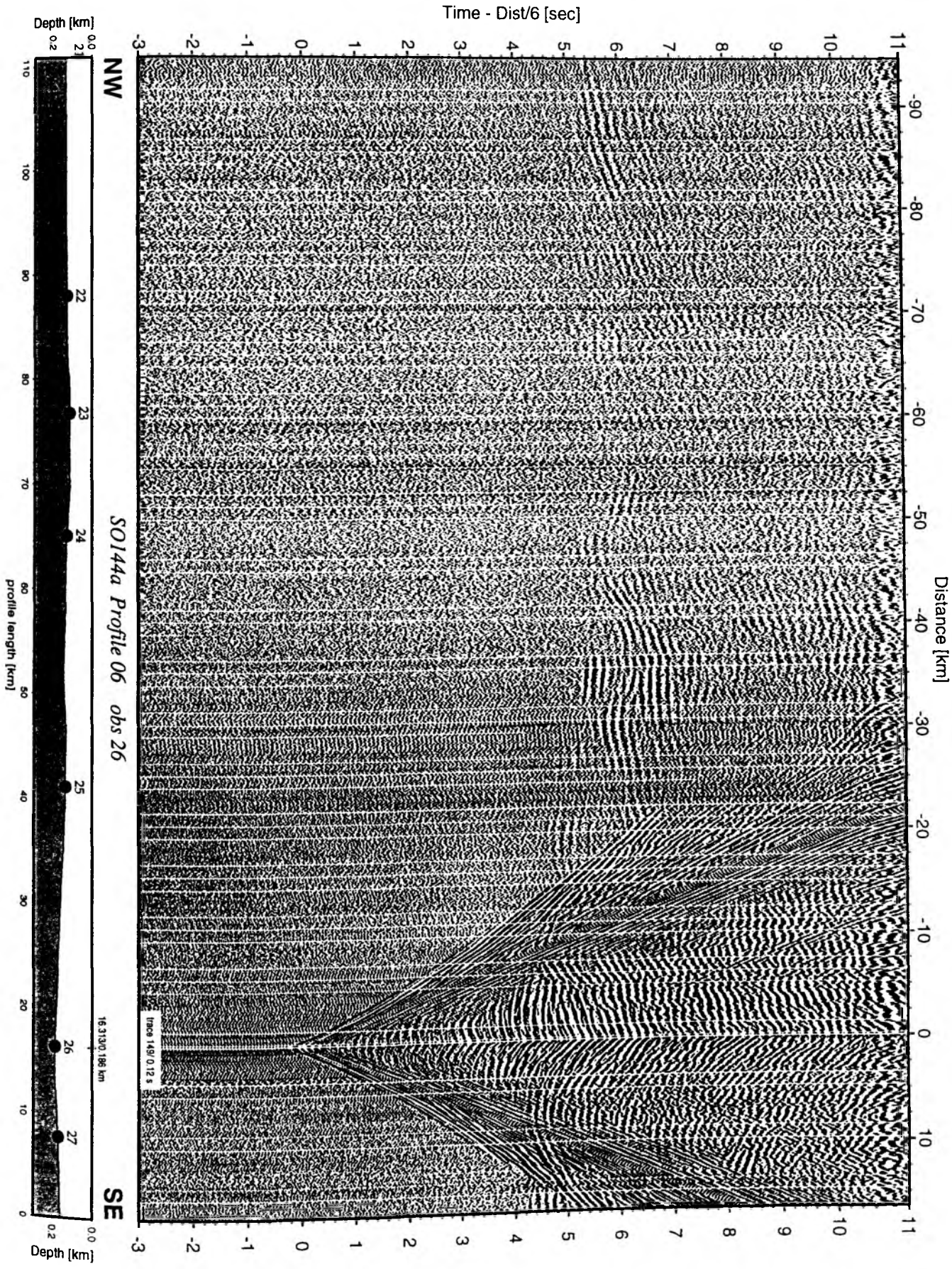

Figure 6.2.4.1.25: Record section from obs 26 hydrophone, Profile 06.

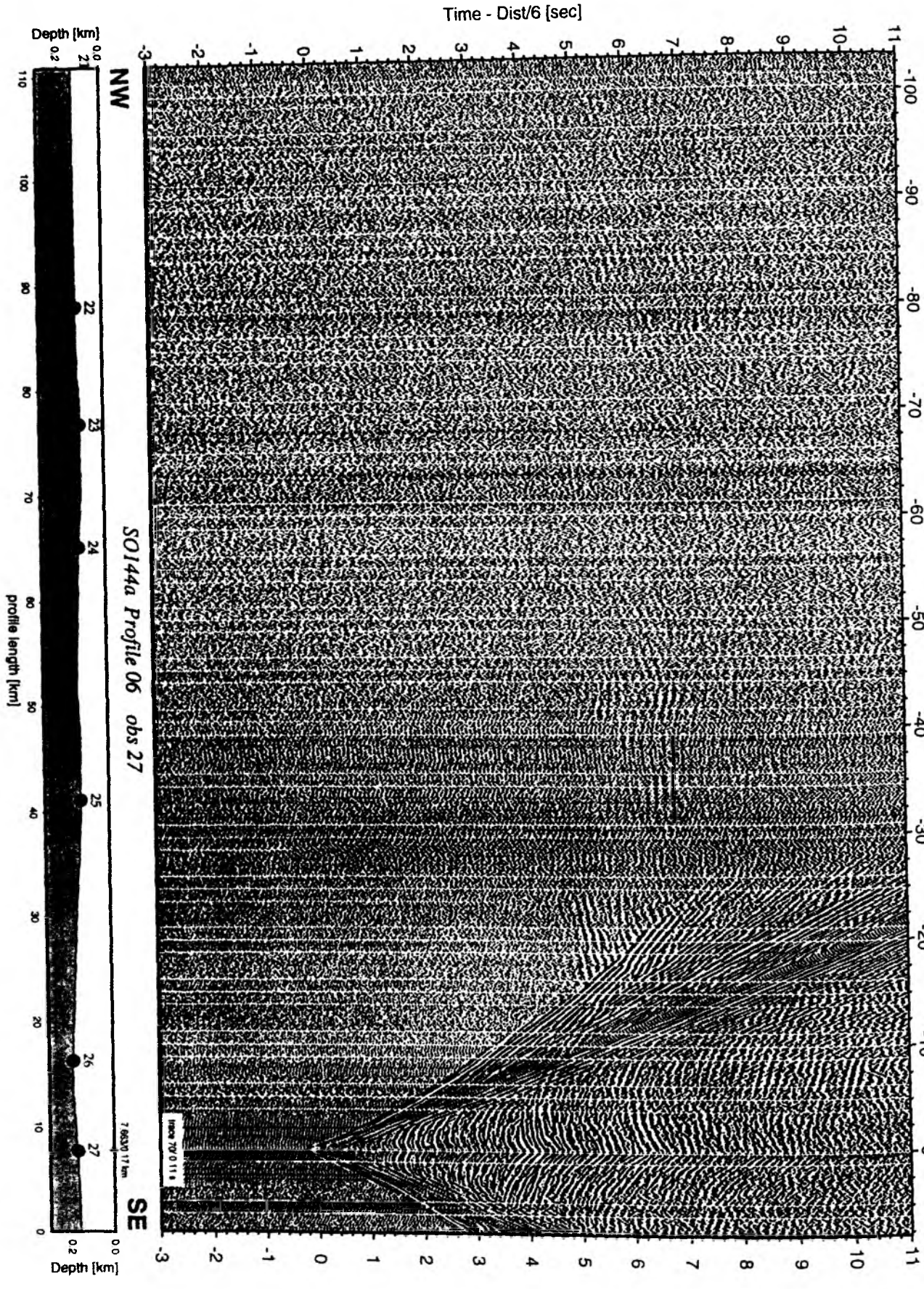

Figure 6.2.4.1.26: Record section from obs 27 hydrophone, Profile 06.

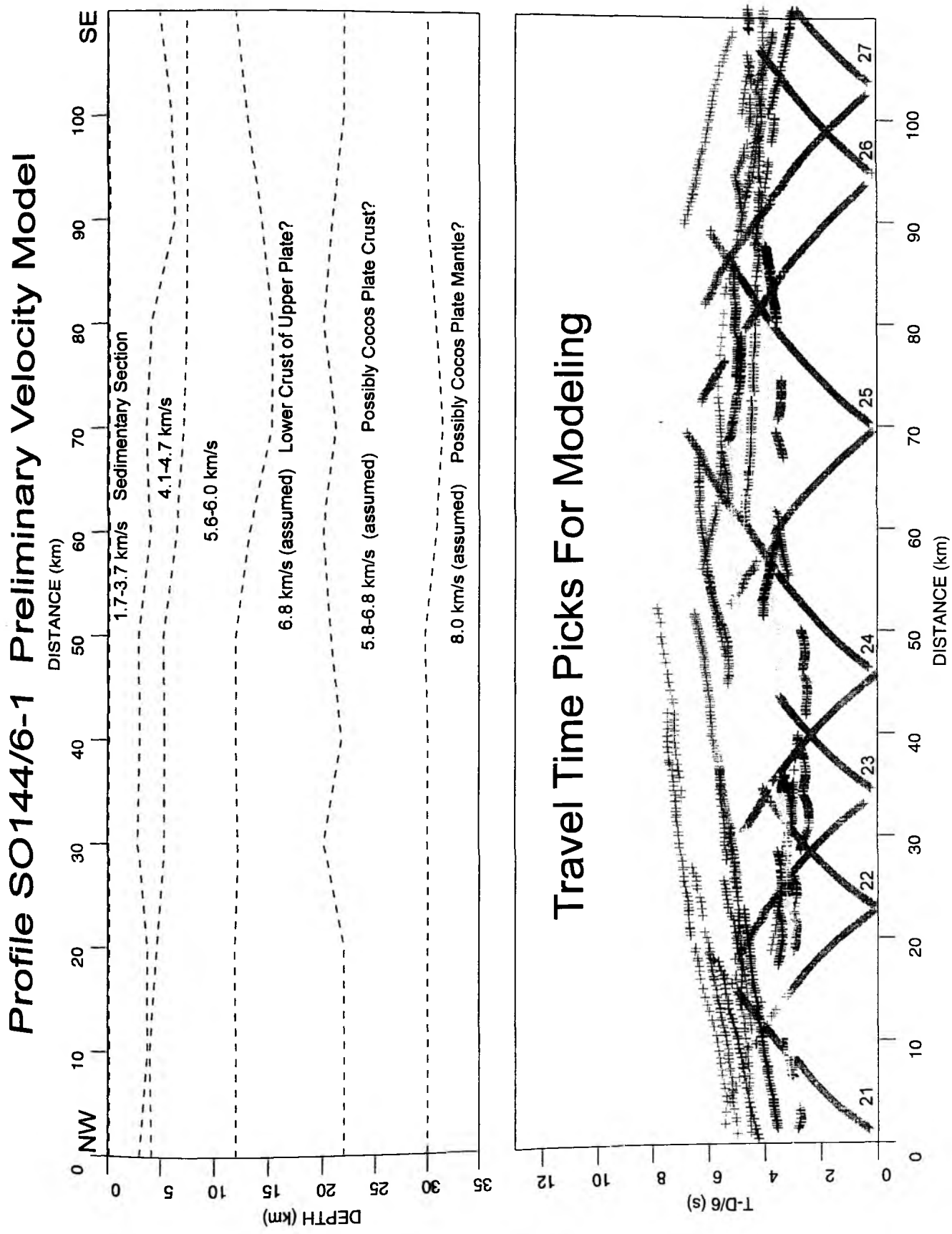

Figure 6.2.4.1.27 Preliminary velocity model and travel time picks for profile SO144/6-1. This is a strike line along the shelf of the Nicaragua continental margin.

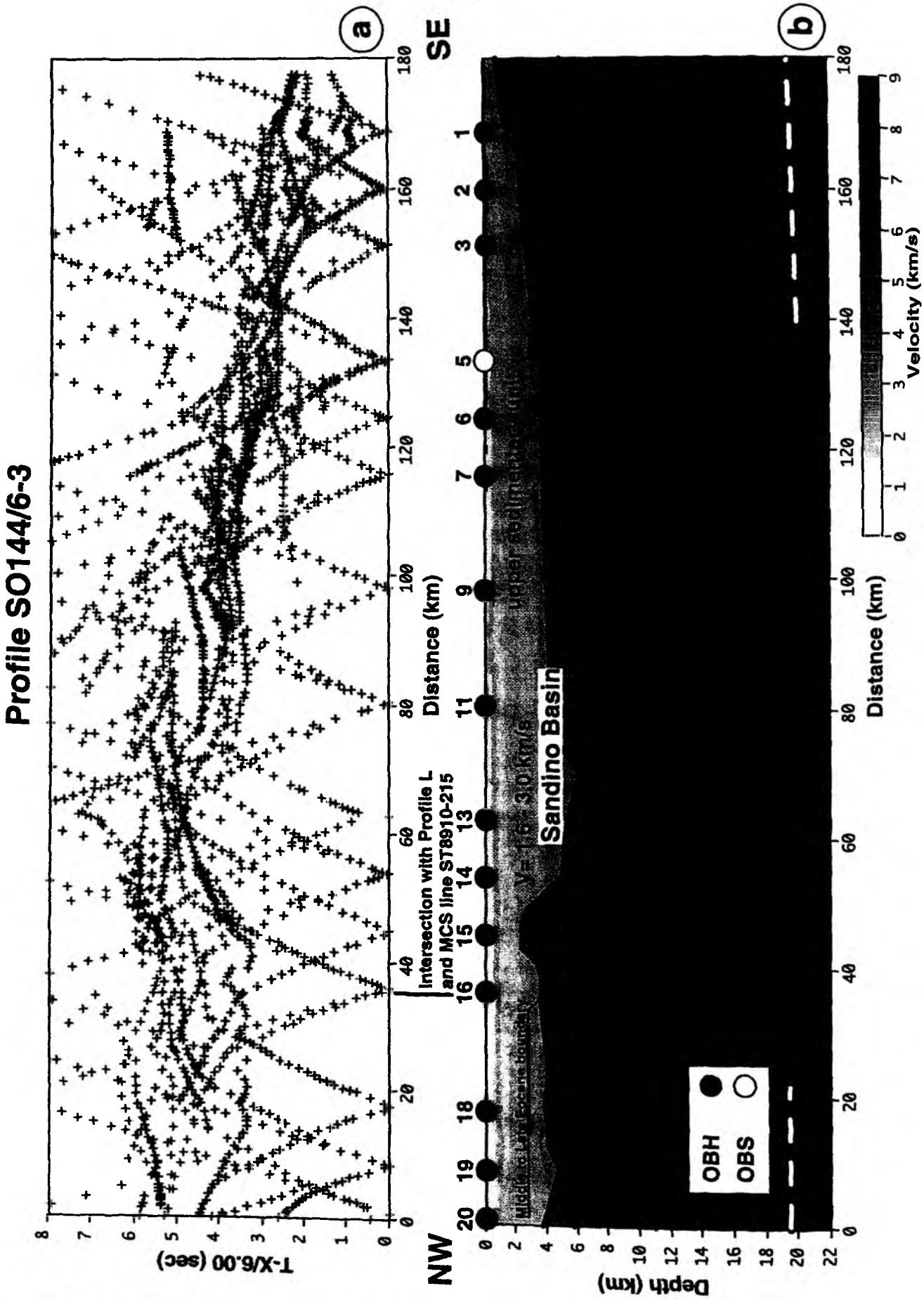

Figure 6.2.4.1.28 a) Picks extracted from the record sections of Profile 6-3 show the deepening Sandino Basin from SE to NW.
b) Crustal cross section for Profile 6-3 from preliminary analysis of wide-angle data.

6.2.4.2 BSR EXPERIMENT – PROFILES 9–12

On the MCS lines of cruise SO81, Bottom Simulating Reflectors (BSR) were identified within sedimentary sequences and on top of subducted seamounts. Because of shelf uplift and following slope failure, these are locations where methane may be released into the water. Within the sections, the reflection event could be traced up to the almost vertical scarp, where the sediment has been uplifted during the seamount's passage. During leg SO144-1a, five OBS were deployed along two rectangular profiles on top of a subducted seamount to further investigate the physical properties above and below the BSR. We chose the MCS line SO081-13 for this experiment (Fig. 6.2.4.2.1). The three Géo Azur and two GEOMAR OBS were deployed 2 nm apart. Airgun shooting was performed with a 7-gun array, only 4 guns of which could be operated simultaneously (s.ch. 5.5). Because the gun array was deployed from the port gun-slide, a three-channel streamer (s.ch. 5.9) could be operated from the center aft deck of SONNE.

The first shot was fired on 23 September at 12:14 UTC, with airguns 1, 2, 3 and 4, providing a total volume of 3.2 l (s.ch. 5.5). Shots were fired at 18-s-intervals at a speed of 3.5 kn - a shot spacing of about 32 m. At 13:27 UTC, airgun 4 was switched off after uncontrolled auto-triggers and gun 5 engaged, raising the total volume to 3.35 l. Line 09 terminated at 14:27 UTC. Line 10 was shot between OBS 31 and OBS 30 (s. Figure 6.2.4.2.10 and 6.2.4.2.1) and terminated at 15:43 UTC. Owing to a time delay at the beginning, line 11 could not be shot across OBS28. The release time preprogrammed for the GÉO Azur OBS caused shooting to stop on 23 September at 17:30 UTC. After recovery of airguns and streamer, the ship headed for OBH28's position. A flag was, for the first time, attached to the radio beacon of the GÉO Azur instruments making them easy to detect before the Zodiac was sent out for recovery. The GEOMAR OBS were released from distance and they were already floating when SONNE arrived. Unfortunately, several fishing vessels were around and OBS32 surfaced opposite a fishing rope. These ropes are deployed over several kilometers and float at the surface. Passing with SONNE would cut them and might cause danger to the ship's propeller if it was turning slowly. Therefore, it was decided to use the Zodiac and tow the instrument to the vessel.

After a short transit, OBS33 and OBS34 were deployed along a 6 nm section of line SO081-17, where no seamount is interpreted. Airguns and streamer were deployed on 23 September at 23:51 UTC and again, the array of airguns 1, 2, 4 and 5 was shot over 18-s-intervals at 3.5 kn. On 14/10, 00:50 UTC, airgun 5 (0.3 l) was changed with airgun 7 (1.25 l), lifting the total volume to 4.25 l (s. Figure 6.2.4.2.12). On 14 October at 01:58 UTC, shooting was terminated and the OBS were recovered without further problems. The record sections of the GEOMAR instruments are shown in Figures 6.2.4.2.2 to 6.2.4.2.8 for the profile 9 and 12. The MCS data of profile 9, 10, 11, and 12 are shown in Figures 6.2.4.2.9 to 6.2.4.2.12. The record section of the GÉO Azur instruments are shown in Figures 6.2.4.2.13 to 6.2.4.2.25 for the profiles 9 and 11. Further details on shots and receivers can be found in Appendices 9.1.2 and 9.1.3.

No interpretation of the collected data was attempted during the cruise.

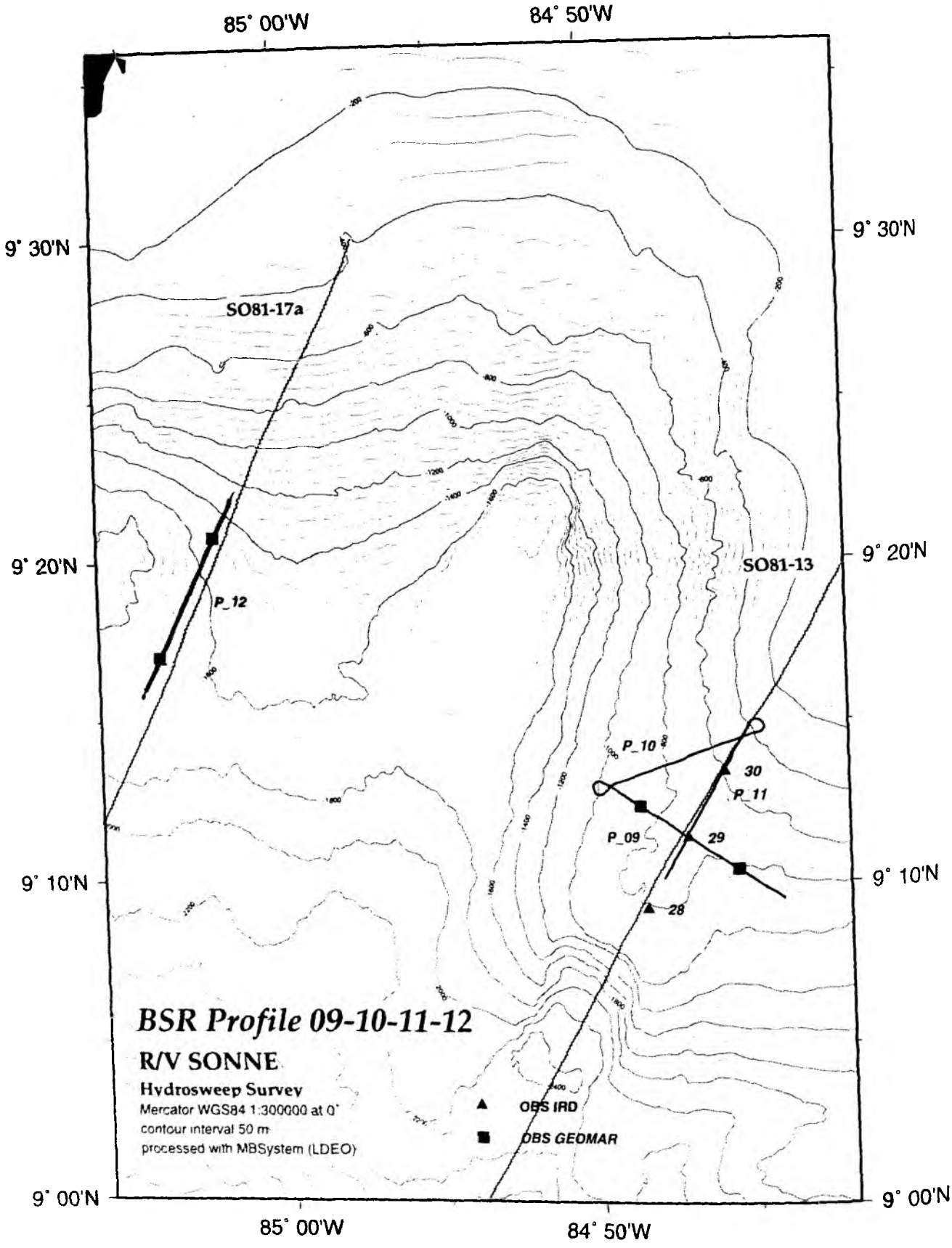

Figure 6.2.4.2.1: Profiles SO144 09-12, Location map

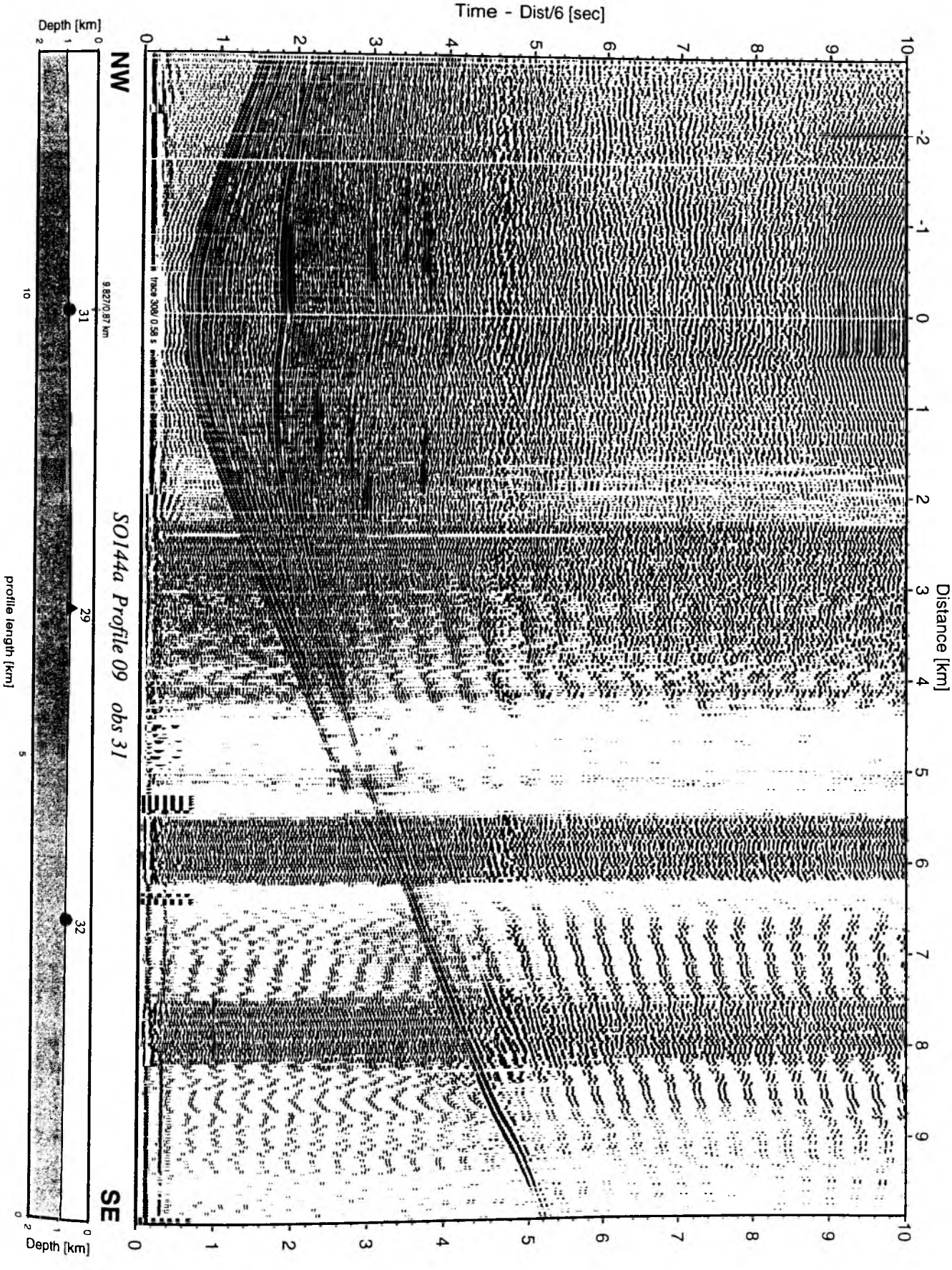

Figure 6.2.4.2.2: Record section from obs 31 hydrophone, Profile 09.

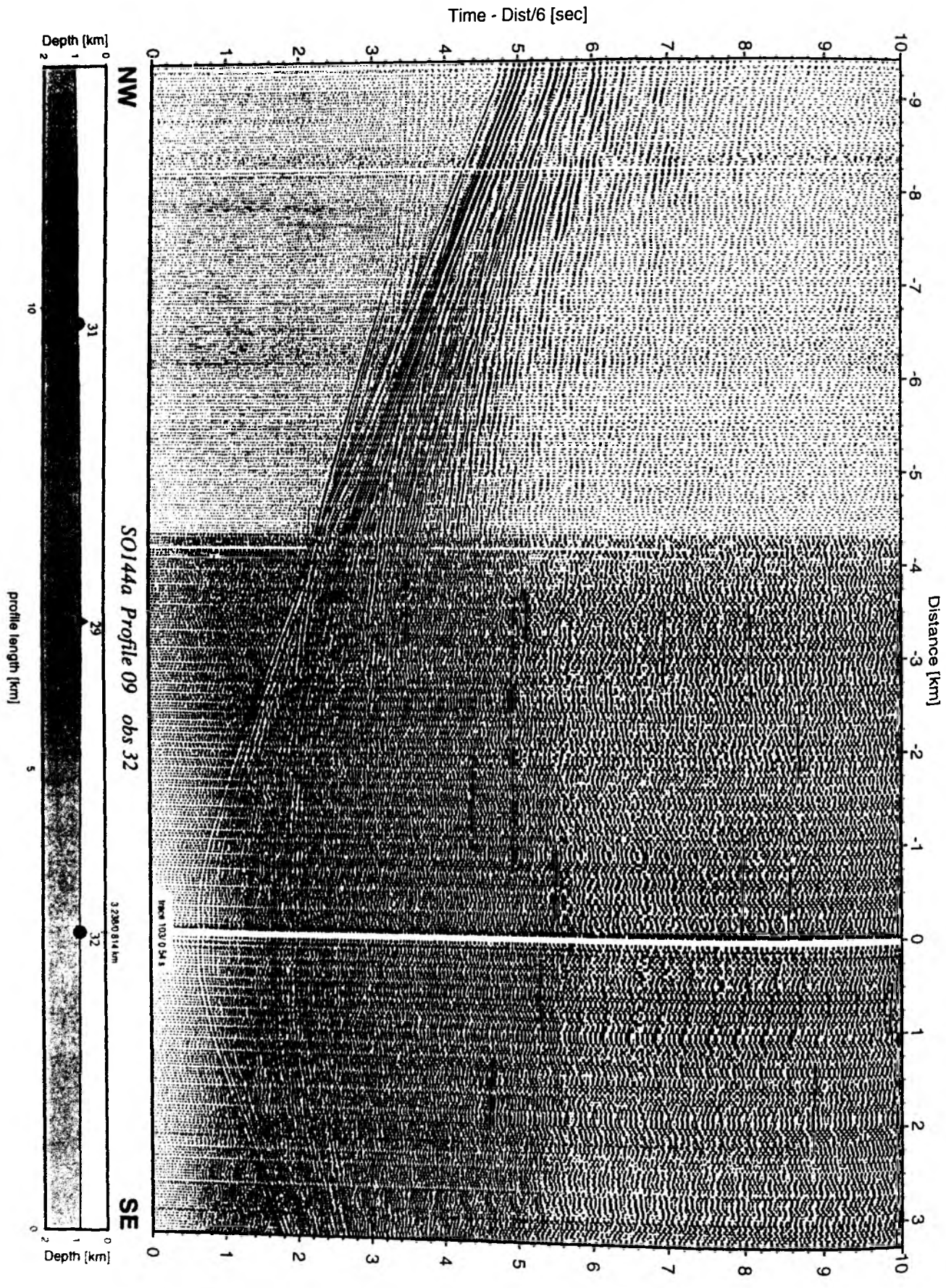

Figure 6.2.4.2.3: Record section from obs 32 hydrophone, Profile 09.

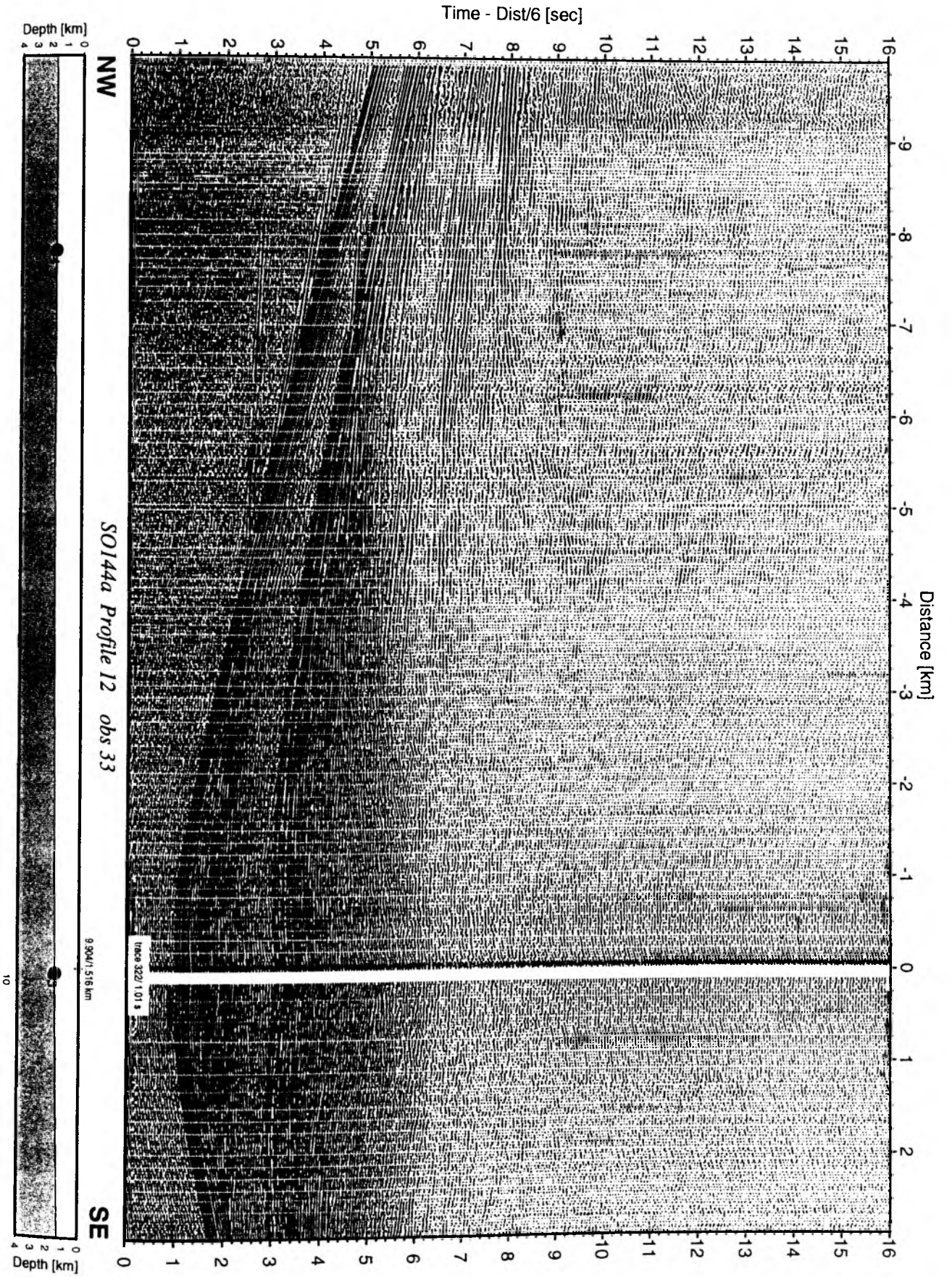

Figure 6.2.4.2.4: Record section from obs 33 hydrophone, Profile 12

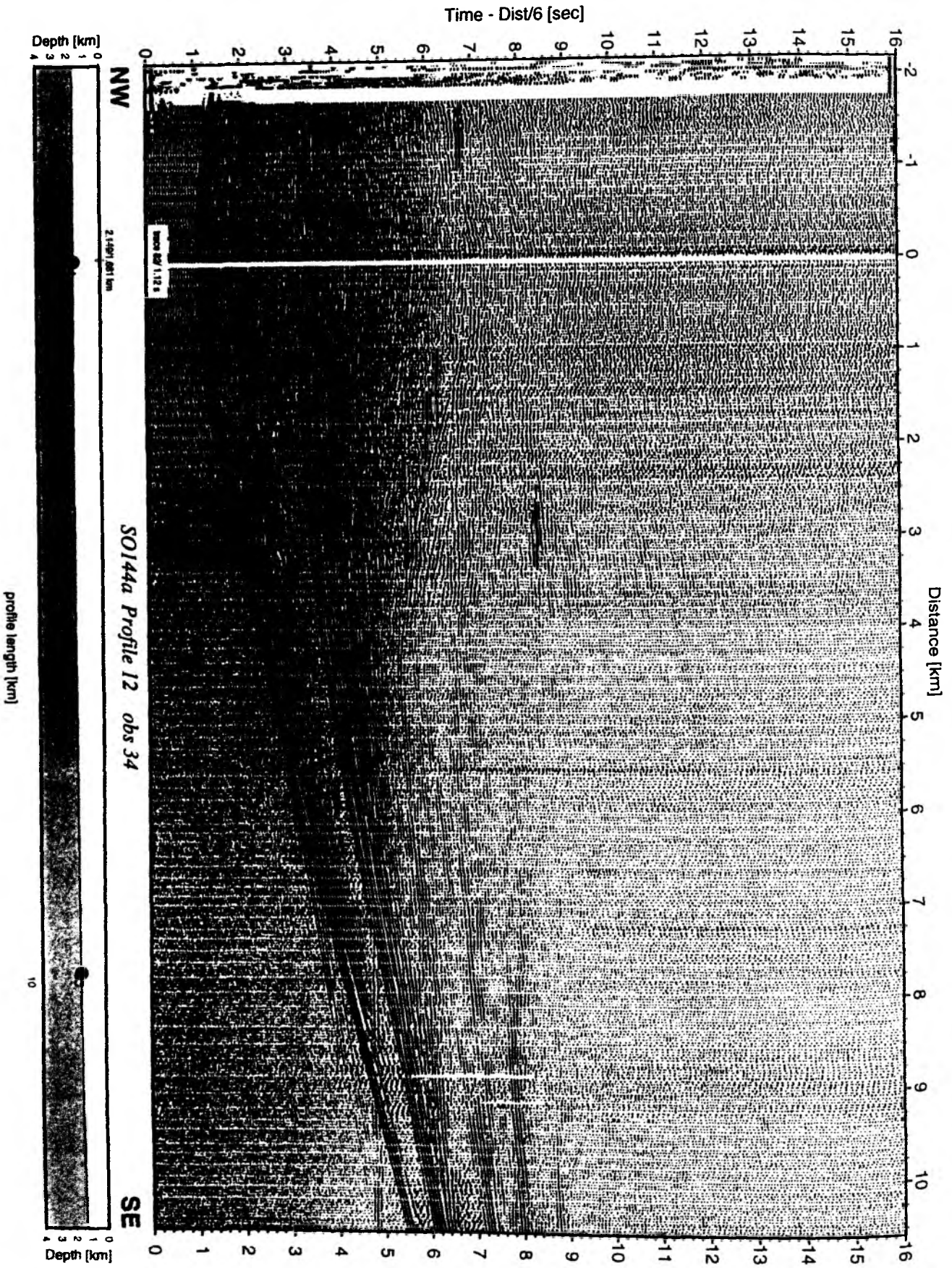

Figure 6.2.4.2.5: Record section from obs 34 hydrophone, Profile 12

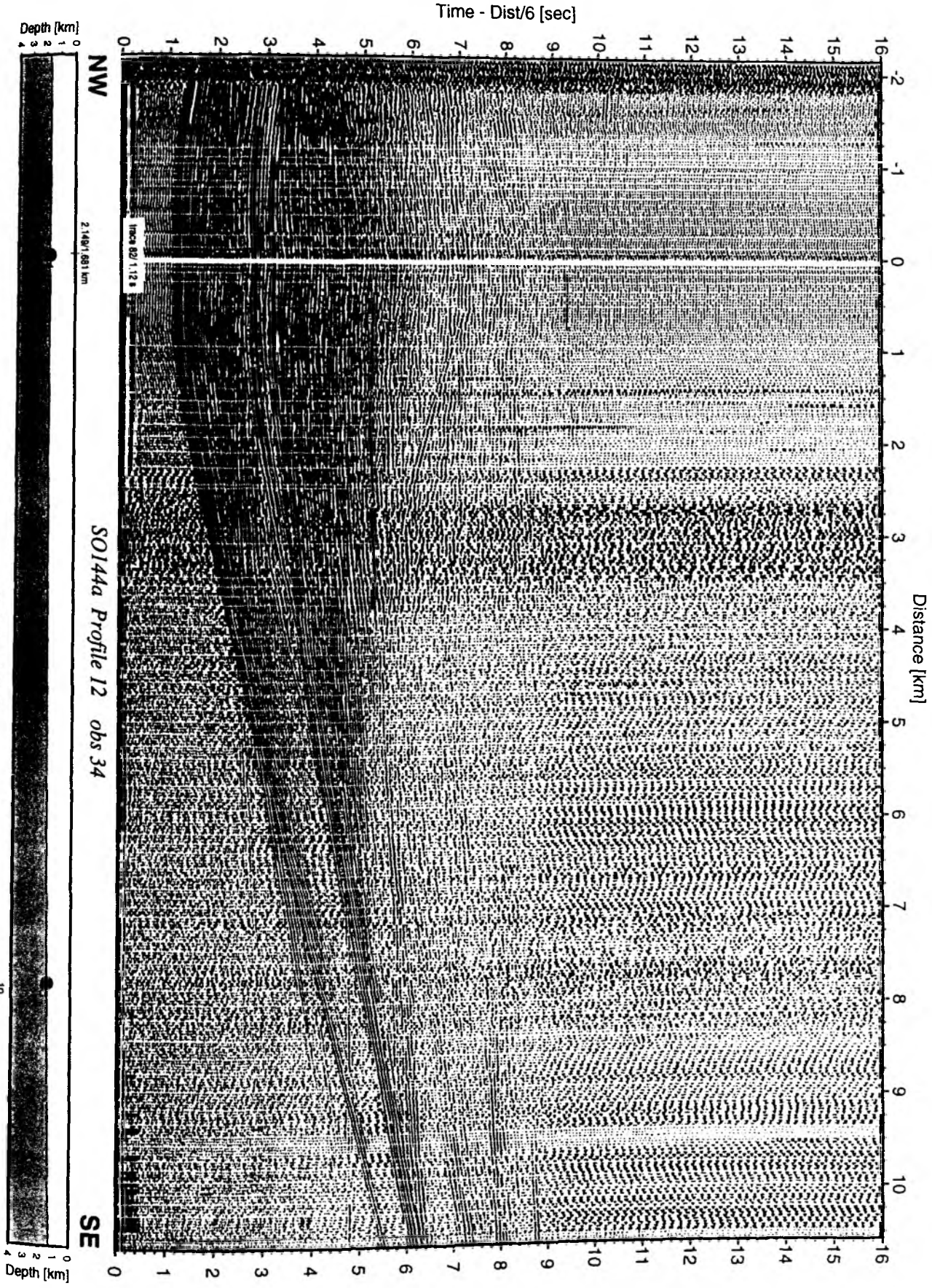

Figure 6.2.4.2.6: Record section from obs 34 vertical component, Profile 12

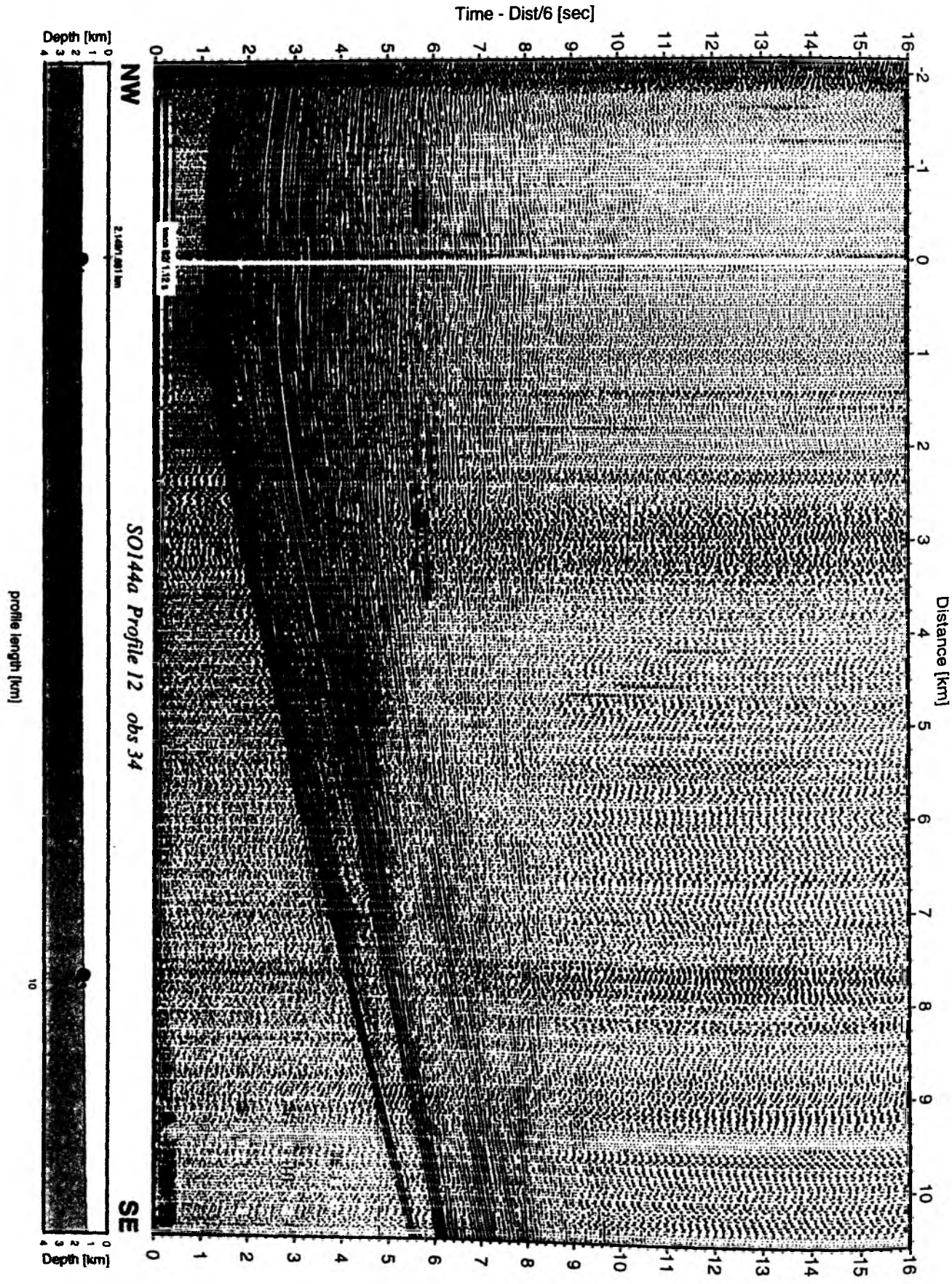

Figure 6.2.4.2.7: Record section from obs 34 horizontale component 1, Profile 12

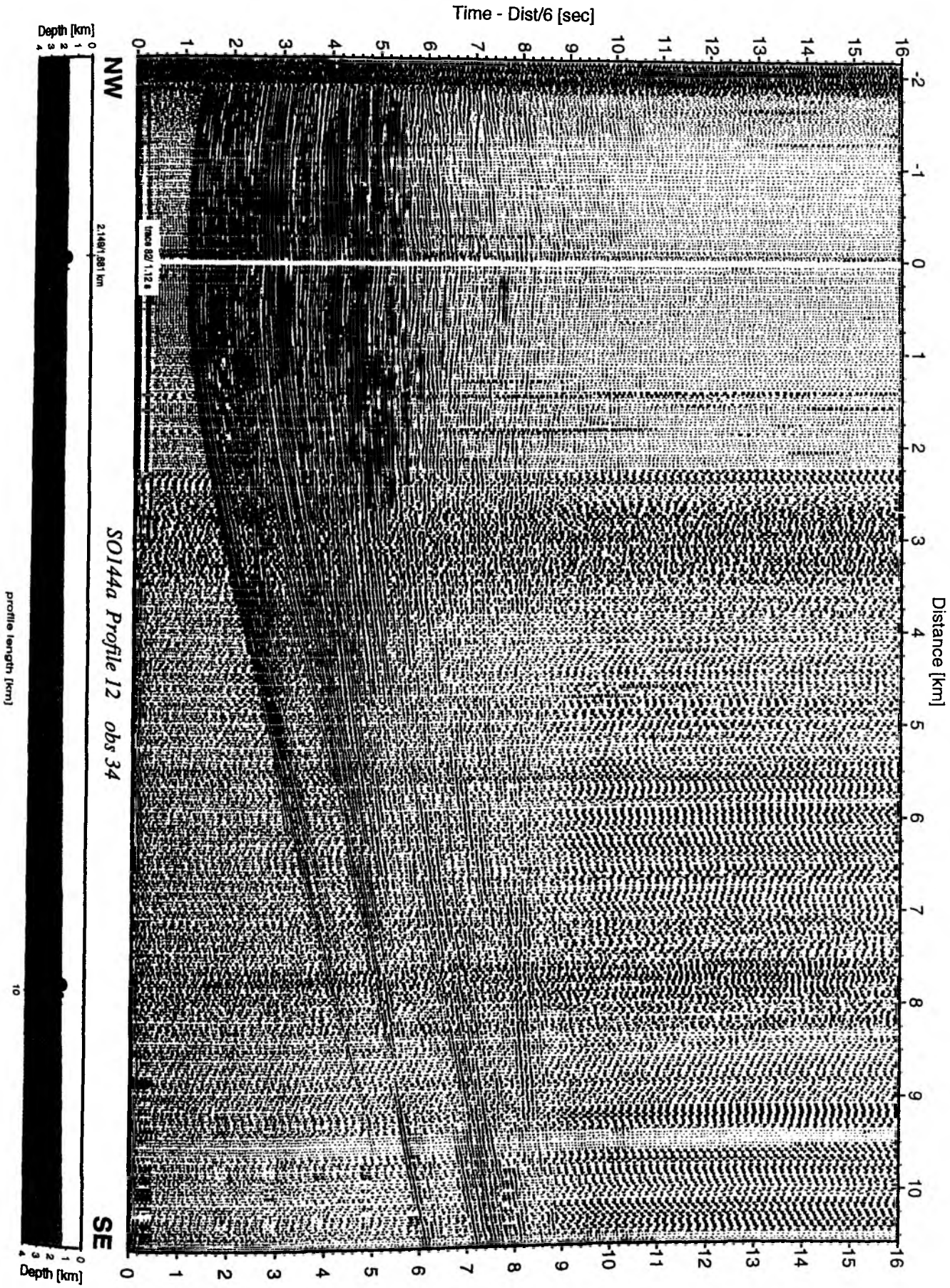

Figure 6.2.4.2.8: Record section from obs 34 horizontale component 2, Profile 12

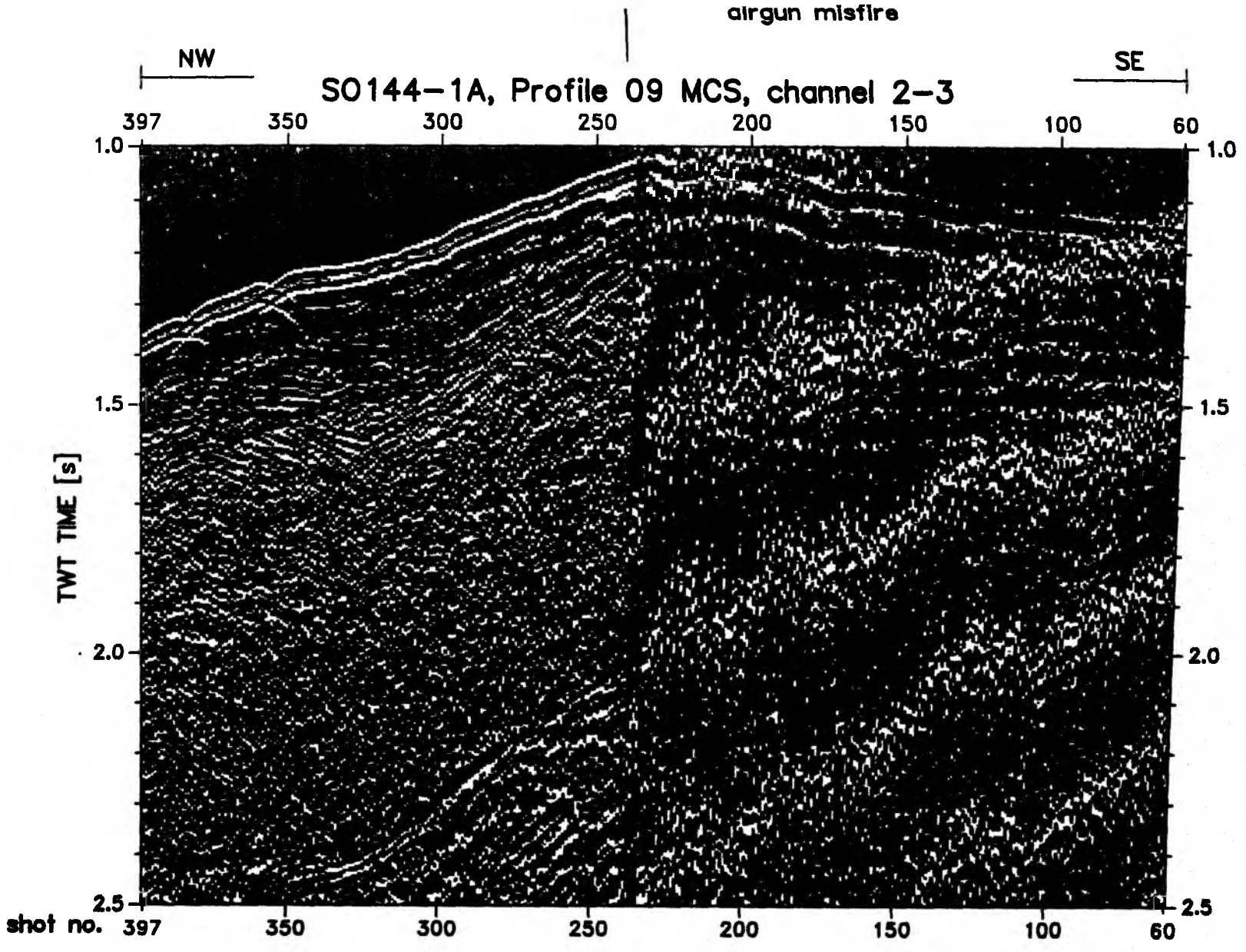

Figure 6.2.4.2.9: Seismic section of MCS data of Profile 09

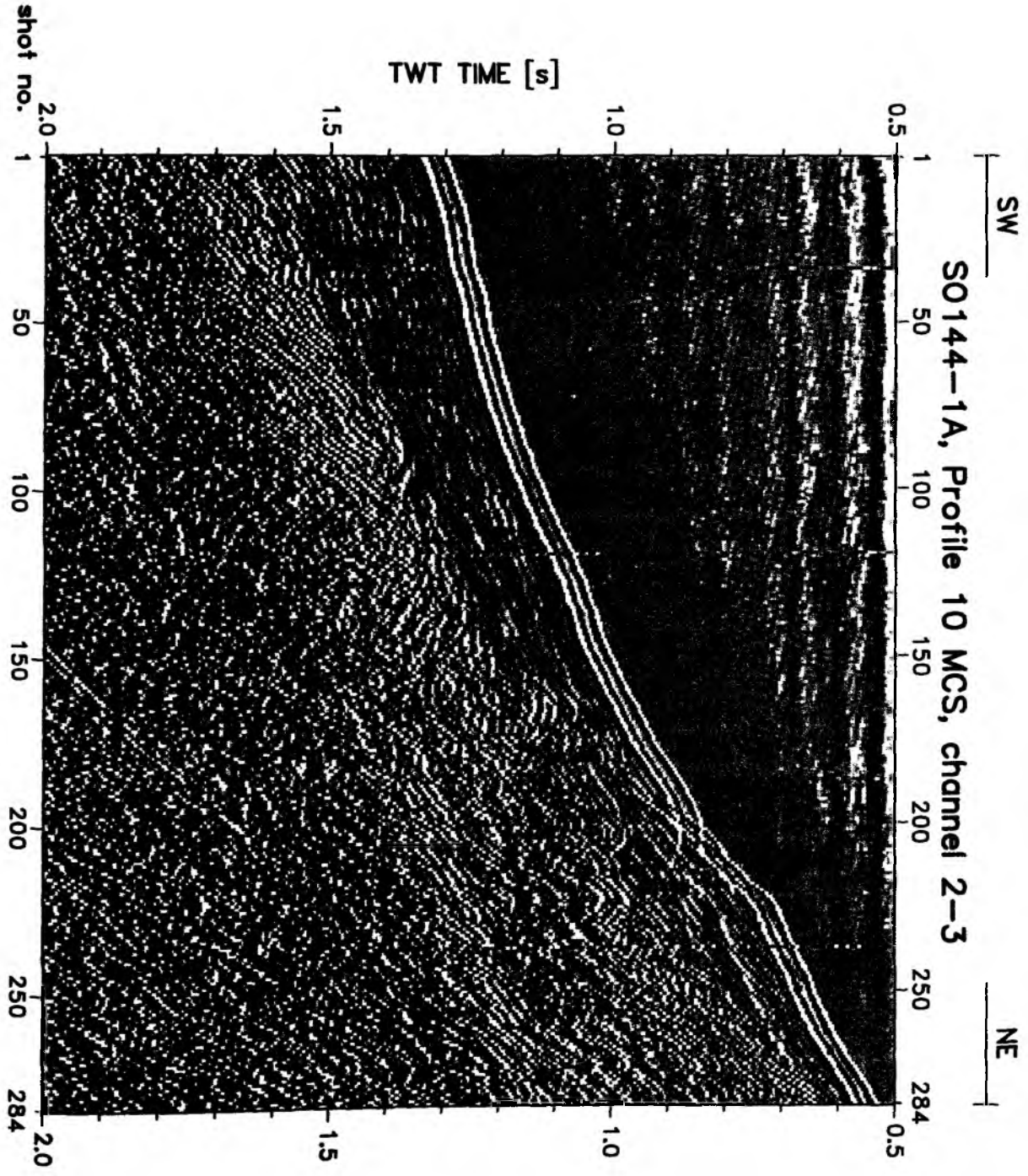

Figure 6.2.4.2.10: Seismic section of MCS data of Profile 10

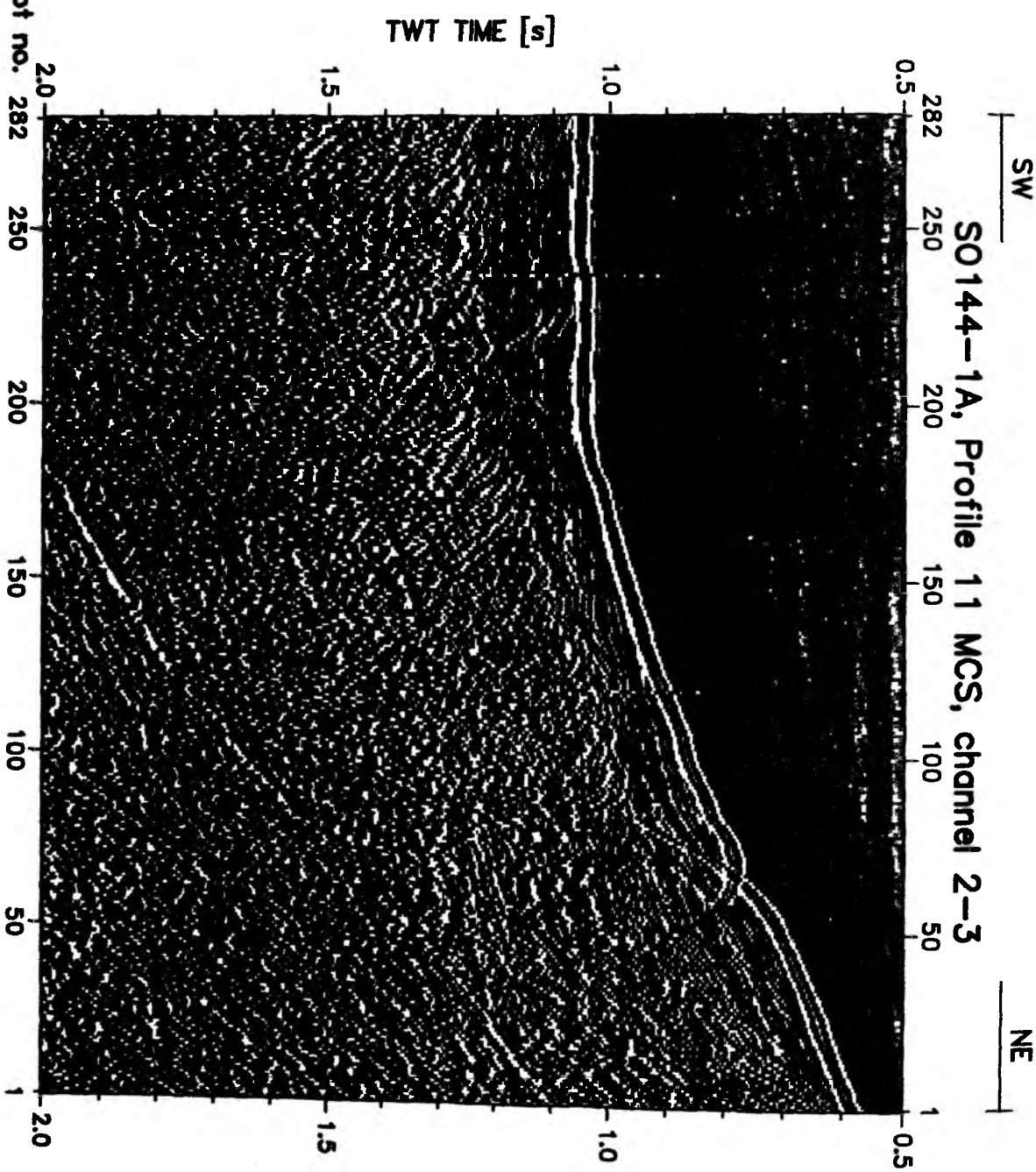

Figure 6.2.4.2.11: Seismic section of MCS data of Profile 11

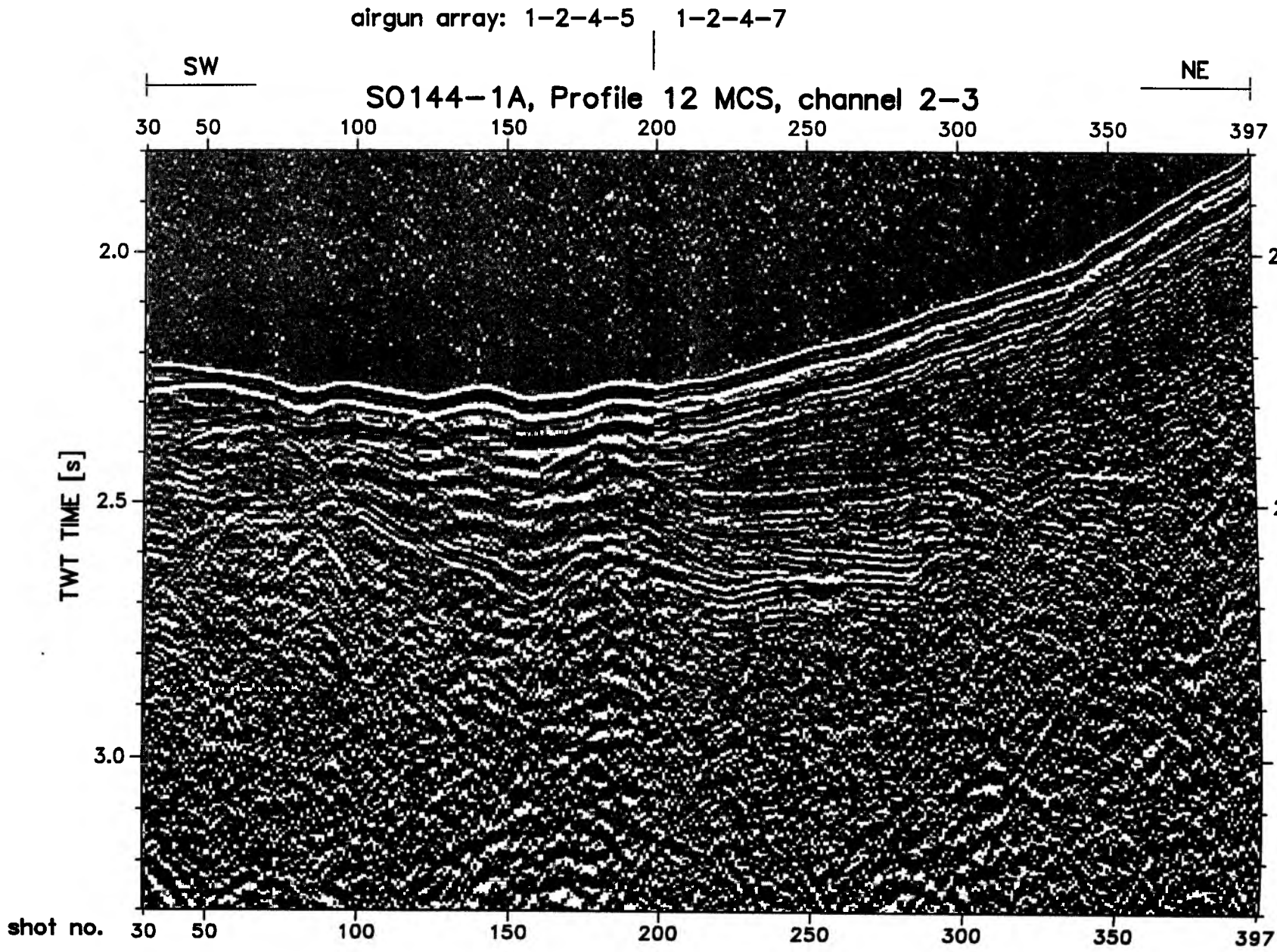

Figure 6.2.4.2.12: Seismic section of MCS data of Profile 12

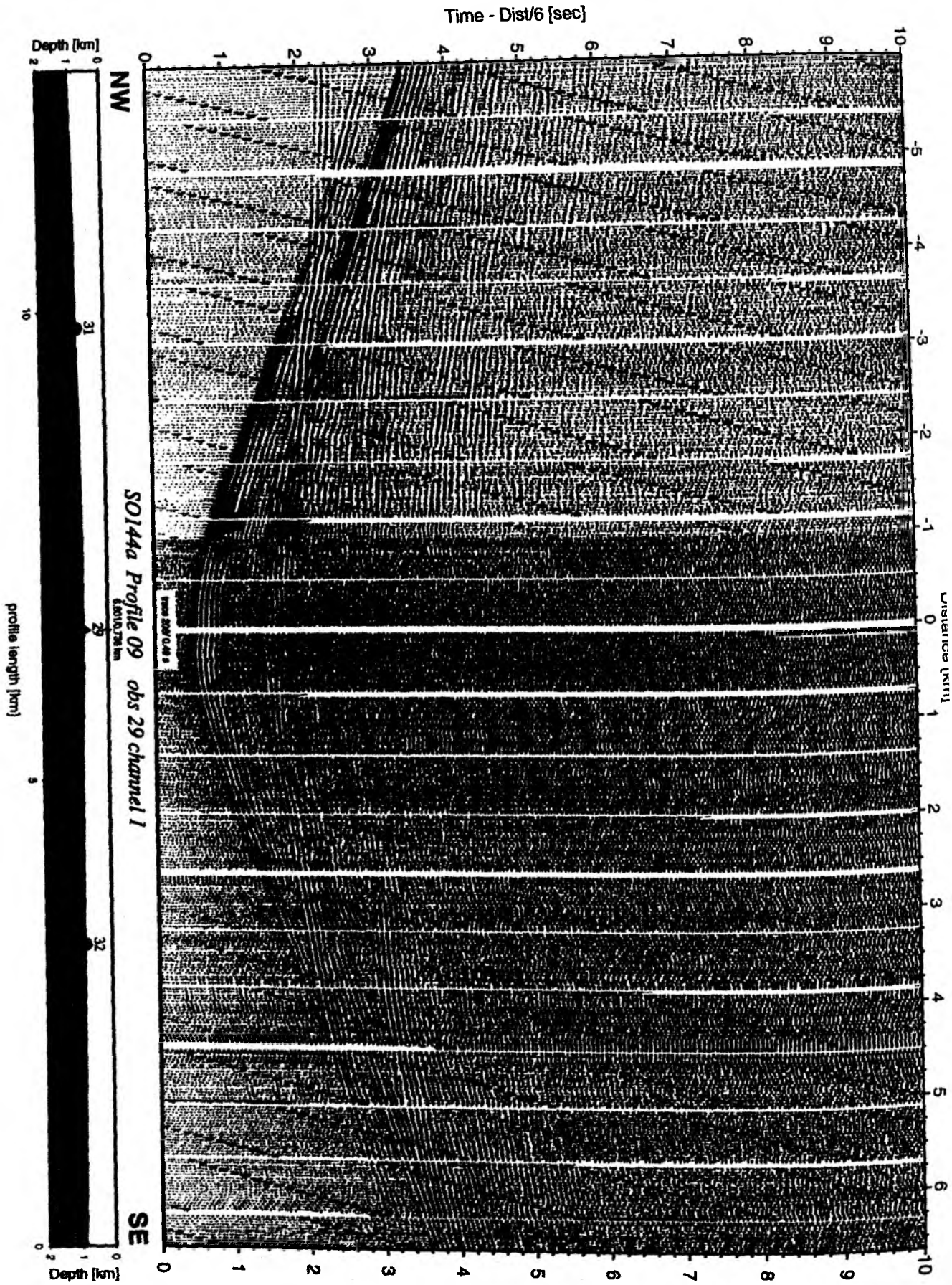

Figure 6.2.4.2.13: Record section from obs 29 vertical component, Profile 09.

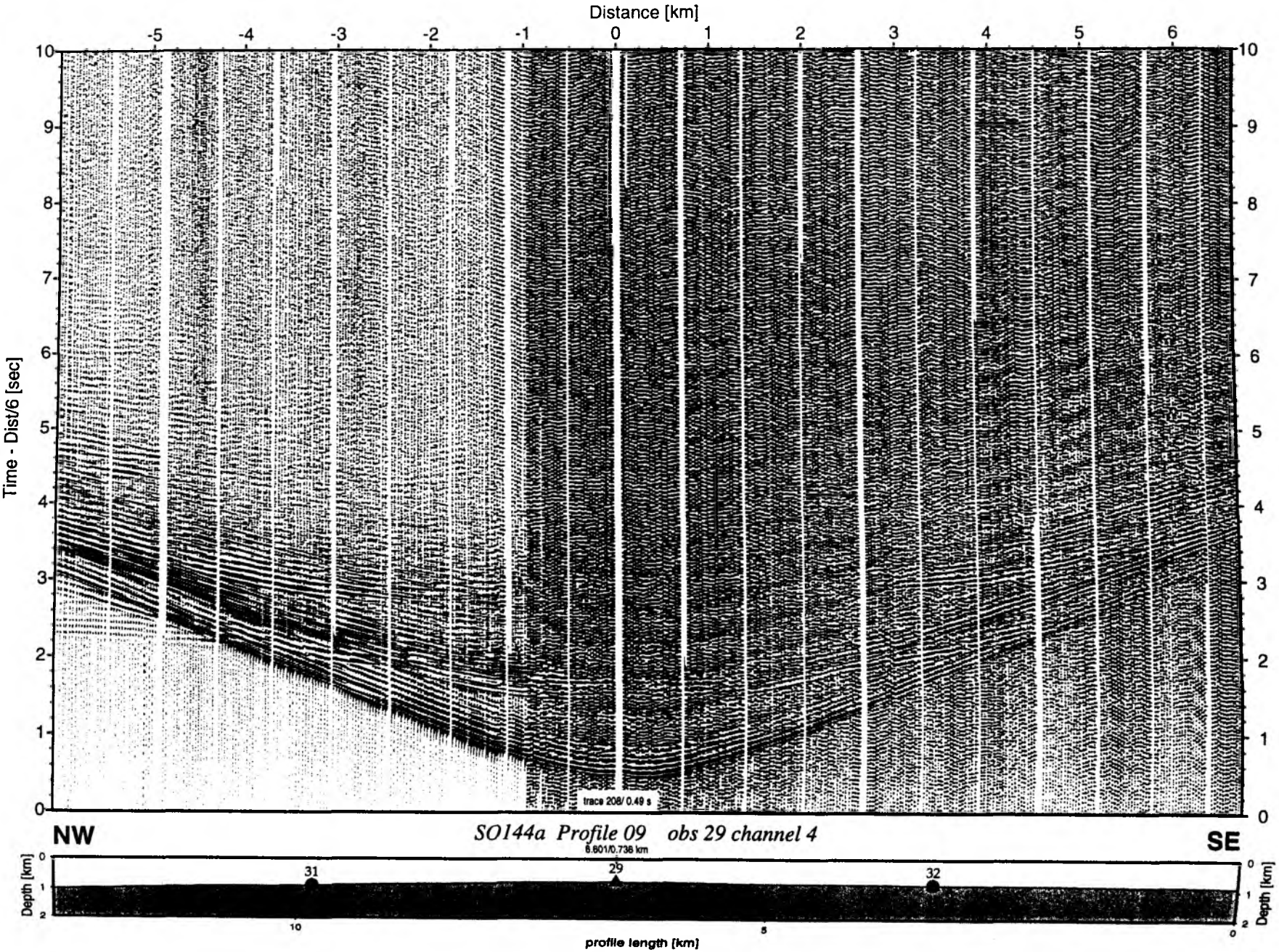

Figure 6.2.4.2.14: Record section from obs 29 hydrophone, Profile 09.

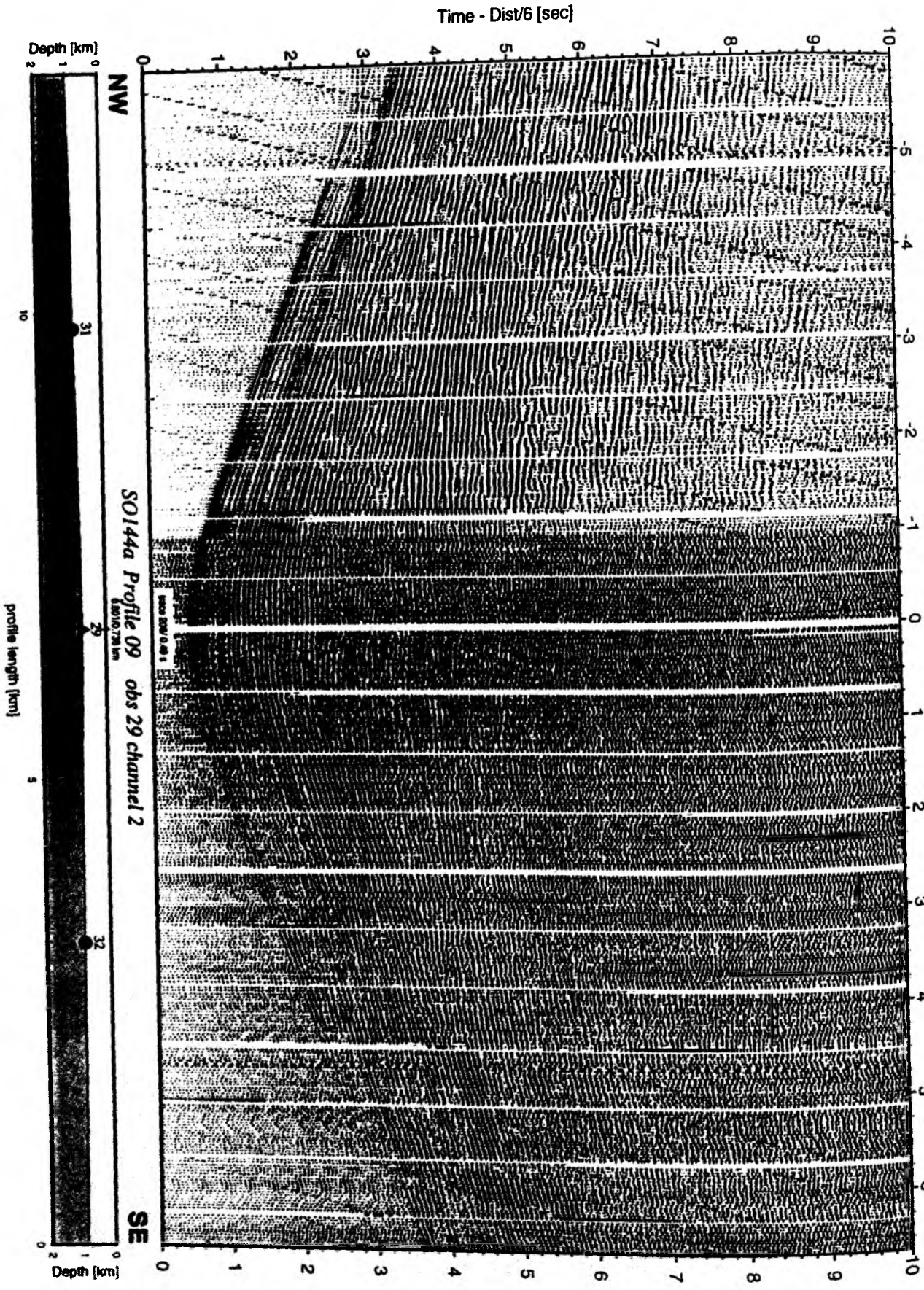

Figure 6.2.4.2.15: Record section from obs 29 horizontal component 1, Profile 09.

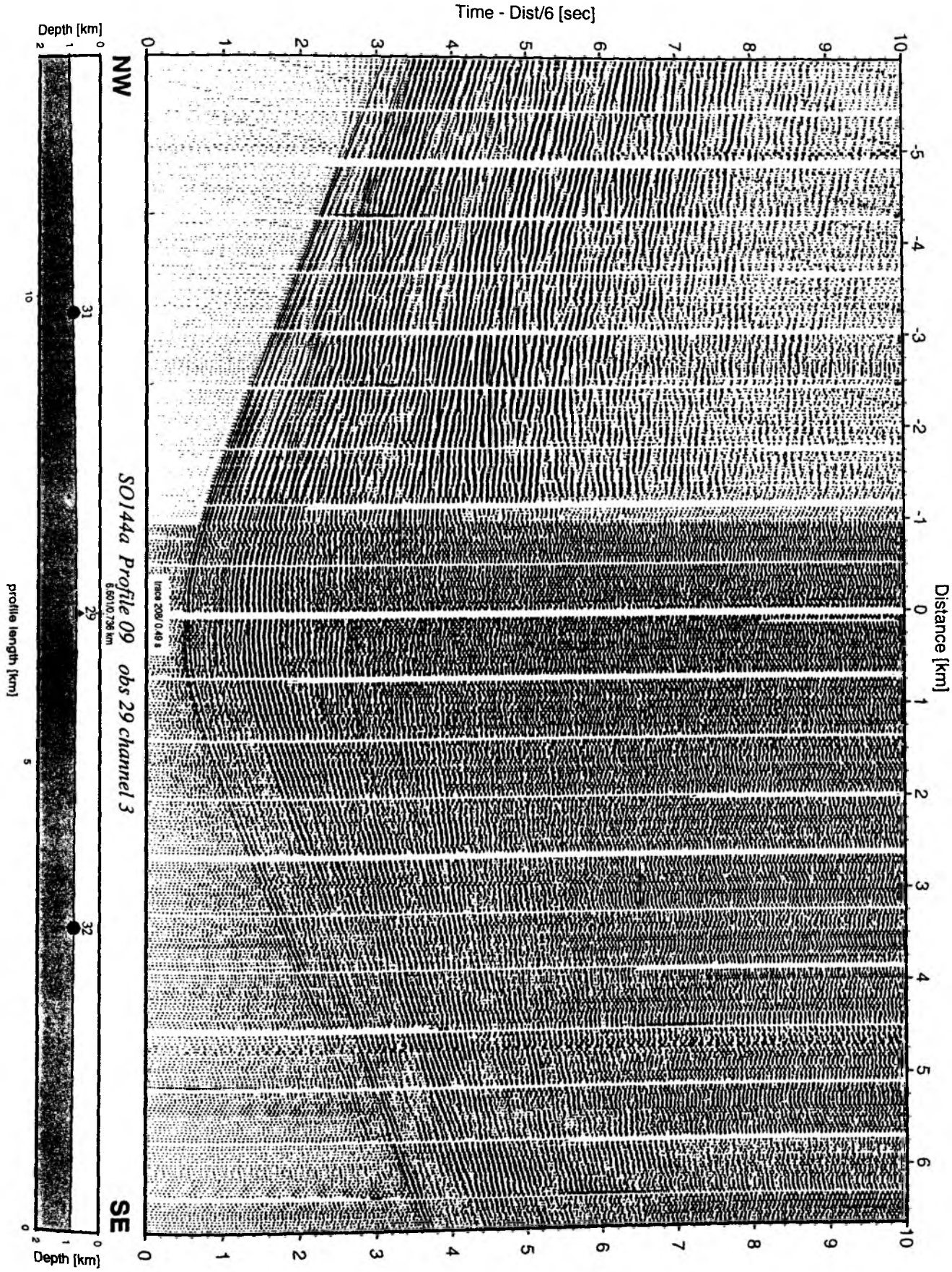

Figure 6.2.4.2.16: Record section from obs 29 horizontal component 2, Profile 09.

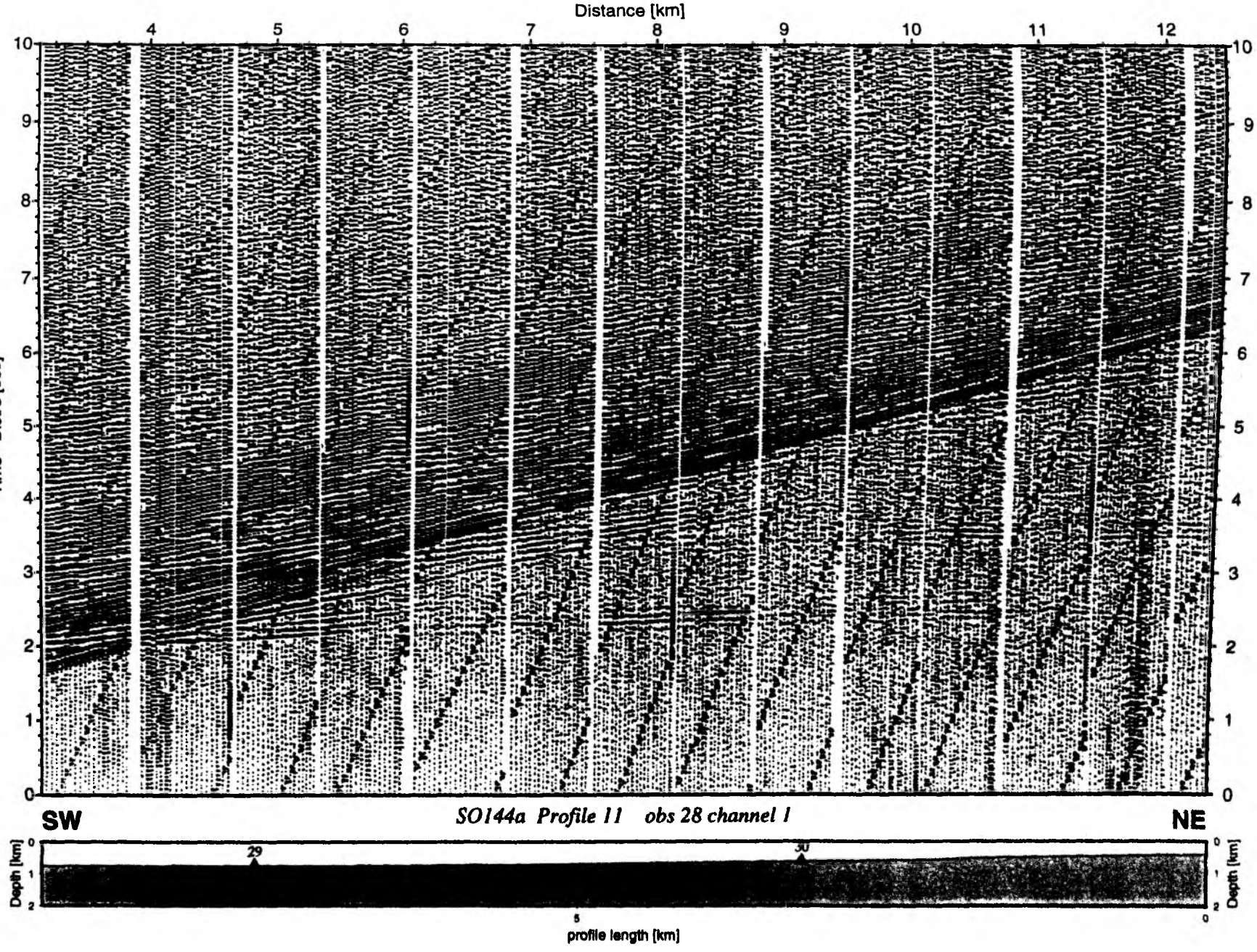

Figure 6.2.4.2.17: Record section from obs 28 vertical component, Profile 11.

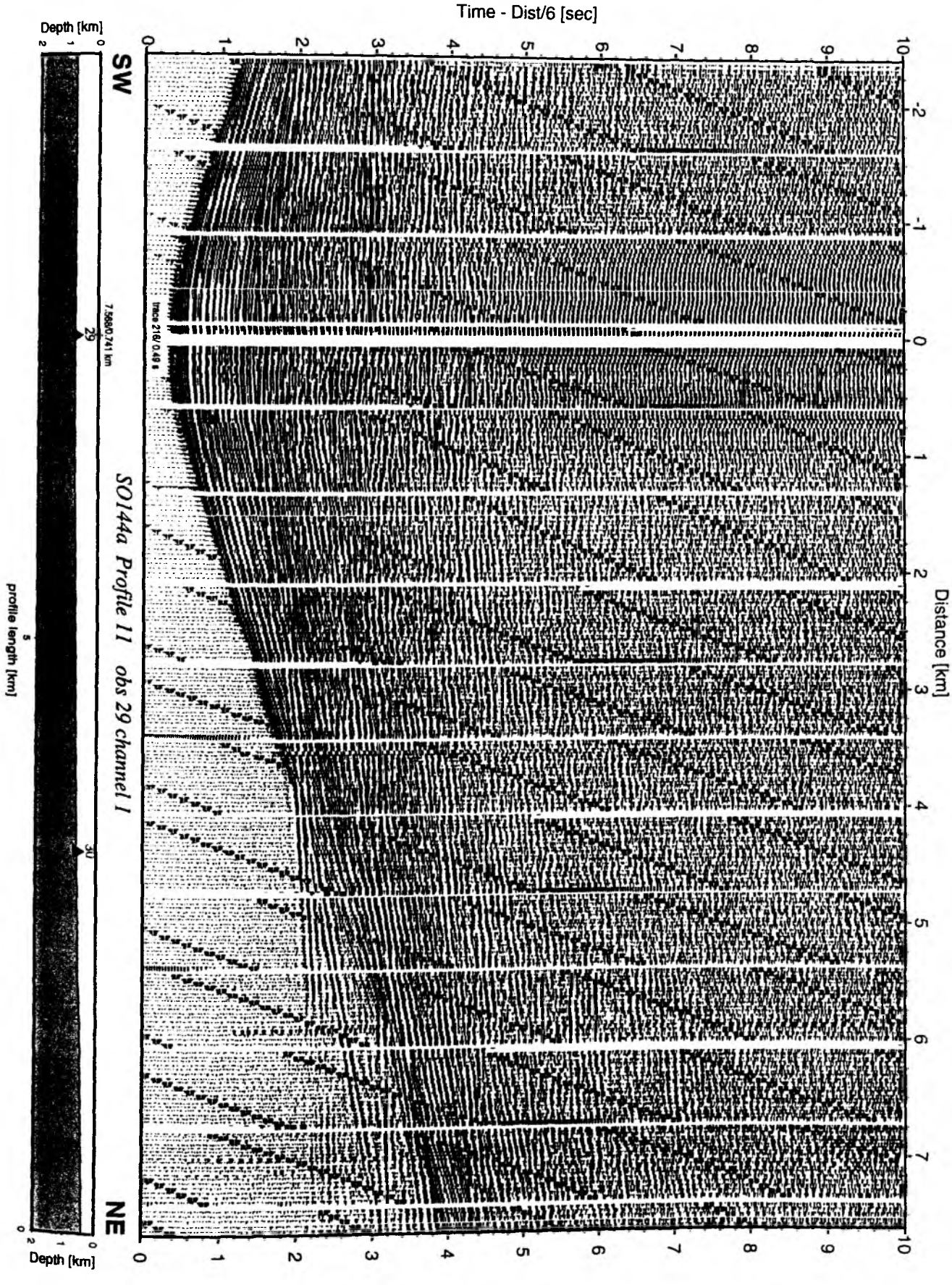

Figure 6.2.4.2.18: Record section from obs 29 vertical component, Profile 11.

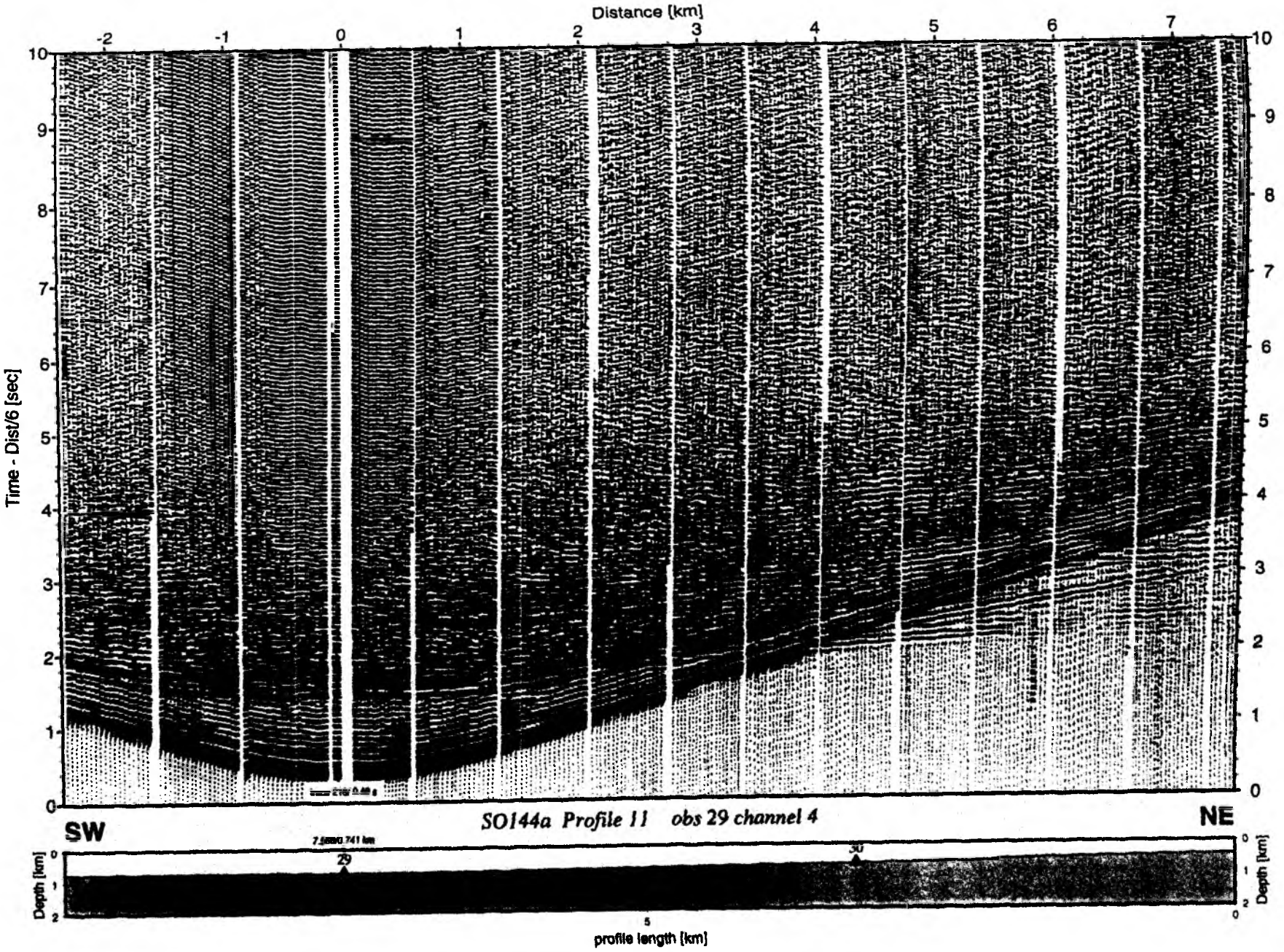

Figure 6.2.4.2.19: Record section from obs 29 hydrophone, Profile 11.

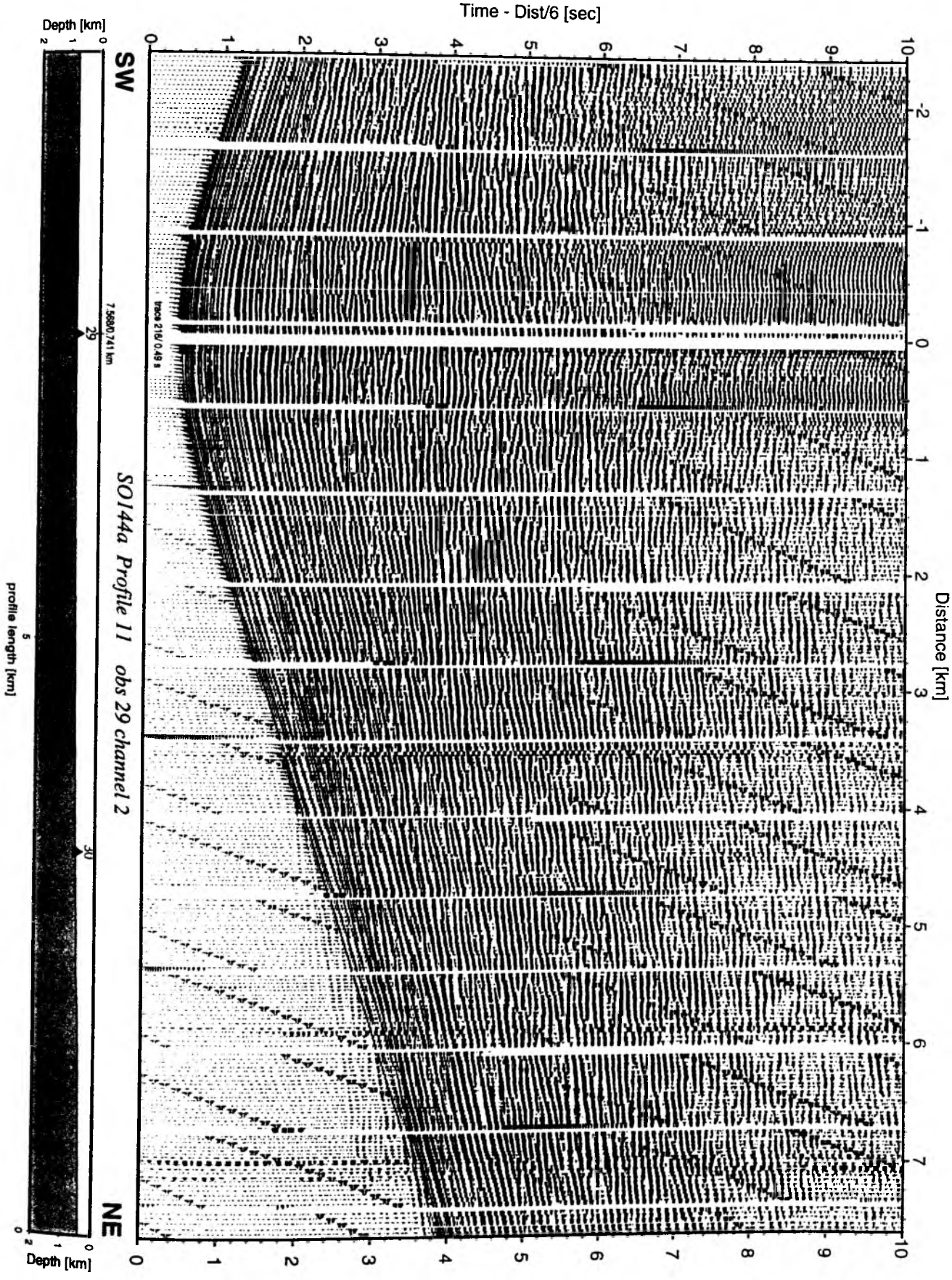

Figure 6.2.4.2.20: Record section from obs 29 horizontal component 1, Profile 11.

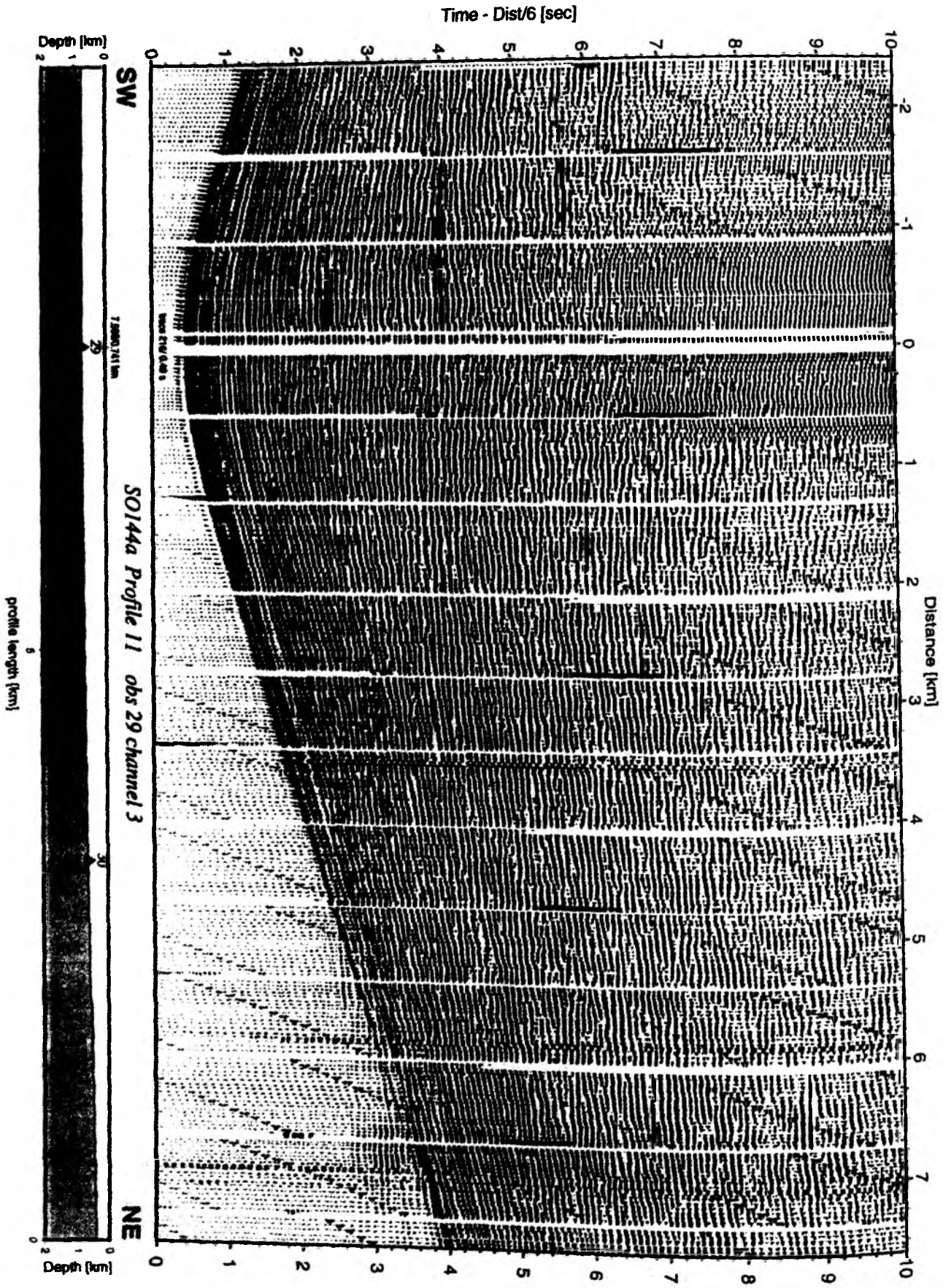

Figure 6.2.4.2.21: Record section from obs 29 horizontal component 2, Profile 11.

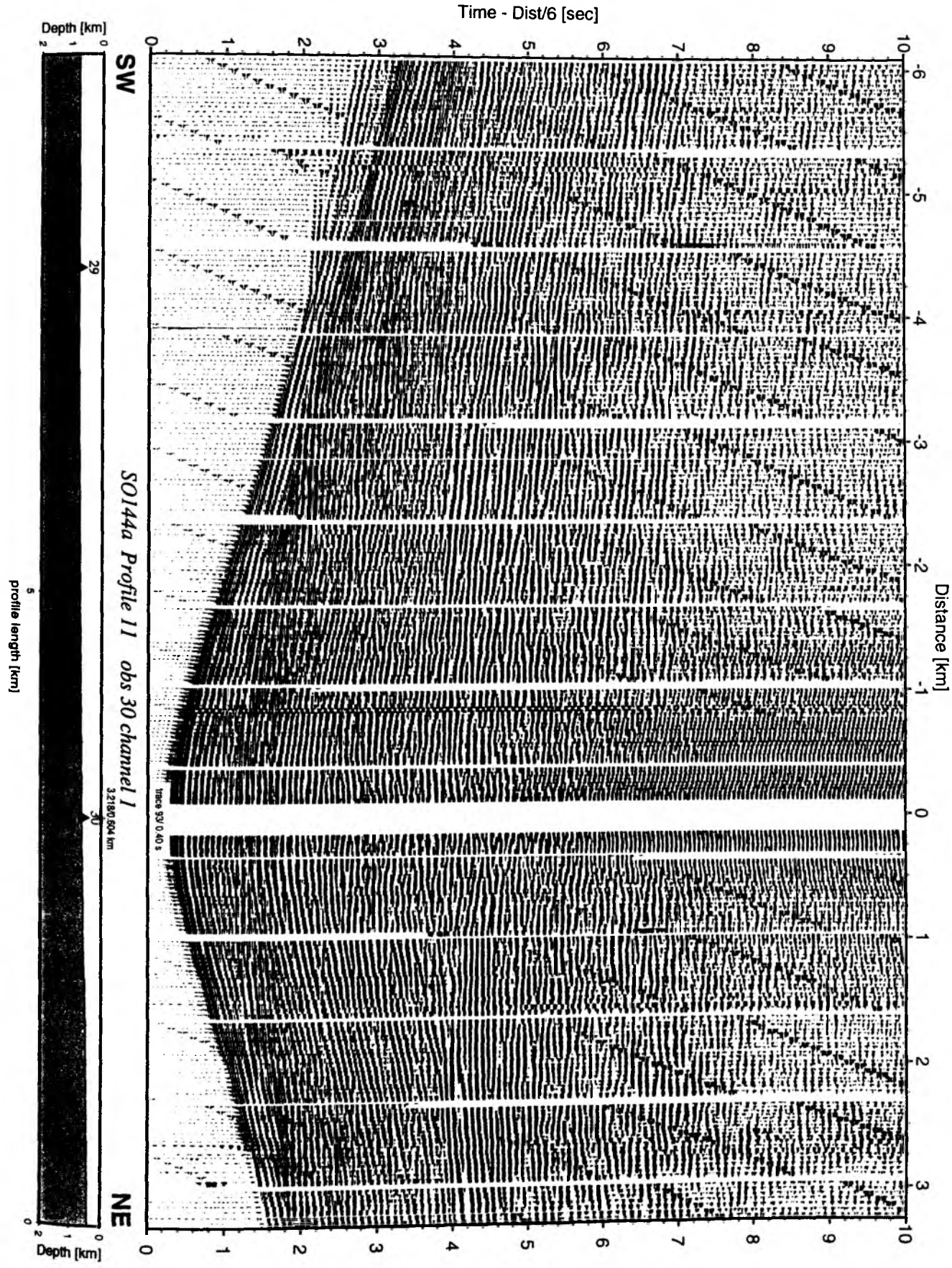

Figure 6.2.4.2.22: Record section from obs 30 vertical component, Profile 11.

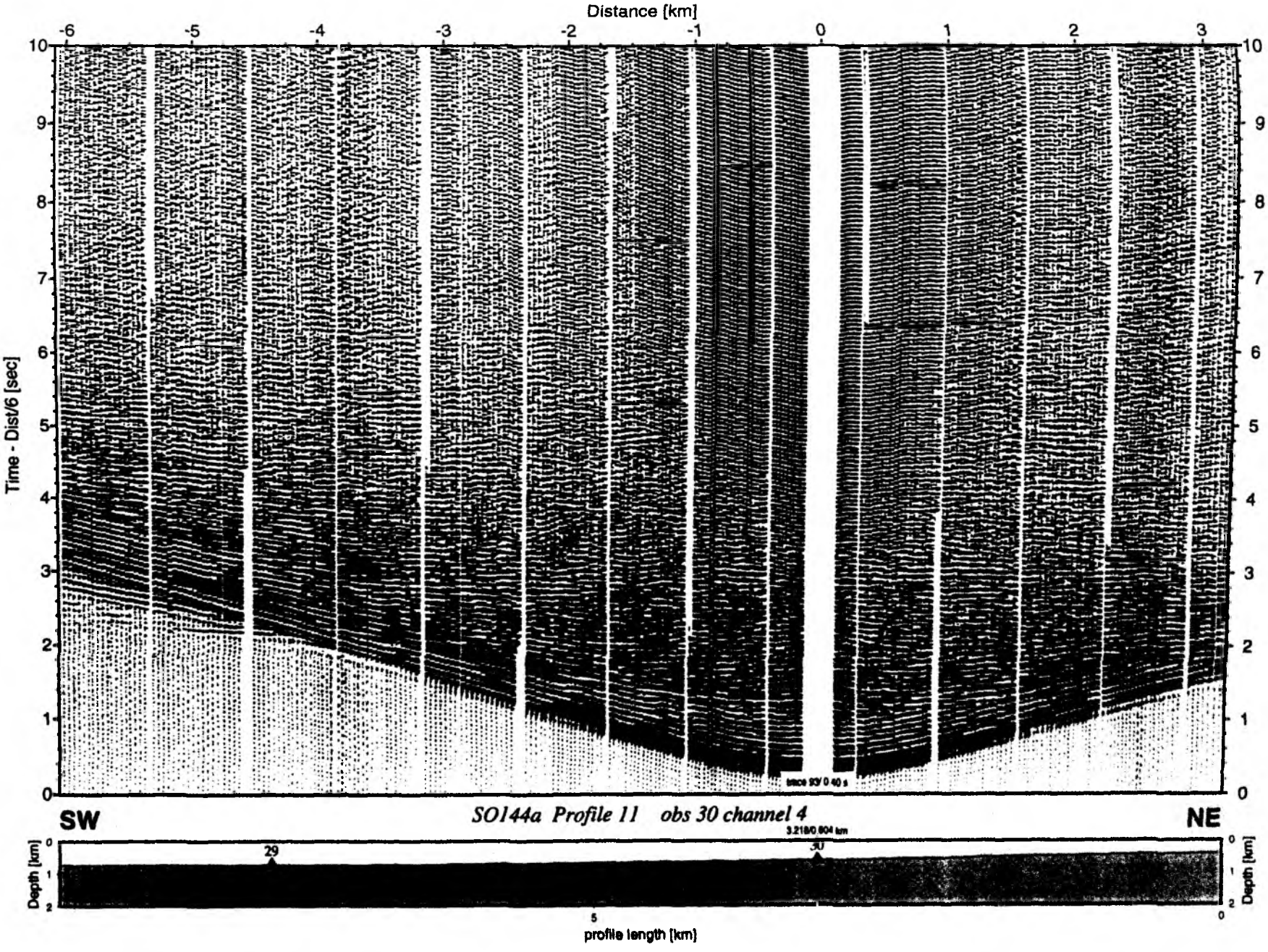

Figure 6.2.4.2.23: Record section from obs 30 hydrophone, Profile 11.

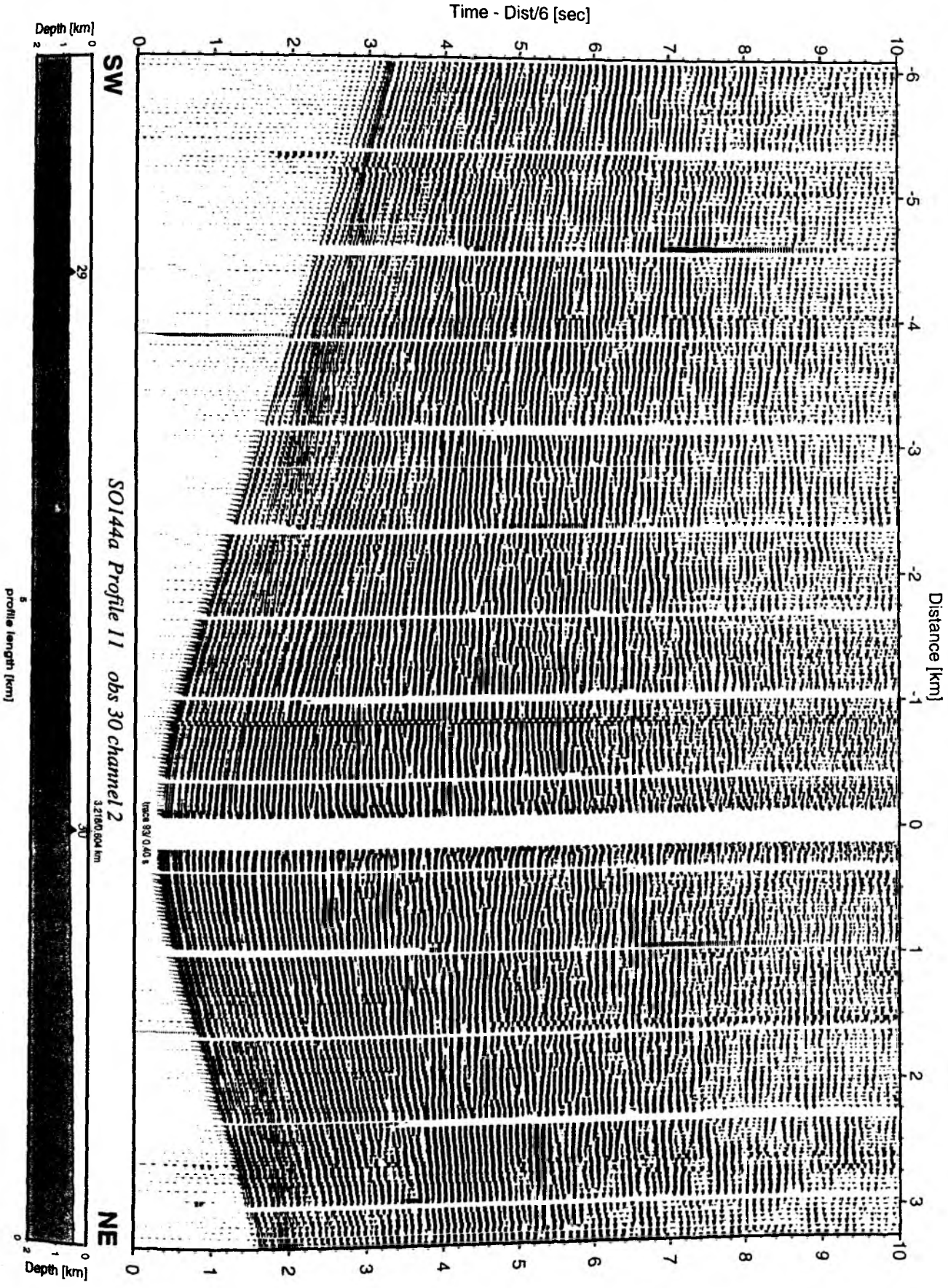

Figure 6.2.4.2.24: Record section from obs 30 horizontal component 1, Profile 11.

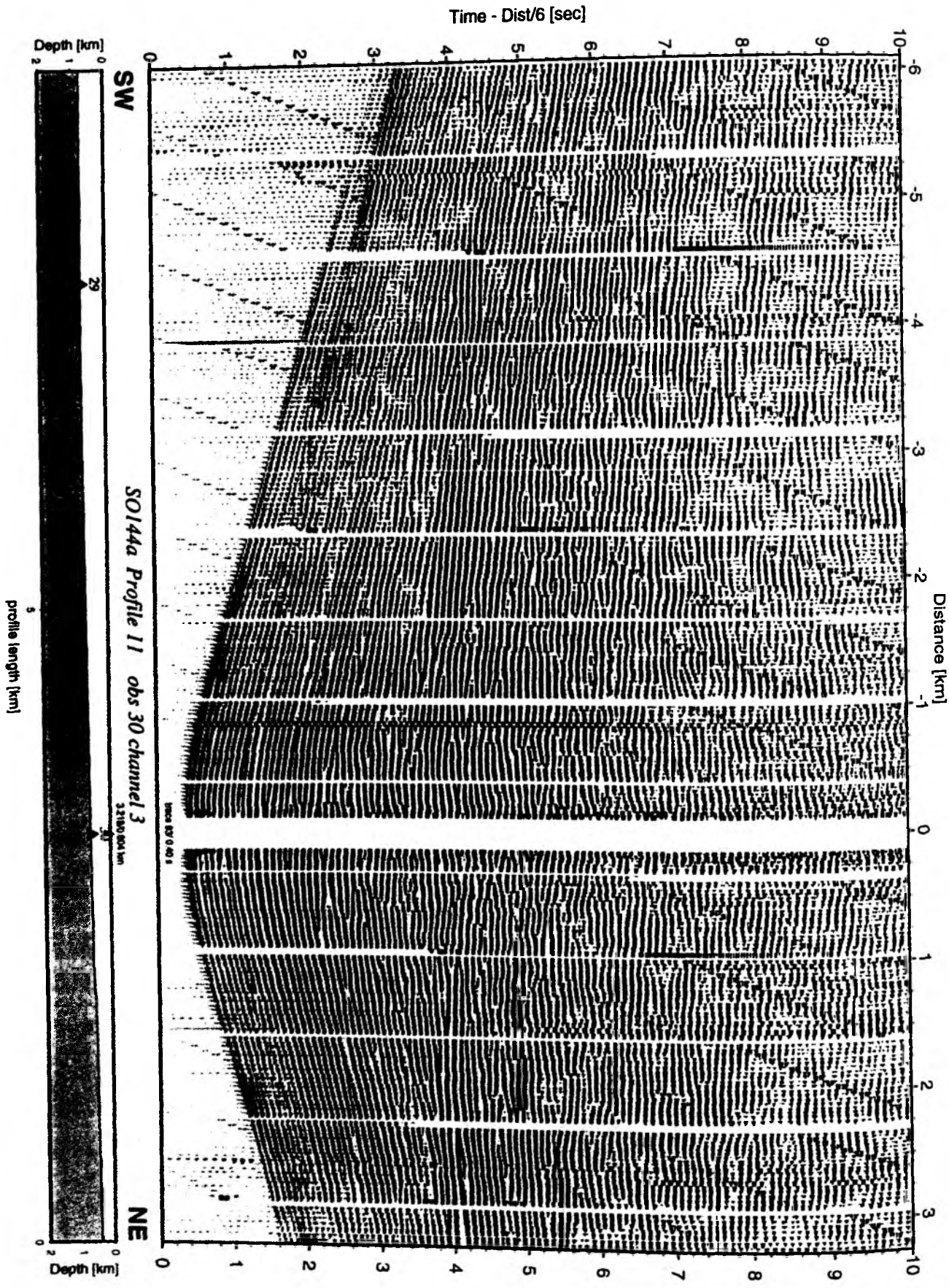

Figure 6.2.4.2.25: Record section from obs 30 horizontal component 2, Profile 11.

6.2.4.3 PROFILE SO144-01

Profile SO144-01 is located seaward of the Middle America Trench, offshore Costa Rica and crosses Quepos Plateau and Cocos Ridge (Fig. 6.2.4.3.1). The aim behind this profile was to investigate crustal variations (thickness and velocity) of the incoming plate, which may have a profound effect on earthquake generation and be the cause for asperities. In addition, the amount of underplated material and the ratio of intrusive to extrusive volcanics is unknown for the Quepos Plateau and Cocos Ridge, as well as for neighbouring structures. The profile was chosen coincident with two MCS lines recorded in 1992 during cruise SO81. A poststack time migration of these lines (Hinz et al., 1996) is presented in Fig. 6.2.4.3.3. Along the profile, 33 instruments were deployed (OBS 35 to 67) - 13 IRD OBS in the southeast followed by 20 GEOMAR OBH/OBS to the northwest. The IRD instruments were deployed on 24 September, and the release times were set to 00:00 - 15:00 on 04.October. The GEOMAR instruments were deployed on 26 September before SONNE left for its call to the port of Caldera on 27/28 September. Shooting started on leg SO144-1b on 28 September at 17:00 at a speed of 3.5 kn with a 60-secshot interval, terminating the 140-nm-long profile at 09:00 on 30.09. The shooting line started and terminated about 10 nm before and after the recording array. All three airguns worked well for the first 12 hours, but later problems with the airhoses and trigger lines caused repair times during which only one or two guns stayed operational. Details on instruments and shots are given in Appendices 9.1.3 and 9.2. During shooting the magnetometer was also deployed. The GEOMAR instruments were recovered immediately after shooting, between 16:00 on 30 September and 11:00 01 October, during which a track-parallel line with magnetics and hydroacoustics was also collected. About one hour after shooting had terminated the 7.4 magnitude Oaxaca earthquake in Mexico occurred and was well recorded by most of the instruments, which were more than 1600 km away. The record section from this event is shown in Figure 6.3.4.2.2. On a few instruments the batteries were low and some other problems occurred (see Appendix 9.1.3), but the data quality is generally very good, with clear arrivals seen beyond 150 km offset. The IRD instruments were all safely recovered in time on 04 October between 00:00 an 15:00 and had also recorded the airgun shots along profile SO144-02-1. Record sections are shown in Figures 6.2.4.3.3 to 6.2.4.3.33.

Modelling and interpretation

The most prominent seismic phases were picked for every GEOMAR OBH/OBS and for every other IRD OBS. The picking accuracy was better than 50 ms in the near offset range where apparent velocities stay below 6 km/s. deteriorated to 100 ms in the far offset range and could exceed 200 ms for phases with weak and isolated appearance of energy. From MCS lines the basement reflection was picked in two-way travel time. In the end, 8600 traveltimes were picked out of the wide-angle recordings and 230 from the two MCS lines (Fig 6.2.4.3.34 a).
2-D ray tracing was done from top to bottom. A starting model comprised only the morphology. Sediment coverage was modeled with the MCS picks and the appearance of the first basement refraction. A very low velocity of 1.6 – 1.9 km/s had to be taken for the sediment because almost no precursor appears near the water wave phase.
Results of the preliminary modeling from top to bottom and NW to SE (Fig. 6.2.4.3.34 b):

- The MCS lines from SO81 clearly show the boundary between sediment and basement and the wide-angle modeling adds a prominent velocity contrast to this boundary. Sediment velocities seldom exceed 2.0 km/s. Basement velocities start with 3.8 km/s or more. Sediment thickness reaches a maximum of 1 km in the Cocos Ridge central graben structure and 0.8 km in the basin between the Cocos Ridge and the Quepos Plateau. An 0.8 km sediment thickness is also found at the northeastern flank of the graben structure, whereas on the southeastern flank of the ridge only 0.5 km is present.
- From wide-angle modeling the Quepos Plateau appears as a compact block with a homogeneous velocity structure. Values are 3.8 km/s at the top, with a gradient of 0.2 s^{-1}. The top of the plateau exibits a high impedance contrast giving rise to some additional multiples (2 sec) generated by shots over this feature, in addition to the usual multiples generated near the OBHs. They are visible in the record sections of OBHs 67, 62, 60, 59 and OBS 61.
- The basement consists of three layers, units a, b, c (Fig. 6.2.4.3.34 b). From their appearance in the record sections, there may be a more gradual transition between them than that of a first order boundary.
- The uppermost basement, unit a, has average velocities between 4.2 - 4.7 km/s. There appears to be a difference between the two flanks of the Cocos Ridge. At the northwestern side, from the central graben to the Quepos Plateau, velocities increase from 3.8 – 4.0 km/s at the top to 4.3 – 4.5 km/s at the bottom. At the southeastern flank, the values are higher and increase from 4.4 – 4.5 km/s to 4.8 – 4.9 km/s. Showing a highly variable thickness from a 2.2 km maximum to almost zero below the central graben, unit a also thins out remarkably northwest of the Quepos Plateau.
- Basement unit b has average velocities between 5.3 – 5.7 km/s. Again, velocities are slightly higher (+0.15 km/s) SE of the Cocos Ridge center, although this layer is shallower than the other flank. Layer thickness is almost constant between 1.5 – 2.0 km.
- Basement unit c best exhibits the thickened crust of the Cocos Ridge. In the NW part of the profile, this unit deepens from 6 km to 11 km. From km 40 on the lower boundary deepens further and reaches a maximum depth of more than 20 km at km 140. This deep crust-mantle boundary can be followed by the wide-angle data to km 230, where depth is slightly less. The maximum thickness of 16 km is reached below the central graben structure. Velocity values do not vary much and range vertically from 6.4 – 7.0 km/s in the thinner northwestern part to 6.6 – 7.2 km/s in the thickened crust. These values reveal some difference in the velocities of the upper part of this layer, whereas the lateral increase in the lower part can be easily attributed to increasing pressure.
- Mantle velocities are 8.0 – 8.1 km/s.

In summary, an almost normal oceanic crust was found in the NW of Profile 01, where unit b closely resembles layer-2, with almost 2 km thickness and velocities of 5.3 – 5.4 km/s. Unit c resembles layer-3 with 5 km thickness and velocities of 6.4 – 7.0 km/s. The crust-mantle boundary is at 11 km depth. Within 60 km, this boundary dramatically deepens to the SE to more

than 20 km in the center of the Cocos Ridge. The expected shallowing of the crust-mantle boundary on the SE flank of the ridge was not detected by our data and must, therefore, lie still farther to the SE. In the record sections, the strong lateral change in MOHO depth is reflected in distinct shadow zones of the PmP-phase. On OBH 48 to 55, they occur to the NW; on OBH/OBS 59 to 67, to the SE. The upper basement of the Cocos Ridge, represented by unit a in the model, shows a reduced velocity of 3.8 – 4.9 km/s compared to the 5 – 6 km/s of normal oceanic upper crust.

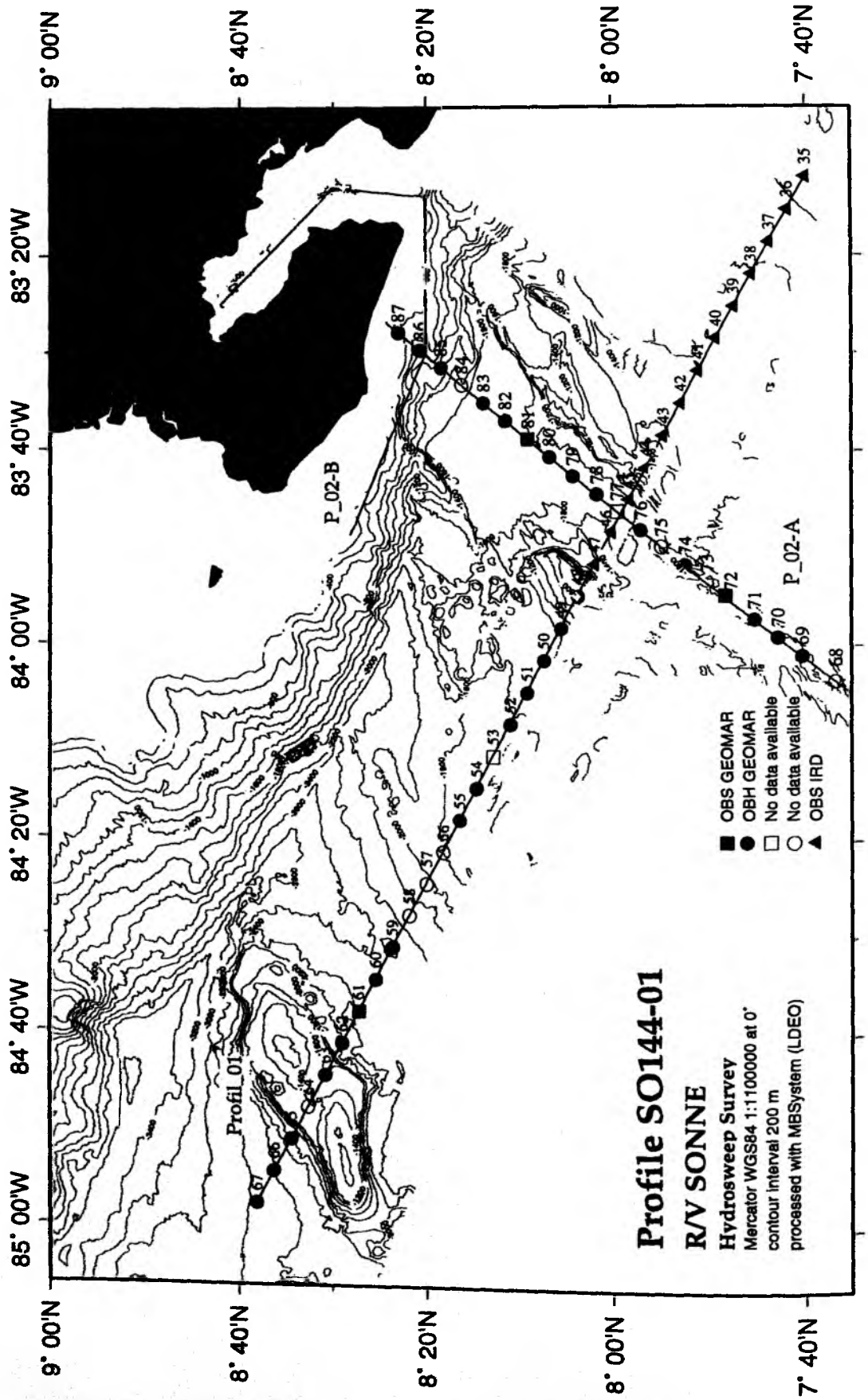

Figure 6.2.4.3.1: Profiles SO144-01, Location map

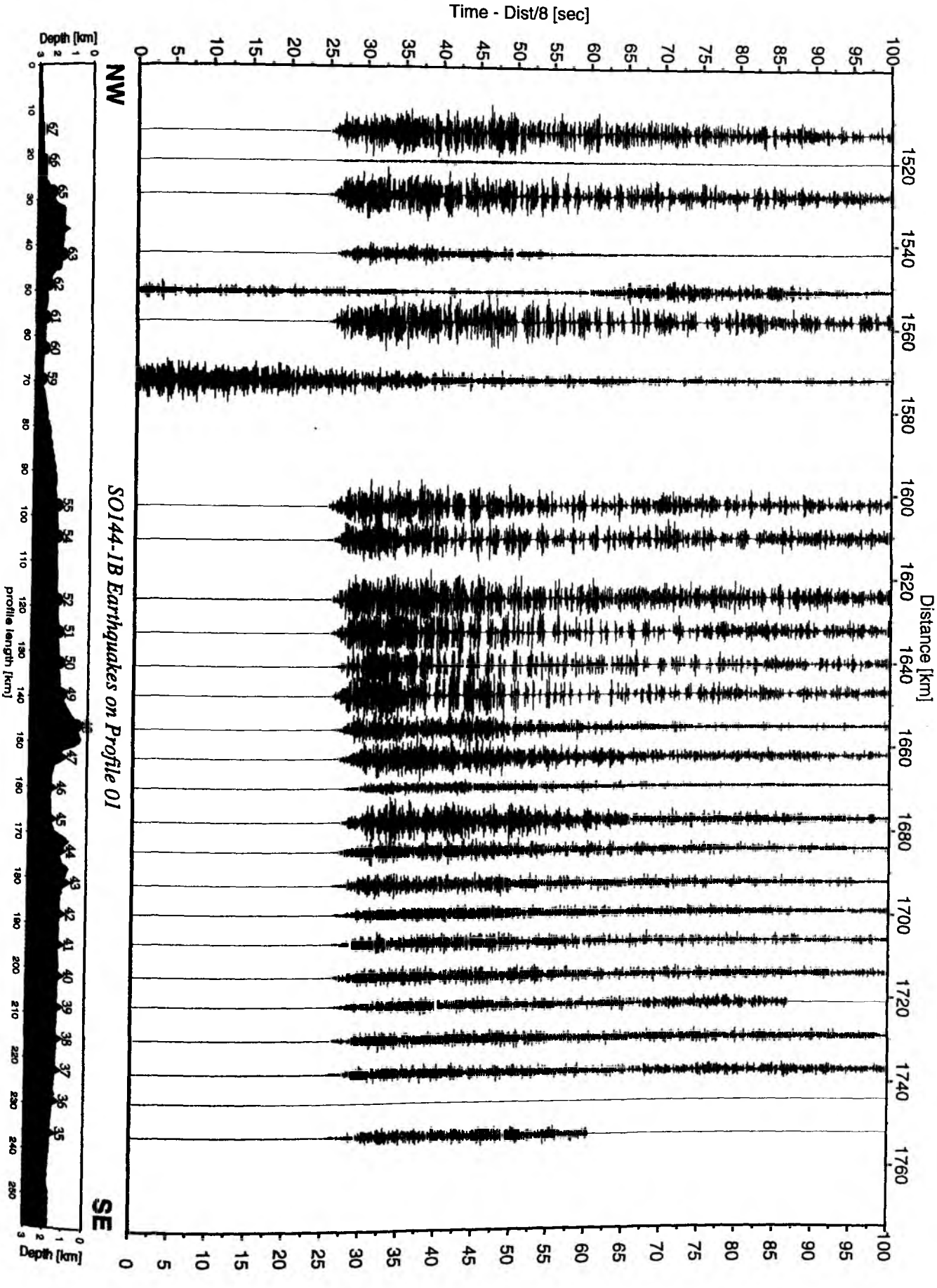

Figure 6.2.4.3.2: Earthquake seismogram from OBH/S station 35 to 67, Profile 01.

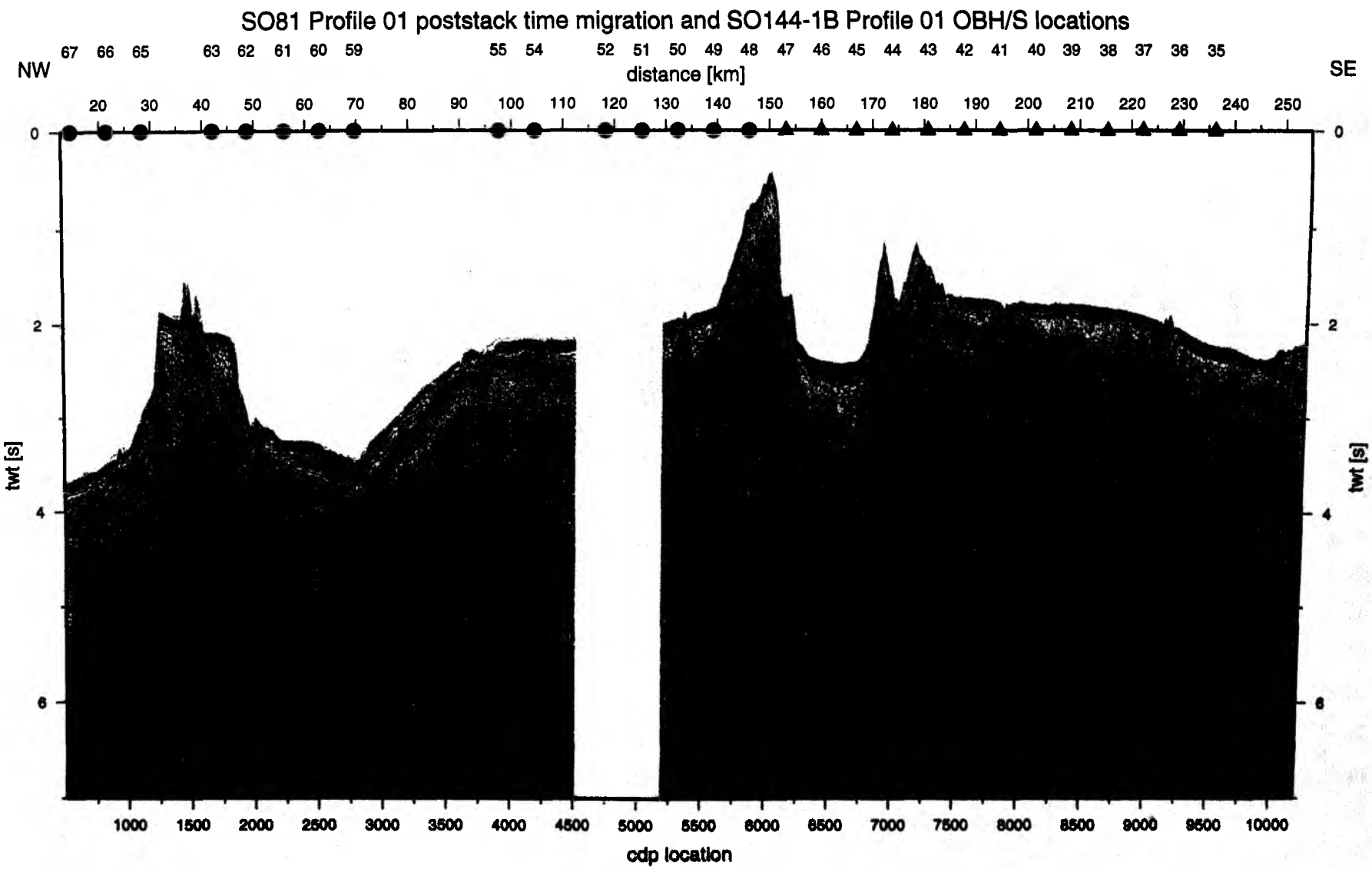

Figure 6.2.4.3.3: Poststack time migration from SO81 Profile 01, and OBH/S locations from Profile 01.

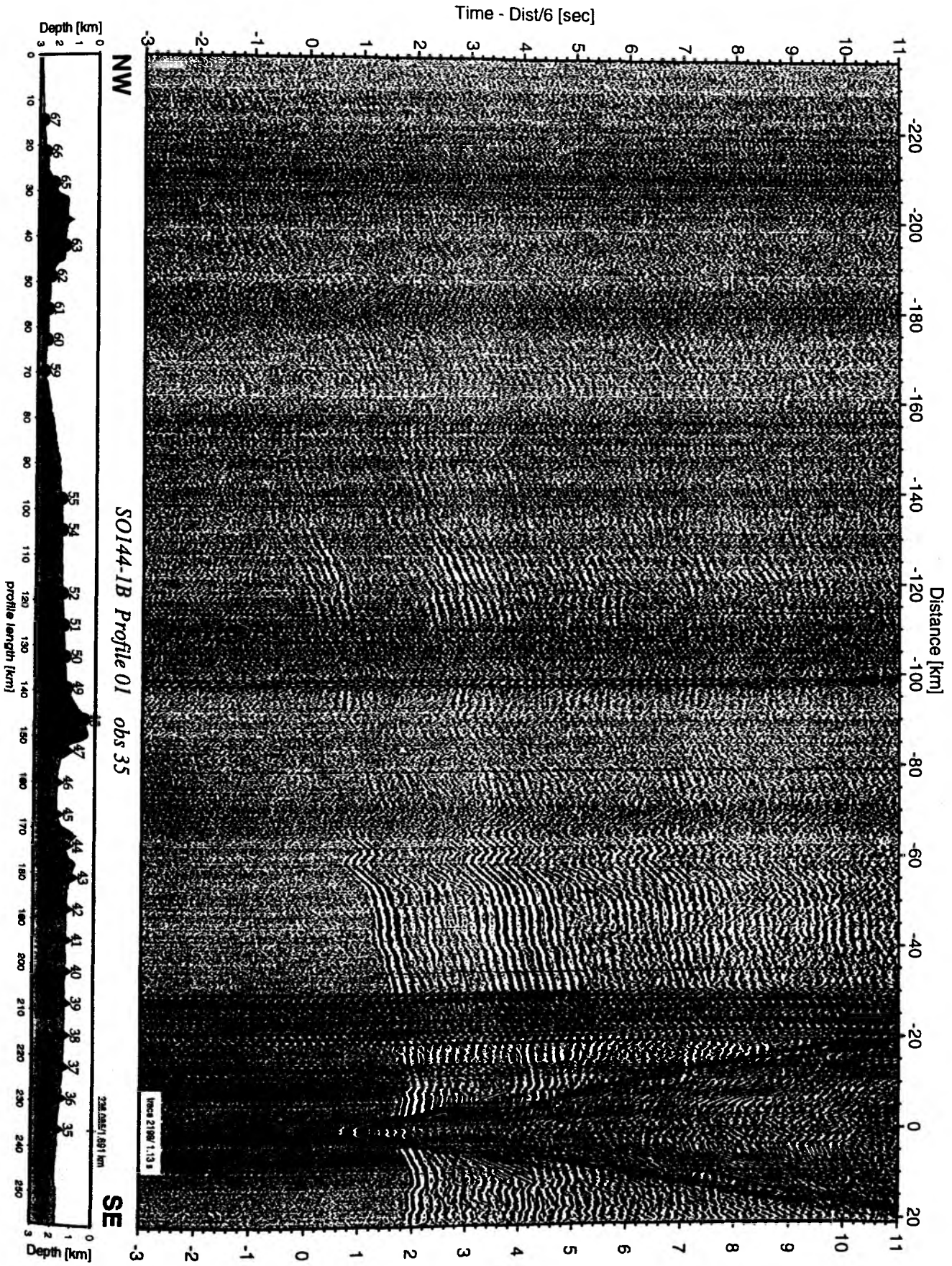

Figure 6.2.4.3.4: Record section from obs 35 vertical component, Profile 01.

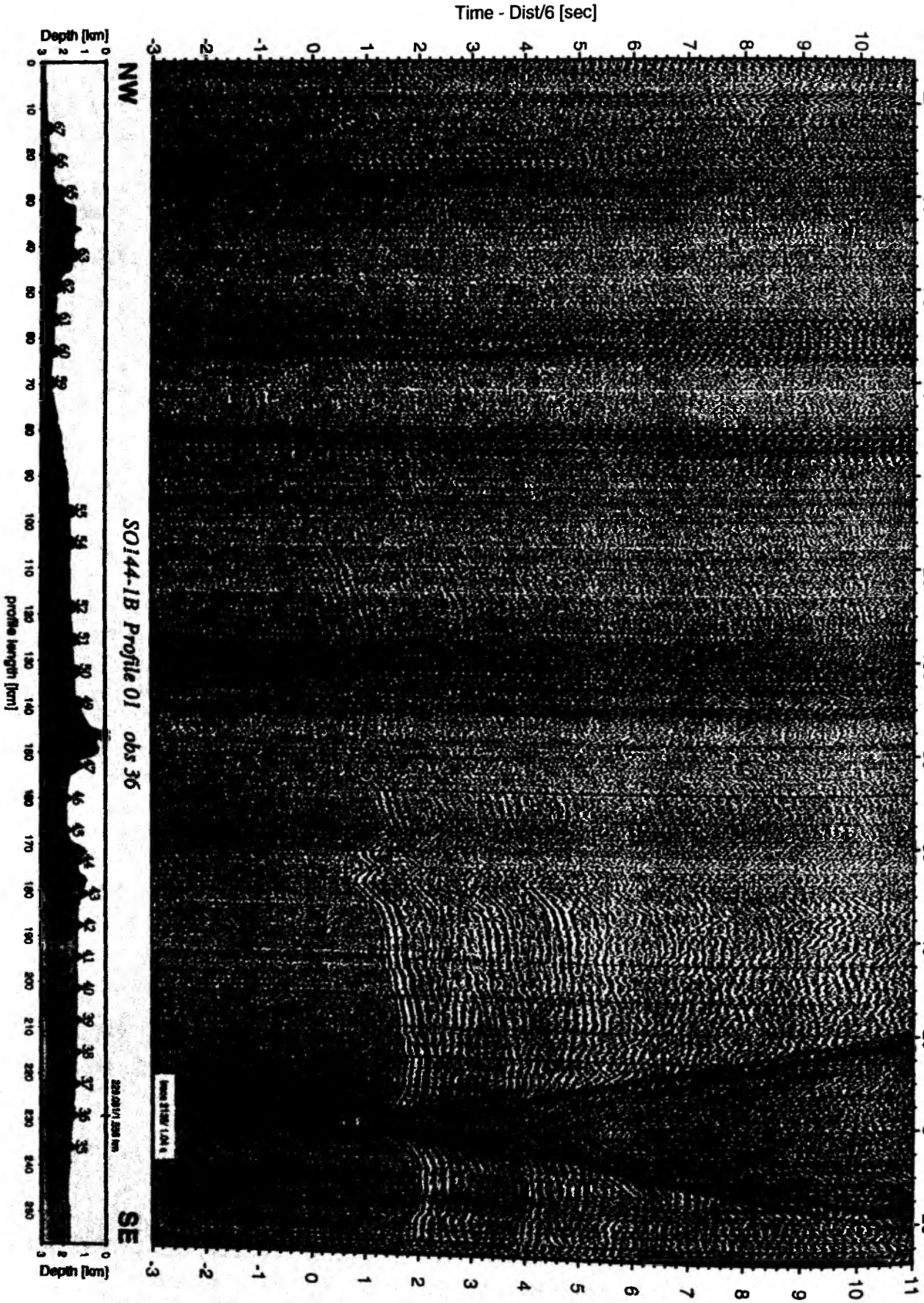

Figure 6.2.4.3.5: Record section from obs 36 vertical component, Profile 01.

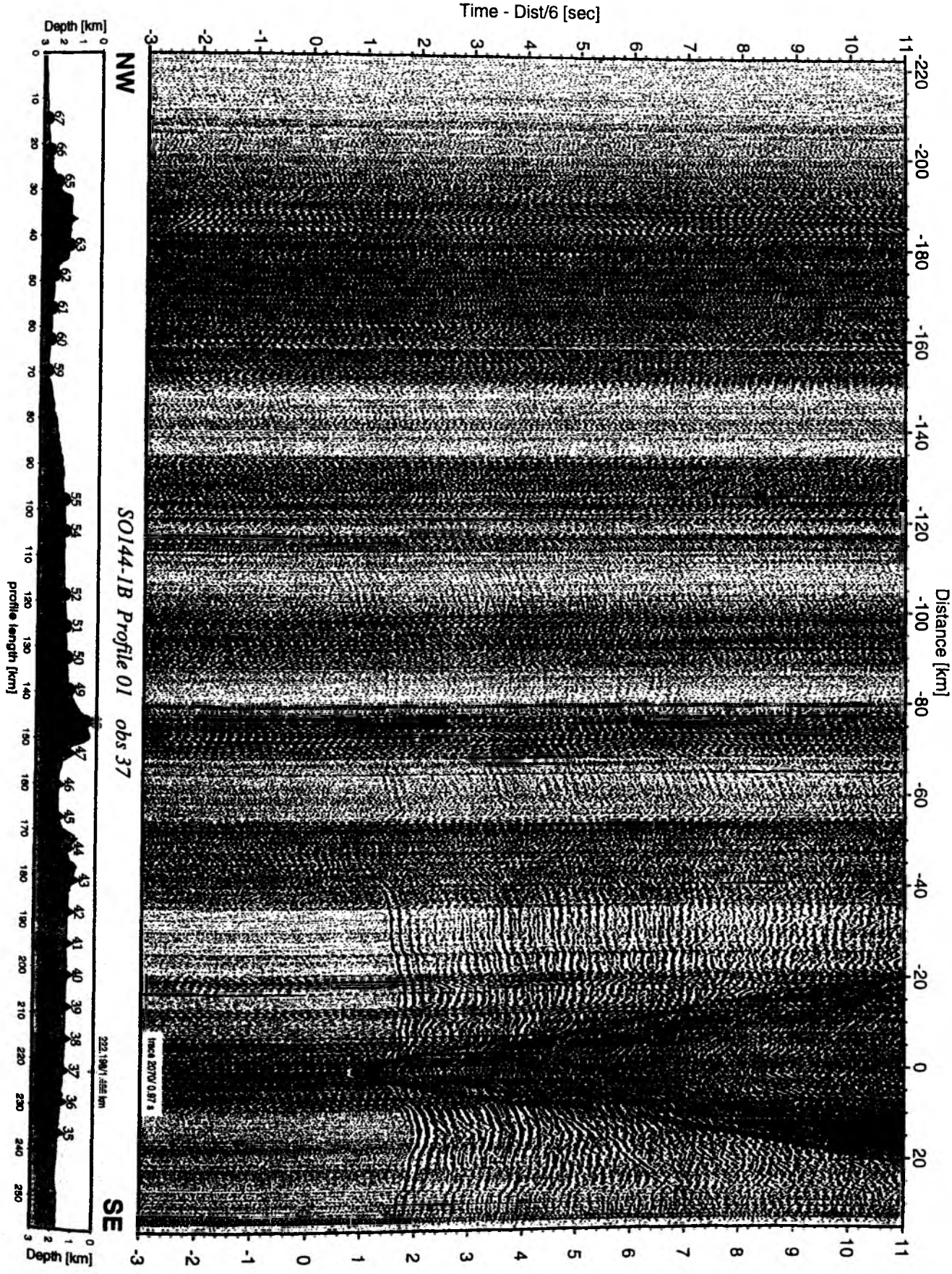

Figure 6.2.4.3.6: Record section from obs 37 vertical component, Profile 01.

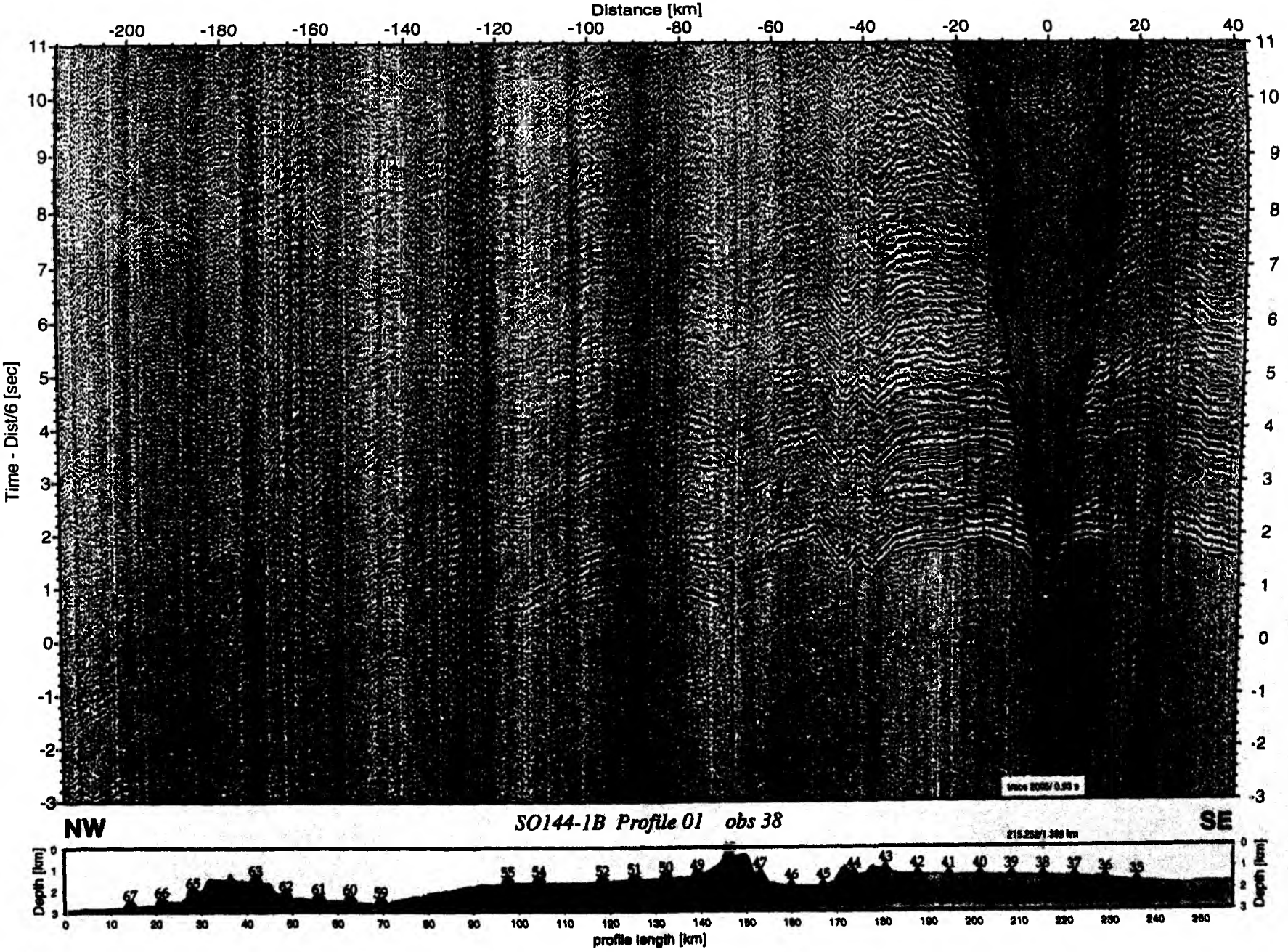

Figure 6.2.4.3.7: Record section from obs 38 vertical component, Profile 01.

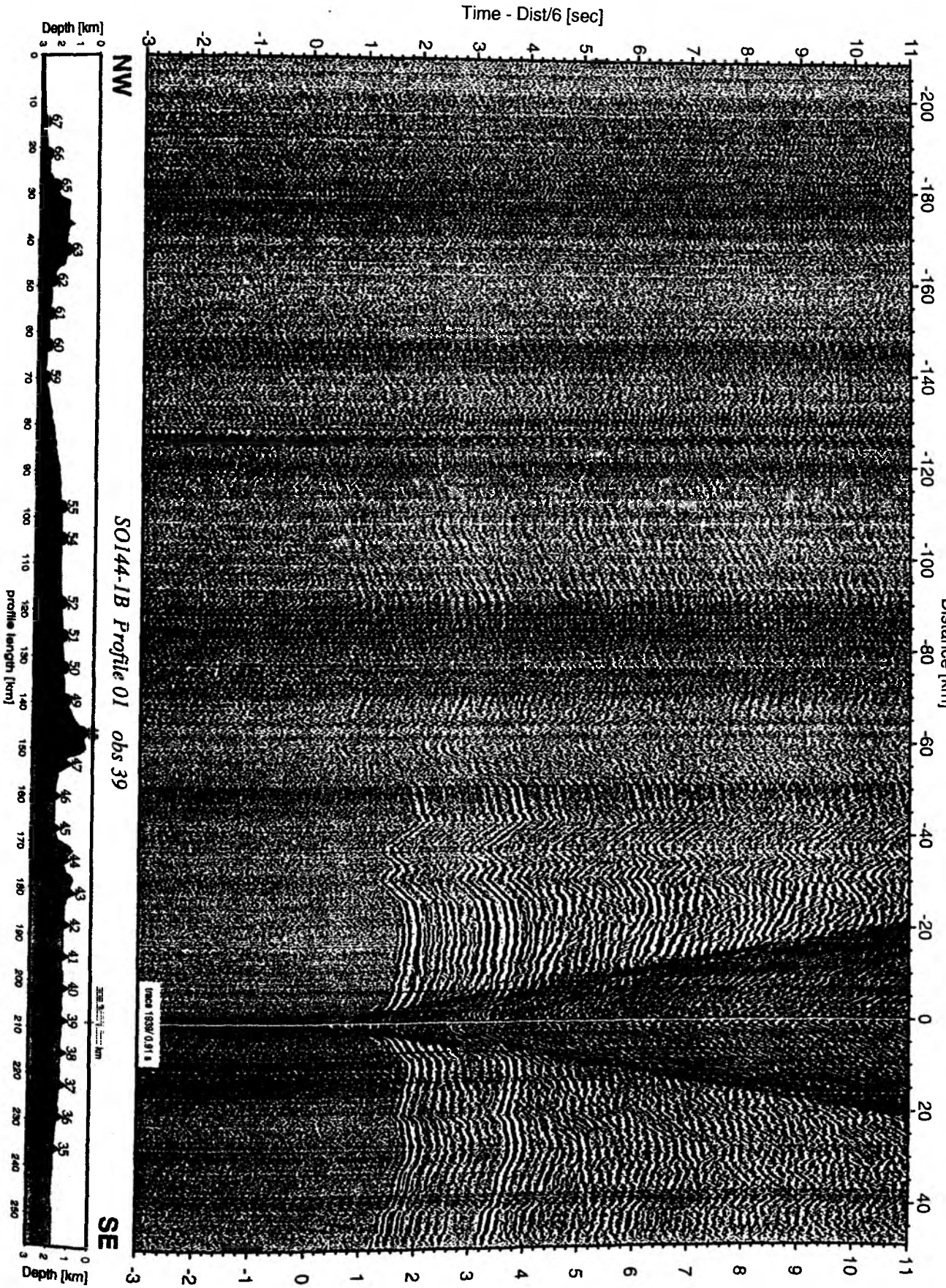

Figure 6.2.4.3.8: Record section from obs 39 vertical component, Profile 01.

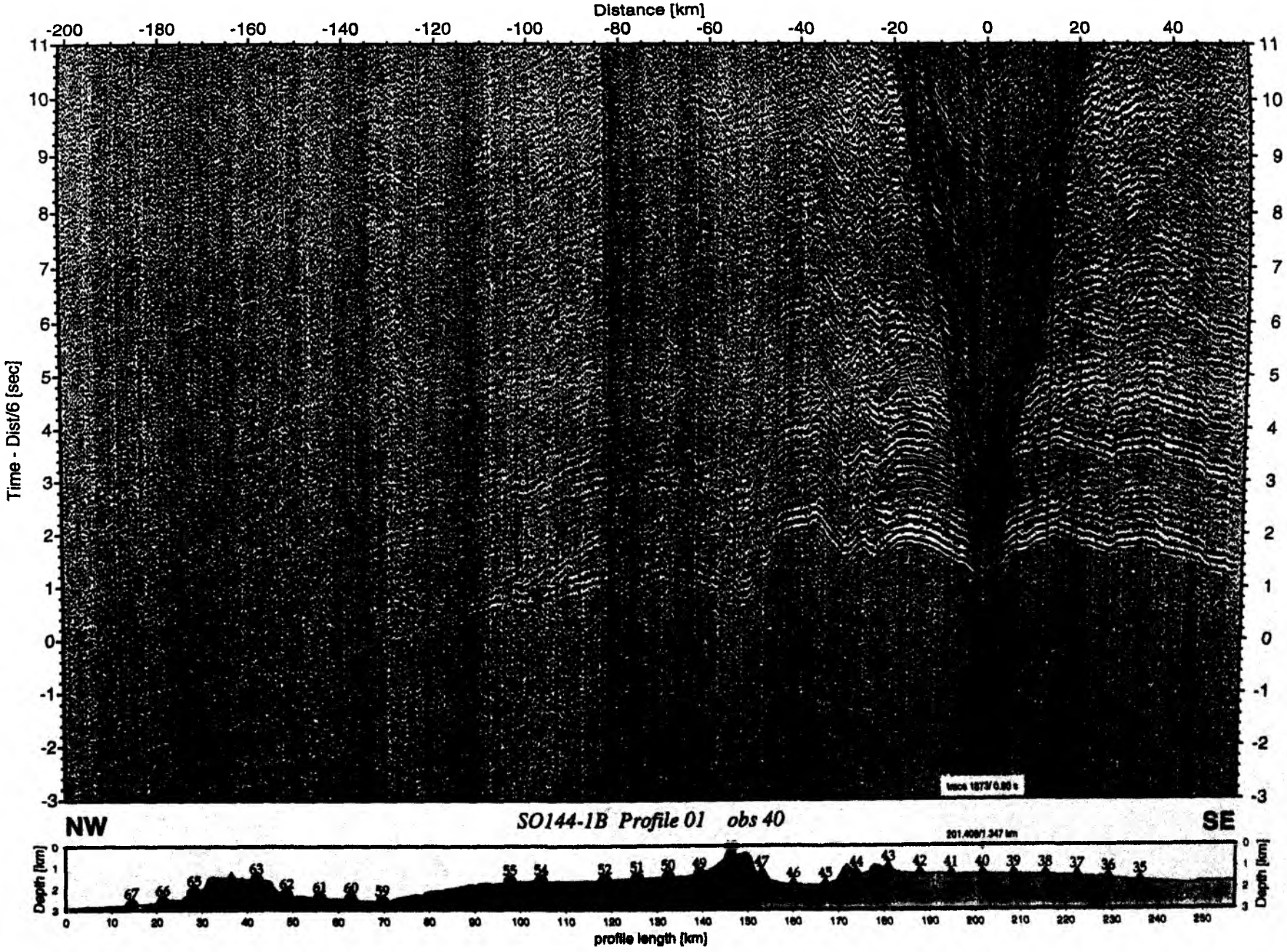

Figure 6.2.4.3.9: Record section from obs 40 vertical component, Profile 01.

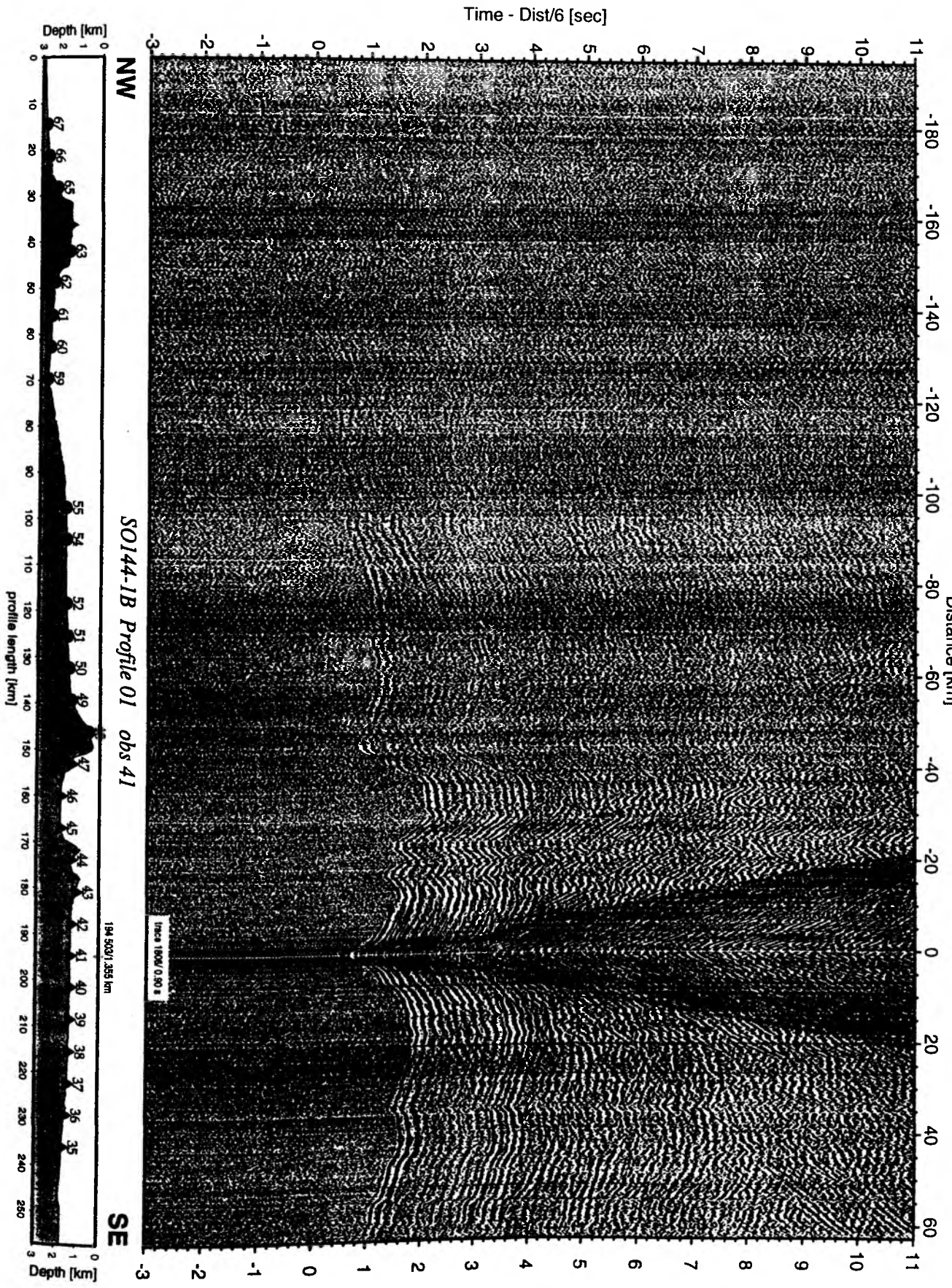

Figure 6.2.4.3.10: Record section from obs 41 vertical component, Profile 01.

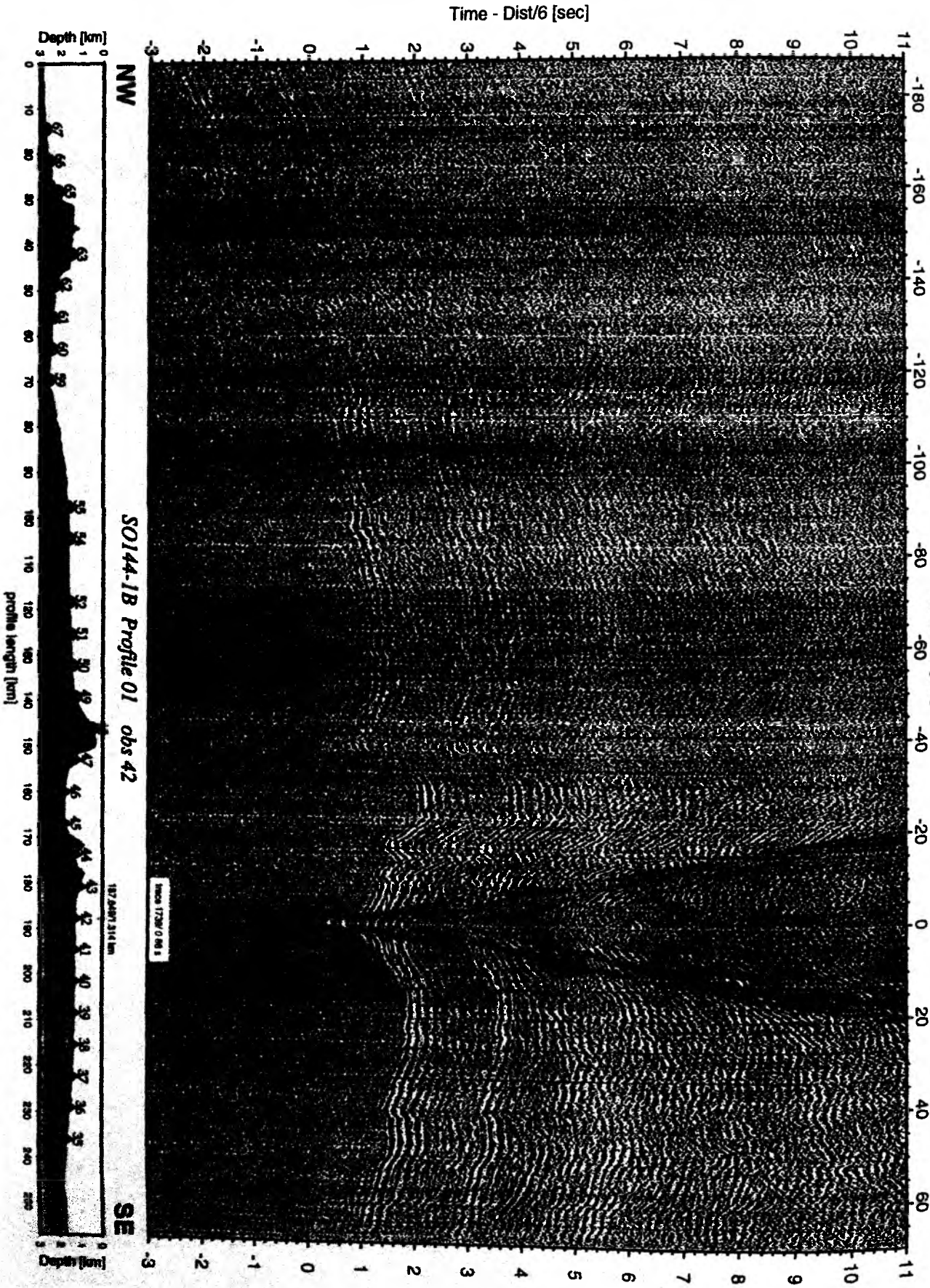

Figure 6.2.4.3.11: Record section from obs 42 vertical component, Profile 01.

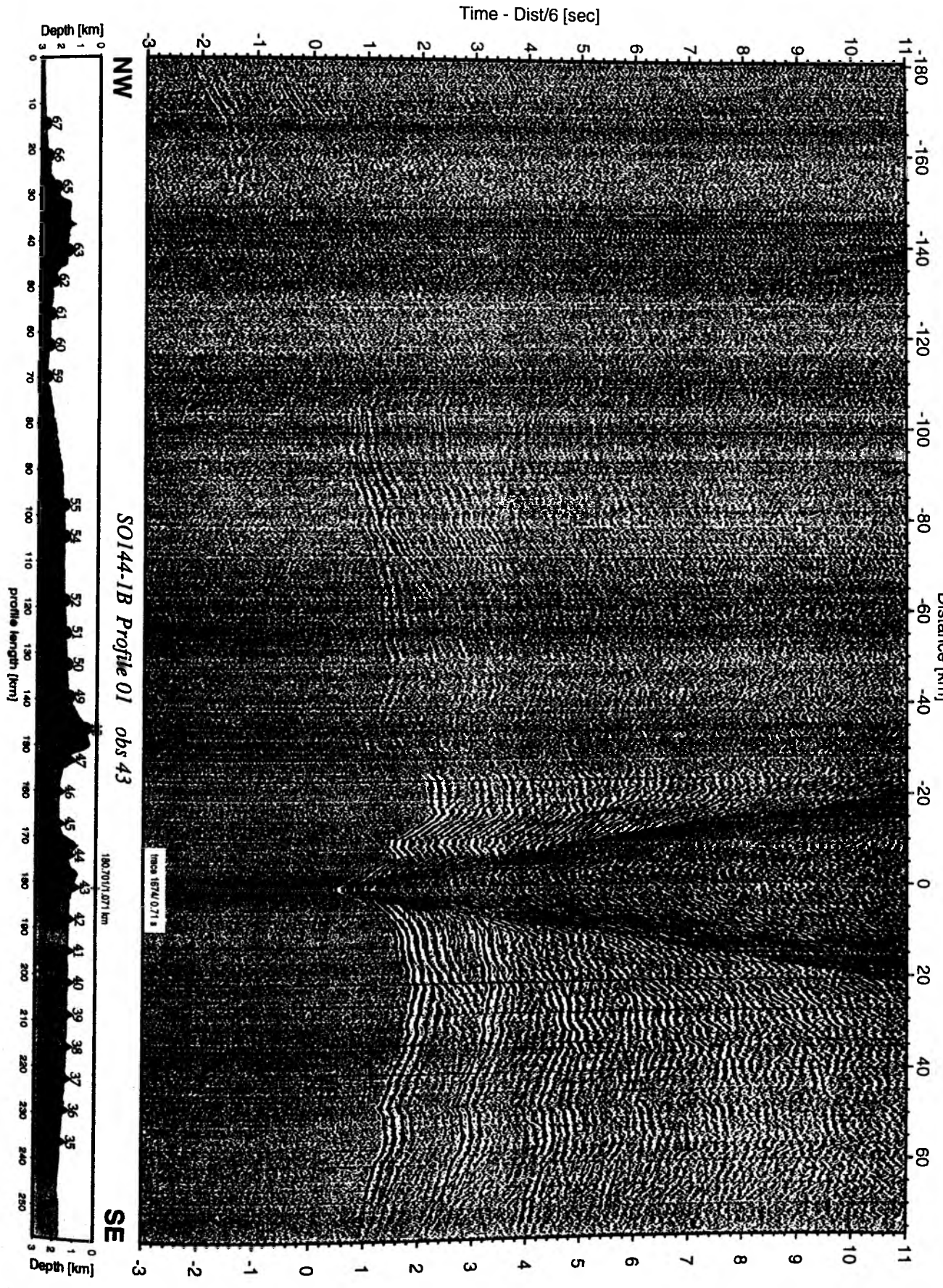

Figure 6.2.4.3.12: Record section from obs 43 vertical component, Profile 01.

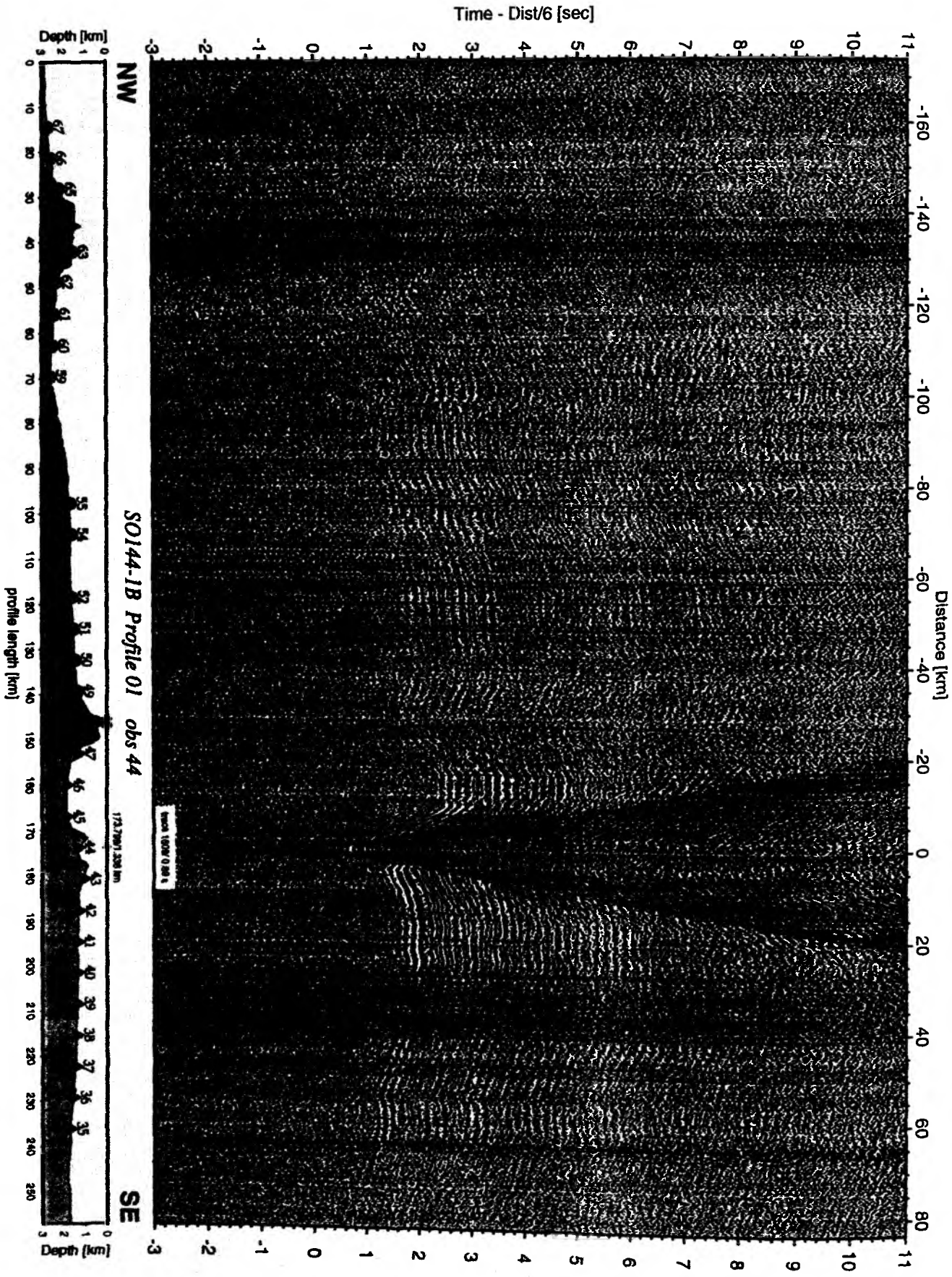

Figure 6.2.4.3.13: Record section from obs 44 vertical component, Profile 01.

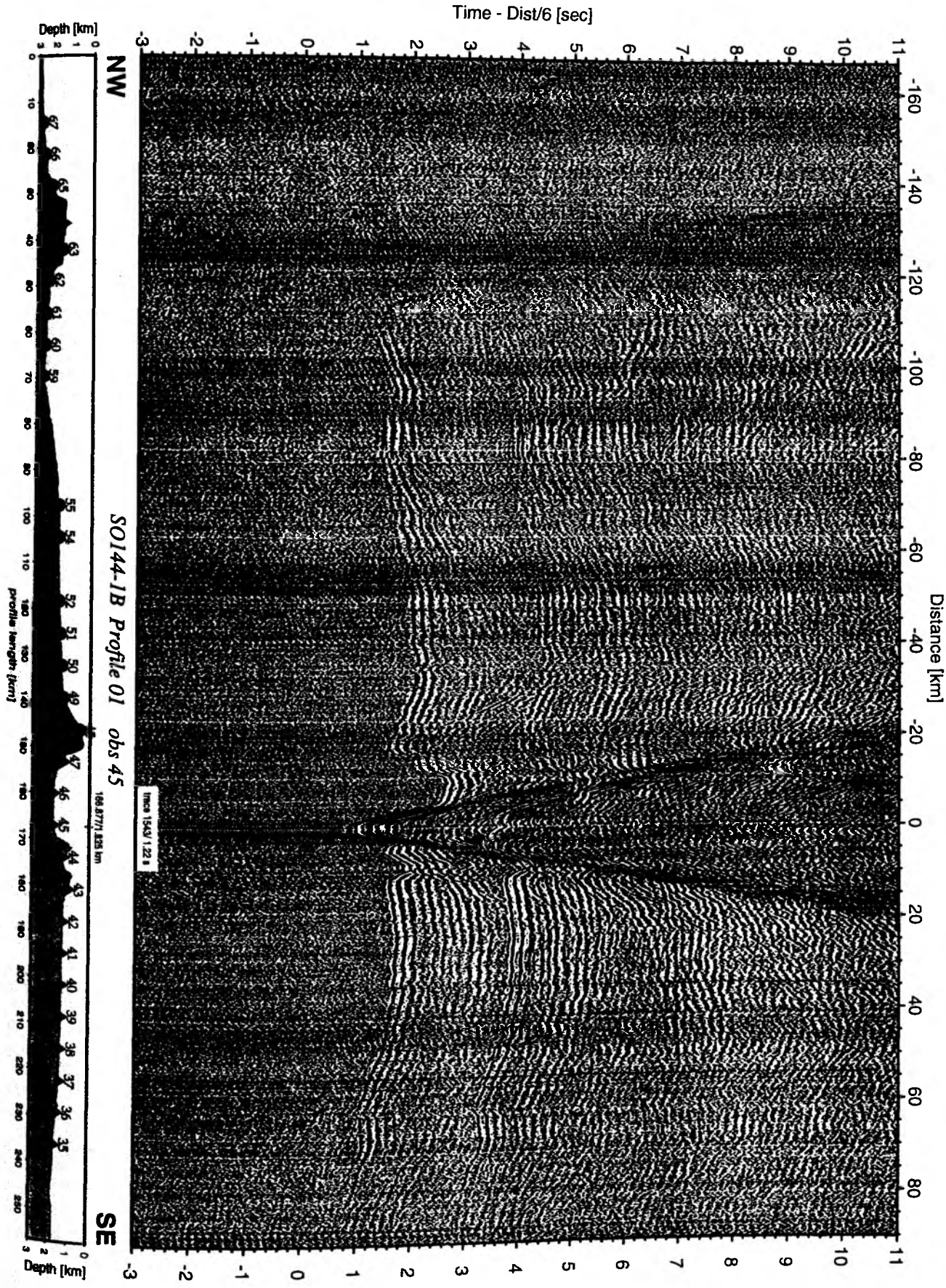

Figure 6.2.4.3.14: Record section from obs 45 vertical component, Profile 01.

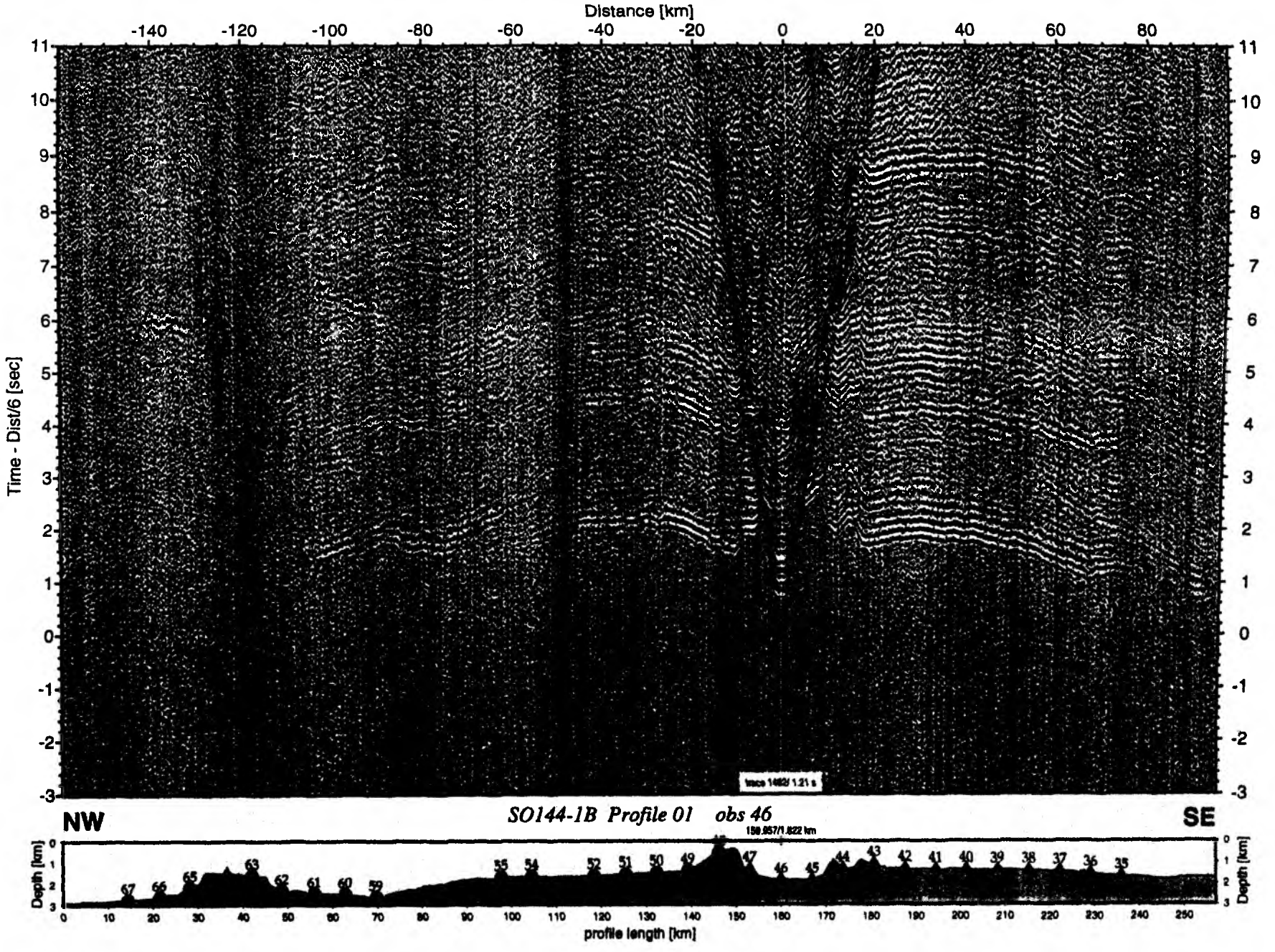

Figure 6.2.4.3.15: Record section from obs 46 vertical component, Profile 01.

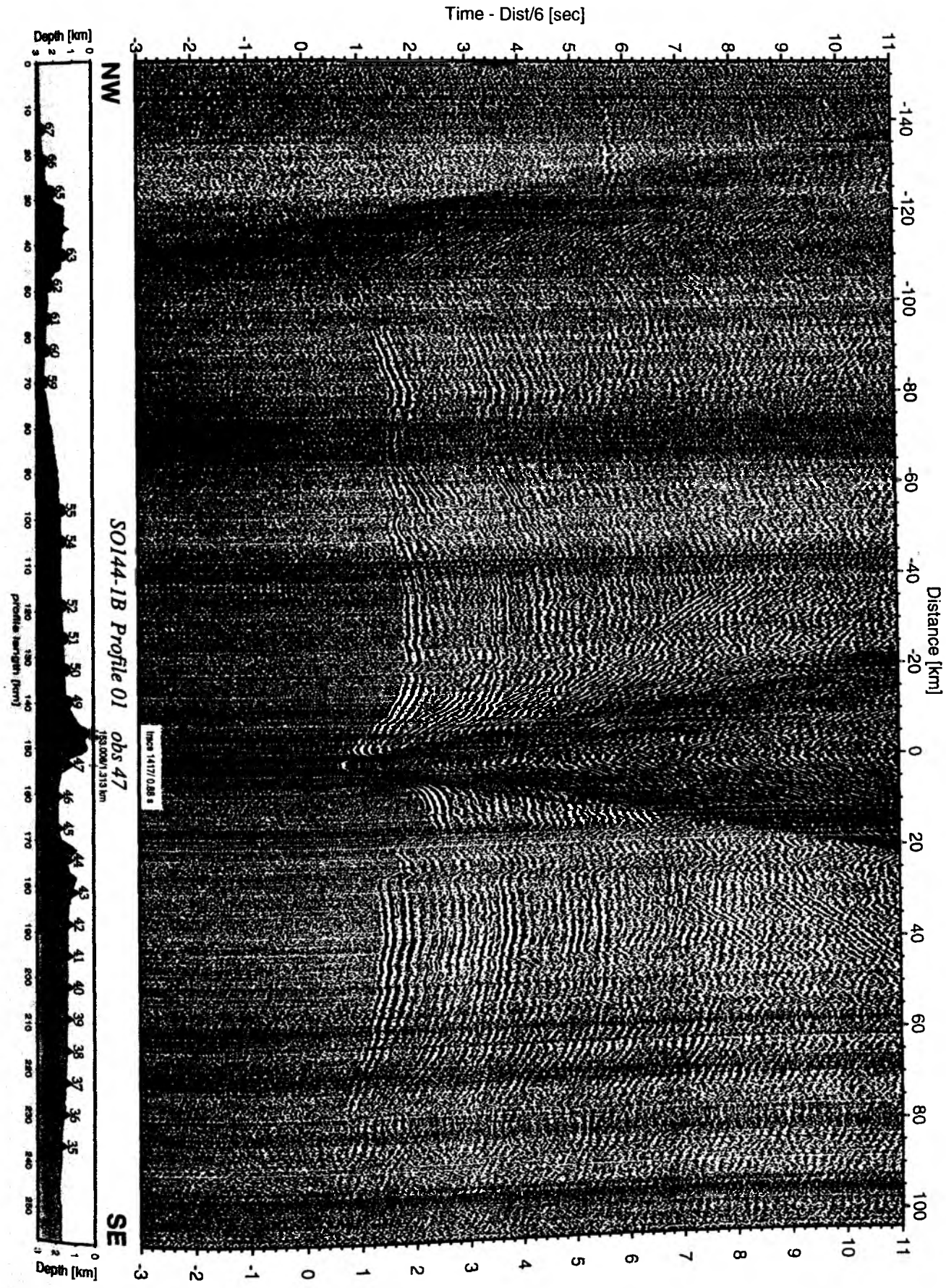

Figure 6.2.4.3.16: Record section from obs 47 vertical component, Profile 01.

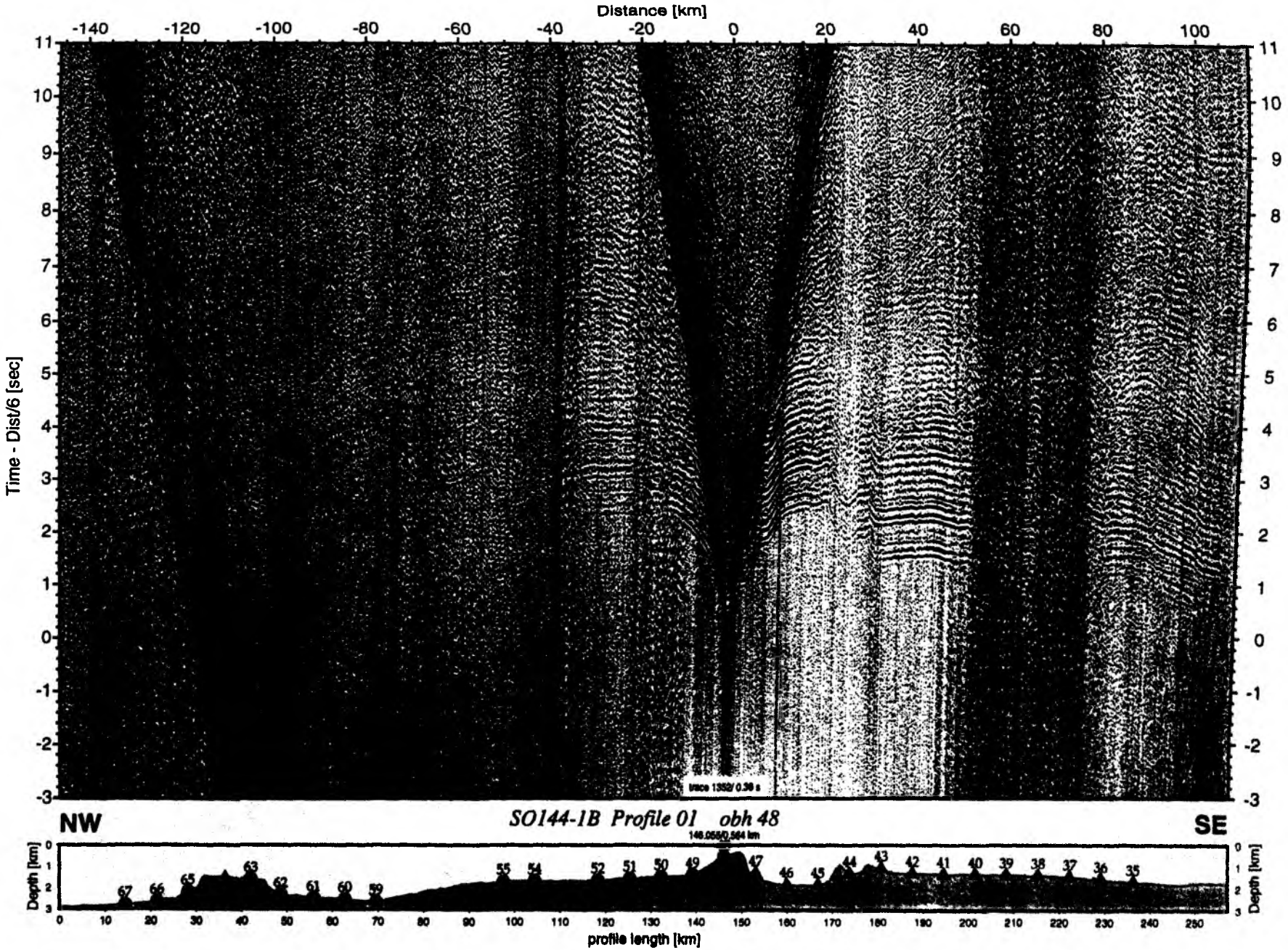

Figure 6.2.4.3.17: Record section from obh 48 , Profile 01.

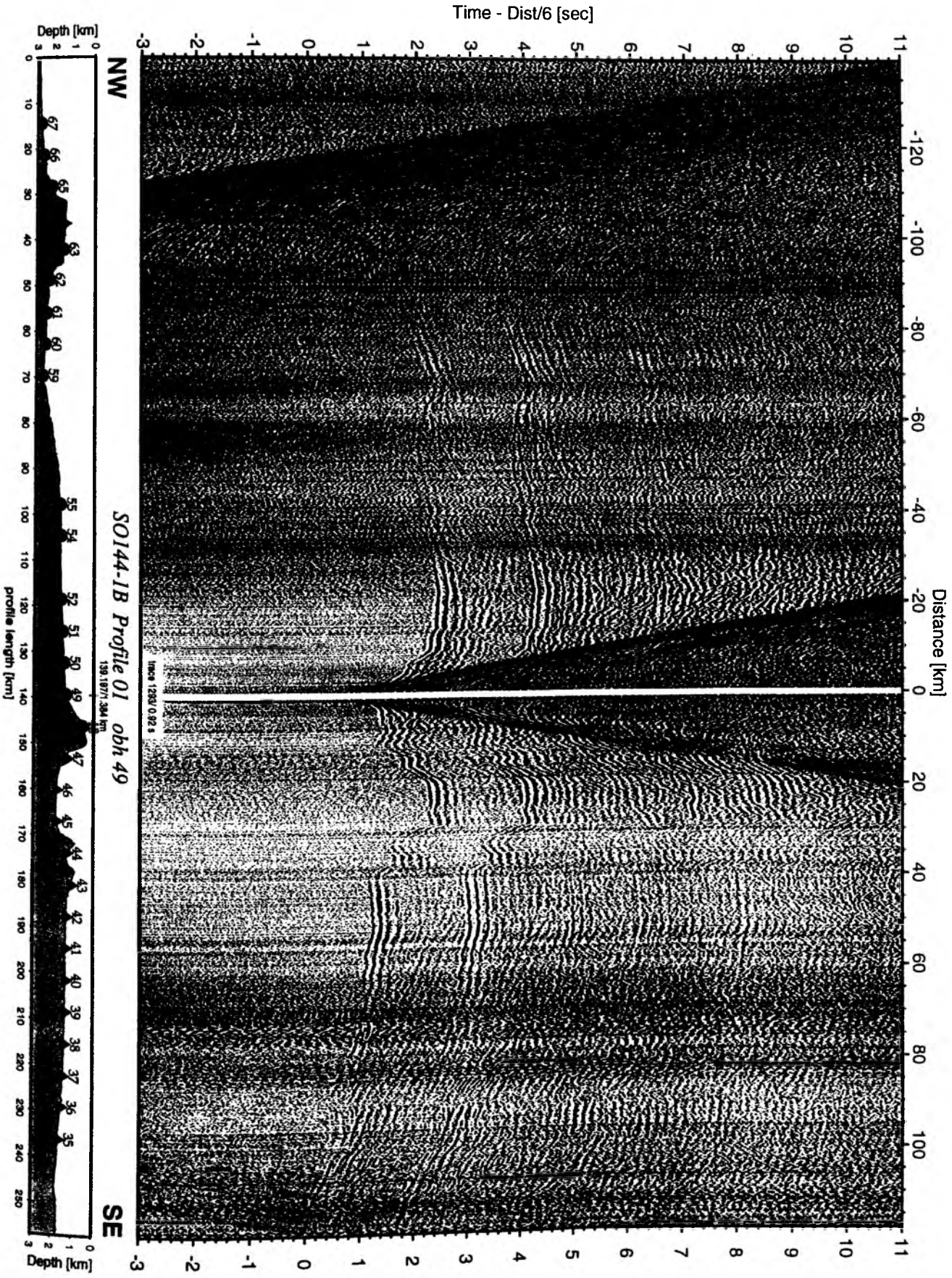

Figure 6.2.4.3.18: Record section from obh 49 , Profile 01.

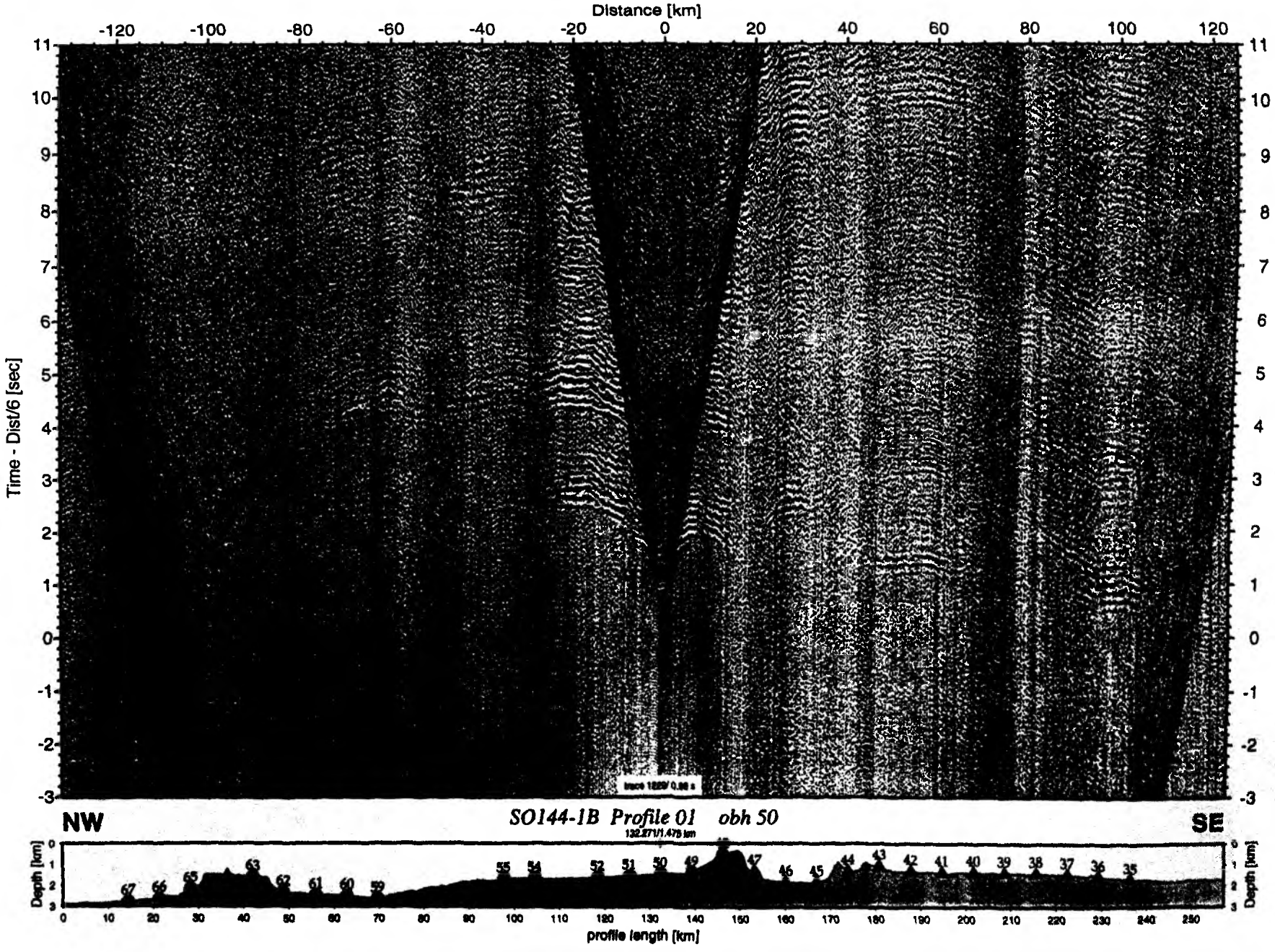

Figure 6.2.4.3.19: Record section from obh 50 , Profile 01.

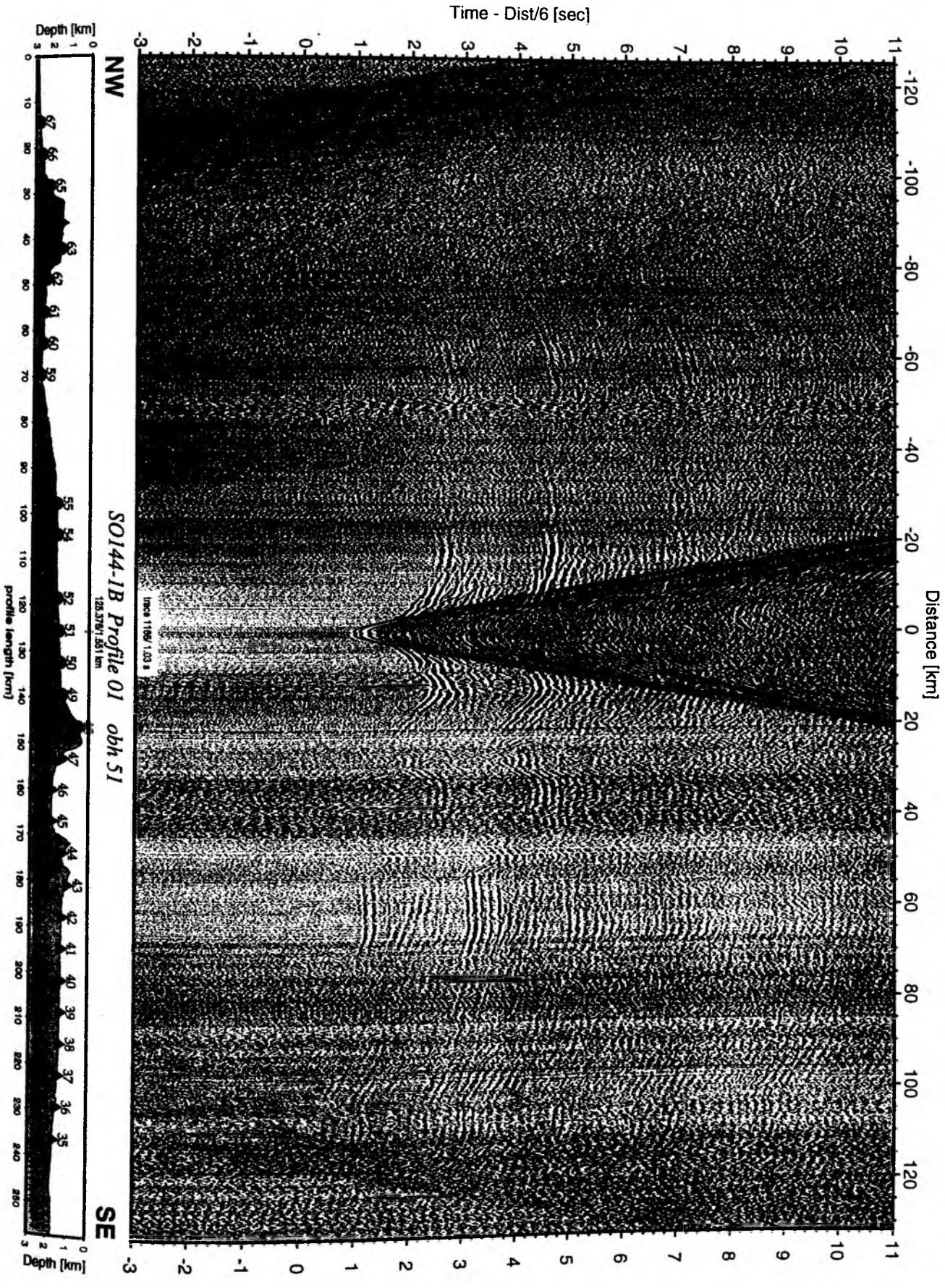

Figure 6.2.4.3.20: Record section from obh 51 , Profile 01.

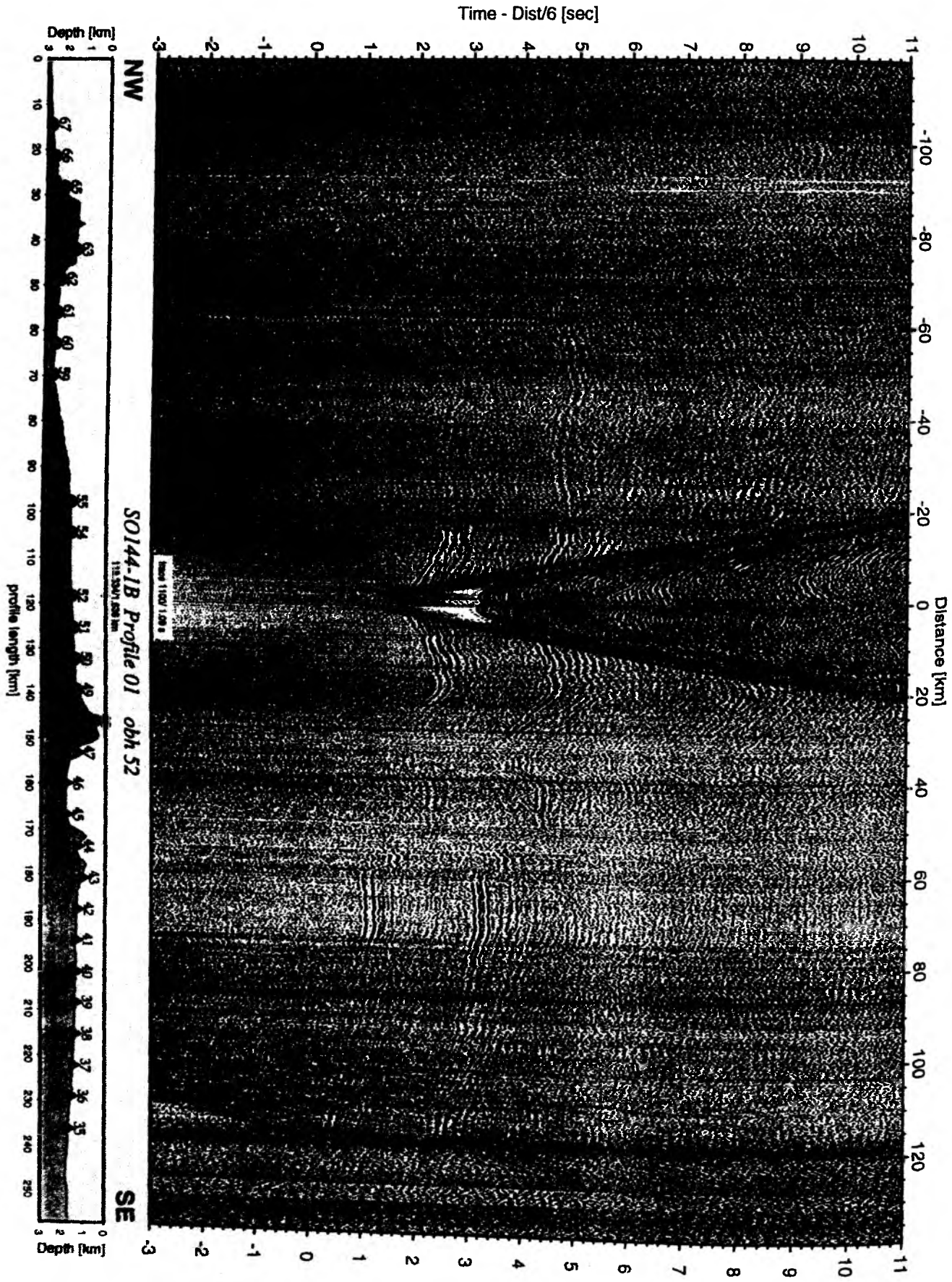

Figure 6.2.4.3.21: Record section from obh 52 , Profile 01.

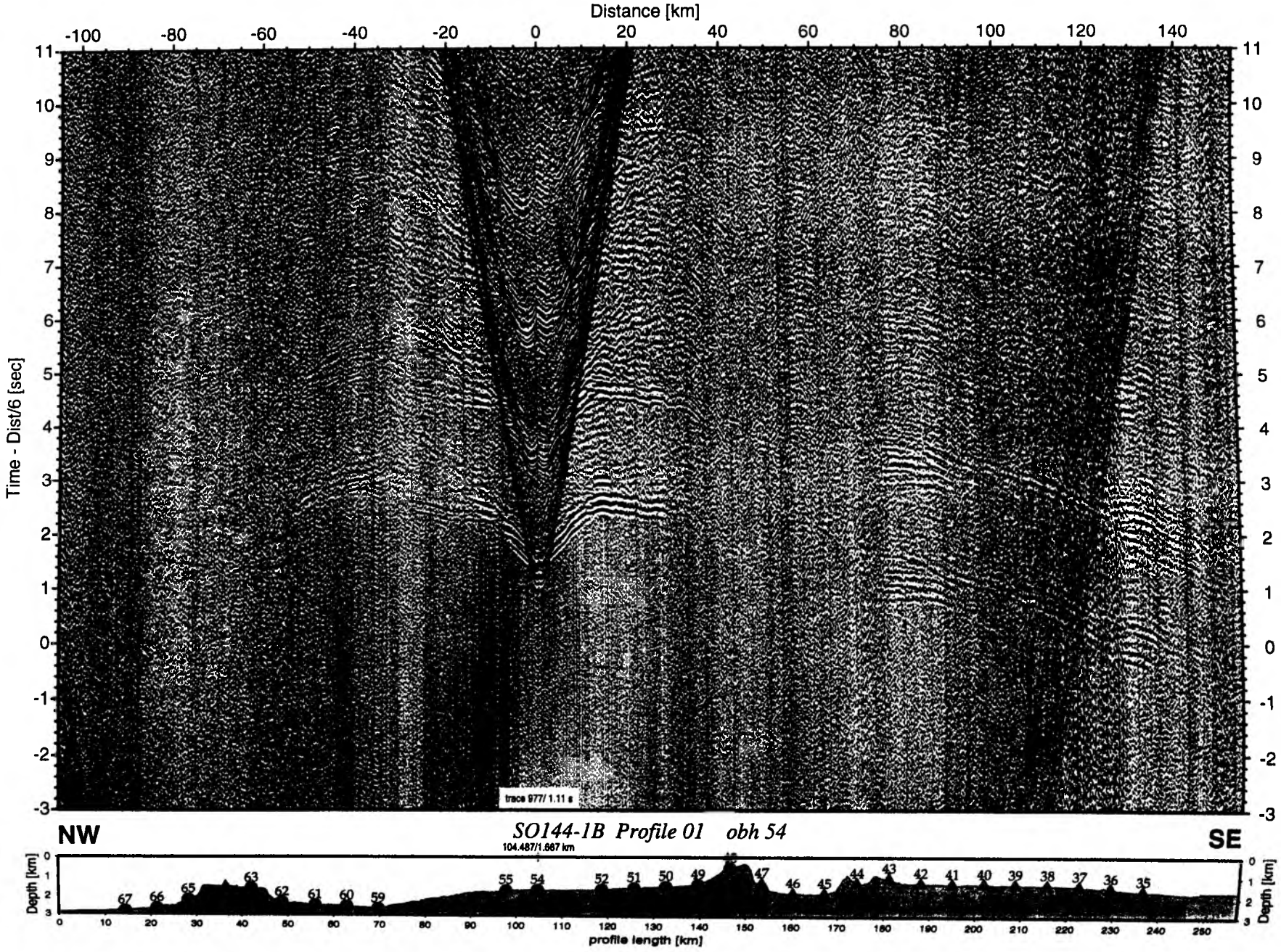

Figure 6.2.4.3.22: Record section from obh 54 , Profile 01.

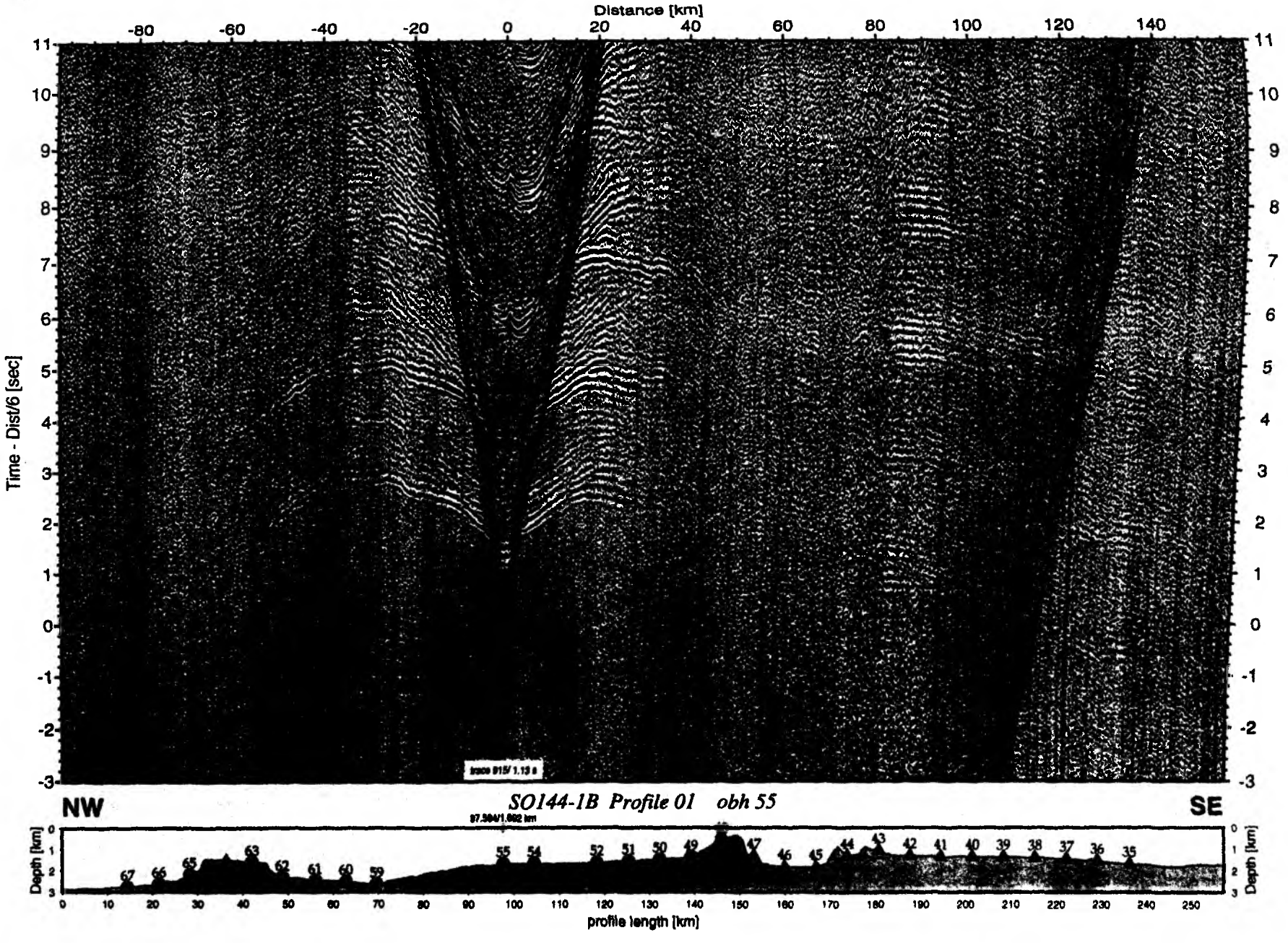

Figure 6.2.4.3.23: Record section from obh 55 , Profile 01.

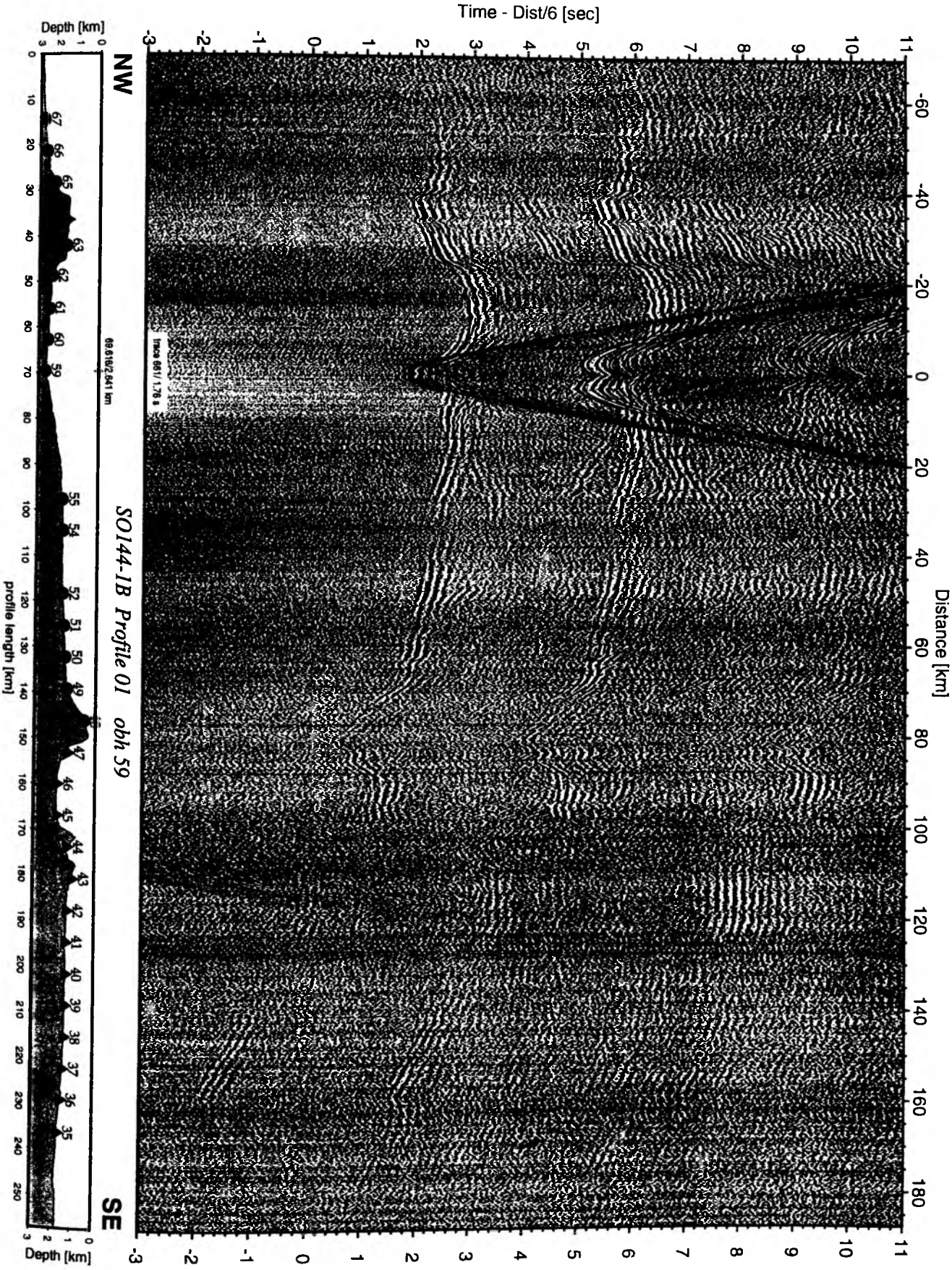

Figure 6.2.4.3.24: Record section from obh 59 , Profile 01.

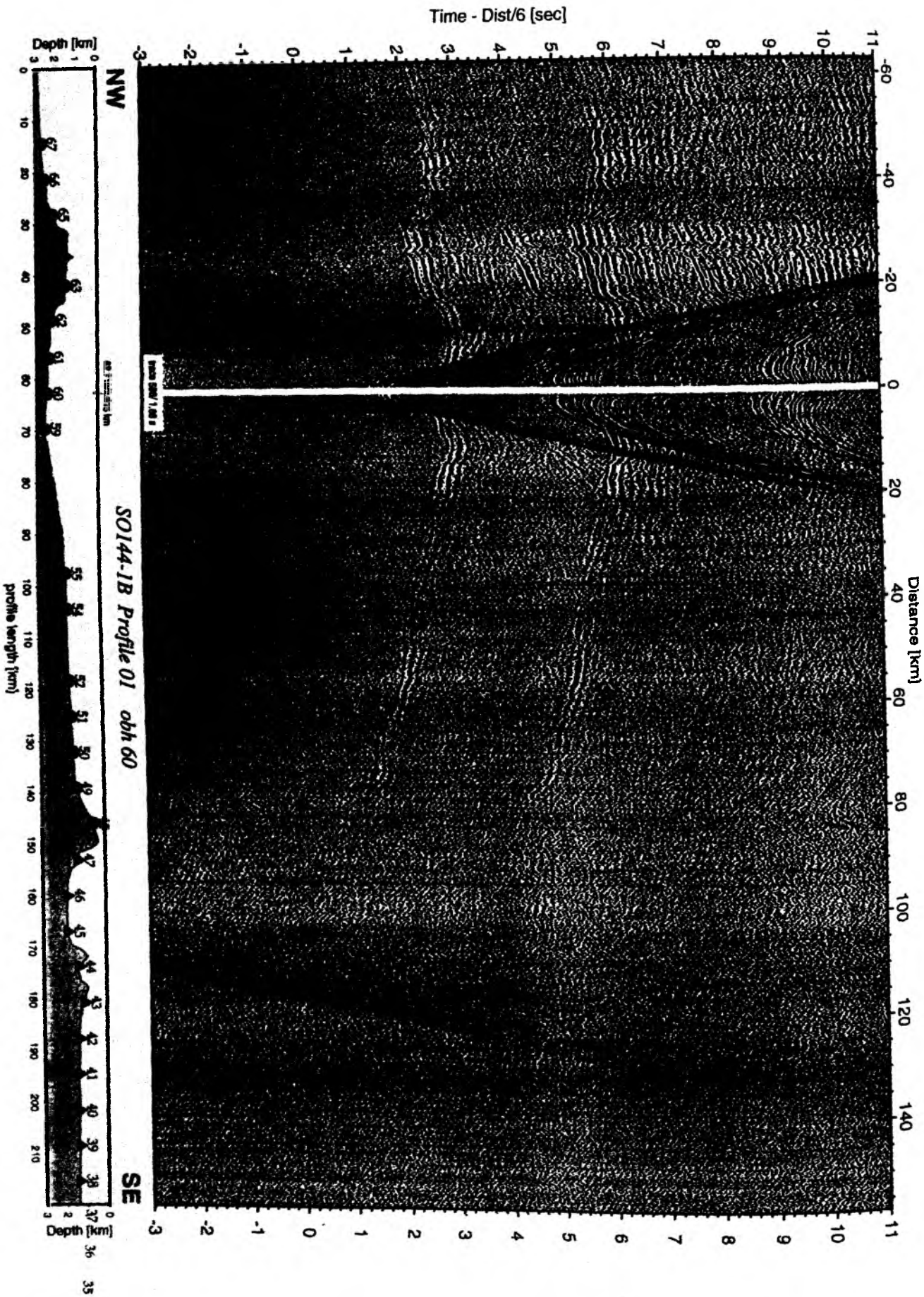

Figure 6.2.4.3.25: Record section from obh 60 , Profile 01.

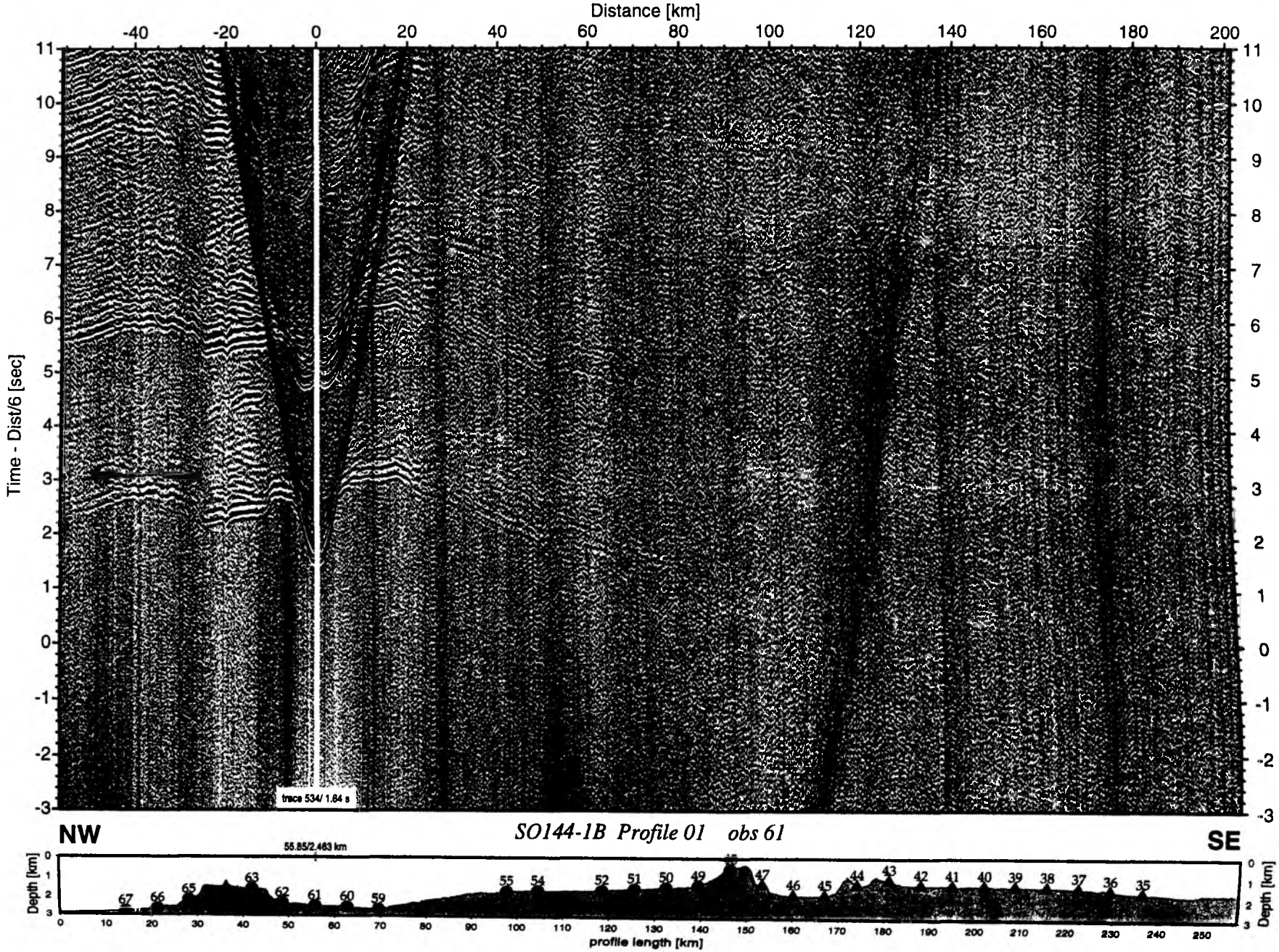

Figure 6.2.4.3.26: Record section from obs 61 hydrophone, Profile 01.

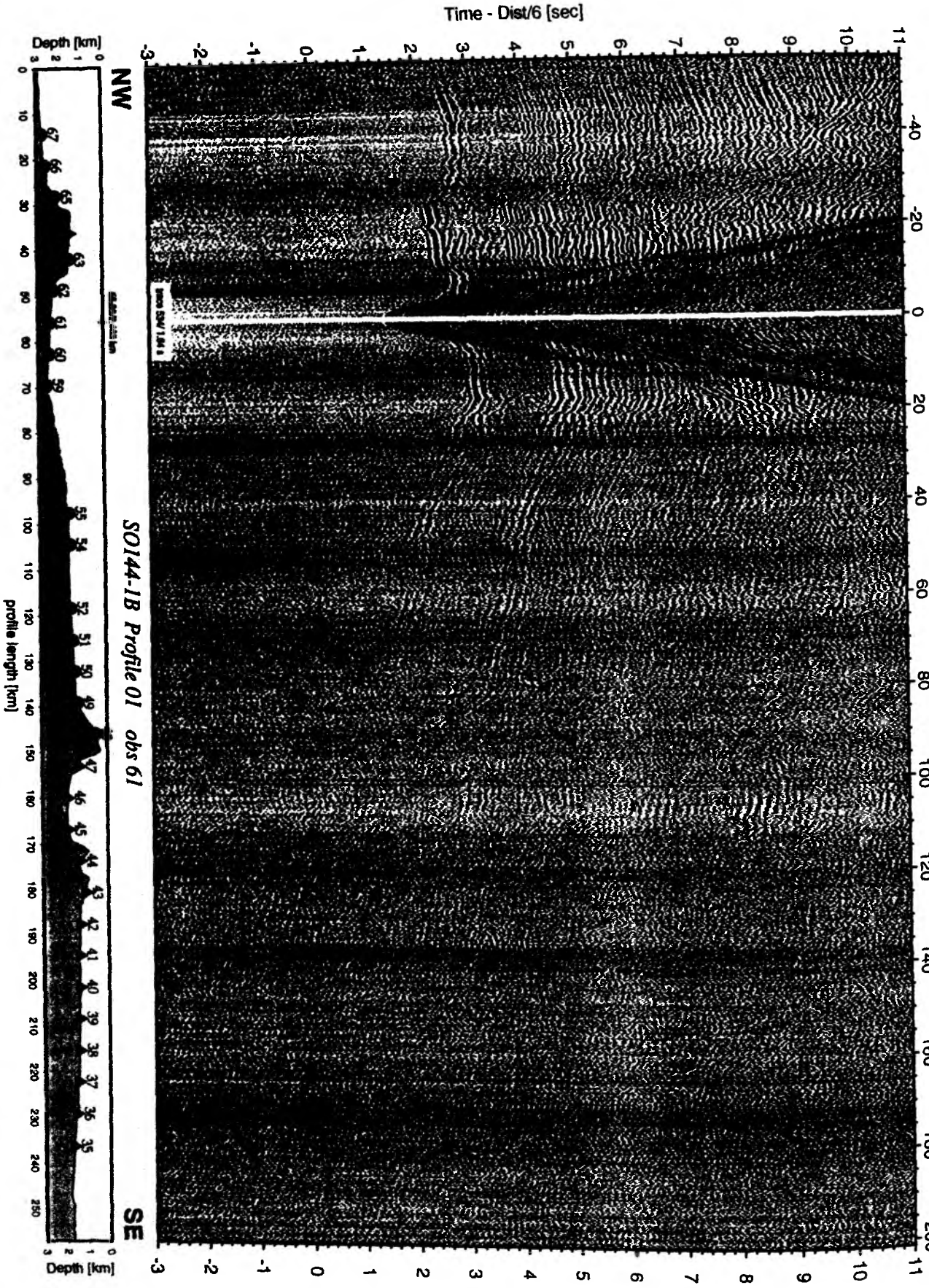

Figure 6.2.4.3.27: Record section from obs 61 vertical component, Profile 01.

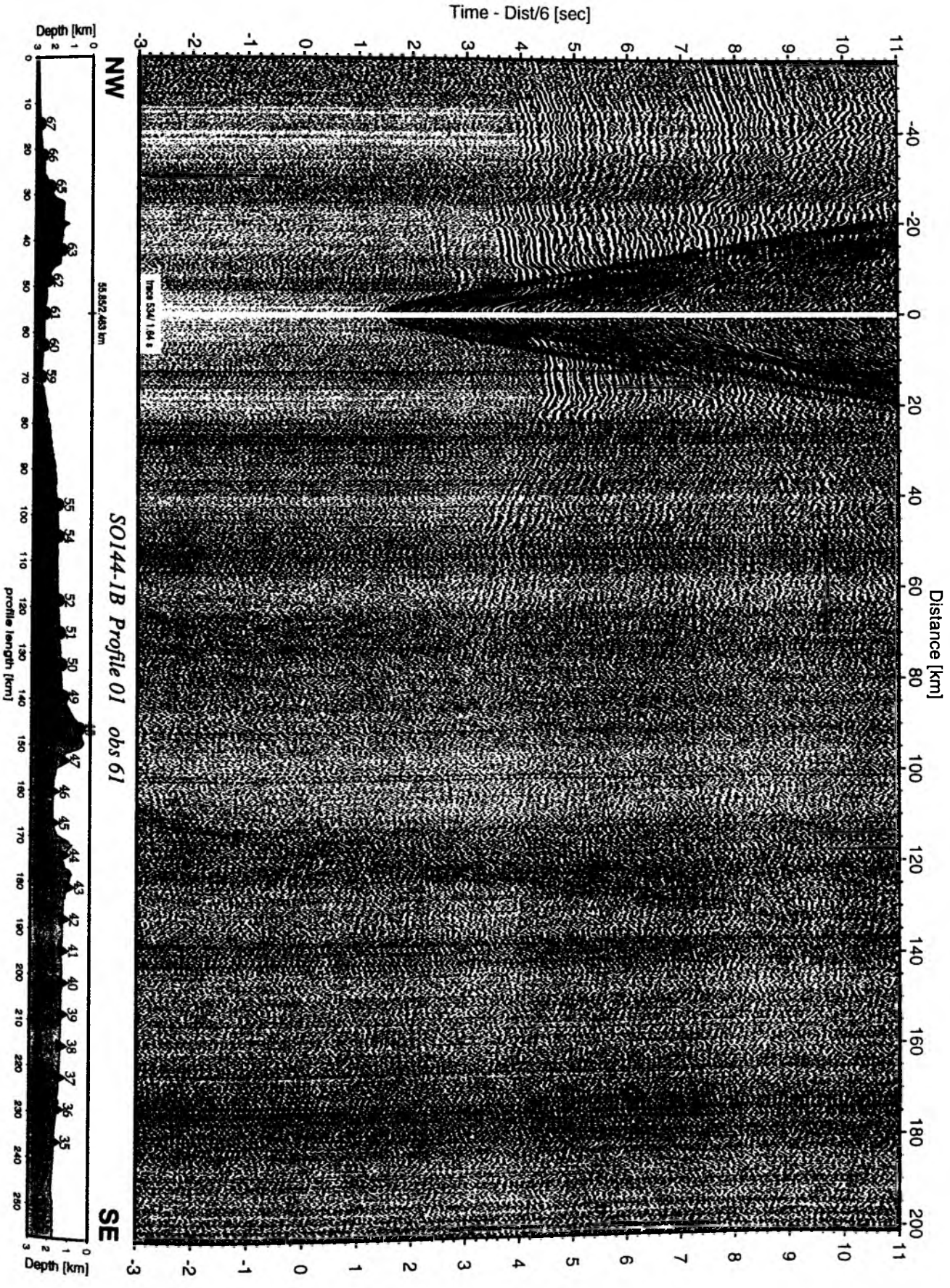

Figure 6.2.4.3.28: Record section from obs 61 horizontal component 1, Profile 01.

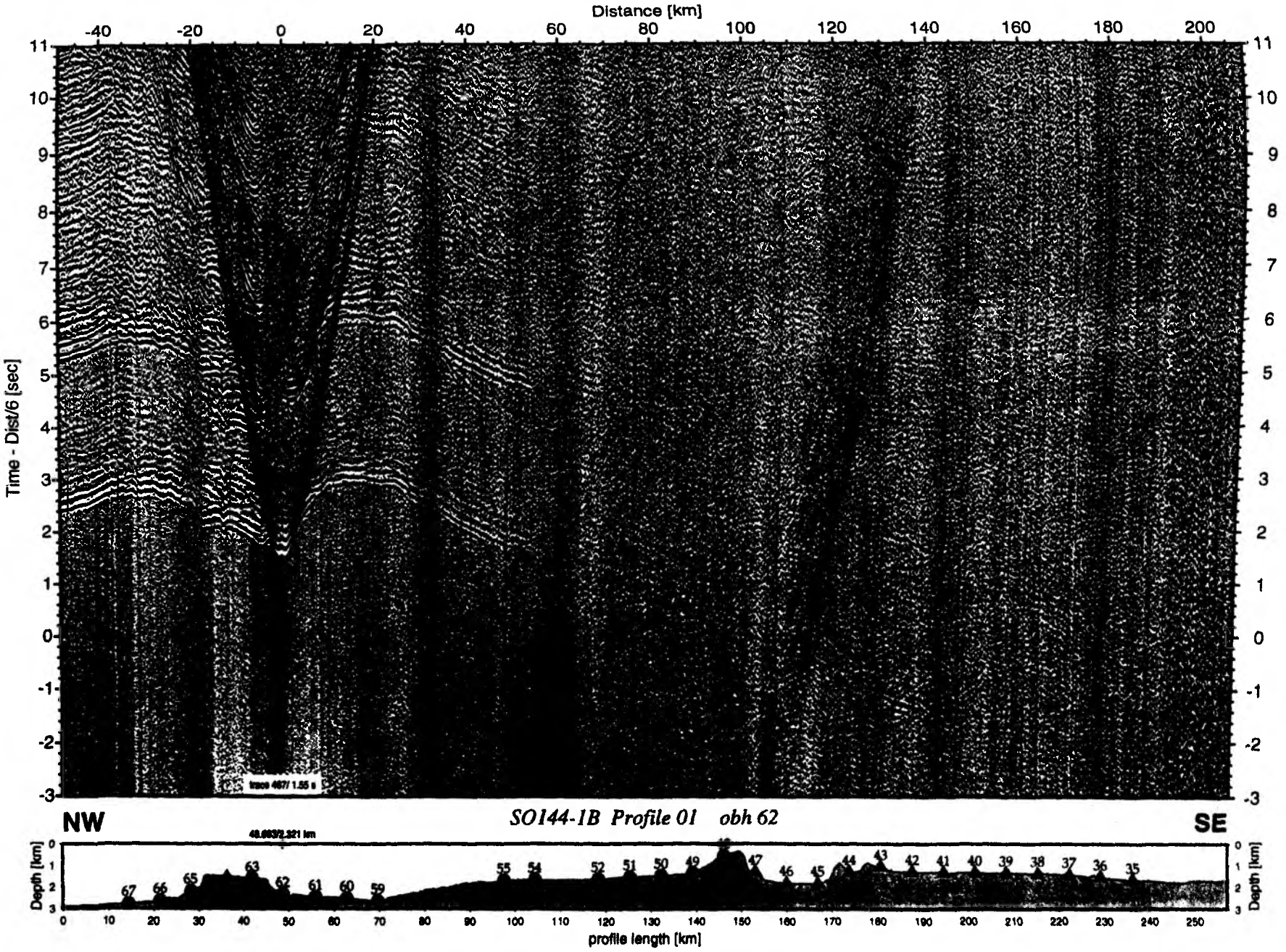

Figure 6.2.4.3.29: Record section from obh 62 , Profile 01.

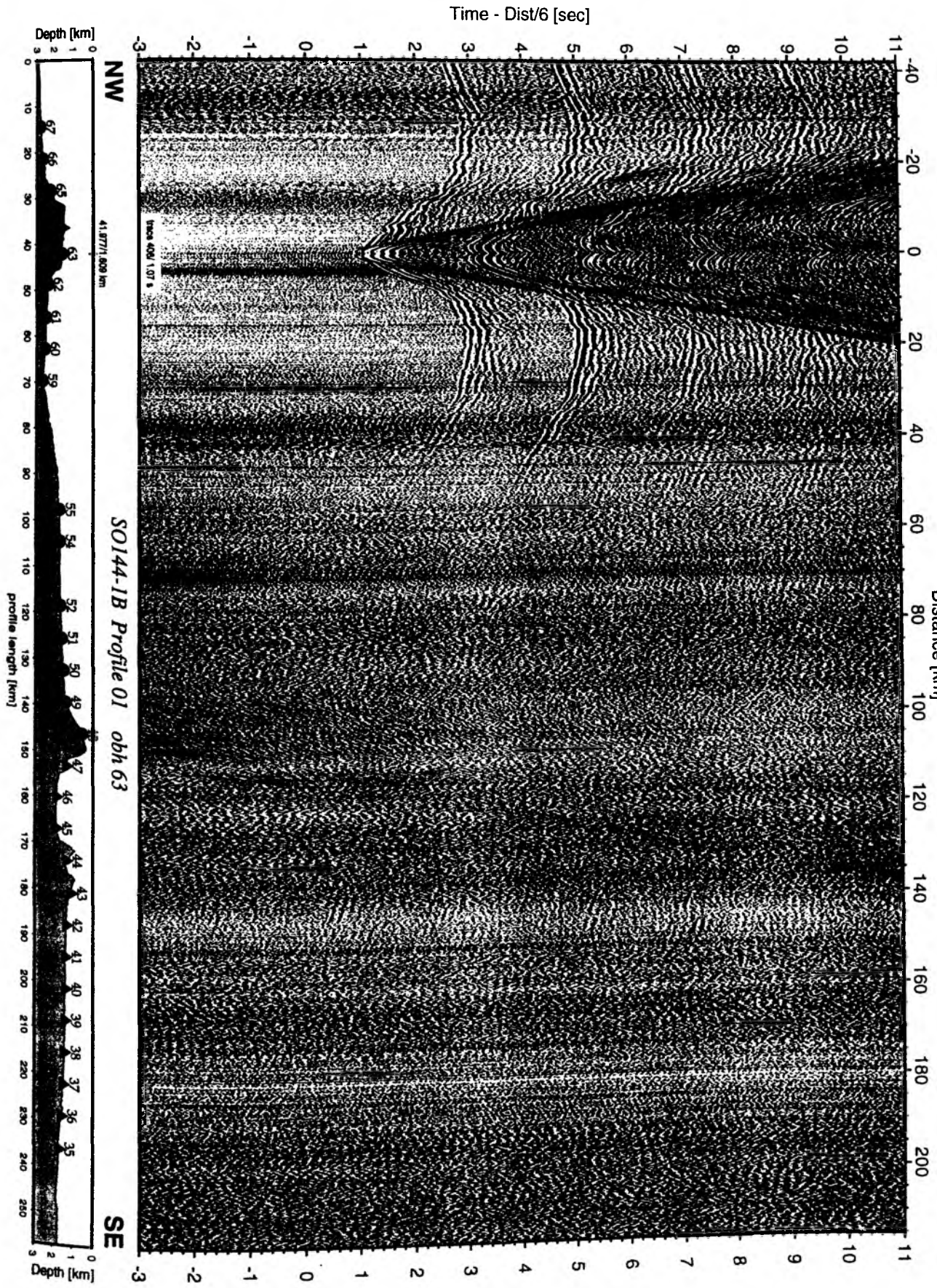

Figure 6.2.4.3.30: Record section from obh 63 , Profile 01.

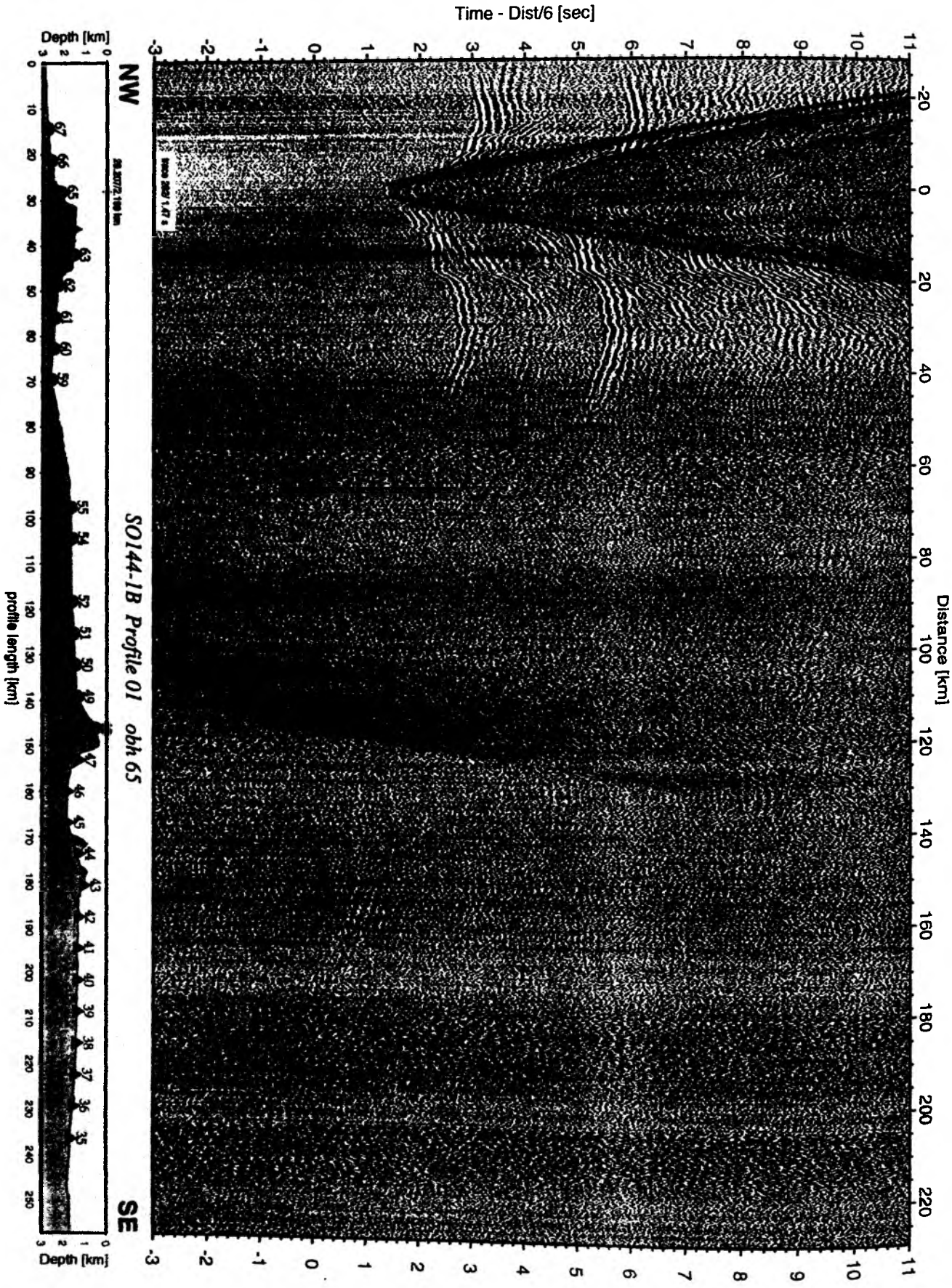

Figure 6.2.4.3.31: Record section from obh 65 , Profile 01.

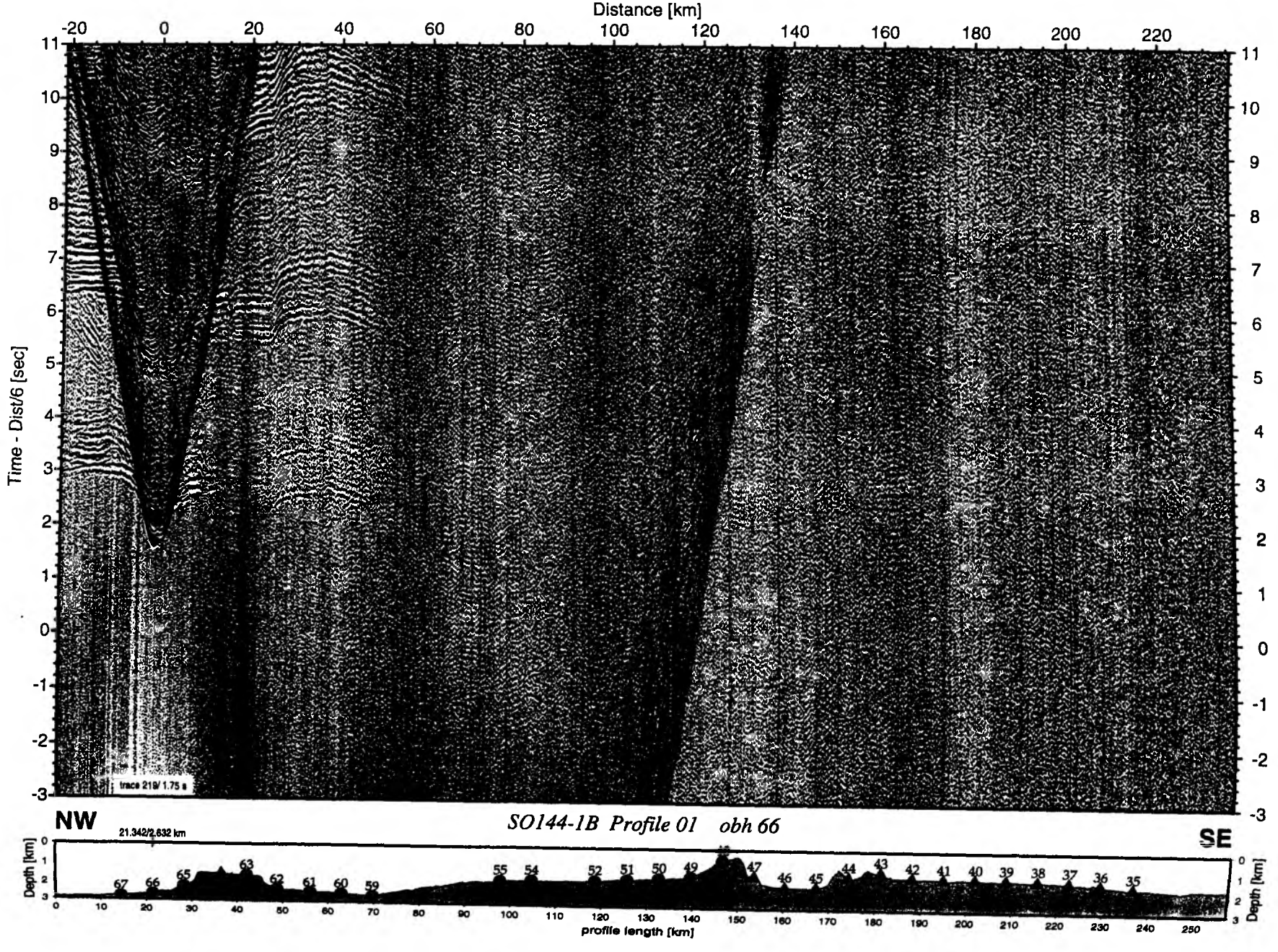

Figure 6.2.4.3.32: Record section from obh 66 , Profile 01.

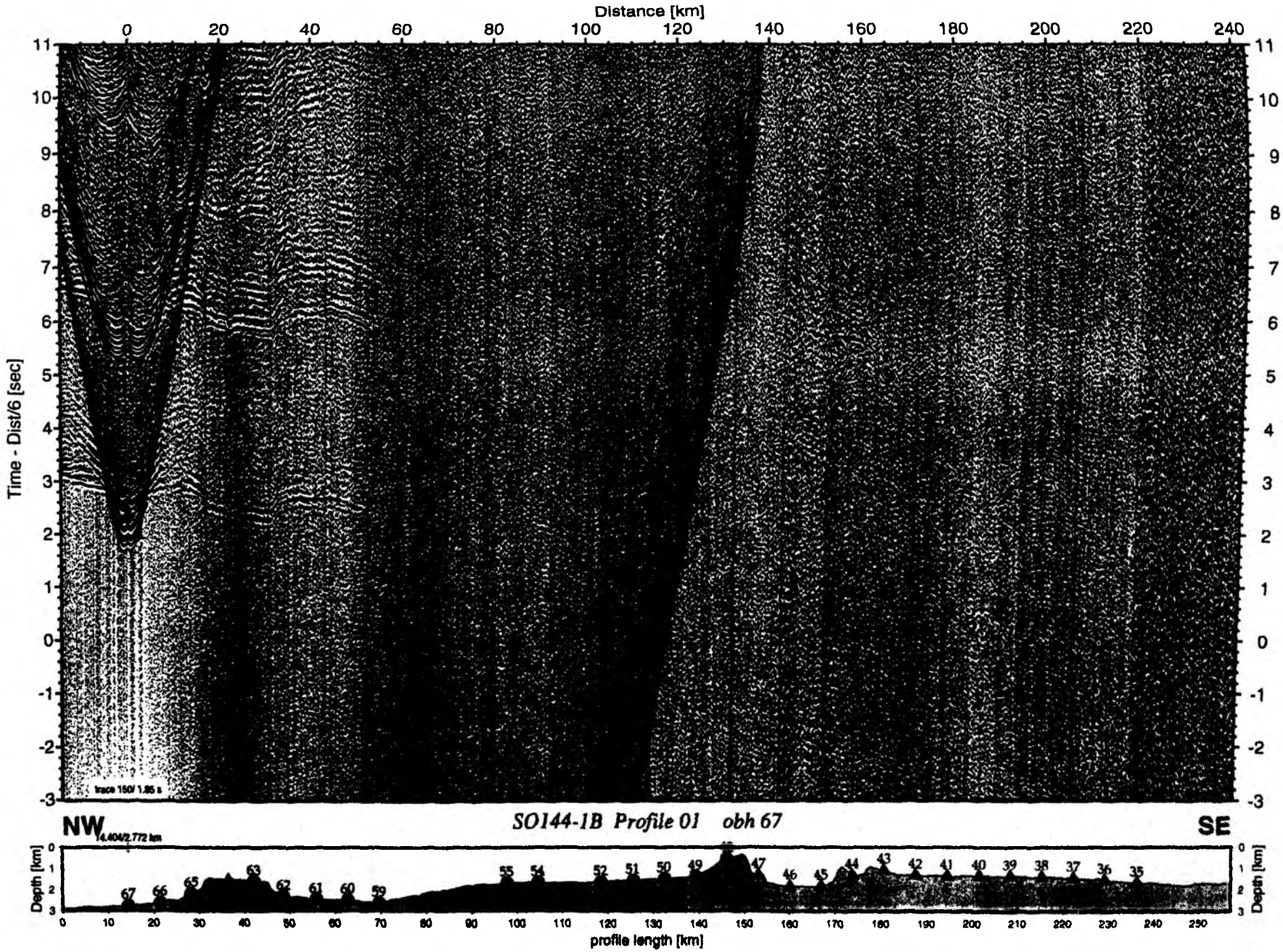

Figure 6.2.4.3.33: Record section from obh 67 , Profile 01.

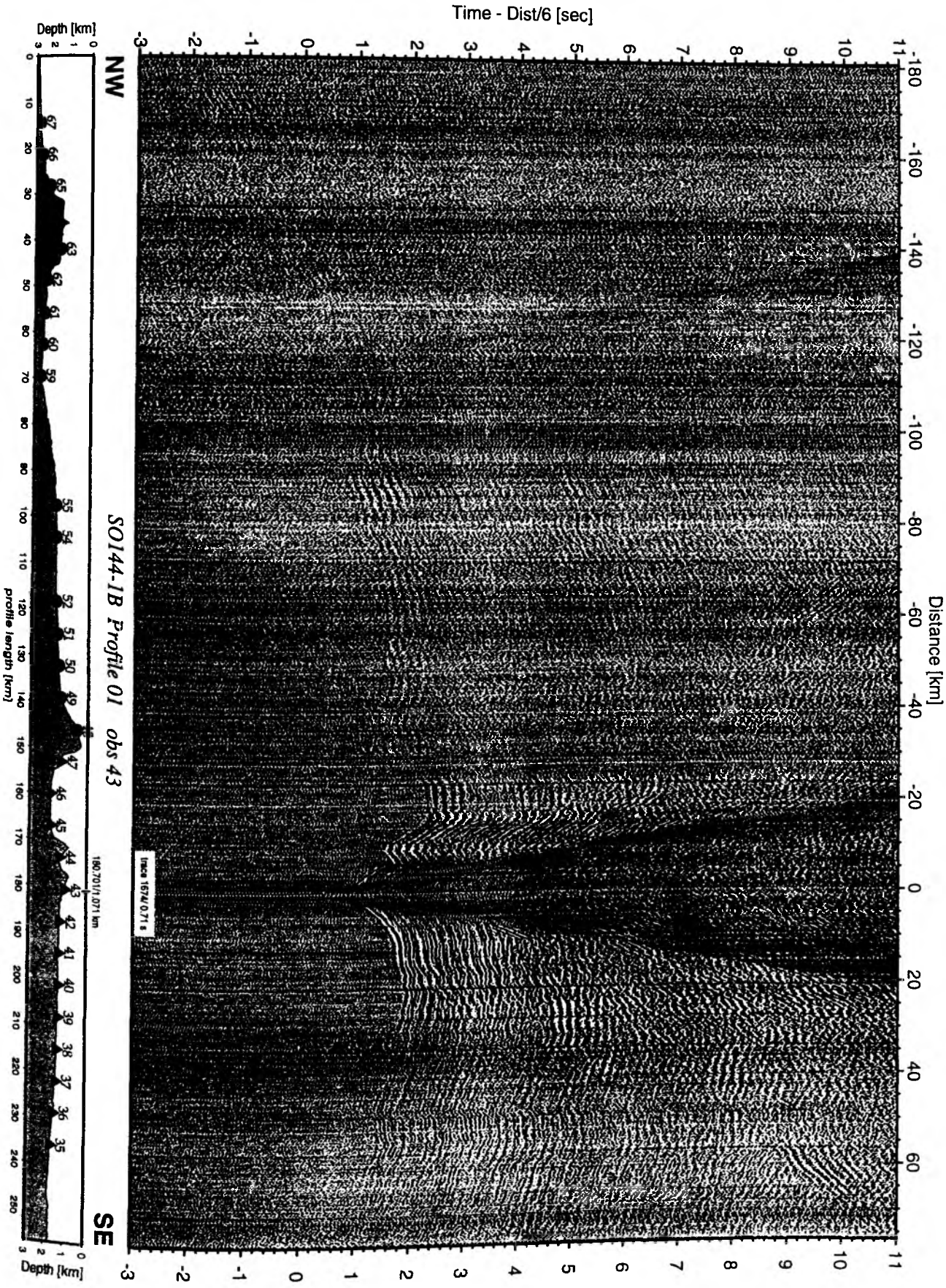

Figure 6.2.4.3.35: Record section from obs 43 horizontal component 2, Profile 01.

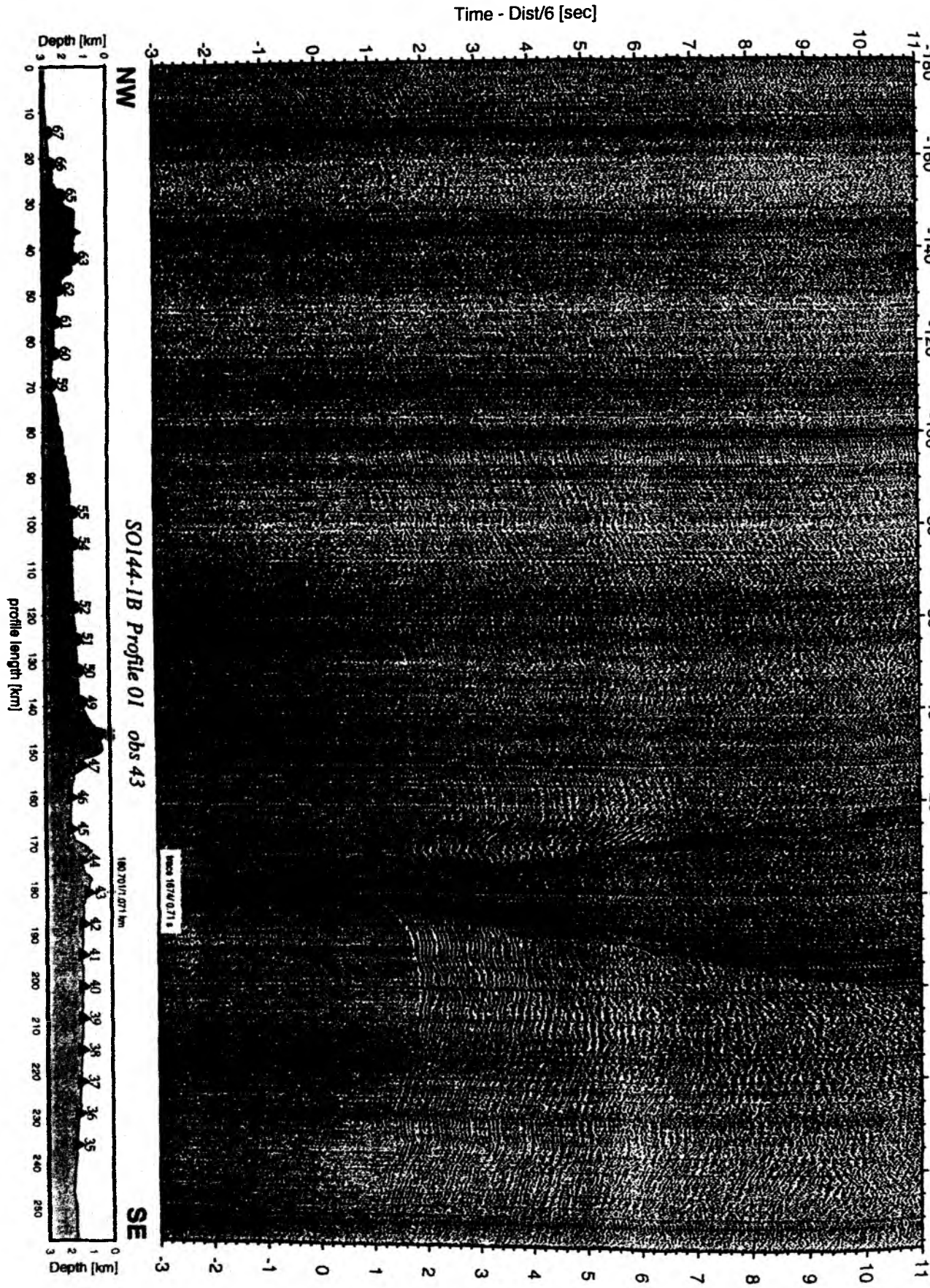

Figure 6.2.4.3.34: Record section from obs 43 horizontal component 1, Profile 01.

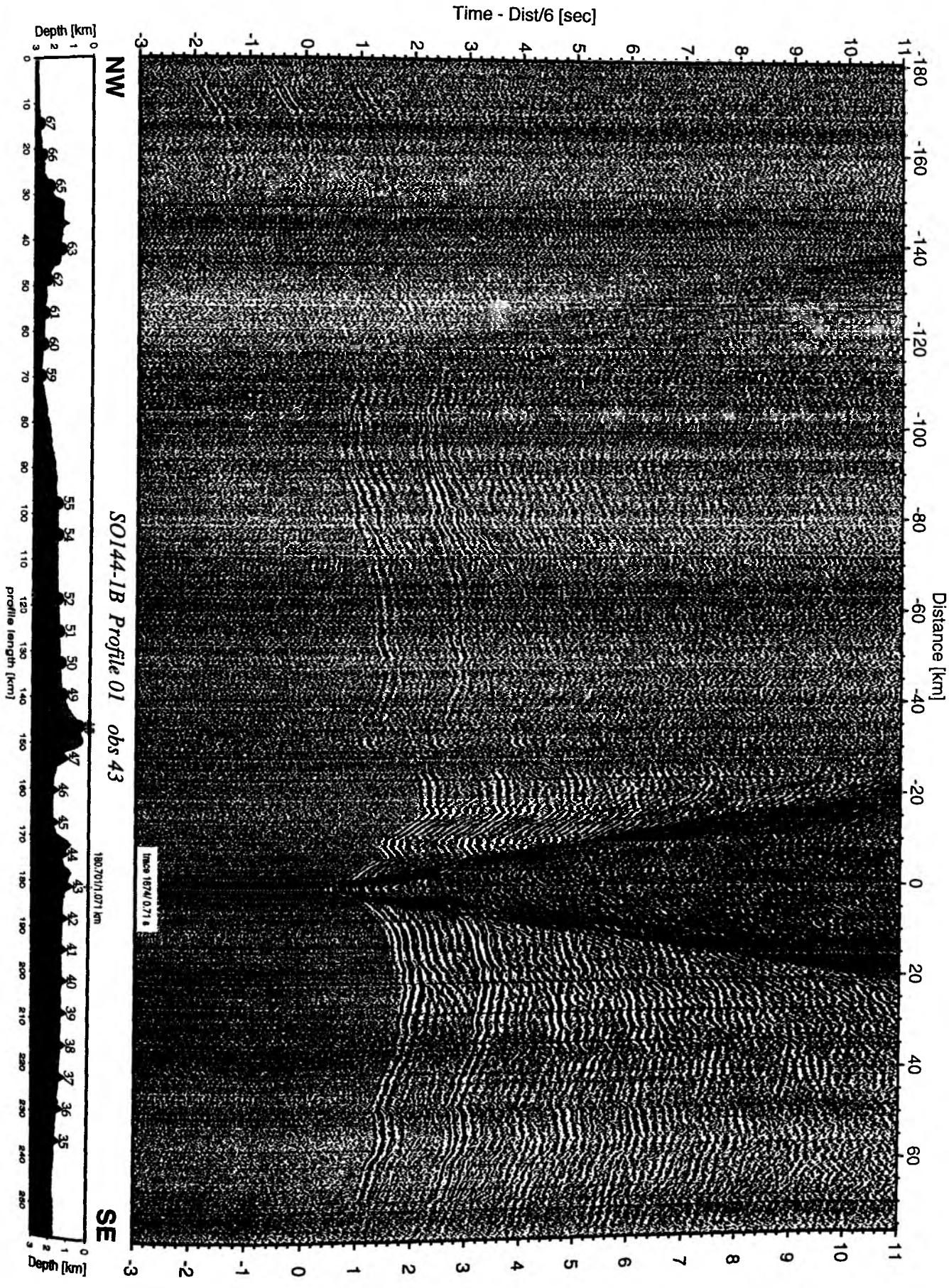

Figure 6.2.4.3.36: Record section from obs 43 hydrophone, Profile 01.

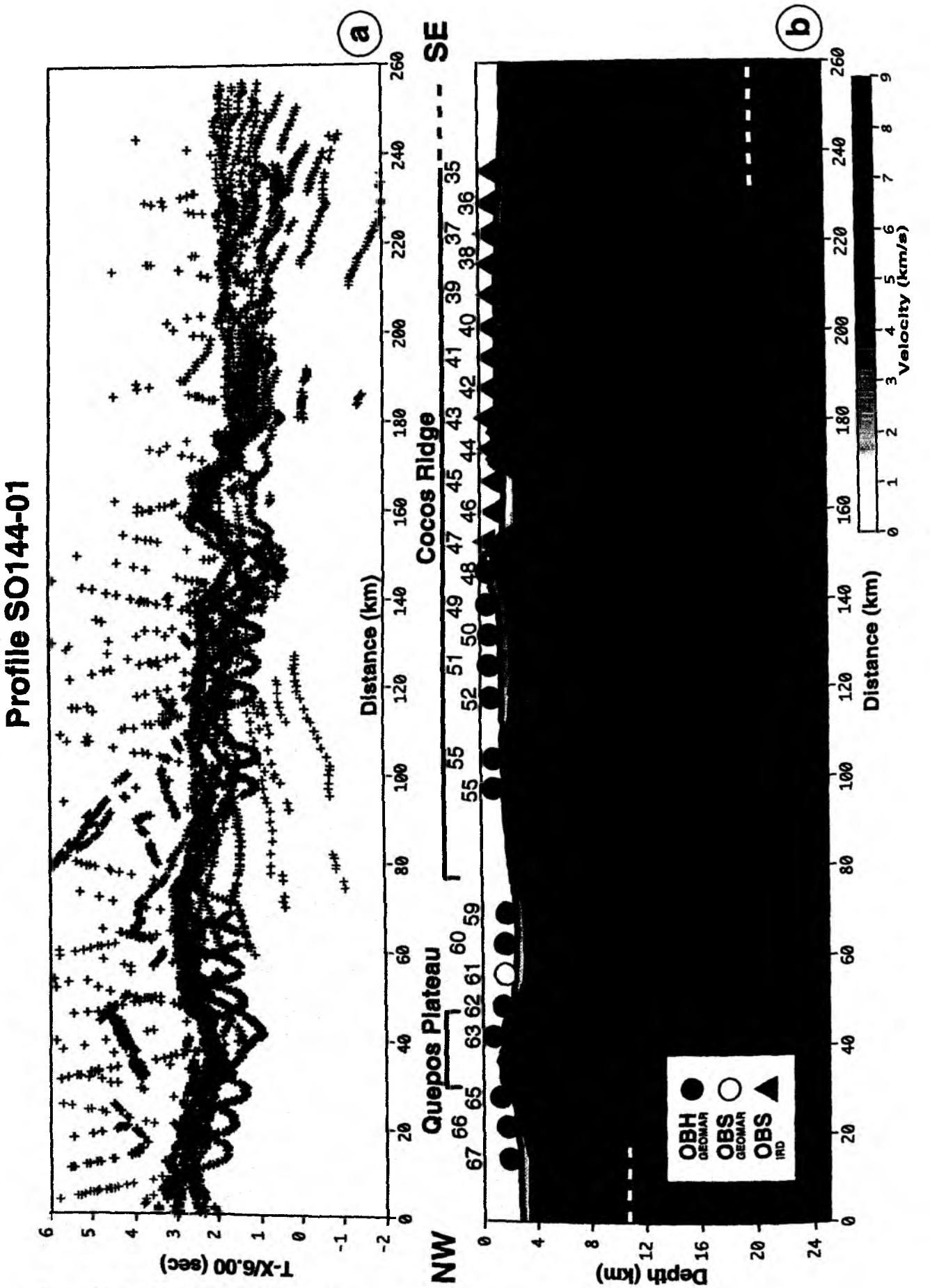

Figure 6.2.4.3.37 a) Picks extracted from the record sections of Profile 01
b) Crustal cross section for Profile 01 from preliminary analysis of wide-angle data.

6.2.4.4 PROFILE SO144-02

Profile SO144-02 is located along the crest of Cocos Ridge and reaches close to the coast of the Osa Peninsula. It also includes an attempt to map the subduction zone underneath the Osa Peninsula in 3-D. This was possible due to the facts that a.) the seismological network of the Scripps instruments was operational, the IRD instruments along profile SO144-01 were still operational and that the Gulfo Dulce is deep enough so that Sonne could enter and fire its airguns. 20 GEOMAR OBH (OBH68 to 87) were deployed along the crest of the ridge at about 3 nm spacing between 14:00 and 23:00 on 01 October. Shooting started on a profile around the Osa Peninsula into Gulfo Dulce from 20:00 on 2 October to 16:00 on 3 October (Profile SO144-2B, see Figure 6.3.4.3.1). After this segment was shot, the IRD instruments from Profile SO144-01 had to be recovered and shooting was resumed on 04 October at 18:00 to 15:00 on 05 October. The GEOMAR instruments were recovered immediately afterwards until 03:00 on 06 October. Shooting was done at about 3.5 kn with a 60 s trigger interval, and the magnetometer was deployed throughout shooting, except in the very shallow parts of Gulfo Dulce. Record sections from Profile SO144-02a and one representative section from line SO144-02B (sorted by shot number) are shown in Figures 6.2.4.4.2 to 6.4.4.4.17.

Modelling and interpretation:

The record sections obtained along Profile SO144-2A are of moderate quality, although arrivals can be followed to the end of the profile on most sections. They all show high velocity first arrivals starting at offsets in excess of 20 to 30 km. The three stations (OBH85 to 87) deployed landward of the trench show a pronounced asymmetry of the first arrivals due to the rapidly changing water depth. In addition, there are the only three sections where low velocity arrivals (sedimentary strata) can be seen. Unlike many other data sets obtained from the Costa Rican Pacific margin (Ye et al., 1996), no clear plate boundary reflection is evident. Those record sections obtained along the crest of Cocos Ridge show a large degree of self-similarity, with a few exceptions. The presence of considerable sediment, in places more than 1000 m, can easily be inferred due to the delay of the first arrivals. Since no refracted waves from these sediment can be seen in the data, a rather low velocity (1.7 km/s) was assumed for modelling and the sediment thickness was adjusted in a way that travel times of first arrivals were matched. Considerable variability of the sedimentary thickness is clearly indicated by a strong asymmetry on some record sections (e.g. OBH69, 74, 76, and 81). No intracrustal reflections are evident in the record sections, and only on some stations are later arrivals, such as the crust mantle boundary (PMP) visible.

Preliminary modelling was done using ray tracing techniques. The first arrivals out to large distances of more than 80 km were easily fit by two upper crustal layers (3.7 to 5.4 km/s and 5.0 to 5.8 km/s) with high velocity gradients. These layers are underlain by a high velocity layer (6.6 km/s). The scarcity of crust mantle reflections makes it difficult to determine the velocity of the lower crust, but high velocities (up to 7.5 km/s) seem to better match the PmP curvature than lower velocities. Assuming such a high velocity in the lower crust would place the Moho at a depth of 23 km, thus resulting in a 20-km-thick crust. This is in good agreement with the results from profiles SO144-01 and SO144-03.

The continental slope of the Osa Peninsula is generally made up of high velocities, with the exception of a small basin near the foot. The slope velocities range from 3.7 near the surface to 4.7 at a depth of 10 km, where the plate boundary is assumed to be, and closely resemble values obtained by Stavenhagen et al. (1998) on a nearby profile. As stated above, no clear plate boundary reflections are evident, but from the travel time delay on stations OBH85 to 87 and the depth of the 5.5 km/s and the 6.6 km/s layers, the boundary can be inferred. This suggests a very moderate dip angle, in agreement with earlier observations. A sketch of the crustal structure inferred from onboard interpretation is shown in Figure 6.2.4.4.18.

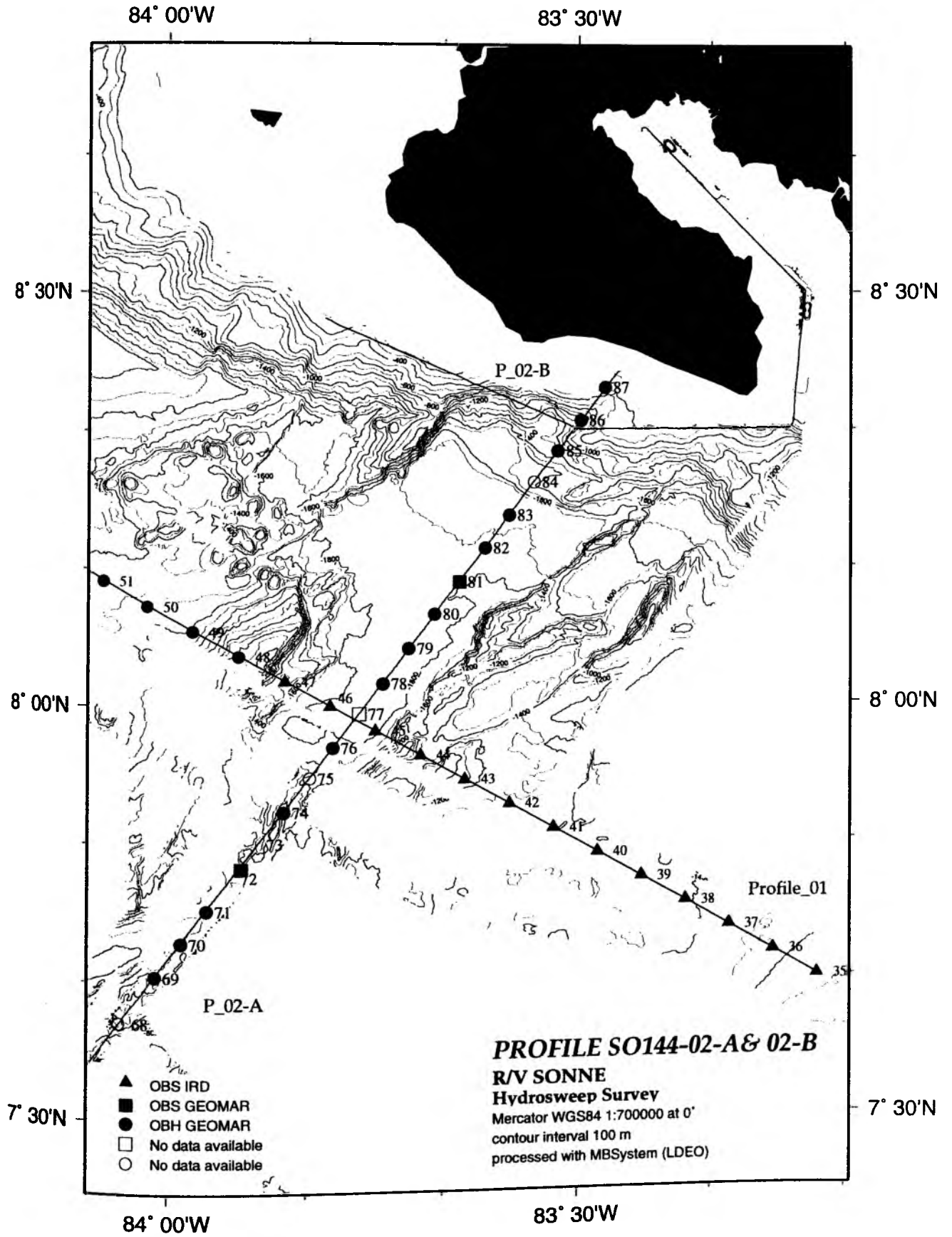

Figure 6.2.4.4.1: Profiles SO144-02-A& 02-B, Location map

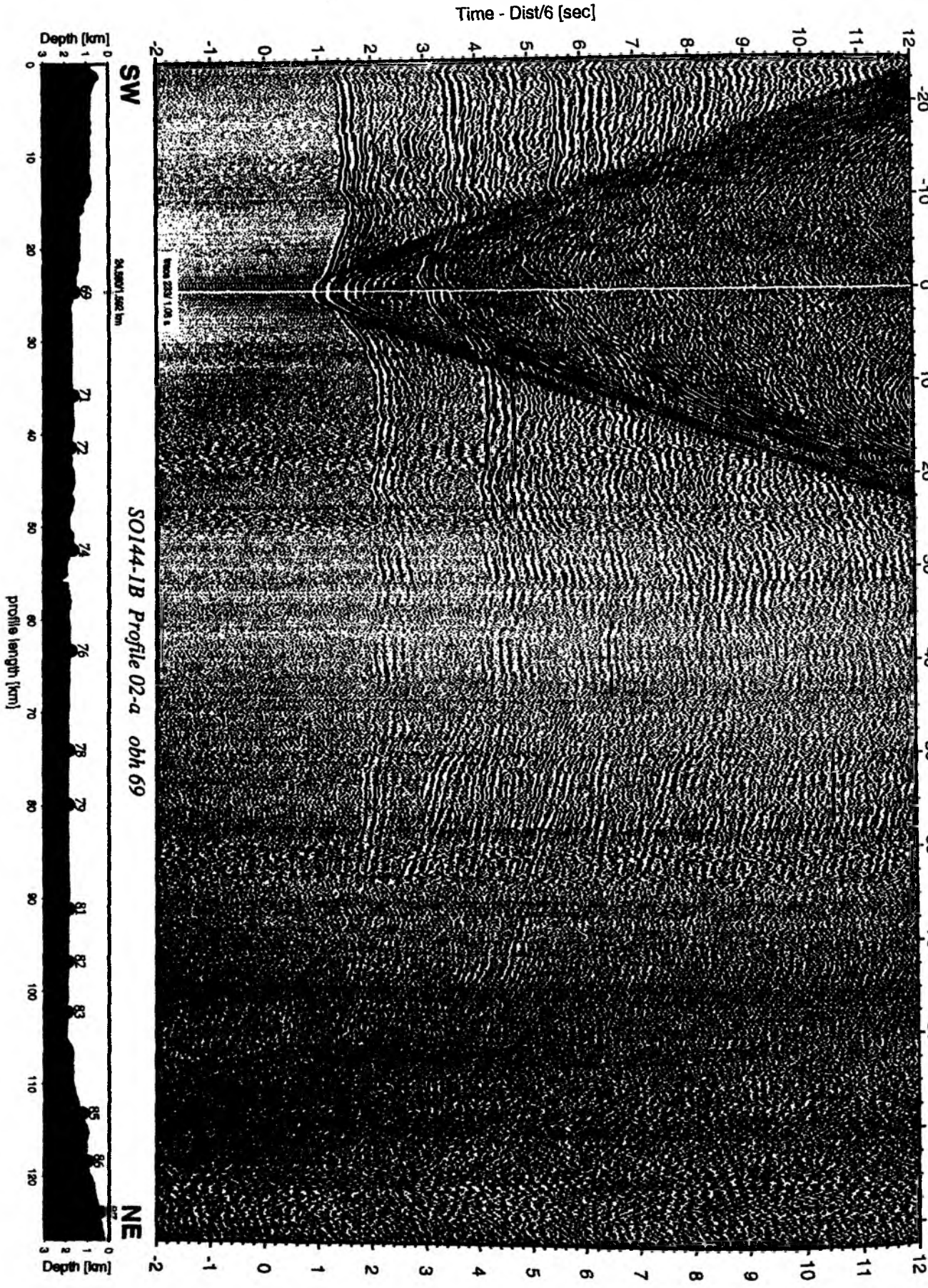

Figure 6.2.4.4.2: Record section from obh 69 , Profile 02-a.

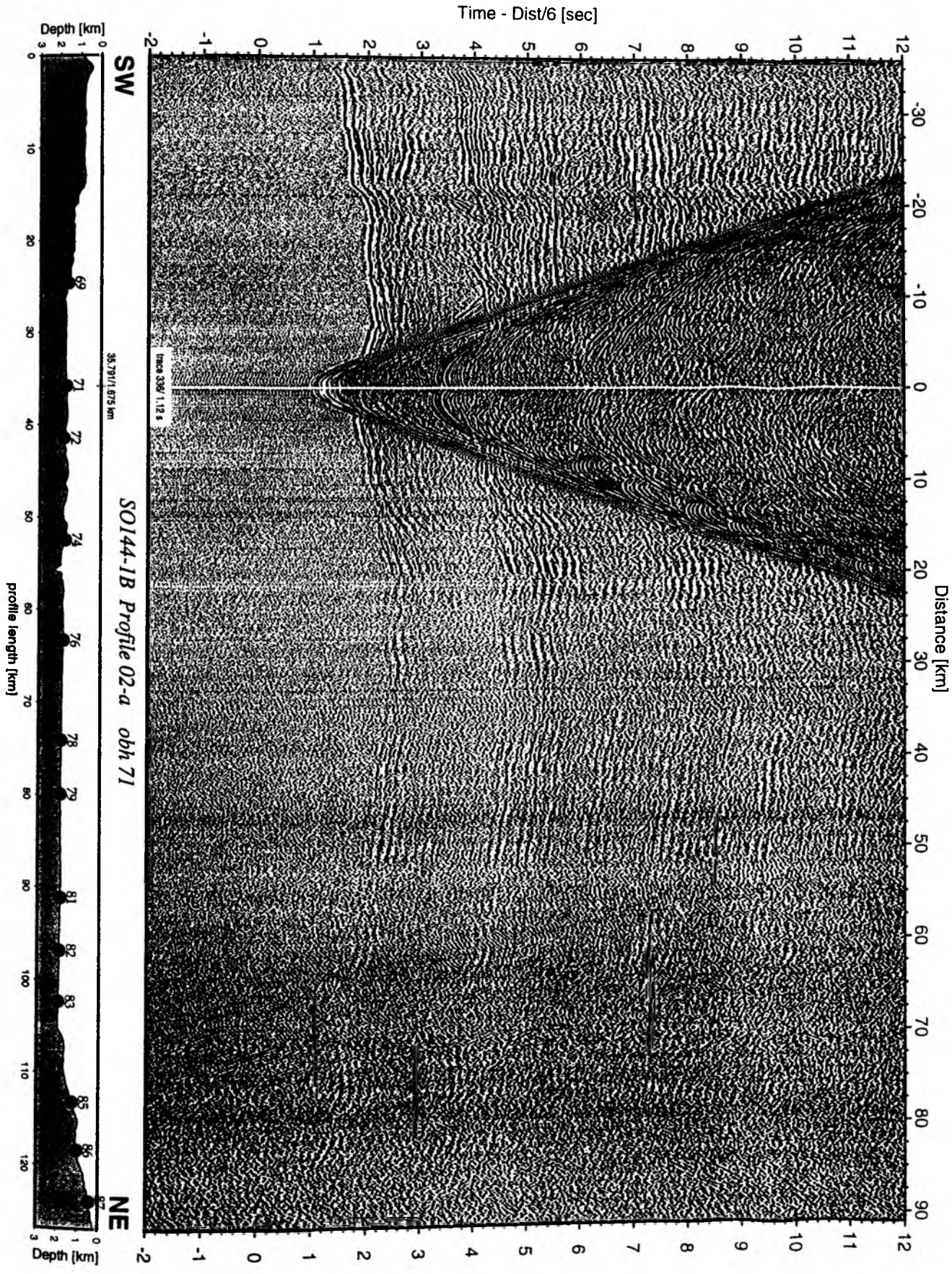

Figure 6.2.4.4.3: Record section from obh 71 , Profile 02-a.

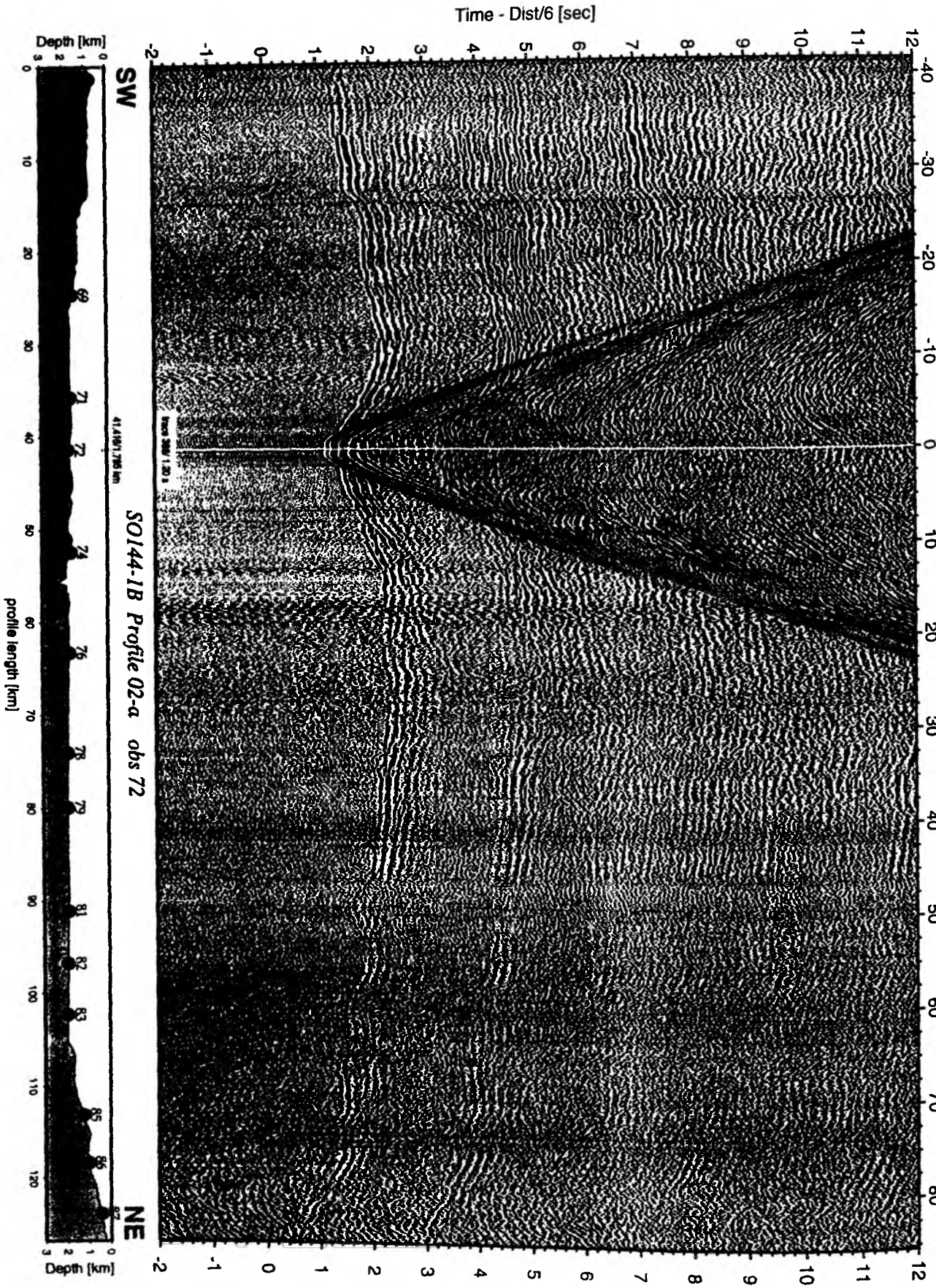

Figure 6.2.4.4.4: Record section from obs 72 hydrophone, Profile 02-a.

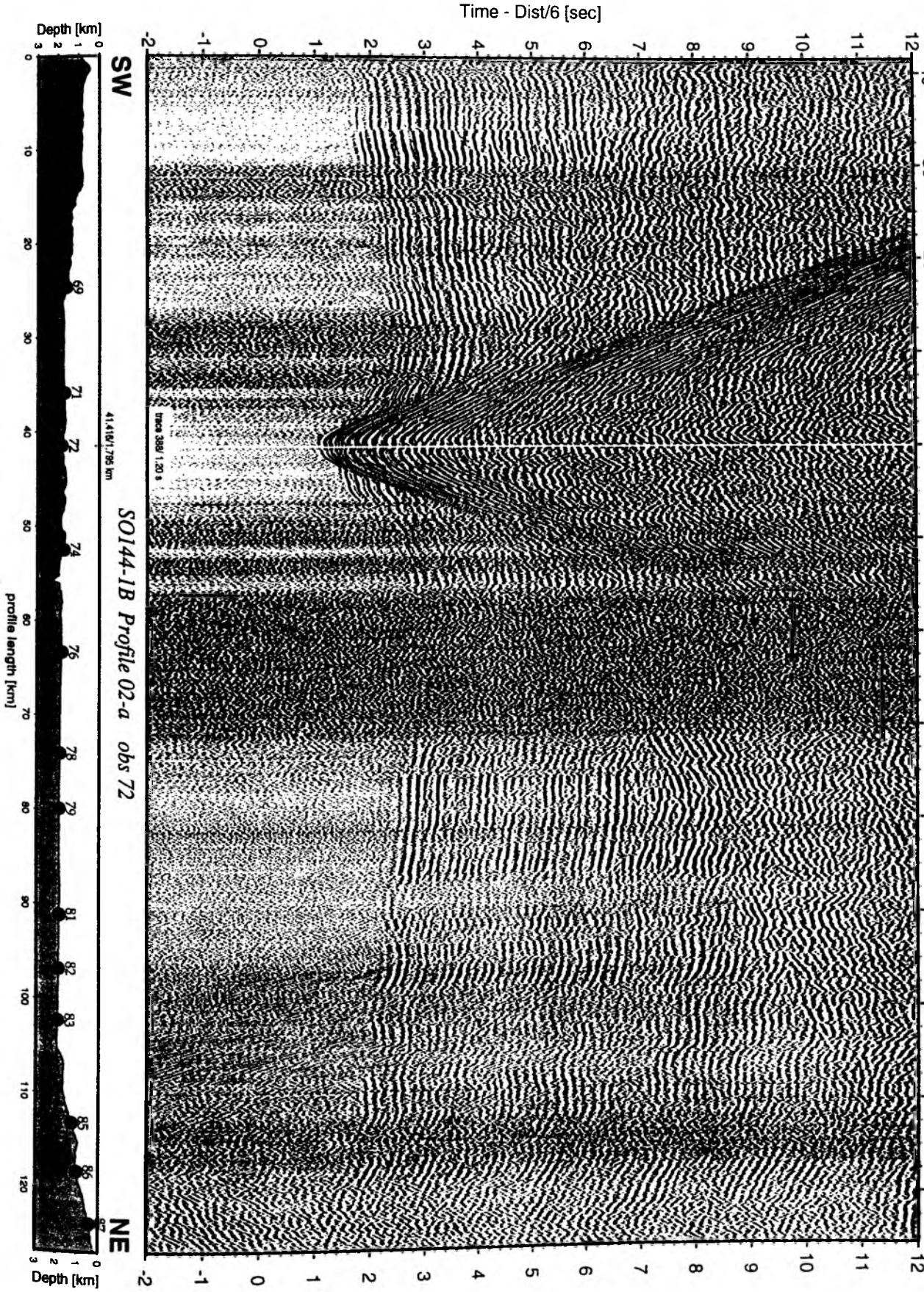

Figure 6.2.4.4.5: Record section from obs 72 horizontal component 1, Profile 02-a.

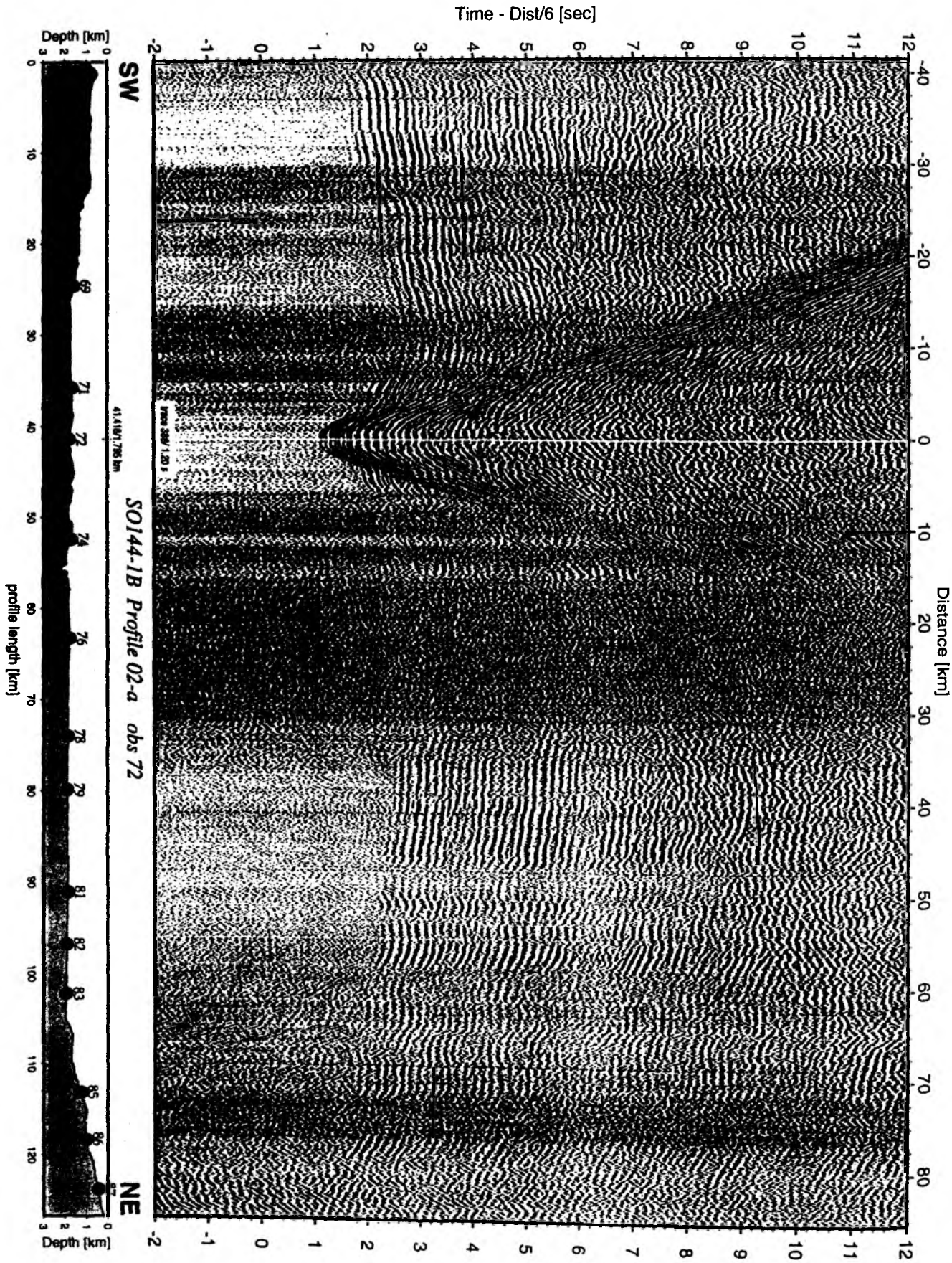

Figure 6.2.4.4.6: Record section from obs 72 horizontal component 2, Profile 02-a.

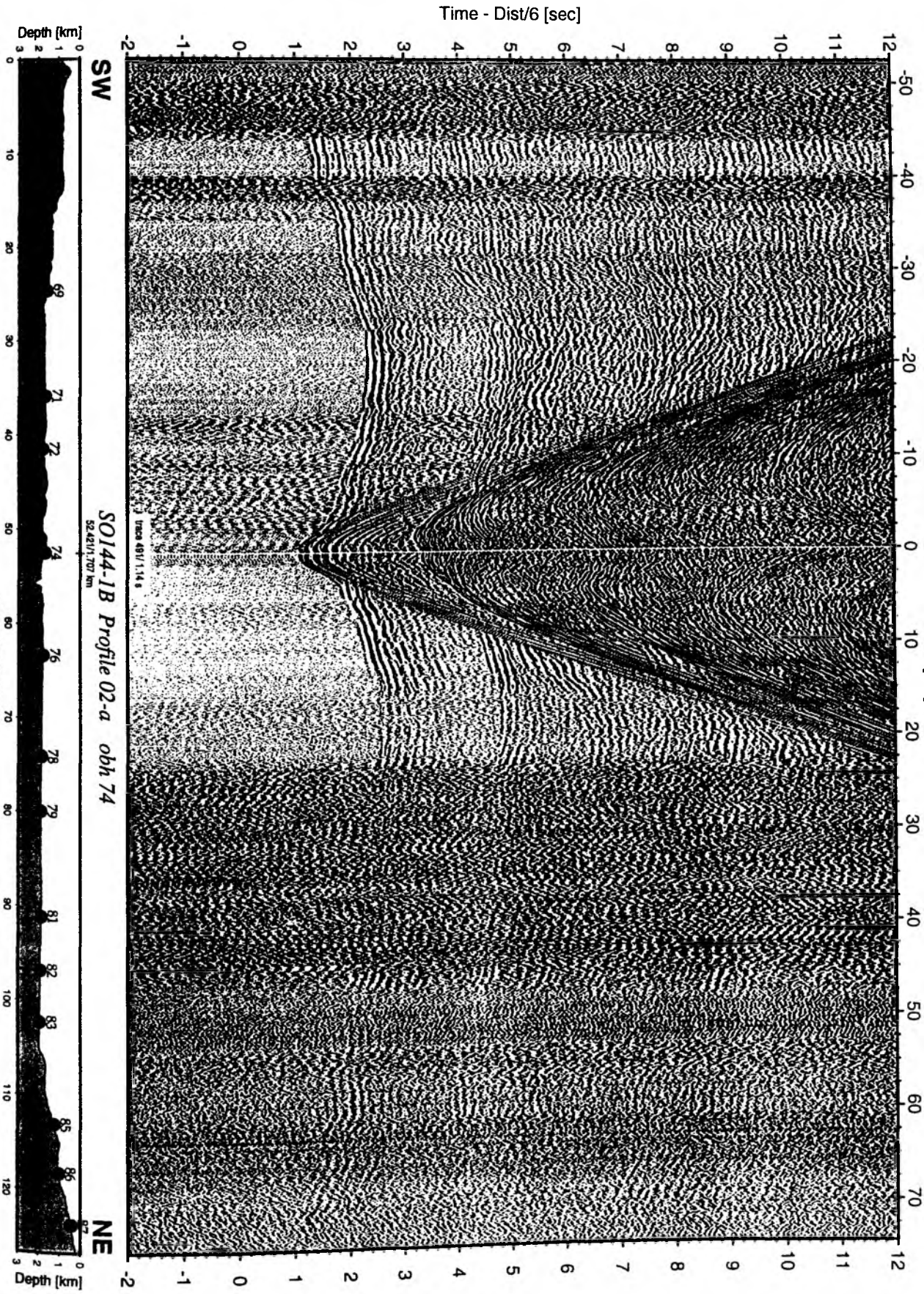

Figure 6.2.4.4.7: Record section from obh 74 , Profile 02-a.

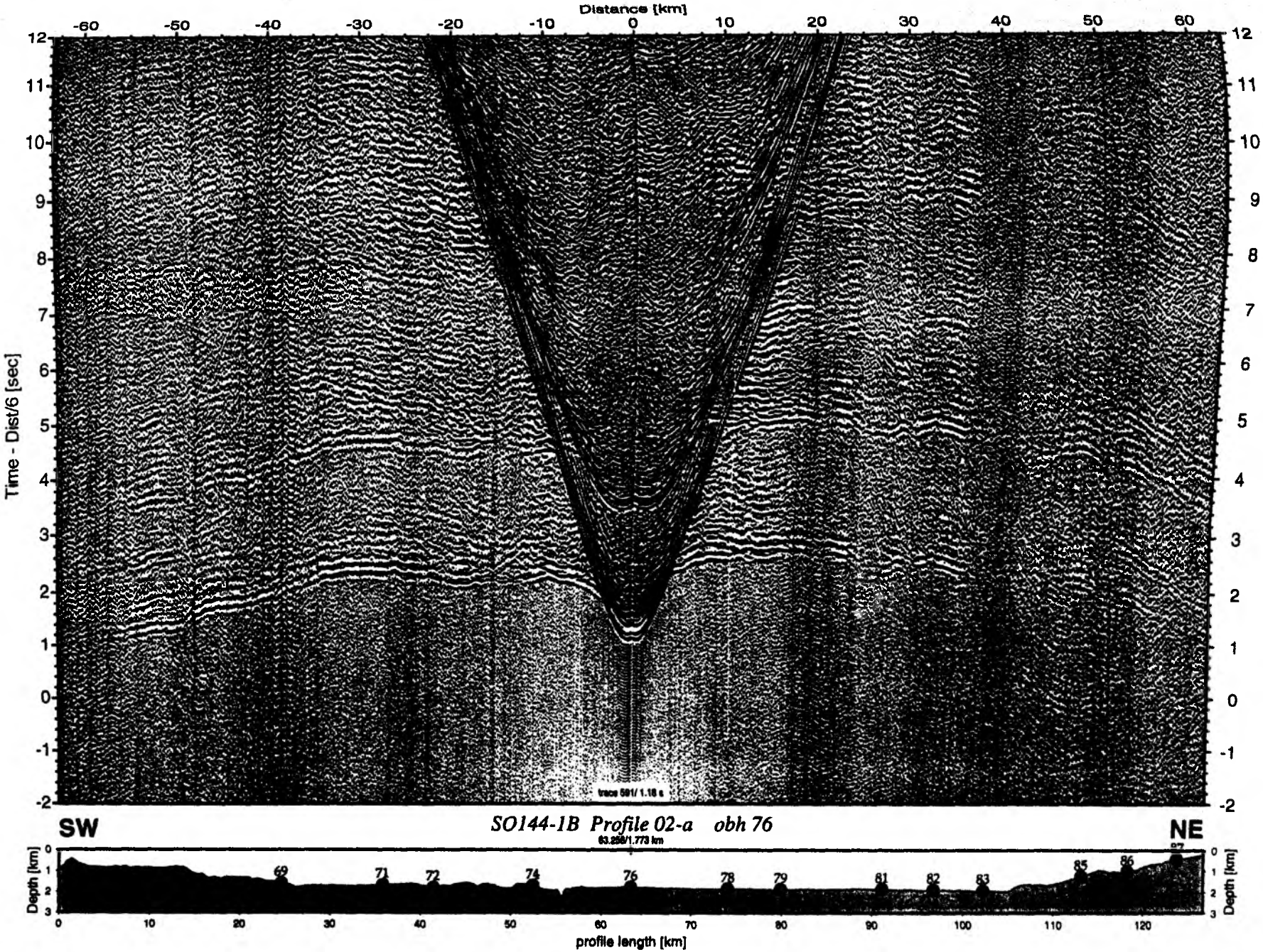

Figure 6.2.4.8: Record section from obh 76 , Profile 02-a.

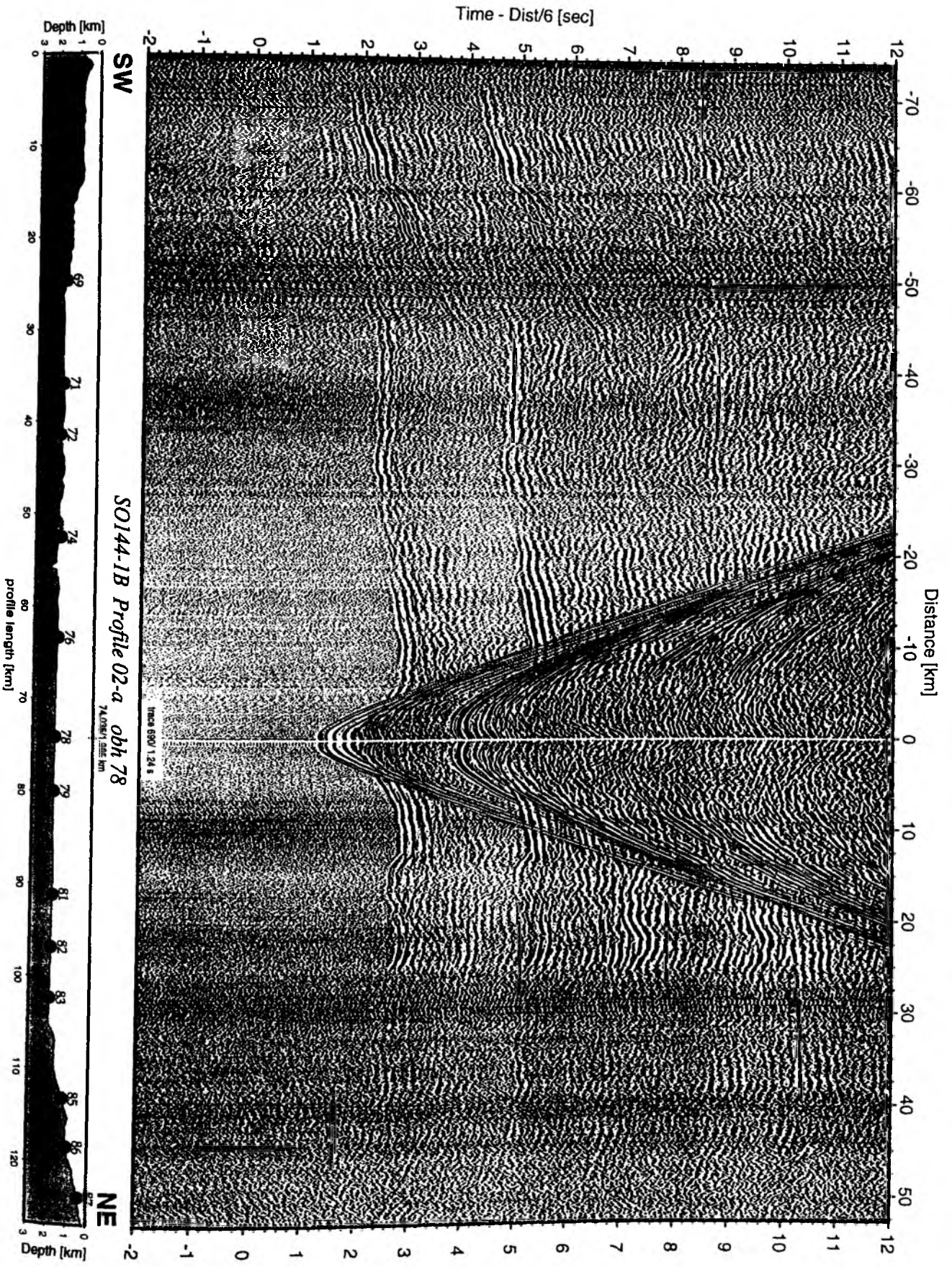

Figure 6.2.4.4.9: Record section from obh 78 , Profile 02-a.

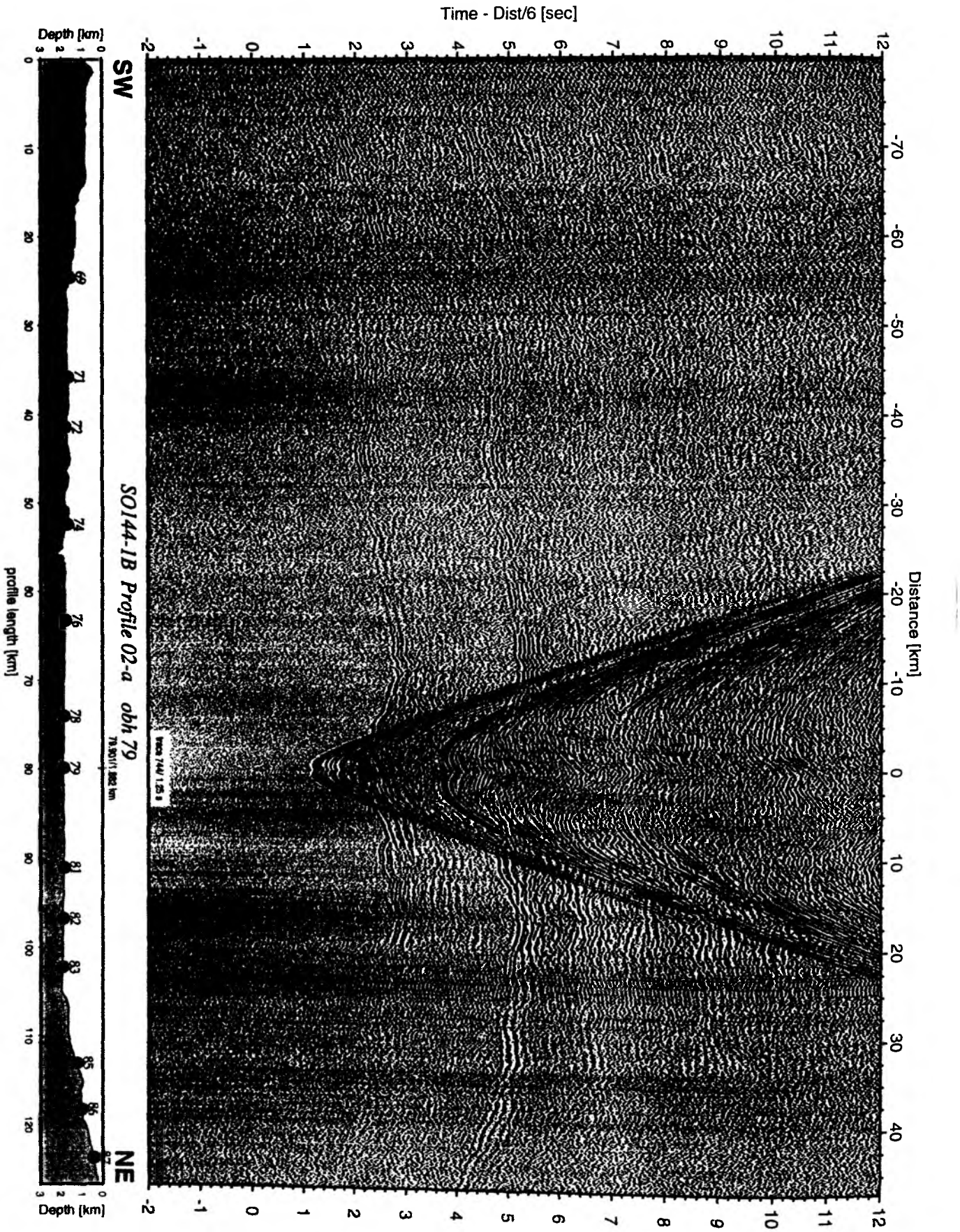

Figure 6.2.4.4.10: Record section from obh 79 , Profile 02-a.

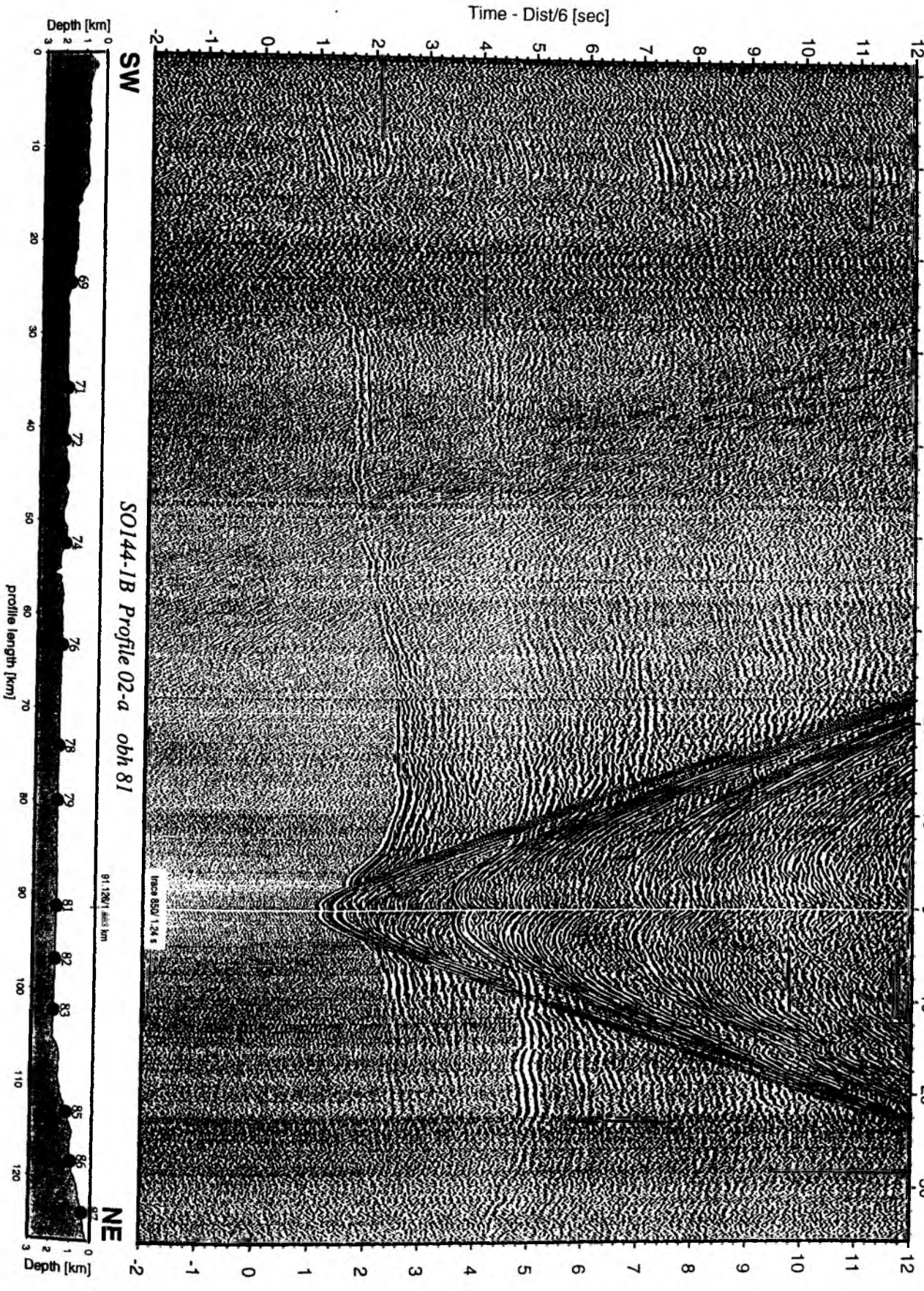

Figure 6.2.4.4.11: Record section from obh 81 , Profile 02-a.

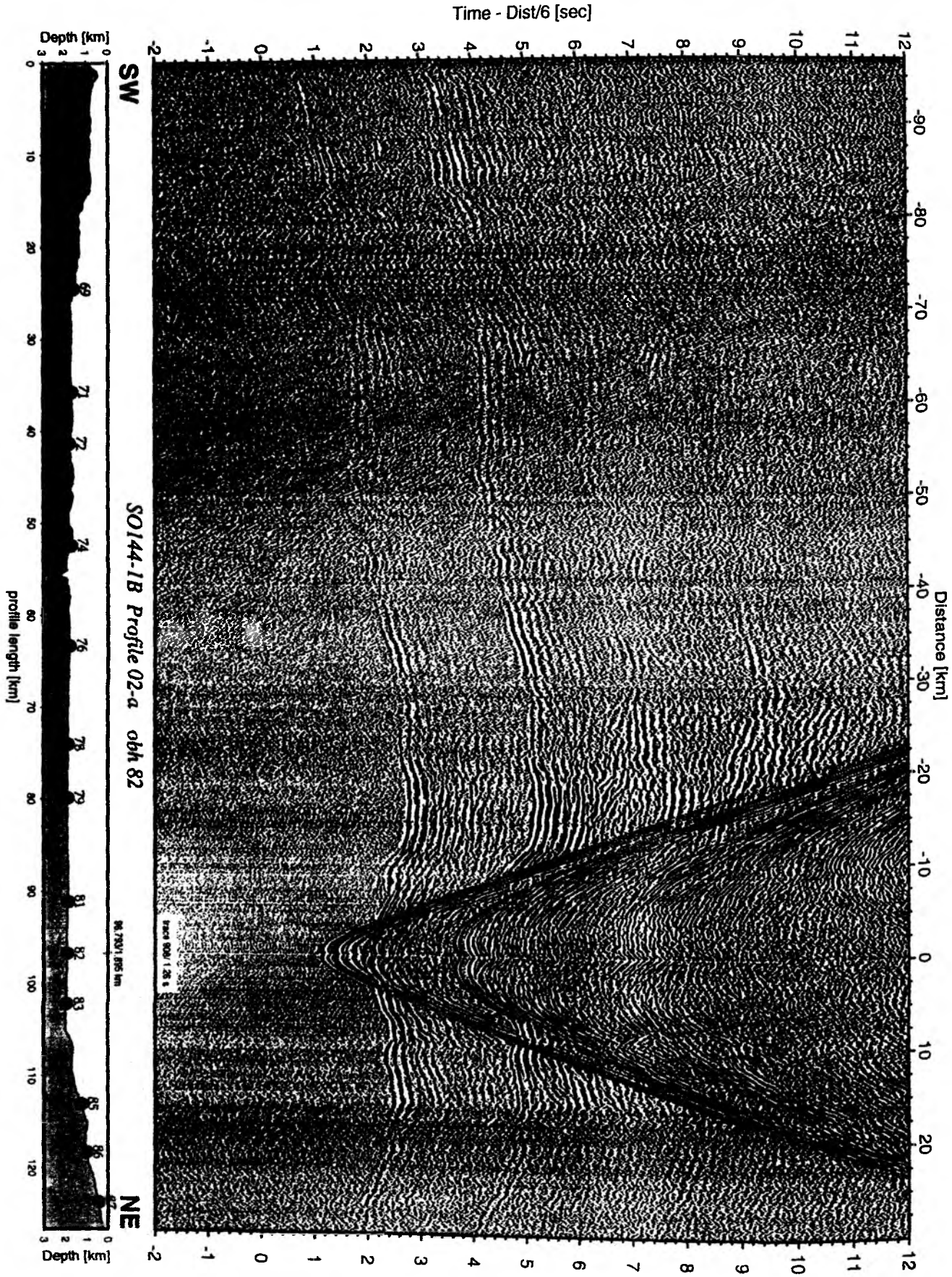

Figure 6.2.4.4.12: Record section from obh 82 , Profile 02-a.

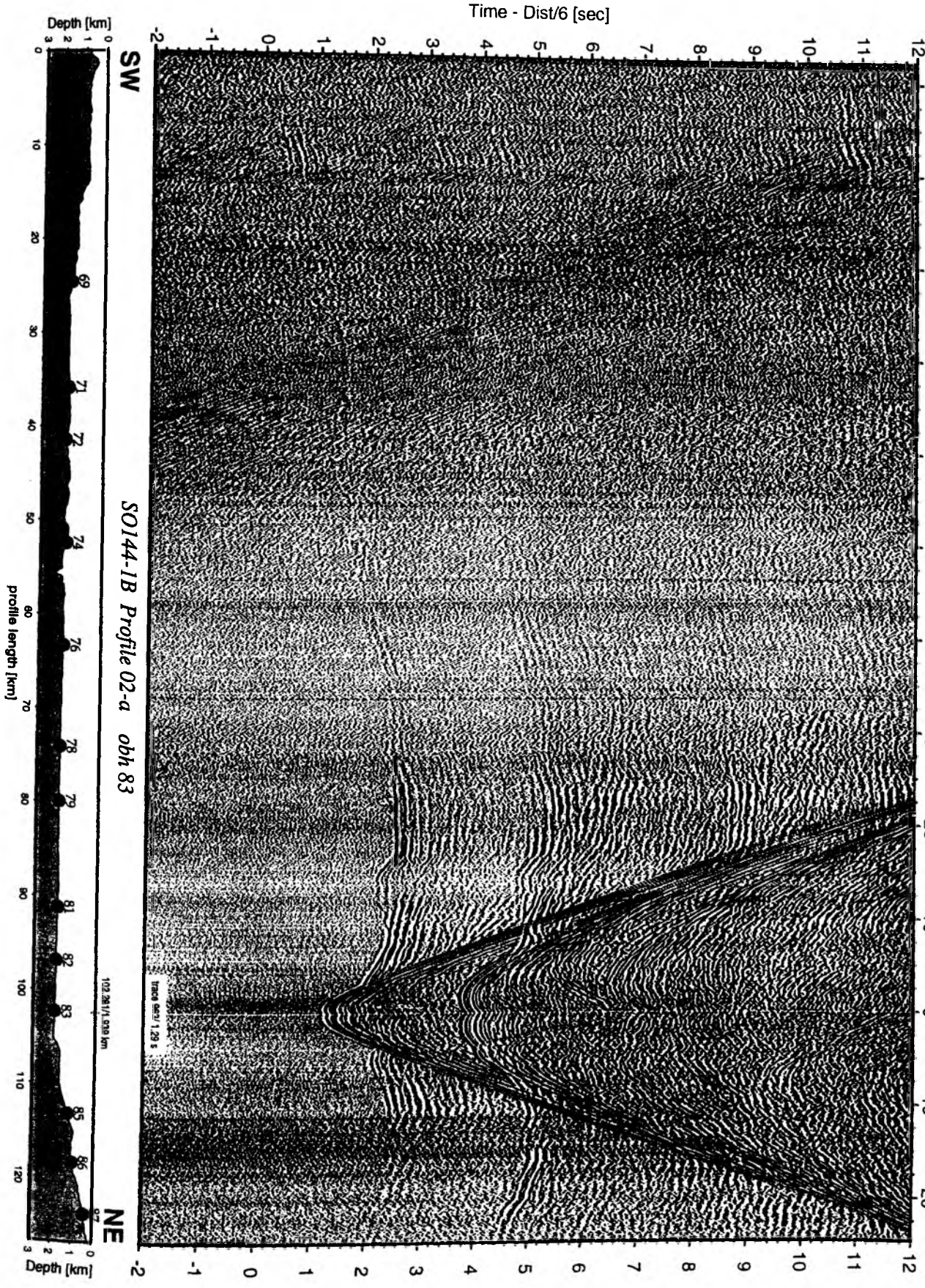

Figure 6.2.4.4.13: Record section from obh 83 , Profile 02-a.

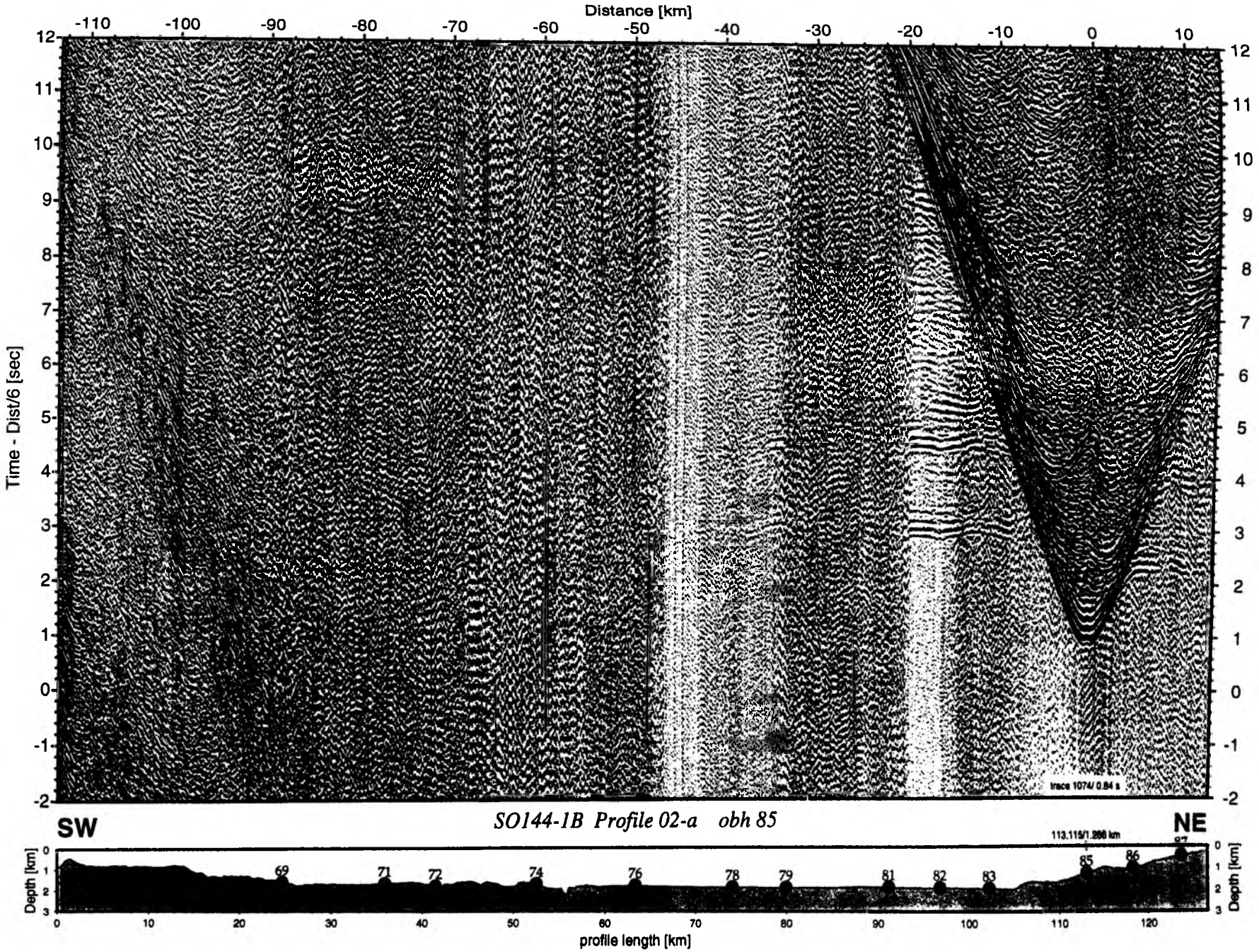

Figure 6.2.4.14: Record section from obh 85 , Profile 02-a.

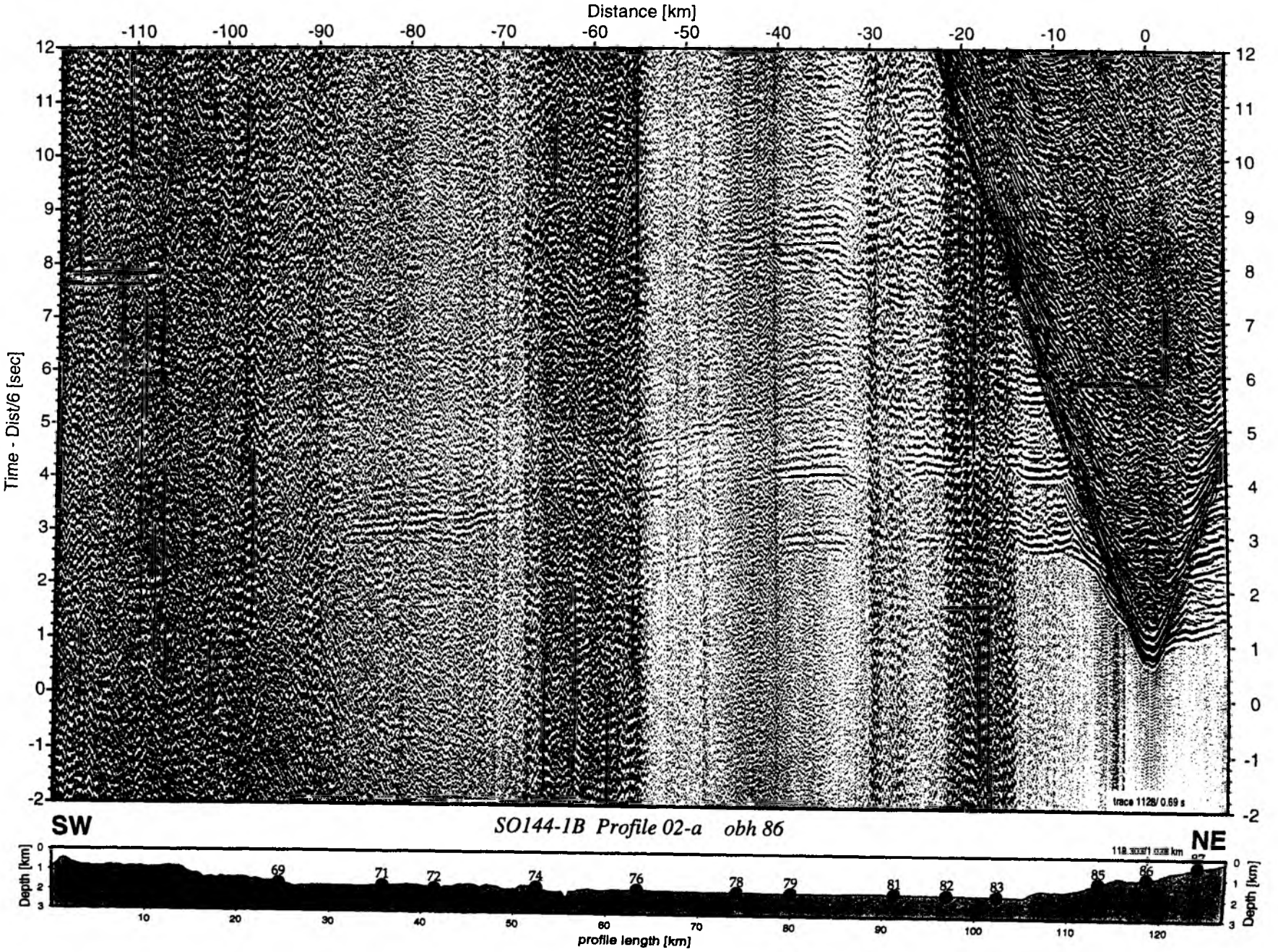

Figure 6.2.4.4.15: Record section from obh 86 , Profile 02-a.

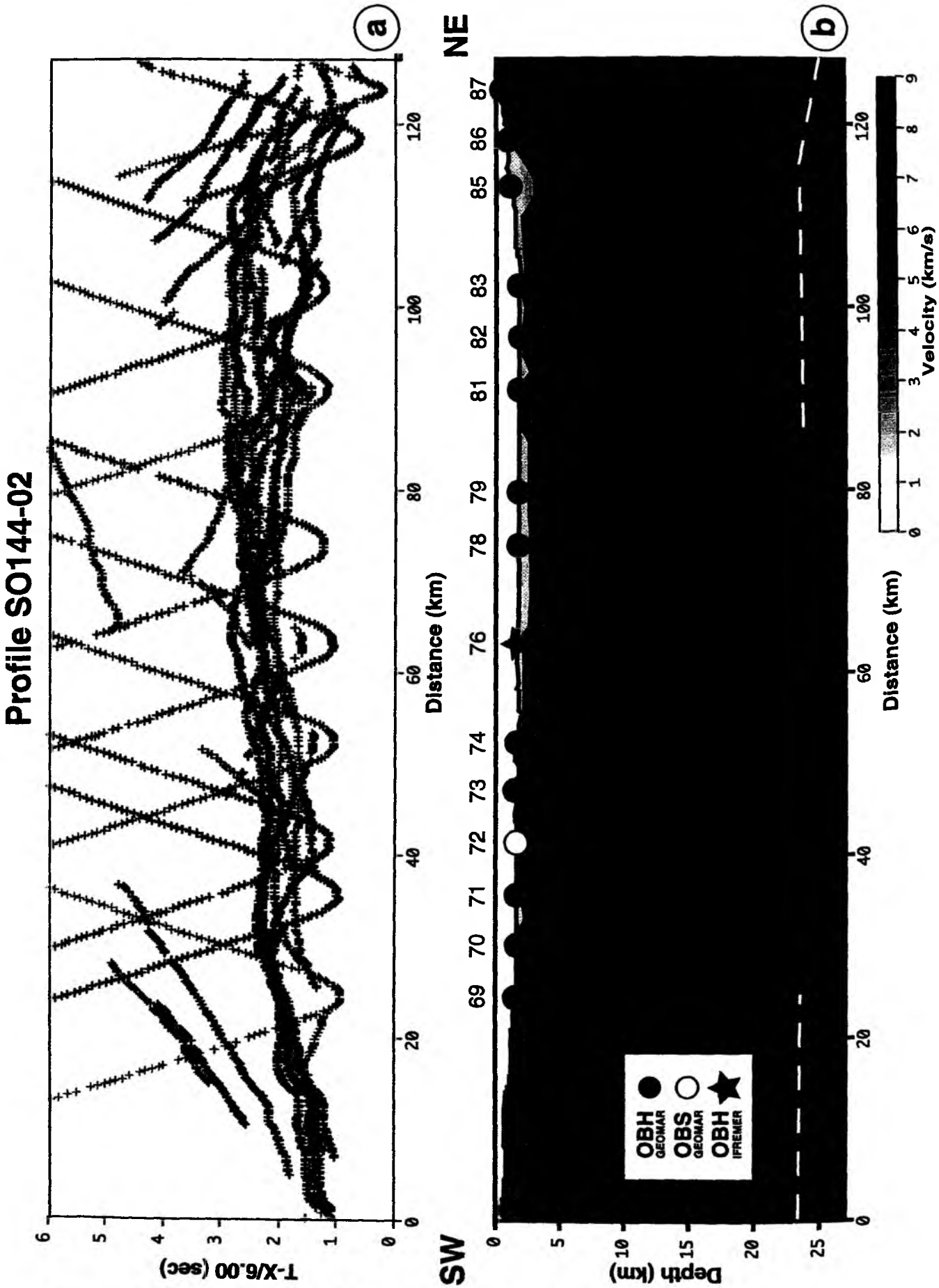

Figure 6.2.4.4.18 a) Picks extracted from the record sections of Profile 02
b) Crustal cross section for Profile 02 from preliminary analysis of wide-angle data.

6.2.4.5 PROFILE SO144-03

The Malpelo Ridge is a NE-SW trending bathymetric high, ca. 300 km long and 100 km wide, located between the Panama Fracture Zone and the Yaquina Graben. The top of the ridge is typically 1 to 2 km deep but emerges locally at Malpelo Island. Profile SO144-03 is a dip line across the Malpelo Ridge offshore Colombia. It is oriented 135° and passes Malpelo Island at a distance of approximately 30 nm. It is nearly coincident with a profile collected in the early seventies during Projecto Narino (Meissner et al., 1976). More important, this profile will be continued with MCS and wide-angle data during the SISTEUR project in August 2000. The line will be continued to the port of Tumaco at the Colombian/Ecuadorian border, and supplementary land stations will be operated. The origin of the Malpelo Ridge remains controversial. Though it is generally accepted to have been generated at the Galapagos Hotspot, two conflicting ideas have been proposed. One group of authors claim that the Malpelo ridge is part of the northern extension of the Cocos Ridge (e.g. von Huene and Flueh, 1994). According to this idea, the Malpelo Ridge has been shifting south relative to the Cocos Ridge along the Panama Fracture Zone for 8 Ma. Another group (e.g. Gutscher et al., 1999) interprets weak magnetic anomalies between the Malpelo Ridge and the Carnegie Ridge as an indication that the Malpelo Ridge rifted away from the Carnegie Ridge. These two models cannot unambigously be differentiated by a seismic profile, however, the southern margin of Malpelo ridge is expected to show possible structures that could be used to support one of the two models.

SONNE reached Colombian waters around midnight 07 October, and a track-parallel line with magnetics and hydroacoustics (profile 117) was run to the southeast, where deployment of a 33 element linear array began at 07:00 on 07 October. All 33 instruments (OBH/S 90 to 122) were deployed by 22:00, and shortly after midnight two airguns were operational, the third one being added about 12 hours later. Shooting was done at 3.5 kn with a shot interval of 60 s, the 140-nm-long line being terminated at 14:00 on 09 October. The magnetometer was also deployed throughout shooting, although it failed for a few hours in the beginning. The GEOMAR instruments were recovered between 16:30 and 03:30 on 10 October, leaving 4 hours before the IRD instruments were to be at surface. These hours were used for additional magnetic and hydroacoustic profiles (profile 120), and at 20:00 the last IRD OBS was safely recovered. The location of the profile is shown in Figure 6.2.4.5.1, representative record sections are shown in Figures 6.2.4.5.2 to 6.2.4.5.35. Further information on instruments and shots is given in Appendices 9.1.4 and 9.2.

Modelling and Interpretation:

Seismic sections recorded on the Malpelo Ridge and in the adjacent basin exhibit an excellent signal-to-noise ratio with clear seismic arrivals visible as far as 220 km. A strong reflection, most probably from the base of the crust (PmP) is visible as a second arrival between 70 and 110 km. A further arrival with high apparent velocities (>8.0 km/s) can be interpreted as a refraction from the upper mantle (Pn). Horizontal components of OBS exhibit clear converted S-waves (see example in Figure 6.2.4.5.35).

Preliminary interpretations of the data attempted onboard show a high gradient upper crust below a sedimentary cover of variable thickness. This thickness variation is indicated by the

1000 m thick in places. To facilitate modelling, an upper and a lower crustal layer were introduced. The upper one has a velocity increasing from 4.7 to 5.7, while in the lower crust the velocity increases from 6.5 to 6.8 km/s. In the northwest part of the profile, the lower crustal velocities seem to be somewhat higher, ranging from 6.6 to 7.0 km/s. Most pronounced on the record section is the PmP reflection, which also varies considerably along the profile. Its critical distance and the crossover point of the Pn phase changes from 40 to 80 km for the critical distance and from 80 to 120 km for the Pn. In an attempt to model these characteristics, a crustal model as shown in Figure 6.2.4.5.36 has been developed. This model shows normal oceanic crust on both sides of the Malpelo ridge, and a pronounced layer with higher velocities in the lower crust (6.8 to 7.2 km/s), reflecting the change in topography. The maximum crustal thickness is about 22 km on the northwestern side of the ridge. It is noteworthy that the preliminary modelling suggests a gradual decrease of crustal thickness to the southeast, but a sharp decrease to the northwest. Although this should be interpreted with great care for the moment, it will be a feature that shall be further investigated during post-cruise interpretation.

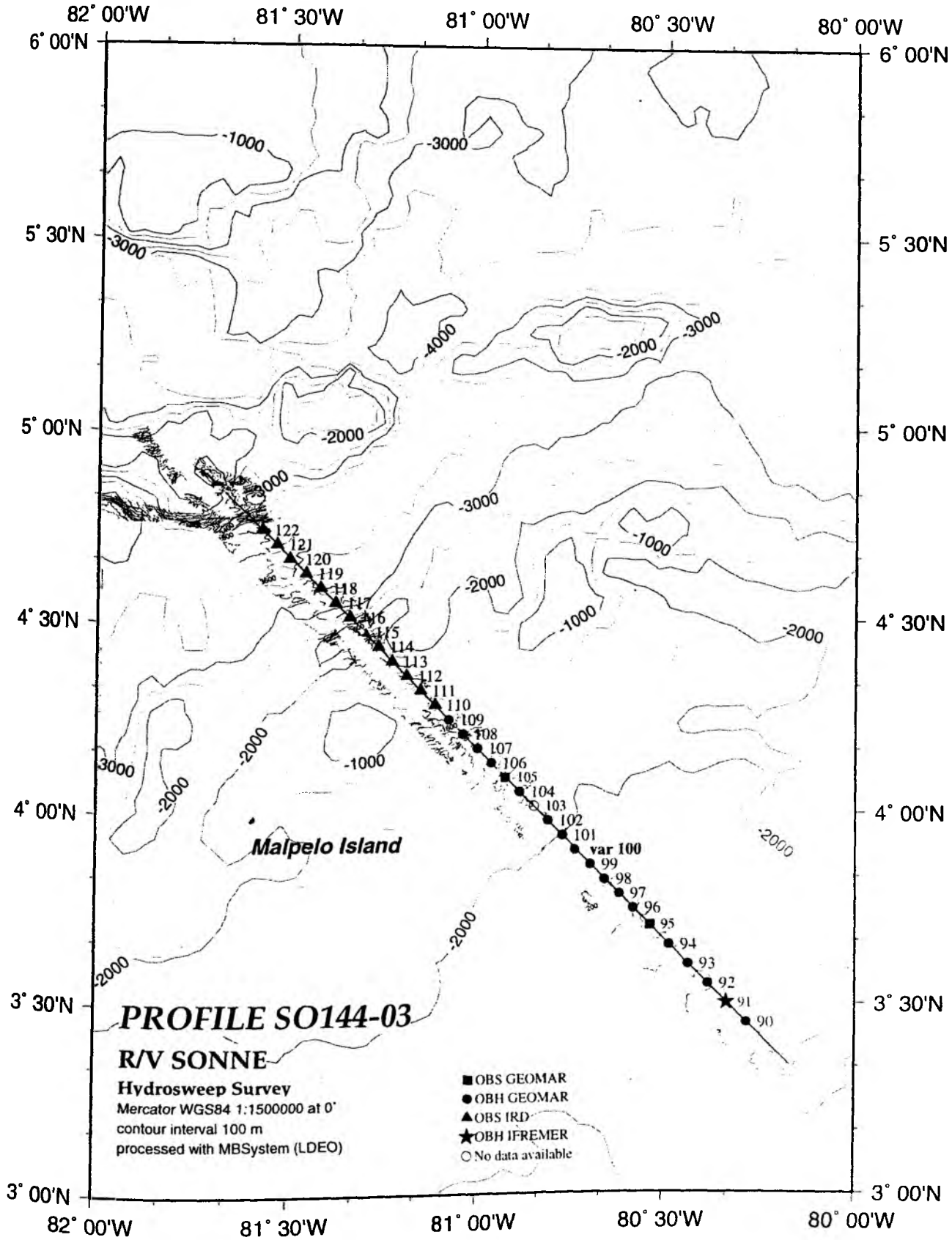

Figure 6.2.4.5.1: Profile SO144-03, Location map

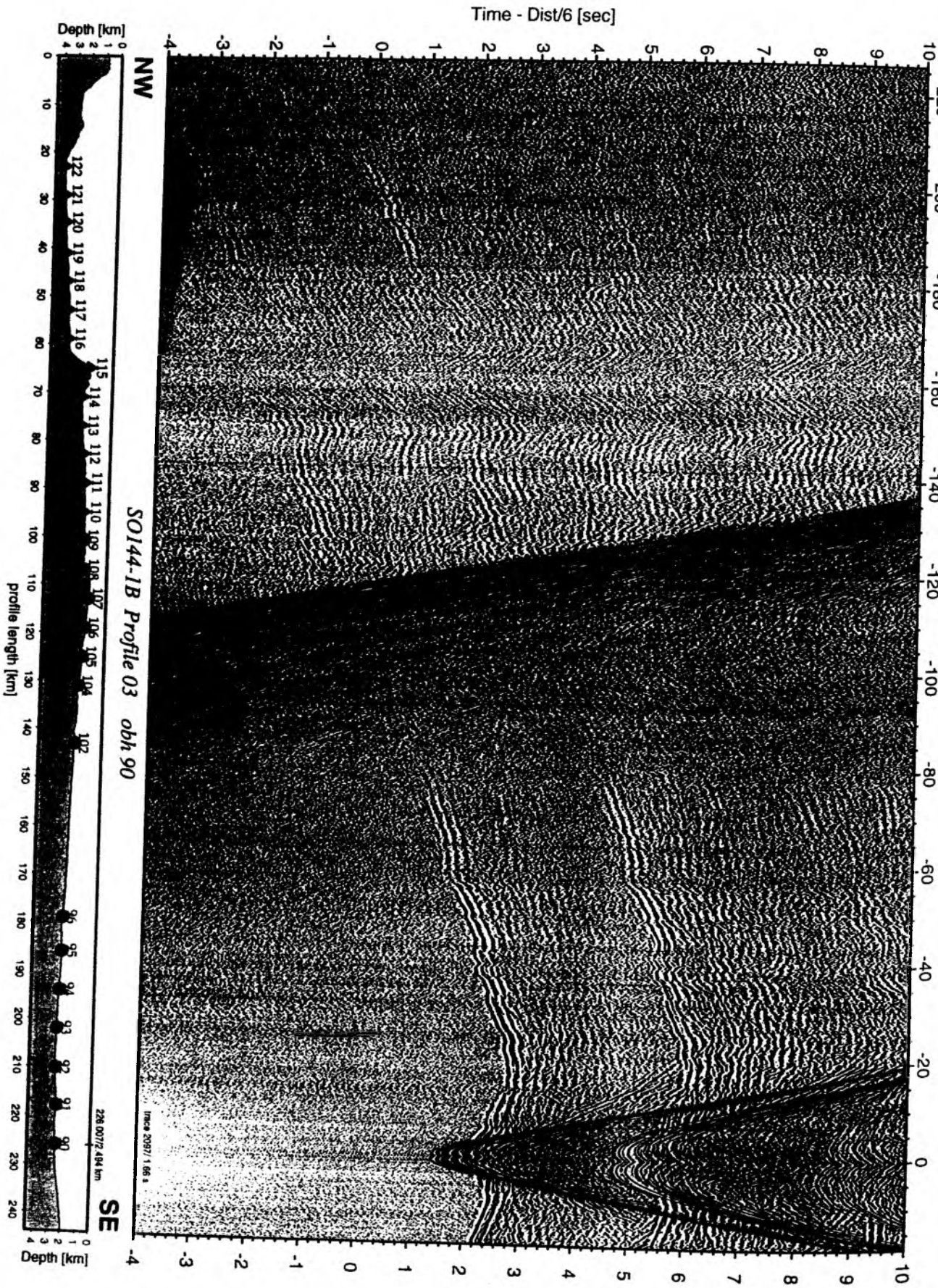

Figure 6.2.4.5.2: Record section from obh 90 , Profile 03.

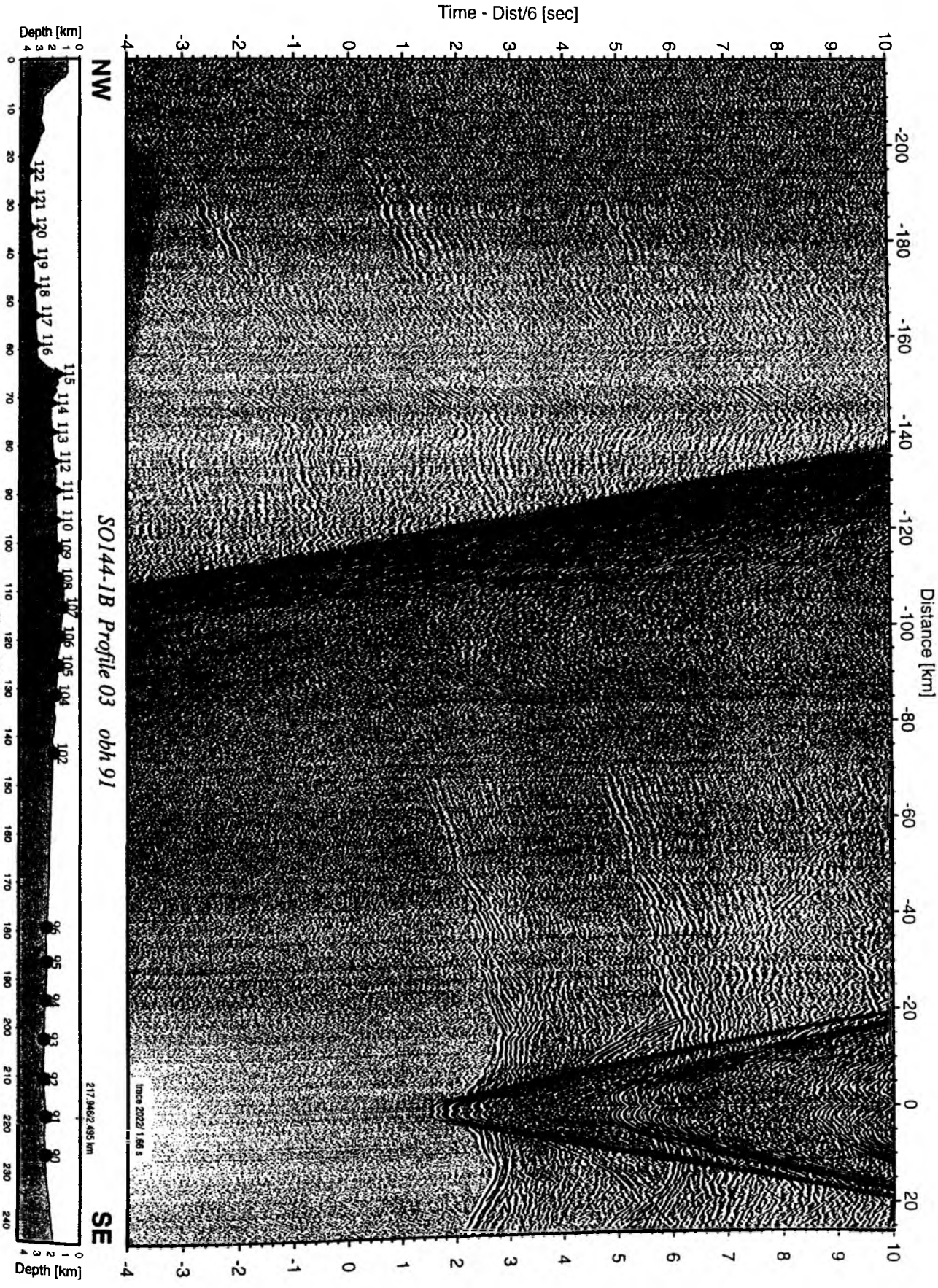

Figure 6.2.4.5.3: Record section from obh 91 , Profile 03.

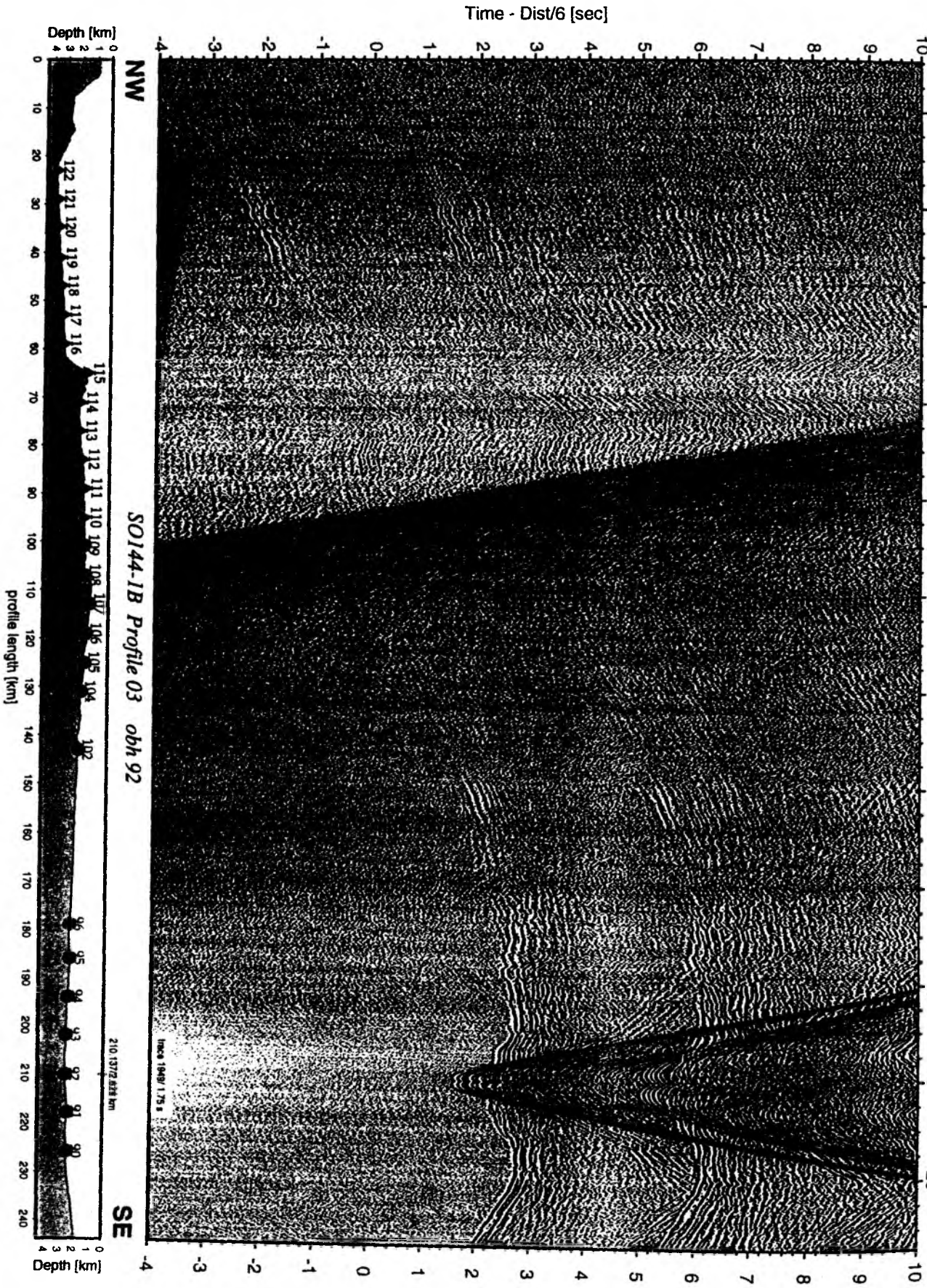

Figure 6.2.4.5.4: Record section from obh 92 , Profile 03.

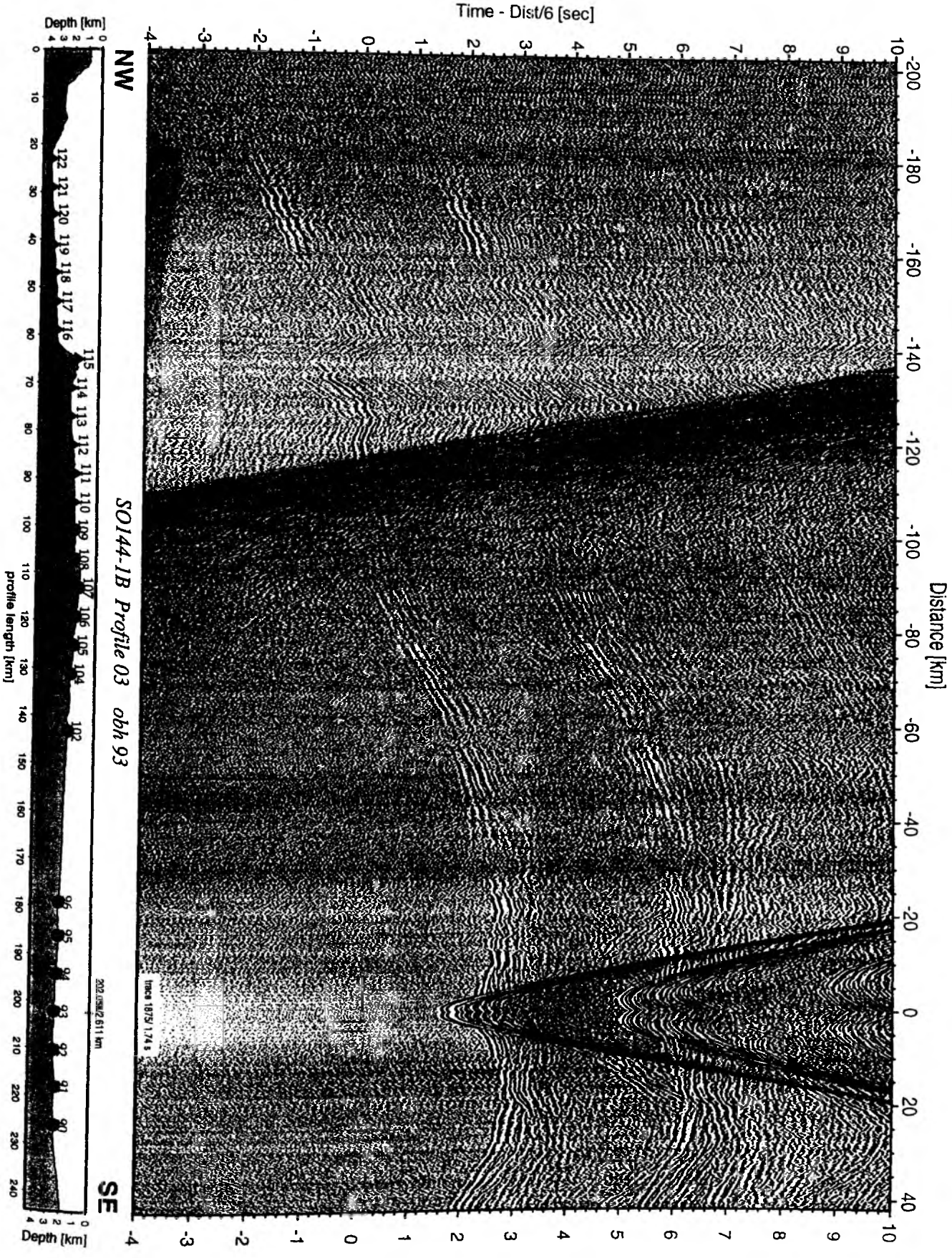

Figure 6.2.4.5.5: Record section from obh 93 , Profile 03.

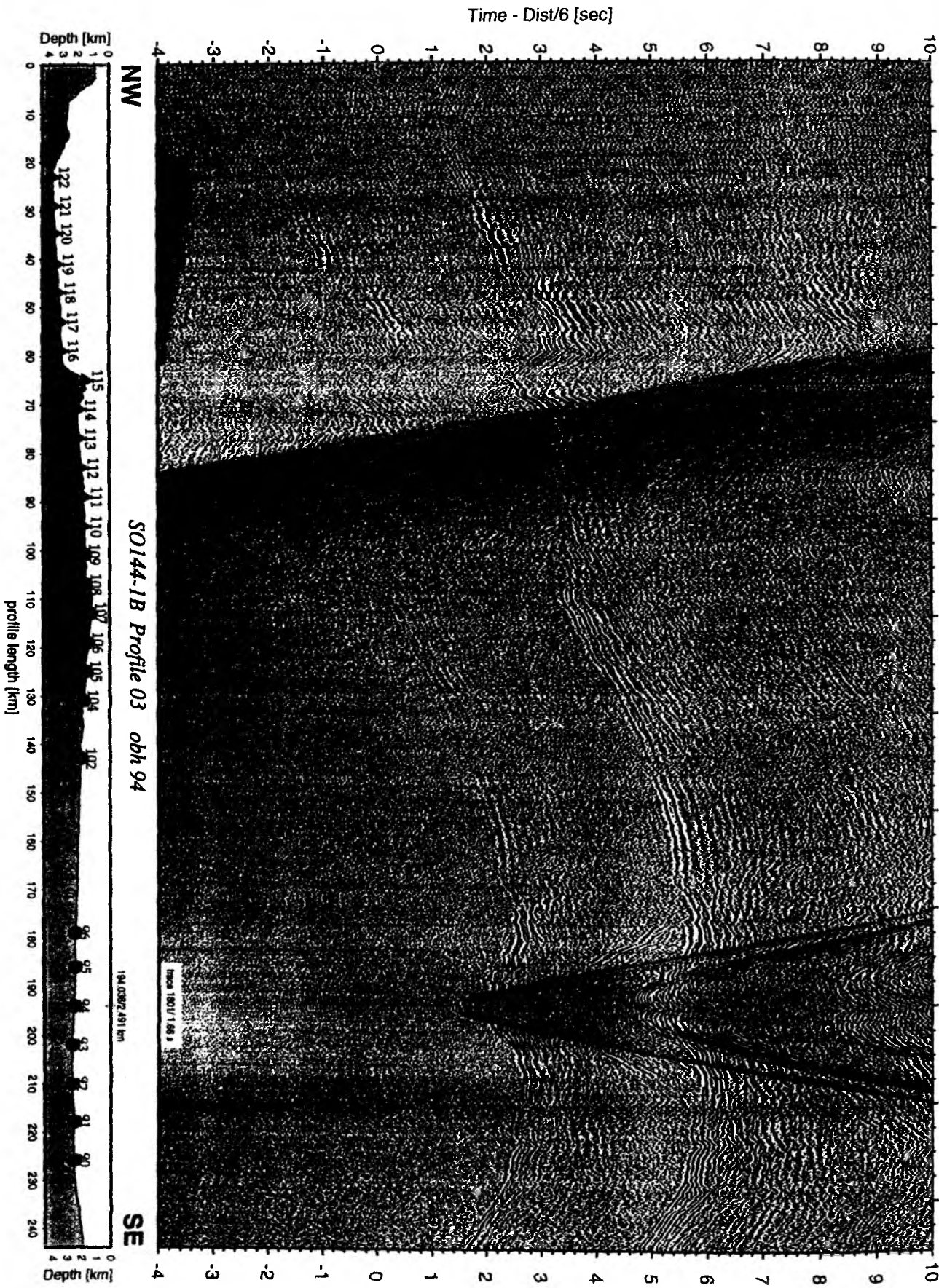

Figure 6.2.4.5.6: Record section from obh 94 , Profile 03.

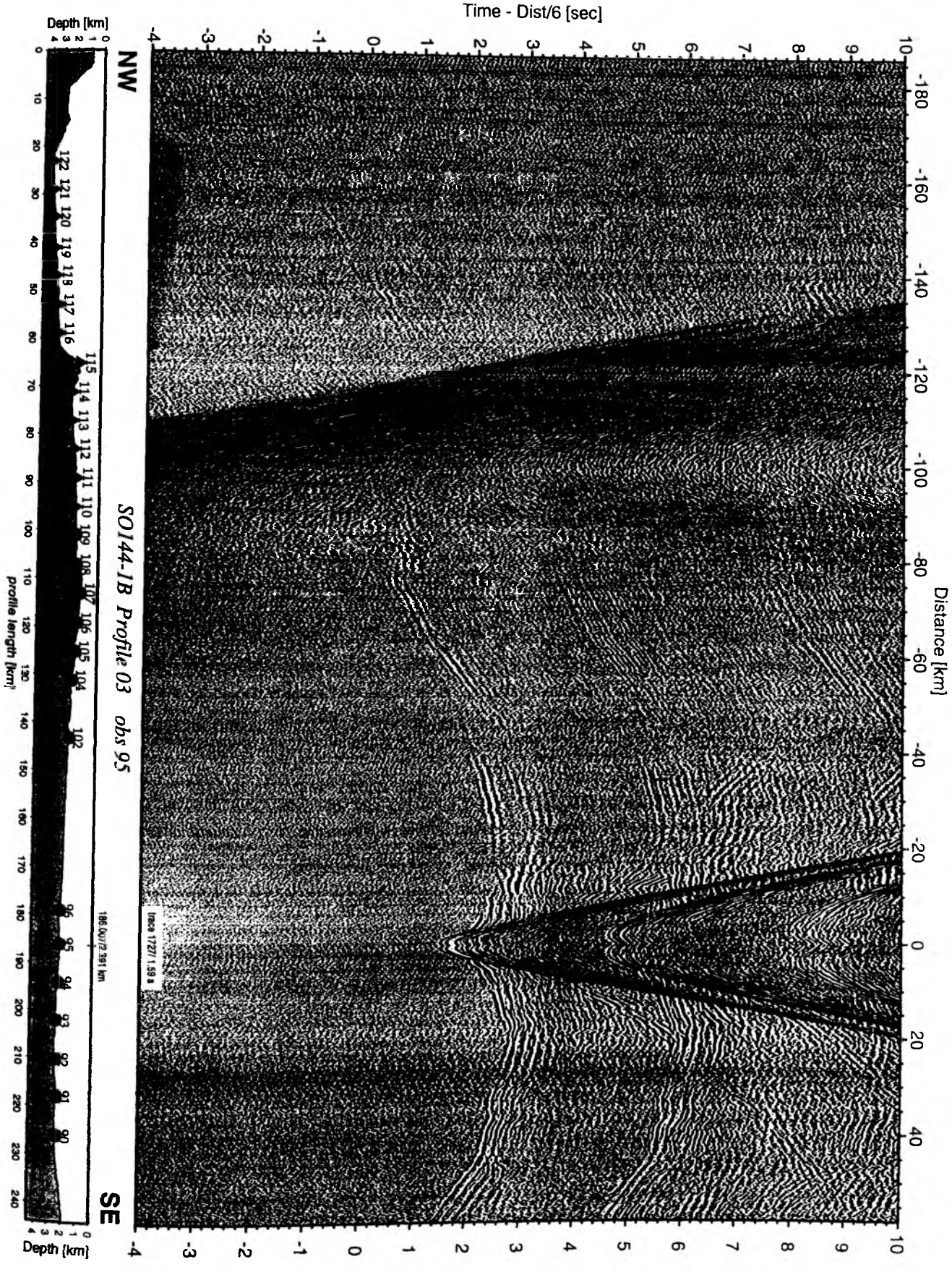

Figure 6.2.4.5.7: Record section from obs 95 hydrophone, Profile 03.

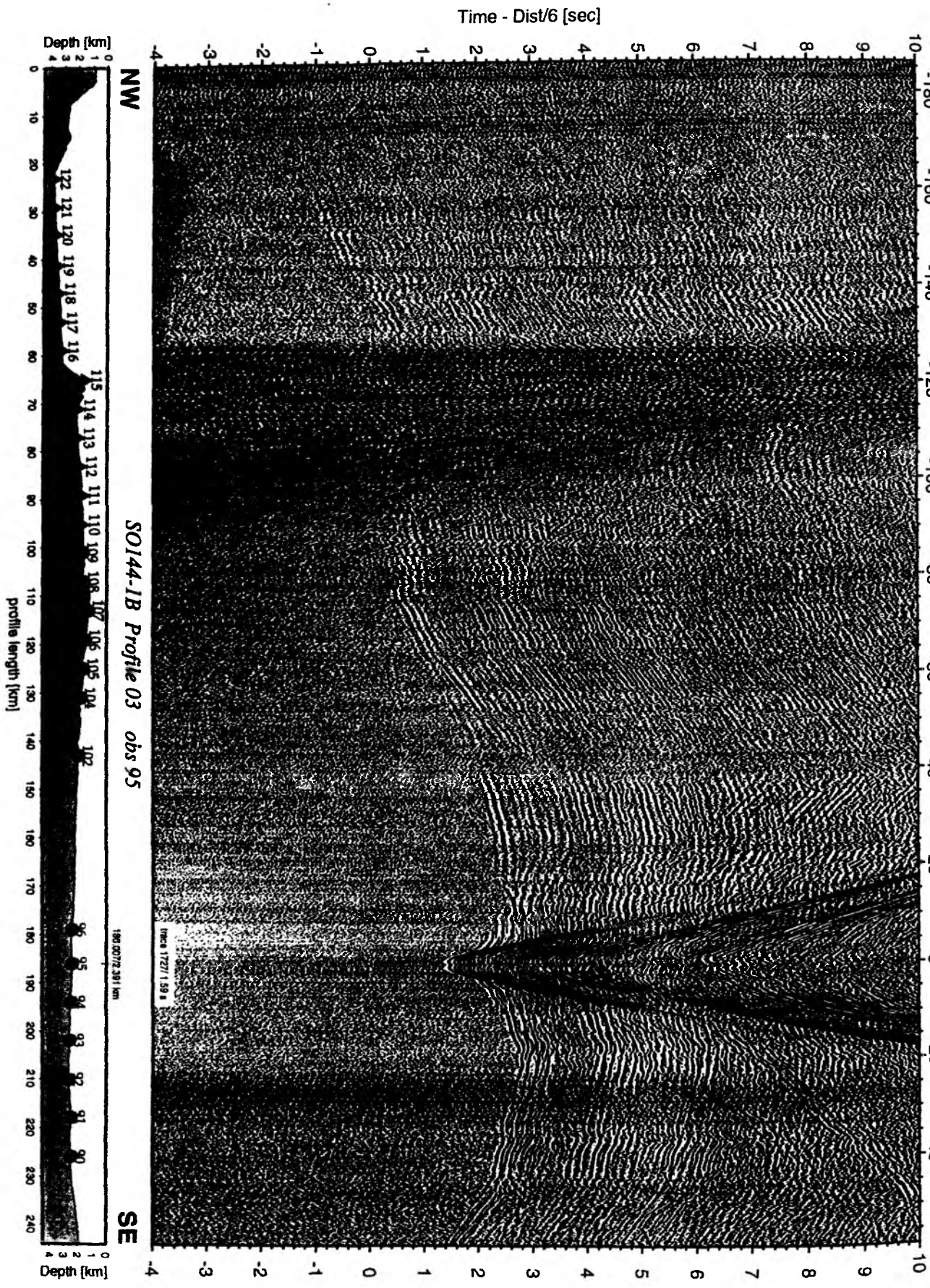

Figure 6.2.4.5.8: Record section from obs 95 vertical component, Profile 03.

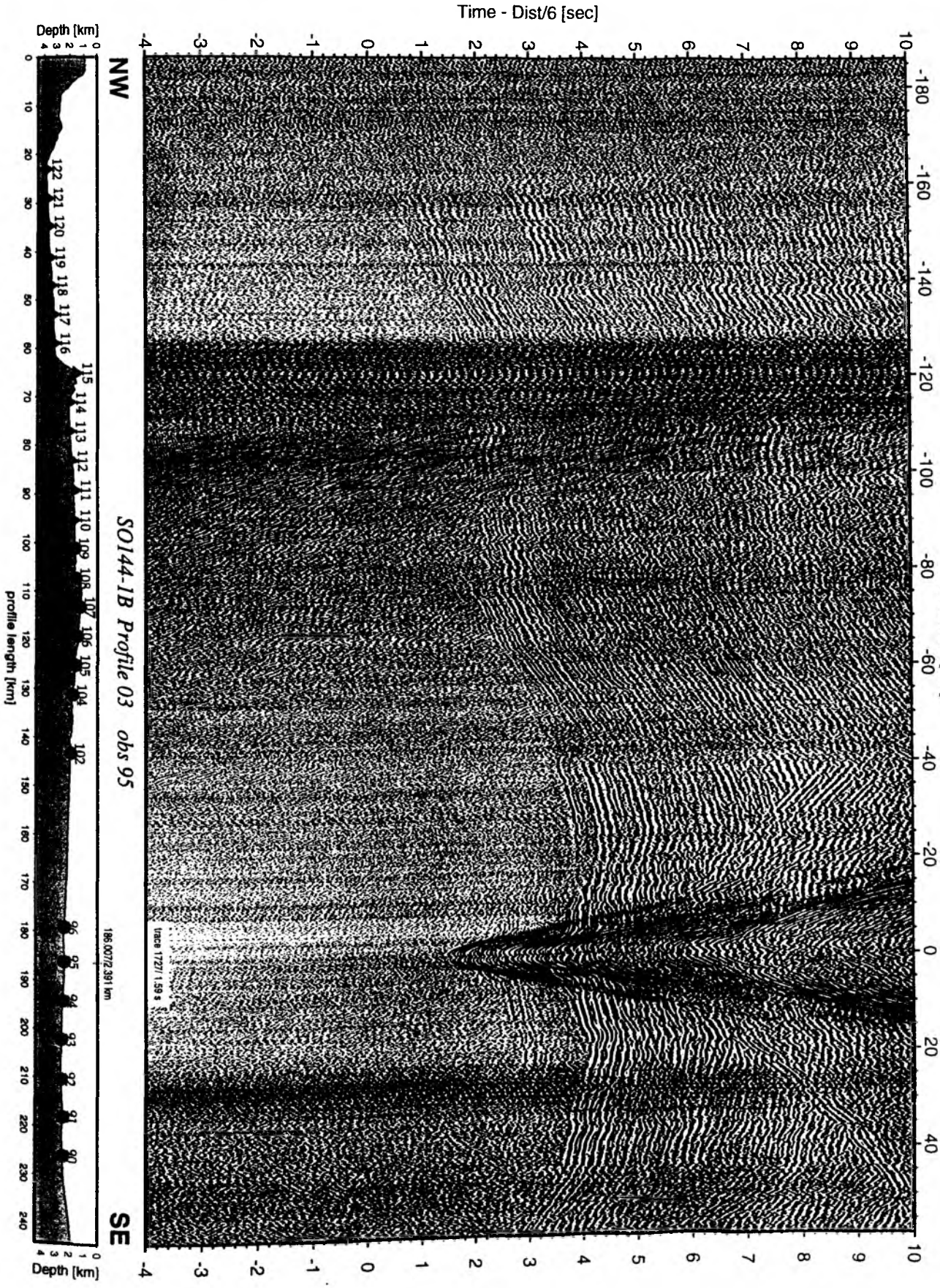

Figure 6.2.4.5.9: Record section from obs 95 horizontal component 1, Profile 03.

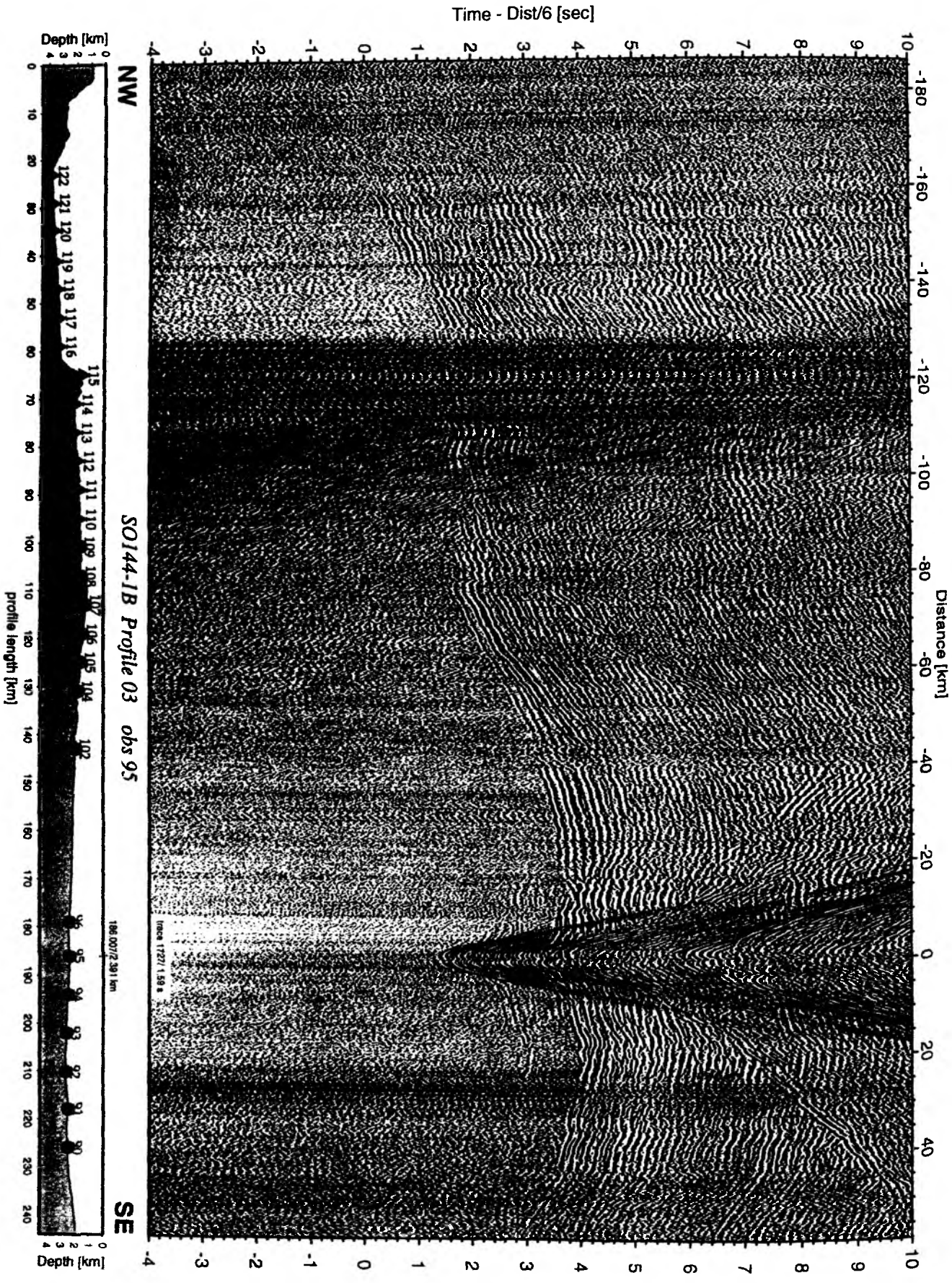

Figure 6.2.4.5.10: Record section from obs 95 horizontal component 2, Profile 03.

Figure 6.2.4.5.11: Record section from obh 96 , Profile 03.

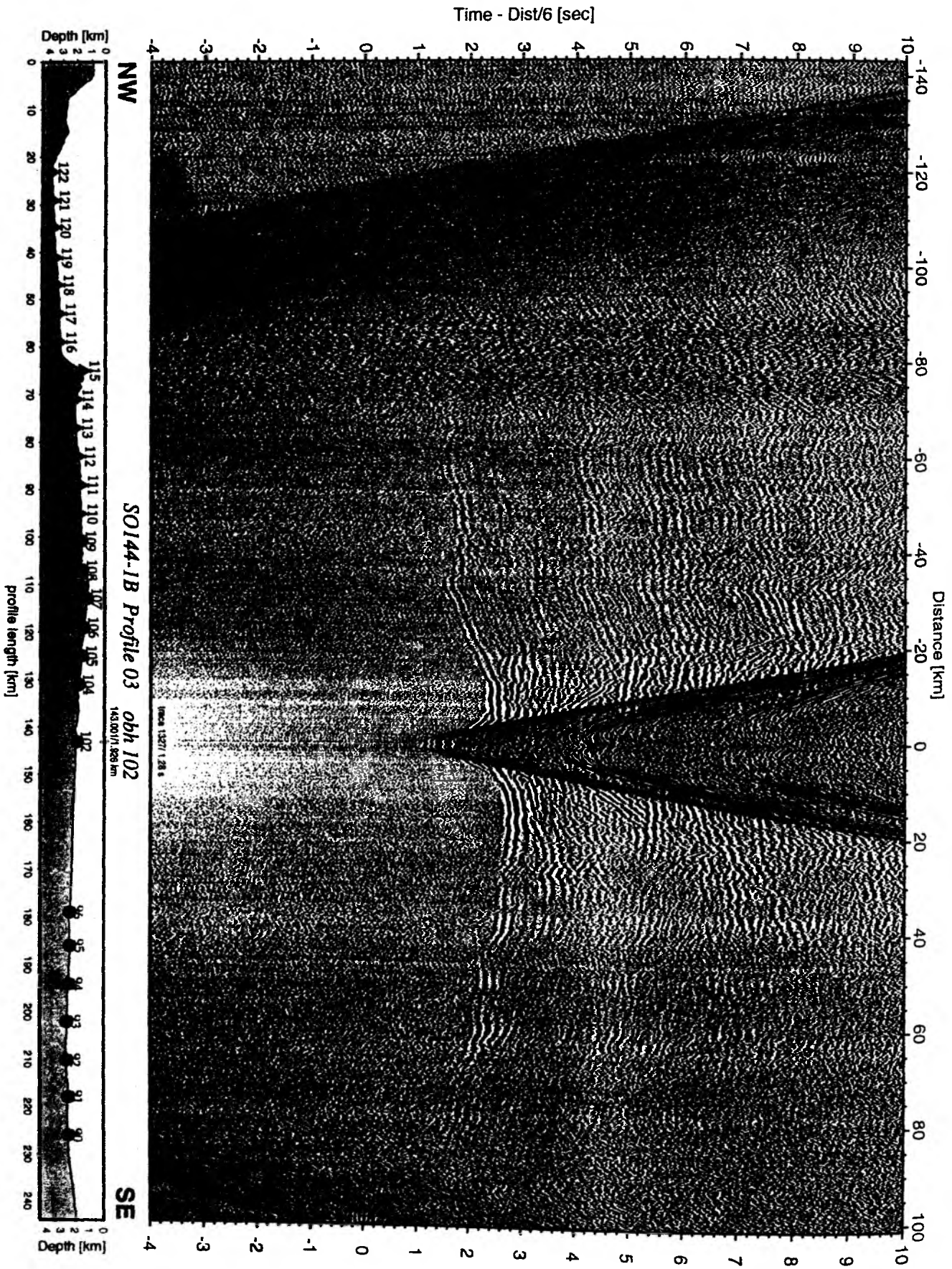

Figure 6.2.4.5.12: Record section from obh 102 , Profile 03.

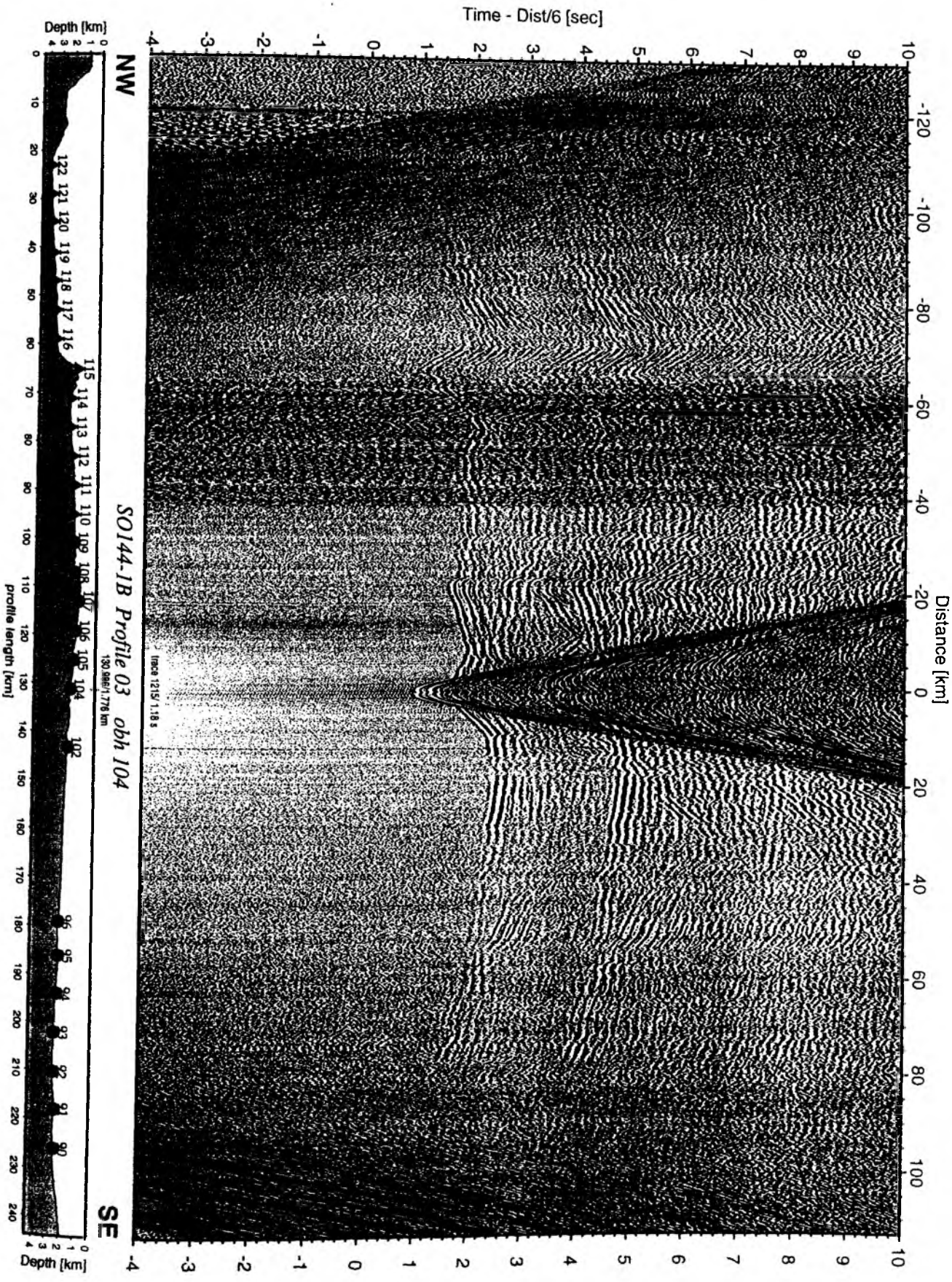

Figure 6.2.4.5.13: Record section from obh 104 , Profile 03.

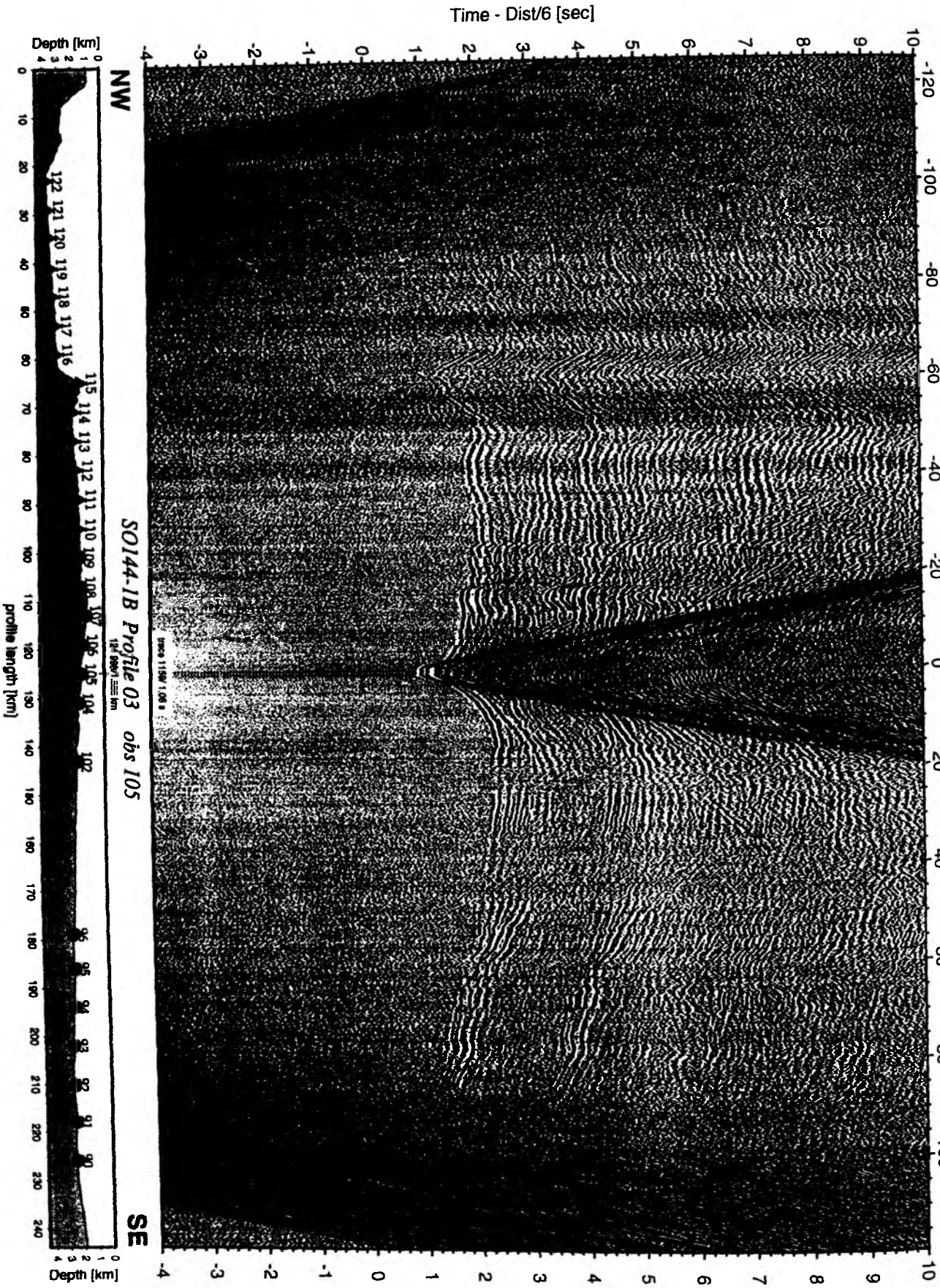

Figure 6.2.4.5.14: Record section from obs 105 hydrophone, Profile 03.

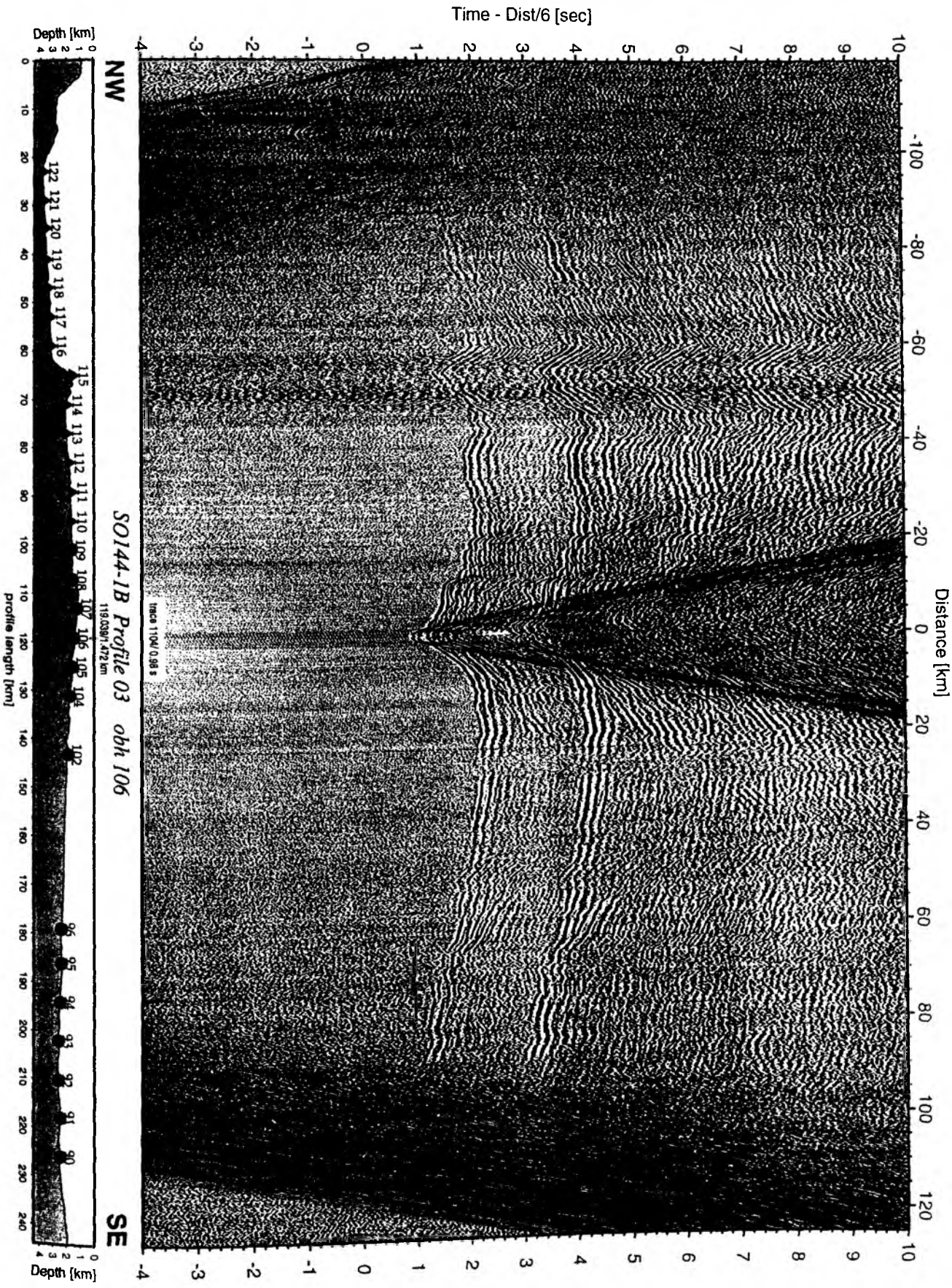

Figure 6.2.4.5.15: Record section from obh 106 , Profile 03.

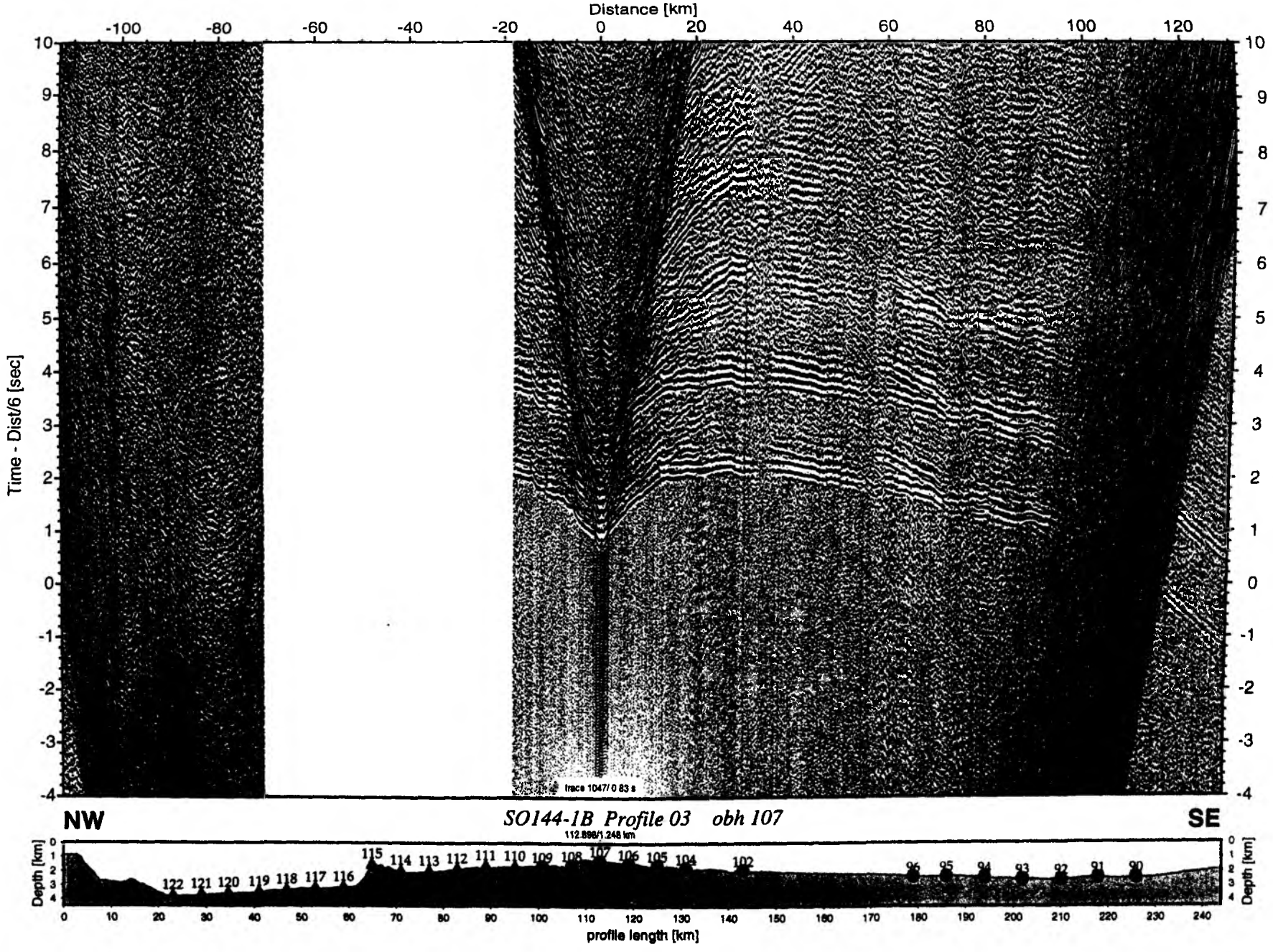

Figure 6.2.4.5.16: Record section from obh 107 , Profile 03.

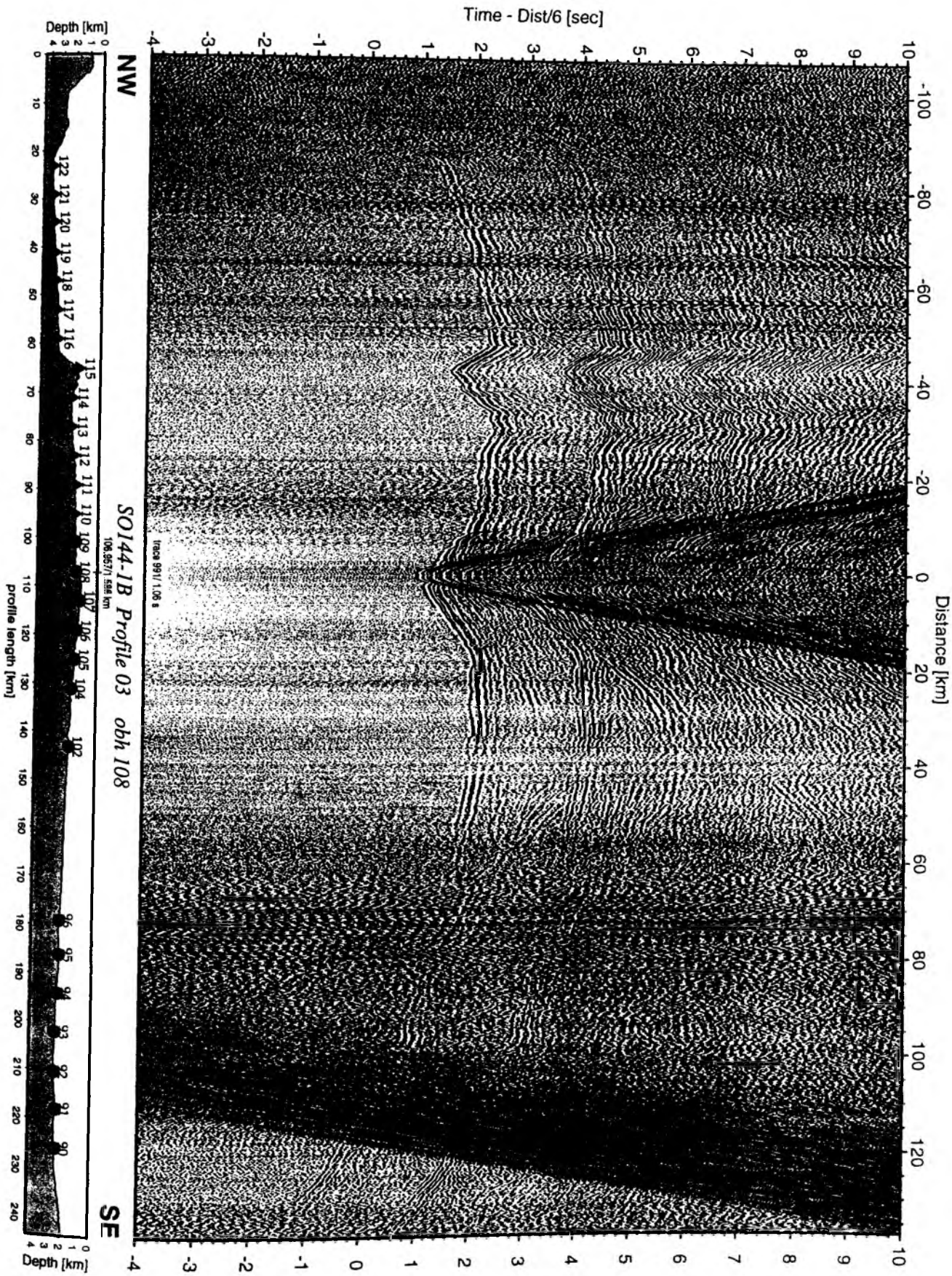

Figure 6.2.4.5.17: Record section from obh 108 , Profile 03.

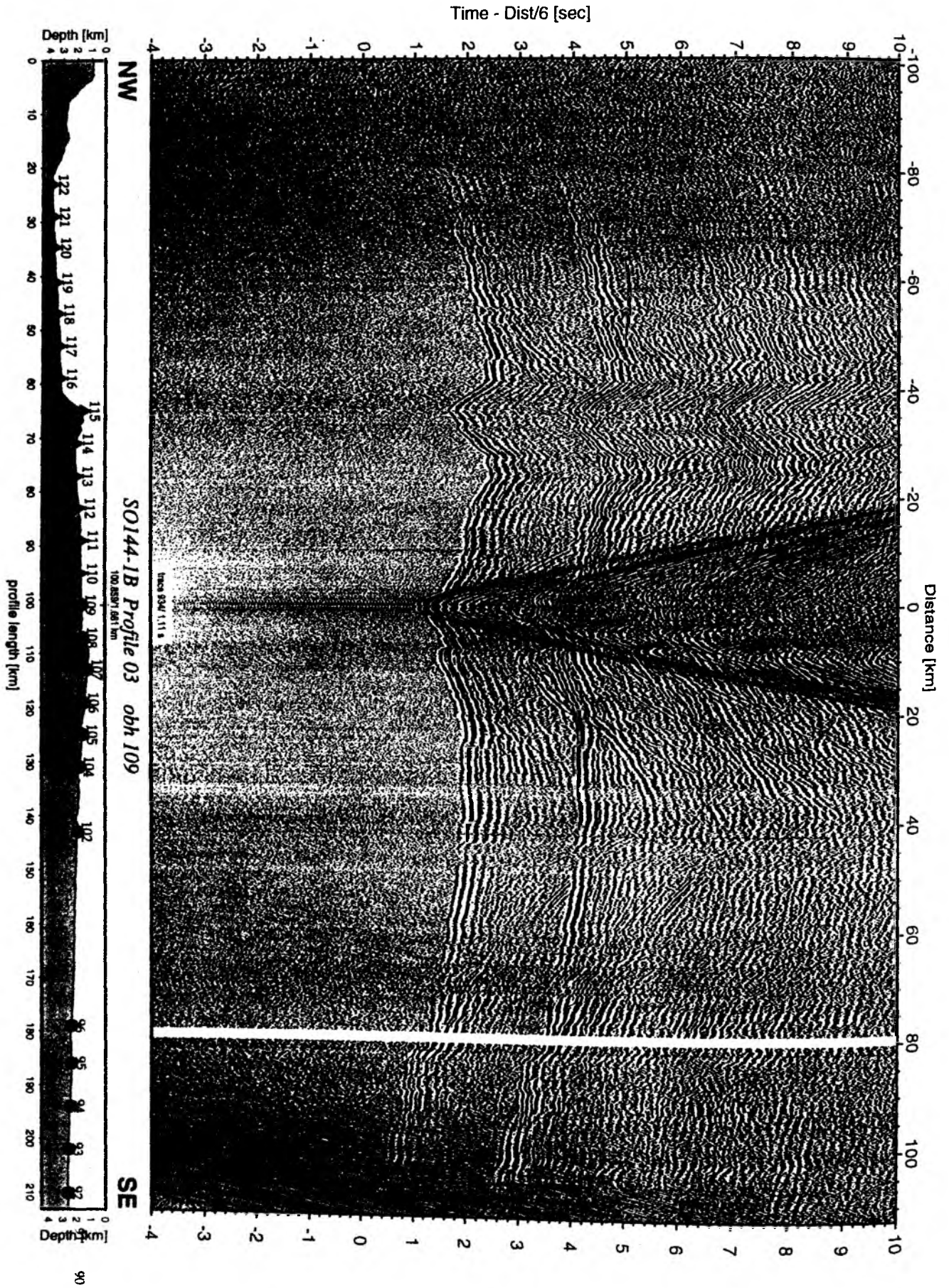

Figure 6.2.4.5.18: Record section from obh 109 , Profile 03.

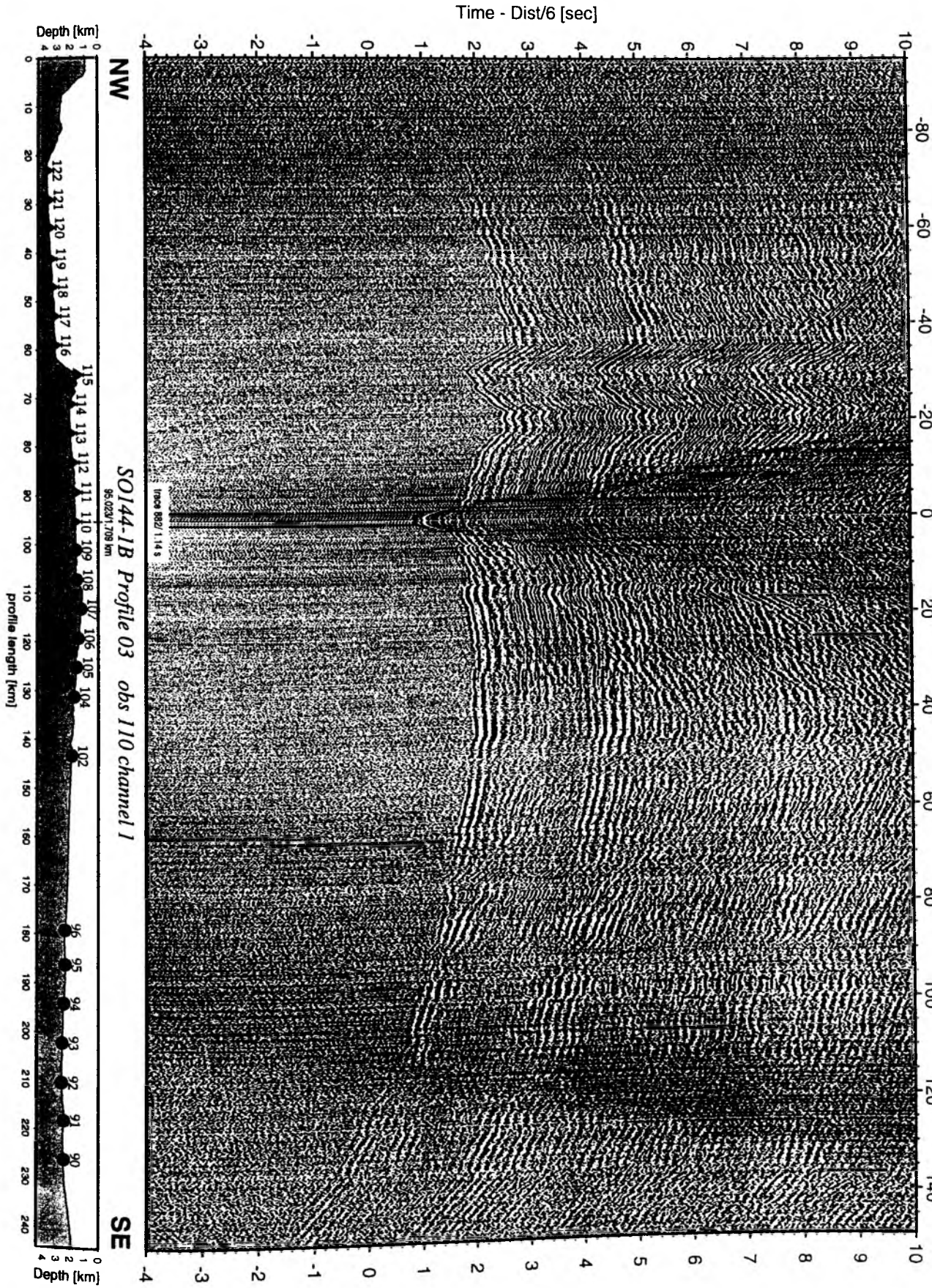

Figure 6.2.4.5.19: Record section from obs 110 vertical component, Profile 03.

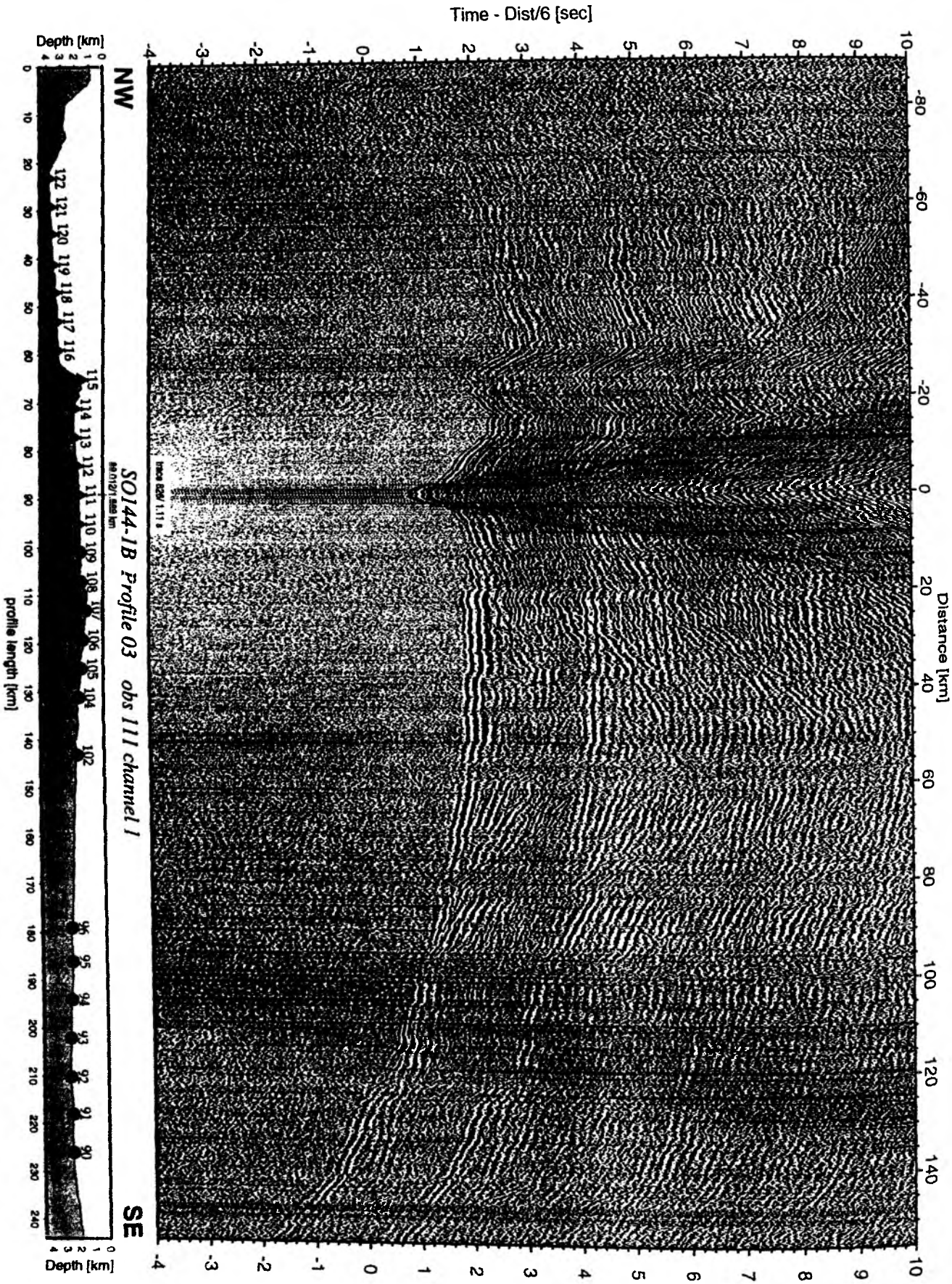

Figure 6.2.4.5.20: Record section from obs 111 vertical component, Profile 03.

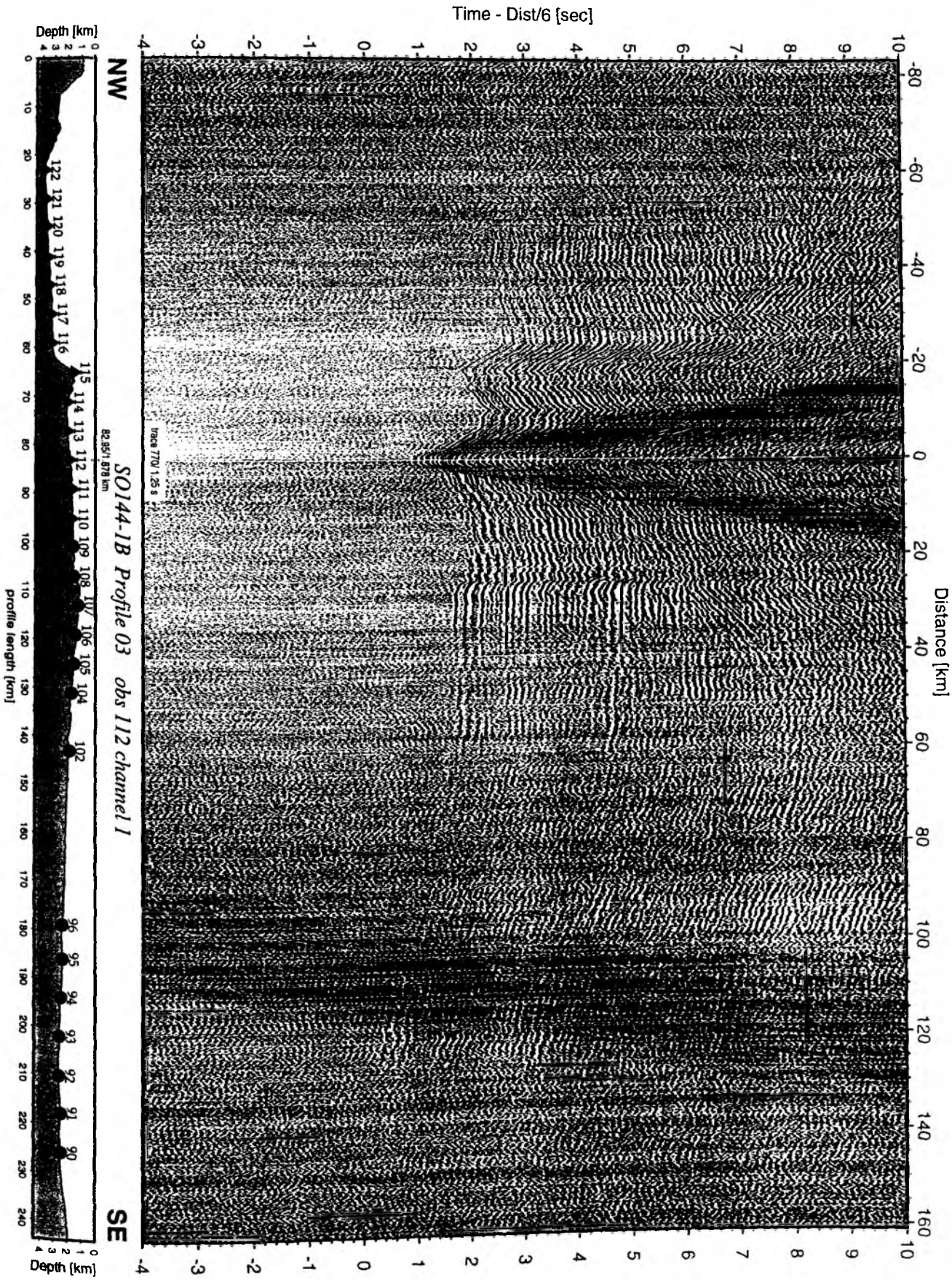

Figure 6.2.4.5.21: Record section from obs 112 vertical component, Profile 03.

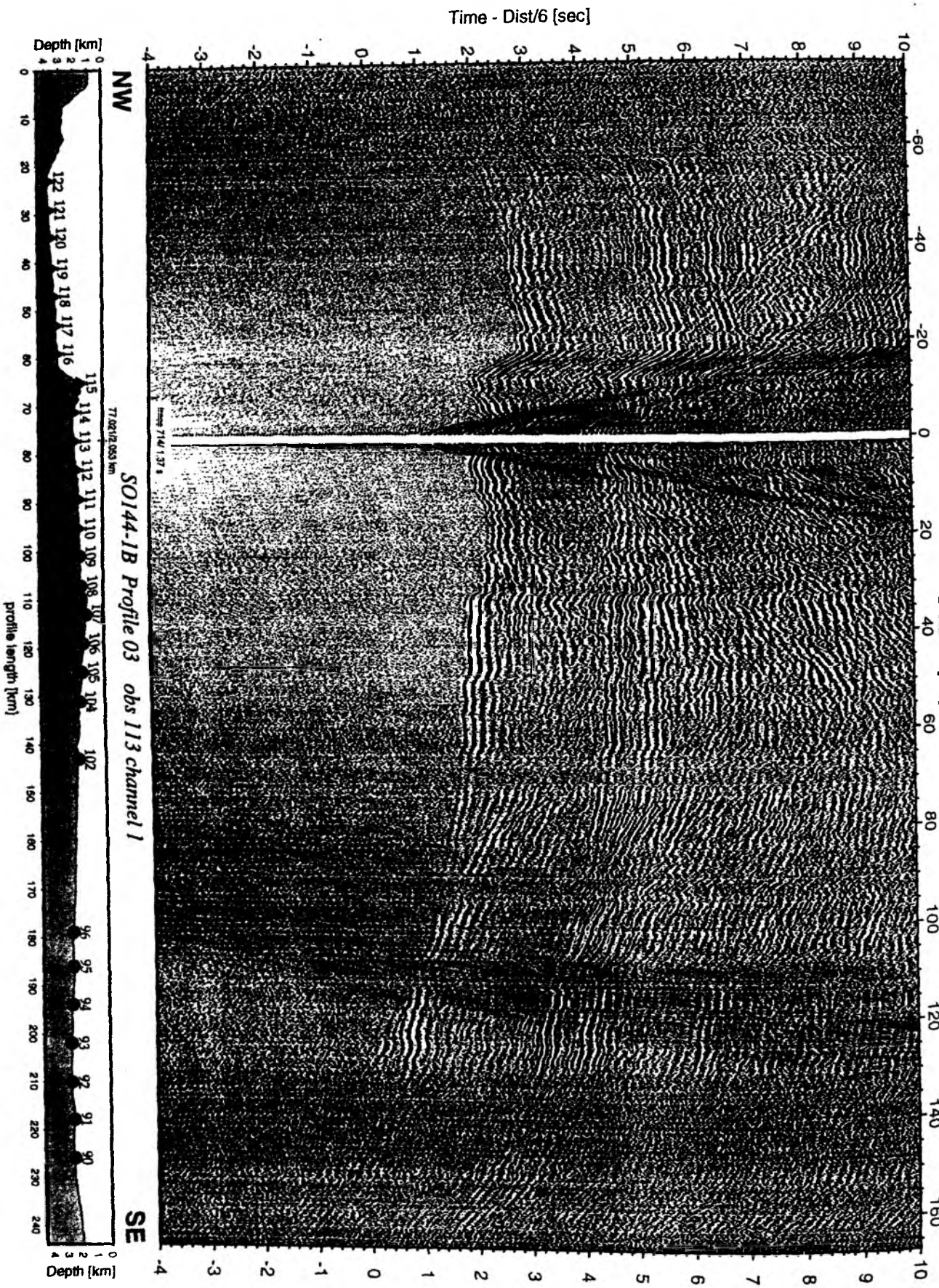

Figure 6.2.4.5.22: Record section from obs 113 vertical component, Profile 03.

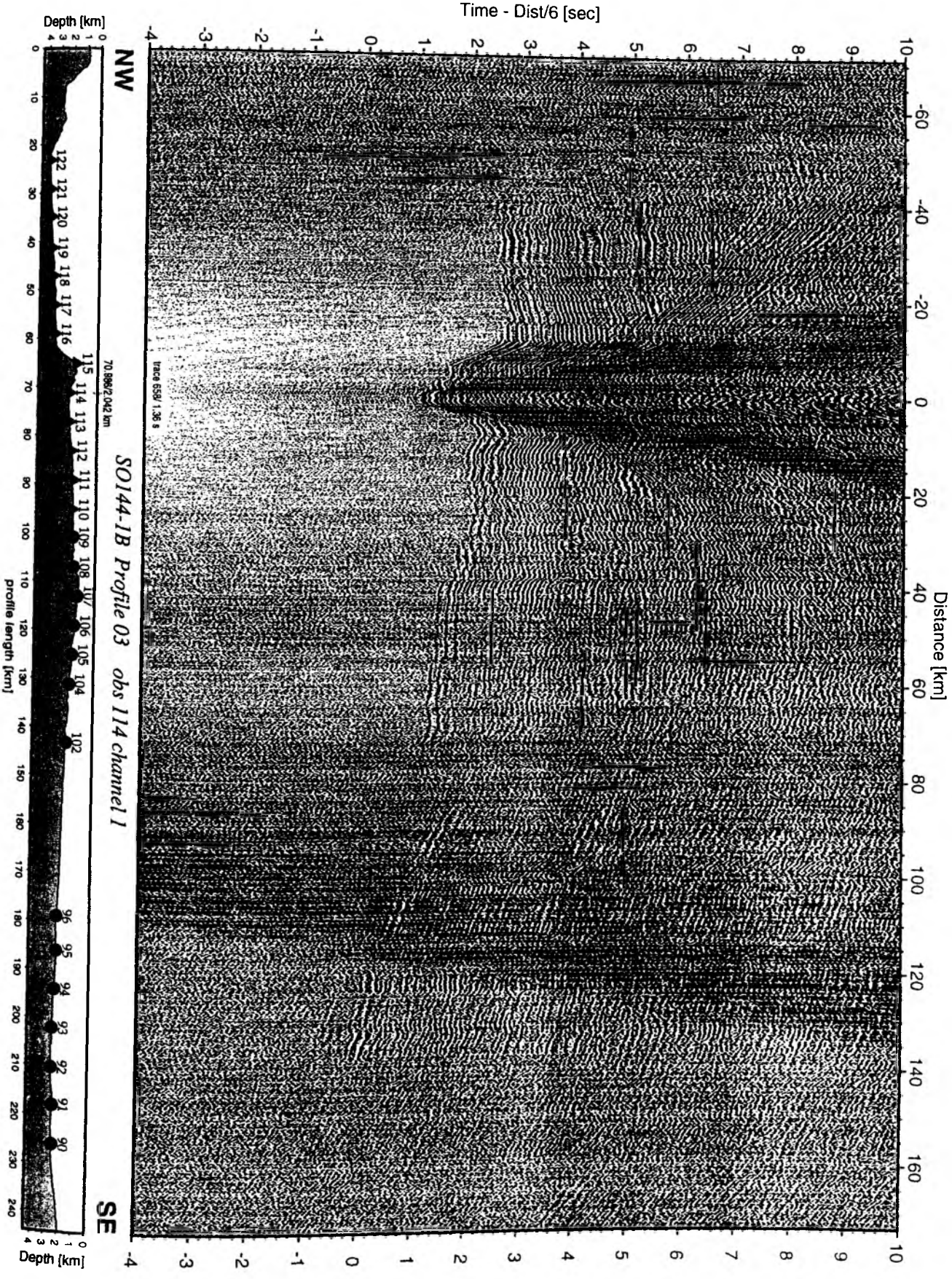

Figure 6.2.4.5.23: Record section from obs 114 vertical component, Profile 03.

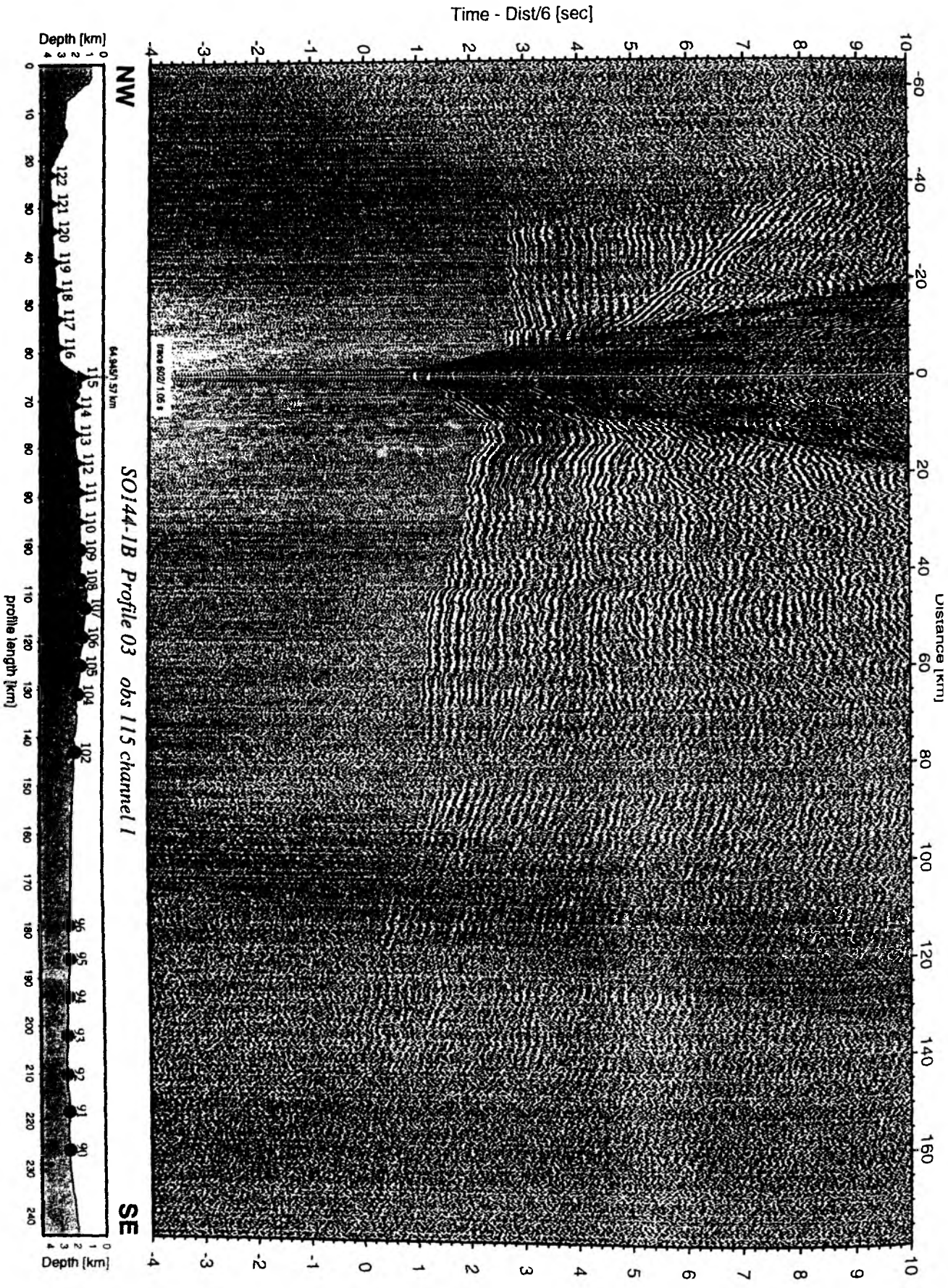

Figure 6.2.4.5.24: Record section from obs 115 vertical component, Profile 03.

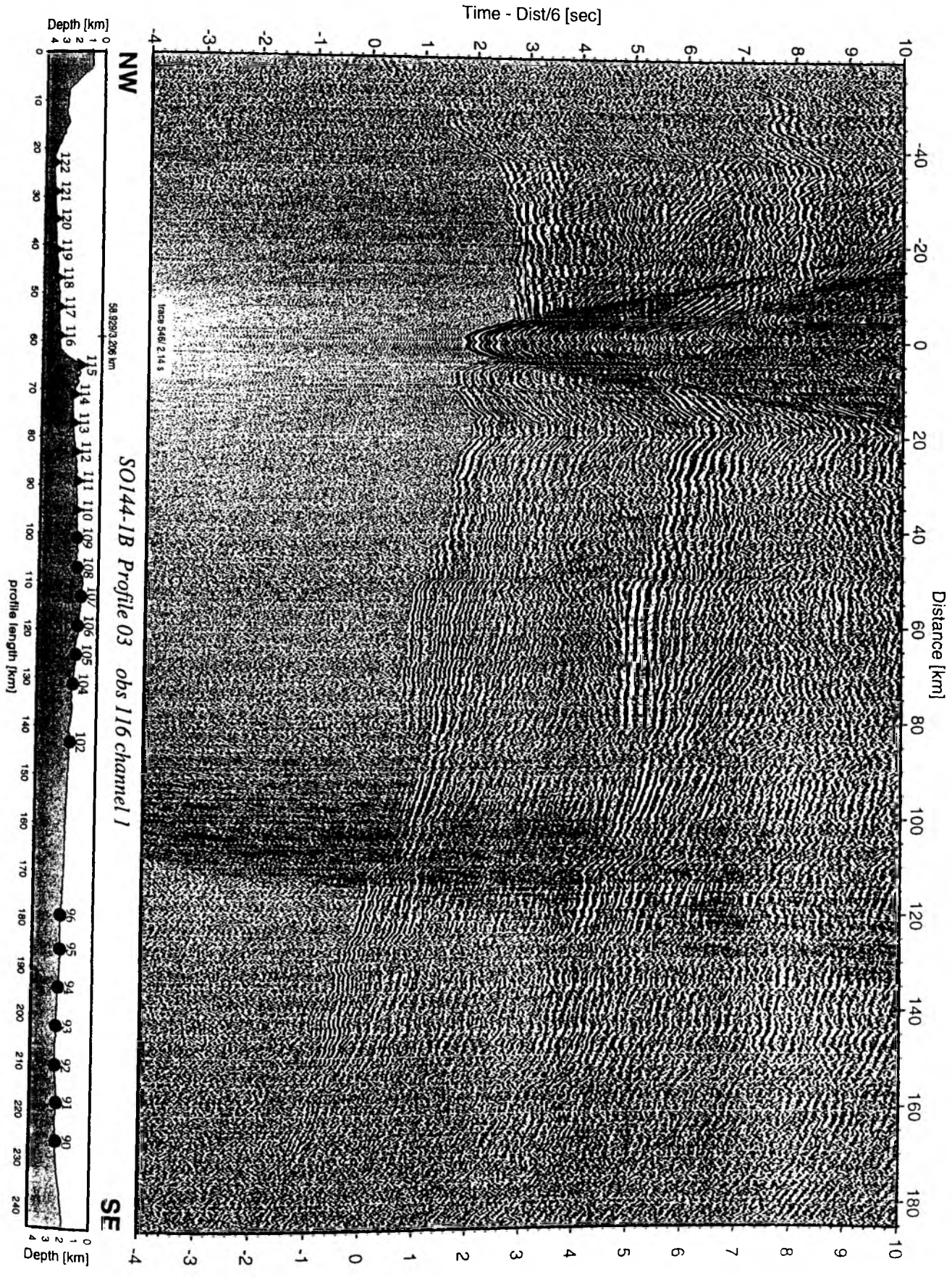

Figure 6.2.4.5.25: Record section from obs 116 vertical component, Profile 03.

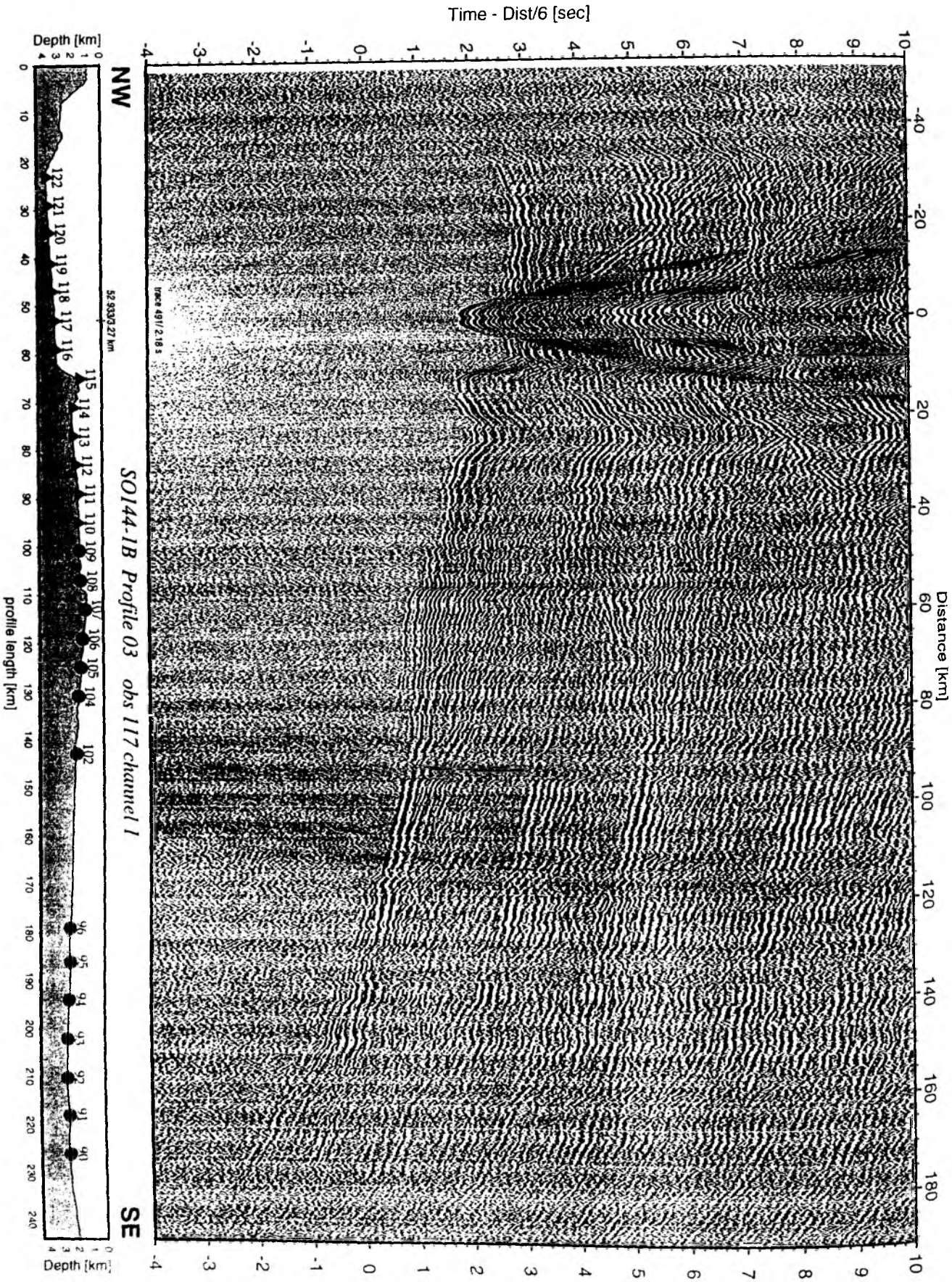

Figure 6.2.4.5.26: Record section from obs 117 vertical component, Profile 03.

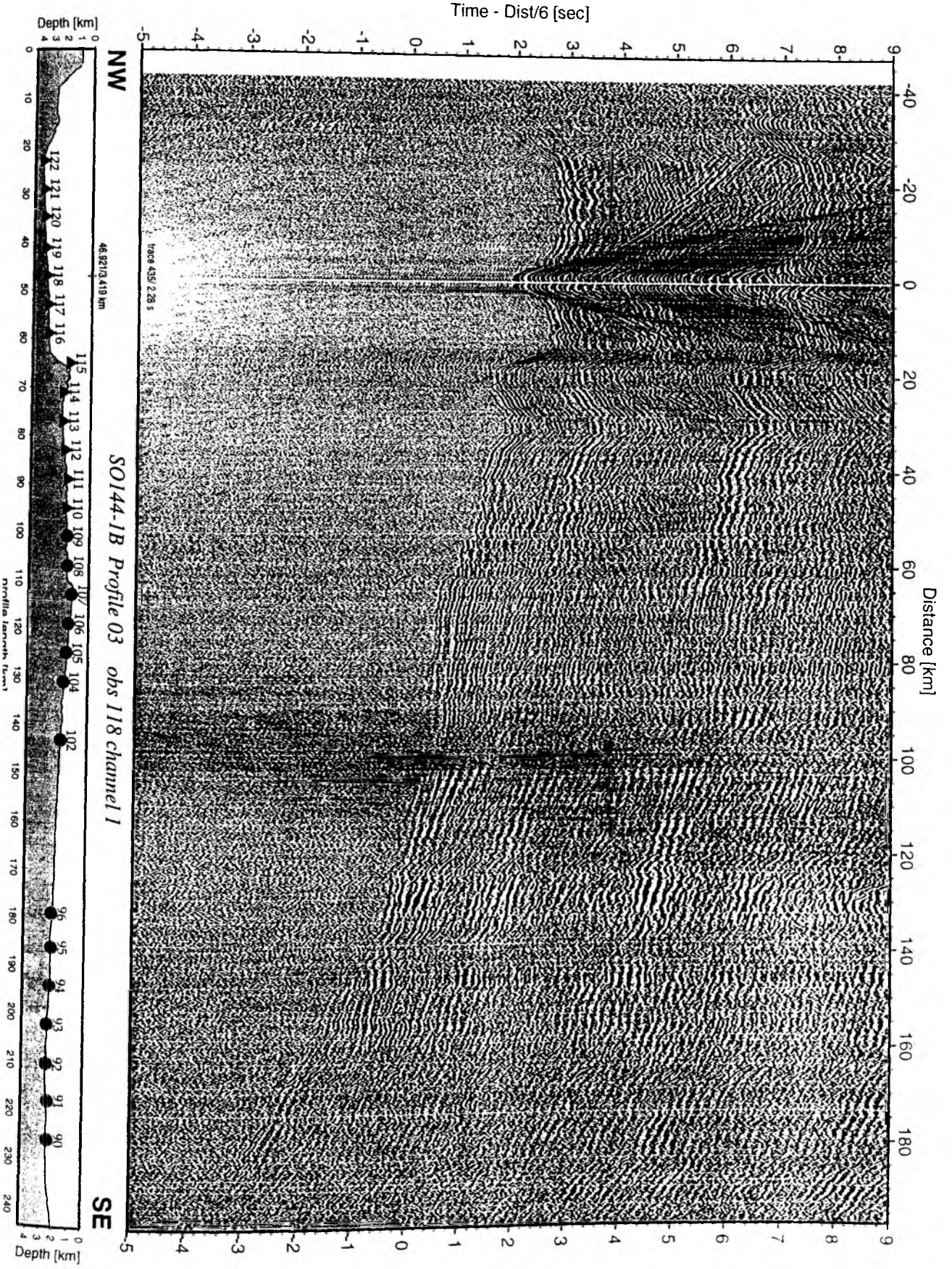

Figure 6.2.4.5.27: Record section from obs 118 vertical component, Profile 03.

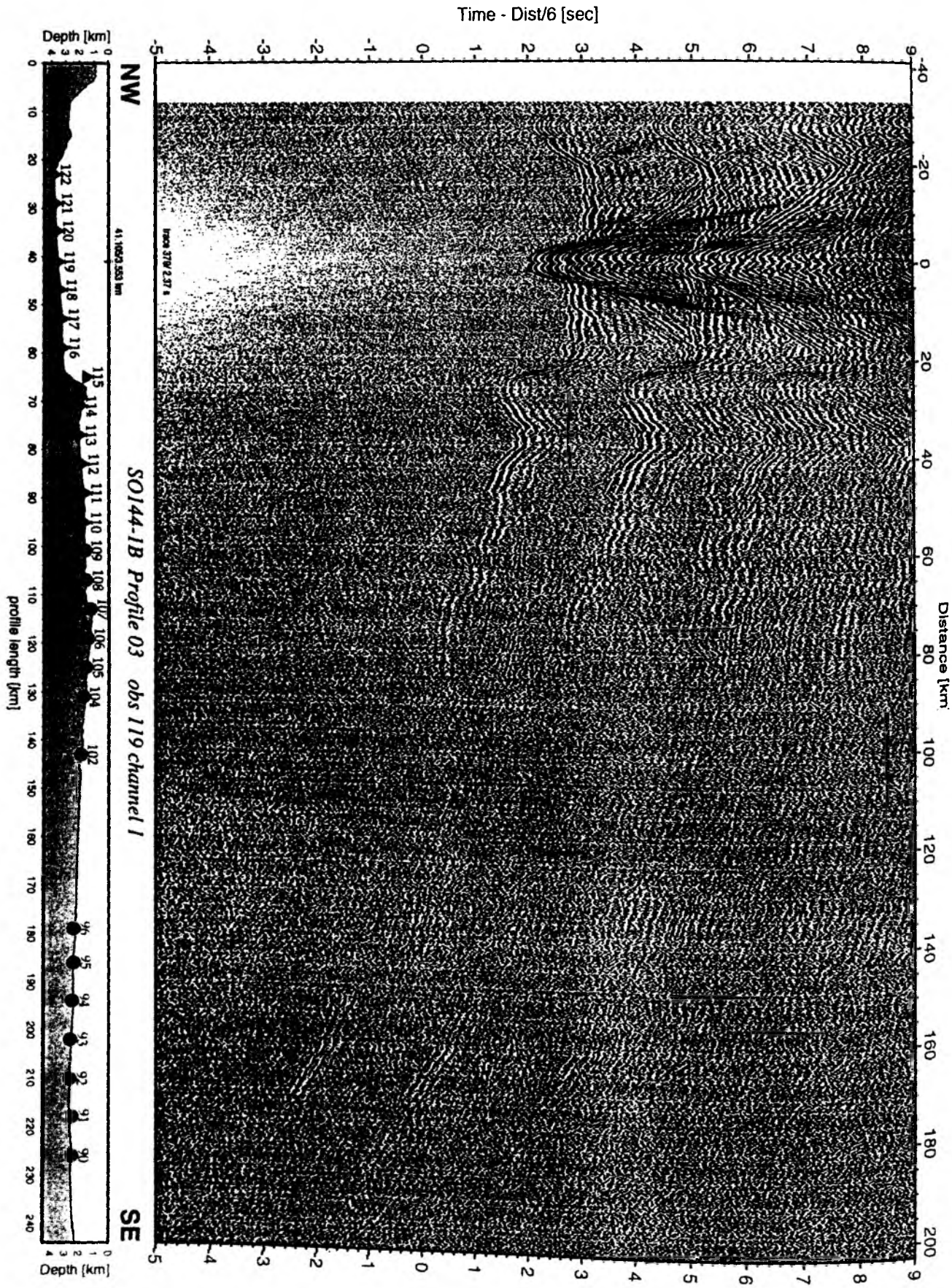

Figure 6.2.4.5.28: Record section from obs 119 vertical component, Profile 03.

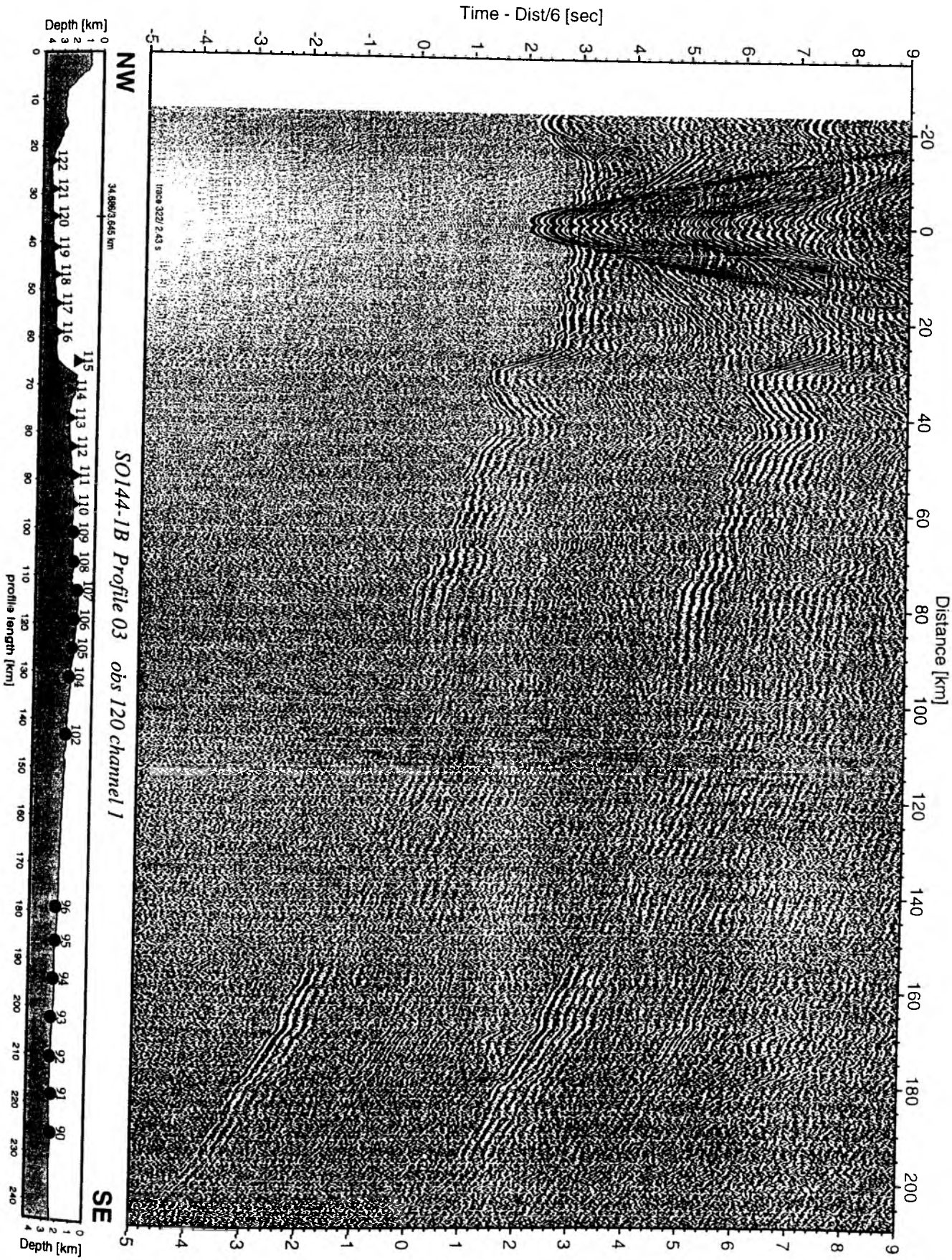

Figure 6.2.4.5.29: Record section from obs 120 vertical component, Profile 03.

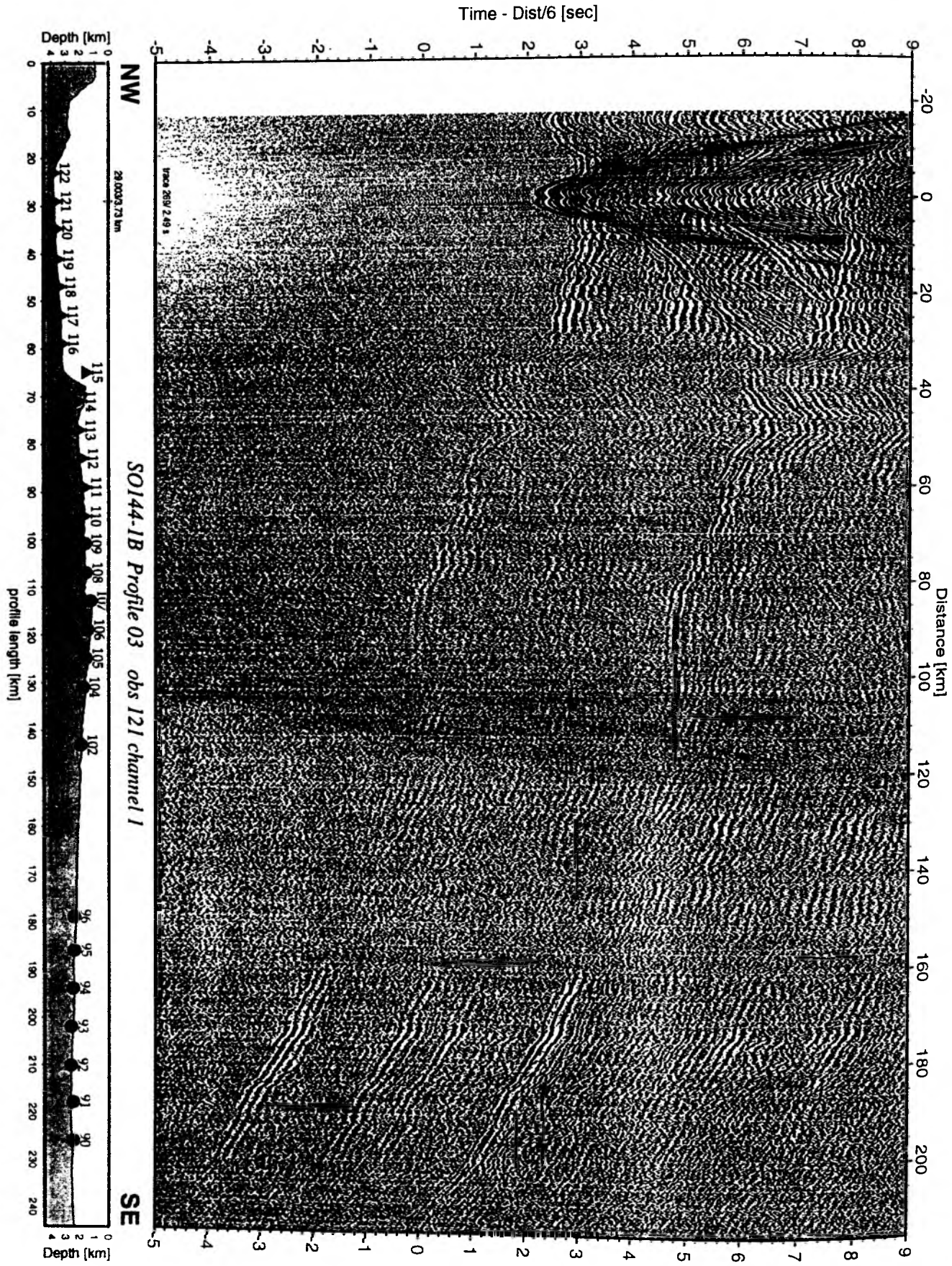

Figure 6.2.4.5.30: Record section from obs 121 vertical component, Profile 03.

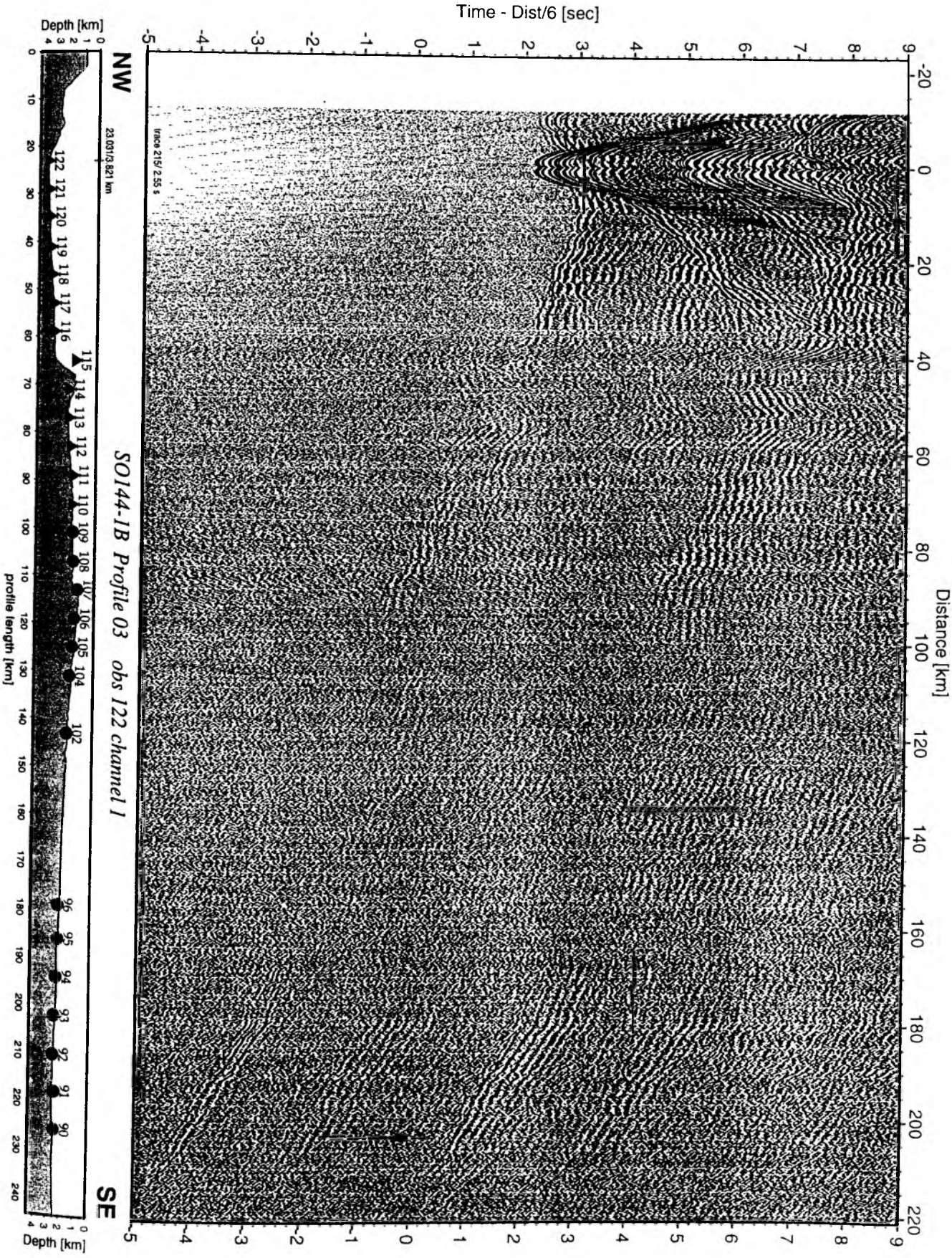

Figure 6.2.4.5.31: Record section from obs 122 vertical component, Profile 03.

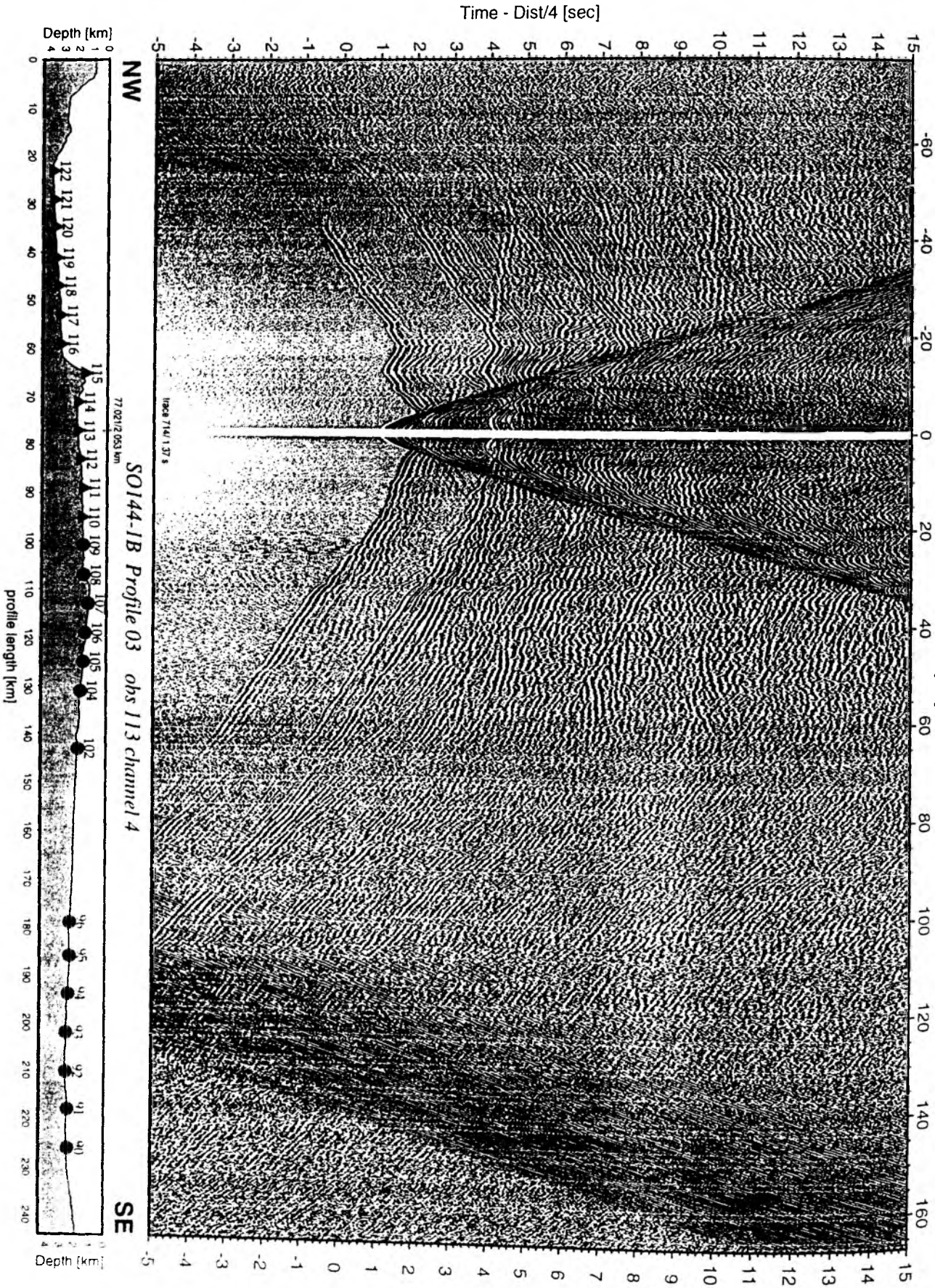

Figure 6.2.4.5.32: Record section from obs 113 hydrophone, Profile 03.

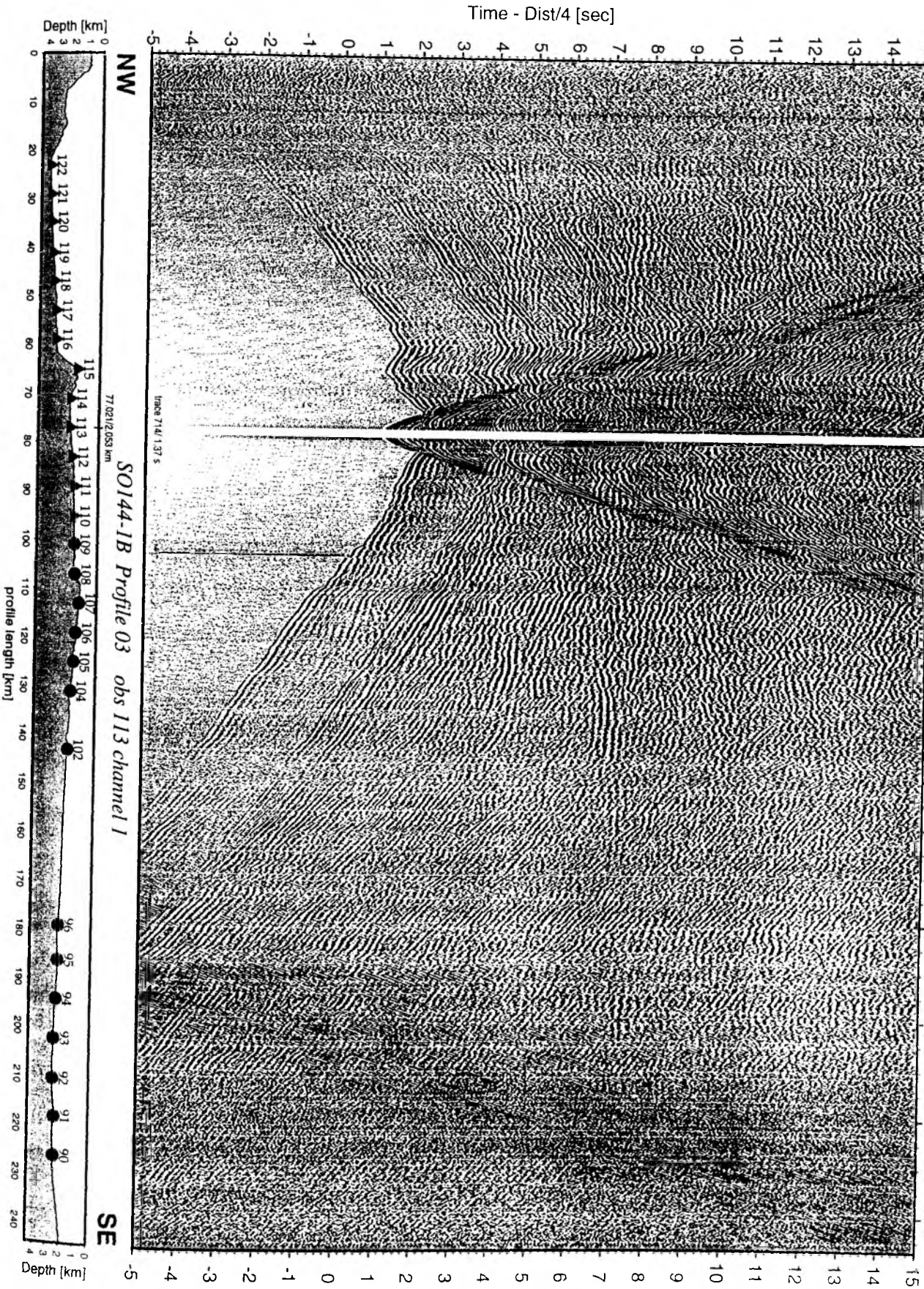

Figure 6.2.4.3.33: Record section from obs 113 vertical component, Profile 03.

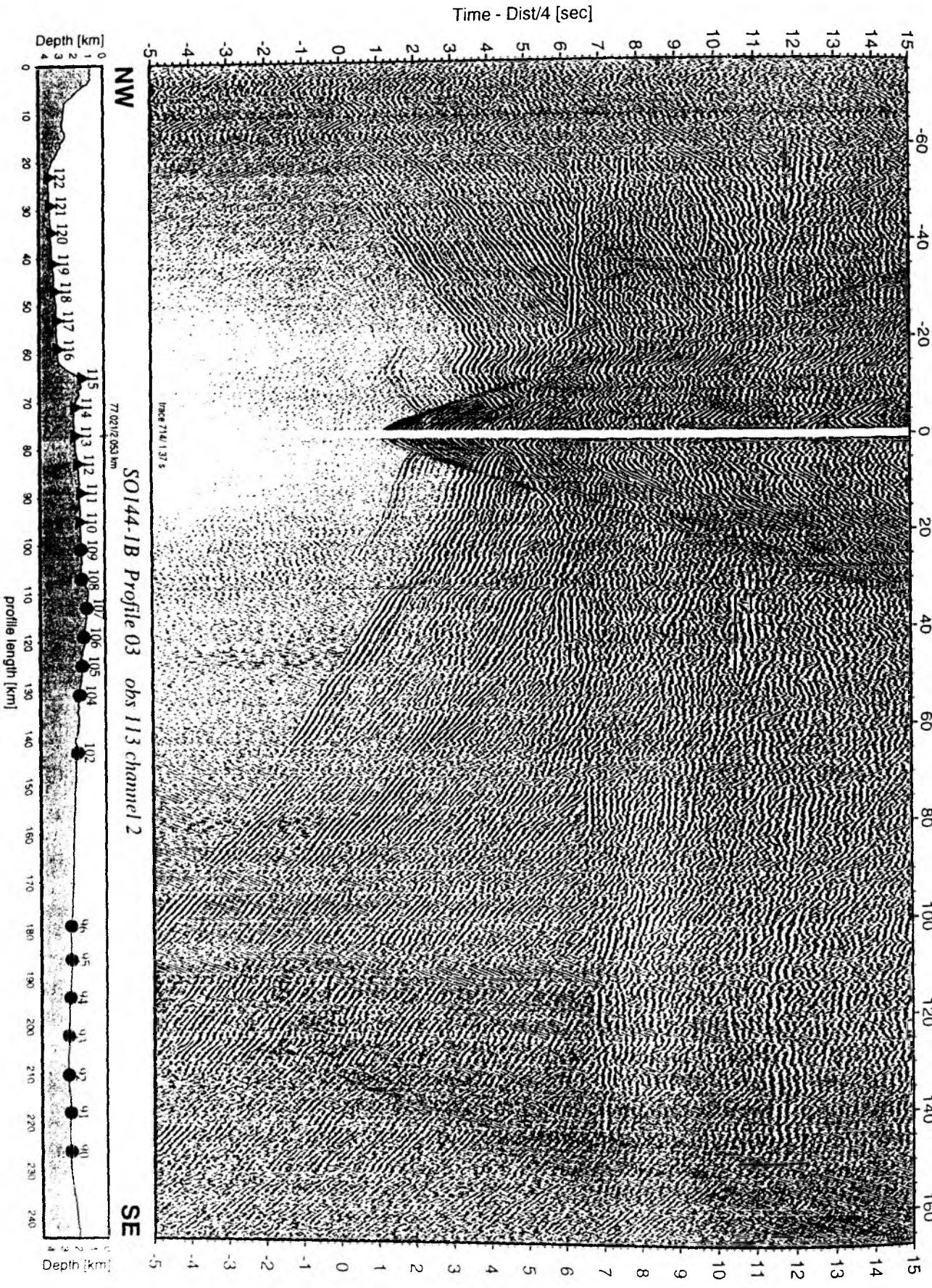

Figure 6.2.4.3.34: Record section from obs 113 horizontal component 1, Profile 03.

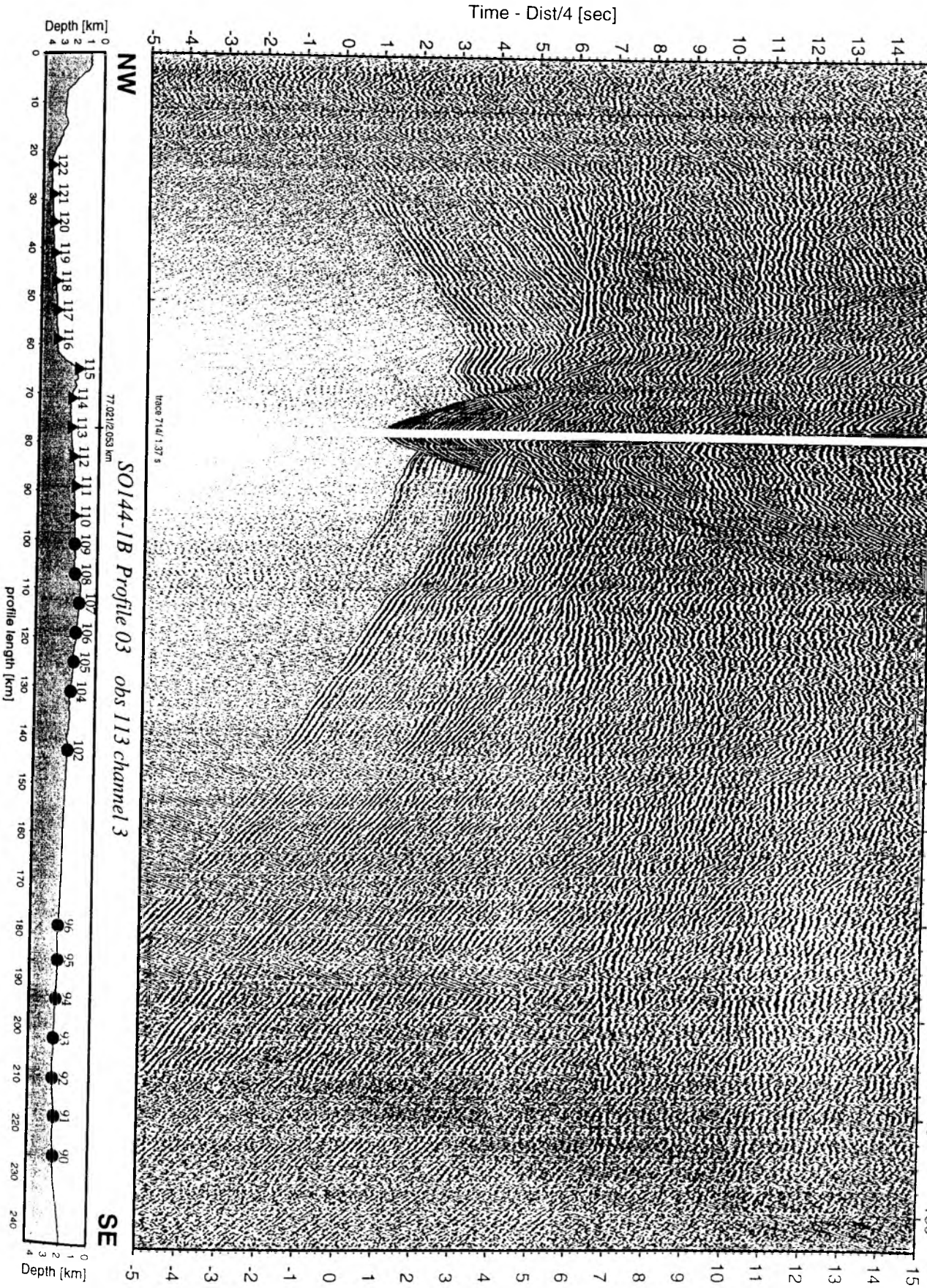

Figure 6.2.4.3.35: Record section from obs 113 horizontal component 2, Profile 03.

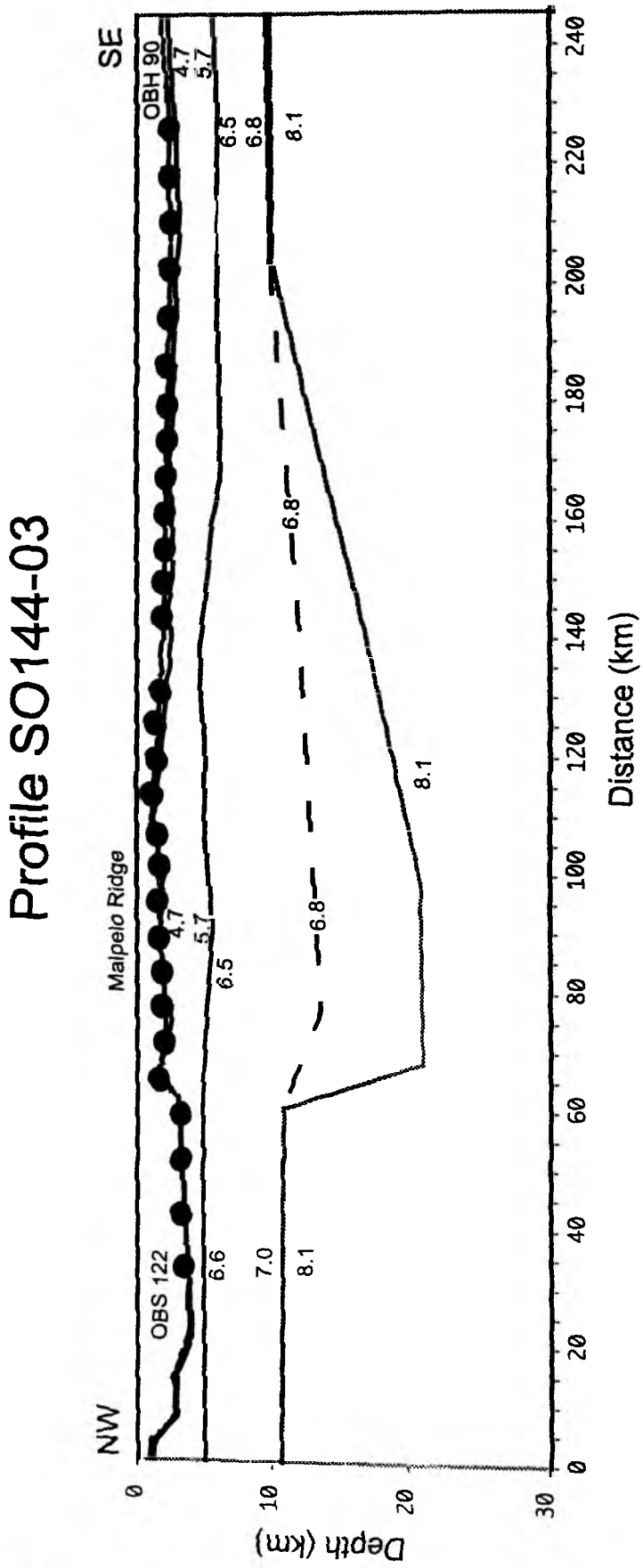

Figure 6.2.4.5.36: Preliminary model of crustal velocity structure along profile SO144-03 based on PmP arrivals.

6.2.4.6 PROFILE SO144-04

Profile SO144-04 is a second dip line across the Cocos Ridge (like SO144-01), but located on a crustal segment that is presumably about 3 to 5 ma younger thatn profile SO144-01. One of the goals of this profile is to investigate if there are major differences between the different age provinces. This would allow a generalization of results from one profile for the entire Cocos Ridge. Between 14:00 on 11 October and 06:00 on 12 October, a total of 27 instruments (OBH123 to OBS149) were deployed along the profile at variable spacing, including the IFREMER OBH, the vertical array and the breadband seismometer with the GEOLON recorder (see chapter 5.2). Two airguns were available for this profile and shooting started on 12 October at 07:00 and lasted until 18:00 on 13 October. It was interrupted for a few minutes on 12 October at 18:00 when a landshot was expected to be fired. The magnetometer was deployed during shooting and was recovered on 13 October at 20:00, when instrument recovery started with OBH123. Because the time release for the IRD instruments (OBS 144 to 149) was set for 1=:00 on 14 October, three GEOMAR instruments could not be recovered before them and were left until the last IRD instrument had been picked up. The transit was used for another magnetic profile, and by 22:00 on 14 October all instruments were safely recovered, and SONNE headed northward for the final seismic experiment. The location of the profile is shown in Figure 6.2.4.6.1, representative record sections are shown in Figures 6.2.4.6.2 to 6.2.4.6.24. Details on instruments and shots are given in Appendices 9.1 and 9.2.

Modeling and interpretation

The most prominent P-wave phases were picked for all GEOMAR OBH/OBS and the OBH from IFREMER, but not for the IRD instruments. The picking accuracy was usually better than 50 ms and deteriorated to 100 ms only in the very far offset range or weak phases. 2900 travel times were picked out of the wide-angle recordings and are shown in Figure 6.2.4.6.25a.

2-D ray tracing was done layer by layer from top to bottom. The starting model comprised only the morphology. A very low velocity of 1.6 – 1.9 km/s was taken for the sediment because almost no precursor appears near the water wave phase. Because picks from the IRD recordings were unavailable, the model resolution deteriorates in the northwest part, from 0 – 60 km. Results of the preliminary modeling from top to bottom (Fig. 6.2.4.6.25 b):

- On top of the igneous oceanic crust of the Cocos Ridge sediment thickness reaches 0.5 km, while at the southeastern flank of the ridge it increases to almost 1 km. The velocities in the sediment remain below 2.0 km/s.
- The igneous oceanic crust can be divided into an upper and lower crustal layer.
- The upper crustal velocities start with 3.8 km/s or more and increase to 4.9 km/s at the bottom. The average thickness of this layer is 2.2 km.
- Crustal thickening under the Cocos Ridge appears only in the lower igneous crust. Depth change from normal to anomalous crust appears very rapidly within 20 km on the NW flank of the ridge and 40 km in the SE. Although not well resolved by the present evaluation without the IRD instruments, the base of the normal oceanic crust NW and SE of the ridge is

about 9 – 10 km deep, whereas the crust-mantle boundary deepens to 19 km under the ridge. It stays at this depth for over 100 km and gives the Cocos Ridge structure a flat bottom. Lower crustal thickness is 4.7 km in the normal part and 15 km in the thickened part.

- The velocities in the normal lower crust increase from 6.4 km/s at the top to 6.8 km/s at the crust-mantle boundary and reach from 6.4 to 7.6 km/s respectively in the area of the Cocos Ridge, a difference that is mostly due to the influence of increasing pressure with depth.
- In the present study no internal structure is encountered in the lower crust.
- The mantle velocities are 8.0 – 8.1 km/s.

In summary, the lateral extent and internal structure of the Cocos Ridge are well imaged by our data. The major depth change of the crust-mantle boundary occurs in the NW within only 20 km and in the SW within 40 km. The crust-mantle boundary deepens from 9 – 10 km to 19 km depth under the ridge. It stays there for over 100 km giving the ridge a bathtub-like sectional form. Crustal thickening appears only in the lower crust, which is three times thicker than the normal lower oceanic crust to both sides. No internal structure is found in the lower crust under the Cocos Ridge. Similar values in depth, velocities and in shape are found on Profile 01 (see Chapter 6.2.4.3 and Fig. 6.2.4.3.37). It seems that crustal differences between the Cocos Ridge and neighbouring oceanic crust are mainly a matter of difference in depth of the crust-mantle boundary.

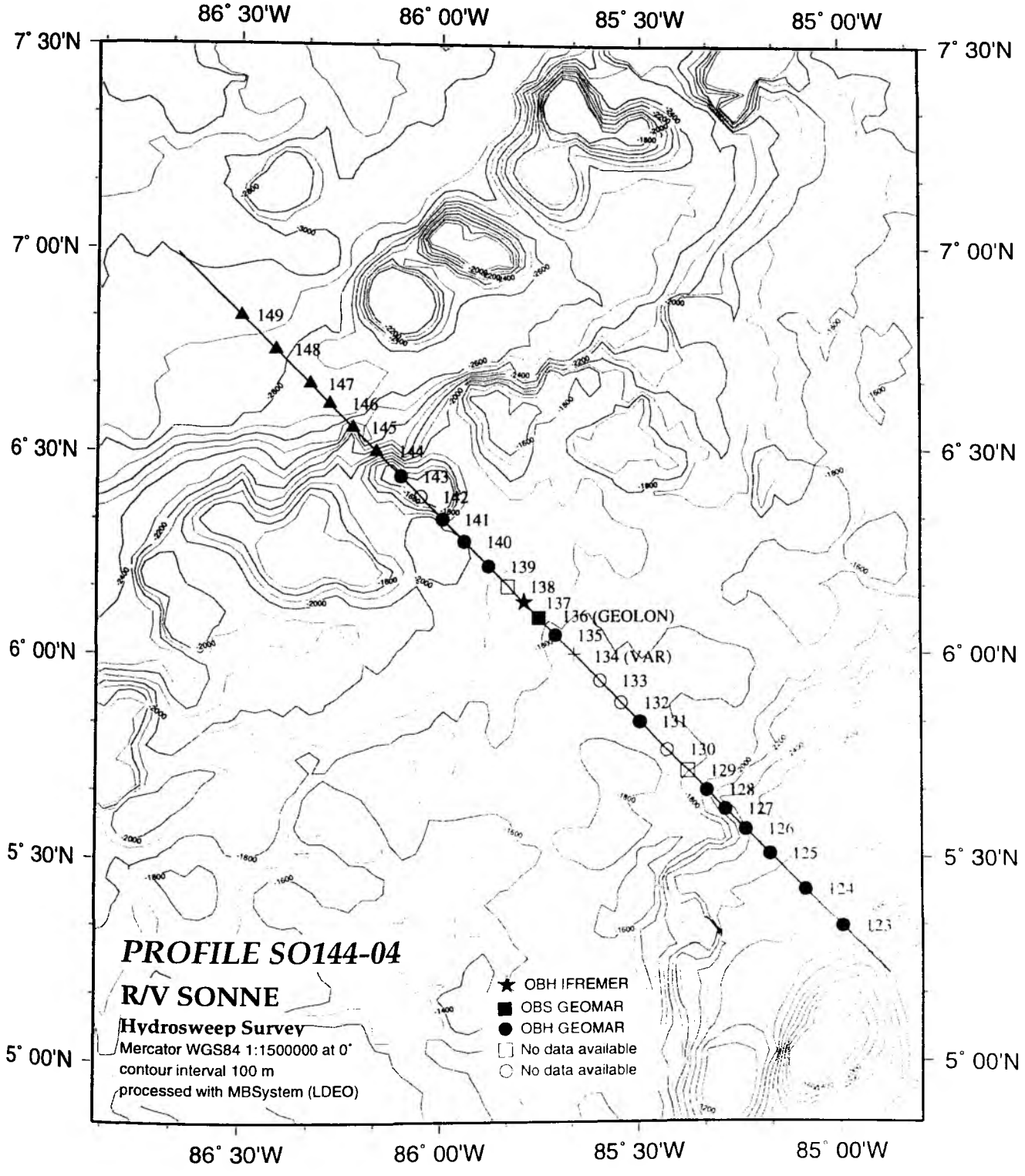

Figure 6.2.4.6.1: Profile SO144-04, Location map

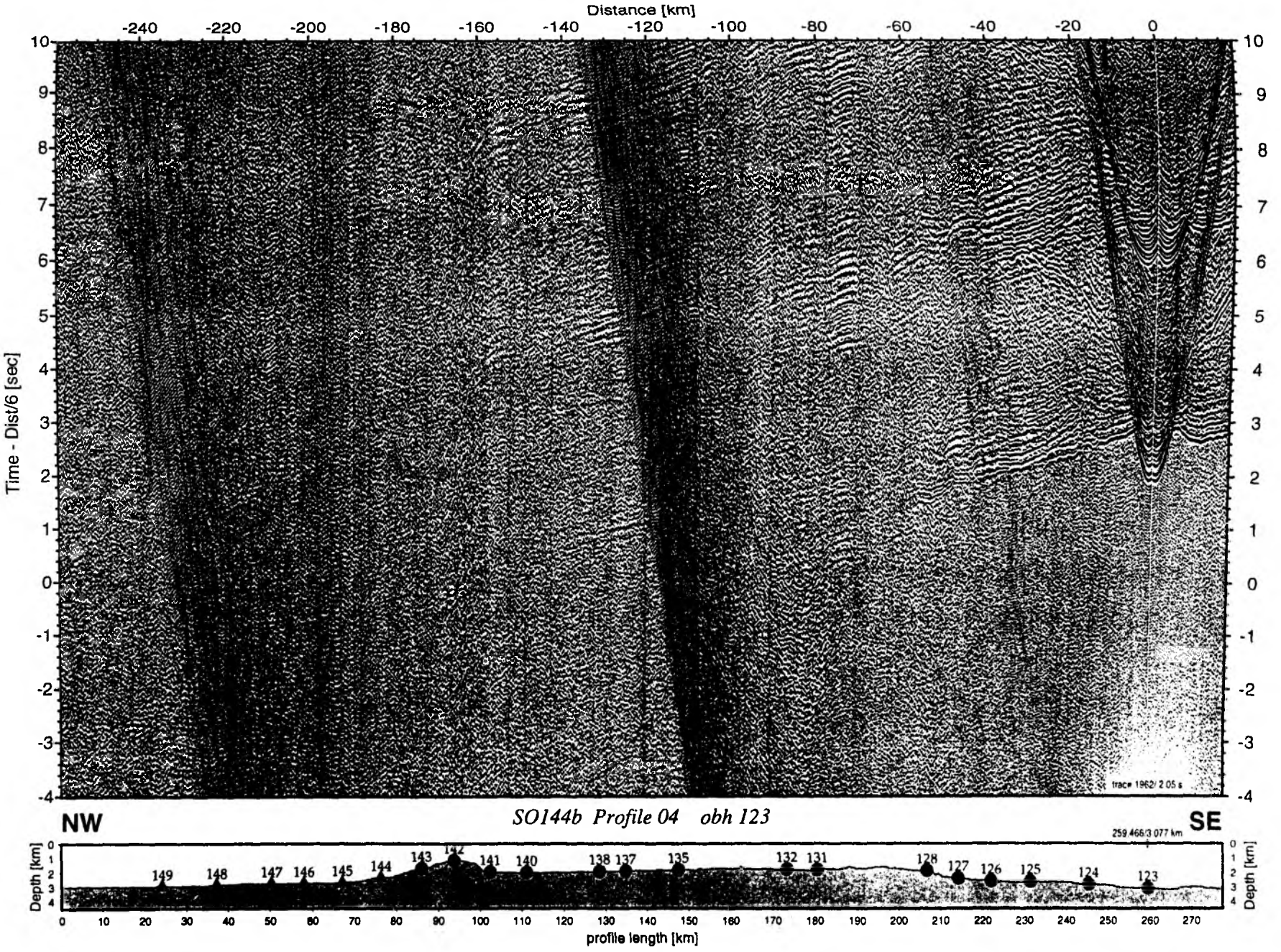

Figure 6.2.4.6.2: Record section from obh 123 , Profile 04.

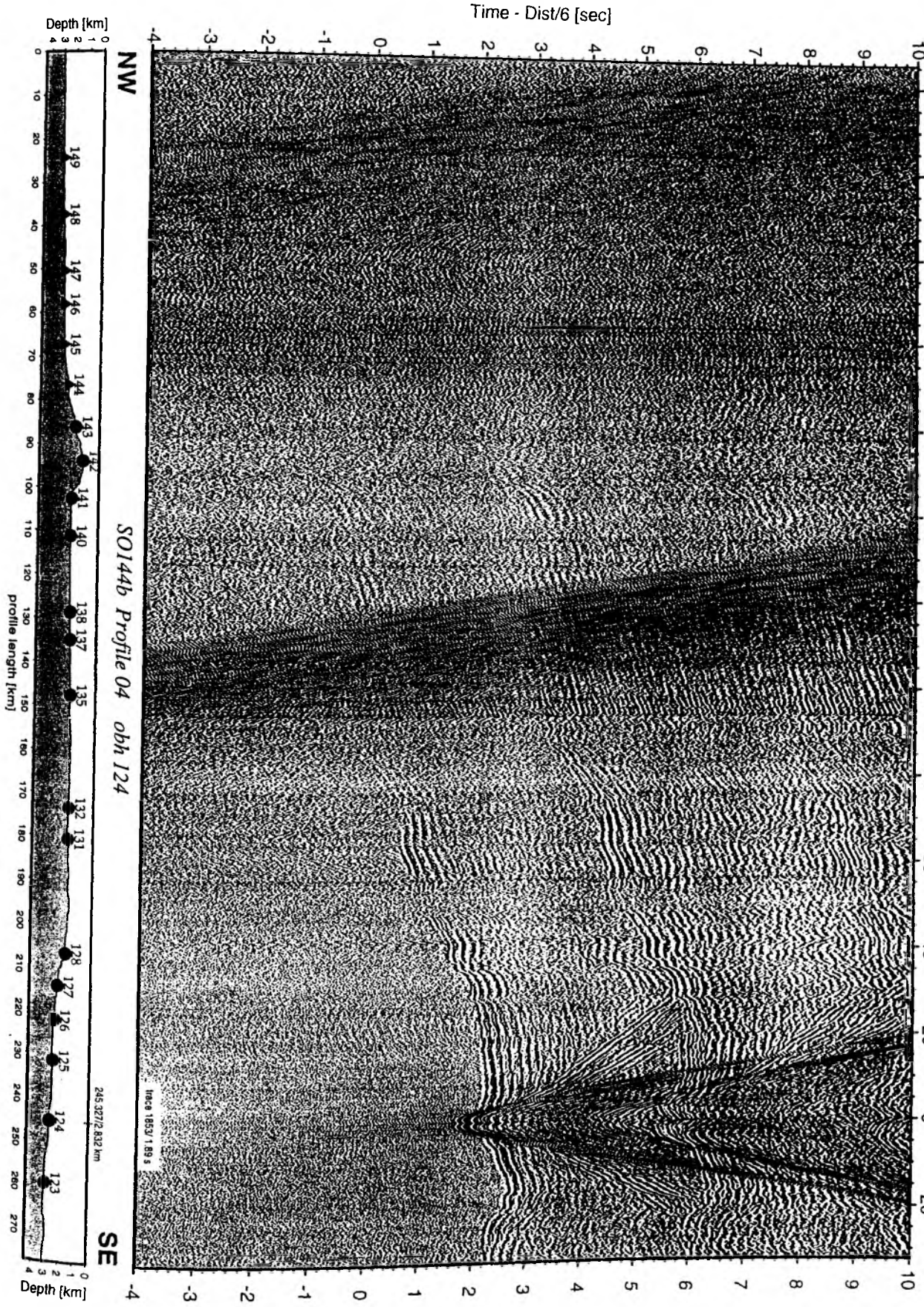

Figure 6.2.4.6.3: Record section from obh 124 , Profile 04.

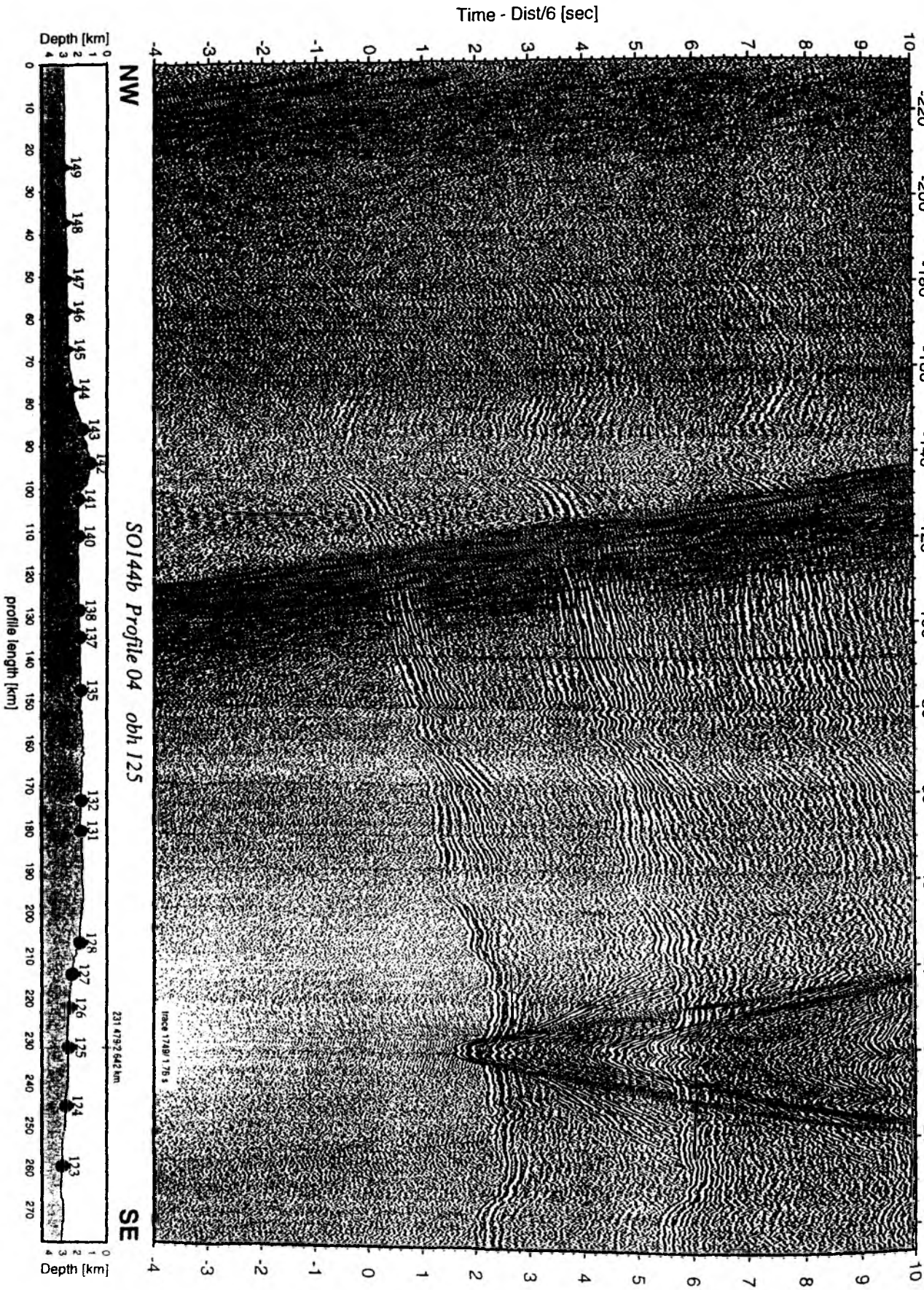

Figure 6.2.4.6.4: Record section from obh 125 , Profile 04.

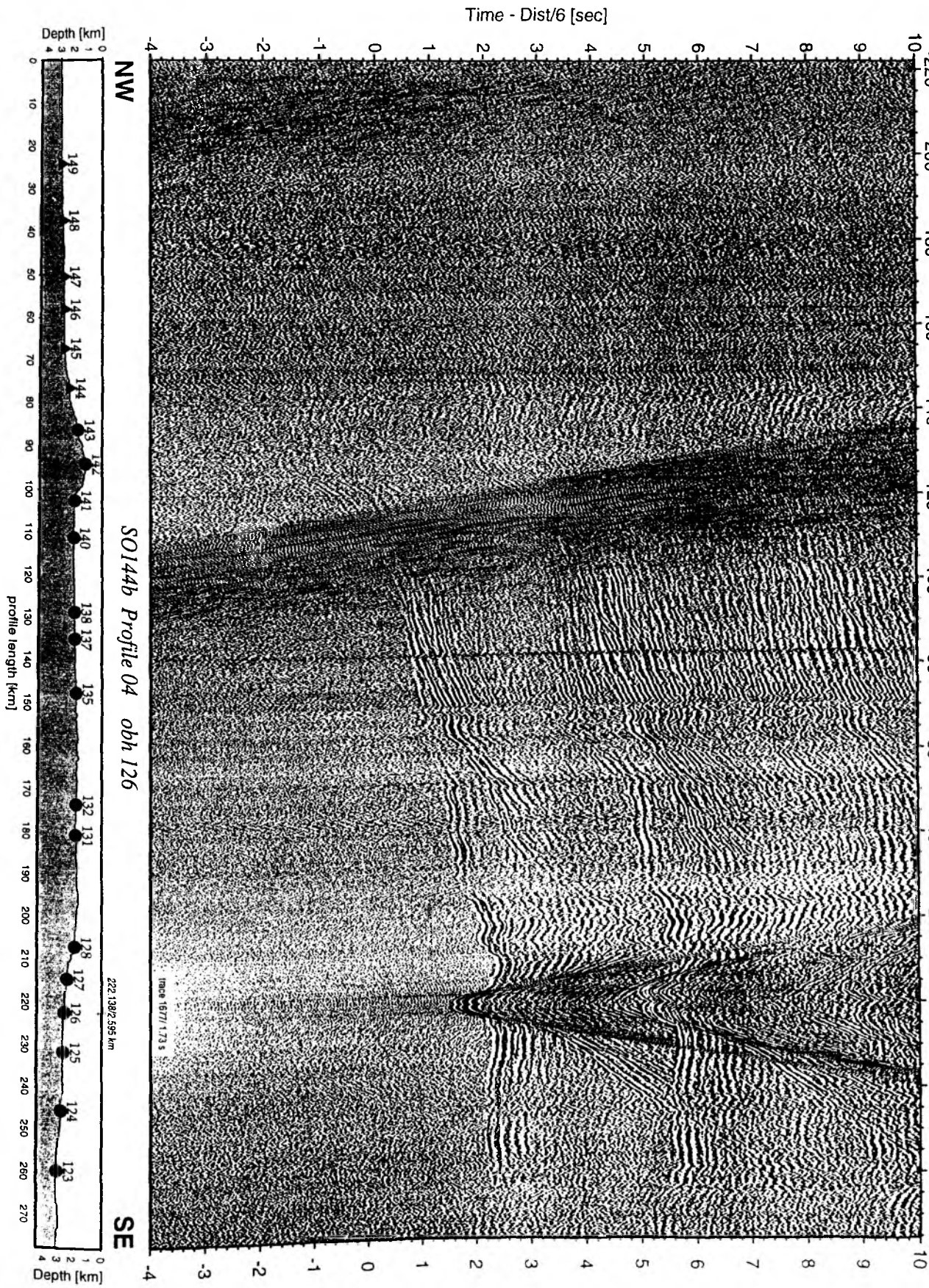

Figure 6.2.4.6.5: Record section from obh 126 , Profile 04.

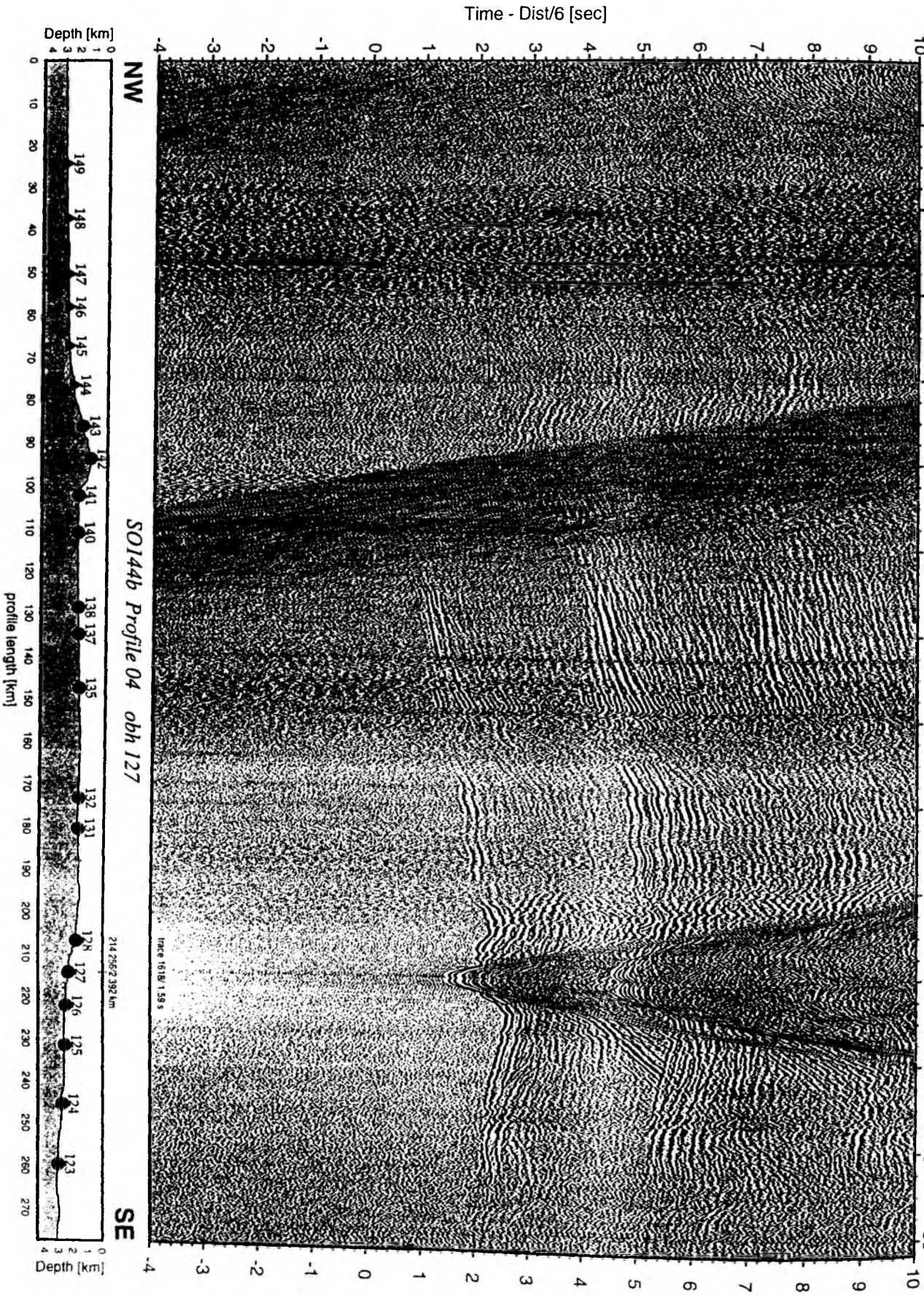

Figure 6.2.4.6.6: Record section from obh 127 , Profile 04.

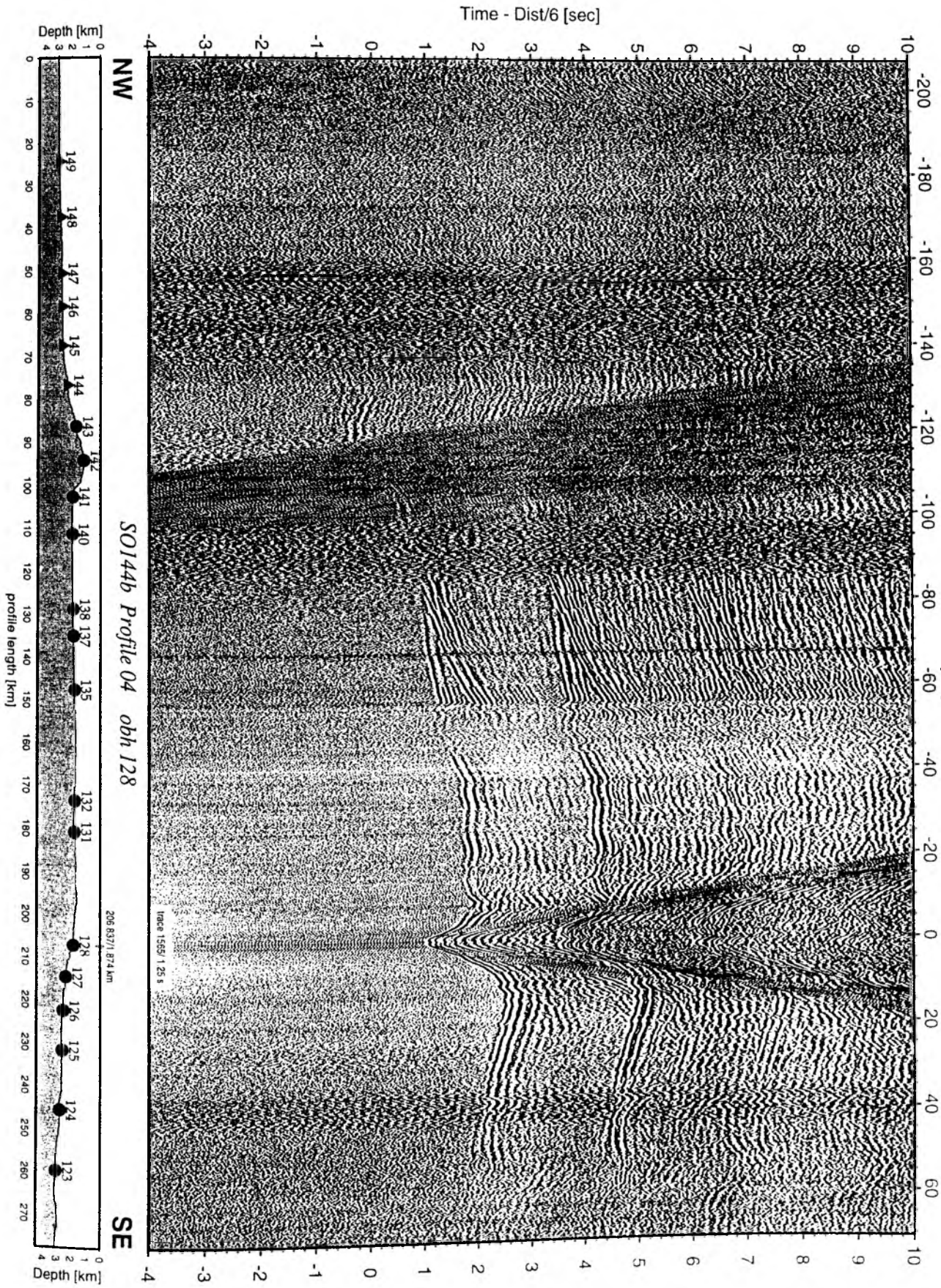

Figure 6.2.4.6.7: Record section from obh 128 , Profile 04.

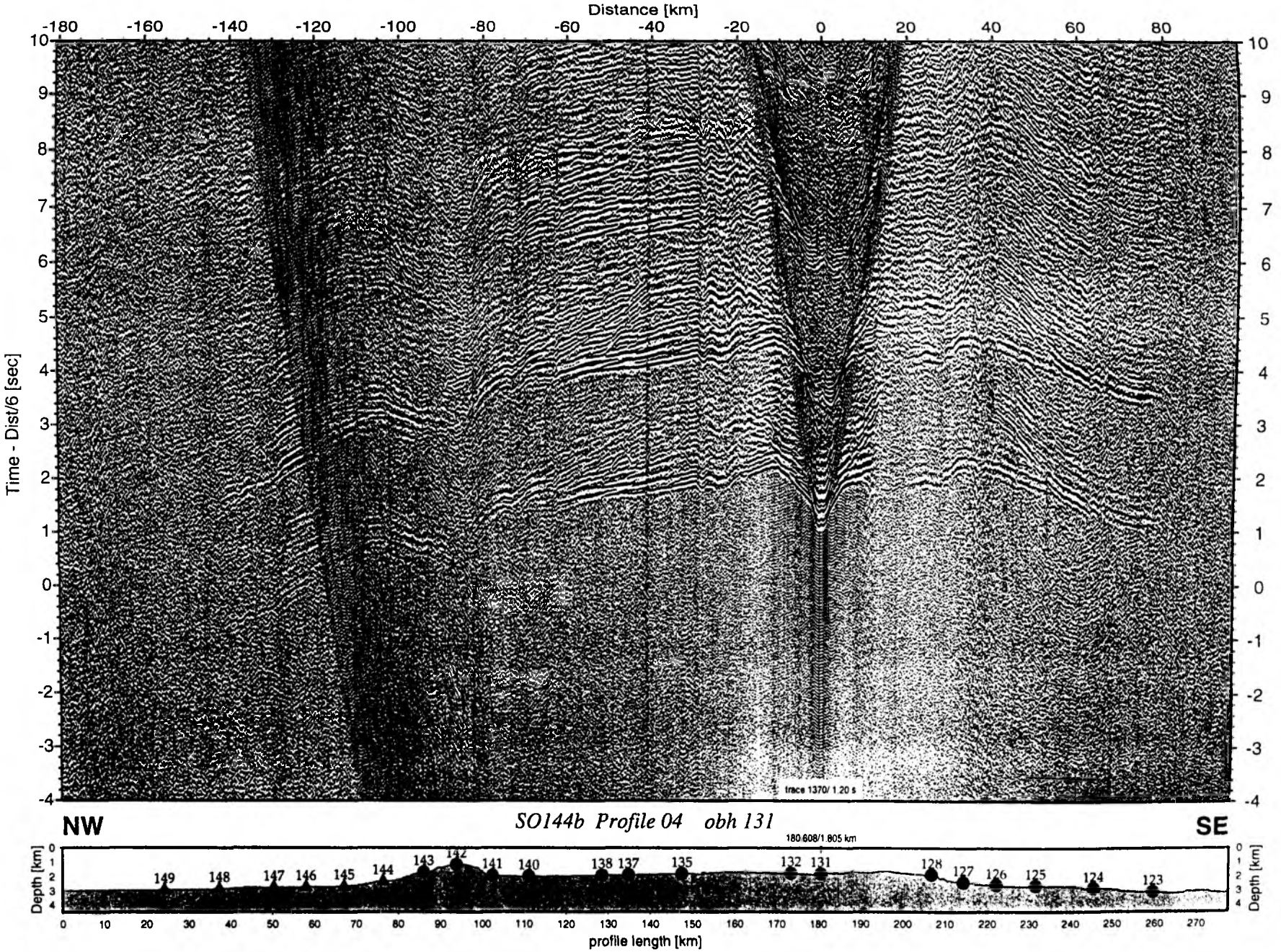

Figure 6.2.4.6.8: Record section from obh 131 , Profile 04.

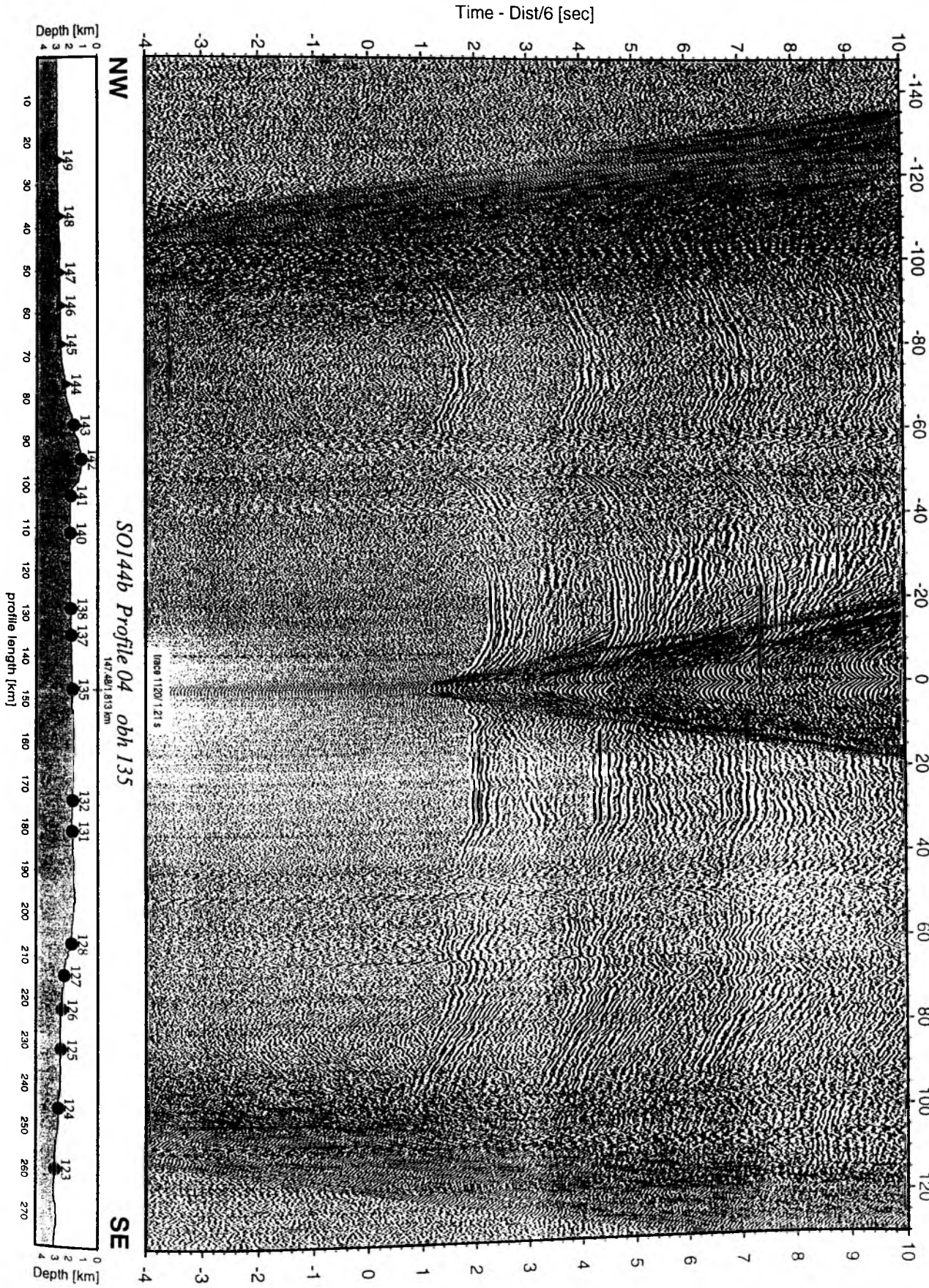

Figure 6.2.4.6.9: Record section from obh 135 , Profile 04.

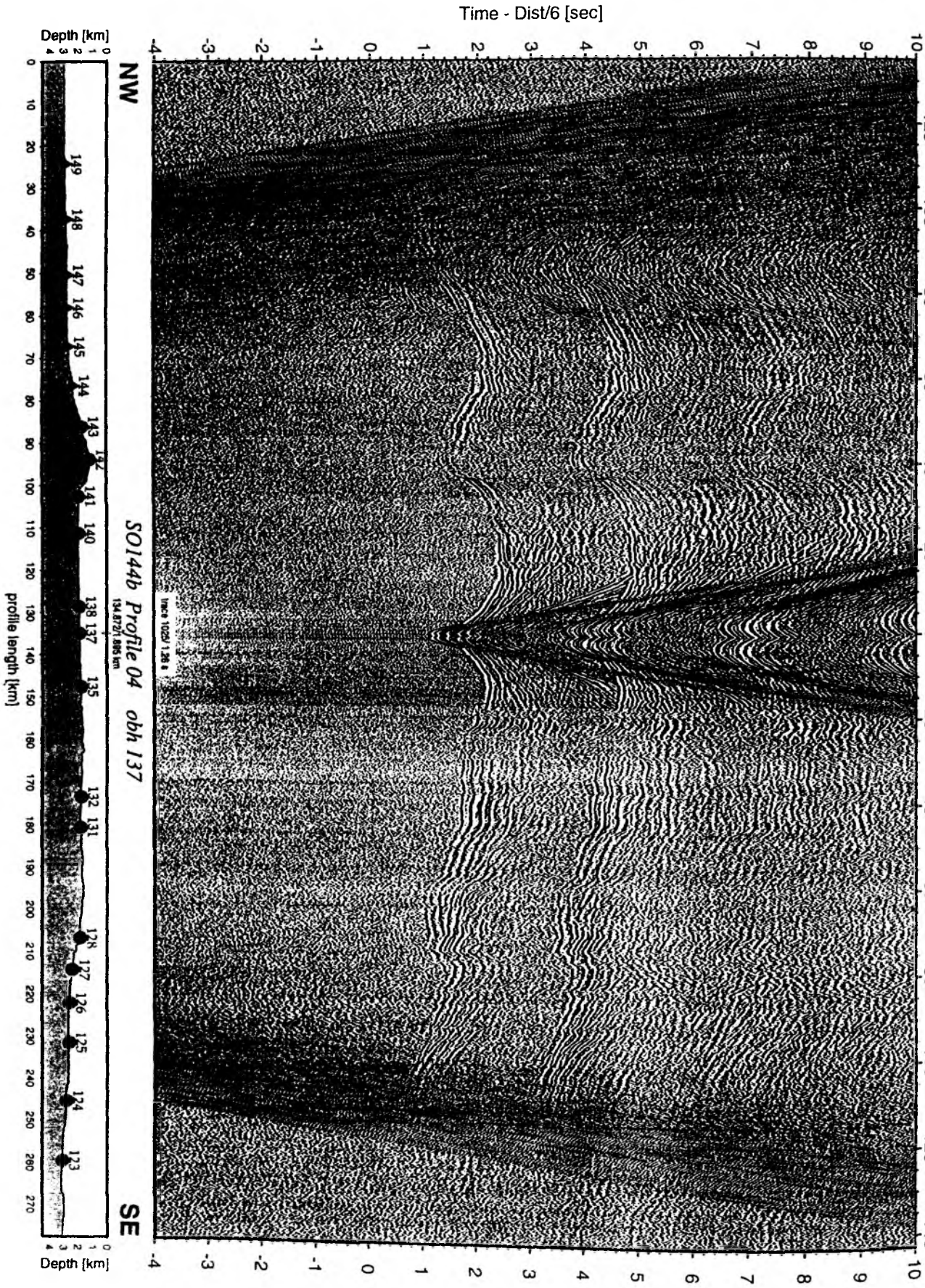

Figure 6.2.4.6.10: Record section from obh 137 , Profile 04.

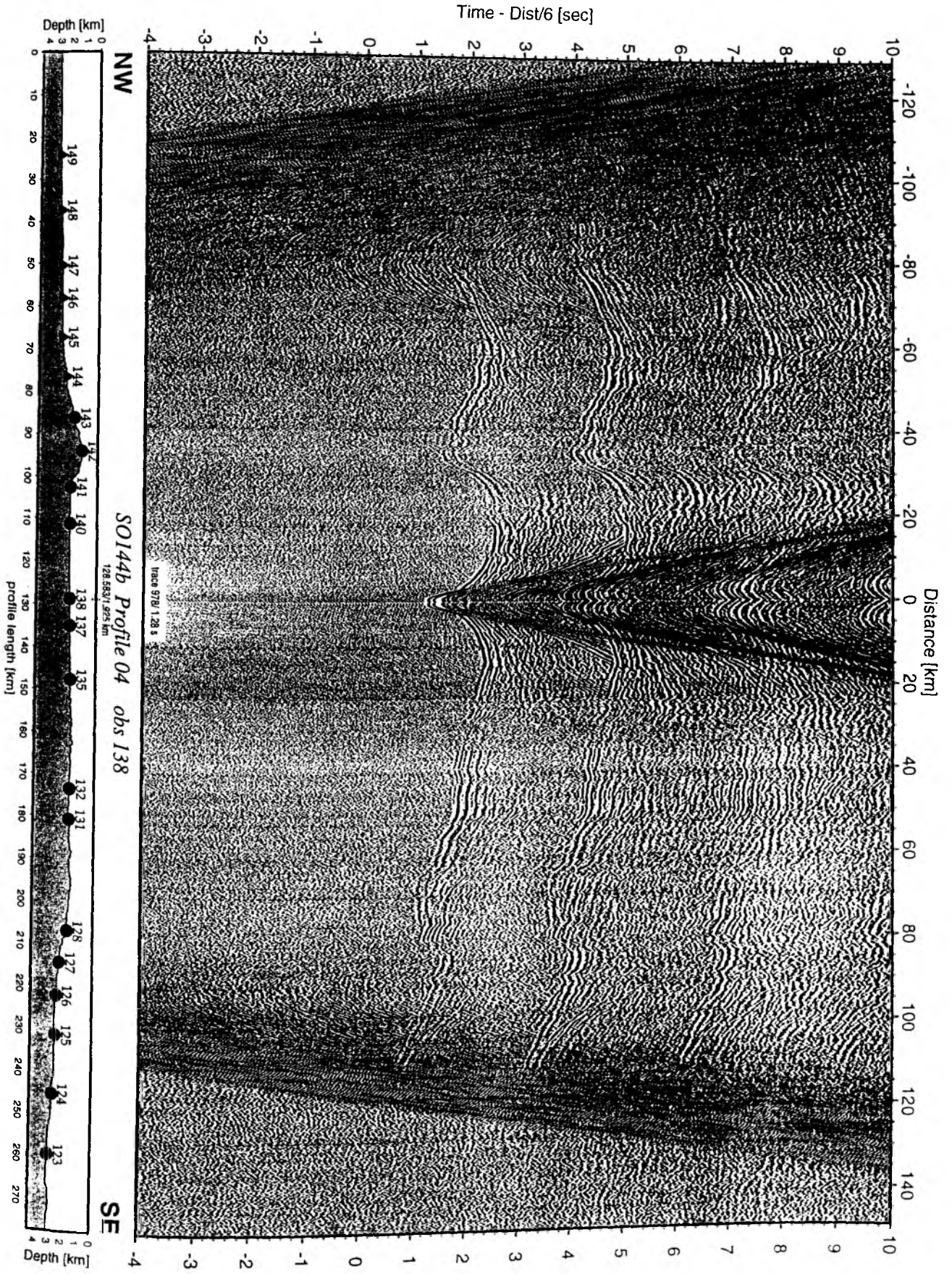

Figure 6.2.4.6.11: Record section from obs 138 hydrophone, Profile 04.

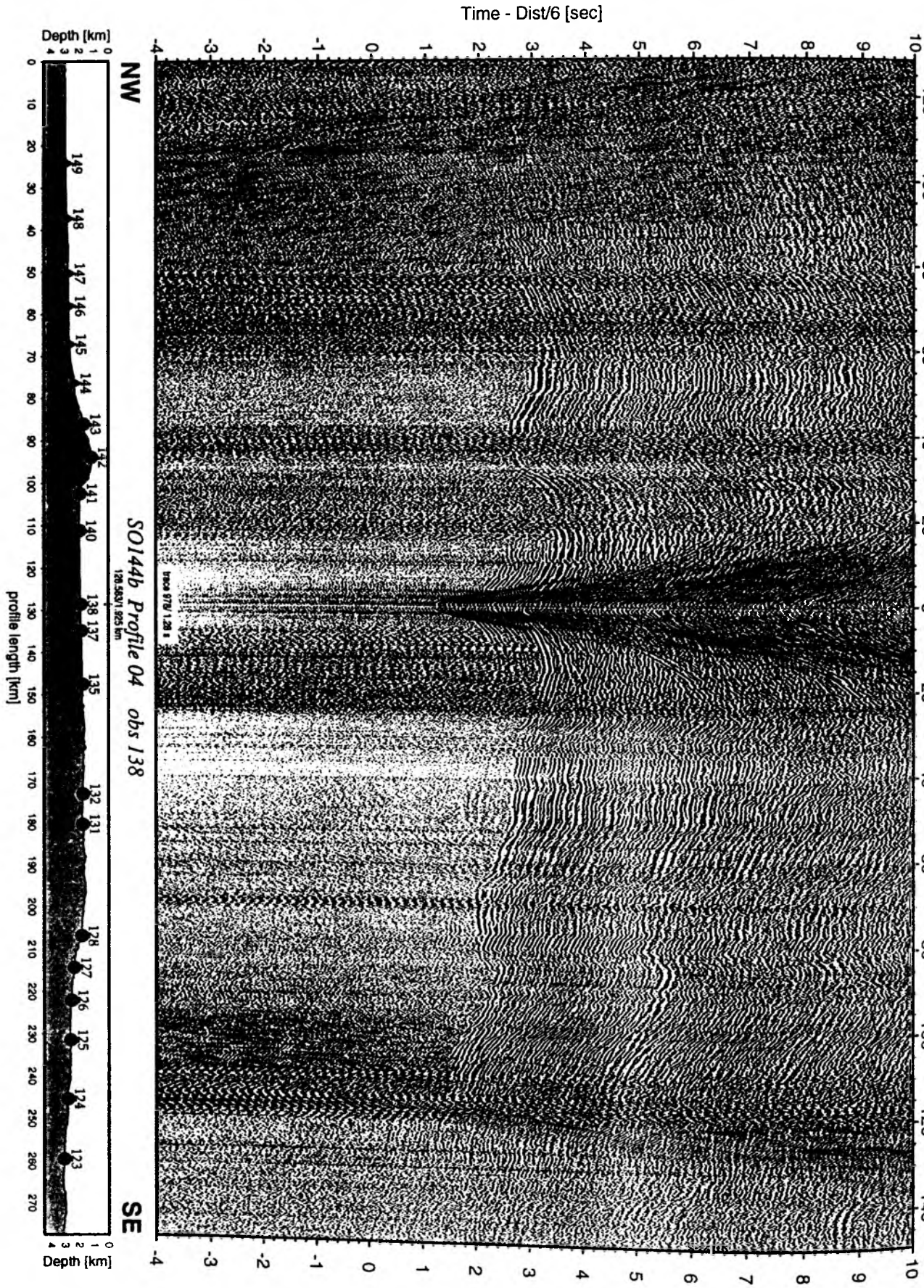

Figure 6.2.4.6.12: Record section from obs 138 vertical component, Profile 04.

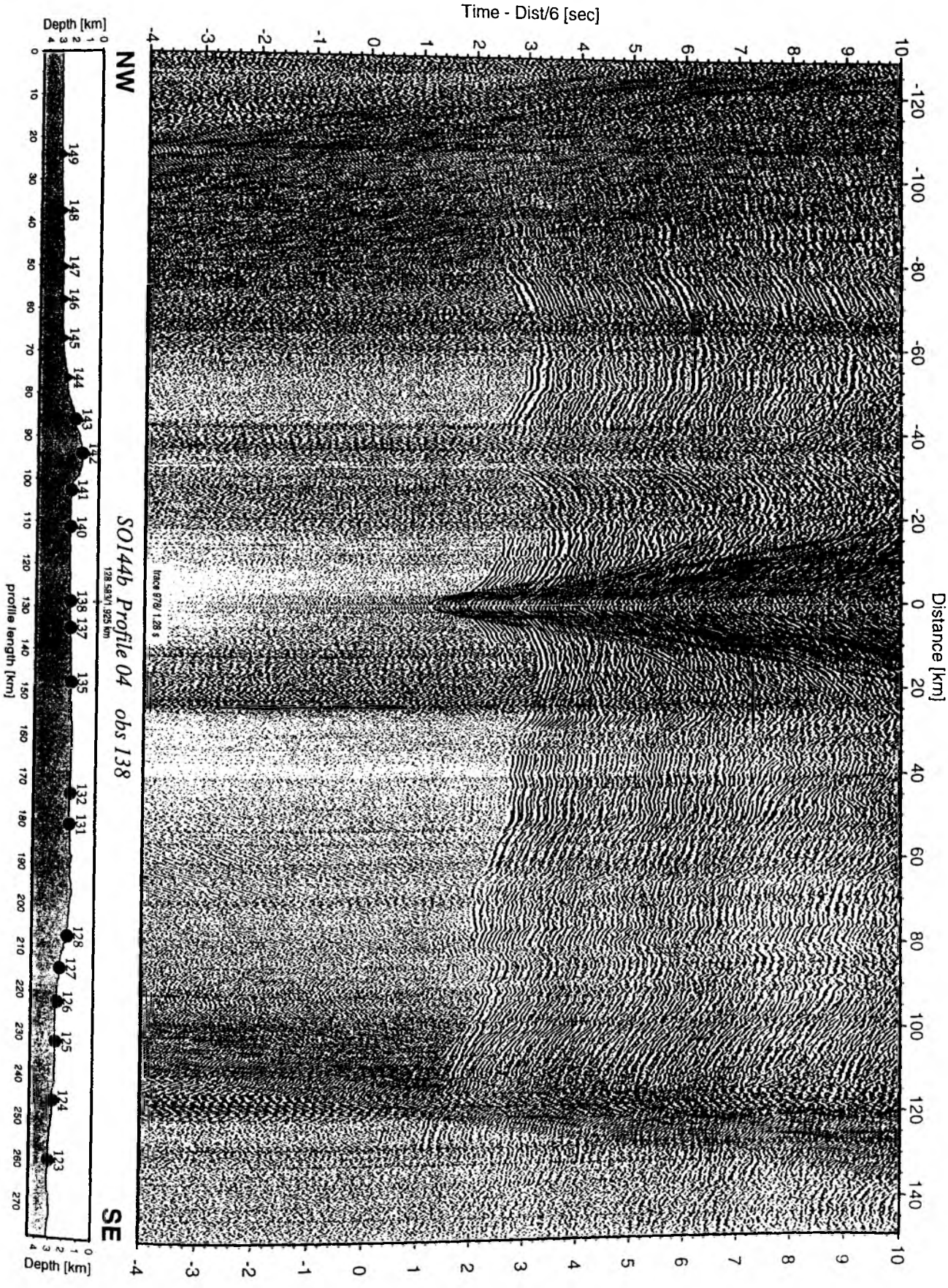

Figure 6.2.4.6.13: Record section from obs 138 horizontal component 1, Profile 04.

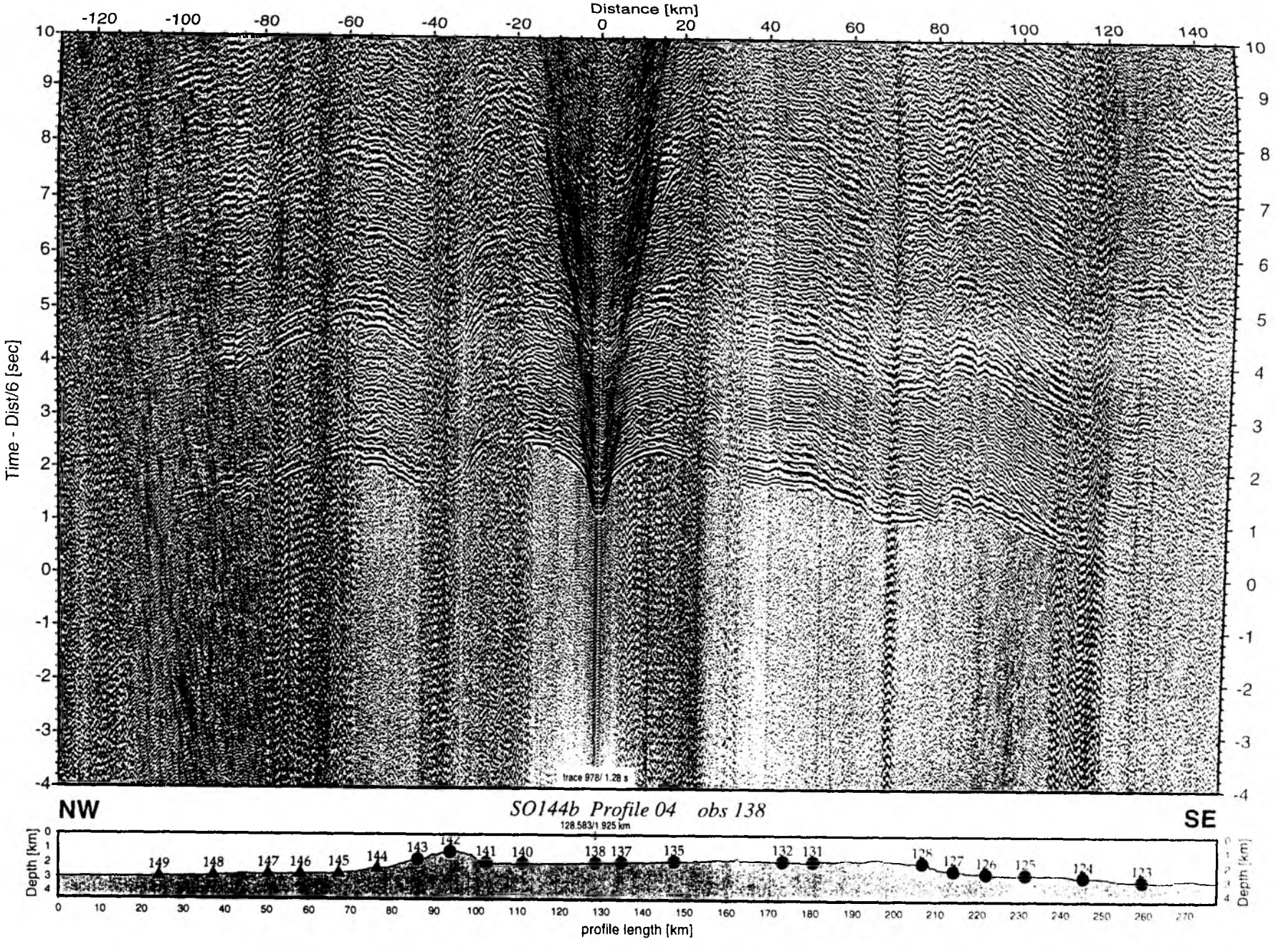

Figure 6.2.4.6.14: Record section from obs 138 horizontal component 2, Profile 04.

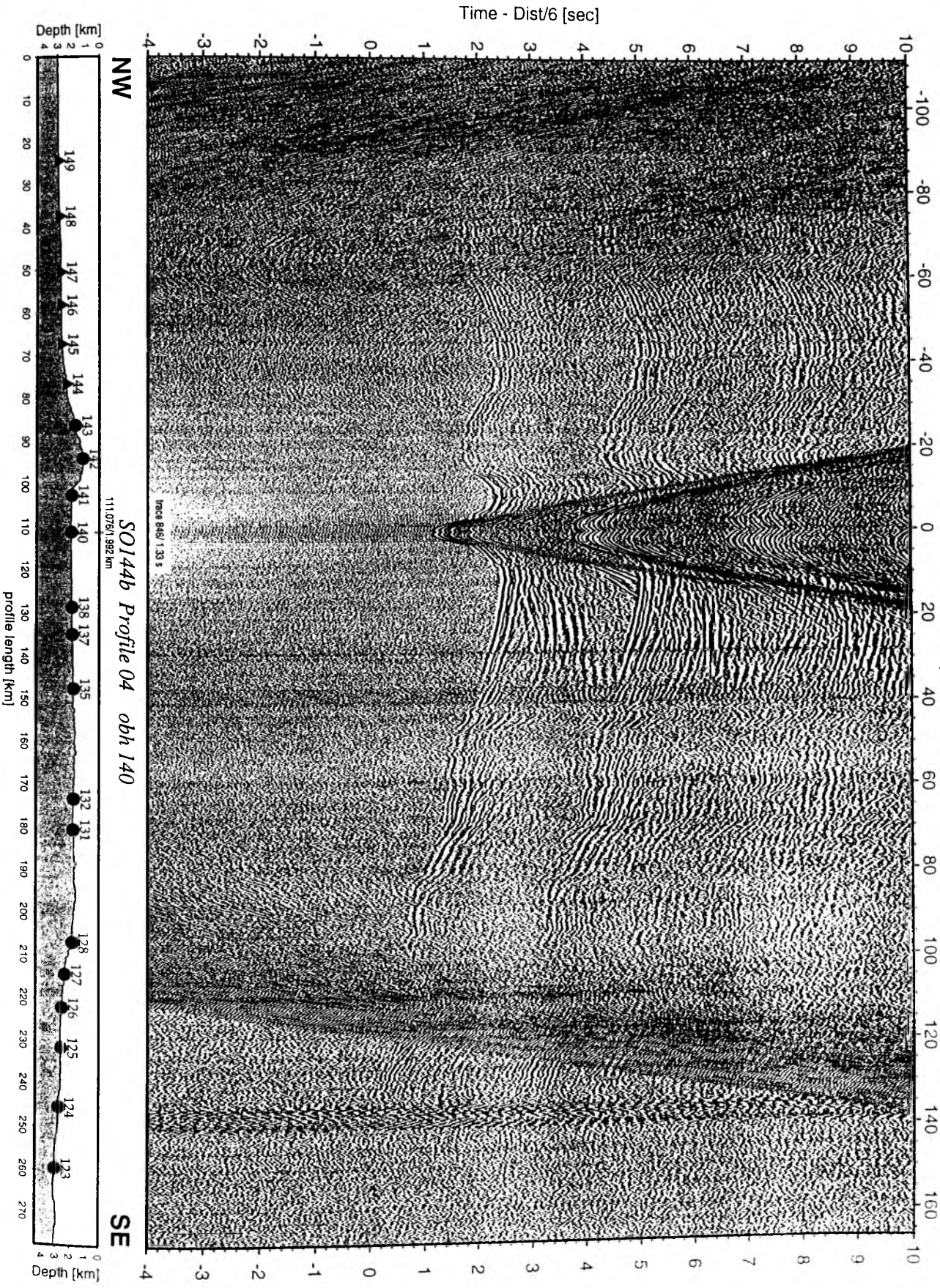

Figure 6.2.4.6.15: Record section from obh 140 , Profile 04.

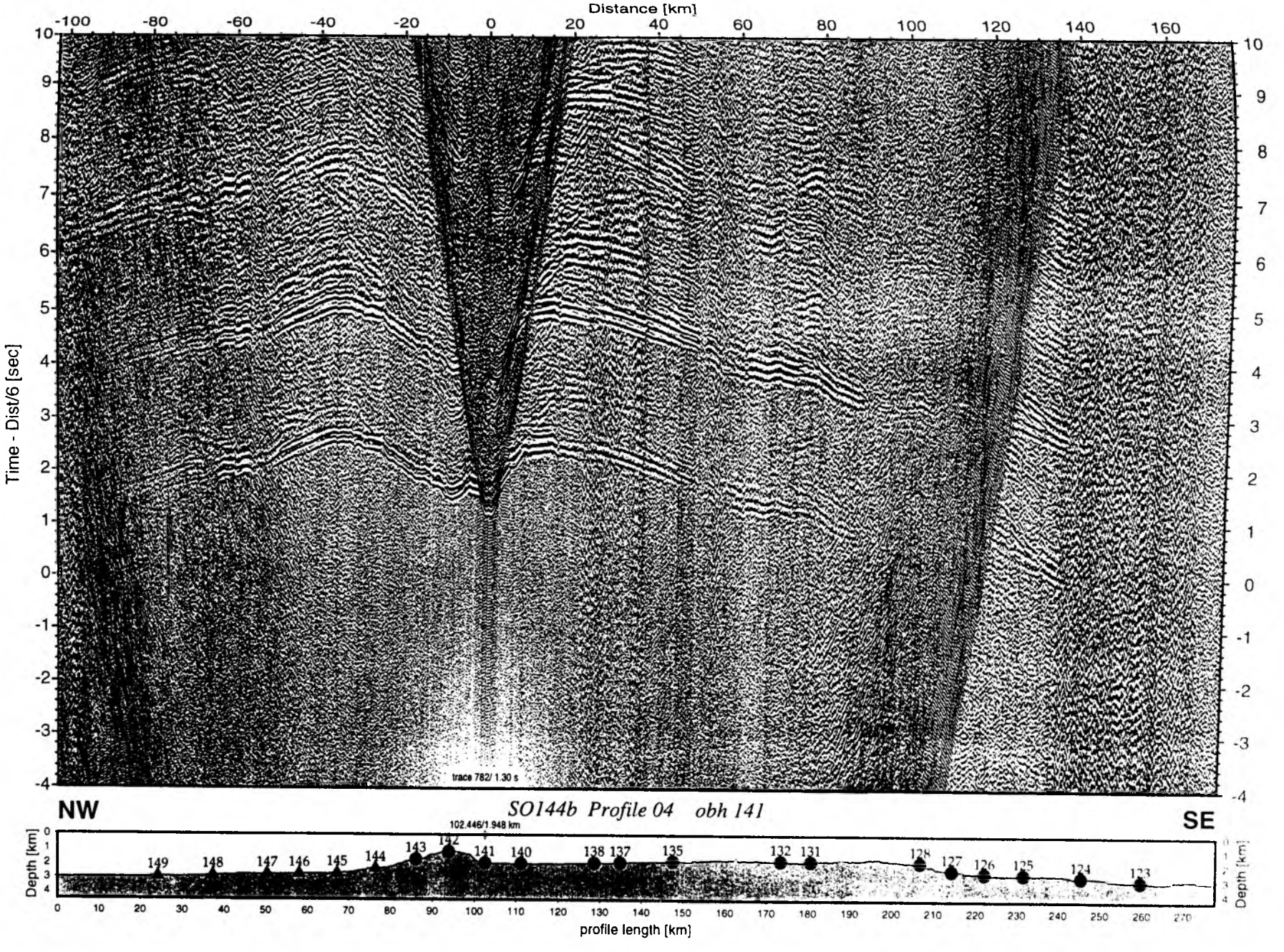

Figure 6.2.4.6.16: Record section from obh 141 , Profile 04.

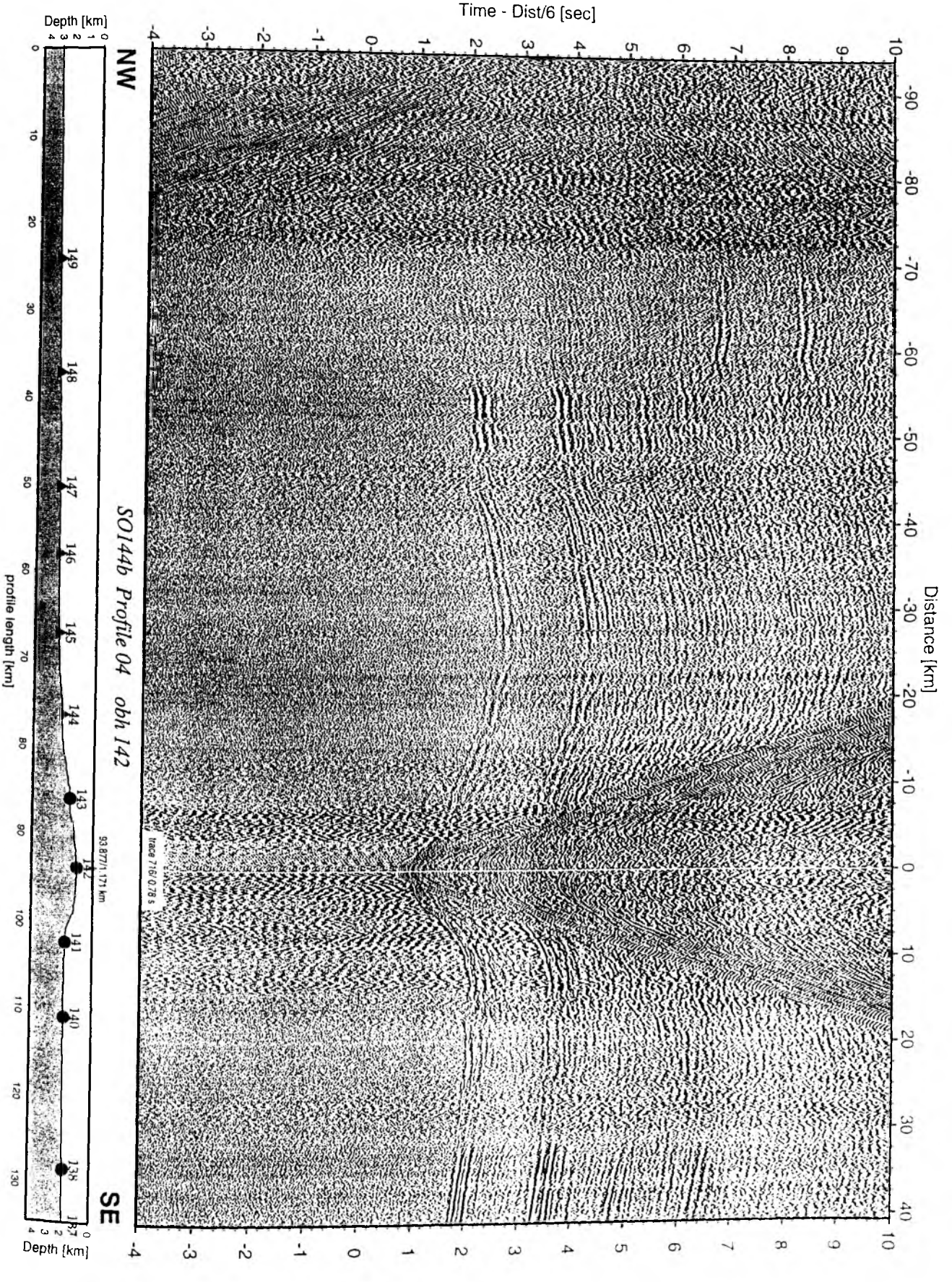

Figure 6.2.4.6.17: Record section from obh 142 , Profile 04.

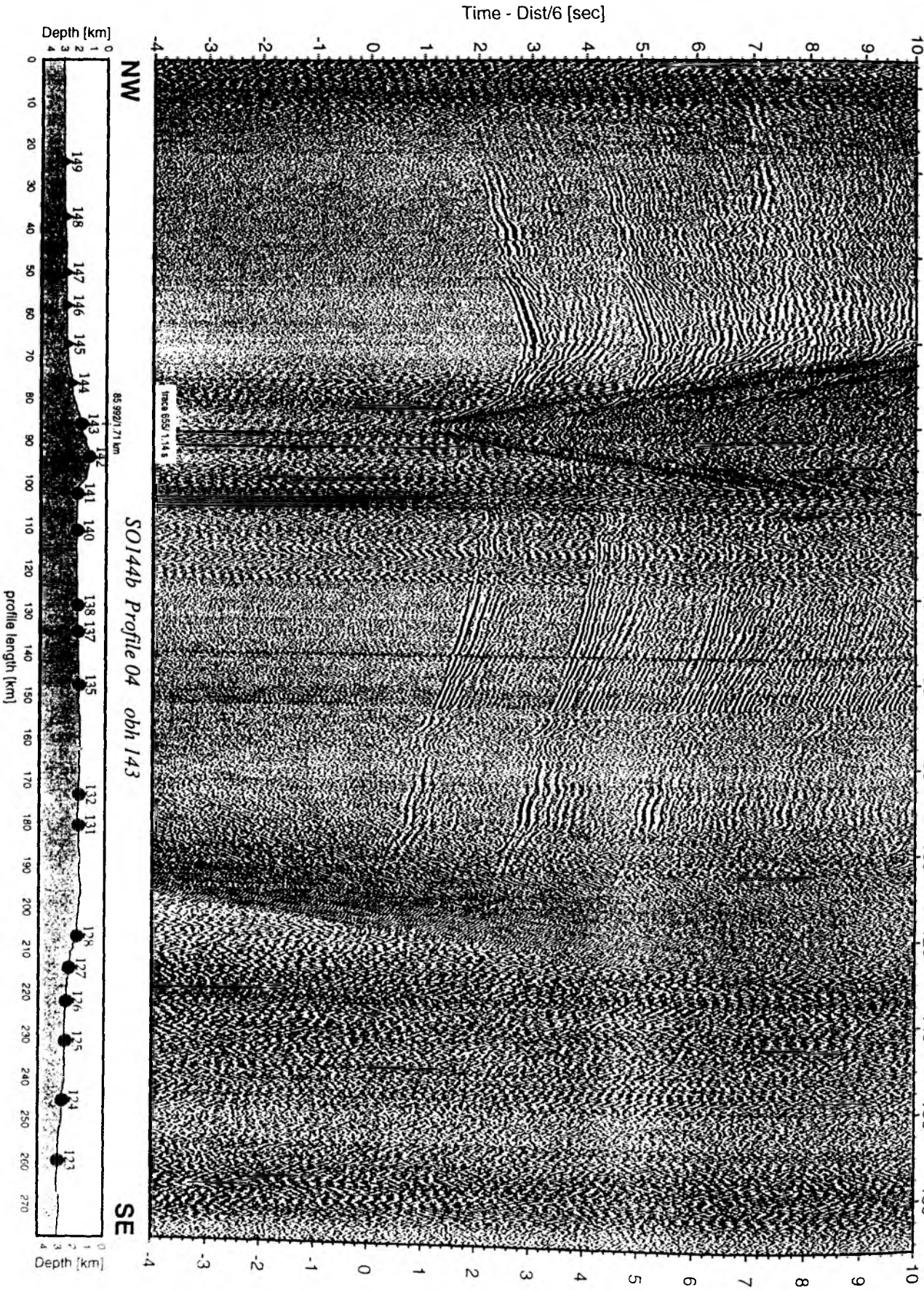

Figure 6.2.4.6.18: Record section from obh 143 , Profile 04.

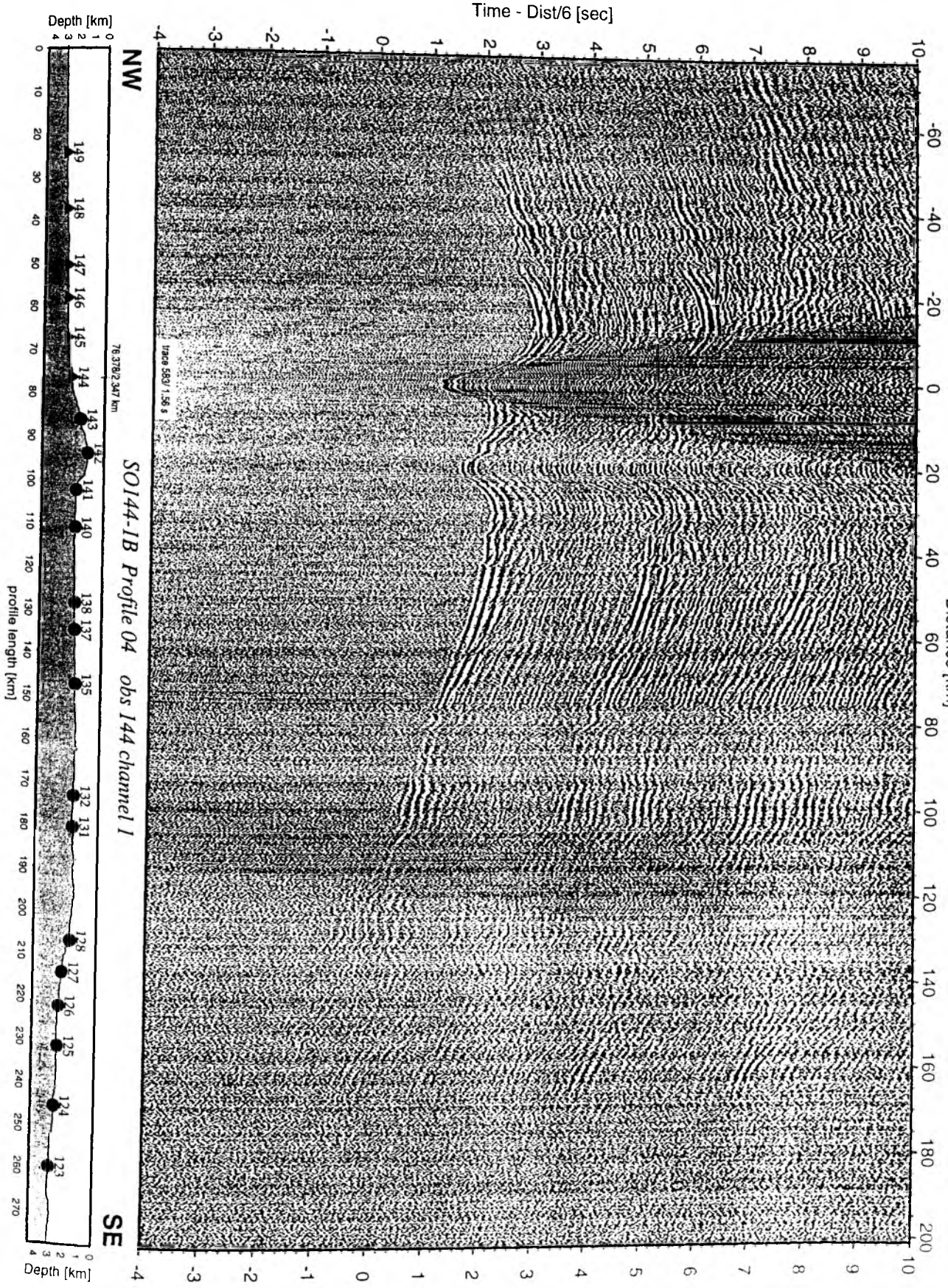

Figure 6.2.4.6.19: Record section from obs 144 vertical component, Profile 04.

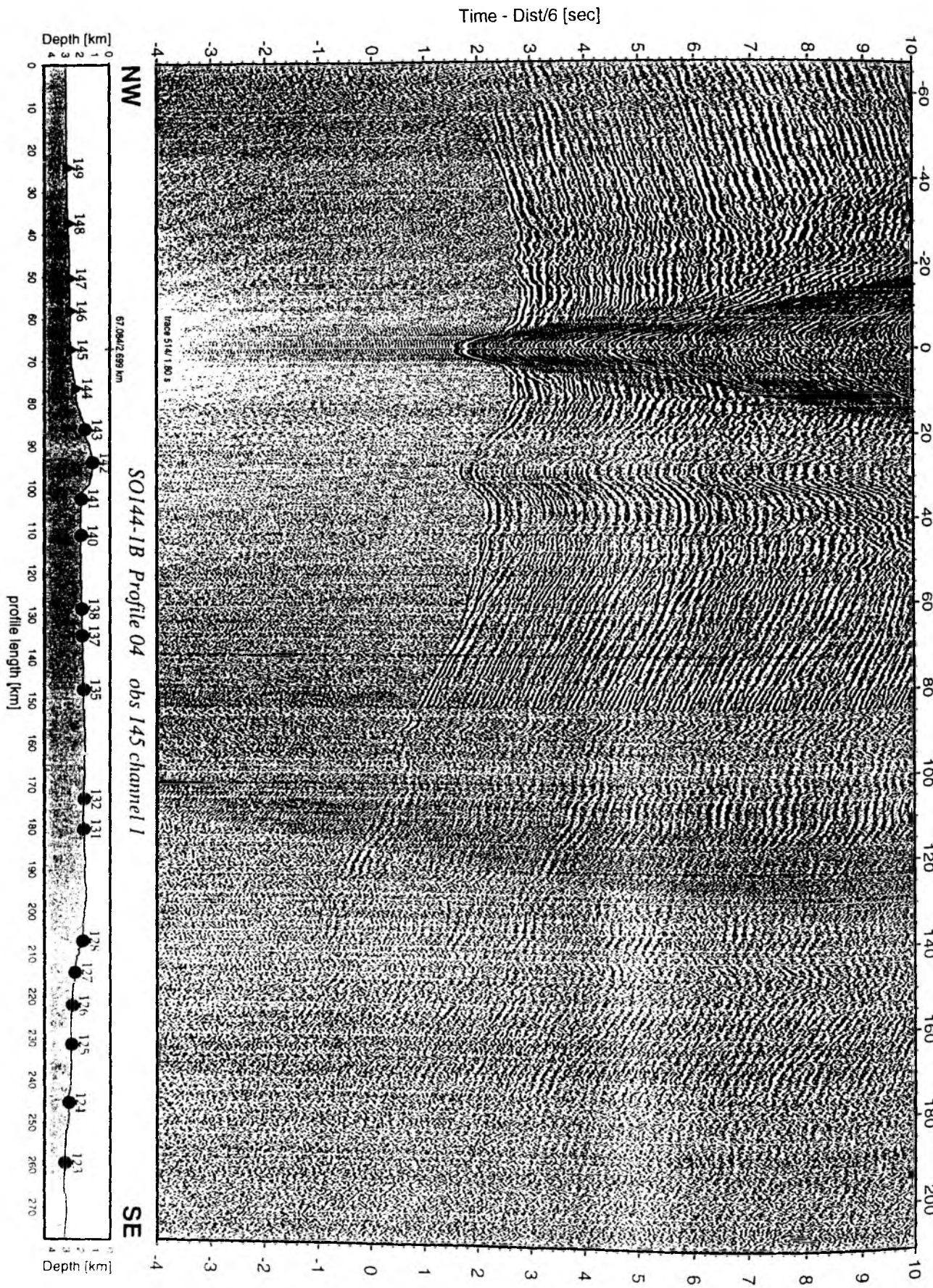

Figure 6.2.4.6.20: Record section from obs 145 vertical component, Profile 04.

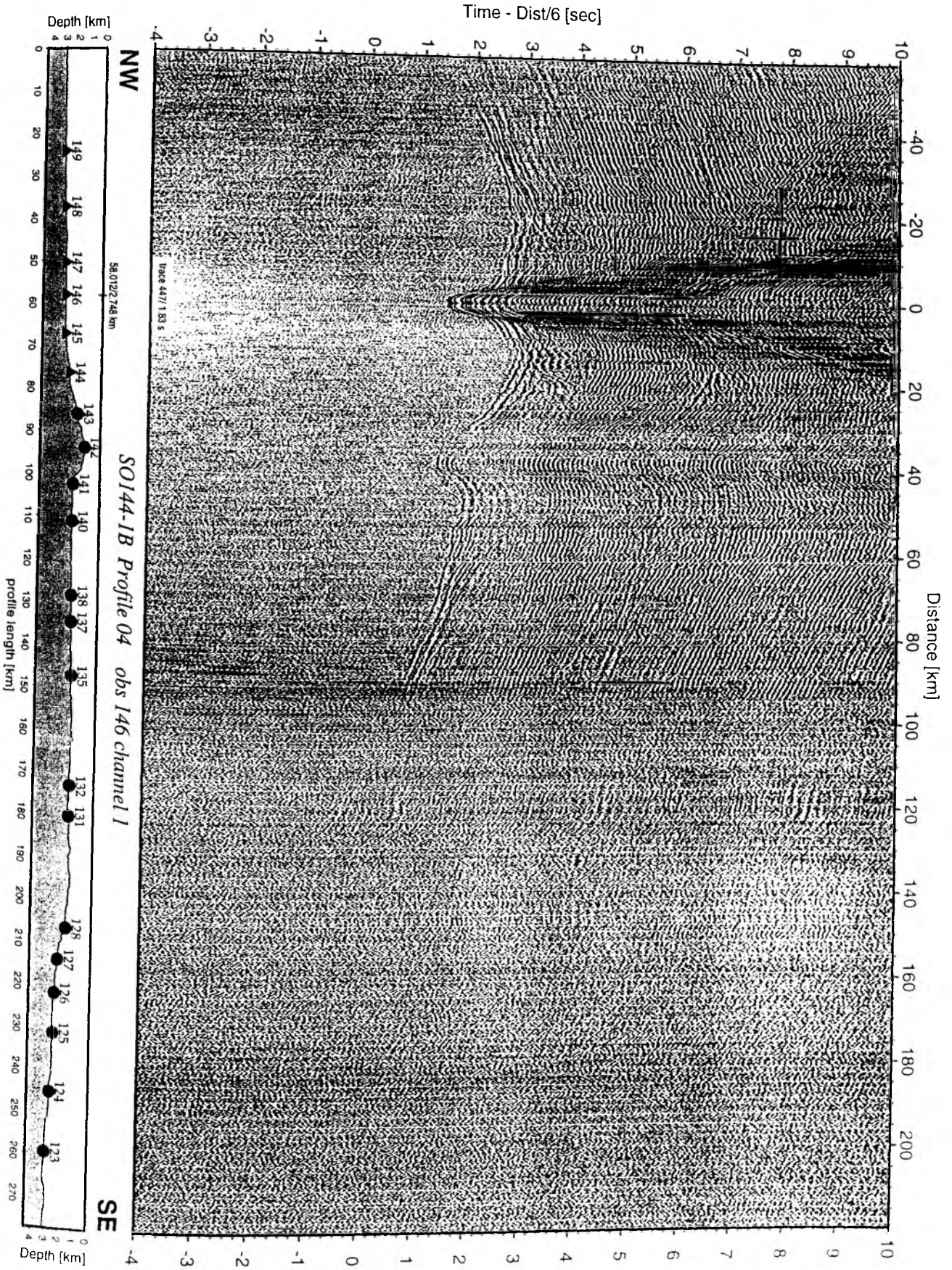

Figure 6.2.4.6.21: Record section from obs 146 vertical component, Profile 04.

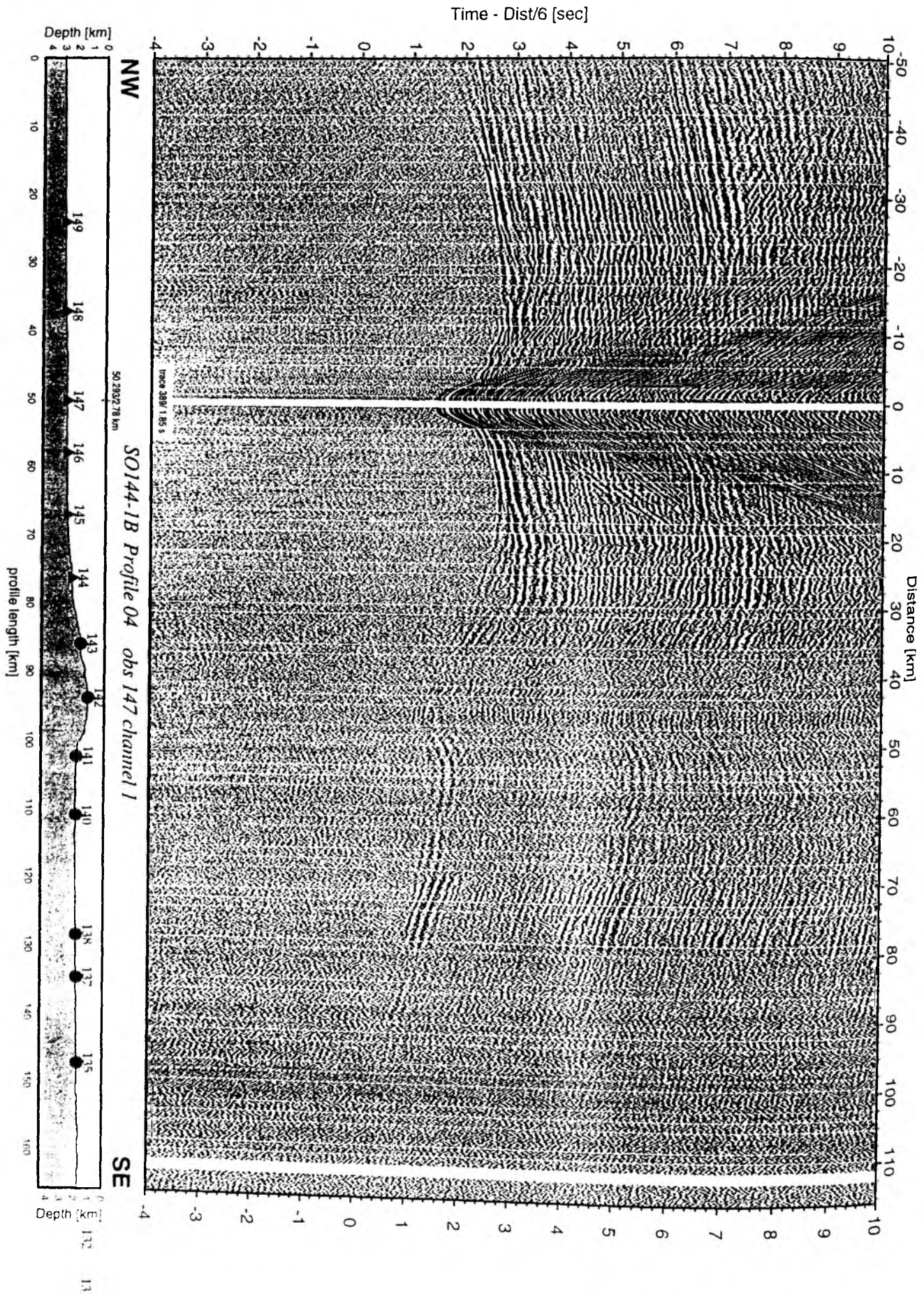

Figure 6.2.4.6.22: Record section from obs 147 vertical component, Profile 04.

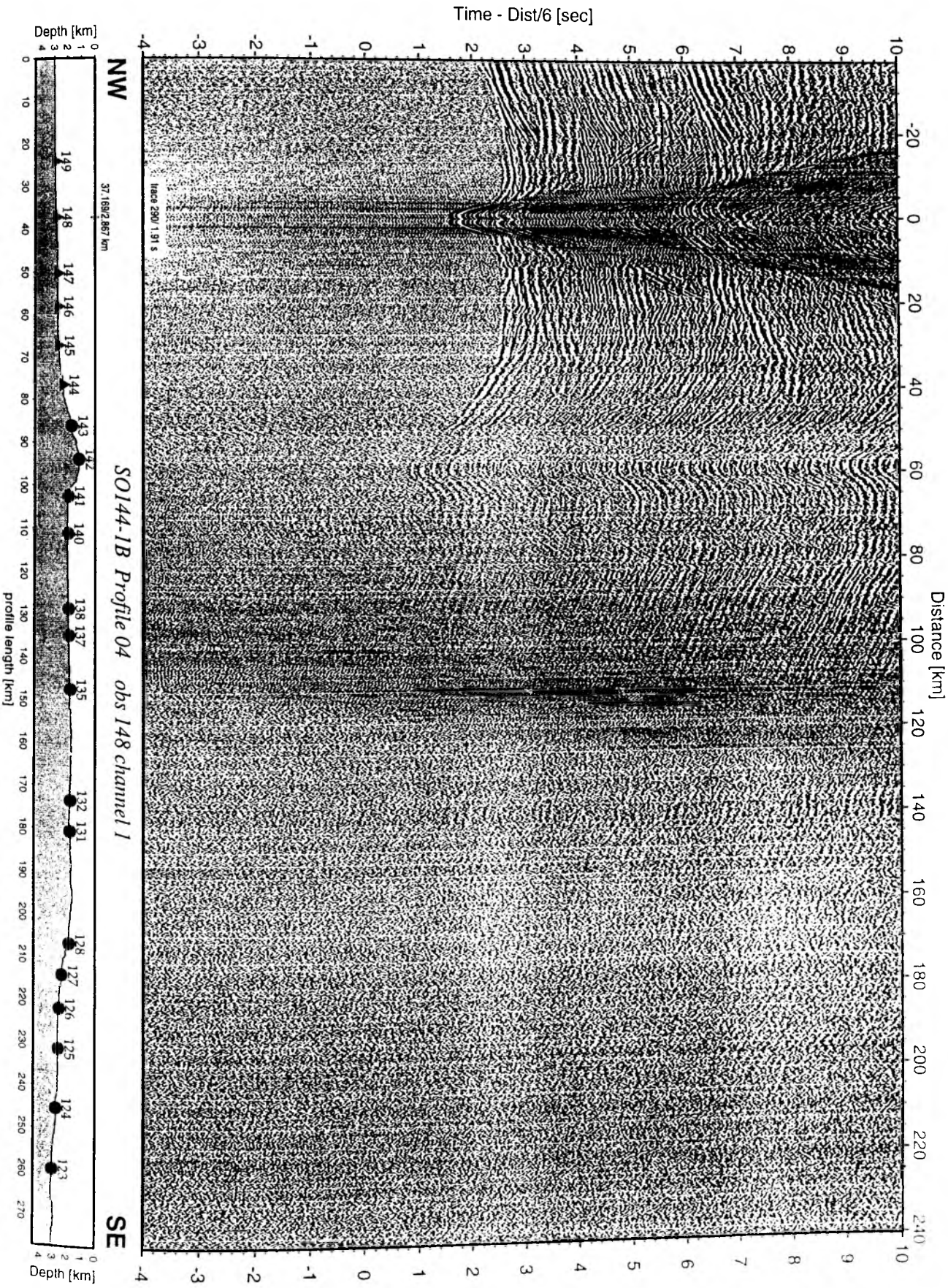

Figure 6.2.4.6.23: Record section from obs 148 vertical component, Profile 04.

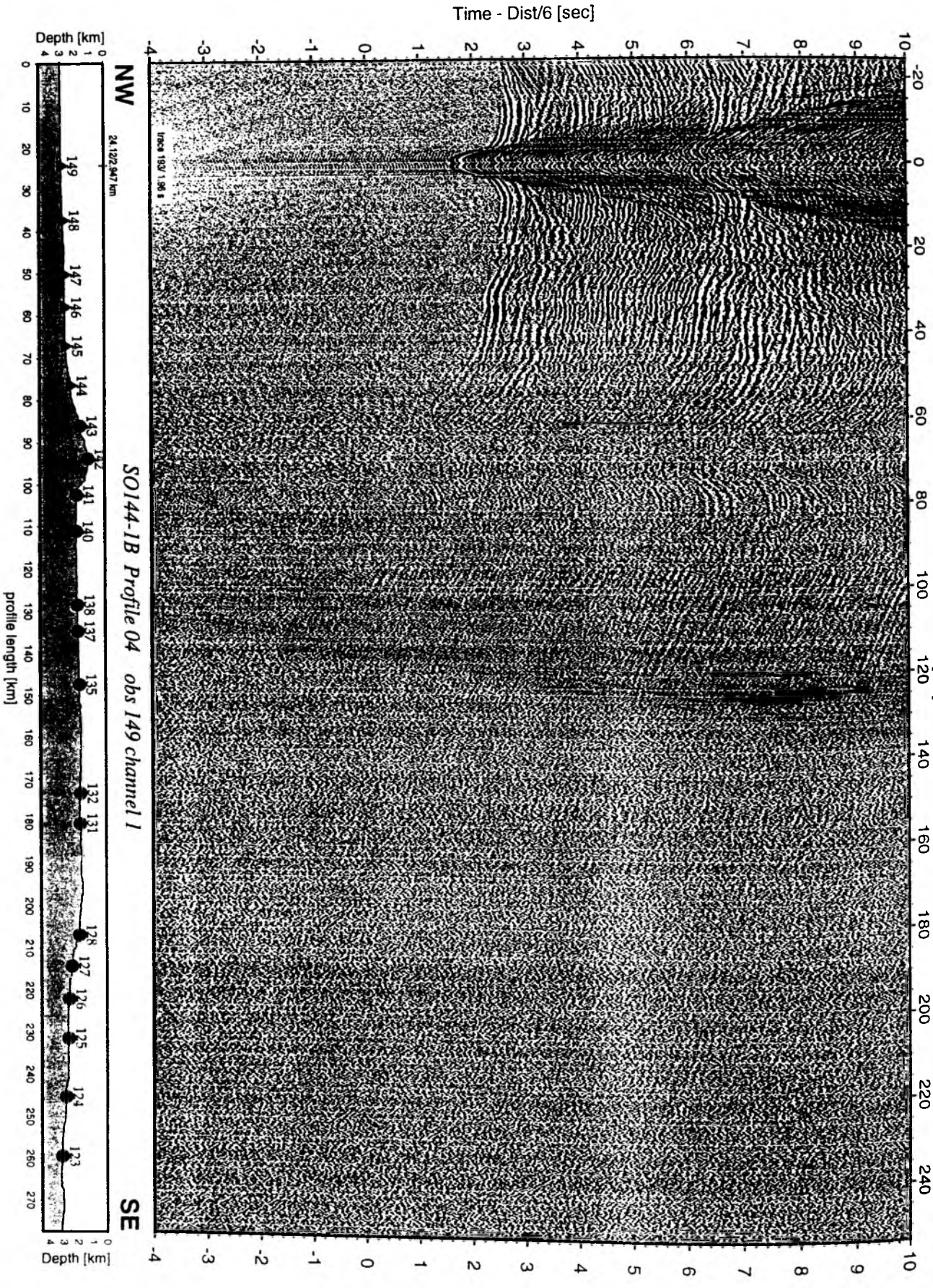

Figure 6.2.4.6.24: Record section from obs 149 vertical component, Profile 04.

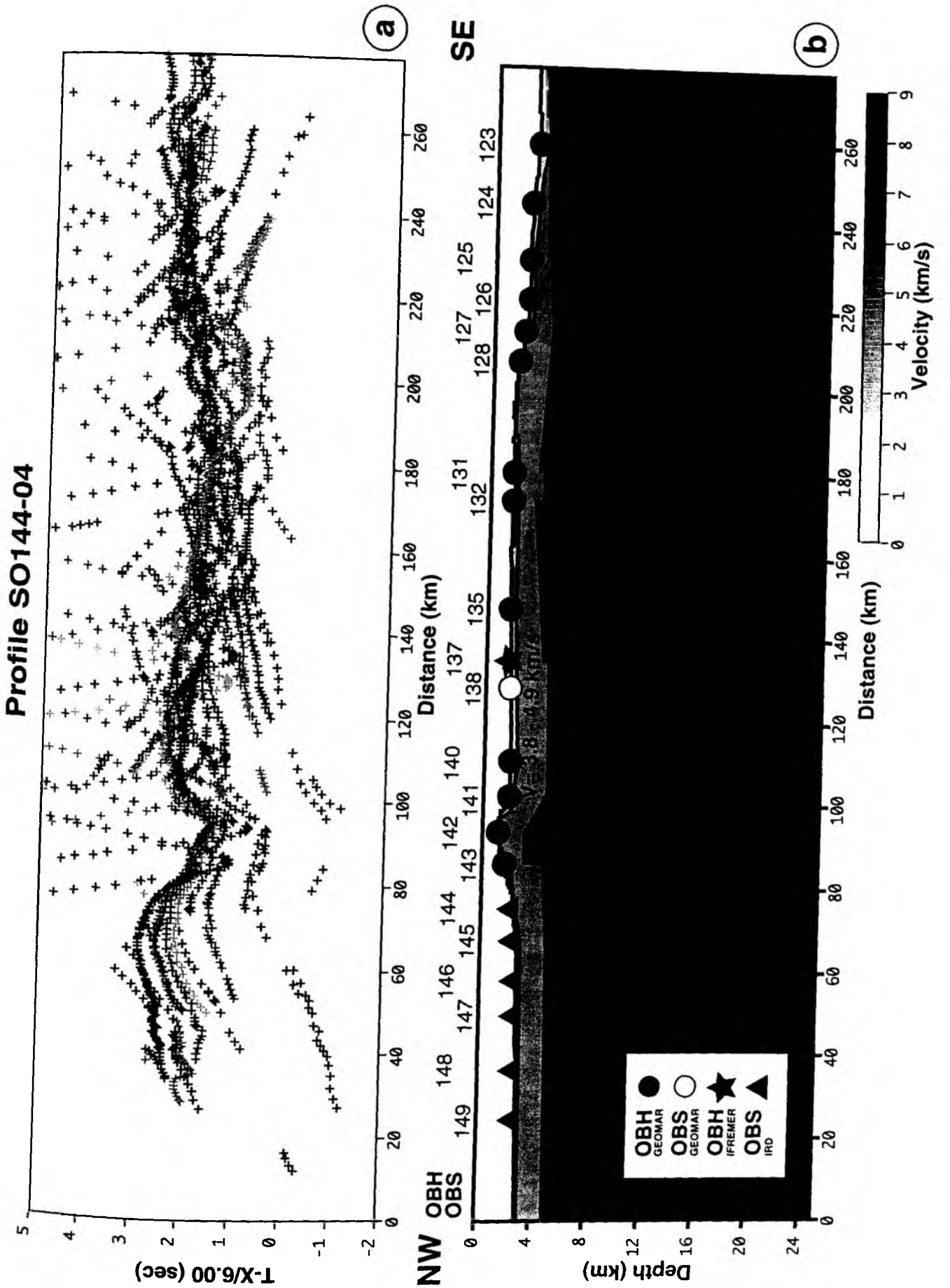

Figure 6.2.4.6.25 a) Picks extracted from the record sections of Profile 04
b) Crustal cross section for Profile 04 from preliminary analysis of wide-angle data.

6.2.4.7 PROFILE SO144-05

Profile SO144-05 is a short line shot seaward of the trench facing the Nicoya Peninsula, where the transition from crust generated at the East Pacific Rise to the crust generated at the Galapagos Spreading Centre is believed to occur (von Huene et al., in press). This hypothesis is mainly supported by magnetic anomalies, clearly related to the Galapagos spreading centre to the south, and some tectonic evidence. Along this line, 13 GEOMAR OBH (OBH150 to 162) were deployed on the 15.10 in the afternoon. A 60 nm long line was shot at 3.8 kn with a 60 s shot interval from 20:00 on 15 October to 12:00 on 16 October. The magnetometer was deployed during shooting. The location of the profile and the instruments is shown in Figure 6.2.4.7.1, details of shots and receivers can be found in Appendices 9.1.7 and 9.2.

Seismic sections (Figures 6.2.4.7.2 to 6.2.4.7.13) exhibit clear arrivals of up to 50 km offset. The bathymetry and the sediment thickness being more or less constant along the line we can infer some qualitative information on the crustal structure from the apparent seismic velocity. A wide-angle reflection, which could be interpreted as the PmP reflected from the Moho, appears on most of the seismic sections. To the southeast the reflection is clear from 15 to 35 km range (OBH159 to 162, figures 6.2.4.7.10 to 6.2.4.7.13) whereas it is less clear and probably at larger offset (> 25 km) to the northwest (OBH151 to 156, figures 6.2.4.7.3 to 6.2.4.7.8). This suggests that the crust could be thicker to northwest of the line than to the southeast supporting a different origin related to the activity of the East Pacific Rise and the Galapagos spreading centre respectively.

On all the record sections, second arrivals with a low apparent velocity are clear between 5 and 25 km range. These phases could be interpreted as PSP, converted from P to S beneath the shot point, travelling the crust as S waves and converted to P beneath the instrument. The conversion could occur at the sediment-basement interface. These phases will be used to process an S velocity model for the crust along this line.

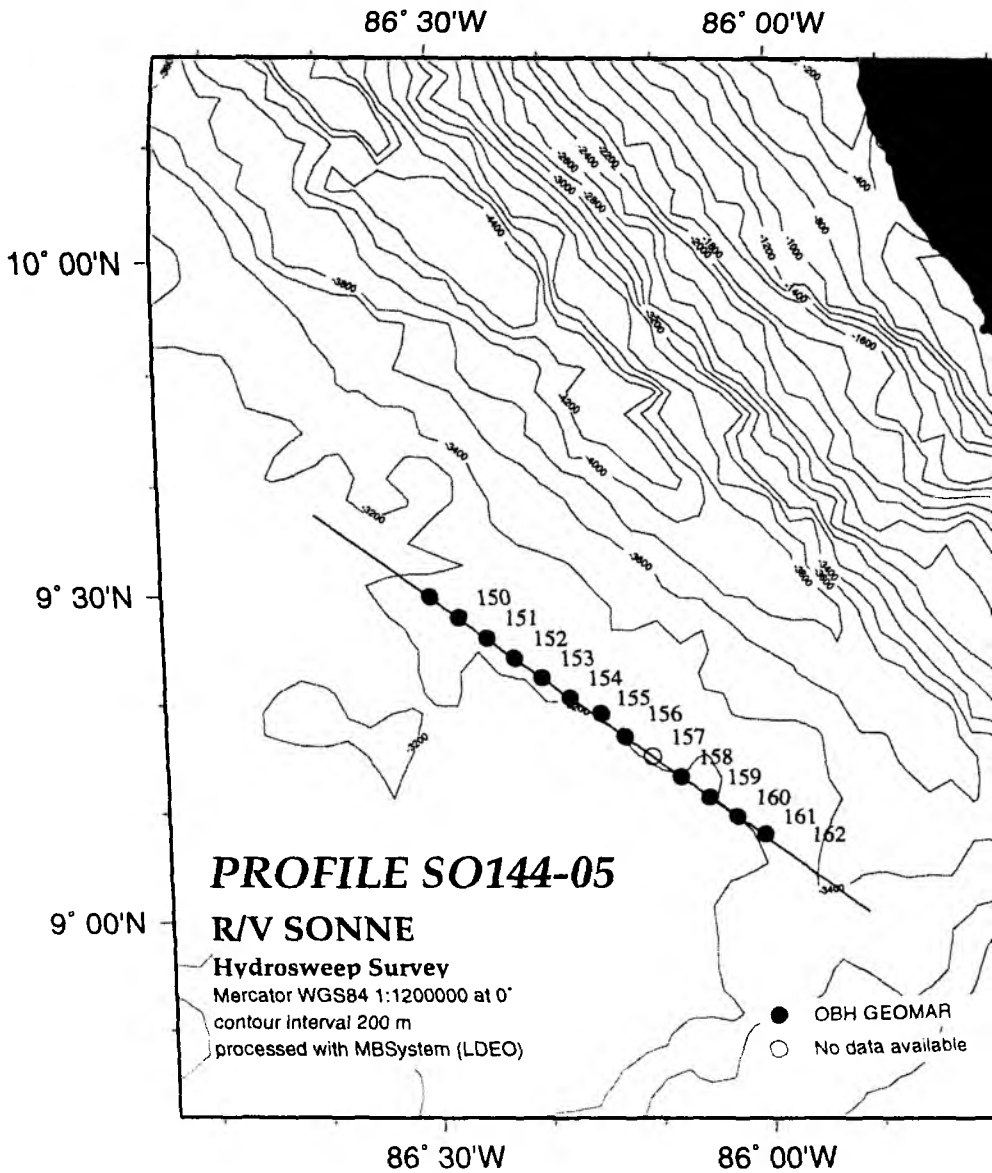

Figure 6.2.4.1: Profile SO144-05, Location map

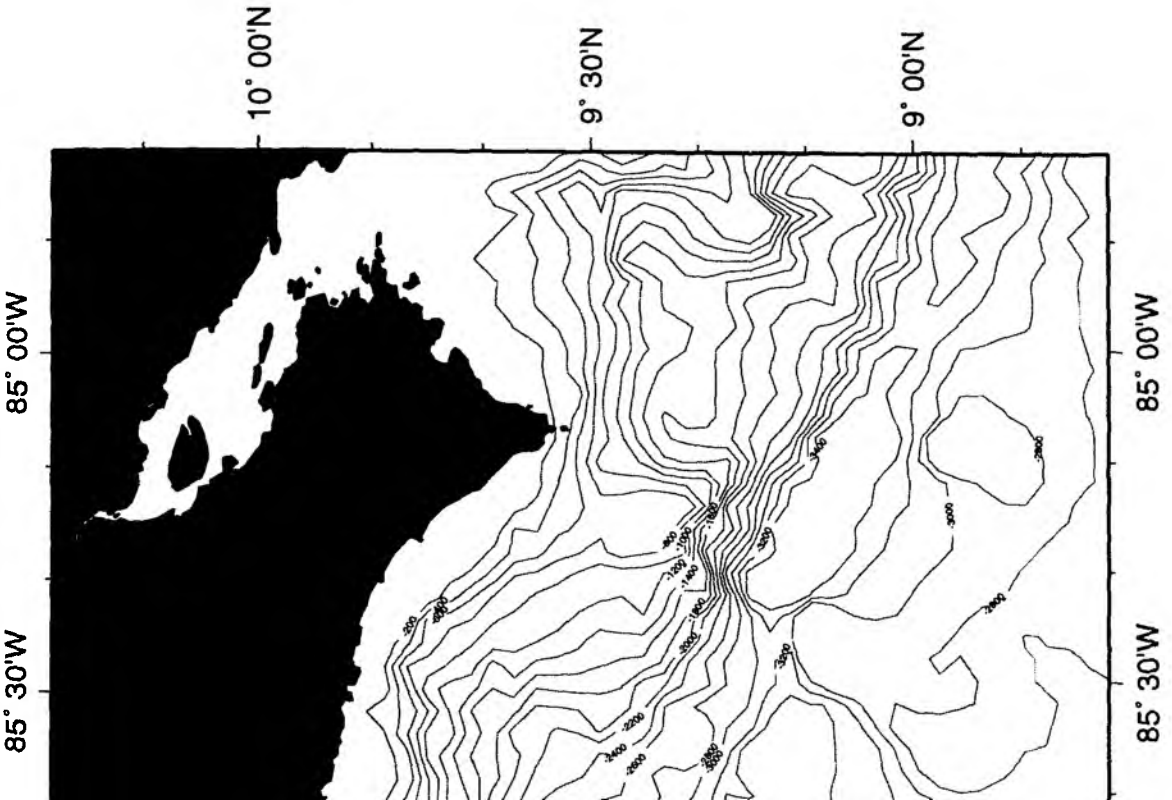
10° 00'N
9° 30'N
9° 00'N
85° 00'W
85° 30'W

6.2.4.7 PROFILE SO144-05

Profile SO144-05 is a short line shot seaward of the trench facing the Nicoya Peninsula, where the transition from crust generated at the East Pacific Rise to the crust generated at the Galapagos Spreading Centre is believed to occur (von Huene et al., in press). This hypothesis is mainly supported by magnetic anomalies, clearly related to the Galapagos spreading centre to the south, and some tectonic evidence. Along this line, 13 GEOMAR OBH (OBH150 to 162) were deployed on the 15.10 in the afternoon. A 60 nm long line was shot at 3.8 kn with a 60 s shot interval from 20:00 on 15 October to 12:00 on 16 October. The magnetometer was deployed during shooting. The location of the profile and the instruments is shown in Figure 6.2.4.7.1, details of shots and receivers can be found in Appendices 9.1.7 and 9.2.

Seismic sections (Figures 6.2.4.7.2 to 6.2.4.7.13) exhibit clear arrivals of up to 50 km offset. The bathymetry and the sediment thickness being more or less constant along the line we can infer some qualitative information on the crustal structure from the apparent seismic velocity. A wide-angle reflection, which could be interpreted as the PmP reflected from the Moho, appears on most of the seismic sections. To the southeast the reflection is clear from 15 to 35 km range (OBH159 to 162, figures 6.2.4.7.10 to 6.2.4.7.13) whereas it is less clear and probably at larger offset (> 25 km) to the northwest (OBH151 to 156, figures 6.2.4.7.3 to 6.2.4.7.8). This suggests that the crust could be thicker to northwest of the line than to the southeast supporting a different origin related to the activity of the East Pacific Rise and the Galapagos spreading centre respectively.

On all the record sections, second arrivals with a low apparent velocity are clear between 5 and 25 km range. These phases could be interpreted as PSP, converted from P to S beneath the shot point, travelling the crust as S waves and converted to P beneath the instrument. The conversion could occur at the sediment-basement interface. These phases will be used to process an S velocity model for the crust along this line.

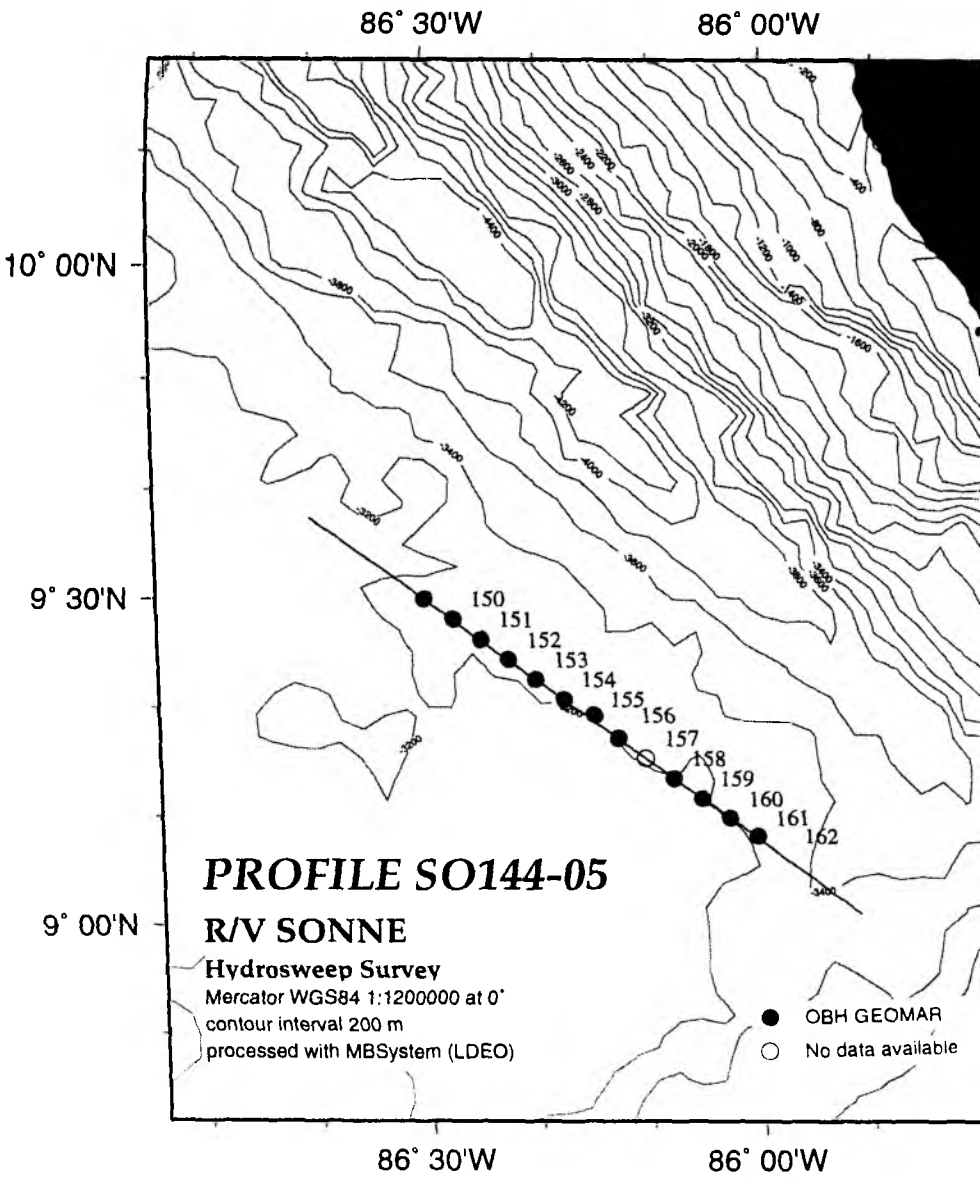

Figure 6.2.4.7.1: Profile SO144-05, Location map

85° 30'W
85° 00'W
10° 00'N
9° 30'N
9° 00'N
85° 30'W
85° 00'W

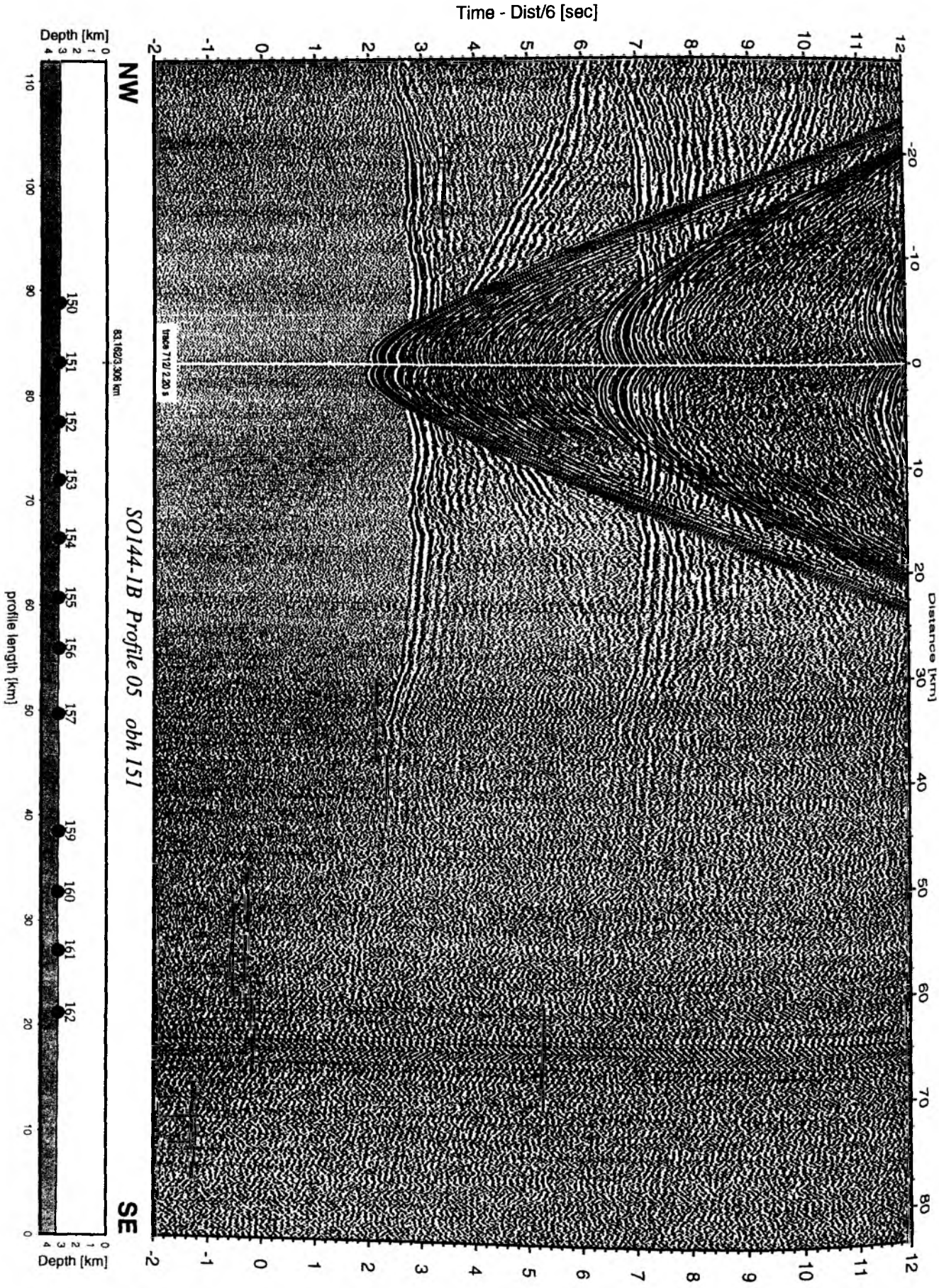

Figure 6.2.4.7.3: Record section from obh 151 , Profile 05.

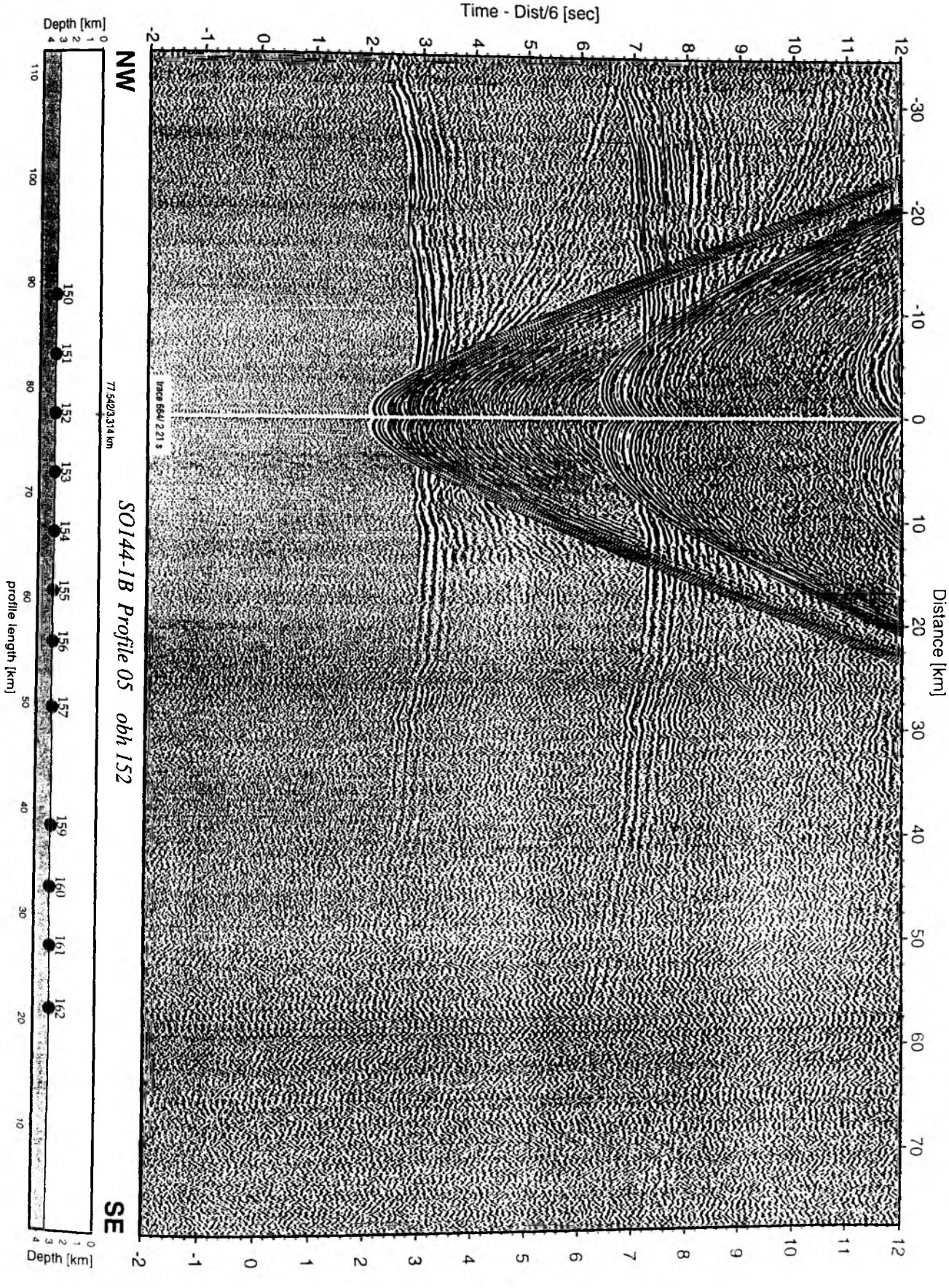

Figure 6.2.4.7.4: Record section from obh 152 , Profile 05.

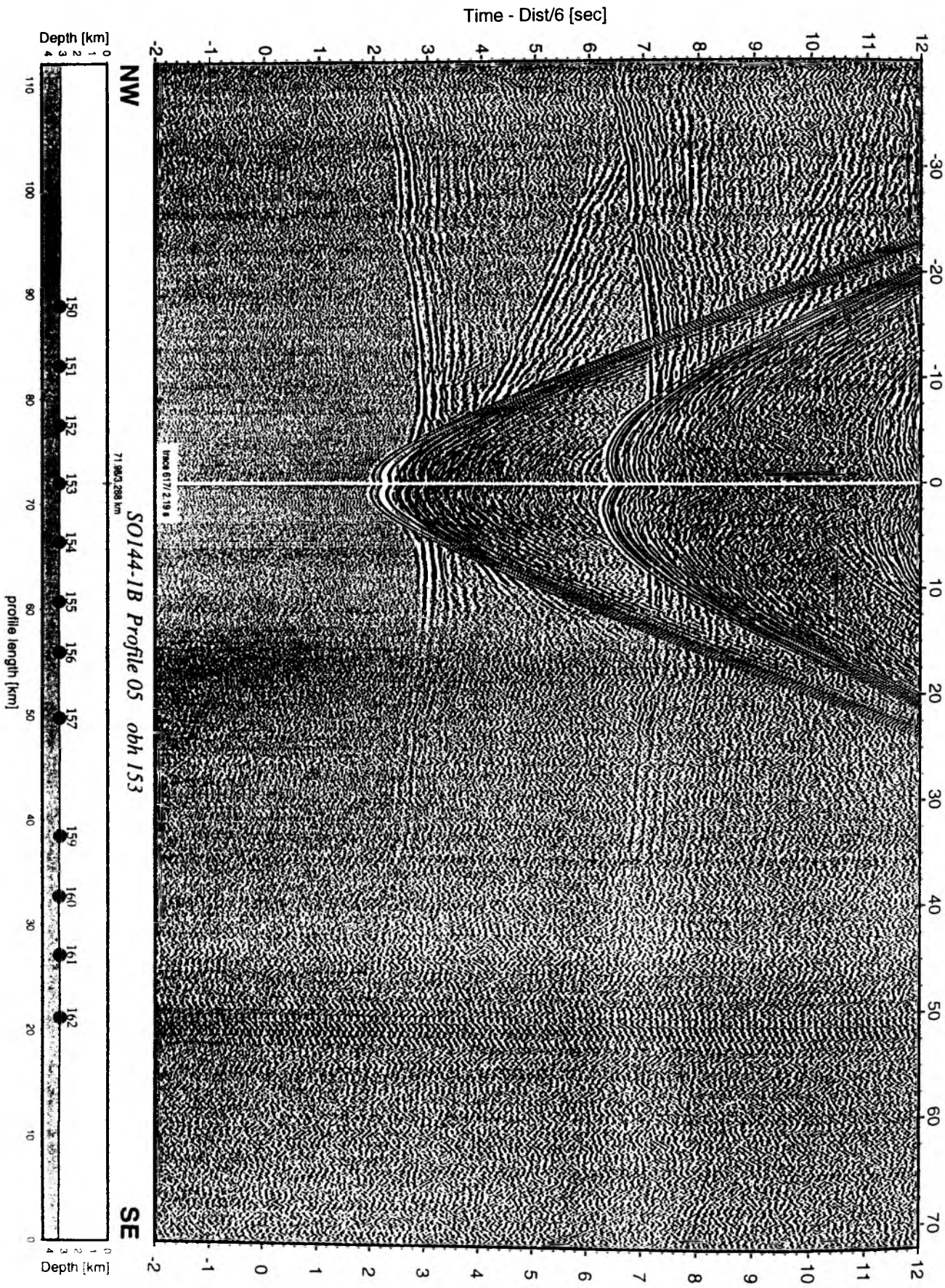

Figure 6.2.4.7.5: Record section from obh 153 , Profile 05.

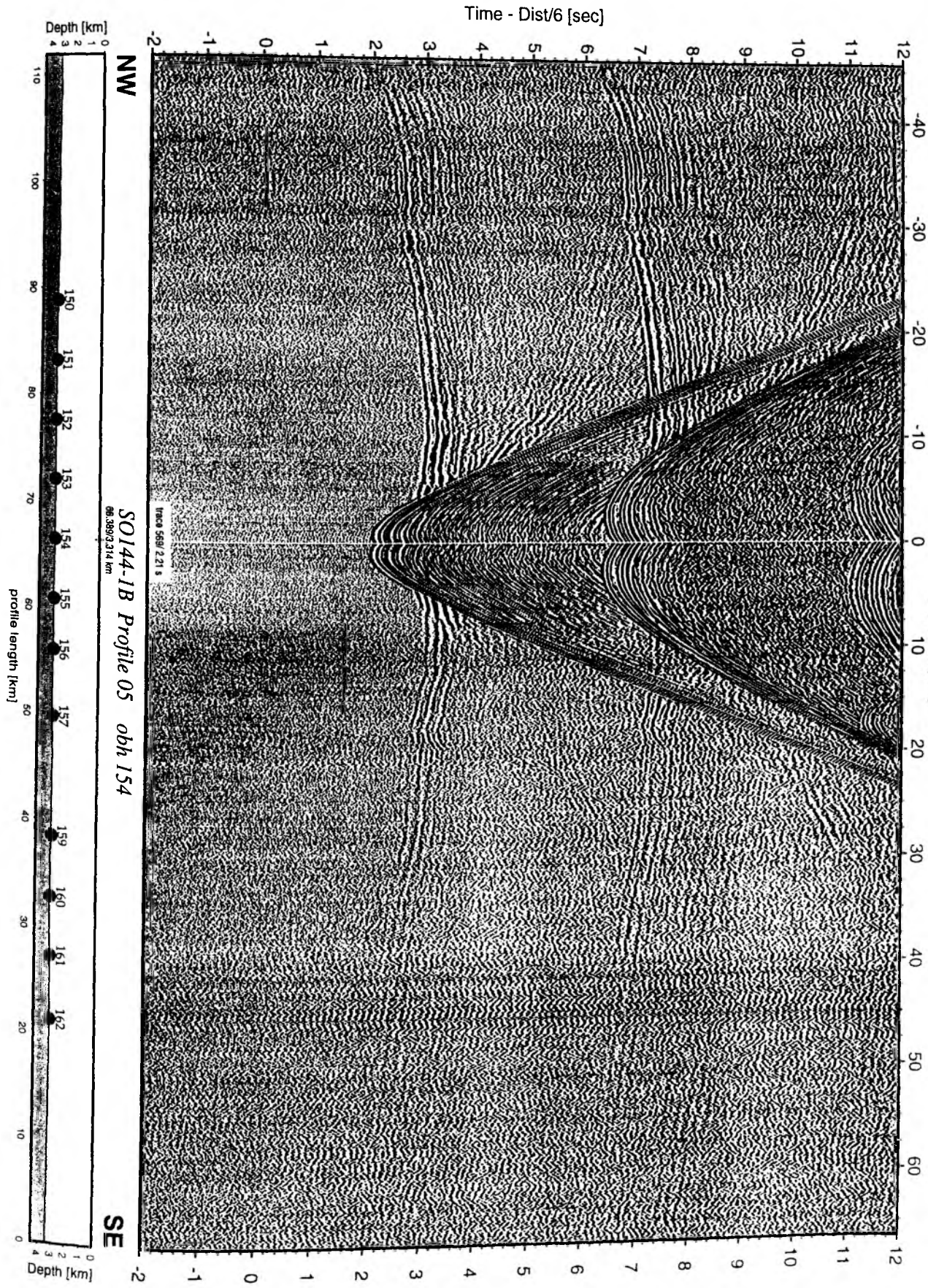

Figure 6.2.4.7.6: Record section from obh 154 , Profile 05.

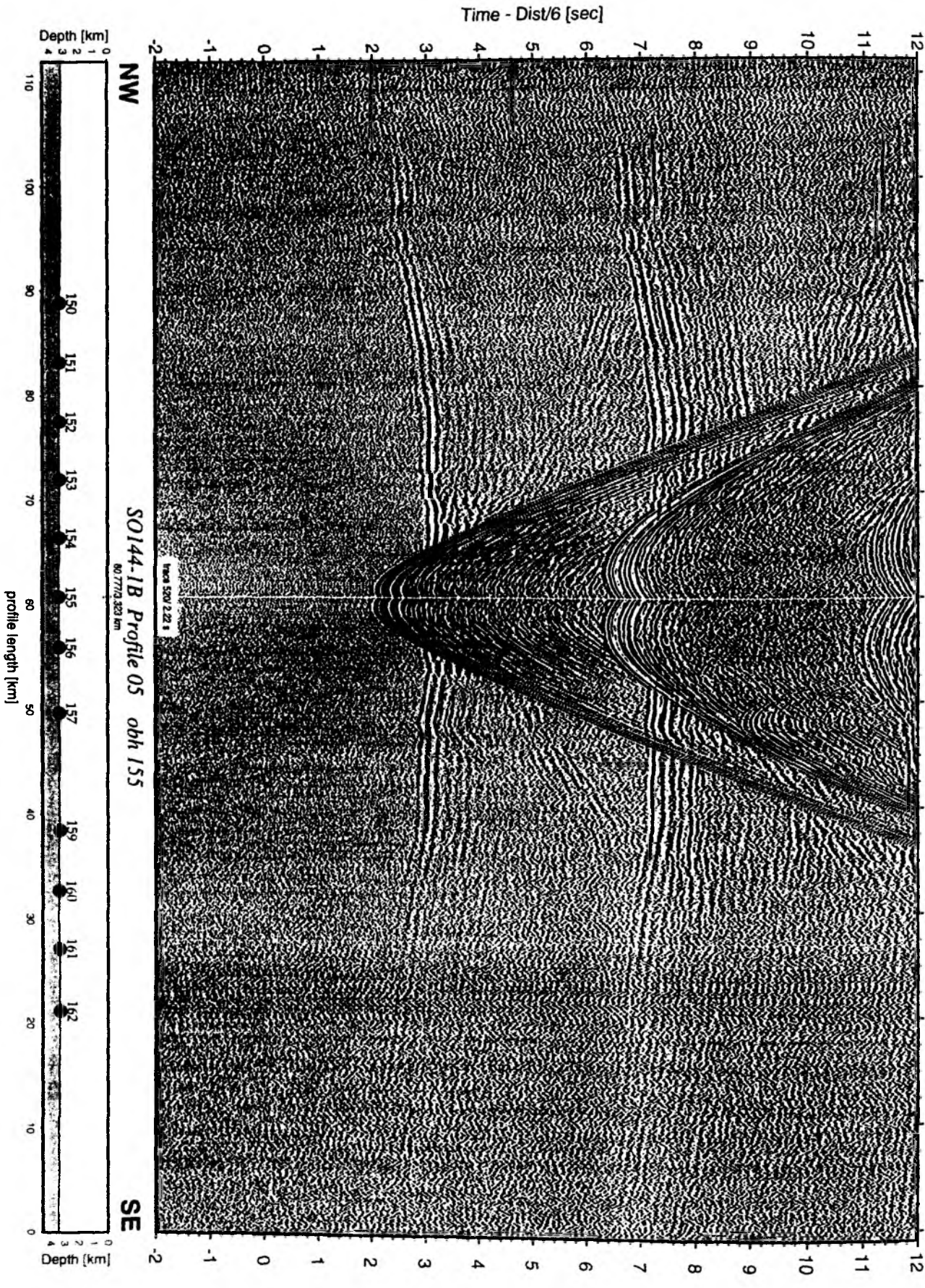

Figure 6.2.4.7.7: Record section from obh 155 , Profile 05.

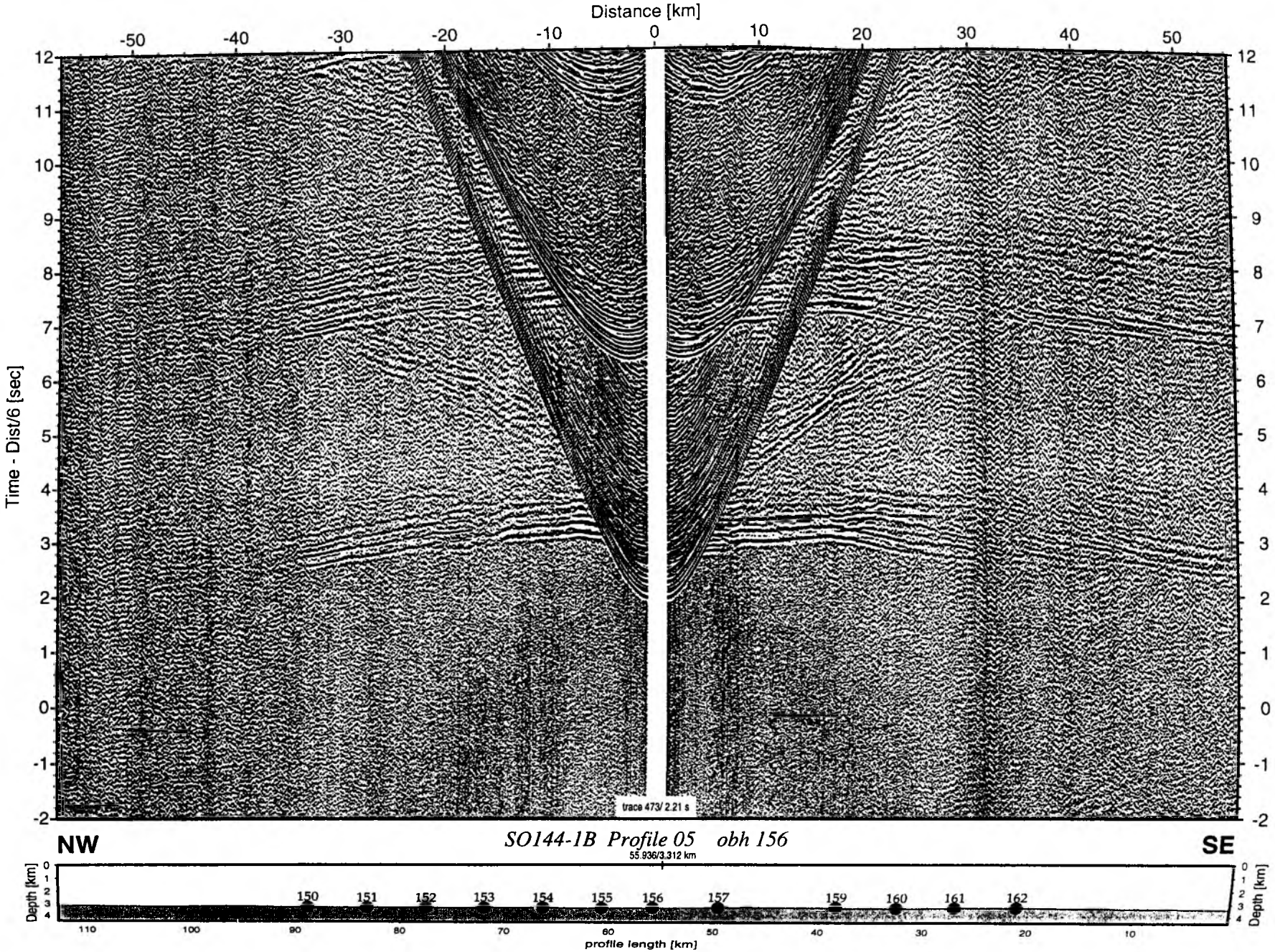

Figure 6.2.4.7.8: Record section from obh 156 , Profile 05.

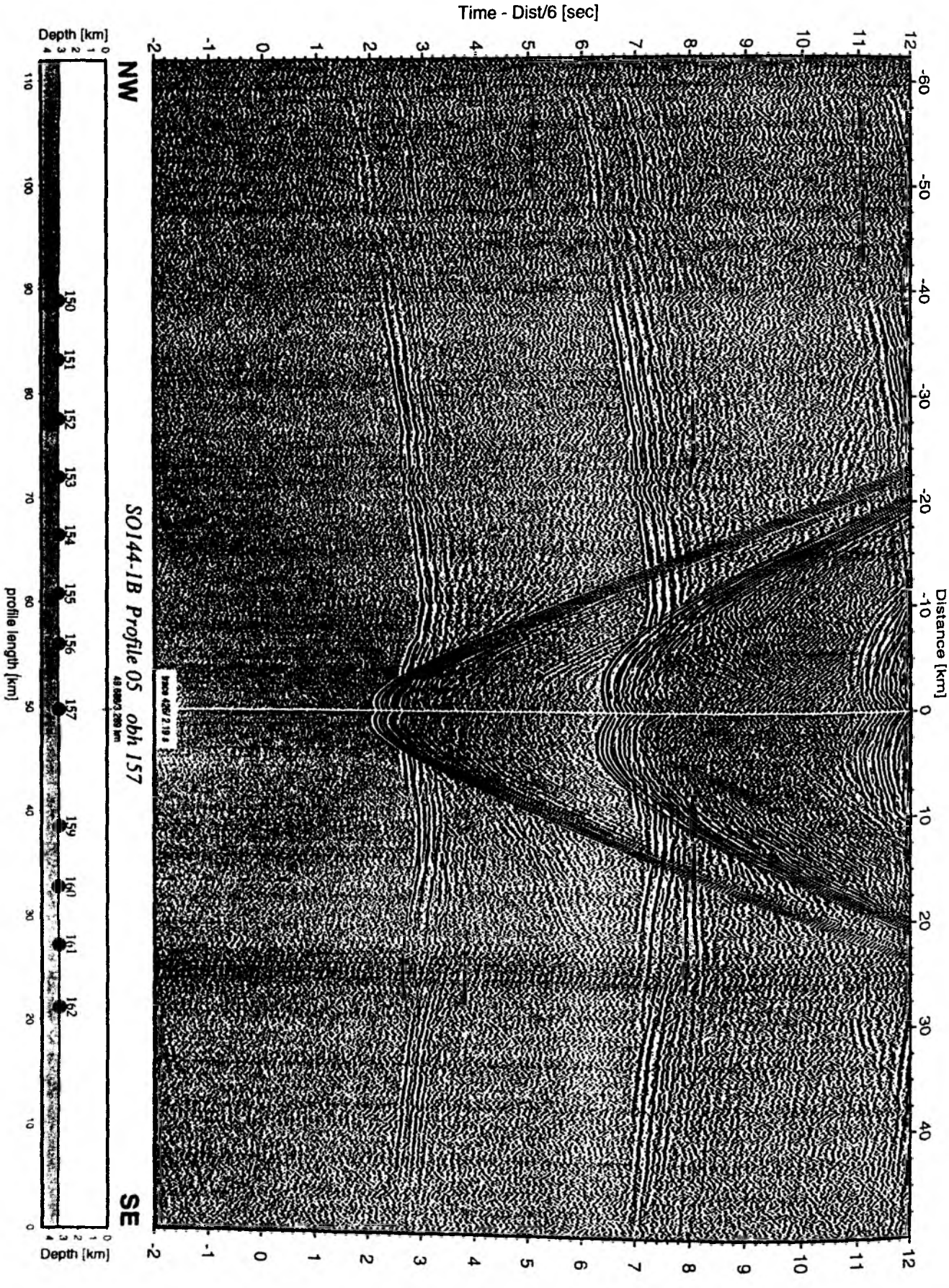

Figure 6.2.4.7.9: Record section from obh 157 , Profile 05.

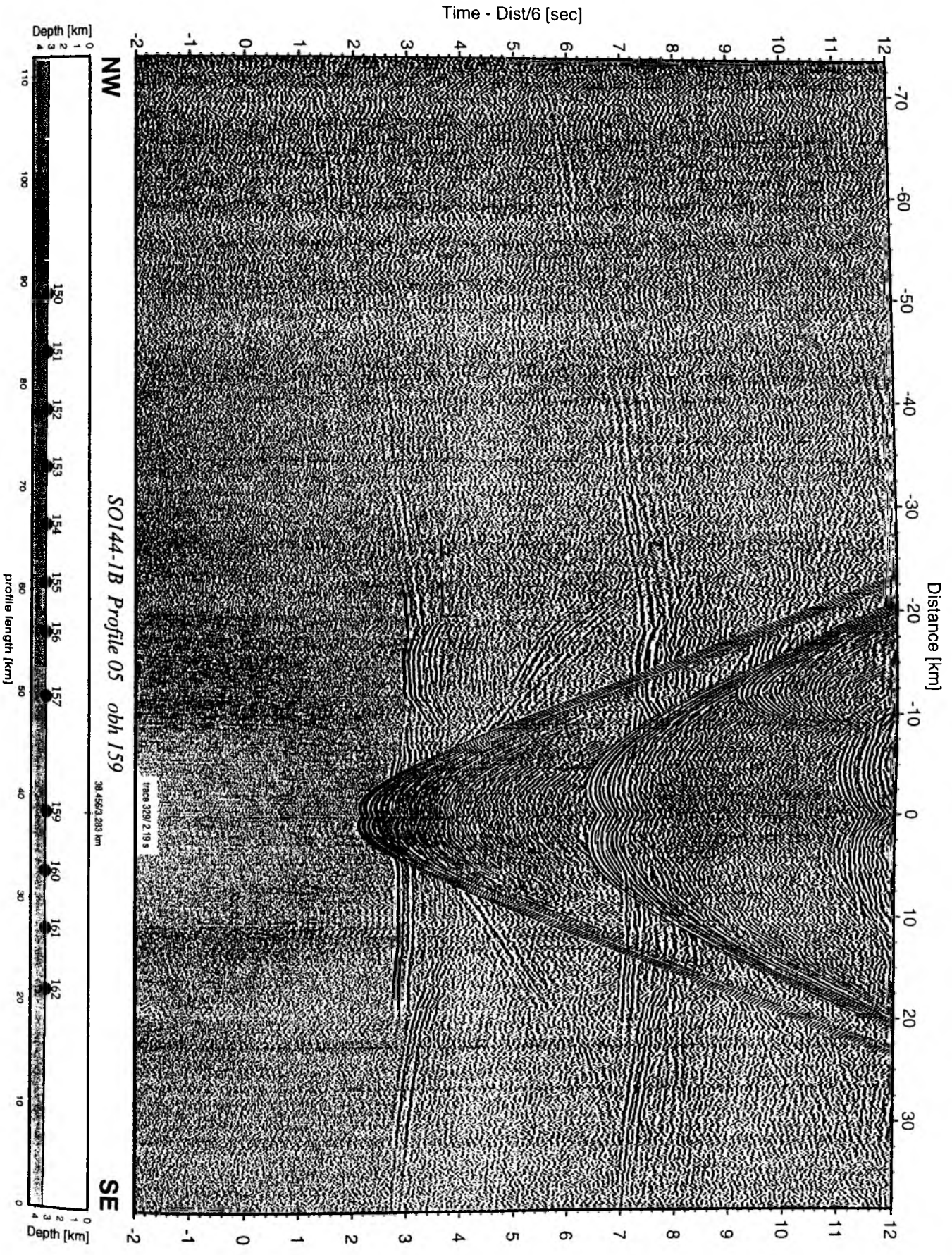

Figure 6.2.4.7.10: Record section from obh 159 , Profile 05.

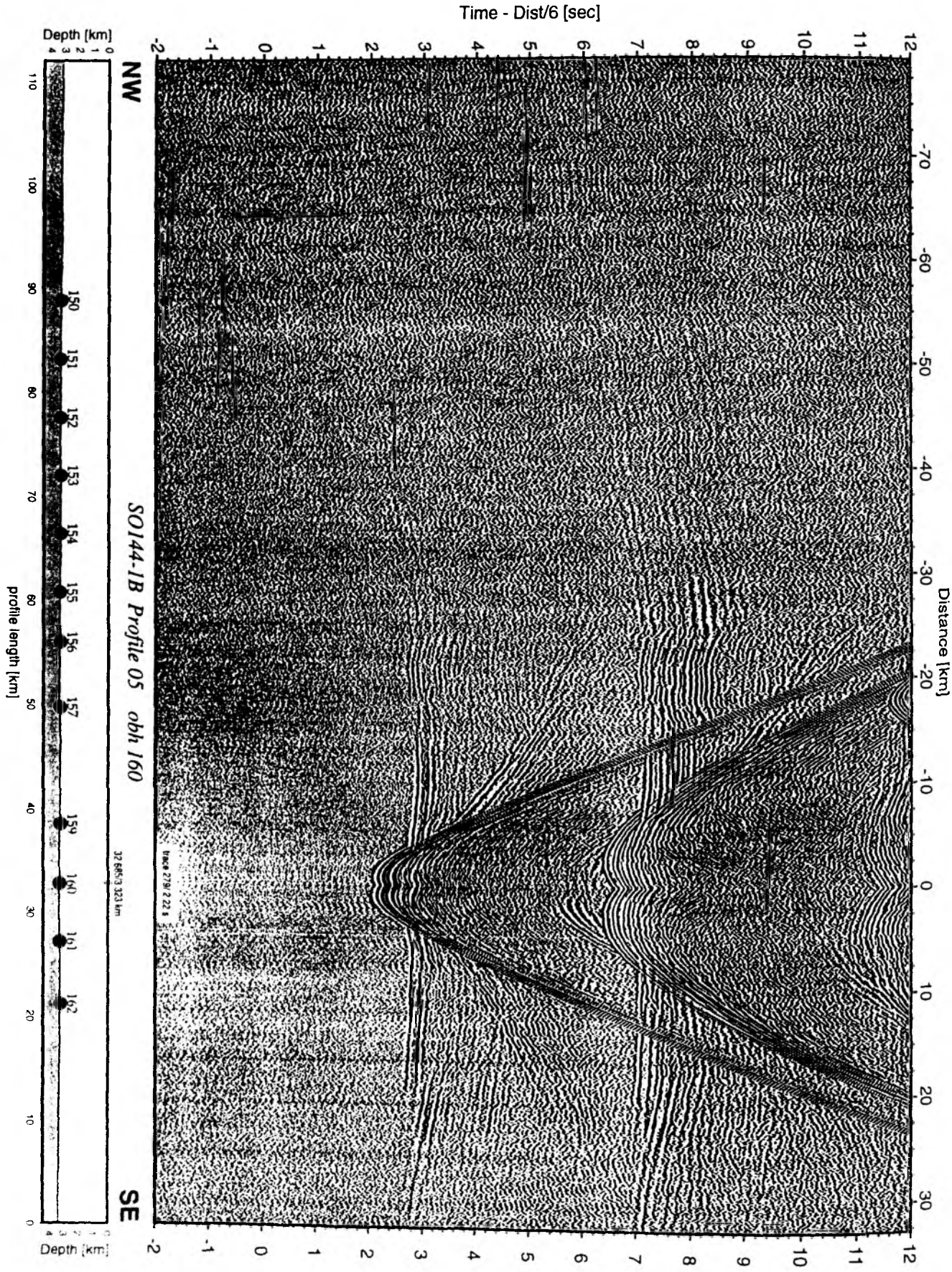

Figure 6.2.4.7.11: Record section from obh 160 , Profile 05.

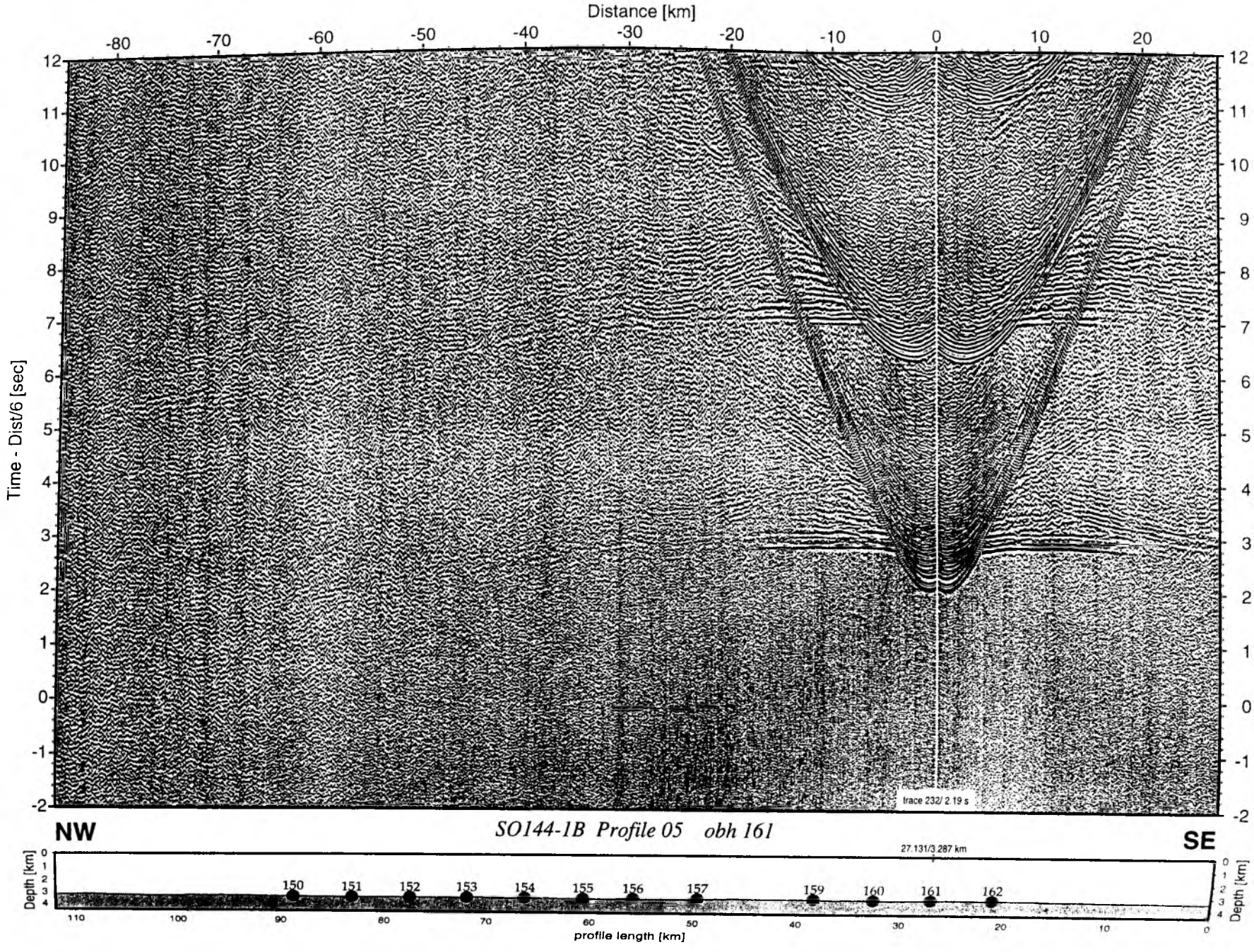

Figure 6.2.4.7.12: Record section from obh 161 , Profile 05.

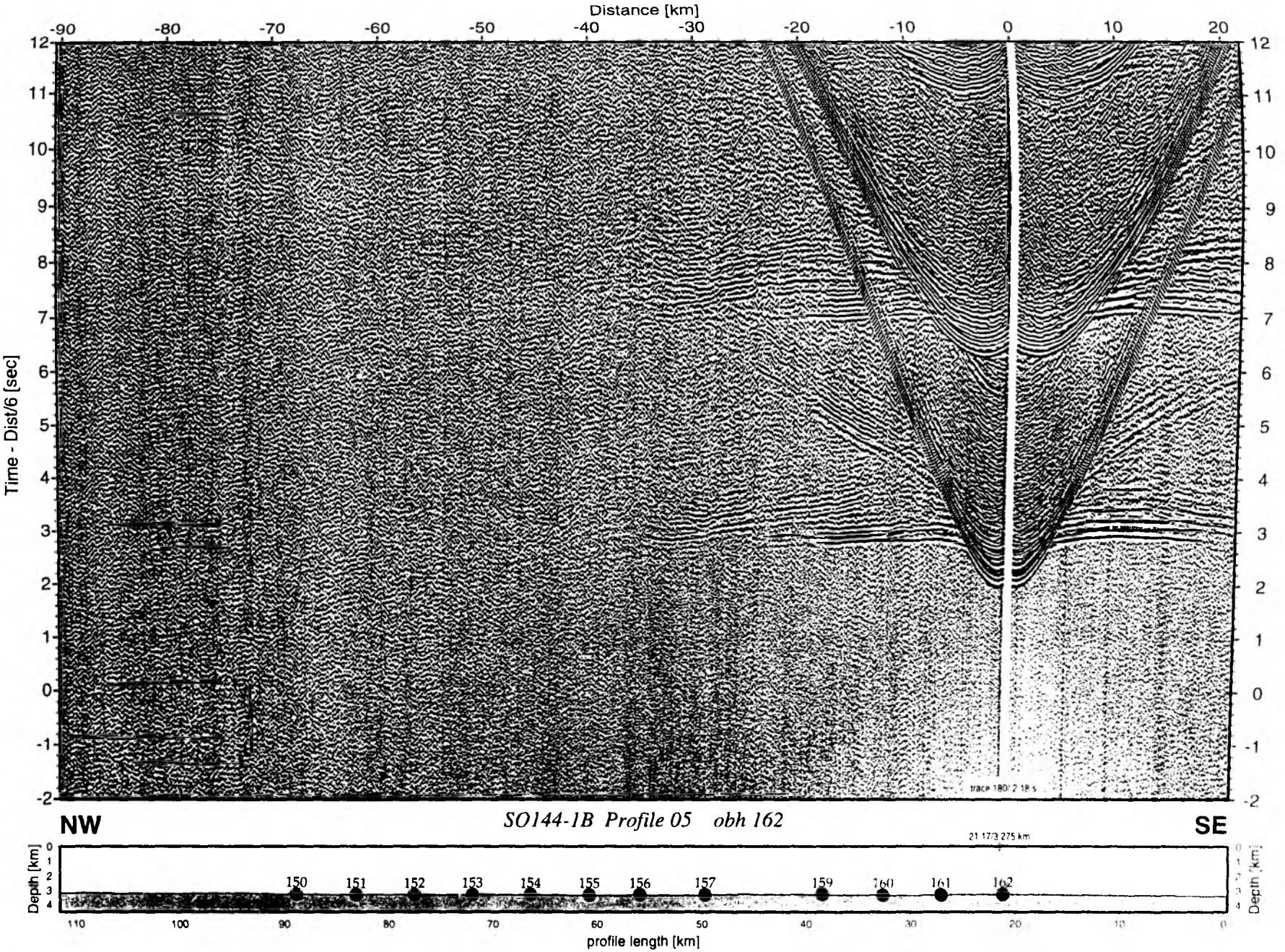

Figure 6.2.4.7.13: Record section from obh 162 , Profile 05.

6.3. MAGNETIC DATA

(J. Petersen, I. Schaffer, C. R. Ranero, R. von Huene, and watchkeepers)

Data Acquisition

For marine acquisition, where recording is carried out at relatively low speed (10 to 12 knots), a sampling rate of 3 seconds was considered sufficient to subsequently process (e.g. filtered) data and to record the long wavelength variation of the magnetic anomalies (5 to 20 km in the area). Magnetic data collected during SO144-1a are shown in Figure 6.3.1 together with tracks from previous cruises (SO76 and SO107). Tracks along which data were collected during SO144-1b and SO144-2 are shown in Figures 6.3.2 and 6.3.3. Magnetic data were acquired systematically only off NW Nicoya Peninsula (Figures 6.3.1 and 6.3.4) and during some transit tracks off Central and Southern Costa Rica, and along profiles across the Cocos and Malpelo Ridges. A total amount of 6363 km of magnetic data was recorded. A list of all profiles is given in appendices 9.3.1 to 9.3.3.

Data Processing

Quality control, preliminary data processing and presentation were done onboard. In order to process the magnetic data, ASCII files of raw data were transferred to a Sun workstation. Processing consisted of filtering, resampling and merging the magnetic data with the differential GPS navigation from the ship. Optimal smoothing was achieved with a median filter of 240 s. The anomalies were plotted along track after merging with the navigation. No corrections for diurnal variations have been carried out so far. Thus, no gridding with pre-existing data sets (Barkhausen, 1998, Barkhausen et al., 1999) was accomplished.

First Results

The data collected off NW Nicoya Peninsula, shown as along track anomalies in Figure 6.3.4 (after removing an arbitrary value of increasing amount with latitude), correlate well with the anomalies along tracks collected during SO107. The track collected south of the low scarp off the central Nicoya Peninsula and possibly marking a boundary in the ocean plate shows anomalies that fit well with the NE - SW anomalies observed on previous tracks. The lines collected NW of the scarp show anomalies that might indicate a roughly NW-SE trend and thus support the interpretation obtained from SO107 and bathymetry that the scarp is the fossil trace of the boundary separating lithosphere formed at the Galapagos and the East Pacific Rise respectively. However, the data will be fully processed ashore by correcting for diurnal variations before this interpretation can be confirmed. Anomalies across the slope have a larger amplitude, but again a better interpretation must await full processing and integration with existing data.

Data were also collected in a gap between the SO76 and SO107 data across the flank of Cocos Ridge along 7 tracks (Fig 6.3.1 and 6.3.2). These data should remove an uncertainty in identifying individual anomalies across the crest of Cocos Ridge.

During the second leg of SO144-1 further magnetic data were collected raising the total alongtrack length to 5670 km. In addition to the first leg, a reduction for the Earth's magnetic field of internal origin, i.e. subtraction of the International Geomagnetic Reference Field (IGRF), was applied.

However, using a single sensor, the data are inherently affected by charged particle flows in the Earth's magnetic field rising from the solar wind. Thus, a quality check was performed with data obtained on parallel tracks. In Figure 6.3.5, total magnetic field intensity (a), IGRF (b), remaining anomalies after IGRF reduction (c) and bathymetry (d) are displayed for three profiles running across the flank of Cocos Ridge. The correlation of the anomalies between the lines is reasonably good, therefore a malfunction of the magnetometer can be excluded. However, some amplitudes in the western part show a considerable degree of deviation (up to 400 nT). This could display the complex magnetic structure typical for ridges, but the impact of diurnal variations (S_q variation) and magnetic storms is also clearly visible. Parallel profiles lying along strike of Cocos Ridge display good correlations as well (Figures 6.3.6, 6.3.7).

When approaching Malpelo Ridge during profile 117, data quality increasingly deteriotated. Therefore it was decided to renew the gasoline filling, after which the magnetometer worked well again until the end of cruise SO144-1b. Data acquired along parallel tracks running perpendicular to Malpelo Ridge are displayed in Figure 6.3.8 and reveal a good correlation of amplitudes.

On cruise SO144-2 magnetic data were collected during TOBI surveys and on transit profiles. At the beginning of the 2nd TOBI profile suddenly unrealistic values were measured. Since another refilling of gasoline did not improve the results, the cable and all the connections were tested for possible failures. Unfortunately, the sensor got lost when approaching a Costa Rican fishing vessel during a rescue manoever. It took one more day to reinstall an older sensor available with a cable length of 200m. Data quality was surprisingly good until the end of the cuise. Fig. 6.3.9 shows alongtrack anomalies acquired during TOBI profile 6. As on cruise SO144-1b, a reduction for the Earth´s magnetic field (IGRF) was applied. In fig. 6.3.10 some of the calculated anomalies for parallel profiles can be seen. They show a good correlation of amplitudes which also seem to correlate well with topography. Data of profile 6, for example, clearly characterize Fisher seamount (fig. 6.3.11). Due to the lack of data in the middle of the TOBI survey (see also fig. 6.3.3) no 2-D interpretation of the data was done so far.

Magnetic anomalies tend to correlate with seafloor topography along some profiles showing negative anomalies at locations where the seafloor shallows abruptly (Figures 6.3.5, 6.3.6, 6.3.8). In general however, the anomalies seem to arise from the specific remnant magnetisation of the oceanic crust. Thus, it should be possible, after further corrections, to identify specific magnetic anomalies compared with a synthetic line calculated after the geomagnetic polarity time scale of Cande and Kent (1995).

The figures clearly show the necessity to correct for the above mentioned variations. To this effect, a southern Costa Rican magnetic observatory will provide the land-based reference station to enable correction for the variation in the Earth's magnetic field.

Figure 6.3.1: Track chart with magnetic data from SO76, SO107 (black) and SO144-1a (grey).

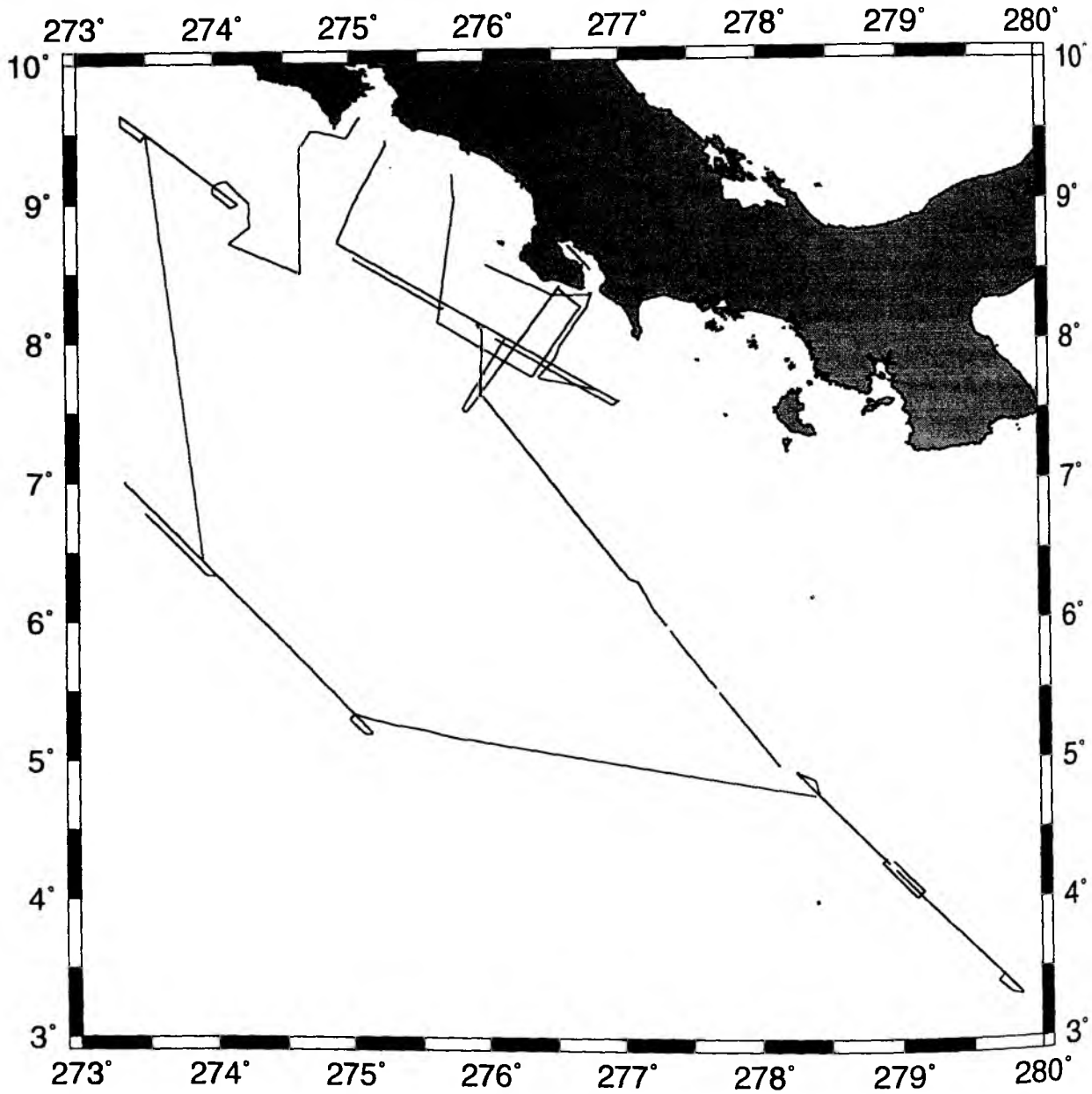

Figure 6.3.2.: magnetic tracks during SO144-1b.

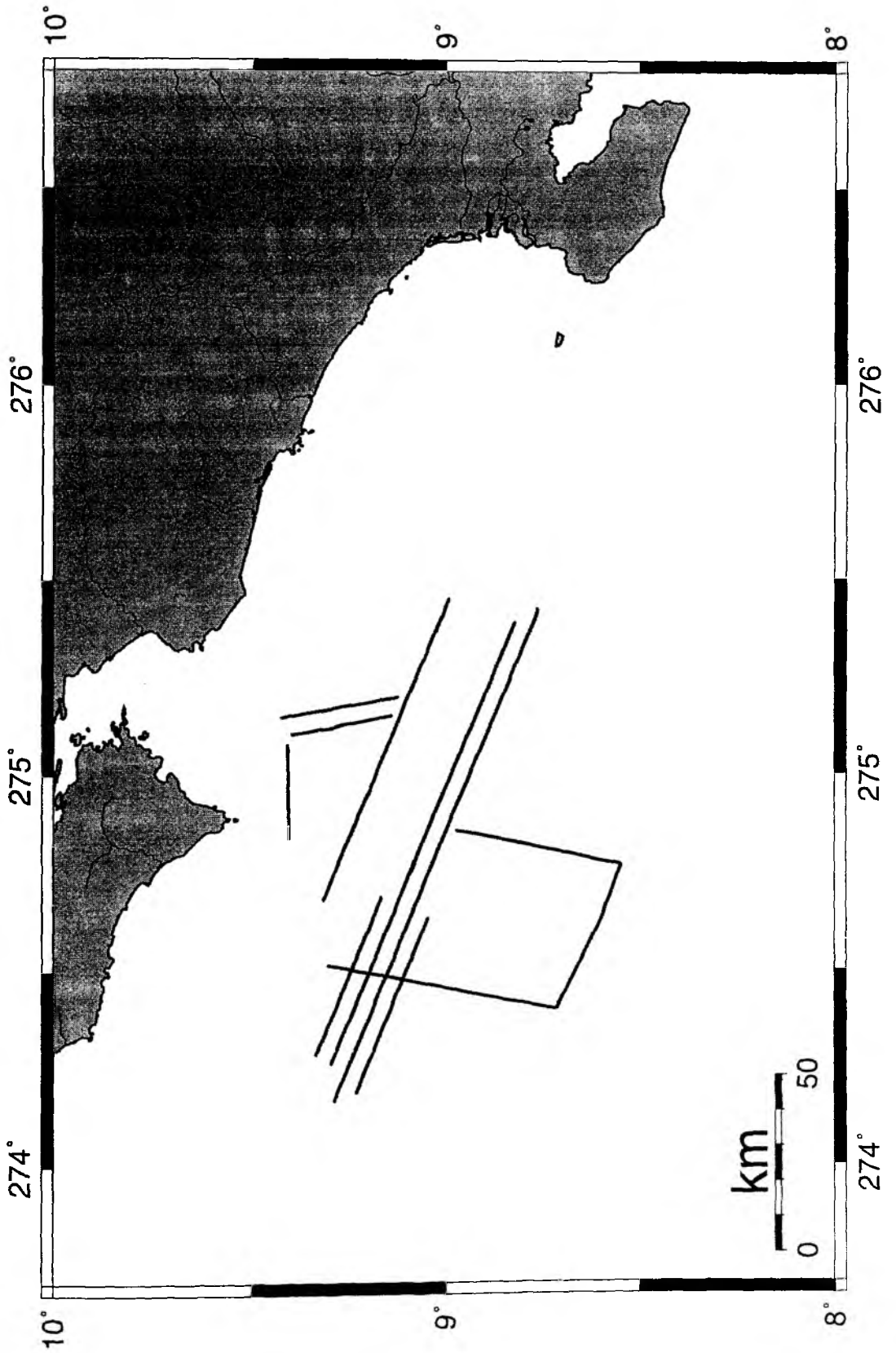

Figure 6.3.3: magnetic tracks during SO144-2

Figure 6.3.4: Alongtrack magnetic anomalies collected during SO107 and SO144.

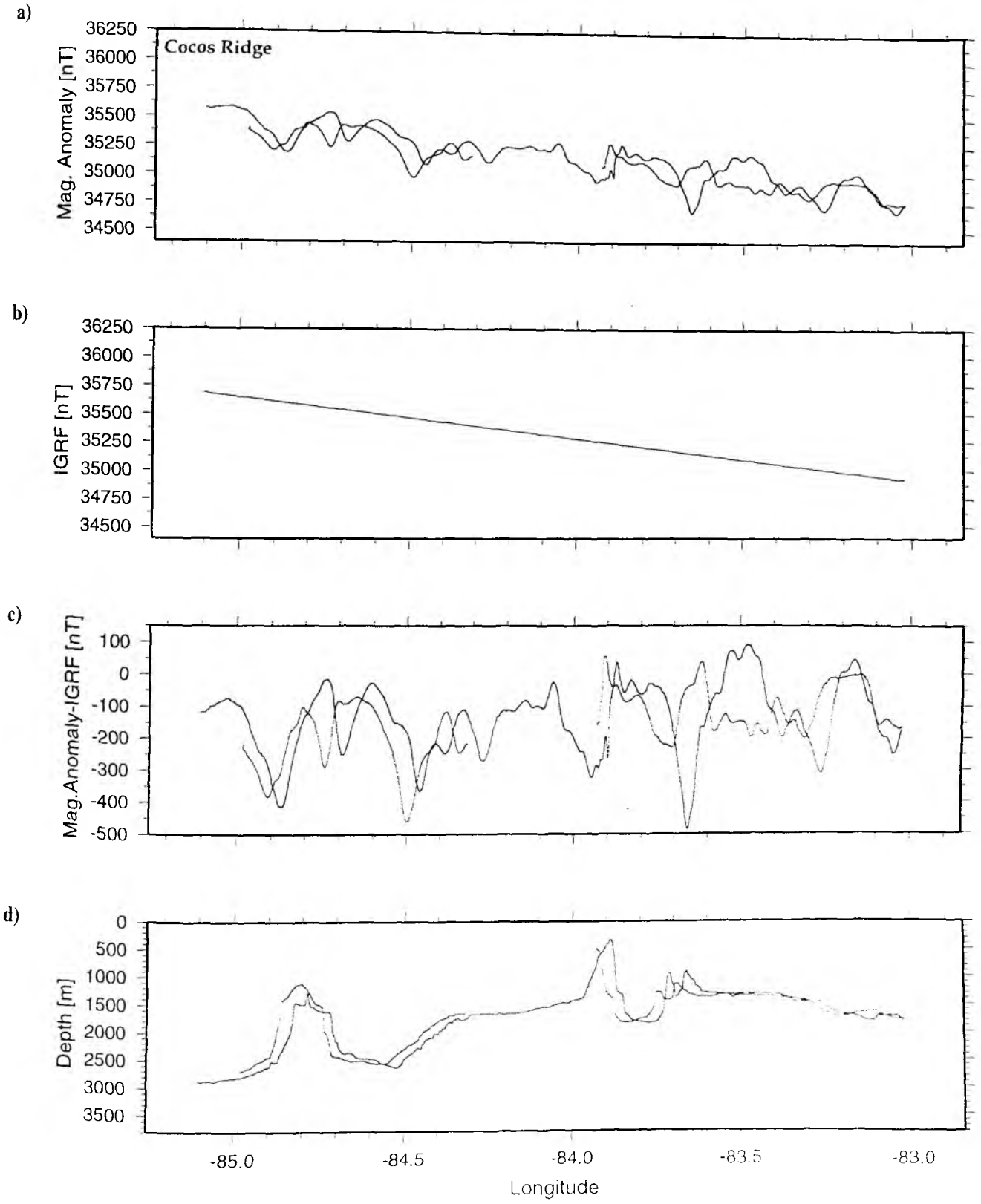

Figure 6.3.5: magnetic anomalies obtained on parallel running profiles 102, 103 and 104

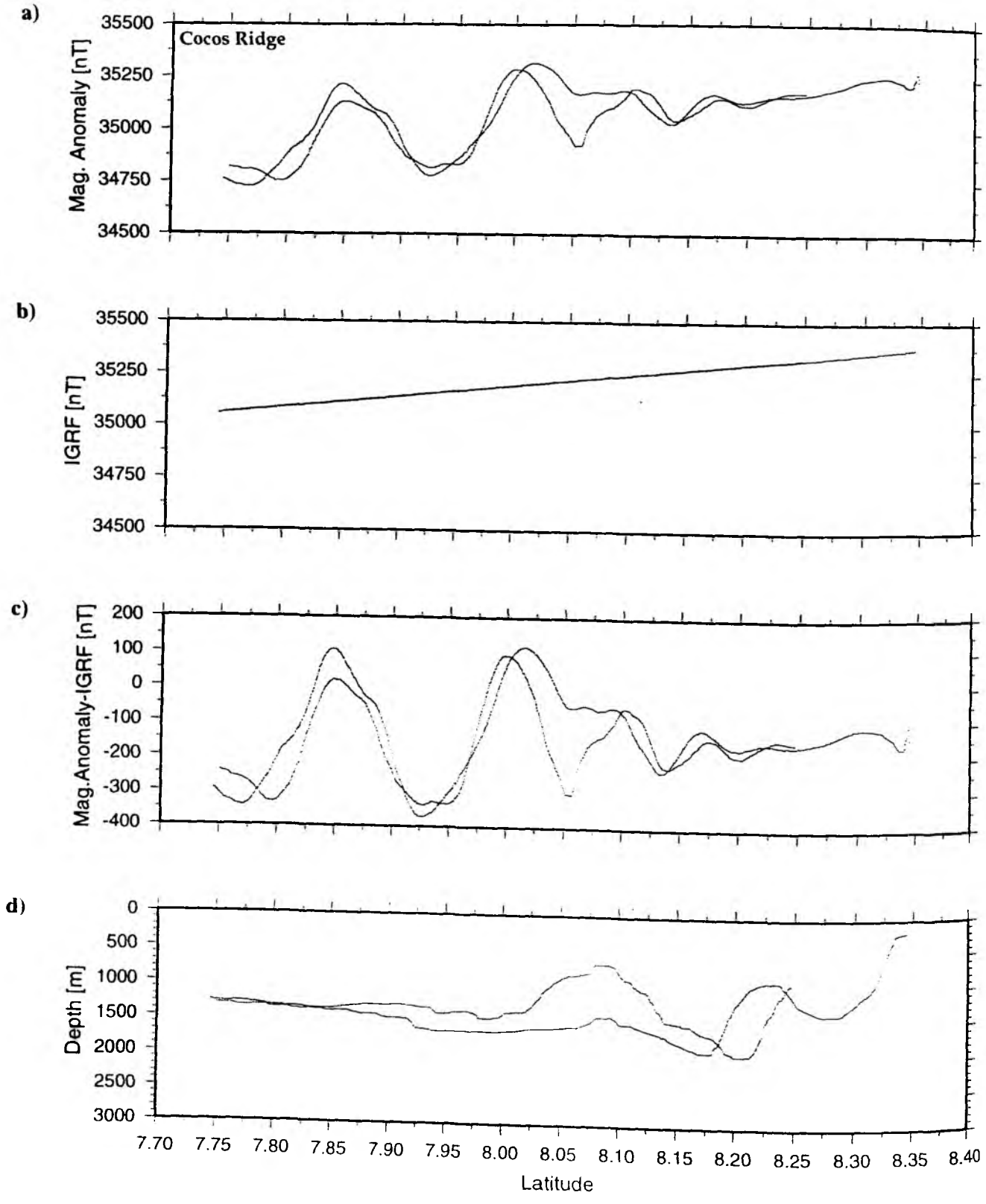

Figure 6.3.6: magnetic anomalies obtained on parallel running profiles 107 and 112b.

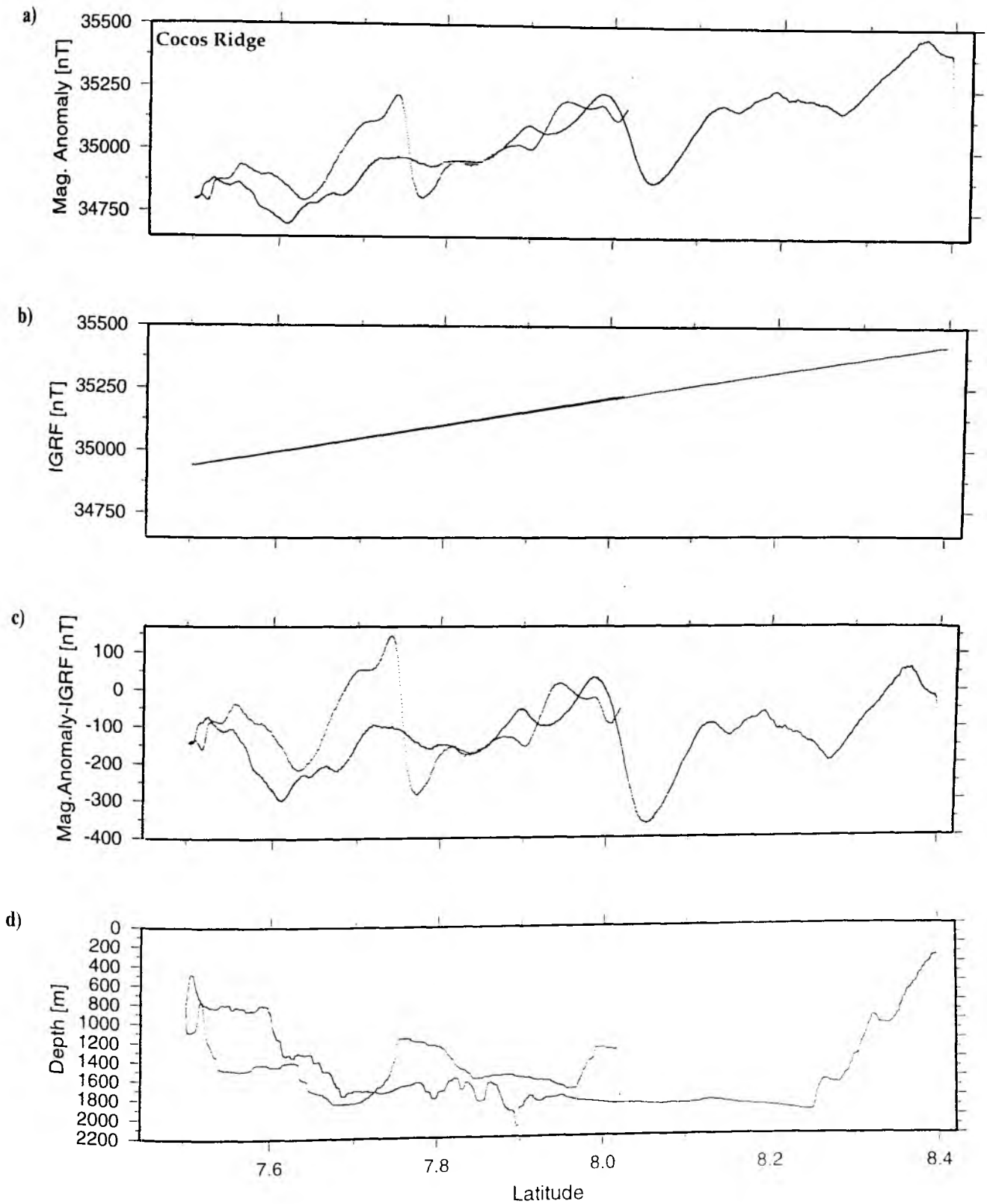

Figure 6.3.7: magnetic anomalies obtained along profile 116

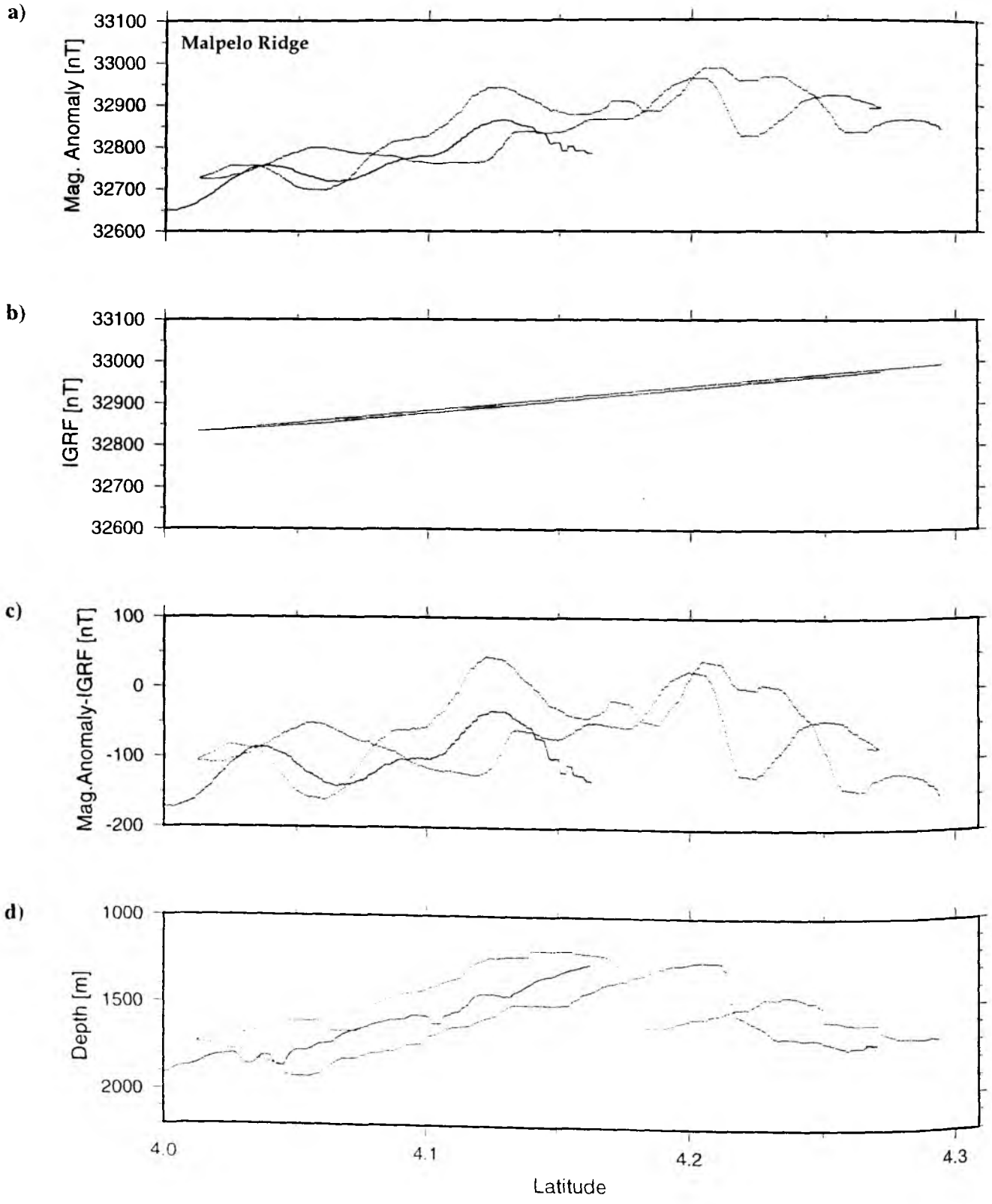

Figure 6.3.8: magnetic anomalies obtained on parallel running profiles 118 and 120

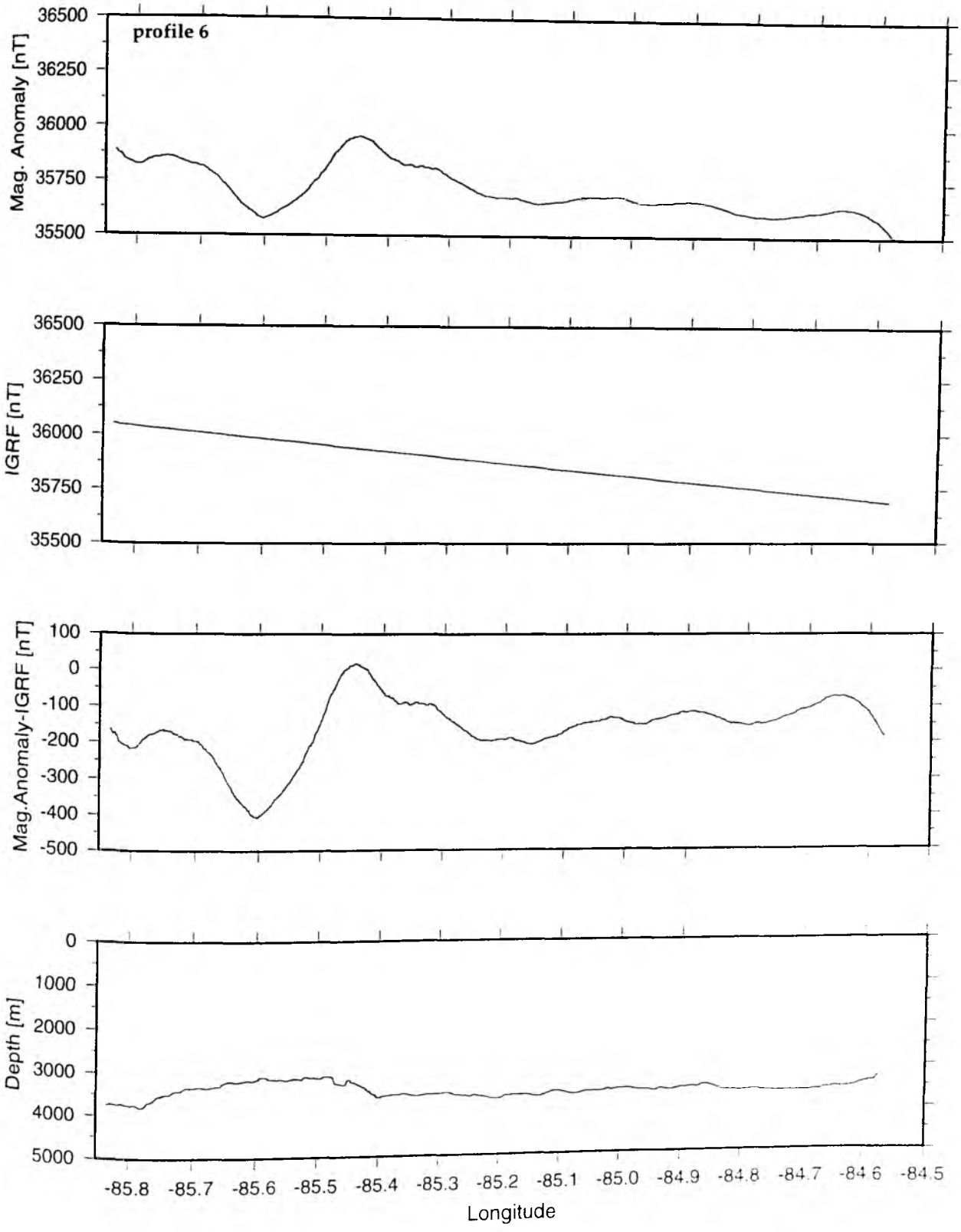

Abb.6.3.9: magnetic anomalies along profile 6 of TOBI survey

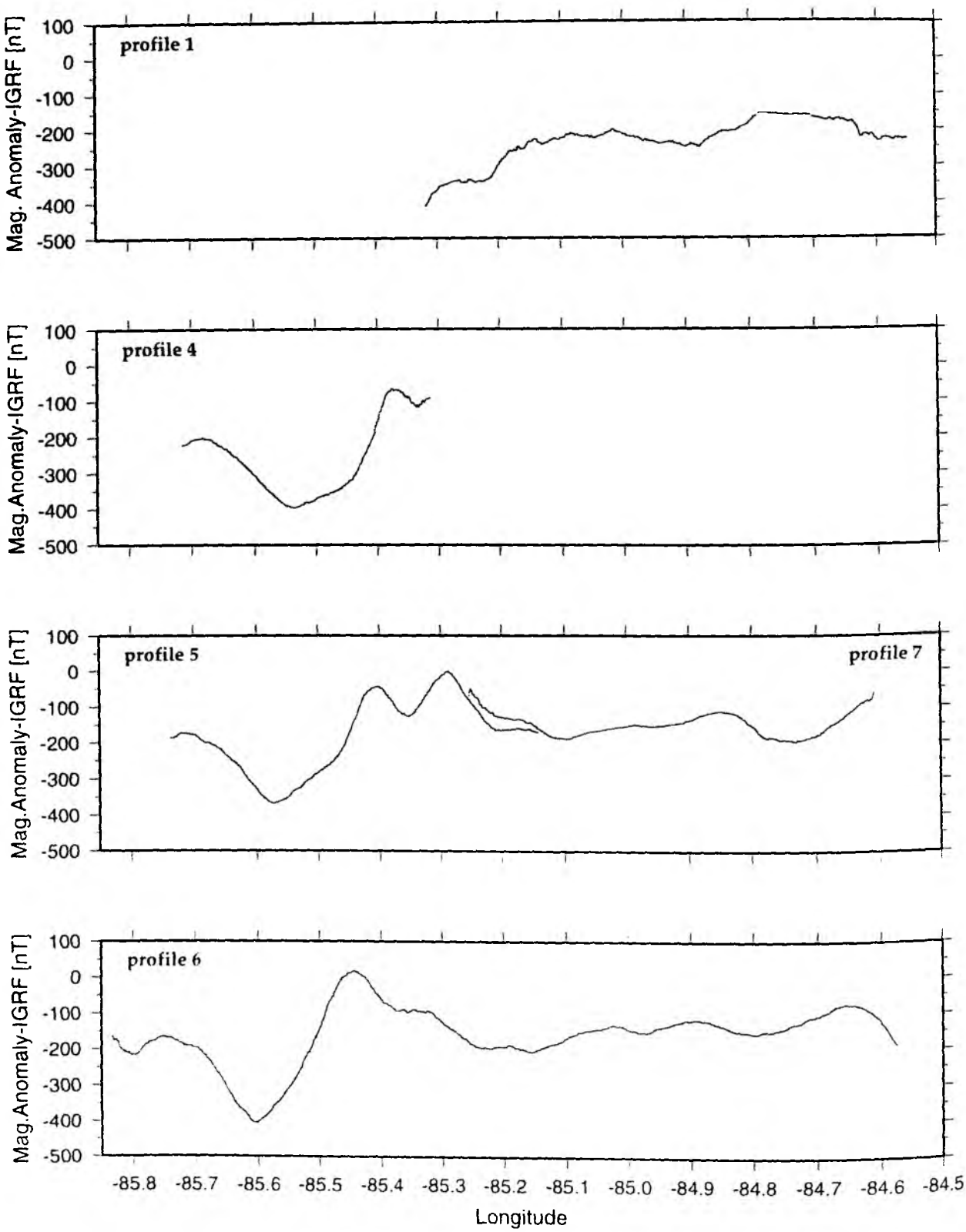

Figure 6.3.10: magnetic anomalies along profiles 1, 4, 5, 6 and 7 of TOBI survey

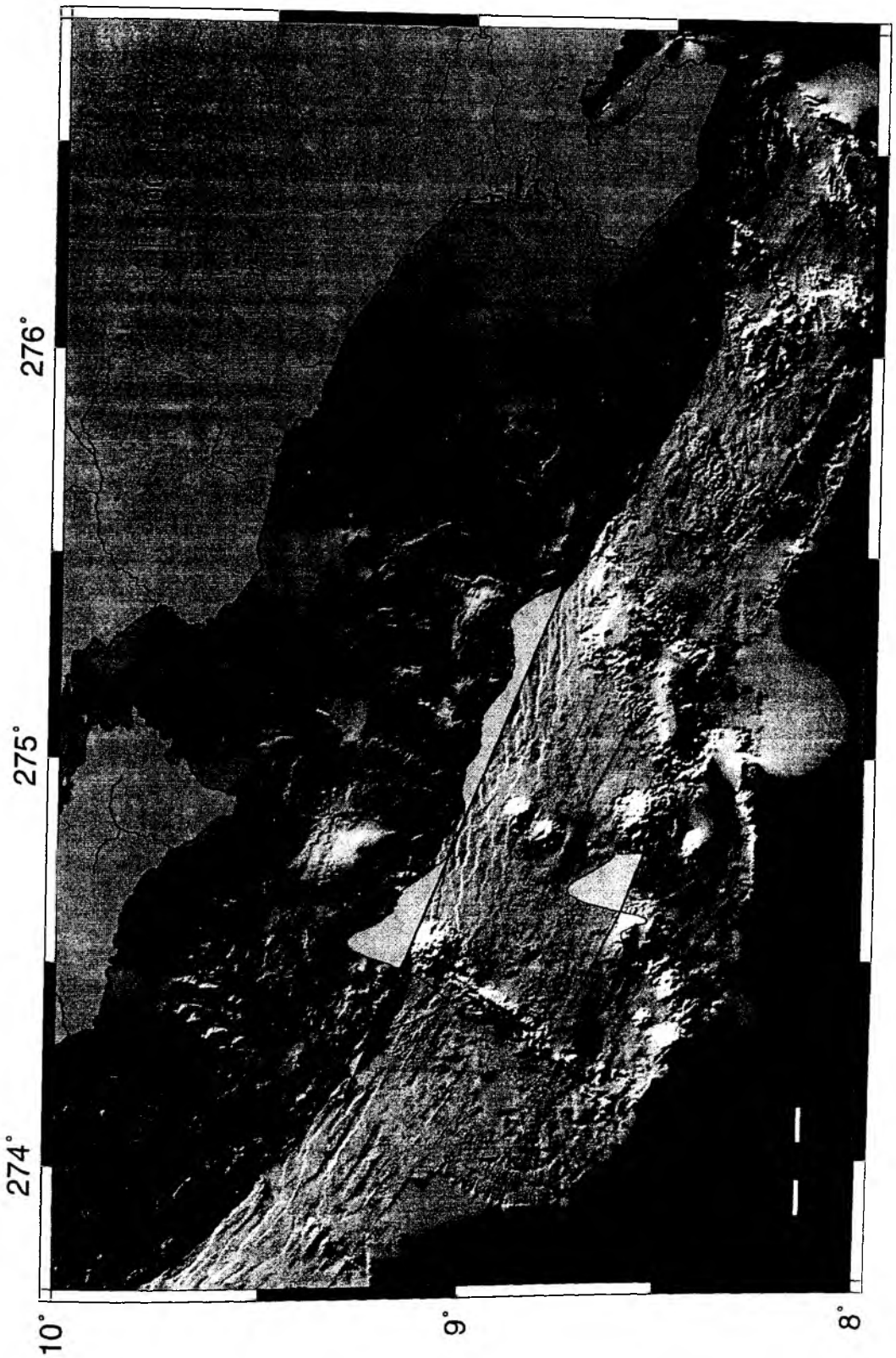

Figure 6.3.11: examples of alongtrack magnetic anomalies collected during TOBI surveys

6.4 SEISMOLOGICAL NETWORK

(LeRoy Dorman)

The goals of PAGANINI and the US NSF MARGINS programs overlap at the continental margin of Costa Rica. The US participation in PAGANINI comes about through the project called "Imaging the Seismogenic Zone with Geodesy and Seismology: Two Land-Ocean Transects Across Costa Rica and the Middle America Trench" which is a part of the SEIZE (Seismogenic investigations) which is, in turn, part of the MARGINS initiative of the National Science Foundation. The Principal Investigators of this project are: Timothy Dixon and Edmundo Norabuena, Rosenstiel School of Marine and Atmospheric Sciences University of Miami; LeRoy Dorman, Scripps Institution of Oceanography, University of California, San Diego; Ernst Flueh, GEOMAR; Paul Lundgren, Jet Propulsion Laboratory, California Institute of Technology; Marino Protti, OVISICORI-UNA; Susan Schwartz, University of California, Santa Cruz.

This project is focussed on understanding the three-dimensional distribution and nature of the seismogenic zone (the locked or partly locked plate interface which generates large or great earthquakes). This is of great societal relevance since these large shallow thrust-zone earthquakes are ones which generate destructive tsunamis. The tools which we use are GPS, optical leveling, seismographs on land and Ocean-Bottom Seismographs offshore.

The deformation of the earth (especially the vertical motion) above a locked plate interface can provide some information about the extent of the locked zone and the effectiveness of the locking (whether it is completely locked, or allows some limited slip). The region which shows the largest geodetic signal is the region immediately above the locked zone. This makes the Nicoya and Osa peninsulas particularly attractive since GPS sites can be placed on land there, in contrast with other locations where the region above the locked zone is under water.

The geodetic signal is most sensitive to the downdip extent of the locked zone and to the percentage of locked slip, so we will attempt to use an OBS array to outline the seismically active slipping zone, and, hopefully, the updip boundary of the seismogenic zone.

The passive seismic program: what it takes to locate earthquakes well.

As pointed out above, the seismogenic zone on the Costa Rican margin is close to land, but not beneath it. The fact that land is close by allows us to emplace land seismometers as part of an array to obtain precise definition of the seismogenic zone. A glance at the distribution of seismicity off the Osa and Nicoya peninsulas reveals a pattern which is best described as a cloud, rather than a planar slip surface, which one might expect (or at least hope) to see. The earthquakes are not, in fact, well-located, a consequence of the geometry of the seismic network used to locate the earthquakes. The earthquakes which define the active zone are not large enough to be recorded all around the world, so the locations are a product of the local network, which is confined to land which is to the northeast of the source region. The ideal seismic array for location of earthquakes is symmetric about the source area. This symmetry leads to the cancellation of errors due to poor knowledge of the seismic structure, and to the fact that we must solve for the source time as well as the source location. The physics of the earthquake location process lead to a tradeoff between source time and depth. The pattern of P-wave arrival times from an earthquake at some depth is not very different from the pattern of arrival times from an earthquake occurring slightly deeper and slightly

earlier in time. The effects of this tradeoff are exacerbated for asymmetric arrays, consequently locations of events whose epicenters are outside the array are poorly determined, especially in depth. So we see then, that we must have a seismic array whose area contains the epicenters of the events which we hope to locate precisely.

After symmetry, the next most important factor in the design of an array for locating earthquakes is station density or, put another way, the distance between stations. We have used a simple earth model, a half-space, but the salient features of the graphs also apply when a more realistic earth model is used. The most obvious feature of all the travel-time curves is that they become indistinguishable at epicentral distances of a few times the source depth. So the lesson to be learned from this graph is that for high depth resolution, we must have a station not much more than the source depth away from the epicenter. If we are interested in earthquakes whose depths are, say 20 km, we must use an array whose elements are separated by distances of the scale of 20 km. The offshore array is laid out in this manner.

Of course, we are limited in the number of instruments we have available, and not all locations are suitable instrument sites. In particular, the shallowest sites are poor choices because ocean waves create seismic noise readily in very shallow water and the instruments themselves are at risk from the activities of the fishing industry.

In the Osa region, we were fortunate to experience a large earthquake on 20 Aug, 1999. This event had a Mw of 6.9 and promises to supply a bountiful level of aftershock activity. We have placed our array to cover this aftershock activity, as well as the proposed deep drilling site.

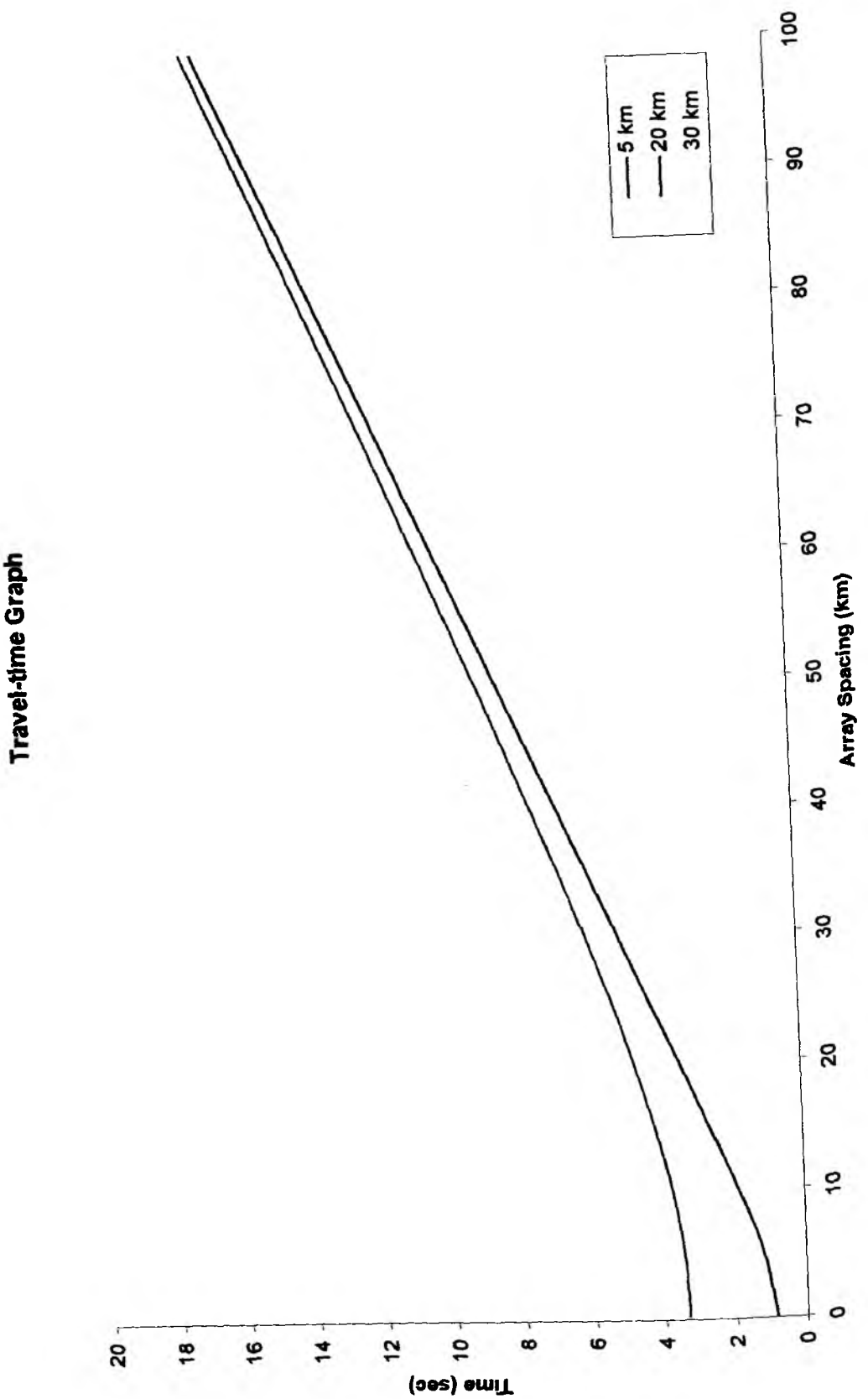

Figure 6.4.1: Travel-time graphs for different epicenter depth showing the depth dependance of array spacing

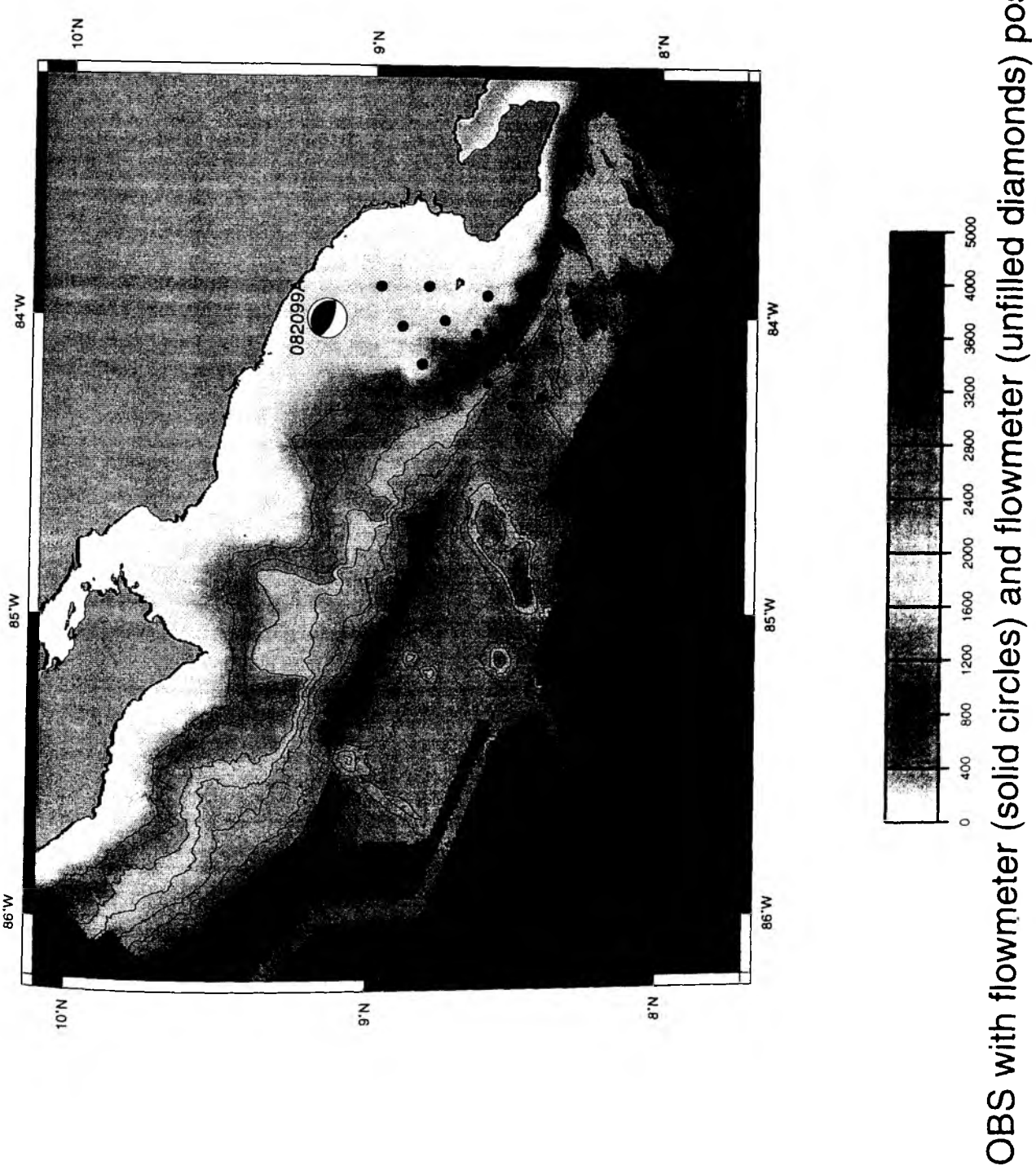

Figure 6.4.2: Deployment positions of SCRIPPS OBS and flowmeter

soild circle	OBS with flowmeter
open diamond	flowmeter
half filled circle	20 Aug. 99 earthquake

6.5. TOBI OPERATIONS AND INITIAL DATA INTERPRETATION

(D. Masson, I. Rouse, V. Huhnerbach, D. Matthew, B. Wallace)

During Sonne 144-2, TOBI was used to obtain detailed sidescan sonar images of the continental slope, the deformation front at the foot of the slope and the immediately adjacent oceanic crust. The objectives were :

(i) to examine the structure of embayments in the continental slope, previously interpreted as slide scars related to the subduction of seamounts

(ii) to understand the overall contribution of slope failure and sliding to the evolution of the Costa Rica margin

(iii) to search for features, such as mud volcanoes, areas of carbonate crust or areas of anomalous sonar backscatter which might relate to fluid venting or the presence of gas hydrates at the seafloor

(iv) to examine surficial deformation structures on the continental slope, with the aim of understanding the deformation processes that create these structures

Four TOBI deployments, totalling 243.4 hours (10.15 days), were undertaken during SO144-2 (Table 6.5.1). Runs 1 and 2 both had to be terminated prematurely, run 1 due to the flooding of the CTD unit, run 2 due to water entry into the swivel unit, causing it to short. Despite these minor setbacks, the planned programme of TOBI work was completed in full, and all the survey objectives were addressed.

TOBI Run No	SONNE Station No	TOBI Line No	Start	End	Track Length	Comments
1	5-7	1-3	19:50 22 Oct	11:00 26 Oct	360 km	Terminated by CTD failure
2	16-17	4-5	22:00 28 Oct	04:45 31 Oct	200 km	Terminated by Swivel failure
3	20-23	6-9	04:10 01 Nov	09:00 04 Nov	295 km	Successfully Completed
4	24-26	10-12	15:20 04 Nov	15:05 05 Nov	95 km	Successfully completed

Table 6.5.1. Summary of TOBI deployments undertaken during SO144-2.

All TOBI data was recorded on magneto-optical disks in real time. Two copies of each data disk were later produced on CD-ROM as backup archives. TOBI sidescan sonar data were displayed on paper in real time and preliminary digital processing was carried out offline. Sidescan sonar processing was undertaken using PRISM software developed at the Southampton Oceanography Centre (SOC) and the commercial ERDAS image manipulation package. Processing improves the quality of the displayed image and allows it to be accurately placed on a map. Processed data is essential for quantitative image analysis (e.g. texture mapping) and also allows the sidescan data to be merged with other data sets (e.g. multibeam bathymetry). Digital sidescan processing involves both

geometric and radiometric corrections. Geometric corrections change the relative position of pixels in the imagery, and include slant-range correction, anamorphosing, and geo-referencing. Radiometric corrections change the relative values of neighbouring pixels. Radiometric corrections include shading corrections to compensate for the decrease in signal strength across the swath, the removal of surface reflections, line dropout removal, filtering for speckle noise and deblurring.

The TOBI 7 kHz profiles were corrected for variations in depth of the vehicle along track and displayed as continuous paper records. 950 line km of TOBI profile data were collected during Sonne 144-2. Phase data from the TOBI sidescan signals (from which swath bathymetry can be derived) and magnetic field data were stored in raw form on the data disks and will be processed as required after the cruise.

The sidescan sonar data collected using TOBI was of excellent quality. In total, the survey covers approximately 4950 km^2. It extends from the upper part of the continental slope, in approximately 500 m water depth, to the trench floor, at about 3700 m water depth, covering the area of the continental slope between 84° 35' and 85° 45' W (Fig. 6.5.1). The major features observed can be grouped under the following headings :

(i) Slide scars and deposits
(ii) Deformation structures in the overriding plate
(iii) Structure of the oceanic plate
(iv) Features possibly related to fluid venting
(v)

Slide scars and deposits

Several spectacular slide scars were imaged during the TOBI survey. A number of discrete scars in the central and western parts of the survey area show the progressive effects of seamount subduction beneath the slope (see Section 4.3, Fig. 4.3.1. for a map showing scar locations and names).

The top of the headwall of the Parrita scar, centred at 08° 58' N, 84° 38' W, is located only 6 km upslope from the deformation front. A pronounced erosional scar up to 7 km in width extends downslope from this point, at 1100 water depth, to 3000 m water depth. The structure of this headwall is a highly complex, and is characterised by several cross-cutting down-to-the-trench normal fault trends (Fig. 6.5.2). Immediately upslope from the headwall, a pronounced bathymetric high is seen. This high is characterised by normal faults downthrowing in an upslope direction. Downslope from the headwall scarp, evidence of discrete debris flow lobes, each characterised by a surface fabric of pressure ridges, is seen. Where the scar opens into the trench, the trench floor is characterised by a field of debris covering some 10 km^2 (Fig. 6.5.3).

The top of the headwall of the Jaco scar, centred at 09° 08' N, 84° 50' W, is located 15 km from the deformation front. The scar is between 5 and 6 km in width. In contrast to the Parrita scar, the Jaco headwall is a relatively simple escarpment which extends from 1000 to 2200 m (Fig. 6.5.4.). The bathymetric high upslope from the headwall is less pronounced than that associated with the Parrita scar, but characterised by similar normal faults downthrowing upslope. A single small debris lobe can be identified immediately downslope of the headwall region (Fig. 6.5.4). However, further downslope, the trace of the Jaco scar is heavily sedimented, and in this area it appears to be an inactive structure. No debris associated with this scar is seen in the trench.

It is notable that in the case of both the Jaco and Parrita scars, the bathymetric highs upslope from the scar headwalls and also the areas adjacent to the lateral walls of the scars are highly faulted. Although complex cross-cutting fracture patterns are seen, many faults

downthrow in an upslope direction. It appears that these faults form in an extensional regime due to uplift as a seamount travels beneath the overriding plate, and that the area affected by uplift and extension is wider than that later affected by collapse over the trailing flank of the seamount.

In contrast to the Parrita and Jaco scars, the Cabo Blanco and Tarcoles scars, respectively 43 and 53 km upslope from the deformation front, appear to be relatively inactive structures. TOBI images show some high backscatter features corresponding to the steep scar headwalls, but there is little evidence for either active faulting or active slides.

A large slide complex, the Nicoya Slide, occupies the lower slope in the west of the study area between 85° 10' and 85° 45' W. The western part of the slide headwall lies at about 2500 m water depth, but it gradually shallows until it lies at about 1000 m water depth in the east. The headwall is a complex feature, in some places appearing as a single scarp, in others as a series of steps defined by complex normal fault patterns (Fig. 6.5.5). The body of the slide is also a complex mixture of flow units and blocky seafloor. Near the trench there is much evidence for a compressional fabric of ridges and troughs. This might result either from compression at the foot of the slide or from folding of the slide mass as it was accreted back onto the overriding plate after the slide had occurred. It is clear that the Nicoya Slide is composed of multiple flow units which were emplaced at different times. The topography of the western part of the slide is much subdued and here the slide mass appears to have a considerable sediment cover. In the east, the degree of seabed disruption is much greater and the slide also appears very fresh. In this area, a number of discrete flow units are separated by distinct lineaments oriented downslope. North of Fisher Seamount, the ocean floor seaward of the Nicoya Slide is covered by a huge blanket of debris, which extends for at least 40 km along the strike of the margin (Fig. 6.5.6). This debris is partially buried by later sediments, particularly in the area of the trench, which might indicate that it is relatively old. At the present time, it is not clear whether it has been derived from the Nicoya Slide, or from an older, perhaps even larger slide.

Deformation structures in the overriding plate

In general, compressional structures, such as folds and the surface traces of thrust faults, are only easily recognisable in a narrow band parallel to, and just landward of, the deformation front. The deformation front itself is easily recognised as a distinct boundary between the smooth, flat-lying trench sediments (showing low backscatter on TOBI images) on the oceanward side and the rough, corrugated material of the lowermost slope (showing high backscatter on TOBI images) (Fig. 6.5.7). Immediately landward of the deformation front, the toe of the overriding plate is generally characterised by a series of small-scale ridges or corrugations, oriented parallel to the front. Fold wavelengths are typically 100 to 300 m. Asymmetric folds, recognisable on TOBI images, may relate to the outcrop of thrust faults.

Further upslope, the overriding plate is characterised by a highly complicated surficial fabric resulting from folding, faulting (probably both normal and thrust faults) and sliding. Most lineaments trend parallel or sub-parallel to the deformation front. This however, is a highly complex area, and interpretation of the TOBI data will require a more detailed study than has been possible to date.

Structure of the oceanic plate

Most of the oceanic plate shows a smooth, low-backscatter sedimented surface. South of Fisher Seamount, this is cut by normal faults related to the bending of the oceanic plate as it enters the trench. Faulting of the plate north of Fisher Seamount is, however, much less prominent. Extensional normal faults downthrow both towards the north and south, although those with the largest throws face towards the north.

Features possibly related to fluid venting

Much of the backscatter variation seen on the TOBI images can be interpreted in terms of the topography and sedimentology of the study area and, in turn, related to tectonic and sedimentological processes. However, some areas exhibit anomalous backscatter patterns which might tentatively be interpreted as evidence for fluid venting or seepage. In particular, irregular patches of anomalous high backscatter occur in many places on the lower slope. Some are associated with areas of faulting (e.g. scar headwall areas) or folding, but others occur within relatively flat-lying sedimented areas. Several OFOS tracks crossed such high-backscatter patches. These photographic transverses will be used to test the hypothesised link between high backscatter and fluid venting, by relating the distribution of biological and chemical manifestations of venting at the seabed to the observed backscatter patterns. However, further processing of the sidescan imagery and detailed comparison between the sidescan imagery and the OFOS photographs will be required to complete this study.

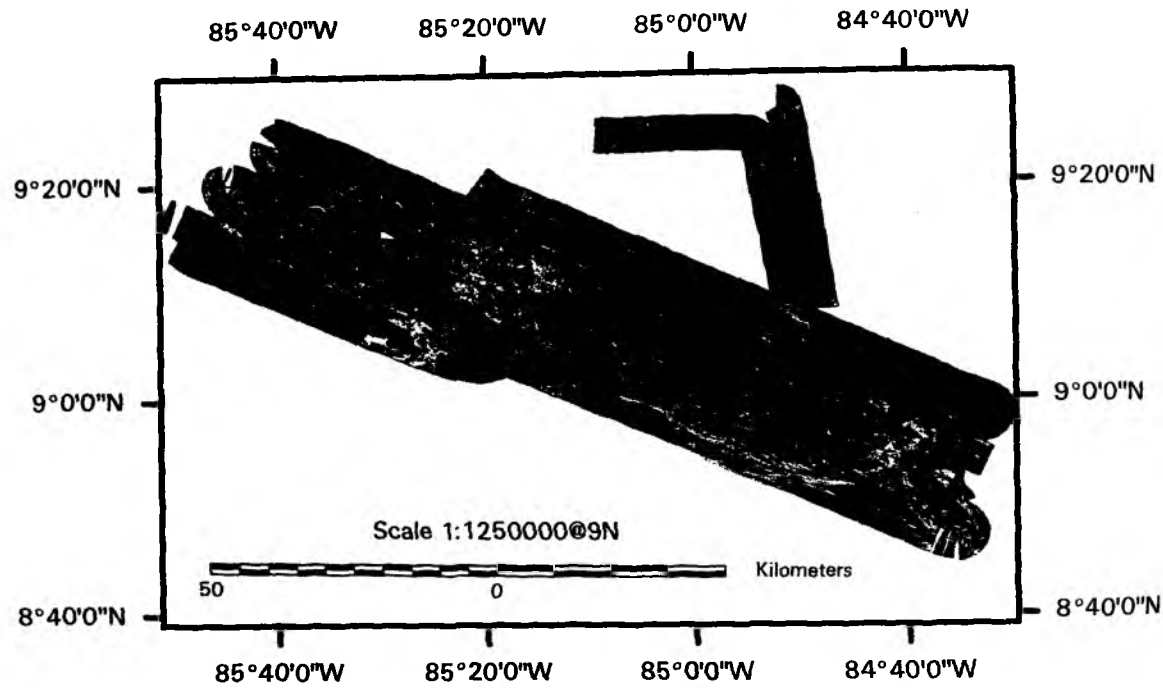

Figure 6.5.1 Regional overview of the sidescan sonar coverage obtained with TOBI.

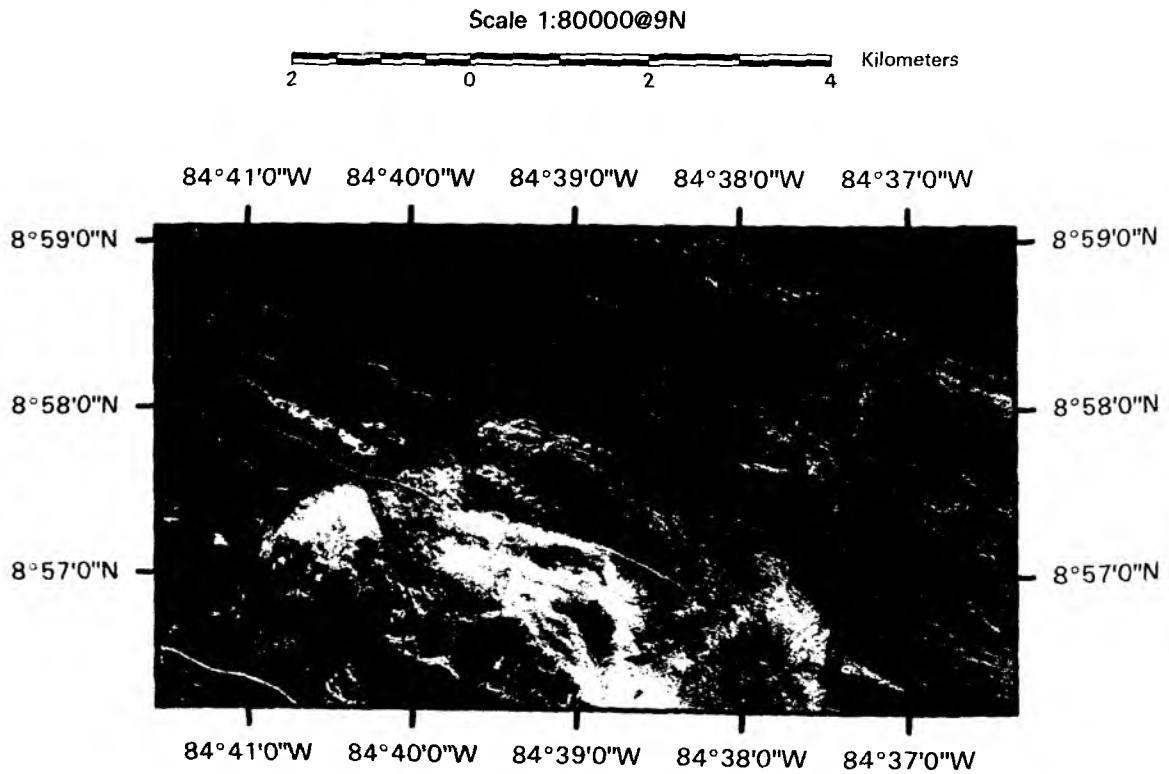

Figure 6.5.2 TOBI sidescan sonar image showing complex fault patterns at the headwall of the Parrita Scar.

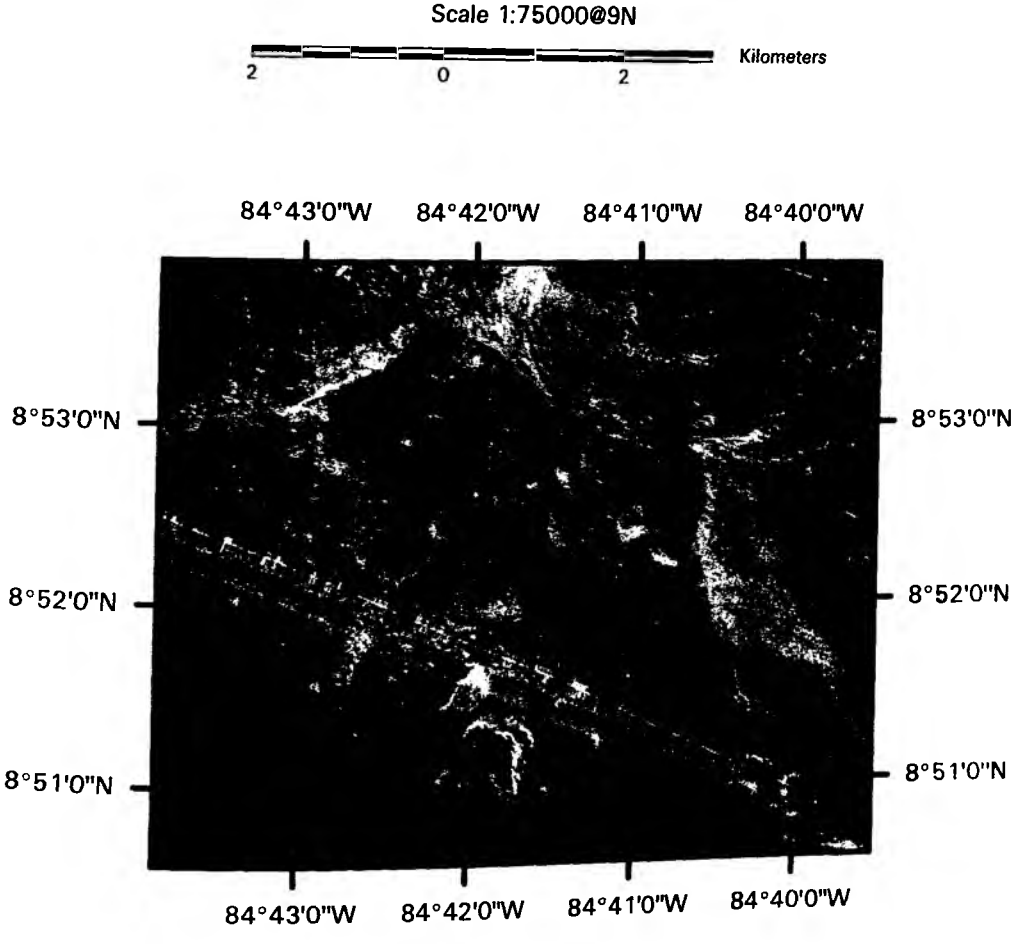

Figure 6.5.3 TOBI sidescan sonar image showing debris deposit in the trench below the Parrita Scar.

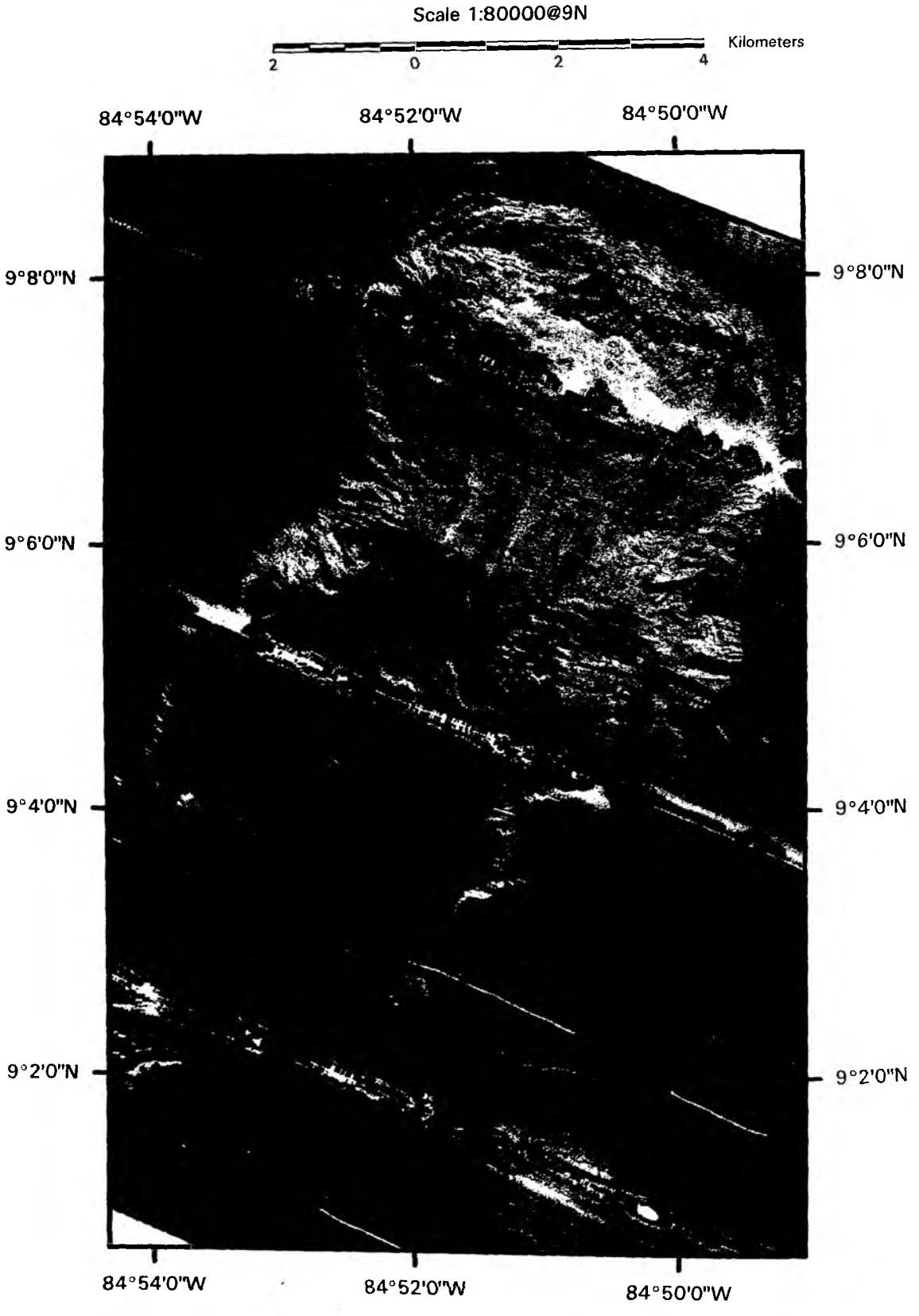

Figure 6.5.4 A mosaic of TOBI sidescan sonar images showing Jacor Scar.

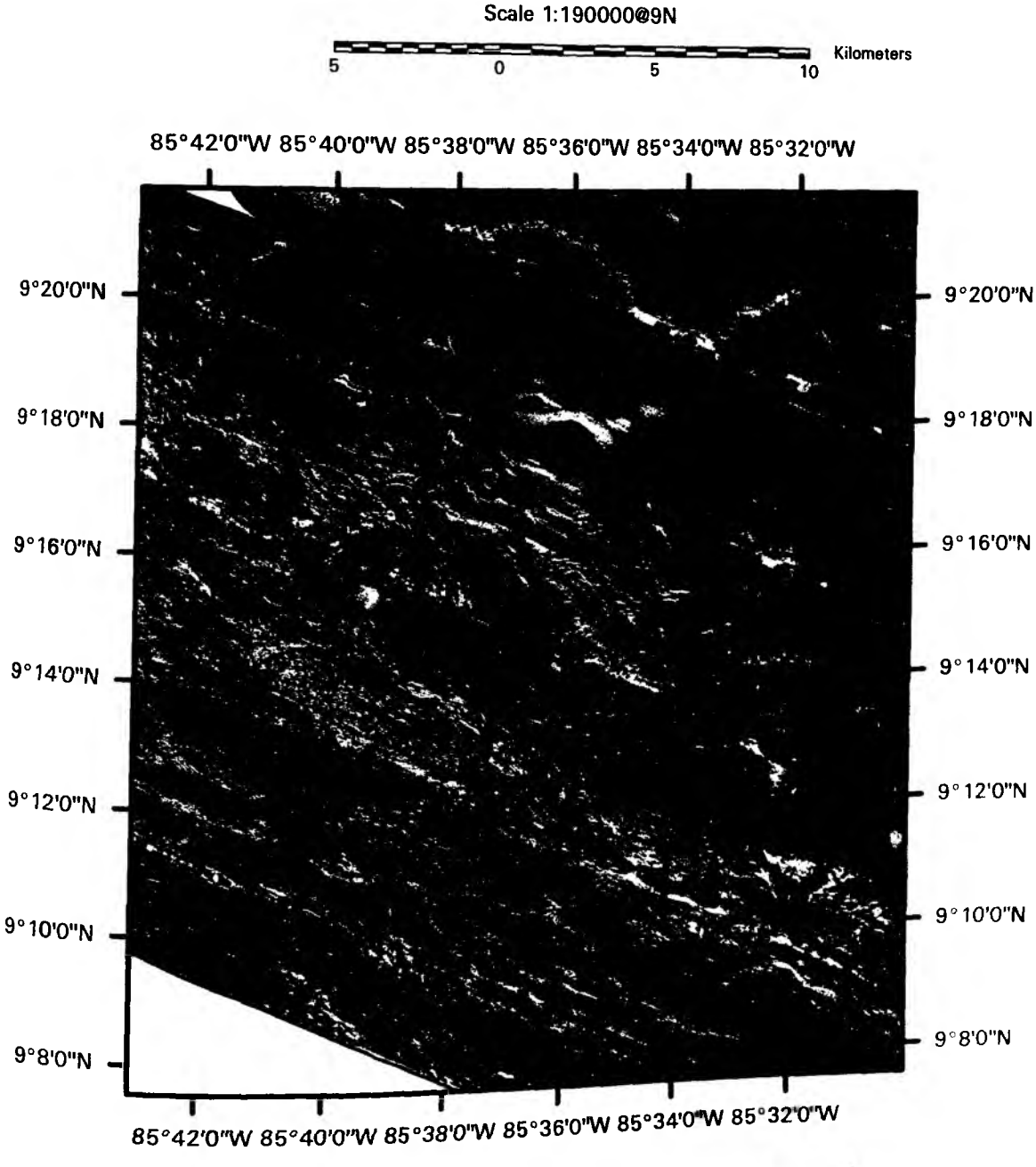

Figure 6.5.5 A mosaic of TOBI images showing part of the Nicoya Slide.

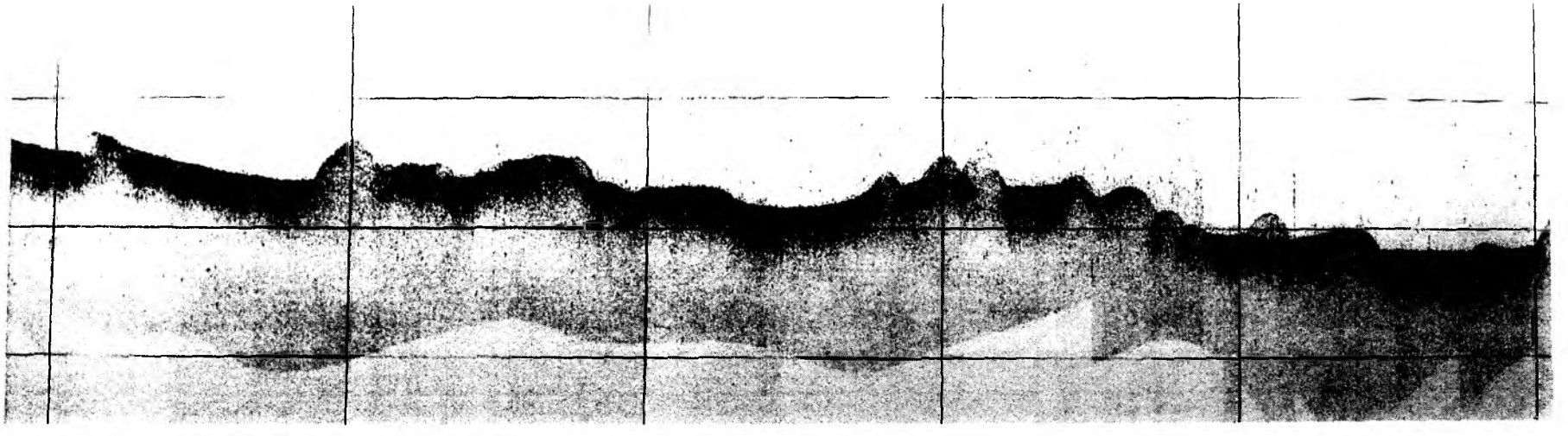

Figure 6.5.6 An example of a subbottom profile obtained using the 7 kHz profiler mounted on TOBI. Profile shows the debris flow deposit which covers the oceanic plate seaward of the Nicoya slide. High areas along the profile correspond to individual debris blocks. Layered sediments between the blocks, up to 25 m in thickness, postdate the emplacement of the slide. Horizontal lines are 75 m apart, vertical lines are approximately 2 km apart.

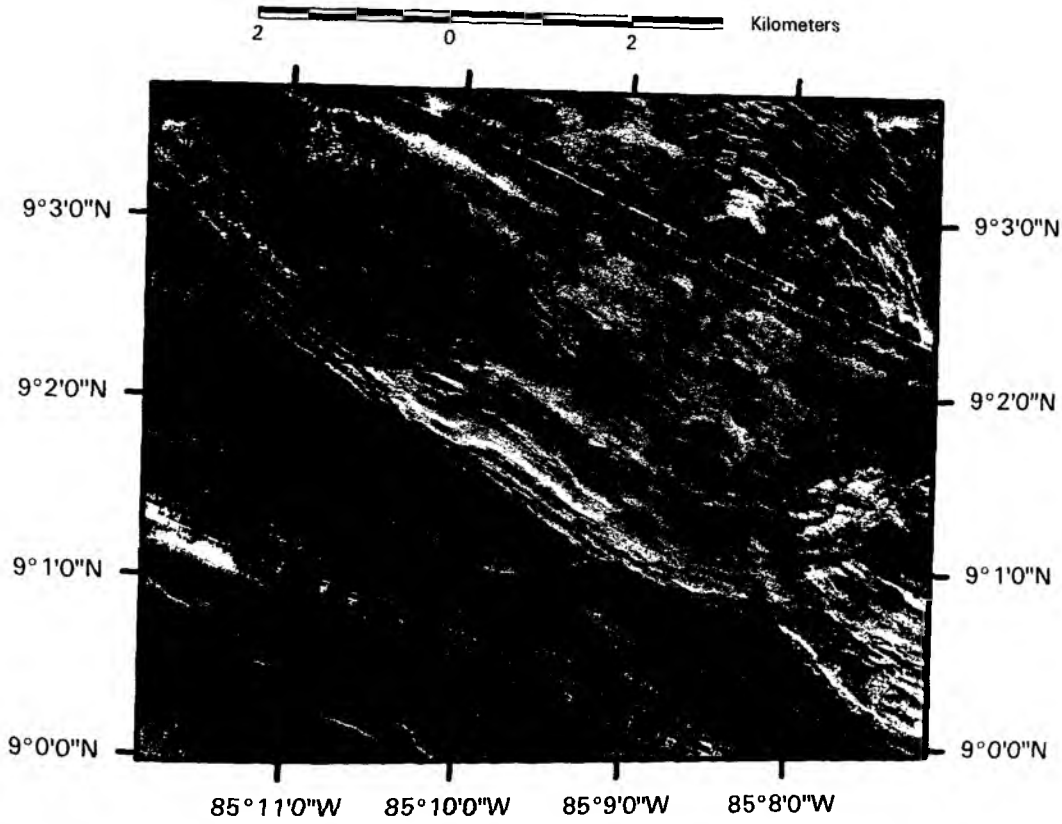

Figure 6.5.7 TOBI sidescan sonar image showing the typical structure of the deformation front. Note the contrast between the smooth low backscatter trench floor to the south and the variable backscatter deformed to the north.

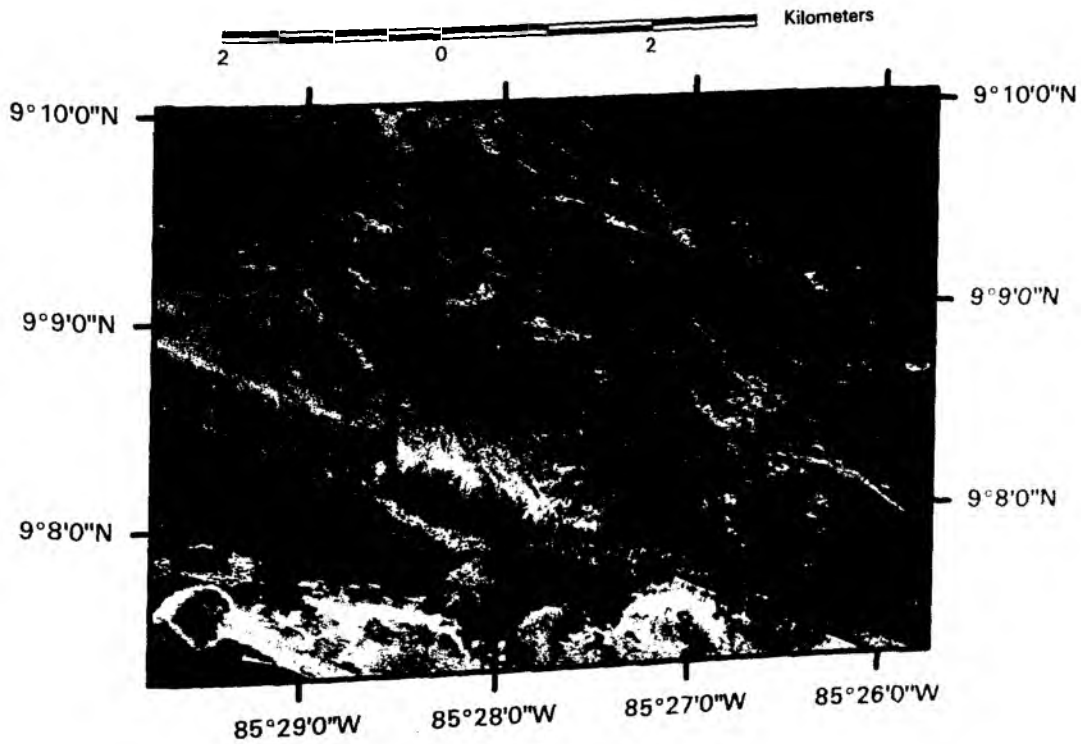

Figure 6.5.8 TOBI sidescan sonar image showing complex deformation of the lower slope adjacent to Fisher seamount.

6.6. Ocean bottom observation by OFOS

(C. Jung, B.V. Baranov, H. Florianova, T. Kath and G. Bohrmann)

The use of OFOS, the Ocean Floor Observation System, is one of the first attempts to view the shape and development of the seafloor. The OFOS surveys on cruise SO 144-2 were designed and conducted to map the distinct morphological, geological and biological features that occur in gas hydrate and active fluid venting regions. 10 OFOS (Fig. 6.6.1; Table 6.6.1) surveys were completed during SONNE cruise 144-2, their locations dispersed throughout the Costa Rican Pacific continental margin.

The Pacific continental margin region off Costa Rica is characterized by the tracks of subducted seamounts, forming scarp and land slide structures. During OFOS tracks, several land slide areas located on the Middle American Trench continental slope off Costa Rica, were investigated. These slides originated and continued to develop from slope uplift and eventual failure on account of seamount subduction (von Huene et al., 1995). Many fractures and weak zones appeared during slide development and such areas can be the preferential pathways for the different manifestations connected with fluid expulsion. The aims of using OFOS were to investigate the destabilization of gas hydrates uplifted over subducting seamounts. The dissociation of gas hydrates releases methane gas. The areas of rising gases and fluids are indicated by authigenic precipitates and chemoautotrophic organisms. A typical vent is characterised by clams and clam fields (*Calyptogena* and *Acharax*), tube worms (*pogonophora*) and especially by bacterial mats.

Further objectives were to discover new cold vent and gas and areas of near-surfface occurence of hydrates, and new chemoautotrophic organisms in order to verify previous results.

The tracks **OFOS 01** (SO144/2-2) and OFOS 02 (SO144/2-3) run along multichannel seismic line 13, which crosses the Jacó scar and slide structure, located within the middle slope of the continental margin (Fig. 6.6.1). This slide represents a head of seamount track (Huene et al., submitted). OFOS 01 was cancelled after one hour due to a technical defect of the electric power cable. OFOS 02 continued the planned track. The OFOS 01 track shows typical seafloor sedimentation without any indication of seepage.

The **OFOS 02** track begins at 09°10.75' N, 84°48.42' W at 778 m water depth and ends at 09°04.64' N of 84° 52.28' W at 2438 m depth (Fig. 6.6.2). Over the first part the seafloor is characterized by soft sediments and small patches of carbonates and boulders with little to no sediment drape (Fig. 6.6.3). The smooth bottom surface is disturbed by several scarps with outcrops of carbonate. The scarps face upslope and are up to 40 m high. These features are connected with fracturing due to uplift (Ranero et al., in press). Scattered tube worms appear near the carbonate outcrops. The carbonate surfaces are rough and irregular like chemoherm carbonates. Some doughnut carbonates were also observed.

The headwall consists of two scarps connected with shallow faults developed during slope failure. The dip of the lower one is shallower indicating rotation. Both scarps are 280 m high and many outcrops of grey/green sedimentary rocks are present. The rocks appeared massive and are strongly jointed in some places. A comparison with multichannel seismic profile 13 shows that these outcrops correspond to the uppermost layer of stratified reflectors (see Fig. 6.6.3). The BSR inside this sequence outcrops in the middle of the first scarp where several bacterial mat colonies were observed. The composition of the lower layer in this acoustically turbid sequence is still undecided due to a lack of outcrop on slope. Smaller bacterial mats as well as some living clams and shells of dead clams are dispersed at the headwall and at the site of slide deposition.

The lower part of the track is dominated by talus deposition covered by a thin blanket of sediments. Three extensive clam fields were observed, the first at 1400 m depth connected with bacterial mats, the second at 1800 m and the third and most extensive clam field at 1900 m. The lower debris avalanche may be older than the upper one, indicated by the presence of boulders - probably carbonate - coated black with manganese oxide suggesting longer exposition on the seafloor. Dispersed sea anaenomes, crinoides, corals, brittle stars, crabs and rattail fish were identified on the seafloor throughout the area. Sea urchins, sponges and cucumbers only appear at the upper part of the track and no clams were observed. The corals typically attach themselves to hard, substrates usually exposed boulders or carbonates. The corals and crinoids are also oriented in the dominant sea-bottom current direction.

The third survey, **OFOS 03** (SO144/2-9), was conducted across Parrita Scar, another scarp southeast from the former OFOS lines. The track begins at 09° 00.14' N, 84° 36.20' W at 1391 m water depth and ends at 08° 55.40' N, 84° 36.29' W at 2766 m water depth (Fig. 6.6.4). The upper part of the profile is characterized by soft, bioturbated sediment and an extensive area of fractured sedimentary rocks (Fig. 6.6.5). Several scarps that form a saw-like sea bottom profile are the remarkable features of this area. The scarps are up to 20-25 m high and they face in the direction of the track, SSE. Because of the scarps' morphology, they are thought to originate from extension and normal faulting of the upper sediment layers due to uplift connected with seamount subduction (von Huene et al., 1995). There are light grey/greenish bedrock outcrops on these scarps. Stratification exists where the outcrop begins. but is lost further to the southwest where the rocks become more massive with joints appearing along two orientations. Benthic life observed along track OFOS 03 consists of crinoids, sea cucumbers, sponges, star fish and sea urchins. Reaching the slope area, sedimentary rocks alternate with talus and soft sediment.

The head wall begins at around 1000 m depth and was studied down to a depth of 2600 m. It consists of several scarps, each separated by a flatter surface. The grey/green massive, jointed sedimentary rocks outcrop on all scarps. Only minor outcrop with visible stratification was observed at 1380 m. The most continuous outcrop is located at 1620-1840 m, where the OFOS track ran along the SW strike of a small ridge. This ridge is thought to be connected with transcurrent shears originating during slope failure and development of large landslides. Talus was observed at the base of most scarps, and also continuing downslope where it is slightly overlapped with sediments. Even near the scarp base talus is covered by a thin veneer of sediments, possibly indicating a relatively older age for the scarp. Fresh talus was observed only in one location (2400m) and here bacterial mats had developed as well. At depths of 1100 m to 1300 m on the upper slope, several clam shells, clams and clam fields were present within a large field of talus. Scattered clams and clam-shell debris occur at 1700 m and at 1800 m, several *pogonophoras* were observed. Reaching the end of the cross-section at 2500 m, dispersed bacterial mats were discovered surrounded by scattered clams.

OFOS 04 (SO144/2-11) was recorded in the working area's most southeastern part on the upper continental slope, WNW of the Osa Peninsula (Fig 6.6.1) extending to the southwest. The purpose of OFOS 04 was to investigate an unknown area in shallow water. The track begins at 08° 51.54' N, 84° 12.71' W and ends at 08° 47.52' N, 84° 16.16' W (Fig. 6.6.6.). Starting and ending depths were 214 m and 854 m, respectively. The track starts on a rapidly steepening slope (Fig. 6.6.7), where scattered outcrops of consolidated light grey/green sediments (or sedimentary rocks) are covered by a very thin layer of soft sediments. The rocks show visible stratification with slope-parallel dipping layers. A headwall appears at 270 m and dips down to 420 m. It consists of grey/green sedimentary rocks, which, in the uppermost part, are lighter in colour, stratified and cavernous in structure. The rocks

become massive and jointed downwall and stratifications are not clearly visible. Far better visible, talus covers the scarp base at 365 m (Fig. 6.6.7).

A slide starting at 400 m has remarkable outlines, is convex down to 625 m and its surface consists of several small rises of up to 20 m, which step upslope (saw-like surface). It was observed that these slopes are very steep scarps where sedimentary rocks outcrop. They are antithetic to the main slide plain and can be interpreted as having derived from normal faulting (Fig. 6.6.7). The slide's lower section has a rough wave-like surface with separate small ridges up to 40 m high. The bathymetric map (Fig. 6.6.1) shows the ridges to align along slope in a NW direction, but in fact their strike gradually rotates clockwise downslope. Sedimentary rocks, to those observed upslope outcrop, were also seen where they incline steepest. These structures are interpreted to be compessional ridges appearing in the tail part of slides.

The most extensive presence of bacterial mats was observed from 350 m to 450 m. The bacterial mats extend about 220 m, completely covering the seafloor in white, blue/grey and orange. Many small bacterial mats are dispersed around the slide tail and surrounded by numerous clams, clam-shell debris and *pogonophoras*. Other benthic life includes dispersed snails, crabs, crinoides and aneanomes. Carbonates are exposed on the crest as sedimentary rocks near the cross-section termination. They are rough and irregular and possibly chemoherm carbonates.

The Cabo Blanco Scar on the upper continental slope south of the Nicoya Peninsula was site to **OFOS 05** (SO144/2-13) at water depths of 316 m to 1703 m. The OFOS track begins at 09° 28.47' N, 85° 05.32' W and ends at 09°22.61' N of 85° 07.81' W (Fig. 6.6.8.). The cross-section is dominated by landslides (Fig. 6.6.9). Up to the headwall at 900 m, the seafloor is covered by sediments. At the beginning of the track, ripple marks indicate currents. The headwall has a stepped profile, the steps becoming less steep downslope. Grey/greenish sedimentary rocks are outcropping on scarps, sometimes with distinguishable stratification and jointing increases downslope.

Talus was observed only at the first scarp's base where it is partially covered by sediments (depth 960 m). Sediment blanketing was only down to 1500 m. Below this level appeared much talus material, not only onslope but also on flat areas indicating slumping. On the slide tail, occasional clams and pogonophoras were observed. Dispersed crinoides, snails, star fishes, sponges and many sea cucumbers also exist.

OFOS 06 (SO144/2-15) was conducted across the middle continental slope near Jacó Scar. The track crossed two structures indicated by high backscatter in the TOBI survey. The structures were thought to be mud volcanoes. OFOS 06 begins at 09°00.77' N, 84°44.21' W and ends at 08°56.77' N of 84° 43.00' W (Fig. 6.6.10), positioned west of OFOS 03 (Fig. 6.6.1). Starting depth was 1776 m and end depth was 2494 m.

The slope is stepped and covered by sediments along the whole track especially where steep. Some clams and many clam traces were observed particularly at the mud volcanoes expected where the profile shows smooth elevation. However, neither mud volcanoes nor their indicators were seen. Benthic life at the seafloor consists of crinoids, sea anaenomes, sea cucumbers, star fishes, corals, sea urchins and snails. As seen before, the corals and crinoids were oriented in the dominant sea-bottom current direction.

The survey, **OFOS 07** (SO144/2-19), crossed the middle part of the Nicoya slide, running down the Puerto Coyote Scar slope. The OFOS track begins at 09° 19.60' N, 85° 24.01' W and ends at 09°15.14' N of 85° 25.37' W (Fig. 6.6.11). From start to end, water depths were 1097 m to 2376 m. In the profiles beginning at the 1100 m contour, a diversity of carbonates were observed on the sediment cover. Most characteristic is a hard carbonate crust,

composed of slabs, cobbles, boulders and typical vent carbonates displaying doughnut, chimney, and skeletal carbonate structures as well as chemoherm carbonates. These are older precipitates because there were no signs of active venting. Outcrops of carbonates were also seen on small scarps.

Downward the slope smoothly subsides to the beginning of the Nicoya slide headwall at 1780 m. The slope has a very pronounced step shape and consists of several flat surfaces subdivided by scarps up to 100 m high. Sediments cover the scarps with a few minor outcrops of light grey/green rocks with fine stratification. There is minor visible talus near the scarps, but it is only seen to be fresh at 1420 m, where the slope is gouged oblique to its strike. The concave headwall, which dips more steeply than the upper slope, contains small scarps where sedimentary rocks, with some visible stratification, outcrop. The large apron of talus probably originated from partial disintegration of the wall. Scattered clams and clam-shell debris occur at 1800 m to 2300 m. Other observed seafloor-dwelling animals were crinoids, snails, sea cucumbers, brittle stars and sea feathers, as well as unknown white worms appearing on the slide's deeper end.

OFOS 08, OFOS 09 and OFOS 10 are listed in Table 6.6.1.

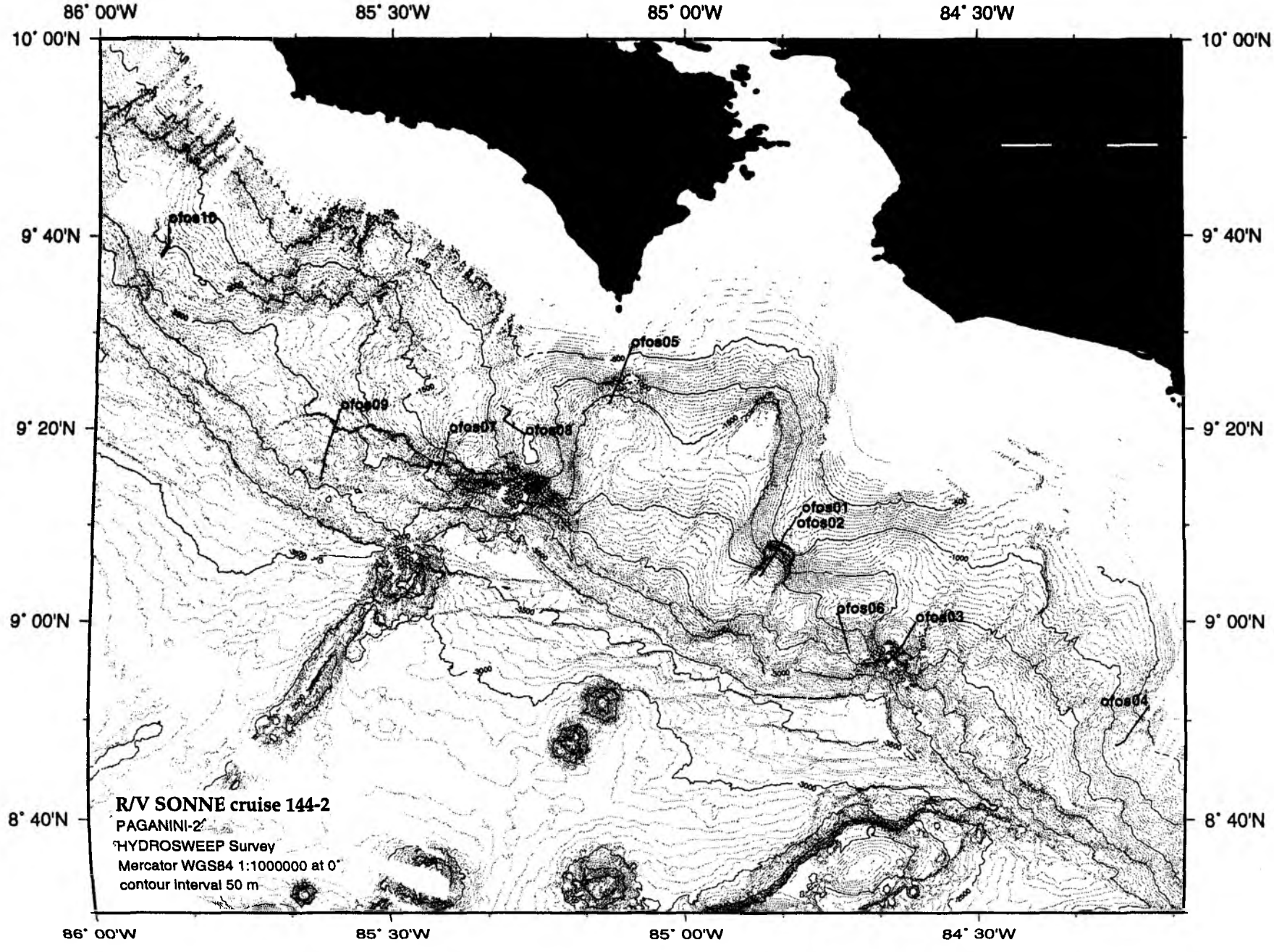

Figure 6.6.1: Bathymetric map of OFOS locations.

Sonne 144-2 OFOS-tracks

Date	Stat. No.	Time (UTC)	Time (UTC)	Start		End		Working area	Observation	slide No:
		at bottom	off bottom	Lat. (NS) at bottom	Long. (EW)	Lat. (NS) off bottom	Long. (EW)			
	144/2-									
21.10.99	2 OFOS 01	5:26	6:20	09°11.318'	84° 47,884'	09° 10,816'	84° 48,199'	Jaco Scar, slide structure at the continental margin of Costa Rica	soft sediment	36
22.10.99	3 OFOS 02	1:04	10:30	09°10.755'	84°48.429'	09°04.646'.	84°52.280'	Jaco Scar, slide structure at the continental margin of Costa Rica	carbonate crust, chemoherm carbonates and pogonophora at the upper part; clams, clam fields and bacterial mats at the lower part	369
26.10.99	9 OFOS 03	18:35	1:48	09°00.146'	84°36.209	08°55.407'	84°36.297'	Parrita Scar, slide structure	soft sediment, talus, clams and clam fields at the upper slope, bacterial mats at the end of the track	324
27.10.99	11 OFOS 04	7:45	14:30	08°51.549'	84°12.716'	08°47.522'	84°16,163'	west-north-west of Osa Peninsula	extensive bacterial mats at water depth of 400m, scattered clams and clam fields as well as bacterial mats, chemoherm carbonates at the end of the track	310
27.10.99	13 OFOS 05	23:35	8:14	09°28.472'	85°05.329'	09°22.616'	85°07.810'	Cabo Blanco Scar, South of Nicoya Peninsula	soft sediment, sedimentary rocks, occasionaly clams and pogonophoras	227
28.10.99	15 OFOS 06	14:27	19:30	09°00.772'	84°44.214'	09°56.771'	84°43.006'	near the Jaco Scar, middle continental slope	looking for mud volcanoes, not much clams	157
31.10.99	19 OFOS 07	18:26	0:46	09°19.608'	85°24.014'	09°15.142'	85°25.372'	middle part of Nicoya slide	carbonate slabs and boulders, chemoherm carbonate, doughnuts, old vent site at the upper part; scattered clams, clam shell debris at the lower part	307
5.11.99	27 OFOS 09	16:24	21:58	09°19.338'	85°16.222'	09°22.410'	85°15.850'	Rio Bongo Scar	clams and clam fields, bacterial mats, chemoherm carbonates	286
6.11.99	29 OFOS 09	2:20	12:45	09°21.855'	85°34.986'	09°14.452'	85°37.028	Nicoya Slide	soft sediment	233
6./7.11.99	31 OFOS	19:59	4:46	09°41.297	85°53.020	09°39.481	85°53.042	Mudvolcanoe	clam fields (Acharax), biggest clams, bacterial mats pogonophora bushes, chemoherm carbonates	269

Table 6.6.1 Summary of OFOS-tracks SO 144/2

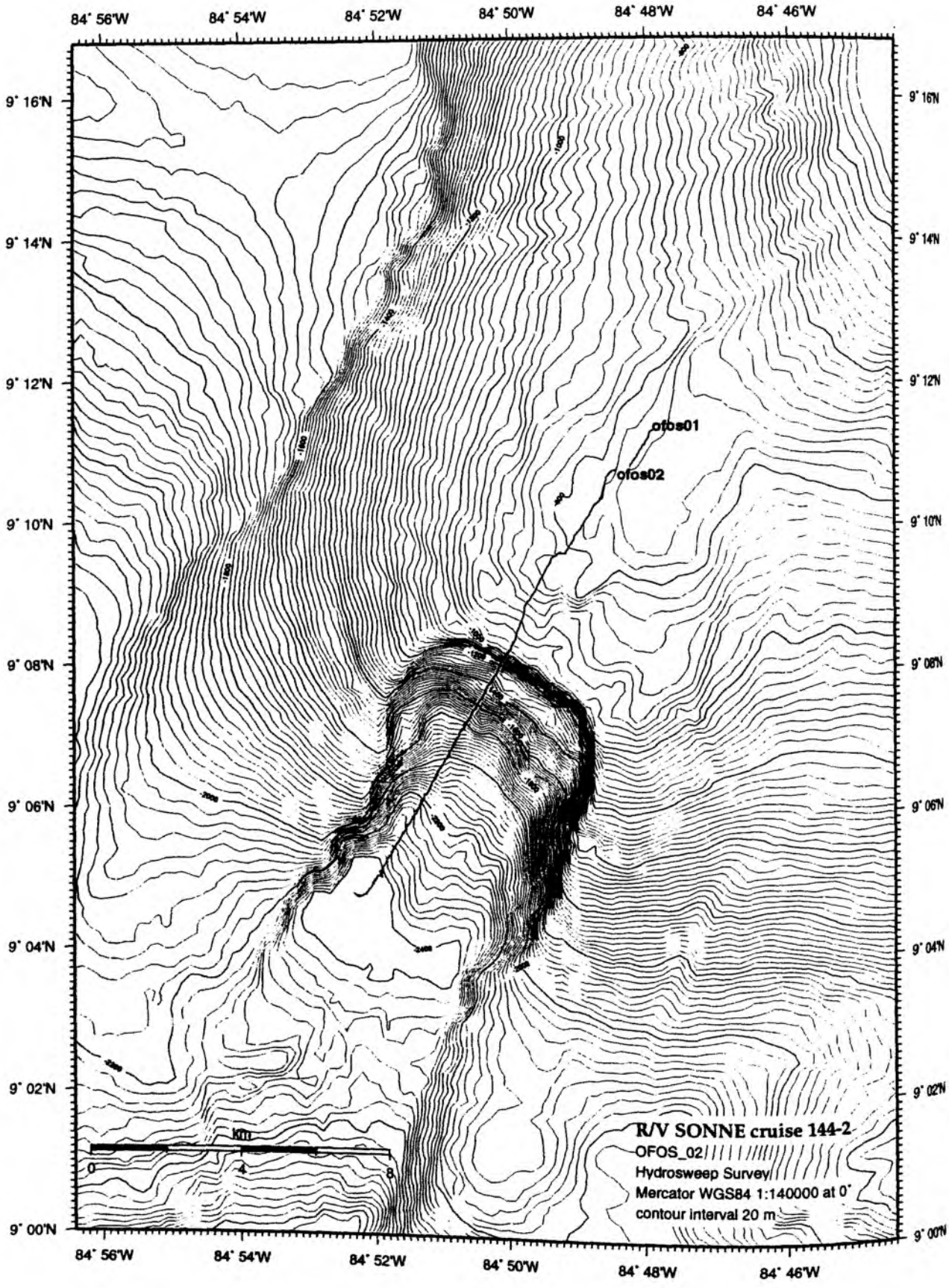

Figure 6.6.2 Position of OFOS 01 and OFOS 02.

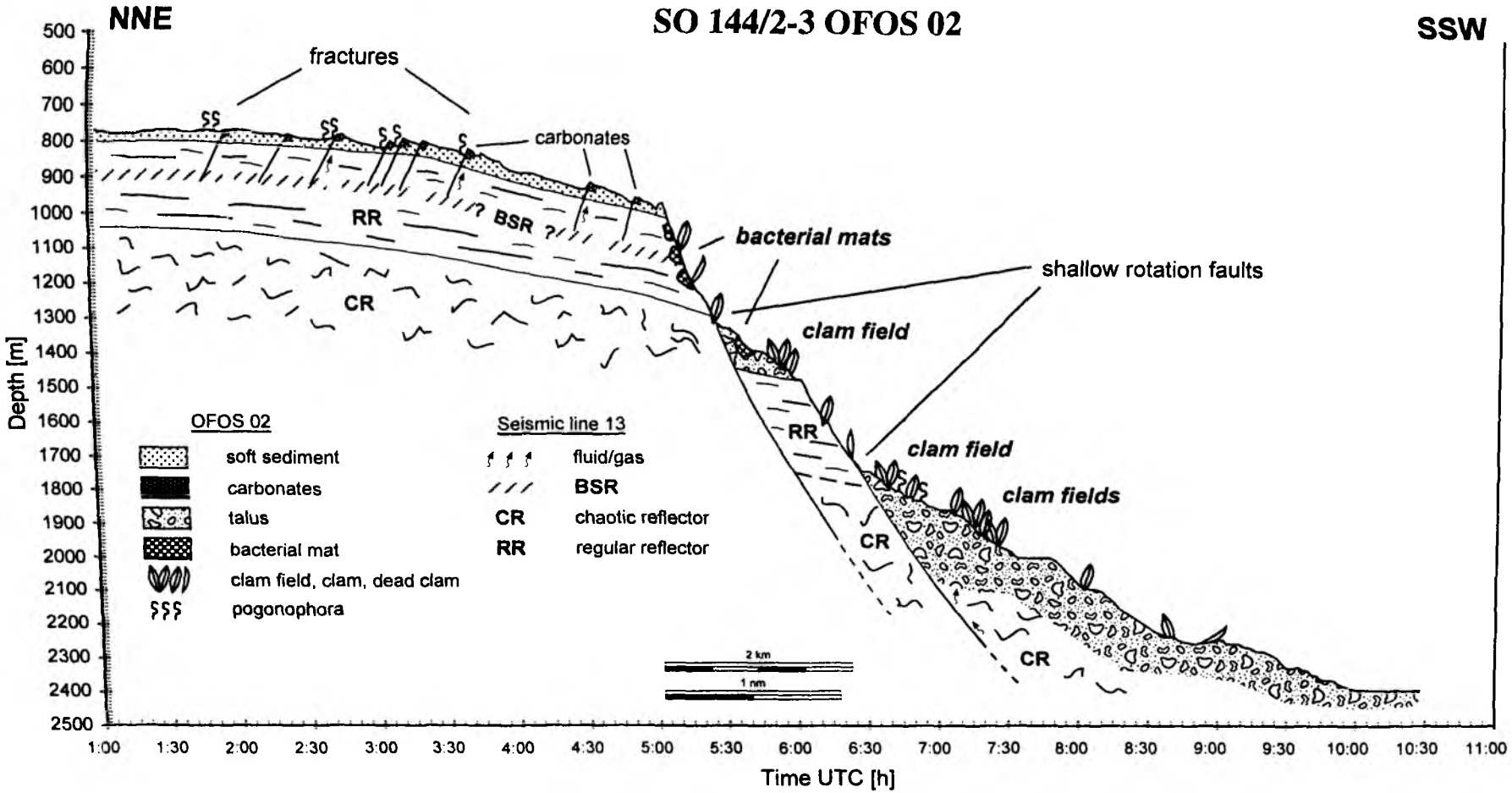

Figure 6.6.3. OFOS observation compiled with the Seismic Line 13. Schematic section.

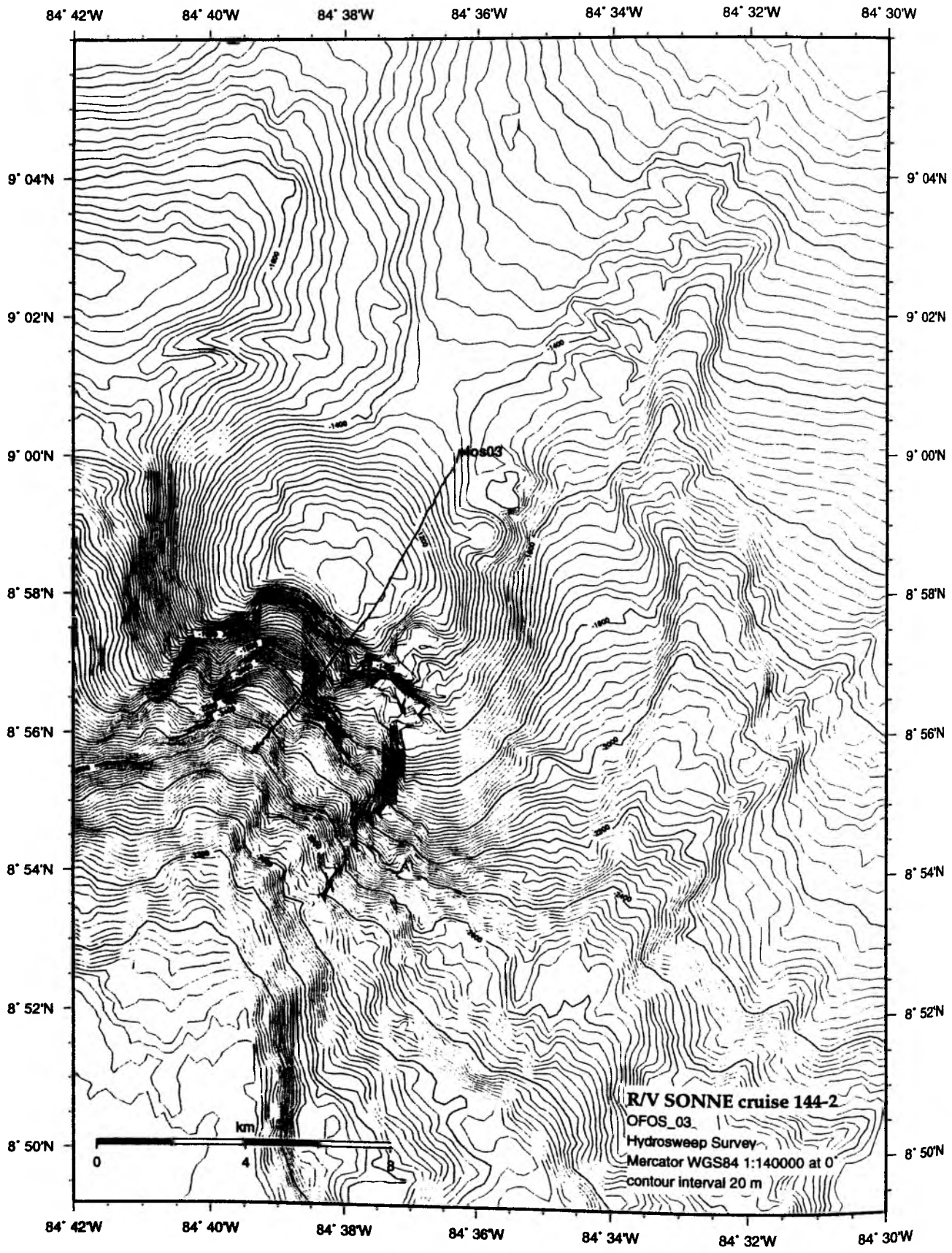

Figure 6.6.4 Position of OFOS 03.

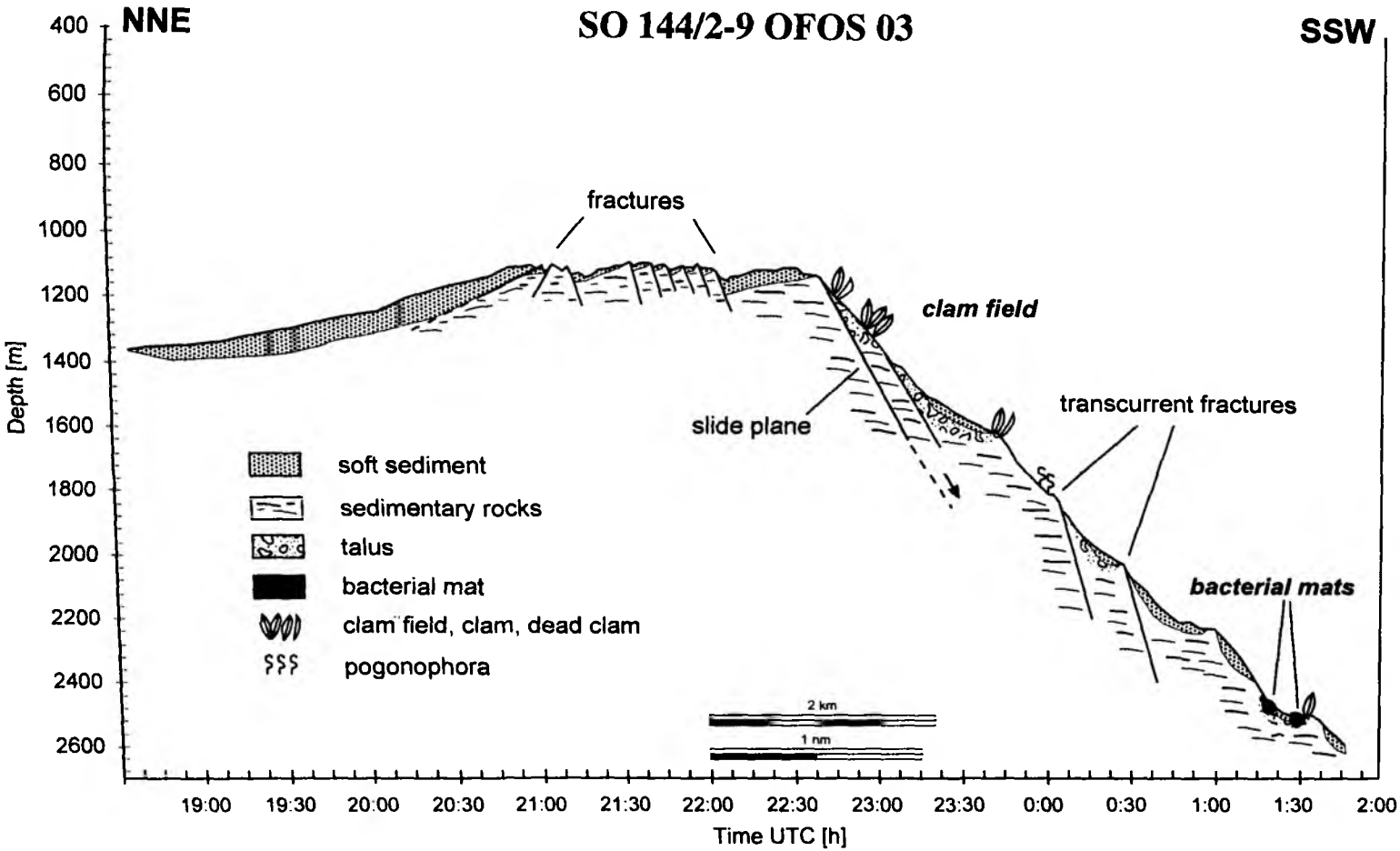

Figure 6.6.5 OFOS 03 observation. Schematic section.

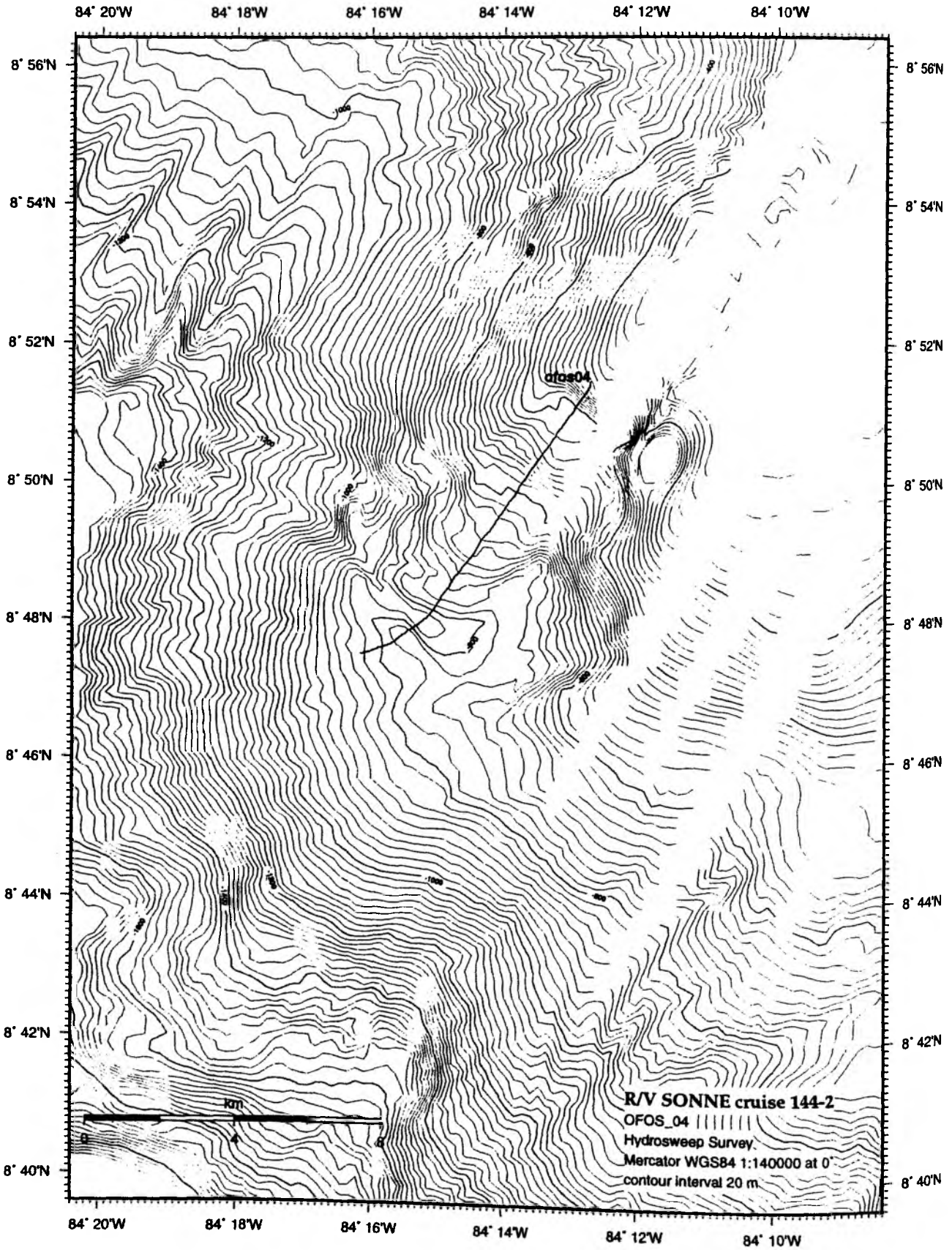

Figure 6.6.6 Position of OFOS 04.

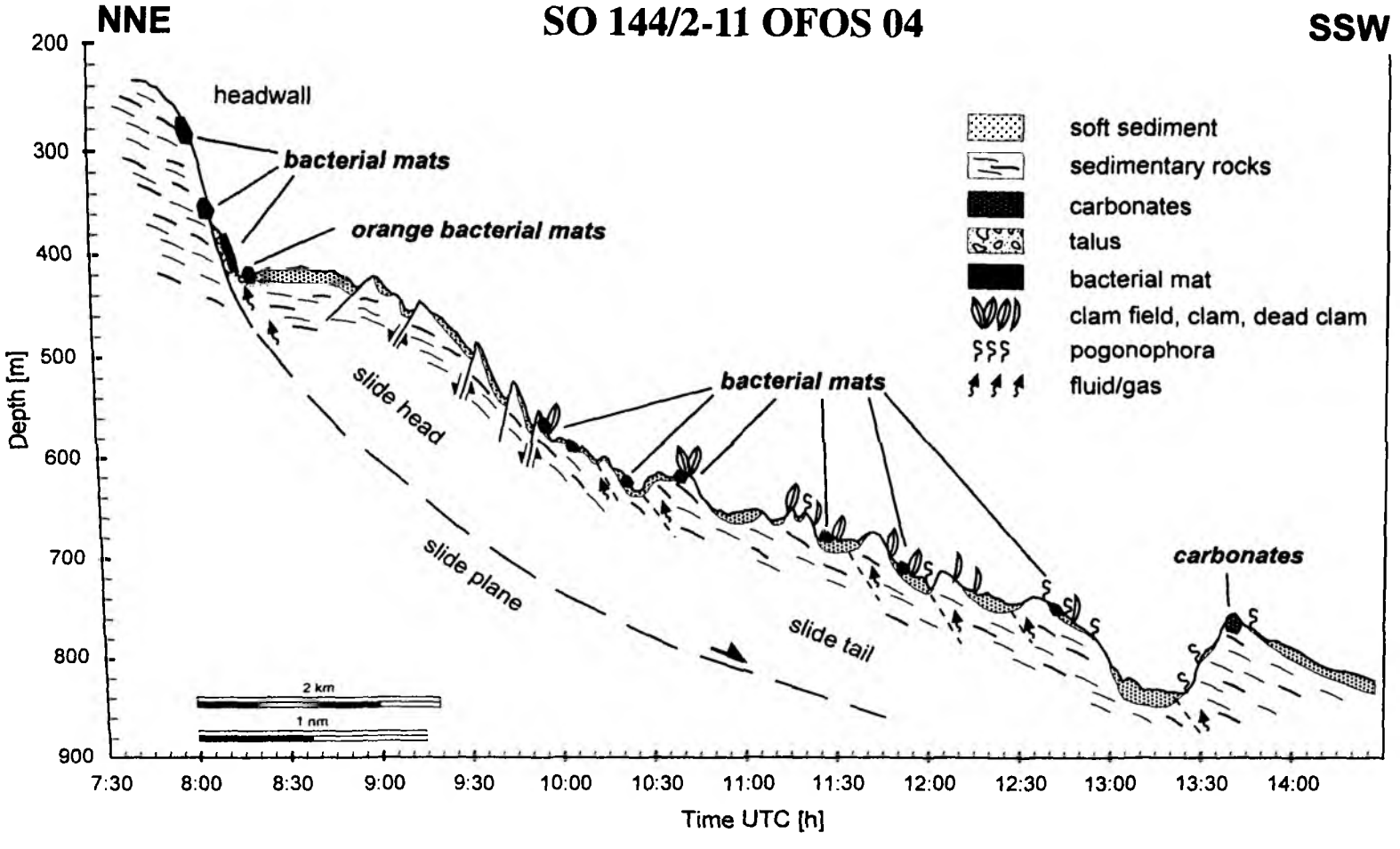

Figure 6.6.7 OFOS 04 observation. Schematic section.

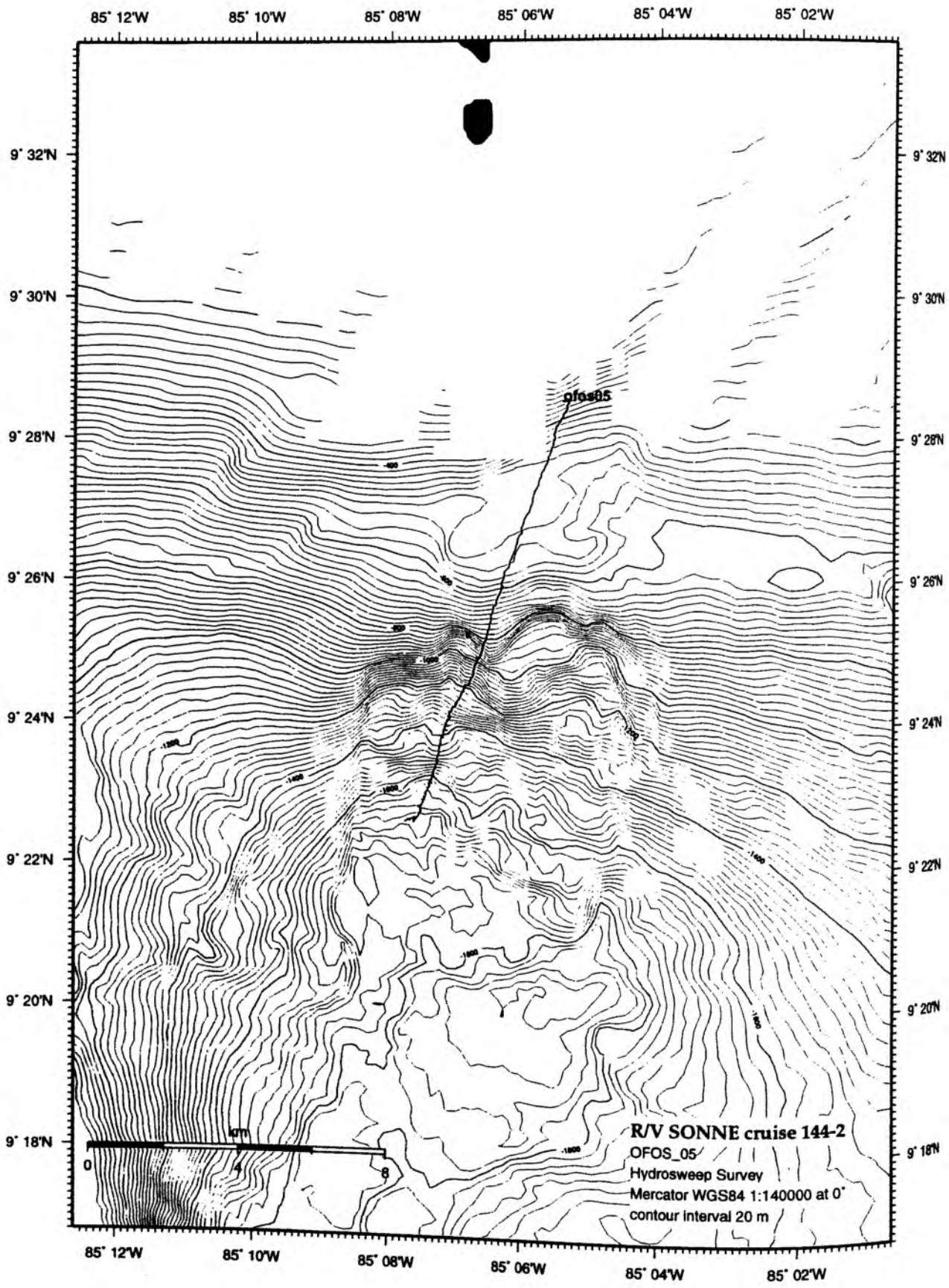

Figure 6.6.8 Position of OFOS 05.

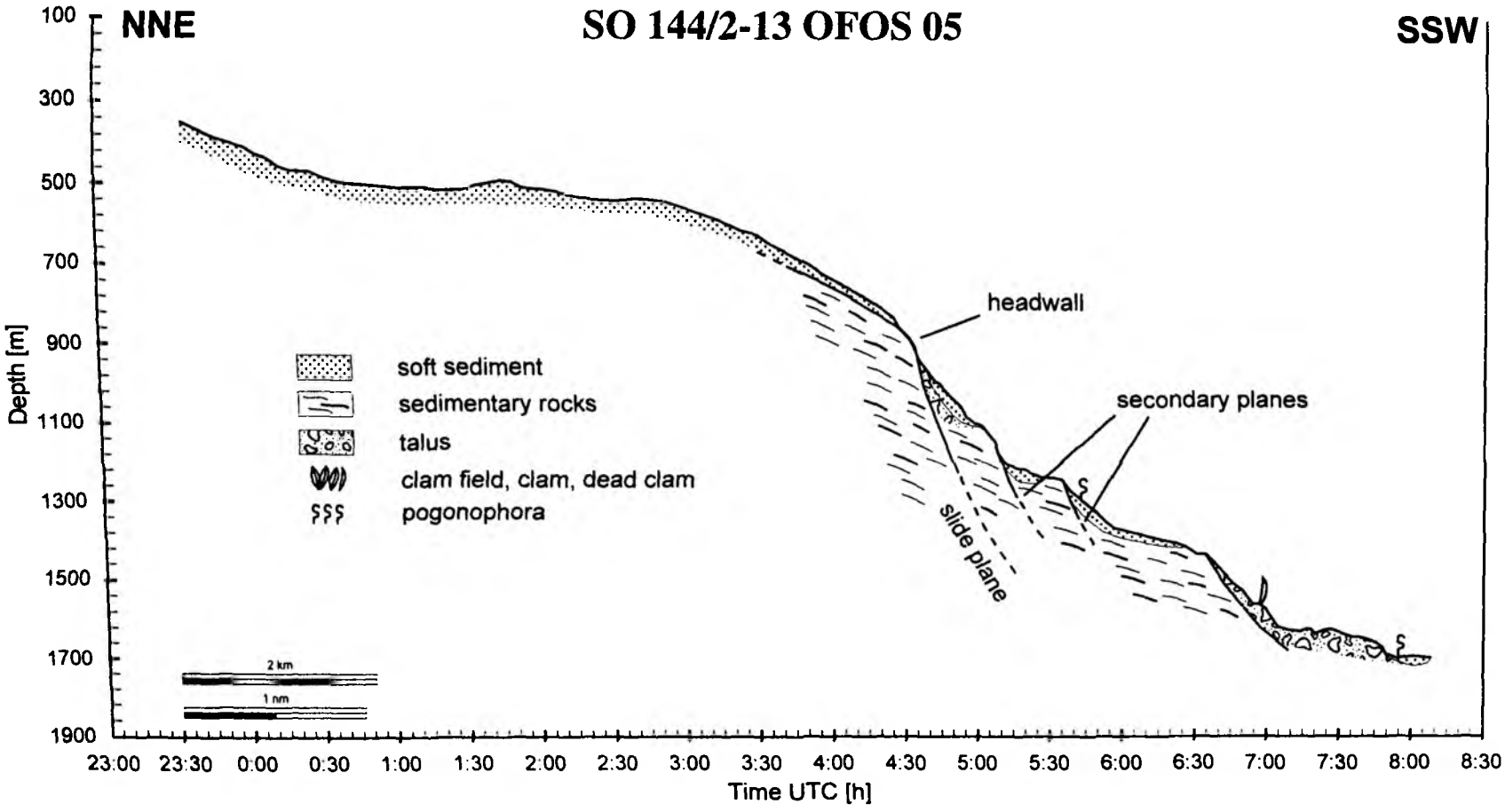

Figure 6.6.9 OFOS 05 observation. Schematic section.

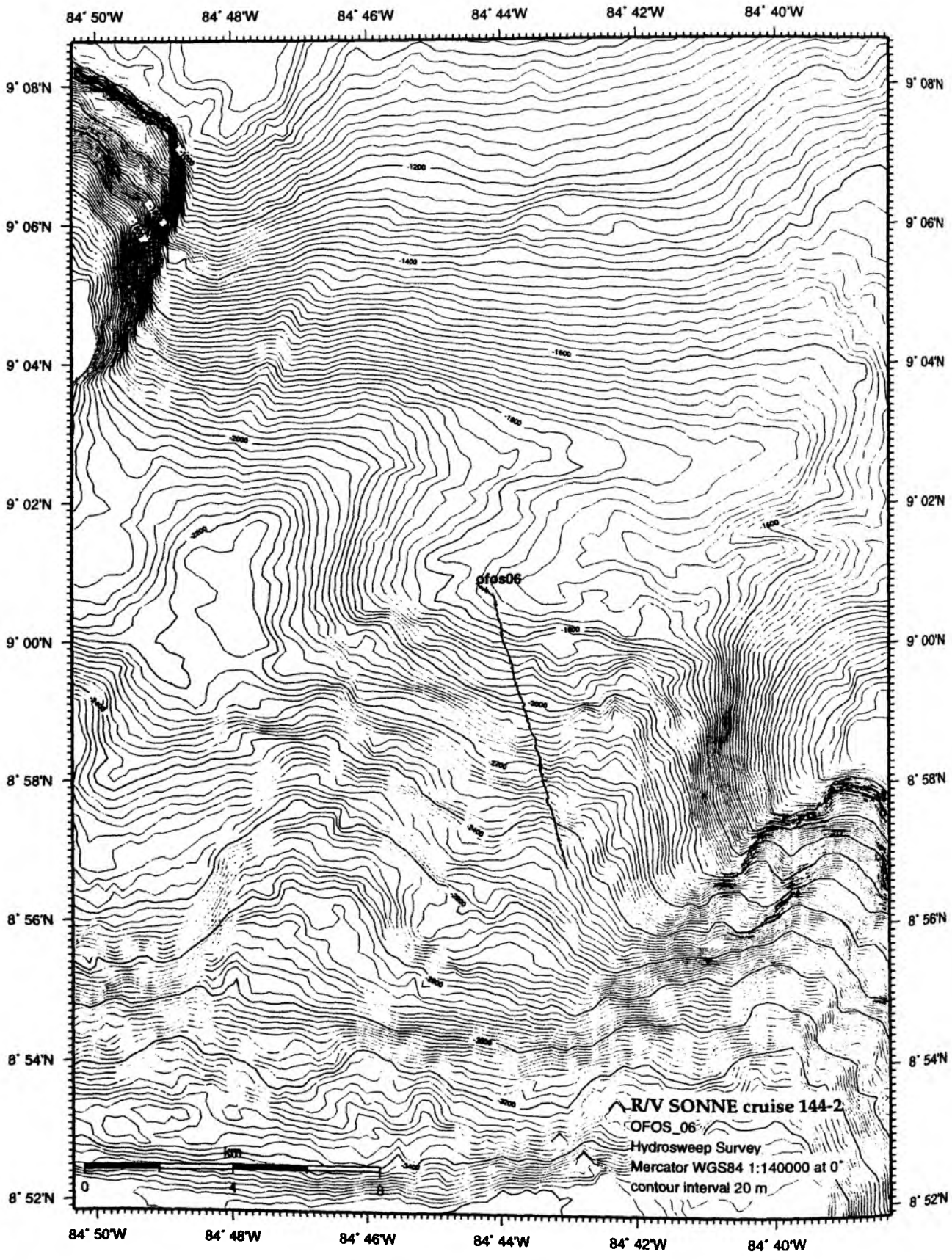

Figure 6.6.10 Position of OFOS 06.

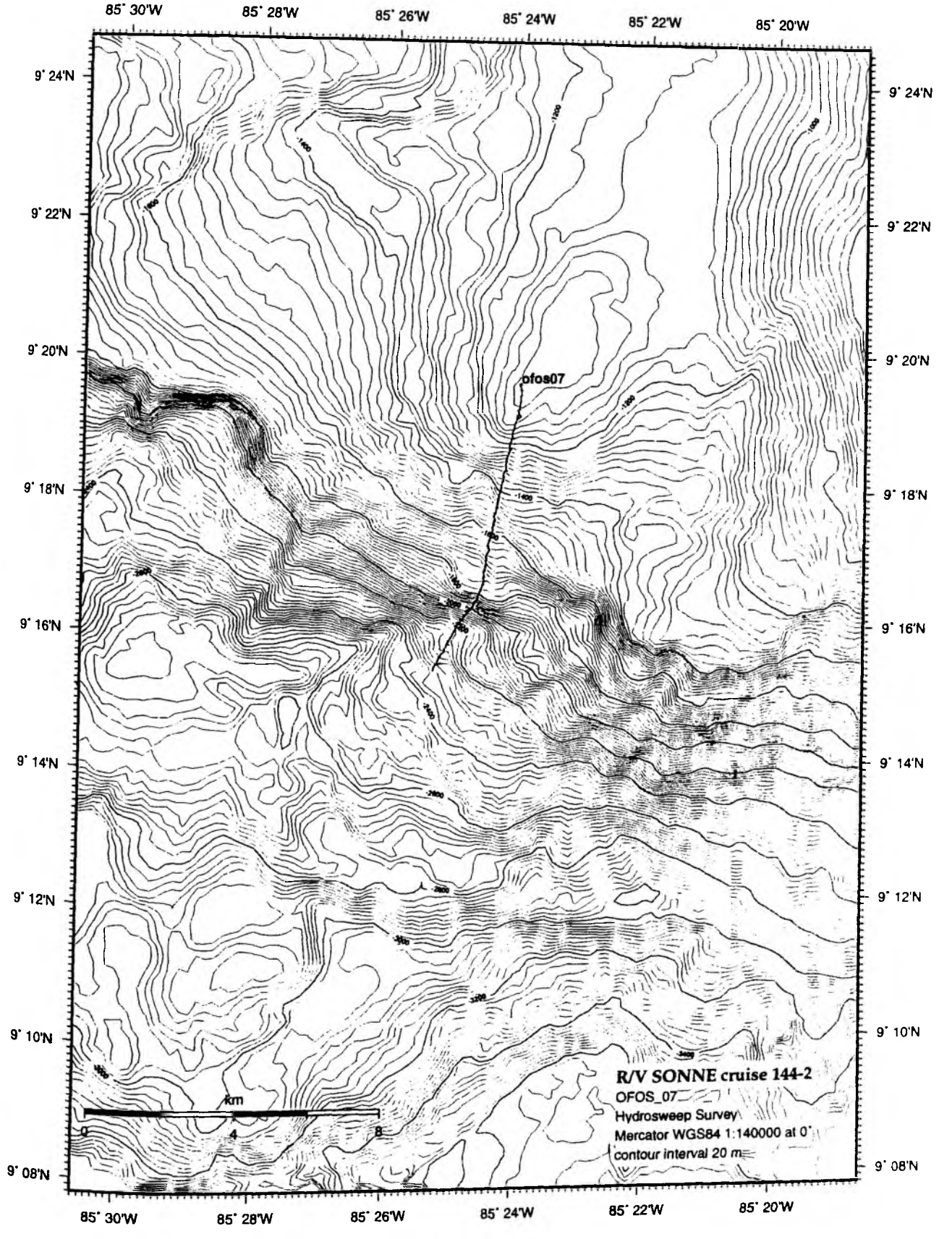

Figure 6.6.11 Position of OFOS 07.

6.7 WATER COLUMN INVESTIGATIONS

(K. Heeschen, C. Röckmann, T. Kath)

In addition to detailed mapping of the seafloor and the occurrence and destabilization of gas hydrates, a major goal of cruise SO 144-2 off the Costa Rican Pacific margin was to investigate fluid and gas expulsion from the sea floor. Along the margin, the morphologically rough, seamount-featuring Cocos Plate is being subducted. With the known existence of a Bottom Simulating Reflector (BSR) and sediment-layer uplift from subduction of seamounts, a wide destabilisation of gas hydrates is expected. Large amounts of vent fluids and methane gas can be emitted from the resulting scars, which may lead to vertical outcrops of sediment layers, once reaching the BSR and free gas zone (see Chapter 2 for details).

Initially, for a general view of the water columns, methane inventor sampling, using SONNE's own CTD/carousel water sampler (see chapter 5.11.5), was performed mainly in the near-bottom water column in morphological depressions. The ship's 18 kHz Parasound system also assisted by allowing detection of free gas bubbles (Chapter 5.11.2 and 6.1.2.2) .

In total, 9 CTDs were deployed (see Fig. 6.7.1 for locations). Positions for the CTDs were partly chosen from results of the OFOS video sled (vent organisms; see chapters 5.11.4, 6.6) or partly from the bathymetric map and TOBI raw data. Plateaus beneath steeper slopes within slump scars or slides were thought to be potentially higher in methane concentrations. The bottom-near water column was sampled at high resolution, with most of the niskin bottles being closed in steps of 10 to 30 m in the first 300 m from the sea floor. Only a few samples were taken in the upper 1000 m. Additionally, the first CTD provided a sound velocity profile down to a depth of 3500 m, which was used for the hydroacoustic work (Chapter 6.1). On the first CTD no methane measurements were taken.

Methane Measurements

During cruise SO144-2, methane in the water column was measured from discrete samples collected directly from the CTD carousel water sampler. For CH_4 analysis, a modified vacuum degassing method was used as described by Lammers and Suess [1994]. 400 ml of seawater were sampled directly from the Niskin bottles using a large glass syringe and were immediately injected into sealed pre-evacuated 600 ml glass bottles. To equilibrate the air and water phases in the sample bottles the latter were shaken for at least 30 min. An evacuated preparation line is used for subsequently recompressing the gas phase by slowly pushing a brine underneath the sample water until atmospheric pressure is reached. The CH_4 mole fraction of the extracted gas was determined by gas chromatography (Shimadzu R-14A) using flame ionization detection. Assuming that N_2 and Ar were 100% saturated relative to their atmospheric partial pressures [Weiss, 1970], the total gas content of the sample was calculated from the measured dissolved oxygen concentration. The dissolved oxygen concentration was derived from the Winkler titration. Finally, the dissolved methane concentration (nmol/l) was calculated as the product of the mole fraction in the extracted gas phase and the amount of total gas (STP) in the sample divided by the molar weight of methane. For the FID calibration, bottled mixtures of 10.00 ppm ± 5% and 904 ± 2% methane in synthetic air were used.

Oxygen Measurements

In addition to using the CTD sensor, oxygen measurements were determined using discrete water samples from the rosette. Calibration against Winkler titration (see *Grasshoff*, 1982) showed an average difference between the oxygen sensor and the oxygen measured by titration of 0.19 ml/l with a standard deviation of 0.1 ml/l. 55 oxygen values from Winkler titration were suitable for use (CTD 02 – 07). Especially at lower concentrations, the

rence can be up to 0.35 ml/l and within double of the oxygen concentration in the oxygen imum zone at 200 - 600 m water depth. For recalculation of the methane concentrations, titrated values were used except for CTD 04, where no oxygen was determined on discrete nples. Corrected values from the sensor were used in this case. For a typical oxygen profile the water column within the investigated area, see Fig. 6.7.2.

'reliminary Results

A typical distribution of temperature, salinity and oxygen is shown in Fig. 6.7.2. Below a very warm and light surface layer of only about 30 m mixed with freshwater from the nearby coast, a layer of higher salinity and more rapid temperature decreases follows. Salinity stabilisation and a more gradual temperature decrease begins at 400 m, continuing to 2000 m. From this depth, temperature, too, nears stability. When comparing the gas hydrate stability curve against the temperature distribution recorded from CTDs 01 – 07, gas hydrates can be expected to destabilize at approximately 600 m (Fig. 6.7.3). Temperature distribution in the sediment may differ slightly. Therefore, if sediments containing gas hydrates are uplifted by seamount subduction above this depth the methane clathrates will free methane gas.

Elevated methane concentrations within the water column were found in 5 of 8 profiles within the water column of land slides and slump scars at the northern Costa Rican Pacific margin. The profiles of all hydrocasts are plotted in Figs. 6.7.4 and 6.7.5. For the most parts, the highest methane concentrations are limited to the bottom near 150 m of the water column. More seldom, slightly higher concentrations are found several hundred metres above the seafloor. They are probably related to vent sites at the slope next to the CTD profile (8-CTD 03, 10-CTD 04). Rather than any specific ocean depth having consistently higher concentrations, the elevated methane values near the ocean floor were found at greatly varying depths (4-CTD 02, 10 CTD 04, 12-CTD 05, 28-CTD 08, 30-CTD 09 – from here on only referred to by the CTD number).

The highest methane concentrations of 237 nmol/l were detected in CTD 02 within only 30 m from the bottom. The two maxima of this hydrocast at 1900 m and 1815 m correspond with vent organisms (*Calyptogena* s.p.) observed with the OFOS video sled at exactly this depth (Chapter 6.6). The maxima are separated by a minimum having half of the methane concentration (93 nmol/l) at 1835 m.

CTD 05, deployed where a huge expansion of bacterial mats blankets the slope of the slump scar, showed high methane concentrations (up to 76 nmol/l) within 10 m from the seafloor. Concentrations remained high in all samples from up to 300 m water depth, where the first bacterial mats were observed. Typically, higher concentrations are found in bacterial mat sites than in clam fields, exemplified in the results from CTD O4, CTD 08 but not CTD 02. However, as only one OFOS track covered each scar much of the area is still unfamiliar.

Methane concentrations in the deepest water samples of CTD 04 reached 34 nmol/l, with bottommost values highest. Nevertheless, slightly higher concentrations were also found at 1500 and 1240 m coinciding with the depth of OFOS-observed vent sites (144/2-9 OFOS 03). CTD 03, deployed before any knowledge of vent sites in the Parrita Scar, did not show elevated values at the bottom, but at 2200 m (20 nmol/l) suggesting another area of vent sites within this depth range. However, nothing was seen here with OFOS. Presently, with no knowledge about the local currents and restricted to only a few hydrocasts, no conclusion can be made regarding more exact source areas of the elevated values within the water column, nor about whether or not they spread over a bigger area within the same depth or are restricted to a local appearance.

CTD 08, deployed at another vent site above the Rio Bongo Scar, showed values comparable with CTD 04, even at only 600 m depth. In the bottommost water column, elevated methane values reaching 94 nmol/l were also found with CTD 09. The main feature

here was a mud mount, which was richly inhabited by all kinds of vent organisms such as clams (*Calyptogena* s.p., *Acharax* s.p.), *pogonophora* s.p. and bacterial mats. Methane concentrations probably vary considerably within a small area, as indicated by the scattered groups of organisms.

CTD 06 was deployed in an area where no vent organisms were found (Cabo Blanco Scar 144/2-13 OFOS 05) and the recorded methane concentrations of no more than 4 nmol/l were not significantly different to background concentrations of 1 – 2 nmol/l, which were found within the same water mass. CTD 07 gained similar values with near-bottom concentrations of 3 nmmol/l. However, CTD 07 was deployed without any former information due to an OFOS deployment right at the bottom of a steep slope at the northern rim of the Nicoya Slide.

Subsurface maxima of methane contents at 50 to 170 m were found in all hydrocasts. This can be attributed to currents from the nearby Costa Rican shelf or to in-situ production of methane within the anoxic environments of particles or digestive systems of marine animals. As a distinct thermocline found at about 30 m decreases the gas exchange between the water column and the atmosphere methane can be enriched to up to 17 nmol/l below this depth. Mean values are about 6 – 8 nmol/l.

There is a considerable scope for more water column investigations in order to obtain a better overview of the methane inventory at the investigated areas and to gain greater knowledge of fluxes within the water column and from the water column to the atmosphere. However, a very important result has been achieved by gaining a picture of the methane concentration distribution along the Costa Rican Pacific margin and relating it to observations from concurrently deployed OFOS investigations on SO 144-2.

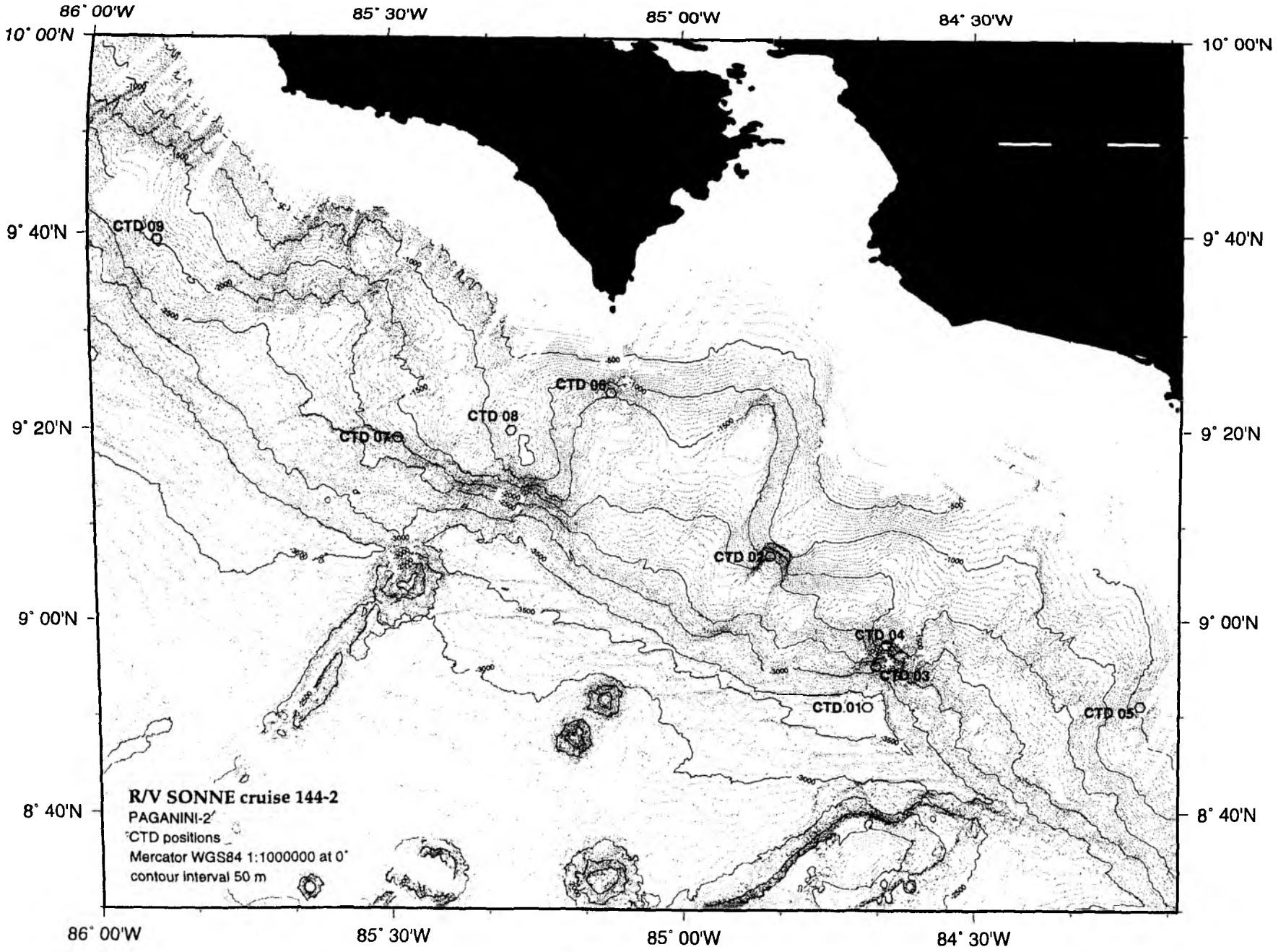

Figure 6.7.1: Positions of CTD deployments on SO144-2.

SO144/2-10 CTD - 04

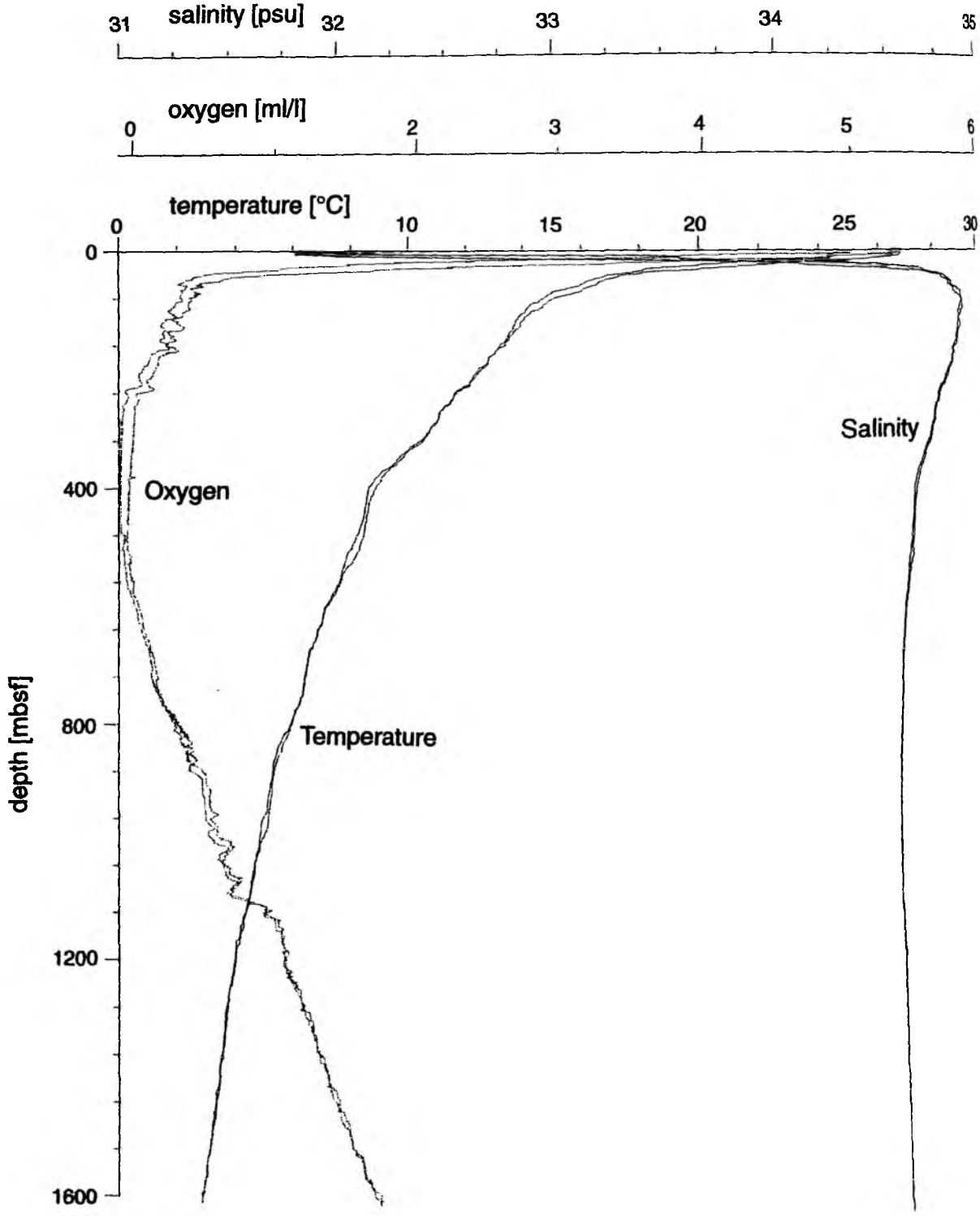

Fig. 6.7.2: Typical water column profils of salinity, temperature and oxygen for the area of Costa Rica Margin; CTD 04 was chosen as an example

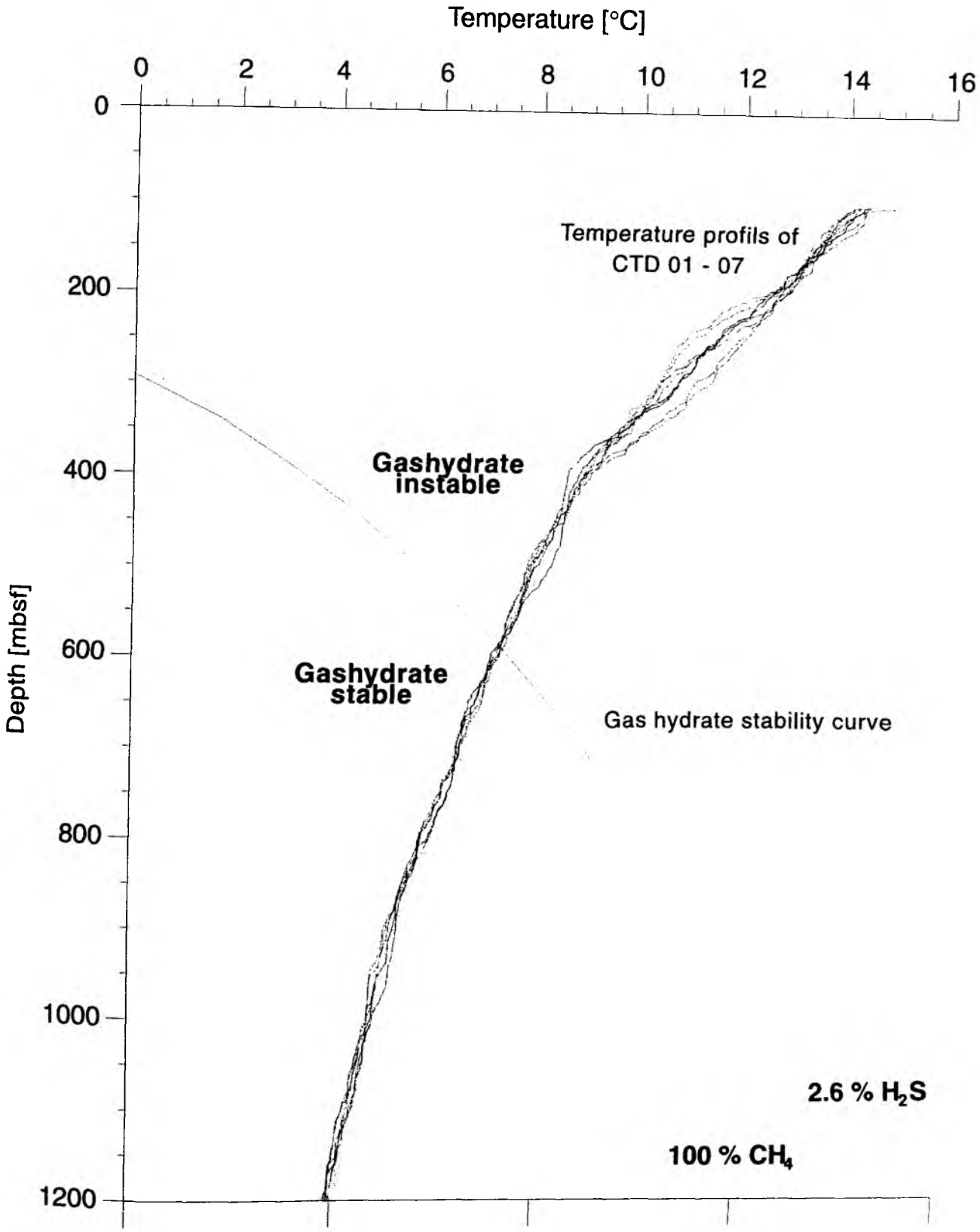

Fig. 6.7.3: Temperature distribution in the water column of CTD 01 - 07 at a depth range between100 -1200 m versus gas hydrate stablitiy curve. Gas hydrate is stable below 580 m.

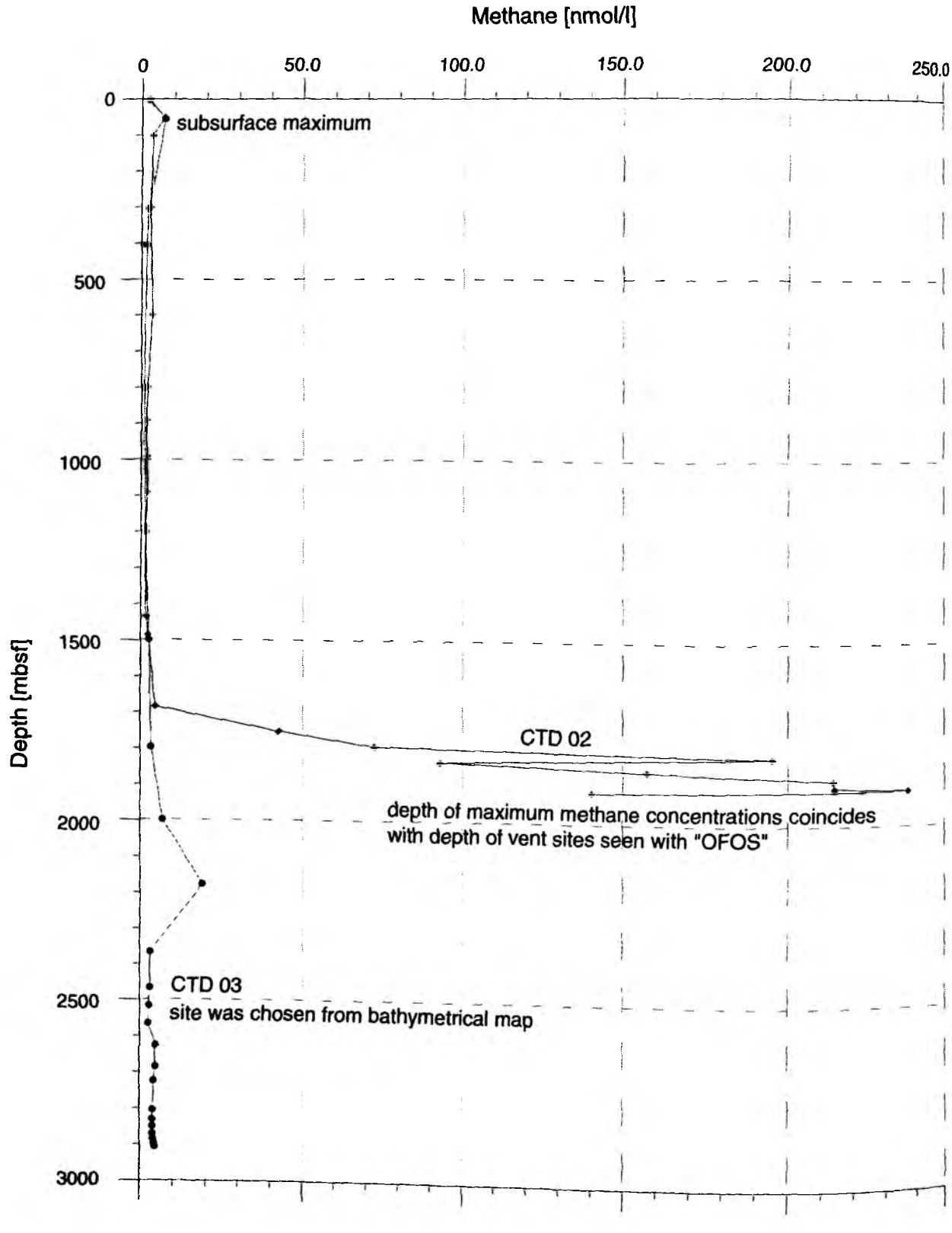

Fig. 6.7.4: Methane distribution in the water column of CTD 02 - 03 with remarks about the results from OFOS investigations at the CTD sites

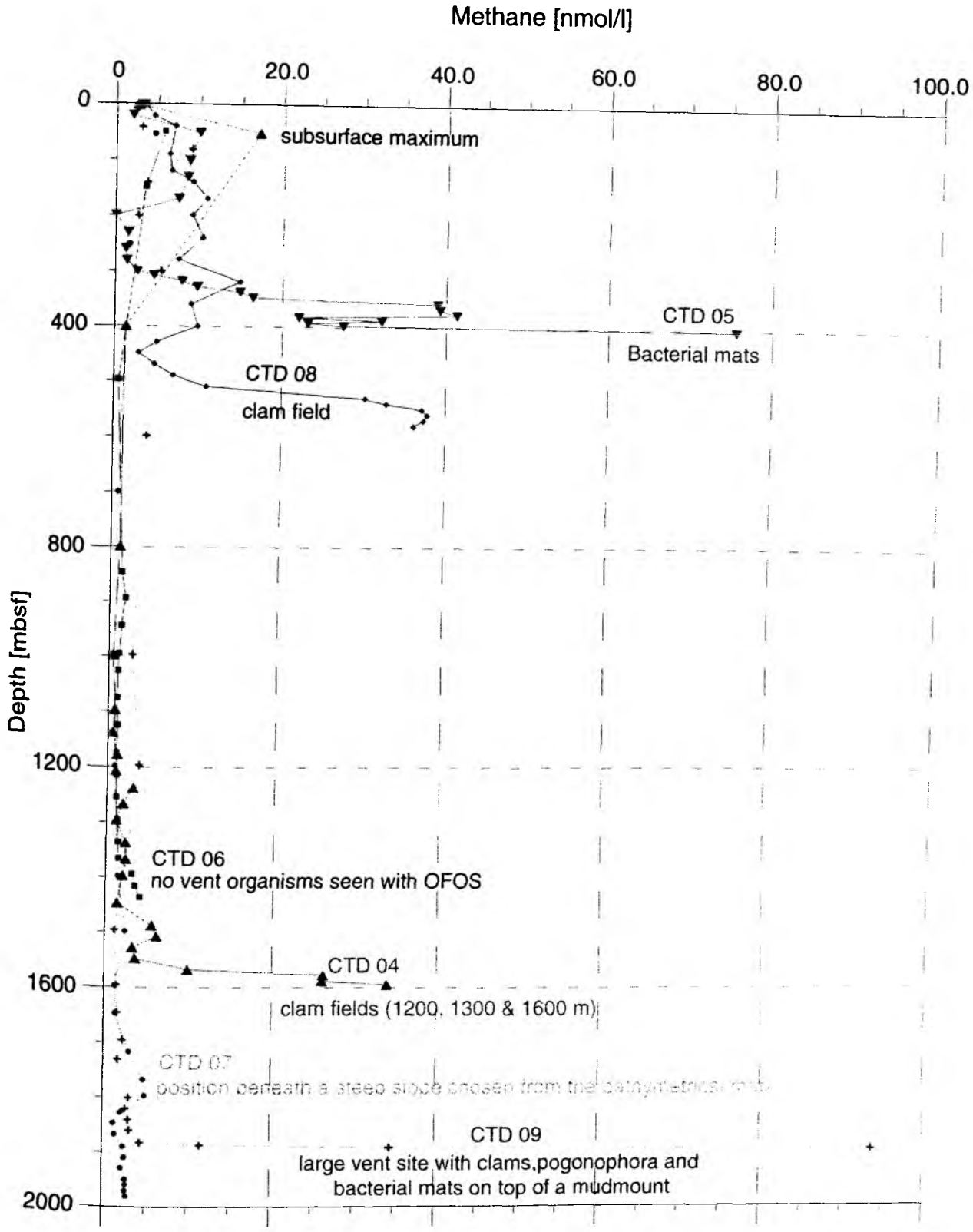

Fig. 6.7.5: Methane distribution in the water column of CTD 04 - 09 with remarks about results from OFOS investigations at the CTD sites

7. ACKNOWLEDGEMENTS

Cruise SO 144-1&2 was funded by the German Ministery of Education, Research, Science, and Technology (BMBF) under project No. 03G144A to GEOMAR within the continued and generous most commendable support for marine sciences with an outstanding research vessel such as SONNE. Additional funding was provided through the Large Scale Facility program of the EU donated to research onboard RV SONNE, which was this time dedicated to support the OBS systems from GÉO AZUR. We also gratefully acknowledge the support of NSF (grant No. OCE-9819204) to the American scientists from SCRIPPS Institution of Oceanography. Luis Geli and Yves Auffret thank IFREMER for supporting their participation to the cruise.

We thank the Challenger Division of Southampton Oceanography Centre (SOC) for financial support for the use of TOBI on the cruise. Technical support for TOBI was provided by the Ocean Technology Division of SOC.

We warmly thank master H. Papenhagen and his crew for their excellent support in all work done and for the splendid working atmosphere throughout the entire and ambitious working program.

8. REFERENCES

Agnew, D. C., J. Berger, W. E. Farrell, J. F. Gilbert, G. Masters, and D. Miller, 1986: Project IDA: a decade in review, EOS, Transactions of the AGU, 67, 203-212,

Ammon, C.J., and J.E. Vidale, 1993: Tomography without rays, Bull. Seism. Soc., Am., 83, 509-528.

Anderson, R.N., Moore, G.F., Schilt, S.S., Cardwell, R.C., Trehu, A. and Vacquier, V., 1976: Heat flow near a fossil ridge on the north flank of the Galapagos spreading center, J. Geophys. Res., 81, 1828-1838.

Barash, T. W., C. G. Doll, J. A. Collins, G. H. Sutton and S. C. Solomon, 1994: Quantitative Evaluation of a Passively Leveled Ocean Bottom Seismometer, Mar Geophys. Res., 16, 347-363.

Barckhausen, U., Ranero, C., von Huene R., and Meschede, M., in prep., Revised tectonic boundaries in the Cocos Plate off Costa Rica and analogous segmentation of the continent.

Barckhausen, U., Roeser, H.A., and von Huene, R., 1997: New insight into the structure of the Cocos plate offshore Costa Rica from seamagnetic measurement, Zentrabl. Geol. Palaeontol., Teil 1, 385-391.

Barckhausen, U., Roeser, H.A. and von Huene, R., 1998: Magnetic signature of upper plate structures and subducting seamounts at the convergent margin off Costa Rica, J. Geophys. Res., 103, 7079-7093.

Barry, K.M., Cavers, D.A. & Kneale, W., 1975: Recommended standarts for digital tape fomats, Geophysics, 40, 344-352.

Batiza, R., 1986: Failed rifts. In: The Eastern Pacific Ocean and Hawaii (ed. by E.L. Winterer, D.M. Hussong and R.W. Decker), The Geology of North America, Vol. N, Ch. 11, pp. 177-186.

Berger, J, D. C. Agnew, R. L. Parker, and W. E. Farrell, 1979: Seismic Calibration: 2. Cross-spectral calibration using random binary signals. Bull. Seismol. Soc. Am., 69, 271-288.

Berrangé, J.P., Thorpe, R.S., 1988: The geology, geochemistry and emplacement of the Cretaceous-Tertiary ophiolitic Nicoya Complex of the Osa Peninsula, southern Costa Rica: Tectonophysics, no. 147, p. 193-220.

Bialas, J. and Flueh, E. R., 1999: Ocean Bottom Seismometers; Sea Technology, 40, 4, 41-46.

Blondel, P. and B.J.Murton, 1997: Handbook of Seafloor Sonar Imagery, John Wiley and Sons, Chichester, 314.

Bohrmann G., Greinert J., Suess E., and Torres M., 1998 Authigenic carbonates from Cascadia Subduction Zone and their relation to gas hydrate stability. Geology 26(7), 647-650.

Boschini, I., 1996: Actividad sísmica superficial en la Región Sureste de Costa Rica: Sus implicaciones para el P.H. Boruca: San Jose-Costa Rica, Instituto Costarricense de Electricidad, Departamento de Geología, Oficina de Sismología y Vulcanología, internal report, 21 p.

Boschini, I., 1989: Incidencia de las fuentes sísmicas en la región Caribe de Costa Rica: San José-Costa Rica, Escuela Centroamericana de Geología, Universidad de Costa Rica, undergraduate thesis, unpublished, 97 p.

Burbach, G.V., Frohlich, C., Pennington, W.D., Matumoto, T., 1984: Seismicity and Tectonics of the Subducted Cocos Plate: Journal of Geophysical Research, vol. 89, no. B9, p. 7719-7735.

Camacho, E., Víquez, V., 1993: Historical seismicity of the North Panama Deformed Belt: Revista Geológica de América Central, no. 15, p. 49-64.

Cande, S.C. and Kent, D.V. J., 1995: Geomagnetic polarity time scale, J. Geophys. Res., 100, B4, 6093-6095.

Christeson, G., 1998: OBSTOOL: software for processing OBS data.

Collins, L.S., 1993: Neogene paleoenvironments of the Bocas del Toro Basin, Panama, J. Paleont., 67, 699-710.

Collins, L.S., Coates, A.G., Jackson, J.B.C. and Obando, J., 1995: Timing and rates of emergence of the Limon and Bocas del Toro basins: Caribbean effects of Cocos ridge subduction? In: Mann, P. (Ed.), Geologic and Tectonic Development of the Caribbean plate boundary in southern Central America, Geol. Soc. Amer., Spec. Pap., 295, 263-289.

Corrigan, J., Mann, P., Ingle, J.C., 1990: Forearc response to subduction of the Cocos Ridge, Panama-Costa Rica: Geological Society of America Bulletin, vol. 102, p. 628-652.

DeBoer, J.Z., Drummond, M.S., Bordelon, M.J., Defant, M.J., Bellon, H. and Maury, R.C., 1995: Cenozoic magmatic phases of the Costa Rican island arc (Cordillera de Talamanca), Geol. Soc. Amer., Spec. Pap., 295, 35-55.

DeMets, C., Gordon, R.G., Argus, D.F. and Stein, S., 1990: Current plate motions, Geophys. J. Int., 101, 425-478.

Drummond, M.S., Bordelon, M., De Boer, J., Defant, M.J., Bellon, and Feigenson, M.D., 1995: Igneous petrogenesis and tectonic setting of plutonic and volcanic rocks of the Cordillera de Talamanca, Costa Rica-Panama, Central American arc, Amer. J. Sci., 295, 875-919.

Flueh, E. R., 1995: Cruise Report SO103, Condor 1B; Geomar Report 41, Kiel, 140 pp.

Flueh, E. R. and Bialas, J., 1996: A digital, high data capacity ocean bottom recorder for seismic investigations; Int. Underwater Sytems Design, 18(3), 18-20.

Flueh, E. R., Kukowski, N., and Reichert, C., 1997: Cruise Report SO123, Mamut; Geomar Report 62, Kiel, 292pp.

Flueh, E. R., 1999: Cruise Report SO142, HULA II; Geomar Report 90, Kiel, 224 pp.

Graefe, K., 1998: Exhumation and thermal evolution of the Cordillera de Talamanca (Costa Rica): Constraints from fission track analysis, ^{40}Ar-^{39}Ar, and ^{87}Rb-^{87}Sr chronolgy, Tüb. Geow. Arb., 39, 113 pp.

González-Viquez, C., 1910: Temblores, terremotos, inundaciones y erupciones volcánicas en Costa Rica 1608-1910: Cartago-Costa Rica, Editorial Tecnológica de Costa Rica, reprinted in 1994 from the original, 239 p.

Gutenberg, B., Richter, C.F., 1954: Seismicity of the earth and associated phenomena: Princeton University Press, 310 p.

Gutscher, M. A., Malavielle, J., Lallemand, S., and Collot, J. Y., 1999: Tectonic segmentation of the north Andean margin: Impact of the Carnegie Ridge collision; Earth Planet. Sci. Lett., 168, 255-270.

Güendel, F., Protti, M., 1998: Sismicidad y sismotectónica de América Central: Física de la Tierra, no. 10, p. 19-51.

Güendel, F., 1986: Seismotectonics of Costa Rica: An analytical view of the southern terminus of the Middle America trench: California-U.S.A., University of California (Santa Cruz), Ph.D. thesis, 113 p.

Havskov, J. (ed.), 1997: The SEISAN Earthquake Analysis Software for the IBM PC and SUN: Bergen-Norway, Institute of Solid Earth Physics, University of Bergen, manual, 235 p.

Hello, Y., Charvis, P., Pontoise, B., Nakamura, Y. & Chen, A.T., 1992: Long-range seismic refraction using digital OBS , European Geophysical Society General Assembly, 10 (suppl), Solid earth geophysics & natural hazards, C51.

Hey, R., 1977: Tectonic evolution of the Cocos-Nazca spreading center, Geol. Soc. Amer. Bull., 88, 1404-1420.

Hinz, K., von Huene, R., Ranero, C. R., and PACOMAR working group, 1996:Tectonic structure of the convergent Pacific margin offshore Costa Rica from multichannel seismic reflection data. Tectonics 15, 54-66.

Hyndman R. D., Foucher J. P., Yamano M., Fisher A., and 131 a. S. t. o. O. L. (1992) Deep sea bottom-simulating reflectors: calibration of the base of the hydrate stability field as used for heat flow estimates. Earth and Planetary Science Letters 109(289-301).

Ihmlé, P. F. 1996: Monte carlo slip inversion in the frequency domain: Application to the 1992 nicaragua slow earthquake. Geophys. Res. Lett., vol. 23, 913-916.

Jacobson, R.S., Dorman, L.M., Purdy, G.M., Schultz, A., Solomon, S., 1991: Ocean Bottom Seismometer Facilities Available, EOS, Transactions AGU, 72, pp506,515.

Kimura, G., Silver, E. A., Blum, P., et al., 1997: Proceedings of the Ocean Drilling Program, Initial Reports, v. 170: College Station, Texas, Ocean Drilling Program.

Knickmeyer, E.T., 1996: Hochgenaues Differential-GPS, Proc. 11th Annual Meeting of the German Hydrographic Society, Glücksburg, 3.-5.6.

Kvenvolden K. A. (1993) Gas hydrates - geological perspective and global change. Reviews of Geophysics 31(2), 173-187.

Langseth, M.G., and Silver, E.A., 1996: The Nicoya convergent margin-a region of exceptionally low heat flow: Geophys. Res. Lett., 23, p. 891-894.

Latraille, S, and L. M. Dorman, 1983: A standard format for the storage and exchange of natural and explosive source seismic data: the ROSE format, Mar. Geophys. Res., 6, 99-105.

Lienert, B.R.E., Berg, E., Frazer, L.N., 1986: Hypocenter: An earthquake location method using cenetered, scaled, and adaptively least squares: Bulletin of the Seismological Society of America, vol. 76.

Lonsdale, P. and Klitgord, K.D., 1978, Structure and tectonic history of the eastern Panama Basin, Geol. Soc. Amer. Bull., 89, 981-999.

Luetgert, J., 1992: Interactive two-dimensional seismic raytracing for the Macintosh, USGS Open File Report, 43.

Matumoto, T., Ohtake, M., Latham, G., Umaña, J., 1977: Crustal structure in Southern Central America: Bulletin of the Seismological Society of America, vol. 67, no. 1, p. 121-134.

McIntosh, K., Silver, E., Shipley, T., 1993: Evidence and mechanisms for forearc extension at the accretionary Costa Rica convergent margin, Tectonics 12, 1380-1392.

Meissner, R., Flueh, E.R., Stibane, F., and Berg, E., 1976: Dynamics of the active plate boundary in southwest Colombia according to recent geophysical measurements. In: O.L. Anderson and B.S. Bolt (Editors), Theory and Experiment Relevant to Geodynamic Processes. Tectonophysics, 34, 115-136.

Meschede, M., Zweigel, P., Frisch, W. and Völker, D., 1999 in press, Mélange formation by subduction erosion: the case of the Osa mélange in southern Costa Rica. In press at Terra Nova.

Meschede, M., Barckhausen, U. And Worm, H.-U., 1998: Extinct spreading on the Cocos Ridge, Terra Nova, 10, 211-216.

Miyamura, S., 1980: Sismicidad de Costa Rica: San Jose-Costa Rica, Editorial Universidad de Costa Rica, 189 p.

Montero, W., 1986: Períodos de recurrencia y tipos de secuencias sísmicas de los temblores interplaca e intraplaca en la región de Costa Rica: Revista Geológica de América Central, no. 5, p. 35-72.

Montero, W., 1994: Neotectonics and related stress distribution in a subduction-collisional zone: Costa Rica: In: Seyfried, H., Hellmann, W. (ed.), Profil, Stuttgart-Alemania, Universität Stuttgart, Institut für Geologie und Paläontologie, vol. 7, 433 p.

Montero, W., Denyer, P., Barquero, R., Alvarado, G.E., Cowan, H., Machette, M.N., Haller, K.M., Dart, R.L., 1998: Map and Database of Quaternary Faults and Folds in Costa Rica and its Offshore Region: USA, Department of the Interior, U.S. Geological Survey, 63 pp (+map).

Montessus de Ballore, F., 1888: Tremblements de terre et éruptions volcaniques en Centre Amérique depuis la conquête espagnole jusqu'à nos jours: Dijon-France, Société de Sciences Naturelles de Saône et Loire, 293 p.

Moore, R. D., Dorman, L. M., Huang, C-Y, Berliner, D. L., 1981: An ocean bottom microprocessor-based seismometer, Mar. Geophys. Res., 4, 451-477.

Morales, L.D., 1986: Historia de la Sismologia en Costa Rica: Rev. Fil. Univ. Costa Rica. XXIV (59): p. 93-104.

Mrazek, J. Spangenberg, T., and von Huene, R., 1996: Geologische und Geophysikalische Untersuchungen vor Costa Rica und Nicaragua - Beiträge zum Versändnis des aktiven ostpazifischen Kontinentalrandes, FS Sonne Fahrtbericht SO 107, Pacomar 3, Balboa/Panama - San Francisco/USA, 10.03. - 14.04.1996, Unpublished report, Geomar, Kiel, Ernst-Moritz-Arndt Universität Greifswald, 172 pp.

Nakamura, Y. & Garmany, J., 1991: Development of upgraded ocean bottom seismograph, University of Texas Institute for Geophysics Technical Report, 111.

Nakamura, Y., Donoho, P.L., Roper, P.H. & McPherson, P.M., 1987: Large-offset seismic surveying using ocean-bottom seismographs and air guns: instrumentation and field technique, Geophysics, 52, 1601-1611.

National Geophysical Data Center, 1996: Marine Geophysical DATA, CD-ROM.

Pacheco, J.F., Sykes, L.R., 1992: Seismic moment catalog of large, shallow earthquakes, 1900-1989: Bulletin of the Seismological Society of America, no. 82, p. 1306-1349.

Parson, T., J. McCarthy, W.M. Kohler, mC.J. Ammon, H.M., Genz, J.A. Hole, and E.E. Criley, 1996: Crustal structure of the Colorado Plateau, Arizona: application of a new long-offset seismic data analysis techniques, J. Geophys. Res., 101, 11173-11194.

Paull C. K., Ussler W., and Dillon W. P. (1991) Is the extent of glaciation limited by marine gas-hydrates? Geophysical Research Letters 18, 432-434.

Pecher, I.A., Ranero, C.R., von Huene, R., Minshull, T.A., and Singh, S.C., 1998: The nature and distribution of bottom simulating reflectors at the Costa Rican convergent margin, Geophys. J. Int. 133, p. 219-229.

Peraldo, G., Montero, W., 1994: Temblores del período colonial de Costa Rica: San José-Costa Rica, Editorial Tecnológica de Costa Rica, 162 p.

Prothero, W. A., 1976: A Digital Event-Recording Ocean Bottom Seismometer Capsule. Mar. Geophys. Res., 3, 119-141.

Protti, M., Güendel, F., McNally, K., 1994: The geometry of the Wadati-Benioff zone under southern Central America and its tectonic significance: results from a high-resolution local seismographic network: Physics of the Earth and Planetary Interiors, vol. 84, p. 271-287.

Ranero, C., von Huene, R., and Pecher, I., 1996: Heat flow patterns modeled from BSRs along the Pacific continental margin of Costa Rica, EOS, v. 77, n. 46, p. F645 (abst).

Ranero, C.R., von Huene, R., Flueh, E., Duarte, M., Baca, D., and McIntosh, K., 1999: A cross section of the convergent Pacific margin of Nicaragua: Tectonics, in press.

Rempel A. W. and Buffett B. A. (1998) Mathematical models of gas hydarte accumulation. In Gas hydrates: Relevance to world margin stability and climatic change (ed. J.-P. Henriet and J. Mienert).

Sandwell, D.T. and Smith, W.H.F., 1997: Marine gravity anomaly from Geosat and ERS 1 satellite altimetry. J. Geophys. Res., B, 102, 10,039-10,054.

Sauter, A. W. and Dorman, L.M., 1986: Instrument calibration of Ocean Bottom Seismometers, Mar. Geophys. Res., 8, 265-275.

Sauter, A. W., Hallinan, J., Currier, R., Barash, T., Wooding, B., Schultz, A., Dorman, L.M., 1990: Proc MTS conf on Marine Instrumentation, 99-104.

Schreiber, R., and H.W. Schencke, 1990: Efficient hydrographic surveying of EEZ with new multibeam echosounder technology for shallow and deep water, Ocean resources, 1, 73-87.

Seeber, G., 1996: Stand und Einsatzmöglichkeiten von GPS - ein Überblick, Proc. 11th Annual Meeting of the German Hydrographic Society, Glücksburg, 3.-5.6.

Shipley, T.H., McIntosh, K.D., Silver, E.A., Stoffa, P.L., 1992: Three dimensional seismic imaging of the Costa Rica accretionary prism: Structural diversity in a small volume of the lower slope. Journal of Geophysical Research, v. 97, B4, p. 4439-4459.

Smith, W. H. F. and Sandwell, D.T., 1997: Global sea floor topography from satellite altimetry and ship depth soundings, Science, 277, 1956-1962.

Spangenberg, Th., 1997: FS SONNE Fahrtbericht SO107 PACOMAR3 Greifswald

Sprechmann, P., Astorga, A., Calvo, C. and Fernandez, A., 1994: Stratigraphic chart of the sedimentary basins of Costa Rica, Central America, Profil, 7, 427-433.

Stavenhagen, A. U., et al., 1998: Seismic wide-angle investigations in Costa Rica -a crustal velocity model from the Pacific to the caribbean Coast. ZBL. Geol. Palaont. 1, 393-408.

Suárez, G., Pardo, M., Domínguez, J., Ponce, L., Montero, W., Boschini, I., Rojas, W., 1995: The Limon, Costa Rica earthquake of April 22, 1991: Back arc thrusting and collisional tectonics in a subduction environment: Tectonics, vol. 14, no. 2, p. 518-530.

Suess E., Torres M., Bohrmann G., Collier R., Greinert J., Linke P., Rehder G., Trehu A., Wallmann K., Winckler G., and Zuleger E., 1999: Gas hydrates destabilization: Enhanced dewatering, benthic material turnover and large methane plumes at the Cascadia convergent margin. Earth and Planetary Science Letters 170, 1-15.

Trehu A., Torres M., Moore G., Suess E., and Bohrmann G. (1999) Temporal and spatial evolution of a gas hydrate-bearing accretionary ridge on the Oregon continental margin. Gelogy 27(10), 939-942.

Tristán, J. F., 1916: The Costa Rica Earthquake of February 27, 1916: Bulletin of the Seismological Society of America, no. 6, 232-235.

Tristán, J. F., Biolley, P., Cots, C., 1912: The Sarchí Earthquake, Costa Rica: Bulletin of the Seismological Society of America, no. 2, 201-208.

Vidale, J.E., 1988: Finite-difference calculation of travel times, Bull. Seism. Soc. Am., 78, 2062-2076.

von Huene, R. und Flueh, E. R., 1994: A review of geophysical studies along the Middle America Trench off Costa Rica and the problematic seaward terminus of continental crust; In: H. Seyfried and W. Hellmann (Eds.): Geology of an Evolving Island Arc - The Isthmus of Southern Nicaragua, Costa Rica, and Western Panama., Profil 7, Stuttgart. 143-159.

von Huene, R., Ranero, C. R., Weinrebe, W.; Hinz, K. Quaternary convergent margin tectonics of Costa Rica, segmentation of the Cocos Plate, and Central American volcanism, Tectonics, (in press).

von Huene and Pecher, 1999: Vertical tectonics and the origins of BSRs along the Peru margin, Earth and Planetary Science Letters, 166, p. 47-55.

von Huene, R., Bialas, J., Flueh, E., Cropp, B., Csernok, T., Fabel, E., Hoffmann, J.L., Emeis, K., Holler, P., Jeschke, Leandro M., C., Peréz Fernandéz, I., Chavarria S., J., Florez H., A., Escobedo Z., D., León, R., and Barrios L., O., 1995: Morphotectonics of the Pacific convergent margin of the Caribbean plate boundary in southern Central America: Geological Society of America Special Paper 295, p. 291-307.

von Huene. R., J. Aubouin, et al., 1985: Initial Rep. DSDP 84, 21-77.

Walther, C.H.E., Flueh, E.R., Ranero, C.R., von Huene, R. and Strauch, W., An unusual crustal structure across the Pacific Margin of Nicaragua. submitted to Geophys. J. Int.

Walther, C.; Flueh, E.R.; Ranero, C. R. & von Huene, R., 1997: Seismic investigations offshore Nicaragua. EOS AGU Fall Meeting (San Francisco).

Weinrebe, W., 1997: Fahrtbericht SO-112 HIRESBAT, GEOMAR-Report 64, GEOMAR-Kiel.

Wessel, P., and W.H.F. Smith, 1991: Free software helps map and display data, EOS Trans. Am. Geophys. Un., 72, 441, 445-446.

Wessel, P. and Smith, W. H. F., 1995: The Generic Mapping Tools (GMT) version 3.0, Technical Reference and Cookbook, SOEST/NOAA.

Wilson, D.S., 1996: Fastest known spreading on the Miocene Cocos-Pacific plate boundary, Geophys. Res. Lett., 23, 3003-3006.

Wilson, D.S. and Hey, R., 1995: History of rift propagation and magnetization intensity for the Cocos-Nazca spreading center, J. Geophys. Res., 100, B7, 10,041-10,056.

Ye, S., et al., 1996: Crustal structure of the subduction zone off Costa Rica derived from OBS refraction and wide-angle reflection seismic data. Tectonics 15, 1006-1021.

Zelt, C.A., and R.B. Smith, 1992: Seismic travel time inversion for 2-D crustal velocity structure, Geophys. J. Int., 108, 16-34.

INSTRUMENT	LAT (N)	LONG (W)	DIST. TO	DEPTH	RELEASER	ANT.	RECORDER	SKEW	REMARKS	FIGURE #
	D.M	D.M	NEXT (nm)	(m)	CODE	CH.	NUMBER	(ms)		
OBH 01	10 : 58.856	86 : 03.605	4.78	117	4949	D	980902	6		6.2.4.1.2
OBH 02	11 : 02.113	86 : 07.145	4.78	122	D654	B	980908	-3		6.2.4.1.3
OBH 03	11 : 05.369	86 : 10.656	4.78	122	6969	A	980402	-11		6.2.4.1.4
OBH 04	11 : 08.625	86 : 14.283	4.78	121	B214	D	980901	5	dc-bias	
OBH 05	11 : 11.881	86 : 17.851	4.78	117	5934	A	990712	-6	seismometer poor	6.2.4.1.5
OBH 06	11 : 15.137	86 : 21.442	4.78	112	5924	C	980903	-4		6.2.4.1.6
OBH 07	11 : 18.394	86 : 24.998	4.78	113	B559	D	980401	-14		6.2.4.1.7
OBH 08	11 : 21.650	86 : 28.591	4.78	108	6A29	B	980907	-2	dc-bias	
OBH 09	11 : 24.907	86 : 32.149	4.78	102	C444	A	980403	-2		6.2.4.1.8
OBH 10	11 : 28.163	86 : 35.740	4.78	93	D674	C	06.96	15	tape read error	
OBH 11	11 : 31.419	86 : 39.317	4.78	85	6959	A	02.95	-6		6.2.4.1.9
OBH 12	11 : 34.675	86 : 42.898	4.78	89	4954	B	92.01	-22	tape read error	
OBH 13	11 : 37.931	86 : 46.466	4.78	91	D649	D	08.94	-76		6.2.4.1.10
OBH 14	11 : 41.188	86 : 50.029	4.78	97	A324	B	03.96	-5		6.2.4.1.11
OBH 15	11 : 44.444	86 : 53.730	4.78	103	D634	A	91.14	-34		6.2.4.1.12
OBH 16	11 : 47.701	86 : 57.218	5.00	105	4979	D	990706	-10		6.2.4.1.13
OBH 17	11 : 51.107	87 : 00.955	5.00	107	C464	D	990709	2	dc-bias on hydrophone	6.2.4.1.14/16
OBH 18	11 : 54.512	87 : 04.687	5.00	108	C679	A	15.93	-70		6.2.4.1.17
OBH 19	11 : 57.914	87 : 08.438	5.00	110	6A24	A	980905	-9		6.2.4.1.18
OBH 20	12 : 01.297	87 : 12.203	13.57	110	5929	B	990705	-10		6.2.4.1.19
OBS 21	11 : 51.303	87 : 21.587	12.71	135	time	D	94-4		IRD instruments	6.2.4.1.20
OBS 22	11 : 42.539	87 : 12.202	6.05	126	time	C	93-11			6.2.4.1.21
OBS 23	11 : 38.364	87 : 07.691	6.30	105	time	B	93-14			6.2.4.1.22
OBS 24	11 : 34.062	87 : 02.970	12.97	127	time	A	93-10			6.2.4.1.23
OBS 26	11 : 25.089	86 : 53.408	13.36	135	time	D	93-12			6.2.4.1.24
OBS 28	11 : 15.897	86 : 43.480	4.71	189	time	C	94-1			6.2.4.1.25
OBS 27	11 : 12.651	86 : 40.013		172	time	B	94-5			6.2.4.1.26
TRIGGER							990712	1		

von Huene, R., Bialas, J., Flueh, E., Cropp, B., Csernok, T., Fabel, E., Hoffmann, J.L., Emeis, K., Holler, P., Jeschke, Leandro M., C., Peréz Fernandéz, I., Chavarria S., J., Florez H., A., Escobedo Z., D., León, R., and Barrios L., O., 1995: Morphotectonics of the Pacific convergent margin of the Caribbean plate boundary in southern Central America: Geological Society of America Special Paper 295, p. 291-307.

von Huene. R., J. Aubouin, et al., 1985: Initial Rep. DSDP 84, 21-77.

Walther, C.H.E., Flueh, E.R., Ranero, C.R., von Huene, R. and Strauch, W., An unusual crustal structure across the Pacific Margin of Nicaragua. submitted to Geophys. J. Int.

Walther, C.; Flueh, E.R.; Ranero, C. R. & von Huene, R., 1997: Seismic investigations offshore Nicaragua. EOS AGU Fall Meeting (San Francisco).

Weinrebe, W., 1997: Fahrtbericht SO-112 HIRESBAT, GEOMAR-Report 64, GEOMAR-Kiel.

Wessel, P., and W.H.F. Smith, 1991: Free software helps map and display data, EOS Trans. Am. Geophys. Un., 72, 441, 445-446.

Wessel, P. and Smith, W. H. F., 1995: The Generic Mapping Tools (GMT) version 3.0, Technical Reference and Cookbook, SOEST/NOAA.

Wilson, D.S., 1996: Fastest known spreading on the Miocene Cocos-Pacific plate boundary, Geophys. Res. Lett., 23, 3003-3006.

Wilson, D.S. and Hey, R., 1995: History of rift propagation and magnetization intensity for the Cocos-Nazca spreading center, J. Geophys. Res., 100, B7, 10,041-10,056.

Ye, S., et al., 1996: Crustal structure of the subduction zone off Costa Rica derived from OBS refraction and wide-angle reflection seismic data. Tectonics 15, 1006-1021.

Zelt, C.A., and R.B. Smith, 1992: Seismic travel time inversion for 2-D crustal velocity structure, Geophys. J. Int., 108, 16-34.

PAGANINI / SO144-1 - PROFILE 06

INSTRUMENT	LAT. (N) D:M	LON. (W) D:M	DIST. TO NEXT (nm)	DEPTH (m)	RELEASER CODE	ANT. CH	RECORDER NUMBER	DRIFT (m)	REMARKS	
OBH 01	10 : 58.856	86 : 03.605	4.78	117	4949	D	980902	6		6.2.4.1.2
OBH 02	11 : 02.113	86 : 07.145	4.78	122	D654	B	980908	-3		6.2.4.1.3
OBH 03	11 : 05.369	86 : 10.656	4.78	122	6969	A	980402	-11		6.2.4.1.4
OBH 04	11 : 08.625	86 : 14.283	4.78	121	B214	D	980901	5	dc-bias	
OBH 05	11 : 11.881	86 : 17.851	4.78	117	5934	A	990712	-6	seismometer poor	6.2.4.1.5
OBH 06	11 : 15.137	86 : 21.442	4.78	112	5924	C	980903	-4		6.2.4.1.6
OBH 07	11 : 18.394	86 : 24.998	4.78	113	B559	D	980401	-14		6.2.4.1.7
OBH 08	11 : 21.650	86 : 28.591	4.78	108	6A29	B	980907	-2	dc-bias	
OBH 09	11 : 24.907	86 : 32.149	4.78	102	C444	A	980403	-2		6.2.4.1.8
OBH 10	11 : 28.163	86 : 35.740	4.78	93	D674	C	06.96	15	tape read error	
OBH 11	11 : 31.419	86 : 39.317	4.78	85	6959	A	02.95	-6		6.2.4.1.9
OBH 12	11 : 34.675	86 : 42.898	4.78	89	4954	B	92.01	-22	tape read error	
OBH 13	11 : 37.931	86 : 46.466	4.78	91	D649	D	08.94	-76		6.2.4.1.10
OBH 14	11 : 41.188	86 : 50.029	4.78	97	A324	B	03.96	-5		6.2.4.1.11
OBH 15	11 : 44.444	86 : 53.730	4.78	103	D634	A	91.14	-34		6.2.4.1.12
OBH 16	11 : 47.701	86 : 57.218	5.00	105	4979	D	990706	-10		6.2.4.1.13
OBH 17	11 : 51.107	87 : 00.955	5.00	107	C464	D	990709	2	dc-bias on hydrophone	6.2.4.1.14/16
OBH 18	11 : 54.512	87 : 04.687	5.00	108	C679	A	15.93	-70		6.2.4.1.17
OBH 19	11 : 57.914	87 : 08.438	5.00	110	6A24	A	980905	-9		6.2.4.1.18
OBH 20	12 : 01.297	87 : 12.203	13.57	110	5929	B	990705	-10		6.2.4.1.19
OBS 21	11 : 51.303	87 : 21.587	12.71	135	time	D	94-4		IRD instruments	6.2.4.1.20
OBS 22	11 : 42.539	87 : 12.202	6.05	126	time	C	93-11			6.2.4.1.21
OBS 23	11 : 38.364	87 : 07.691	6.30	105	time	B	93-14			6.2.4.1.22
OBS 24	11 : 34.062	87 : 02.970	12.97	127	time	A	93-10			6.2.4.1.23
OBS 25	11 : 25.089	86 : 53.408	13.36	135	time	D	93-12			6.2.4.1.24
OBS 26	11 : 15.897	86 : 43.480	4.71	189	time	C	94-1			6.2.4.1.25
OBS 27	11 : 12.651	86 : 40.013		172	time	B	94-5			6.2.4.1.26
TM OBH							990712	1		

PAGANINI / SO144-1 - PROFILE 09-12

9 : 09.170	84 : 48.353	824	time	D	93-15		IRD instruments	6.2.4.2.17
9 : 11.389	84 : 47.012	742	time	B	94-2			6.4.2.13/16 and 18/21
9 : 13.440	84 : 45.828	594	time	C	94-3			6.2.4.2.22/23
9 : 12.361	84 : 48.514	867	C464	B	990907	1		6.2.4.2.2
9 : 10.432	84 : 45.460	813	5934	D	990708	-1		6.2.4.2.3
9 : 20.788	85 : 02.130	1526	5934	D	990708	0		6.2.4.2.4
9 : 17.016	85 : 04.005	1681	C464	B	990709	0		6.2.4.2.5/8
					990712	0		

INSTRUMENT	LAT (S)	LON (W)	DIST (NM)	DEPTH (m)	RELEASE					
	DIM	DIM	NEXT (nm)	(m)	CODE	CH	NUMBER	(s)		
OBS 35	7 : 40.009	83 : 11.984	3.75	1692	time	A	94-4		IRD instruments	6.2.4.3.4
OBS 36	7 : 41.834	83 : 15.299	3.75	1555	time	C	93-11			6.2.4.3.5
OBS 37	7 : 43.620	83 : 18.600	3.75	1457	time	B	93-14			6.2.4.3.6
OBS 38	7 : 45.469	83 : 21.908	3.75	1398	time	A	93-10			6.2.4.3.7
OBS 39	7 : 47.274	83 : 25.211	3.75	1368	time	D	93-12			6.2.4.3.8
OBS 40	7 : 49.087	83 : 28.527	3.75	1345	time	B	94-1			6.2.4.3.9
OBS 41	7 : 50.909	83 : 31.818	3.75	1355	time	A	94-5			6.2.4.3.10
OBS 42	7 : 52.729	83 : 35.112	3.75	1315	time	C	93-16			6.2.4.3.11
OBS 43	7 : 54.545	83 : 38.434	3.75	1073	time	D	92-3			6.2.4.3.12
OBS 44	7 : 56.358	83 : 41.727	3.75	1306	time	B	93-16			6.2.4.3.13
OBS 45	7 : 58.178	83 : 45.020	3.75	1826	time	A	93-15			6.2.4.3.14
OBS 46	8 : 00.007	83 : 48.327	3.75	1819	time	D	94-3			6.2.4.3.15
OBS 47	8 : 01.817	83 : 51.643	3.75	1308	time	B	94-2			6.2.4.3.16
OBH 48	8 : 03.643	83 : 54.942	3.75	562	A324	D	980905	-7		6.2.4.3.17
OBH 49	8 : 05.455	83 : 58.247	3.75	1393	D649	B	990706	-12		6.2.4.3.18
OBH 50	8 : 07.266	84 : 01.561	3.75	1478	D634	A	990705	6		6.2.4.3.19
OBH 51	8 : 09.103	84 : 04.841	3.75	1555	4979	B	980907	2		6.2.4.3.20
OBH 52	8 : 10.925	84 : 08.145	3.75	1640	C679	A	980403	-1		6.2.4.3.21
OBS 53	8 : 12.737	84 : 11.472	3.75	1686	5934	A	990708	-7	no data	
OBH 54	8 : 14.533	84 : 14.758	3.75	1673	5929	C	980901	27		6.2.4.3.22
OBH 55	8 : 16.363	84 : 18.050	3.75	1691	6A29	A	980402	-11		6.2.4.3.23
OBH 56	8 : 18.178	84 : 21.365	3.75	1810	6959	D	980903	-1	dc-bias	
OBH 57	8 : 20.002	84 : 24.667	3.75	2045	6A24	B	980401	-20	data gaps	
OBH 58	8 : 21.819	84 : 27.966	3.75	2312	D674	D	980908	6	data read error	
OBH 59	8 : 23.635	84 : 31.260	3.75	2639	B559	A	91.14	-42		6.2.4.3.24
OBH 60	8 : 25.000	84 : 34.616	3.75	2504	C444	C	03.96	-10		6.2.4.3.25
OBS 61	8 : 27.700	84 : 37.881	3.75	2458	C464	A	990709	7		6.2.4.3.26/28
OBH 62	8 : 29.101	84 : 41.179	3.75	2346	5924	D	06.96	-60		6.2.4.3.29
OBH 63	8 : 30.914	84 : 44.490	3.75	1610	4954	B	08.94	-100		6.2.4.3.30
OBH 64	8 : 32.740	84 : 47.785	3.75	1493	B214	C	02.95	6	tape error	
OBH 65	8 : 34.555	84 : 51.092	3.75	2224	6969	A	980902	13		6.2.4.3.31
OBH 66	8 : 36.359	84 : 54.397	3.75	2637	D654	D	92.01	-60		6.2.4.3.32
OBH 67	8 : 38.189	84 : 57.702		2773	4949	A	990712	4		6.2.4.3.33
TRIGGER							990711	-8		

PAGANINI / SO144-1 - PROFILE 02-A AND B

7 : 37.000	84 : 02.000	3.00	1314	4979	A	08.94		no data	
7 : 40.393	84 : 00.892	3.00	1597	5929	D	980907	2		6.2.4.4.2
7 : 42.766	83 : 59.042	3.00	1706	D674	B	980902	13	poor data	
7 : 45.166	83 : 57.179	3.05	1675	C679	C	06.96	-35		6.2.4.4.3
7 : 47.589	83 : 55.298	3.00	1794	C464	A	990709	6		6.2.4.4.4/6
7 : 50.012	83 : 53.489	3.00	1617	A324	A	980401	-25	poor signal	
7 : 52.347	83 : 51.636	3.05	1722	B559	C	980901	23		6.2.4.4.7
7 : 54.784	83 : 49.816	2.85	1766	C444	A	02.95	?	data gaps	
7 : 57.050	83 : 48.060	3.00	1774	3A02		980905	-1		6.2.4.4.8
7 : 59.429	83 : 46.188	2.95	1846	5934	B	990711		power failure	
8 : 01.815	83 : 44.326	3.00	1867	6A24	C	03.96		not synchronized	6.2.4.4.9
8 : 04.197	83 : 42.575	3.00	1882	5924	A	980403	-4		6.2.4.4.10
8 : 06.610	83 : 40.680	3.00	1871	B214	D	990712	3	partly dc-bias	
8 : 08.982	83 : 38.831	3.00	1862	4954	A	990706	-12		6.2.4.4.11
8 : 11.397	83 : 36.978	2.95	1895	D654	B	990705	5		6.2.4.4.12
8 : 13.754	83 : 35.170	3.00	1937	6969	A	980402	-11		6.2.4.4.13
8 : 16.135	83 : 33.328	2.95	1642	4949	B	92.01	-54	poor data	
8 : 18.449	83 : 31.522	2.95	1267	6A29	D	990707	-13		6.2.4.4.14
8 : 20.820	83 : 29.696	2.75	1007	D634	A	01.96		not synchronized	6.2.4.4.15
8 : 22.998	83 : 28.005		464	D649	C	04.96	-32		6.2.4.4.16/17
						990708	17		

INSTRUMENT	LAT. (N)	LON. (E)	DIST. TO NEXT (nm)	DEPTH (m)	RELEASE CODE	RELEASE CH	RECEIVER NUMBER	RECEIVER (m)	REMARKS	C.T.
	D:M	D:M								
OBH 90	3 : 26.922	80 : 16.904	4.35	2496	D674	A	04.96	-20		6.2.4.5.2
OBH 91	3 : 29.965	80 : 20.032	4.25	2493	3A02	71	980905	0	IFREMER OBH	6.2.4.5.3
OBH 92	3 : 33.017	80 : 22.958	4.35	2626	6959	C	980907	2		6.2.4.5.4
OBH 93	3 : 36.084	80 : 26.075	4.30	2611	B559	D	980901	14		6.2.4.5.5
OBH 94	3 : 39.150	80 : 29.150	4.30	2489	C444	A	06.96	-21		6.2.4.5.6
OBH 95	3 : 42.213	80 : 32.234	3.80	2390	5934	C	990711	-6		6.2.4.5.7/10
OBH 96	3 : 44.901	80 : 34.899	3.25	2403	6A24	B	980908	6		6.2.4.5.11
OBH 97	3 : 47.209	80 : 37.181	3.25	2258	C679	D	990706	-9	in part dc-shift	
OBH 98	3 : 49.488	80 : 39.470	3.25	2194	A324	B	980403	-2	dc-shift	
OBH 99	3 : 51.795	80 : 41.793	3.25	2153	5924	A	990705	2	in part dc-shift	
OBH 100	3 : 54.103	80 : 44.317	3.25	2101	4A44	A	15.93	-81	weak signal	
OBH 101	3 : 56.414	80 : 46.345	3.25	2026	B214	B	980401	-14	weak signal	
OBH 102	3 : 58.716	80 : 48.658	3.25	1927	4954	A	980902	7		6.2.4.5.12
OBH 103	4 : 00.986	80 : 50.951	3.25	1827	4949	D	08.94	-51	rec. error, no data	
OBH 104	4 : 03.293	80 : 53.281	3.25	1771	D654	A	03.96	-25		6.2.4.5.13
OBS 105	4 : 05.614	80 : 55.545	3.25	1580	C464	C	990709	3	seismometer poor	6.2.4.5.14
OBH 106	4 : 07.891	80 : 57.831	3.25	1471	6969	B	980402	-7		6.2.4.5.15
OBH 107	4 : 10.190	81 : 00.127	3.25	1250	6A29	D	92.01	-255		6.2.4.5.16
OBH 108	4 : 12.476	81 : 02.498	3.20	1585	D634	C	990707	-7		6.2.4.5.17
OBH 109	4 : 14.776	81 : 04.775	3.25	1674	D649	D	01.96	-263		6.2.4.5.18
OBS 110	4 : 17.090	81 : 07.030	3.25	1716	time	A	94-4			6.2.4.5.19
OBS 111	4 : 19.390	81 : 09.330	3.25	1667	time	B	93-11			6.2.4.5.20
OBS 112	4 : 21.690	81 : 11.630	3.25	1868	time	C	93-14			6.2.4.5.21
OBS 113	4 : 23.980	81 : 13.930	3.25	2050	time	A	93-10			6.2.4.5.22/32-35
OBS 114	4 : 26.280	81 : 16.230	3.25	2038	time	D	93-12			6.2.4.5.23
OBS 115	4 : 28.570	81 : 18.530	3.25	1579	time	B	94-1			6.2.4.5.24
OBS 116	4 : 30.870	81 : 20.870	3.20	3205	time	A	94-5		IRD instruments	6.2.4.5.25
OBS 117	4 : 33.170	81 : 23.130	3.25	3271	time	C	93-16			6.2.4.5.26
OBS 118	4 : 35.460	81 : 25.430	3.25	3415	time	D	92-3			6.2.4.5.27
OBS 119	4 : 37.760	81 : 27.730	3.45	3543	time	B	93-16			6.2.4.5.28
OBS 120	4 : 40.050	81 : 30.300	3.05	3636	time	A	93-15			6.2.4.5.29
OBS 121	4 : 42.350	81 : 32.330	3.25	3721	time	D	94-3			6.2.4.5.30
OBS 122	4 : 44.640	81 : 34.630		3818	time	B	94-2			6.2.4.5.31
TRIGGER							990708	-3		

*VAR: vertical array

PAGANINI / SO144-1 - PROFILE 04

5 : 19.777	84 : 59.746	7.55	3079	D649	D	980405	-6		6.2.4.6.2
5 : 05.175	85 : 05.175	7.45	2833	D634	B	01.96	-18		6.2.4.6.3
5 : 30.507	85 : 10.477	5.05	2646	6969	D	980901	14		6.2.4.6.4
5 : 34.082	85 : 14.062	4.30	2597	D654	C	06.96	-20		6.2.4.6.5
5 : 37.111	85 : 17.075	3.95	2390	6A29	A	980907	3		6.2.4.6.6
5 : 39.963	85 : 19.910	4.00	1876	4954	C	03.96	-16		6.2.4.6.7
5 : 42.829	85 : 22.740	4.35	1741	C464	D	990709		data error	
5 : 45.882	85 : 25.822	5.85	1708	6A24	D	980908		poor data	
5 : 50.010	85 : 29.972	3.90	1813	4979	A	990706	-8		6.2.4.6.8
5 : 52.780	85 : 32.729	4.55	1771	4949	C	92.01	-27	poor data	
5 : 56.040	85 : 35.960	5.60	1719	B214	A	990707		power failure	
5 : 59.913	85 : 39.955	3.80	1740	4A44	A	15.93	-71	poor data	
6 : 02.722	85 : 42.662	3.65	1813	A324	B	980403	-2		6.2.4.6.9
6 : 05.306	85 : 45.250	3.20	1849	D674	C	990903	-1	GEOLON-Recorder	5.2.5-8
6 : 07.544	85 : 47.509	3.40	1895	3A02	71	980905	-1	IFREMER OBH	6.2.4.6.10
6 : 09.967	85 : 49.909	4.25	1925	5934	B	990711	-7		6.2.4.6.211/14
6 : 12.982	85 : 52.922	5.20	1973	C679	A	980401	-14	poor data	
6 : 16.683	85 : 56.620	4.65	1995	6959	B	980903	0		6.2.4.6.15
6 : 19.980	85 : 59.934	4.60	1945	5924	A	990705	1		6.2.4.6.16
6 : 23.274	86 : 03.222	4.25	1175	C444	D	04.96		not sync.	6.2.4.6.17
6 : 26.296	86 : 06.248	5.25	1712	B559	A	980902	-9		6.2.4.6.18
6 : 29.987	86 : 09.974	5.00	2348	time	A	94-4		IRD instruments	6.2.4.6.19
6 : 33.569	86 : 13.508	4.90	2705	time	D	93-10			6.2.4.6.20
6 : 37.043	86 : 16.989	4.15	2748	time	C	93-12			6.2.4.6.21
6 : 39.980	86 : 19.949	7.05	2782	time	B	94-1			6.2.4.6.22
6 : 45.006	86 : 24.967	7.05	2870	time	A	94-5			6.2.4.6.23
6 : 50.008	86 : 29.955	3.20	2948	time	D	92-3			6.2.4.6.24
						990712			

9 : 30.042	86 : 29.940	3.1	3274	C464	D	990706	-3		6.2.4.7.2
9 : 28.184	86 : 27.445	3.1	3305	6969	B	06.96	-11		6.2.4.7.3
9 : 26.339	86 : 25.001		3313	5934	B	980907	1		6.2.4.7.4
9 : 26.339	86 : 25.001	3.0	3313	5934	B	990903	1	DPG	5.29
9 : 24.528	86 : 22.571	3.0	3288	B214	A	03.96	-12		6.2.4.7.5
9 : 22.660	86 : 20.165	3.0	3318	D634	C	980901	7		6.2.4.7.6
9 : 20.836	86 : 17.711	3.0	3328	D654	A	01.96	-11		6.2.4.7.7
9 : 19.627	86 : 15.313	3.0	3322	5924	A	980905	-1		6.2.4.7.8
9 : 17.210	86 : 12.879	3.0	3292	4954	B	980902	-3		6.2.4.7.9
9 : 15.394	86 : 10.482	3.1	3268	6959	D	980903	0	dc-bias	
9 : 13.516	86 : 08.002	3.1	3288	A324	D	980401	-7		6.2.4.7.10
9 : 11.644	86 : 05.477	3.0	3321	6A29	D	980908	3		6.2.4.7.11
9 : 09.851	86 : 03.041	3.0	3286	C444	B	980403	-1		6.2.4.7.12
9 : 07.999	86 : 00.630		3273	B559	D	990705	0		6.2.4.7.13
						990712	0		

PAGANINI / SO144-1a - SEISMIC SOURCES

1	17.09.99	15:14	11 : 09.907	86 : 36.989	60 s	P	320 km	
33	17.09.99	15:46	11 : 11.175	86 : 38.455	60 s	P, S		
233	17.09.99	19:06	11 : 19.387	86 : 47.228	60 s	P		03:30
693	18.09.99	2:46	11 : 37.909	87 : 07.167	60 s	P, S		P gun varying
1678	18.09.99	19:11	11 : 46.786	86 : 56.209	60 s	P, M, S		shooting times
2217	19.09.99	4:00	11 : 25.853	86 : 33.216	60 s	M, S		
2648	19.09.99	11:11	11 : 08.635	86 : 14.297	60 s	S		
2967	19.09.99	16:40	10 : 55.57	85 : 59.944	60 s	S		EOL
1	23.09.99	12:14	9 : 09.560	84 : 44.196	18 s	1-4	11 km	
434	23.09.99	14:27	9 : 13.005	84 : 49.432	18 s	1, 2, 4, 5		EOL
1	23.09.99	14:27	9 : 13.005	84 : 49.432	18 s	1, 2, 4, 5	8 km	
281	23.09.99	15:43	9 : 14.496	84 : 45.244	18 s	1, 2, 4, 5		EOL
1	23.09.99	16:08	9 : 14.759	84 : 45.099	18 s	1, 2, 4, 5	9 km	
273	23.09.99	17:30	9 : 10.135	84 : 47.812	18 s	1, 2, 4, 5		EOL
1	23.09.99	23:51	9 : 16.100	85 : 04.479	18 s	1, 2, 4, 5		
196	24.09.99	0:50	9 : 18.977	85 : 03.017	18 s	1, 2, 4, 7	12 km	
422	24.09.99	1:58	9 : 22.437	85 : 01.271	18 s	1, 2, 4, 7		EOL

*P: portside 32l, M: midside 32l, S: starboard 32l

1 : 2l 2 : 0.6l 3 : 0.3l 4 : 0.3l 5 : 0.6l 6 : 0.3l 7 : 1.2

PROFILE NO.	SHOT NO.	DATE UTC	TIME UTC	LAT (N) D:M	LON (W) D:M	SHOT INT.	GUN POSITION		
SO144-1b	1	28.09.99	23:00	8 : 41.997	85 : 04.711	60 s	S	261 km	
	25	28.09.99	23:24	8 : 41.953	85 : 04.607	60 s	S , P		
	37	28.09.99	23:36	8 : 41.686	85 : 04.168	60 s	S , P , M		
	605	29.09.99	9:04	8 : 25.943	84 : 35.485	60 s	S , P , M		P gun is
	791	29.09.99	12:10	8 : 20.640	84 : 25.815	60 s	S , P , M		irregular
	791	29.09.99	12:10	8 : 20.640	84 : 25.815	60 s	S , M		
	1102	29.09.99	17:21	8 : 11.570	84 : 09.290	60 s	S , P , M		
	1187	29.09.99	18:46	8 : 09.873	84 : 07.127	60 s	S , M		
	1397	29.09.99	22:16	8 : 03.090	83 : 53.846	60 s	S		
	1419	29.09.99	22:38	8 : 02.490	83 : 52.760	60 s	S , P		
	1434	29.09.99	22:53	8 : 02.053	83 : 51.979	60 s	S , M		
	1593	30.09.99	1:32	7 : 52.739	83 : 43.744	60 s	S		
	1638	30.09.99	2:17	7 : 56.273	83 : 41.443	60 s	S , P		
	2396	30.09.99	14:55	7 : 35.131	83 : 03.012	60 s	P		
	2408	30.09.99	15:07	7 : 34.813	83 : 02.271	60 s	P		EOL

PAGANINI / SO144-1b - SEISMIC SOURCES

PROFILE NO.	SHOT NO.	DATE UTC	TIME UTC	LAT. (N) DM	LON. (W) DM	PULSE INT.	GUN POSITION	PROFILE LENGTH	REMARKS
SO 144-1b 1	1	03.10.99	2:22	8 : 28,706	83 : 49,952	60 s	P	112 km	
	12	03.10.99	2:33	8 : 28,446	83 : 49,484	60 s	S , P		
	29	03.10.99	2:50	8 : 28,048	83 : 48,570	60 s	S , P , M		
	58	03.10.99	3:19	8 : 27,324	83 : 47,037	60 s	P , M		
	1104	03.10.99	20:45	8 : 41,551	83 : 24,608	60 s	P		
	1114	03.10.99	20:55	8 : 41,559	83 : 24,800	60 s	P		EOL
SO 144-1b 2A	1	05.10.99	0:29	7 : 30,702	84 : 10,131	60 s	P	162 km	
	12	05.10.99	0:40	7 : 30,217	84 : 09,699	60 s	P , M		
	132	05.10.99	2:40	7 : 35,025	84 : 05,102	60 s	S , P , M		
	158	05.10.99	3:06	7 : 36,317	84 : 04,240	60 s	P , M		
	471	05.10.99	8:19	7 : 50,851	83 : 52,889	60 s	M		
	669	05.10.99	11:37	8 : 00,013	83 : 45,786	60 s	P , M		
	923	05.10.99	15:51	8 : 11,164	83 : 37,158	60 s	S , P , M		
	1119	05.10.99	19:07	8 : 19,696	83 : 30,613	60 s	P		
	1207	05.10.99	20:35	8 : 24,157	83 : 26,832	60 s	P		EOL

PAGANINI / SO144-1b - SEISMIC SOURCES

PROFILE NO	SHOT NO	DATE UTC	TIME UTC	LAT (N) D:M	LON (W) D:M	RATE UNIT	GUN POSITION	LENGTH	REMARKS
	1	08.10.99	6:15	4 : 53.413	81 : 43.393	60 s	P	246 km	
	22	08.10.99	6:36	4 : 52.560	81 : 42.520	60 s	P , M		
	613	08.10.99	16:27	4 : 28.059	81 : 18.012	60 s			missing one shot
	614	08.10.99	16:28	4 : 28.047	81 : 18.001	60 s	P , M		
	873	08.10.99	20:47	4 : 17.539	81 : 07.479	60 s	P , M, S		
	1209	09.10.99	2:23	4 : 03.517	80 : 53.473	60 s	P , M, S		losing M-Gun floats
	1240	09.10.99	2:54	4 : 02.230	80 : 52.210	60 s	P , M, S		
	1279	09.10.99	3:33	4 : 00.652	80 : 50.599	60 s	P , M, S		
	1876	09.10.99	13:30	3 : 37.219	80 : 27.191	60 s	P , M, S		M-gun working part time
	1966	09.10.99	15:00	3 : 22.288	80 : 22.264	60 s	P , M, S		
	2265	09.10.99	19:59	3 : 19.993	80 : 09.990	60 s	P , S		
	2277	09.10.99	20:11	3 : 19.535	80 : 09.644	60 s	P		
	2289	09.10.99	20:23	3 : 19.107	80 : 09.438	60 s	P		EOL

PAGANINI / SO144-1b - SEISMIC SOURCES

1	12.10.99	13:04	6 : 59.260	86 : 39.219	60 s	P	277 km	
16	12.10.99	13:19	6 : 58.490	86 : 38.490	60 s	P, S		
653	12.10.99	23:56	6 : 26.364	86 : 06.202	60 s			land shots
657	13.10.99	0:00	6 : 26.148	86 : 06.074	60 s			
658	13.10.99	0:01	6 : 26.112	86 : 06.026	60 s	P, S		
670	13.10.99	0:13	6 : 25.907	86 : 05.507	60 s	P		
747	13.10.99	1:30	6 : 21.720	86 : 01.721	60 s	P, S		
1137	13.10.99	8:00	6 : 01.832	85 : 41.796	60 s	P, S		losing P-Gun floats
1148	13.10.99	8:11	6 : 01.215	85 : 41.184	60 s	S		
1166	13.10.99	8:29	6 : 00.340	85 : 40.275	60 s	P, S		
1203	13.10.99	9:06	5 : 58.467	85 : 38.428	60 s	S		
1283	13.10.99	10:26	5 : 54.396	85 : 34.264	60 s	P, S		
2095	13.10.99	23:58	5 : 12.760	84 : 52.789	60 s	P, S		EOL
1	16.10.99	1:58	9 : 00.990	85 : 51.292	60 s	P	112 km	
13	16.10.99	2:10	9 : 01.421	85 : 51.000	60 s	P, S		
962	16.10.99	18:00	9 : 37.470	86 : 40.115	60 s	P, S		EOL

APPENDIX 9.3.1 **PAGANINI / SO144-1A - MAGNETIC PROFILES**

Profile number	Date UTC	Time UTC	Lat D : M	Lon D : M	Profile length
Start P06	17.09.1999	23:28	11 : 29.958	86 : 58.590	
			11 : 51.276	87 : 22.158	150.2
			12 : 02.028	87 : 12.072	km
End P06	18.09.1999	23:16	11 : 37.128	86 : 45.612	
Start magnic01	20.09.1999	20:35	11 : 00.450	86 : 50.274	81.3
			10 : 45.948	86 : 56.856	km
End magnic01	21.09.1999	1:04	10 : 23.016	86 : 39.732	
Start magnic02	21.09.1999	3:19	10 : 05.544	86 : 26.772	
			9 : 49.242	86 : 11.448	
			10 : 47.682	86 : 55.182	
			9 : 52.290	86 : 07.134	
			10 : 47.532	86 : 49.572	
			10 : 16.092	86 : 20.136	
			10 : 45.612	86 : 44.148	
			10 : 17.766	86 : 17.634	1358.5
			10 : 44.028	86 : 38.844	km
			10 : 17.718	86 : 16.116	
			10 : 13.260	86 : 20.358	
			9 : 51.342	86 : 03.402	
			9 : 42.420	86 : 14.700	
			9 : 23.190	86 : 16.566	
			9 : 38.412	85 : 58.905	
End magnic02	23.09.1999	9:05	9 : 09.072	84 : 48.210	
Start transit1	24.09.1999	16:40	8 : 32.754	83 : 57.954	129.2
End transit1	24.09.1999	22:23	7 : 39.804	83 : 11.982	km
Start transit2	25.09.1999	5:09	8 : 02.166	83 : 52.260	160.8
			8 : 18.132	84 : 21.006	km
End transit2	25.09.1999	13:21	9 : 12.336	84 : 16.164	
Start Cocos:	26.09.1999	4:03	8 : 27.222	84 : 00.648	
			8 : 16.518	84 : 04.542	
			8 : 25.098	84 : 26.742	
			8 : 17.100	84 : 41.118	280.1
			7 : 44.910	83 : 34.650	km
			7 : 57.990	83 : 56.892	
End Cocos	26.09.1999	17:53	8 : 01.236	83 : 55.710	
Start transit3	27.09.1999	3:46	8 : 35.826	84 : 57.354	
			8 : 25.476	84 : 55.908	193.6
			8 : 38.166	85 : 24.954	km
End transit3	27.09.1999	12:43	9 : 31.542	84 : 52.038	

APPENDIX 9.3.2 **PAGANINI / SO144-1B - MAGNETIC PROFILES**

Profile number	Date UTC	Time UTC	Lat D : M	Lon D : M	Profile length
Start P 101	28.09.1999	18:30	9 : 26.796	84 : 44.730	89.8
End P 101	28.09.1999	22:36	8 : 42.966	85 : 06.252	km
Start P 102	28.09.1999	22:36	8 : 42.858	85 : 06.288	253.5
End P 102	30.09.1999	15:24	7 : 34.710	83 : 01.344	km
Start P 103	30.09.1999	15:24	7 : 34.710	83 : 01.344	111.9
End P 103	30.09.1999	21:44	8 : 01.446	83 : 55.962	km
Start P 104	01.10.1999	2:31	8 : 14.952	84 : 19.164	83
End P 104	01.10.1999	6:43	8 : 36.324	84 : 58.770	km
Start P 105	01.10.1999	17:22	8 : 07.890	84 : 04.104	57.2
End P 105	01.10.1999	19:58	7 : 37.038	84 : 02.580	km
Start P 106	02.10.1999	4:52	8 : 22.902	83 : 27.864	23.5
End P 106	02.10.1999	6:00	8 : 14.880	83 : 17.952	km
Start P 107	02.10.1999	6:00	8 : 14.844	83 : 17.952	68.5
End P 107	02.10.1999	9:06	7 : 45.024	83 : 40.074	km
Start P 108	02.10.1999	9:06	7 : 45.024	83 : 40.098	25.6
End P 108	02.10.1999	10:15	7 : 51.714	83 : 52.086	km
Start P 109	02.10.1999	10:58	7 : 51.210	83 : 52.956	62.8
End P 109	02.10.1999	13:48	8 : 08.742	84 : 21.702	km
Start P 110	02.10.1999	13:48	8 : 08.742	84 : 21.702	116.8
End P 110	02.10.1999	19:01	9 : 12.192	84 : 14.982	km
Start P 111	03.10.1999	1:12	8 : 33.342	84 : 21.702	127.3
			8 : 19.980	83 : 18.900	km
End P 111	03.10.1999	13:22	8 : 21.276	83 : 13.812	
Start P 112a	03.10.1999	21:17	8 : 41.406	83 : 23.466	26
End P 112a	03.10.1999	22:36	8 : 30.918	83 : 13.362	km
Start P 112b	03.10.1999	23:27	8 : 21.156	83 : 12.972	79.7
End P 112b	04.10.1999	3:11	7 : 44.700	83 : 37.140	km
Start P 115	04.10.1999	3:15	7 : 44.400	83 : 36.876	46.6
End P 115	04.10.1999	5:18	7 : 39.546	83 : 11.724	km
Start P 116	04.10.1999	21:19	8 : 00.996	83 : 52.074	191.1
			7 : 30.108	84 : 09.282	km
End P 116	05.10.1999	20:42	8 : 23.868	83 : 27.288	
Start P 117	06.10.1999	9:03	7 : 37.386	84 : 02.016	409.3
End P 117	07.10.1999	3:03	4 : 57.918	81 : 52.434	km

APPENDIX 9.3.2 **PAGANINI / SO144-1B - MAGNETIC PROFILES**

Profile number	Date UTC	Time UTC	Lat D : M	Lon D : M	Profile length
Start P 118a	08.10.1999	4:16	4 : 45.492	81 : 34.896	
			4 : 51.420	81 : 36.732	132.6
			4 : 54.846	81 : 44.850	km
End P 118a	08.10.1999	21:34	4 : 15.414	81 : 05.376	
Start P 118b	08.10.1999	22:38	4 : 18.762	81 : 02.712	
			3 : 18.762	80 : 09.378	178
			3 : 24.456	80 : 19.440	km
End P 118b	09.10.1999	22:01	3 : 27.542	80 : 16.704	
Start P 120	10.10.1999	9:51	4 : 15.948	81 : 03.762	
			4 : 03.606	80 : 50.694	82.5
			4 : 00.750	80 : 53.622	km
			4 : 15.816	81 : 08.334	
End P 120	10.10.1999	13:44	4 : 17.622	81 : 06.546	
Start P 121	11.10.1999	2:20	4 : 44.826	81 : 36.516	380.7
End P 121	11.10.1999	19:51	5 : 19.704	85 : 00.162	km
Start P 124	14.10.1999	22:49	6 : 46.788	86 : 31.260	77.2
End P 124	15.10.1999	2:03	6 : 19.944	85 : 59.436	km
Start P 125	15.10.1999	4:17	6 : 27.246	86 : 06.162	340.2
End P 125	15.10.1999	19:33	9 : 30.048	86 : 30.006	km
Start P 126/7	16.10.1999	0:18	9 : 07.110	86 : 00.636	
			8 : 59.952	85 : 50.028	164.1
			9 : 37.962	86 : 40.902	km
End P 126/27	16.10.1999	19:50	9 : 30.090	86 : 29.856	
Start P 128	17.10.1999	3:52	9 : 08.310	86 : 00.000	
			8 : 59.952	85 : 45.006	142.2
			8 : 43.008	85 : 53.868	km
			8 : 30.060	85 : 23.100	
End P 128	17.10.1999	14:55	9 : 30.594	85 : 13.854	
Start P 129	17.10.1999	15:54	9 : 30.516	85 : 13.914	42.5
			9 : 27.762	85 : 02.184	km
End P 129	18.10.1999	18:00	9 : 36.570	84 : 55.650	

APPENDIX 9.4
Dredge From Five-Faults Seamount

On 16 September at 01:00 UTC RV SONNE arrived at a sheared seamount (Fig. 9.4.1) which had been mapped during the SO107 hydrosweep survey (Spangenberg, 1997) off the coast of Nicaragua. This feature is caracterized by as much as five faults which have caused steep flanks of up to 1 km height. Due to its structure we named this topographic high Five-Faults Seamount. On the enlarged scale map three sites with a large dip angle could be identified to the north, east and south-west. The steepest one dipping to the north was chosen for the first dredge trial. SONNE deployed a 94 cm x 35 cm wide dredge at 11:07.1 N, 87:51.77 W at 3300 m water depth. Moving slowly to the south-east 3374 m of cable were lowered to the ground and kept for the following 2.5 hrs. While dredging SONNE drifted along the line with not more than 1 kn speed through water. At touchdown of the dredge the tow load on the W6 deep sea winch of SONNE was about 4.8 t. Along the line the drag increased several times above 5.5 t with a maximum load of 6.8 t. At about 03:30 UTC SONNE had passed the top of the Five-Faults Seamount at 11:05,93 N, 87:51,73 W, where water depth had decreased to 2550 m and the dredge was expected to be very close at the top. At this point the winch started to pull the chain bag up by 1 m/s. When it showed up at the surface the bag of the dredge was half-filled. Some of the rocks show fresh broken sides. All of them show sharp corners with very little rounding. Therefore it is assumed that even if the rocks were not broken off the ground they have not been deposited far from their origin. This should give the geologist a good basis to retain detailed data about the Five-Faults Seamount.

Dredgeprofile from 15.09.1999, Cruise Sonne-144/1

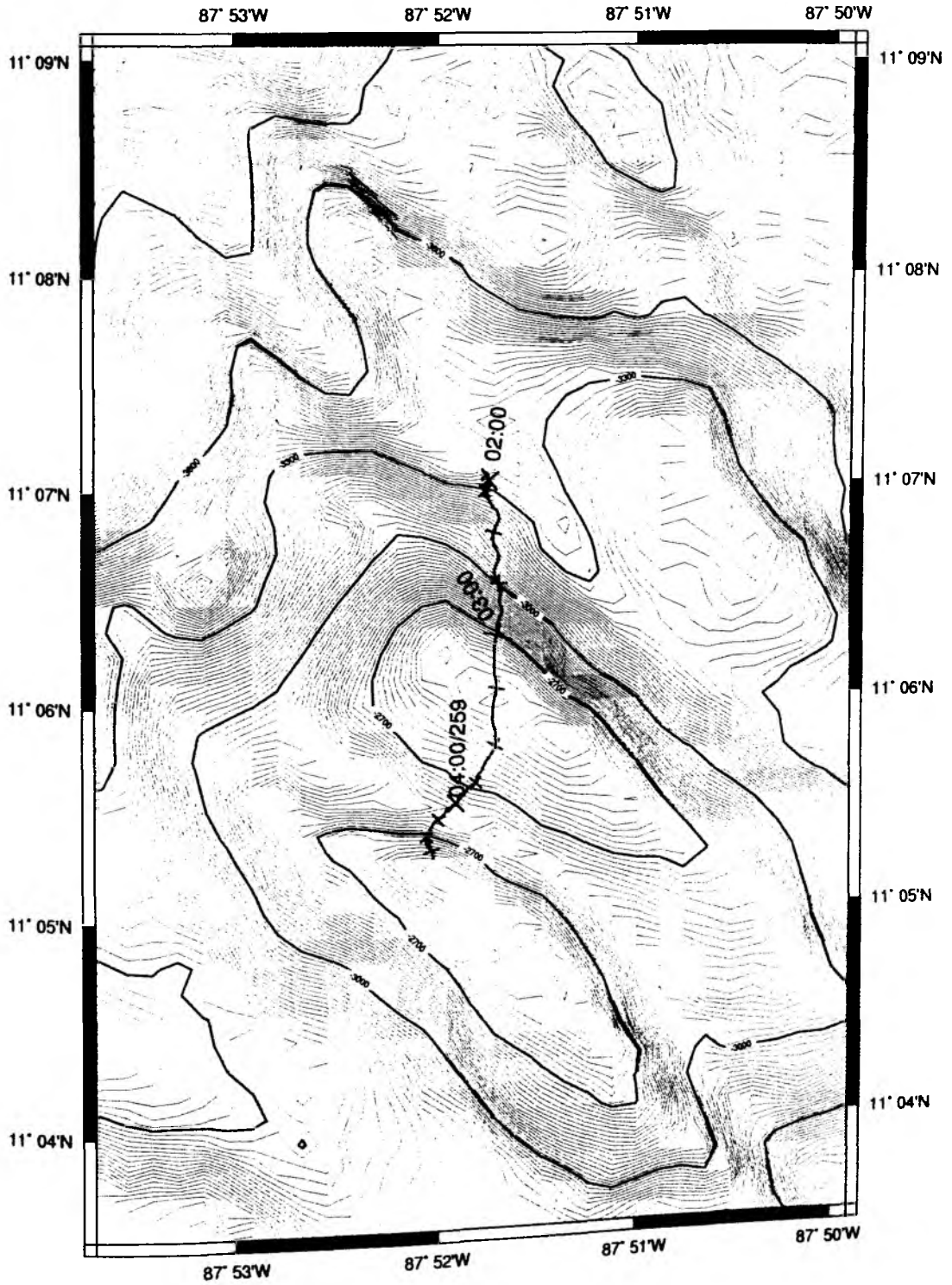

Figure 9.4.1: DREDGE STATION SO144-1a, Location map

SONNE 144/2

Station list

			Time (UTC)					Begin / on seafloor		End / off seafloor				
Date 1999	Station No. SO144/2	Instrument	Begin	on seafloor	off seafloor	End	Duration hh:mm	Latitude N°	Longitude W°	Latitude N°	Longitude W°	Water depth (m)	Recovery	Remarks
21.Okt.	1	CTD-01	00:37	01:53		03:10	2:33	08°50.973	84°41.025	08°51.000	84°41.000	3575	no water samples	test
21.Okt.	2	OFOS-01	05:03	05:26	06:20	06:48	1:45	09°11.318	84°47.884	09°10.816	84°48.199	766		coax cable defect
22.Okt.	3	OFOS-02	00:47	01:04	10:30	11:20	10:33	09°10.755	84°48.429	09°04.646	84°52.280	2438		
22.Okt.	4	CTD-02	12:04	12:35		13:51	1:47	09°06.896	84°50.860	09°06.848	84°50.816	1640		
22./23.Okt.	5	TOBI-01	19:50			16:40	21:50	09°19.110	85°19.290	08°59.600	84°32.47	1834		
23./25.Okt.	6	TOBI-02	19:05			00:58	29:53	08°57.594'	84°35.255'	09°24.510	85°39.290	2616		
25./26.Okt.	7	TOBI-03	02:55			11:00	32:05	09°21.840'	85°40.010'	08°53.800'	84°32.66'	2171		CTD defect
26.Okt.	8	CTD-03	14:17			17:11	02:54	08°55.221	84°40.101	08°55.221	84°40.097	2921		
26./27.Okt.	9	OFOS-03	18:09	18:35	01:48	02:38	08:45	09°00.146	84°36.209	08°55.407	84°36.297	2766		
27.Okt.	10	CTD-04	03:04			05:11	02:07	08°57.508	84°39.027	08°57.503	84°38.991	1626		
27.Okt.	11	OFOS-04	07:36	07:45	14:30	14:48	07:12	08°51.549	84°12.716	08°47.522	84°16.163	854		
27.Okt.	12	CTD-05	15:25			16:34	01:09	08°51.032	84°12.982	08°51.043	84°12.964	408		
27./28.Okt.	13	OFOS-05	23:22	23:35	08:14	08:25	09:03	09°28.472	85°05.329	09°22.616	85°07.810	1703		
28.Okt.	14	CTD-06	09:17			09:58	00:41	09°23.861	85°06.962	09°23.530	85°06.906	1461		
28.Okt.	15	OFOS-06	13:57	14:27	19:30	20:18	07:17	09°00.772	84°44.214	08°56.771	84°43.006	2494		
28./30.Okt.	16	TOBI-04	22:00			05:40	31:40	08°51.810	84°35.340	09°20.780	85°44.600	3090		
30./31.Okt.	17	TOBI-05	07:23			04:44	21:07	09°18.320	85°45.560	09°02.380	85°07.370	3321	TOBI defect	
31.Okt.	18	CTD-07	15:07	15:56		17:18	02:11	09°19.175	85°28.792	09°19.180	85°28.790	2000		
31.Okt.	19	OFOS-07	18:00	18:25	00:46	01:30	06:46	09°19.608	85°24.014	09°15.142	85°25.372	2376		
1./2.Nov.	20	TOBI-06	04:15			16:30	38:15	09°17.620	85°51.220	08°46.070	84°35.150	3396		
2./3.Nov.	21	TOBI-07	19:00			13:30	18:30	08°49.320	84°36.120	09°05.670	85°15.410	3739		
3.Nov.	22	TOBI-08	13:53			16:05	02:13	09°05.750	85°16.180	09°02.780	85°20.370	3430		
3./4.Nov.	23	TOBI-09	16:35			05:10	12:35	09°02.670	85°21.570	09°13.700	85°48.480	3693		
4.Nov.	24	TOBI-10	15:30			23:25	7:55	09°26.960	84°51.560	09°07.500	84°48.000	884		
5.Nov.	25	TOBI-11	01:08			07:29	6:21	09°08.260	84°50.830	09°23.930	84°53.750	1053		
5. Nov.	26	TOBI-12	08:05			13:57	5:52	09°24.690	84°54.830	09°24.290	85°09.570	1136		
5.Nov.	27	OFOS-08	16:15	16:24	21:58		5:43	09°19.338	85°16.222	09°22.410	85°15.850	864		
5.Nov.	28	CTD-08	22:51	23:19		23:58	1:07	09°20.010	85°17.205	09°20.011	85°17.166	592		
6.Nov.	29	OFOS-09	01:39	02:20	12:45	13:33	11:54	09°21.855	85°34.986	09°14.452	85°37.028	2877		
6.Nov.	30	CTD-09	16:46	17:36		18:59	2:23	09°39.382	85°52.938	09°39.425	85°52.945	1919		
6./7.Nov.	31	OFOS-10	19:11	19:59	04:46	05:18	10:07	09°41.297	85°53.020	09°39.481	85°53.042	1962		

APPENDIX 9.6

RF Reedereigemeinschaft
Forschungsschiffahrt GmbH

FS SONNE
SO 144-1

Stationsprotokoll F.S. "S O N N E" Reise SO 144/1

Gebrauchtes Instrumentarium		Anzahl der Einsätze
DR	Kettensackdredge	: 01
OBS	Ocean-Bottom-Seismic-units	
OBH	Ocean-Bottom-Hydrofone-unit	
FLX	Fluxometer	

Eingesetzte Winden:

Winde			RF-Nr.	SO 144/1a Einsatz	Gesamt Einsatz	SO 144/1a S`länge	gefierte max.Sl	Gesamt S`länge	Zust
W 1	LWL	18,2	816233	000 h	0419 h	000000 m	5370 m	156268	2
W 2	LWL	18,2	865017	000 h	1327 h	000000 m	0000 m	834249	5
W 4	NSW	11,0	817141	000 h	0217 h	000000 m	6100 m	136383	3
W 5	NSW	11,0	817164	000 h	0000 h	000000 m	0000 m	000000	1
W 6	Drako	18,2	814150	007 h	0501 h	009374m	7900 m	401528	2

Geräteverluste :

Abkürzungen im Stationsprotokoll:

z.W.	zu Wasser
a.D.	an Deck
Boko	Bodenkontakt
Bosi	Bodensicht
Slmax.	Seillänge
LT	Lottiefe nach Hydrosweep
W x	eingesetzte Winde
HS	Hydrosweep
PS	Parasound
XPNDR	Transponder

Zeit : UTC - 06 Stunden

11.09.1999

Releaser-Test W 6

0805	Beginn Station	LT = 3149 m	20 52,7 N 108 06,3 W
0816	Releaser-units I z.W.		
0915	Slmax = 3000 m	Beginn Releaser-Test	
0934	Ende Test, Beginn hieven		
1032	Releaser a.D.		
1043	Releaser-units II z.W.		
1127	Slmax = 3000 m	Beginn Releaser-Test	
1140	Ende Test, Beginn hieven		
1232	Releaser a.D.		
1238	Beginn Schwimmtest MLS-System am Kran		
1258	Ende Test, Ende Station		

15.09.1999

Station D 1 W 6

1805	Beginn Station	LT = 3305 m	11 07,01 N 87 51,77 W
1807	DK z.W.		

RF Reedereigemeinschaft
Forschungsschiffahrt GmbH

FS SONNE
SO 144-1

2012	Boko SL = 3374 m		LT = 3358 m	11 06,99 N 87 51,77 W
	Kurs = 235 Grad v = 1,0 kn			
2122	Beginn hieven		LT = 2550 m	11 05,93 N 87 51,73 W
2230	DK a.D.			
2250	Ende Station			

Profil 01 – 05 HS/PS

0251	Beginn Profil	1	10 51,57 N 87 03,70 W	
0408	Profilwechsel	1 / 2	11 03,70 N 86 53,93 W	15,5 sml
0416	Profilwechsel	2 / 3	11 02,65 N 86 52,75 N	01,5 sml
0531	Profilwechsel	3 / 4	10 49,88 N 87 01,01 W	15,0 sml
0541	Profilwechsel	4 / 5	10 47,86 N 86 58,98 w^	03,0 sml
0703	Ende Profil	5	11 01,18 N 86 51,41 W	15,0 sml

Profil 06 OBH

1059	OBH 01 z.W.	LT = 117 m	10 58,83 N 86 03,59 W
1141	OBH 02 z.W.	LT =	11 02,11 n 86 07,15 W
1220	OBH 03 z.W.	LT =	11 05,40 N 86 10,68 W
1258	OBH 04 z.W.	LT = 120 m	11 08,60 N 86 14,28 W
1335	OBH 05 z.W	LT = 117 m	11 11,88 N 86 17,85 W
1410	OBH 06 z.W.	LT = 112 m	11 15,12 N 86 21,45 W
1445	OBH 07 z.W.	LT = 113 m	11 18,38 N 86 25,02 W
1520	OBH 08 z.W.	LT = 108 m	11 21,65 N 86 28,59 W
1556	OBH 09 z.W.	LT = 103 m	11 24,91 N 86 32,15 W
1634	OBH 10 z.W.	LT = 92,8 m	11 28,17 N 86 35,74 W
1709	OBH 11 z.W.	LT = 85,3 m	11 31,42 N 86 39,32 W
1742	OBH 12 z.W.	LT = 89,8 m	11 34,66 N 86 42,91 W
1814	OBH 13 z.W.	LT = 92 m	11 37,93 N 86 46,47 W
1852	OBH 14 z.W.	LT = 96 m	11 41,19 N 86 50,03 W
1931	OBH 15 z.W.	LT = 102 m	11 44,47 N 86 53,61 W
2006	OBH 16 z.W.	LT = 106 m	11 47,69 N 86 57,21 W
2043	OBH 17 z.W.	LT = 108 m	11 51,10 N 87 00,95 W
2119	OBH 18 z.W.	LT = 107 m	11 54,51 N 87 04,69 W
2157	OBH 19 z.W.	LT = 110 m	11 57,91 N 87 08,44 W
2232	OBH 20 z.W.	LT = 110 m	11 01,30 N 87 12,20 W
17.09.1999			
0153	OBS 21 z.W.	LT = 135 m	11 51,30 N 87 21,59 W
0308	OBS 22 z.W.	LT = 127 m	11 42,54 N 87 12,20 W
0347	OBS 23 z.W.	LT = 111 m	11 38,64 N 87 07,69 W
0431	OBS 24 z.W.	LT = 127 m	11 34,06 N 87 02,98 W
0543	OBS 25 z.W.	LT = 134 m	11 25,10 N 86 53,41 W
0659	OBS 26 z.W.	LT = 188 m	11 15,89 N 86 43,49 W
0737	OBS 27 z.W.	LT = 172 m	11 12,66 N 86 40,00 W

0820	Beginn aussetzen airguns		
0836	airgun Mitte z.W.		
0856	airgun Bb z.W.		
0908	airgun M a.D.		
0938	airgun Stb z.W.		
0946	Beginn Profil 06/1		11 11,17 N 86 38,42 W
	Kurs = 313 Grad v = 3,5 kn		
1056 - 1117	Stb-airgun klariert		
1314	Stb-airgun a.D.		
1600			11 26,44 N 86 54,83 W
1712	Magnetometer z.W.		11 31,24 N 87 00,00 W
2043	Stb-airgun z.W.		
2400			11 45,73 N 87 15,59 W

RF Reedereigemeinschaft
Forschungsschiffahrt GmbH

FS SONNE
SO 144-1

18.09.1999

0220	Ende Profil 6/1	11 51,30 N	87 21,60 W	58 sml
0224	Magnetometer aufgekürzt			
0224 – 0244	Schleife			
0244	Magnetometer z.W.			
0245	Beginn Profil 6/2	11 51,30 N	87 21,60 W	
	Kurs = 42 Grad v = 3,5 kn			
0636	Ende Profil 6/2	12 01,30 N	87 12,20 W	14 sml
0640	Magnetometer aufgekürzt			
0642 – 0706	Schleife			
0707	Magnetometer z.W.			
0709	Beginn Profil 6/3	12 01,30 N	87 12,20 W	
	Kurs = 132 Grad v = 3,5 kn			
1302	3. Airgun z.W.			
1713	Magnetometer eingeholt			
2211	Bb-airgun a.D. defekt			
2400		11 21,10 N	86 28,00 W	

19.09.1999

0521	3. Airgun a.D. defekt			
1040	Ende Profil 6/3	10 55,60 N	86 00,00 W	79 sml
1053	airgun a.D.			

Aufnahme OBH 1 – 27 GEOMAR

1122	OBH 01 ausgelöst	1124	gesichtet	1131	a.D.	10 58,76 N 86 03,62 W
1154	OBH 02	1159		1206		11 02,03 N 86 07,15 W
1229	OBH 03	1231		1238		11 05,33 N 86 10,66 W
1302	OBH 04	1304		1312		11 08,51 N 86 13,27 W
1340	OBH 05	1346		1352		11 11,84 N 86 17,84 W
1415	OBH 06	1419		1426		11 15,09 N 86 21,41 W
1450	OBH 07	1451		1500		11 18,34 N 86 24,98 W
1524	OBH 08	1527		1533		11 21,67 N 86 28,55 W
1556	OBH 09	1558		1606		11 24,86 N 86 32,07 W
1630	OBH 10	1634		1638		11 28,14 N 86 35,68 W
1701	OBH 11	1706		1713		11 31,34 N 86 39,24 W

Aufnahme OBS 27 – 21 mit time releaser bestückt, per Schlauchboot aufgenommen

OBH 27	1859	1909	11 12,63 N 86 40,03 W
OBH 26	2045	2052	11 15,86 N 86 43,56 W
OBH 25	2229	2238	11 25,09 N 86 53,43 W

20.09.1999

OBH 24	0014	0021	11 34,04 N 87 03,00 W
OBH 23	0203	0209	11 38,39 N 87 07,73 W
OBH 22	0345	0353	11 42,47 N 87 12,25 W
OBH 21	0552	0600	11 51,38 N 87 21,55 W

Aufnahme OBS 20 – 12 GEOMAR

0706	OBH 20	0711	0718	12 01,26 N 87 12,14 W
0742	OBH 19	0747	0754	11 57,88 N 87 08,34 W
0818	OBH 18	0821	0826	11 54,46 N 87 04,58 W
0847	OBH 17	0849	0859	11 51,07 N 87 00,84 W
0921	OBH 16	0923	0930	11 47,63 N 86 57,06 W
0950	OBH 15	0954	1000	11 44,42 N 86 53,50 W
1022	OBH 14	1024	1039	11 40,95 N 86 49,85 W
1058	OBH 13	1101	1109	11 37,79 N 86 46,34 W
1130	OBH 12	1132	1139	11 34,55 N 86 42,78 W

Vermessung mit Hydrosweep und Parasound

1140	Beginn Profil	01	11 34,55 N 86 42,78 W	
1435	Profilwechsel	1 / 2	11 00,64 N 86 50,26 W	35 sml

RF Reedereigemeinschaft
Forschungsschiffahrt GmbH

FS SONNE
SO 144-1

1610	Profilwechsel	2 / 3	10 46,00 N 86 56,84 W	16 sml	
2340	Profilwechsel	3 / 4	09 47,63 N 86 13,42 W	72 sml	
2355	Profilwechsel	4 / 5	09 49,21 N 86 11,45 W	03 sml	
22.09.1999					
0709	Ende Profil	5	10 47,43 N 86 55,07 W	72 sml	
0737	Beginn Profil	6	10 45,10 N 86 55,08 W		
1427	Profilwechsel	6 / 7	09 50,92 N 86 09,14 W	53 sml	
1442	Profilwechsel	7 / 8	09 52,26 N 86 07,11 W	03 sml	
2135	Ende Profil	8	10 47,24 N 86 49,41 W	69 sml	
2152	Beginn Profil	9	10 47,17 N 86 47,10 W		
23.09.1999					
0111	Profiwechsel	9 / 10	10 14,74 N 86 21,74 W	41 sml	
0120	Profilwechsel	10 / 11	10 16,05 N 86 20,12 W	02 sml	
0424	Profilwechsel	11 / 12	10 45,59 N 86 43,88 W	38 sml	
0445	Profilwechsel	12 / 13	10 44,87 N 86 40,49 W	04 sml	
0734	Ende Profil	13	10 17,04 N 86 18,82 W	35 sml	
0743	Beginn Profil	14	10 18,03 N 86 17,70 W		
1028	Profilwechsel	14 / 15	10 43,82 N 86 38,68 W	33 sml	
1045	Profilwechsel	15 / 16	10 42,57 N 86 36,25 W	03 sml	
1207	Profilwechsel	16 / 17	10 29,67 N 86 25,92 W	16 sml	
1324	Profilwechsel	17 / 18	10 17,76 N 86 16,12 W	15 sml	
1356	Profilwechsel	18 / 19	10 13,29 N 86 23,39 W	06 sml	
1615	Profilwechsel	19 / 20	09 51,32 N 86 03,36 W	28 sml	
1728	Profilwechsel	20 / 21	09 42,43 N 86 14,74 W	14 sml	
1905	Profilwechsel	21 / 22	09 22,96 N 86 16,64 W	21 sml	
2055	Profilwechsel	22 / 23	09 38,42 N 85 58,95 W	23 sml	
23.09.1999					
0303	Ende Profil	23	09 09,20 N 84 48,50 W	76 sml	

Seismikprofile 9 - 11

0353	OBS 01	z.W.	LT = 825 m	09 09,17 N 84 48,36 W
0421	OBS 02	z.W.	LT = 739 m	09 11,39 N 84 47,02 W
0445	OBS 03	z.W.	LT = 596 m	09 13,44 N 84 45,83 W
0515	OBS 04	z.W.	LT = 867 m	09 12,36 N 84 48,52 W
0546	OBS 05	z.W.	LT = 813 m	09 10,43 N 48 45,46 W
0602 – 0609	Bb-airgun-array z.W.			
0611 – 0620	setzen streamer aus			
0621	Beginn Profil 09		09 09,80 N 84 44,50 W	
0804	Ende Profil 09		09 13,00 N 84 49,50 W	6,0 sml
0827	Beginn Profil 10		09 12,97 N 84 49,49 W	
0943	Ende Profil 10		09 14,50 N 84 45,25 W	4,5 sml
1007	Beginn Profil 11		09 14,82 N 84 45,06 W	
1130	Ende Profil 11		09 10,15 N 84 47,80 W	5,0 sml
1130 – 1139	holen streamer ein			
1139 – 1148	holen airguns ein			

1202	OBS 01 gesichtet		1222	a.D.	09 09,06 N 84 48,38 W
1242	OBS 02		1247		09 11,33 N 84 46,98 W
1325	OBS 03		1336		09 13,44 N 84 45,68 W
1340	OBS 04 ausgelöst	1400 gesichtet	1431	a.D.	09 10.´,48 N 84 44,96 W
1436	OBS 05	1520	1530		09 12,36 N 84 48,50 W

Seismikprofil 12

1659	OBS 01 geslipt	LT = 1526 m	09 20,79 N 85 02,13 W
1732	OBS 02 geslipt	LT = 1680 m	09 17,02 N 85 04,00 W
1745 – 1750	setzen Bb-airgun-array aus		
1752 – 1759	sezen streamer aus		

RF Reedereigemeinschaft
Forschungsschiffahrt GmbH

FS SONNE
SO 144-1

1800	Beginn Profil			09 16,33 N	85 04,36 W	
1949	Ende Profil			09 22,00 N	85 01,50 W	07 sml
1950 – 1958	holen streamer ein					
1959 – 2005	holen airguns ein					
2006	OBS 1 ausgelöst	2037	gesichtet	2045	a.D.	
2047	OBS 2	2114		2124		

24.09.1999

Auslegung SCRIPPS-OBS und US-fluxometer

0255	OBS 01 z.W.	LT = 2571 m	08 31,10 N	84 17,58 W
0338	OBS 02 z.W.	LT = 2111 m	08 25,01 N	84 15,99 W
0439	OBS 03 z.W.	LT = 2263 m	08 24,51 N	84 05,20 W
0517	FLUX 01 z.W.	LT = 2261 m	08 27,90 N	84 08,65 W
0537	FLUX 02 z.W.	LT = 1979 m	08 29,00 N	84 07,28 W
0554	FLUX 03 z.W.	LT = 1492 m	08 30,50 N	84 06,60 W
0610	FLUX 04(A) z.W.	LT = 1201 m	08 32,00 N	84 05,89 W
0629	FLUX 05(D) z.W.	LT = 849 m	08 33,91 N	84 05,84 W
0648	FLUX 06(G) z.W.	LT = 1338 m	08 32,80 N	84 07,20 W
0707	OBS 04 z.W.	LT = 1585 m	08 31,29 N	84 07,89 W
0725	FLUX 07(B) z.W.	LT = 2033 m	08 29,79 M	84 08,59 W
0817	OBS 05 z.W.	LT = 1695 m	08 36,30 N	84 13,00 W
0901	OBS 06 z.W.	LT = 744 m	08 42,61 N	84 10,71 W
0952	OBS 07 z.W.	LT = 203 m	08 38,70 N	84 03,21 W

Auslegung ORSTROM-OBS

1635	OBS 01 z.W.	LT = 1691 m	07 40,01 N	83 11,99 W
1714	OBS 02 z.W.	LT = 1554 m	07 41,83 N	83 15,30 N
1742	OBS 03 z.W.	LT = 1458 m	07 43,63 N	83 18,60 W
1811	OBS 04 z.W.	LT = 1397 m	07 45,46 N	83 21,91 W
1841	OBS 05 z.W.	LT = 1366 m	07 47,27 N	83 25,21 W
1910	OBS 06 z.W.	LT = 1345 m	07 49,09 N	83 28,52 W
1942	OBS 07 z.W.	LT = 1356 m	07 50,91 N	83 31,82 W
2017	OBS 08 z.W.	LT = 1315 m	07 52,73 N	83 35,11 W
2047	OBS 09 z.W.	LT = 1072 m	07 54,54 N	83 38,42 W
2118	OBS 10 z.W.	LT = 1309 m	07 56,36 N	83 41,72 W
2151	OBS 11 z.W.	LT = 1826 m	07 58,18 N	83 45,02 W
2224	OBS 12 z.W.	LT = 1821 m	08 00,00 N	83 48,33 W
2255	OBS 13 z.W.	LT = 1307 m	08 01,82 N	83 51,64 W

Profil HS/PS/MG

2256	Beginn Profil	1	08 01,82 N	83 51,64 W	
2308	Magnetometer	z.W.			
25.09.1999					
0200	Profilwechsel	1 / 2	08 18,00 N	84 21,00 W	33 sml
0714	Ende Profil	2	09 11,92 N	84 16,23 W	
0722	Magnetometer	a.D.			

Auslegung SCIPPS - OBS

1601	OBS 21 z.W.	LT = 0086 m	08 58,60 N	83 53,60 W
1655	OBS 19 z.W.	LT = 0079 m	08 54,20 N	84 01,64 W
1748	OBS 18 z.W.	LT = 0108 m	08 50,00 N	84 09 19 W
1844	OBS 17 z.W.	LT = 0099 m	08 45,49 N	84 00,50 W
1931	OBS 20 z.W.	LT = 0069 m	08 48,80 N	83 53,60 W
2042	OBS 16 z.W.	LT = 0074 m	08 36,61 N	83 55,49 W
2130	OBS 15 z.W.	LT = 0785 m	08 30,61 N	83 59,50 W

RF Reedereigemeinschaft
Forschungsschiffahrt GmbH

FS SONNE
SO 144-1

Profile HS/PS/MG

2130	Beginn Profil	0	08 30,61 N	83 59,50 W	
2149	Magnetometer z.W.				
2308	Profilwechsel	0 / 1	08 15,00 N	84 05,14 W	17 sml
26.09.1999					
0019	Profilwechsel	1 / 2	08 19,57 N	84 17,50 W	13 sml
0116	Profilwechsel	2 / 3	08 25,14 N	84 26,79 W	11 sml
0244	Profilwechsel	3 / 4	08 17,14 N	84 41,41 W	16 sml
0852	Profilwechsel	4 / 5	07 41,24 N	83 34,94 W	75 sml
0913	Profilwechsel	5 / 6	07 44,97 N	83 34,66 W	04 sml
1134	Ende Profil	6	07 57,86 N	83 56,79 W	25 sml
1204	Magnetometer a.D.				

Auslegung GEOMAR-OBS

1220	OBS 01 z.W.	LT = 0567 m	08 03,64 N	83 54,94 W
1249	OBS 02 z.W.	LT = 1393 m	08 05,43 N	83 58,25 W
1316	OBS 03 z.W.	LT = 1475 m	08 07,27 N	84 01,56 W
1343	OBS 04 z.W.	LT = 1554 m	08 09,10 N	84 04,84 W
1414	OBS 05 z.W.	LT = 1641 m	08 10,92 N	84 08,15 W
1440	OBS 06 z.W.	LT = 1680 m	08 12,73 N	84 11,47 W
1509	OBS 07 z.W.	LT = 1672 m	08 14,53 N	84 14,76 W
1539	OBS 08 z.W.	LT = 1691 m	08 16,37 N	84 18,05 W
1606	OBS 09 z.W.	LT = 1807 m	08 18,18 N	84 21,37 W
1634	OBS 10 z.W.	LT = 2038 m	08 20,00 N	84 24,66 W
1702	OBS 11 z.W.	LT = 2308 m	08 21,82 N	84 27,97 W
1730	OBS 12 z.W.	LT = 2637 m	08 23,64 N	84 31.26 W
1800	OBS 13 z.W.	LT = 2524 m	08 25,46 N	84 34,56 W
1830	OBS 14 z.W.	LT = 2466 m	08 27,27 N	84 37,88 W
1900	OBS 15 z.W.	LT = 2345 m	08 29,10 N	84 41,18 W
1927	OBS 16 z.W.	LT = 1610 m	08 30,92 N	84 44,49 W
1954	OBS 17 z.W.	LT = 1493 m	08 32,73 N	84 47,79 W
2024	OBS 18 z.W.	LT = 2208 m	08 34,55 N	84 51,09 W
2052	OBS 19 z.W.	LT = 2626 m	08 36,36 N	84 54,40 W
2123	OBS 20 z.W.	LT = 2770 m	08 38,19 N	84 57,70 W

Profile HS/PS/MG

2124	Beginn Profil	1	08 38,19 N	84 57,70 W	
2140	Magnetometer z.W.				
2237	Profilwechsel	1 / 2	08 25,51 N	84 55,93 W	13 sml
27.09.1999					
0120	Profilwechsel	2 / 3	08 38,06 N	85 25,00 W	31 sml
0626	Ende Profil	3	09 30,0 N	84 52,50 W	61 sm
0644	Magnetometer a.D.				

Insgesamt wurden :
34 OBS ausgelegt und wieder geborgen

21 OBS ausgelegt für SO 144/3b
07 Flowmeter für SO 144/3b

33 OBS ausgelegt für SO 144/1b

Vermessung mit Hydrsweep, Parasoun und tlw. Magnetik : = 1027 sml
Refraktions- und Weitwinkel-Seismik = 0174 sml

RF Reedereigemeinschaft
Forschungsschiffahrt GmbH

FS SONNE
SO 144-1

Stationsprotokoll F.S. "S O N N E" Reise SO 144/1b

Gebrauchtes Instrumentarium		Anzahl der Einsätze
OBS	Ocean-Bottom-Seismic-units	94 / 18
OBH	Ocean-Bottom-Hydrofone-unit	
	3 x 3 Liter-airguns	
	6 x 0,5 Liter airguns	
MAG	Magnetometer	

Eingesetzte Winden:

Winde			RF-Nr.	SO 144/1b Einsatz	Gesamt Einsatz	SO 144/1b S`länge	gefierte max.Sl	Gesamt S`länge	Zust
W 1	LWL	18,2	816233	000 h	0419 h	000000 m	5370 m	156268	2
W 2	LWL	18,2	865017	000 h	1327 h	000000 m	0000 m	834249	5
W 4	NSW	11,0	817141	000 h	0217 h	000000 m	6100 m	136383	3
W 5	NSW	11,0	817164	000 h	0000 h	000000 m	0000 m	000000	1
W 6	Drako	18,2	814150	000 h	0501 h	009374m	7900 m	401528	2

Geräteverluste : keine

Abkürzungen im Stationsprotokoll:

z.W.	zu Wasser
a.D.	an Deck
Boko	Bodenkontakt
Bosi	Bodensicht
Slmax.	Seillänge
LT	Lottiefe nach Hydrosweep
W x	eingesetzte Winde
HS	Hydrosweep
PS	Parasound
XPNDR	Transponder

Zeit : UTC - 06 Stunden

28.09.1999

Profil 101 / 102 HS/PS/MG

1230 - 1230	setzen Magnetometer aus			
1240	Beginn Profil	101	09 24,70 N 84 44,40 W	
1503	Profilwechsel	101 / 102	09 00,00 N 84 58,70 W	37 sml
1636	Ende Profil	102	08 42,85 N 85 06,27 W	

Profil 01 WS/HS/PS/MG

1700	airgun Bb z.W.		
1720	Stb-airgun z.W.		
1732	airgun M z.W.		
1732	Kurs = 118 Grad	v = 3,5 kn	08 41,79 N 85 04,36 W
2400			08 20,95 N 84 26,38 W

RF Reedereigemeinschaft
Forschungsschiffahrt GmbH

FS SONNE
SO 144-1

29.09.1999

0600		08 20,95 N 84 26,38 W		
0823	Bb airgun a.D.			
1121	Bb airgun z.W.			
1200		08 10,59 N 84 07,58 W		
1508	Bb airgun a.D.			
1636	Bb airgun z.W.			
1722	Bb airgun a.D.			
1800		08 00,27 N 83 48,73 W		
2015	Bb airgun z.W.			
2021	M airgun a.D.			
2144	M airgun z.W.			
2400		07 50,21 N 83 30,48 W		

30.09.1999

0600		07 40,11 N 83 12,05 W		
0807	M airgun a.D.			
0851	Ende Profil	07 35,24 N 83 03,21 W	138	sml
0907	Stb airgun a.D.			
0921	Bb airgun a.D.			

Profil 103 HS/PS/MG

0946	Beginn Profil	07 32,96 N 83 04,51 W		
1543	Ende Profil	08 01,32 N 83 49,21 W	075	sml
1555	Magnetometer a.D.			

Aufnahme OBS von Profil 01

1606	OBH 50	ausgelöst	1612gesichtet	1617a.D.	08 03,56 N	83 54,85 W
1619	OBH 49		1640	1647	08 05,37 N	83 58,10 W
1713	OBH 48		1733	1737	08 07,25 N	84 01,46 W
1937	OBH 55		1958	2010	08 16,21 N	84 18,00 W

Profil 104 HS/PS/MG

2024	Magnetometer z.W.			
2025	Beginn Profil	08 15,43 N 84 18,68 W		

01.10.1999

0037	Ende Profil	08 35,94 N 84 59,02 W	46	sml
0052	Magnetometer a.D.			

Aufnahme OBS von Profil 01

0044	OBH 67	ausgelöst	0113gesichtet	0124a.D.	08 38,07 N	84 57,75 W
0129	OBH 66		0159	0207	08 36,34 N	84 54,36 W
0213	OBH 65		0237	0245	08 34,46 N	84 51,08 W
0252	OBH 64		0306	0322	08 32,55 N	84 47,63 W
0328	OBH 63		0343	0355	08 30,76 N	84 44,41 W
0400	OBH 62		0422	0432	08 28,97 N	84 41,12 W
0439	OBH 61		0520	0526	08 27,16 N	84 37,84 W
0528	OBH 60		0552	0600	08 25,27 N	84 25,52 W
0600	OBH 59		0630	0636	08 23,54 N	84 31,29 W
0636	OBH 58		0703	0711	08 21,77 N	84 28,08 W
0711	OBH 57		0733	0740	08 19,89 N	84 24,76 W

RF Reedereigemeinschaft
Forschungsschiffahrt GmbH

FS SONNE
SO 144-1

0741	OBH 56	0800	0818	08 17,83 N	84 21,47 W
0844	OBH 54	0900	0908	08 14,42 N	84 14,83 W
0908	OBH 53	0932	0943	08 12,63 N	84 111,59 W
0944	OBH 52	1006	1015	08 10,77 N	84 08,20 W
1016	OBH 51	1056	1104	08 09,05 N	84 04,92 W

Profil 105 HS/PS/MG

1115	Magnetometer z.W.			
1116	Beginn Profil	08 08,59 N	84 04,59 W	
1352	Ende Profil	07 37,97 N	84 02,75 W	31 sml

Auslegung OBS Profil 02

1417	OBH 68 z.W.	LT = 1313 m	07 37,99 N 84 02,77 W
1441	OBH 69	LT = 1584 m	07 40,39 N 84 00,92 W
1506	OBH 70	LT = 1692 m	07 42,77 N 83 59,04 W
1528	OBH 71	LT = 1674 m	07 45,16 N 83 57,19 W
1554	OBH 72	LT = 1794 m	07 47,59 N 83 55,30 W
1640	OBH 73	LT = 1619 m	07 49,18 N 83 53,53 W
1704	OBH 74	LT = 1722 m	07 52,35 N 83 51,64 W
1732	OBH 75	LT = 1768 m	07 54,78 N 83 49,8 2 W
1756	OBH 76	LT = 1774 m	07 57,06 N 83 48,06 W
1822	OBH 77	LT = 1845 m	07 59,42 N 83 46,19 W
1843	OBH 78	LT = 1867 m	08 01,81 N 83 44,32 W
1906	OBH 79	LT = 1892 m	08 04,19 N 83 42,57 W
1931	OBH 80	LT = 1870 m	08 06,61 N 83 40,68 W
1954	OBH 81	LT = 1861 m	08 08,97 n 83 38,84 W
2018	OBH 82	LT = 1897 m	08 11,40 N 83 36,97 W
2044	OBH 83	LT = 1937 m	08 13,76 N 83 35,16 W
2110	OBH 84	LT = 1641 m	08 16,12 N 83 33,33 W
2133	OBH 85	LT = 1274 m	08 18,45 N 83 31,51 W
2157	OBH 86	LT = 1006 m	08 20,82 N 83 29,69 W
2248	OBH 87	LT = 0462 m	08 23,00 N 83 28,00 W

Vermessung MG/HS/PS

2257	Magnetometer z.W.			
2257	Beginn Profil 106		08 22,58 N 83 27,46 W	
02.10.1999				
0000	Profilwechsel	106 / 107	08 15,00 N 83 18,00 W	49 sml
0306	Profilwechsel	107 / 108	07 45,00 N 83 40,00 W	37 sml
0419	Ende Profil 108		07 52,06 N 83 52,74 W	15 sml
0422	Magnetometer a.D.			
0447	OBH 73 z.W.	LT = 1619 m	07 50,01 N 83 53,49 W	
0457	Magnetometer z.W.			
0503	Beginn Profil 109		07 52,06 N 83 52,74 W	
0747	Profilwechsel	109 / 110	08 08,63 N 84 21,71 W	33 sml
1256	Ende Profil 110		09 11,78 N 84 14,94 W	72 sml
1304	Magnetometer a.D.			
1905	Magnetometer z.W.			
1906	Beginn Profil 111		08 34,43 N 84 00,32 W	
1914	ä.K. auf 114 Grad	v = 3,5 kn	08 34,43 N 84 00,32 W	

2008	Ende Profil 111	08 28,70 N 83 50,05 W	11	sml

Profil 02 HS/PS/MGWS

2022	Bb airgun z.W.			
2033	Stb airgun z.W.	08 28,44 N 85 49,48 W		
2050	M airgun z.W.			
2155	Stb airgun a.D.			
2311	Stb airgun z.W.			
2317	Stb airgun a.D.			
2350	Stb airgun z.W.			
03.10.1999				
0010	Stb airgun a.D.			
0235	ändern Kurs auf 90 Grad	08 20,00 N 83 30,00 W	27	sml
0703	ändern Kurs auf 25 Grad	08 20,00 N 83 14,00 W	16	sml
0730	Magnetometer a. W.			
0955	ändern Kurs auf 315 Grad	08 30,00 N 83 13,00 W	10	sml
1444	Ende Profil 02	08 42,00 N 83 25,00 W	17	sml
1452	M airgun a.D.			
1507	Bb airgun a.D.			

Vermessung HS/PS/MG

1513	Beginn Profil 112	08 42,00 N 83 24,00 W		
1522	Magnetometer z.W.			
1638	Magnetometer a.D.			
1644	Profilwechsel 112 / 113	08 30,00 N 83 12,50 W	17	sml
1728	Profilwechsel 113 / 114	08 21,00 N 83 13,00 W	09	sml
1736	Magnetometer z.W.			
1800	Profilwechsel 114 / 115	08 15,00 N 83 15,00 W	06	sml
2107	ä.K. auf 101 Grad	07 45,00 N 83 37,00 W	37	sml
2313	Ende Profil 115	07,39,67 N 83 12,19 W	25	sml
2321	Magnetometer a.D..			

Aufnahme Orstrom-OBS (mit Schlauchboot)

2355	OBS 35 gesichtet				
04.10.1999					
0006	a.D. 07 39,89 N 83 11,95 W				
0053	OBS 36 gesichtet	0103	a.D.	07 41,72 N	83 15,32 W
0148	OBS 37	0156		07 43,52 N	83 18,71 W
0251	OBS 38	0257		07 45,41 N	83 22,04 W
0349	OBS 39	0356		07 47,21 N	83 25,33 W
0443	OBS 40	0449		07 49,03 N	83 28,63 W
0552	OBS 41	0600		07 50,84 N	83 31,88 W
0719	OBS 42	0725		07 52,71 N	83 35,09 W
0848	OBS 43	0852		07 54,50 N	83 38,39 W
1015	OBS 44	1020		07 56,25 N	83 41,70 W
1155	OBS 45	1200		07 58,10 N	83 45,06 W
1325	OBS 46	1330		07 59,96 N	83 48,45 W
1449	OBS 47	1503		08 01,78 N	83 51,56 W

Profil 116 HS/PS/MG

1518	Beginn Profil	08 01,05 N 83 52,03 W

RF Reedereigemeinschaft
Forschungsschiffahrt GmbH

FS SONNE
SO 144-1

1519	Magnetometer z.W.	SL = 350 m		
1811	Ende Profil	07 31,93 N 84 10,62 W	34	sml

Profil 02 B HS/PS/MG/WS

1830	Bb airgun z.W.			
1840	M airgun z.W.			
1855	Beginn Profil	07 30,25 N 84 08,92 W		
2035	Stb airgun z.W.			
2136	Stb airgun a.D.			
2400		07 44,00 N 83 58,17 W		
05.10.1999				
0247	Bb airgun a.D.			
0528	Bb airgun z.W.			
0600		08 00,86 N 83 45,17 W		
0950	Stb airgun z.W.			
1423	Ende Profil	08 23,01 N 83 27,97 W	66	sml
1435	Stb airgun a.D.			
1443	Magnetometer vorgehievt			
1451	M airgun a.D.			
1505	Stb airgun a.D.			
1510	Magnetometer a.D.			

Aufnahme OBS von Profil 02 B

1508 OBH 87 ausgelöst	1518 gesichtet	1527 a.D.	08 23,14 N	83 27,98 W
1547 OBH 86	1558	1605	08 20,93 N	83 29,72 W
1606 OBH 85	1626	1637	08 18,63 N	83 31,63 W
1638 OBH 84	1655	1702	08 16,22 N	83 33,41 W
1703 OBH 83	1725	1740	08 13,99 N	83 35,13 W
1742 OBH 82	1806	1814	08 11,50 N	83 36,94 W
1814 OBH 81	1843	1854	08 09,07 N	83 38,74 W
1854 OBH 80	1914	1926	08 06,72 N	83 40,53 W
1926 OBH 79	1944	1959	08 04,30 N	83 42,42 W
1959 OBH 78	2015	2028	08 01,89 N	83 44,15 W
2025 OBH 77	2054	2104	07 59,44 N	83 46,08 W
2110 OBH 76	2146	2158	07 57,02 N	83 47,86 W
2150 OBH 75	2213	2229	07 54,84 N	83 49,50 W
2229 OBH 74	2250	2259	07 52,36 N	83 51,48 W
2259 OBH 73	2315	2335	07 50,15 N	83 52,83 W
2349 OBH 72	0017	0031	07 47,61 N	83 55,06 W
06.10.1999				
0032 OBH 71	0049	0106	07 45,25 N	83 56,88 W
0107 OBH 70	0125	0139	07 42,81 N	83 58,79 W
0140 OBH 69	0155	0218	07 40,53 N	84 00,77 W
0219 OBH 68	0234	0248	07 38,11 N	84 02,70 W

Profil 117 HS/PS/MG

0255 - 0311	Magnetometer z.W.		
0302	Beginn Profil	07 37,45 N	84 02,06 W
0600		07 09,5 N	83 39,5 W

1200		06 09,35 N 82 49,26 W		
1308	Magnetometer a.D.			
1322	Magnetometer z.W.			
1554	Unterbecheung Profil	Magnetometer a.D.	05 30,60 N 82 19,02 W	
1558 – 1743	Releaser-Test mit OBH 88/89			
1745	Fortsetzung Profil			
1800			05 29,84 N 82 18,37 W	
2400			04 29,33 N 81 25,41 W	
07.10.1999				
0700	Ende Profil	03 26,10 N 80 17,81 W		300 sml
0712	Magnetometer a.D.			

Auslegen OBS auf Profil 03

0719	OBS 90 z.W.	LT = 2493 m	03 26,92 N 80 16,90 W	
0752	91	2493	03 29,97 N 80 20,02 W	
0822	92	2626	03 33,02 N 80 22,96 W	
0851	93	2607	03 36,08 N 80 26,08 W	
0920	94	2488	03 39,15 N 80 29,15 W	
0949	95	2390	03 42,22 N 80 32,23 W	
1014	96	2403	03 44,90 N 80 34,90 W	
1036	97	2258	03 47,20 N 80 37,17 W	
1100	98	2195	03 49,48 N 80 39,56 W	
1124	99	2158	03 51,79 N 80 41,79 W	
1159	100	2103	03 54,10 N 80 44,28 W	
1229	101 VA	2027 m	03 56,42 N 80 46,35 W	
1253	102	1927	03 58,71 N 80 48,66 W	
1317	103	1824	04 00,99 N 80 50,95 W	
1342	104	1770	04 03,29 N 80 53,28 W	
1406	105	1581	04 05,61 N 80 55,55 W	
1433	106	1472	04 07,90 N 80 57,83 W	
1458	107	1249	04 10,19 N 81 00,13 W	
1520	108	1583	04 12,47 N 81 02,50 W	
1542	109	1671	04 14,78 N 81 04,75 W	
1609	110	1716	04 17,06 N 81 07,03 W	
1630	111	1667	04 19,36 N 81 09,35 W	
1700	112	1865	04 21,69 N 81 11,66 W	
1730	113	2050	04 23,96 N 81 13,95 W	
1802	114	2044	04 26,27 N 81 16,23 W	
1830	115	1577	04 28,55 N 81 18,57 W	
1902	116	3205	04 30,87 N 81 20,85 W	
1931	117	3267	04 33,20 N 81 23,14 W	
2000	118	3267	04 35,49 N 81 25,45 W	
2031	119	3543	04 37,76 N 81 27,73 W	
2100	120	3652	04 40,10 N 81 30,14 W	
2131	121	3721	04 42,39 N 81 32,30 W	
2205	122	3812	04 44,67 N 81 34,61 W	

Profil 118 HS/MG/PS

2215	*Beginn Profil*	*04 45.30 N 81 34.84 W*	
2248	a.K. auf 298 Grad	04 51,49 N 81 36,64 W	06 sml
2345	Ende Profil	04 54,45 N 91 44,41 W	08 sml

Profil 03 *HS/PS/MG/WS*

0014	Bb airgun z.W.		
0035	M airgun z.W.	04 52,55 N 81 42,51 W	
	Beginn Profil v = 3,5 kn	Kurs = 124 Grad	
0600		04 39,40 N 81 29,38 W	
1200		04 24,54 N 81 14,49 W	
1435	Stb airgun z.W.		
1551	Magnetometer a.D.		
1639	Magnetometer z.W.		
1800		04 09,53 N 80 55,55 W	
2102	M airgun a.D.		
2132	M airgun z.W.		
2400		03 54,74 N 80 44,74 W	
09.10.1999			
0600		03 39,84 N 80 29,80 W	
1200		03 25,00 N 80 15,00 W	
1359	Ende Profil	03 20,00 N 80 10,00 W	130 sml
1406	M airgun a.D.		
1423	Stb airgun a.D.		
1433	Bb airgun a.D.		

Porofil 119 *HS/PS/MG*

1434	Beginn Profil	03 18,72 N 80 09,38 W	
1458	a.K. auf 315 Grad	03 19,53 N 80 13,74 W	04 sml
1527	ä.K. auf 45 Grad	03 24,83 N 80 10,18 E	08 sml
1601	Ende Profil	03 27,35 N 80 16,69 W	04 sml
1607	Magnetometer a.D.		

Aufnahme OBS/OBH Profil 03

1541 OBH 90 ausgelöst	1613gesichtet	1623	a.D.	03 26,89 N 80 17,04 W
1605 OBH 91	1715	1722		03 29,89 N 80 20,22 W
1717 OBH 92	1749	1800		03 33,02 N 80 23,03 W
1753 OBH 93	1822	1831		03 36,19 N 80 26,12 W
1827 OBH 94	1853	1903		03 39,23 N 80 29,17 W
1903 OBH 95	1947	1954		03 42,27 N 80 32,28 W
1950 OBH 96	2011	2025		03 45,07 N 80 34,96 W
2024 OBH 97	2049	2057		03 47,36 N 80 37,14 W
2054 OBH 98	2117	2125		03 49,66 N 80 39,41 W
2125 OBH 99	2152	2201		03 51,98 N 80 41,73 W
2202 OBH 100 VA	2220	2238		03 54,25 N 80 44,33 W
2240 OBH 101	2300	2306		03 56,50 N 80 46,30 W
2306 OBH 102	2328	2335		03 58,81 N 80 48,61 W
2338 OBH 103				

10.10.1999

	0017	0024	04 01,17 N 80 51,02 W
	0045	0056	04 03,41 N 80 53,21 W
0025 OBH 104	0127	0134	04 05,72 N 80 53,47 W
0059 OBH 105	0151	0202	04 07,98 N 80 57,77 W
0134 OBH 106	0217	0232	04 10,33 N 81 00,12 W
0203 OBH 107			

0235	OBH 108	0253	0302	04 12,59 N	81 02,50 W
0305	OBH 109	0324	0331	04 14,87 N	81 04,75 W

Profil 120 PS/HS/MG

0350	Magnetometer z.W.				
0350	Beginn Profil	04 15,78 N	08 03,91 W		
0525	ä.K. auf 225 Grad	04 03,69 N	80 50,72 W	18	sml
0546	ä.K. auf 315 Grad	04 00,75 N	80 53,55 W	04	sml
0725	ä.K. auf 45 Grad	04 15,58 N	81 08,00 W	21	sml
0735	Ende Profil	04 17,09 N	81 07,03 W	02	sml
0744	Magnetometer a.D.				

Aufnahme OBH IRD

0811	OBH 110	gesichtet	0816	a.D.	04 17,15 N	81 07,02 W
0907	OBH 111		0912		04 19,35 N	81 09,39 W
1005	OBH 112		1012		04 21,68 N	81 11,61 W
1109	OBH 113		1117		04 24,09 N	81 13,79 W
1211	OBH 114		1217		04 26,30 N	81 16,16 W
1257	OBH 115		1306		04 28,59 N	81 18,47 W
1409	OBH 116		1415		04 30,96 N	81 20,72 W
1454	OBH 117		1501		04 33,43 N	81 22,97 W
1558	OBH 118		1603		04 35,58 N	81 25,36 W
1651	OBH 119		1658		04 37,84 N	81 27,61 W
1802	OBH 120		1811		04 40,15 N	81 30,02 W
1900	OBH 121		1905		04 42,39 N	81 32,23 W
1958	OBH 122		2004		04 44,65 N	81 34,56 W

Profil 121 HS/PS/MG

2005	Beginn Profil	04 45,00 N	81 35,00 W	
2018	Magnetometer z.W.			
2400		04 51,61 N	82 20,27 W	
11.10.1999				
0600		05 02,47 N	83 30,00 W	
1200		05 14,89 N	84 39,41 W	
1351	Ende Profil	05 19,73 N	85 00,04 W	214 sml
1402	Magnetometer a.D.			

Ausbringen OBS/OBH auf Profil 04

1417	OBH 123 z.W.	LT = 3077 m	05 19,77 N	84 59,76 W	
1506	OBH 124	2836	05 25,19	85 05,18	
1553	OBH 125	2647	05 30,51	85 10,48	
1626	OBH 126	2595	05 34,08	85 14,06	
1635	OBH 127	2392	05 37,11	85 17,08	
1724	OBH 128	1872	05 39,96	85 19,91	
1755	OBH 129	1715	05 42,83	85 22,79	
1827	OBH 130	1708	05 45,88	85 25,82	
1910	OBH 131	1813	05 50,00	85 29,97	
1940	OBH 132	1772	05 52,75	85 32,73	
2014	OBH 133	1720	05 56,03	85 35,95	
2056	OBH 134 VA	1734	05 59,94	85 39,91	

2129	OBH 135	1734	06 02,72	85 42,66	
2206	OBH 136	1849	06 05,29	85 45,24	
2231	OBH 137	1897	06 07,53	85 47,49	
2258	OBH 138	1925	06 09,95	85 49,90	
2329	OBH 139	1973	06 12,97	85 52,91	
12.10.1999					
0006	OBH 140	1993	06 16,68	85 56,62	
0039	OBH 141	1947	06 19,98	85 59,94	
0113	OBH 142	1173	06 23,27	86 03,22	
0143	OBH 143	1712	06 26,29	86 06,25	
0217	OBH 144	2347	06 29,99	86 13,51	
0251	OBH 145	2701	06 33,57	86 13,51	
0324	OBH 146	2748	06 37,04	86 16,99	
0353	OBH 147	2784	06 39,98	86 19,95	
0434	OBH 148	2869	06 45,00	86 24,96	
0518	OBH 149	2950	06 50,00	86 29,95	

Profil 122	*HS/PS/MG*			
0522	bringen Magnetometer aus			
0529	Beginn Profil, MM z.W.	06 51,00 N	86 29,95 W	
0540	ä.K. auf 315 Grad	06 53,22 N	86 29,94 W	04 sml
0637	ä.K. auf 227 Grad	07 01,51 N	86 38,35 W	08 sml
0650	Ende Profil	07 00,00 N	86 40,00 W	02 sml

Profil 04	*HS/PS/MG/S*			
0705	Bb airgun z.W. v = 4,0 kn Kurs = 135 Grad			
	Beginn Profil	06 59,19 N	86 39,16 W	
0716	Stb airgun z.W.			
1000	v = 4,3 kn			
1200		06 44,50 N	86 24,49 W	
1800		06 26,07 N	86 06,00 W	
1826	Stb airgun a.D.			
1931	Stb airgun z.W.			
2400		06 08,23 N	85 48,19 W	
13.10.1999				
0214 – 0230	erneuern Auftriebskörper bei Bb airgun			
0329	Bb airgun a.D.			
0425	Bb airgun z.W.			
0600		05 49,65 N	85 29,60 W	
1200		05 31,29 N	85 11,27 W	
1800	Ende Profil	05 12,67 N	84 52,67 W	154 sml
1814	Bb airgun a.D.			
1830	Stb airgun a.D.			

Profil 123	*HS/PS/MG*			
1830	Beginn Profil	05 11,19 N	84 53,34 W	
1845	ä.K. auf 315 Grad	05 11,19 N	84 55,14 W	003 sml
1931	ä.K. auf 045 Grad	05 17,77 N	85 01,83 W	009 sml
1953	Ende Profil	05 19,73 N	84 59,75 W	003 sml
2003	Magnetometer a,D.			

RF Reedereigemeinschaft
Forschungsschiffahrt GmbH

FS SONNE
SO 144-1

Aufnahme OBS/OBH von Profil 04

1936	OBH	123	ausgelöst	2014	gesichtet	2023	a.D.	05 19,78 N 84 59,74 W
2048	OBH	124		2123		2130		05 25,21 85 05,15
2150	OBH	125		2224		2232		05 30,44 85 10,45
2232	OBH	126		2301		2308		05 34,09 85 13,93
2304	OBH	127		2333		2343		05 37,12 85 16,85
2344	OBH	128						
14.10.1999								
				0006		0017		05 39,91 85 17,63
0017	OBH	129		0042		0051		05 42,79 85 22,50
0104	OBH	130		0120		0129		05 45,84 85 25,60
0147	OBH	131		0213		0220		05 49,93 85 29,74
0222	OBH	132		0240		0253		05 52,78 85 32,43
0308	OBH	133		0327		0338		05 55,96 85 35,78
0356	OBH	134	VA	0412		0430		05 59,95 85 39,70
0434	OBH	135		0454		0504		06 02,63 85 42,46
0505	OBH	136		0543		0554		06 05,29 85 44,95
0545	OBH	137		0635		0640		06 07,51 85 47,44
0631	OBH	138		0704		0709		06 09,94 85 49,83
0705	OBH	139		0729		0738		06 12,91 85 52,66
0800	OBH	140		0822		0828		06 16,69 85 56,52
	OBH	144		1003		1013		06 29,84 86 09,76
	OBH	145		1103		1110		06 33,40 86 13,41
	OBH	146		1219		1227		06 36,83 86 16,78
	OBH	147		1331		1337		06 39,85 86 19,84
	OBH	148		1417		1426		06 44,76 86 24,73
	OBH	149		1518		1527		06 49,89 86 29,85

Profil 124 HS/PS/MG

1642	Beginn Profil	06 47,38 N	86 31,81 W	
1649	Magnetometer z.W.			
1937	ä.K. auf 90 Grad	06 20,22 N	86 04,39 W	23 sml
2000	Ende Profil	06 19,97 N	85 59,72 W	05 sml
2013	Magnetometer a.D.			

Aufnahme OBS von Profil 04

1957	OBH	141	2023	2033	06 19,97	85 59,80
2047	OBH	142	2100	2109	06 23,23	86 03,11
2121	OBH	143	2150	2158	06 26,14	86 06,02

Profil 125 HS/PS/MG

2158	Beginn Profil	06 26,14 N	86 06,02 W	
2217	Magnetometer z.W.			
2400		06 46,55 N	86 08,76 W	
15.10.1999				
0600		07 58,23 N	86 18,02 W	
1333	Ende Profil	09 30,00 N	86 30,00 W	185 sml
1341	Magnetometer a.D.			

Auslegen OBH/OBS auf Profil 05

1351	OBS 150 z.W.	LT = 3274 m	09 30,04 N	86 29,94 W

RF Reedereigemeinschaft
Forschungsschiffahrt GmbH

FS SONNE
SO 144-1

1416	OBH 151	3308	09 28,18	86 27,45
1445	OBH 152	3313	09 26,33	86 25,00
1506	OBH 153	3286	09 24,53	86 22,57
1526	OBH 154	3310	09 22,66	86 20,16
1546	OBH 155	3326	09 20,84	86 17,71
1606	OBH 156	3323	09 19,02	86 15,32
1624	OBH 157	3290	09 17,21	86 12,88
1643	OBH 158	3269	09 15,38	86 10,48
1701	OBH 159	3288	09 13,52	86 08,00
1722	OBH 160	3323	09 11,64	86 05,48
1747	OBH 161	3258	09 09,85	86 03,44
1808	OBH 162	3273	09 08,00	86 00,62

Profil 126 HS/PS/MG

1808	Beginn Profil	09 08,00 N	86 00,62 W	
1817	Magnetometer z.W.			
1831	ä.K. auf 128 Grad	09 04,54 N	86 00,64 W	04 sml
1917	ä.K. auf 60 Grad	08 58,28 N	85 52,93 W	10 sml
1932	Ende Profil	08 59,98 N	85 49,98 W	03 sml

Profil 05 HS/PS/MG/S

1943	setzen airguns aus			
1959	Beginn Seismik	09 00,59 N	85 51,31 W	
2009	beide airguns z.W.			
2400		09 10,24 N	86 03,69 W	
16.10.1999				
0600		09 23,58 N	86 21,51 W	
1200	Ende Profil	09 37,48 N	86 40,01 W	62 sml
1210	Bb airgun a.D.			
1219	Stb airgun a.D.			

Profil 127 HS/PS/MG

1220	Beginn Profil	09 38,01 N	86 40,79 W	
1243	ä.K. auf 127 Grad	09 33,81 N	86 40,60 W	04 sml
1332	ä.K. auf 37 Grad	09 27,25 N	86 32,13 W	11 sml
1350	Ende Profil	09 30,02 N	86 29,93 W	04 sml
1400	Magnetometer a.F.			

Aufnahme OBS/OBH von Profil 05

1340	OBH 150	ausgelöst	1410	gesichtet	1416a.D.	09 30,00 N 86 29,81 W
1412	OBH 151		1451		1456	09 28,14 N 86 27,30 W
1452	OBH 152		1536		1544	09 26,29 N 86 24,83 W
1527	OBH 153		1603		1609	09 24,48 N 86 22,35 W
1605	OBH 154		1644		1649	09 22,64 N 86 19,96 W
1624	OBH 155		1704		1711	09 20,84 N 86 17,57 W
1710	OBH 156		1752		1757	09 18,93 N 86 15,20 W
1739	OBH 157		1817		1823	09 17,18 N 86 12,81 W
1823	OBH 158		1900		1907	09 15,32 N 86 10,44 W
1850	OBH 159		1925		1935	09 13,43 N 86 07,93 W
1929	OBH 160		2010		2017	09 11,56 N 86 05,43 W
2000	OBH 161		2034		2048	09 09,75 N 86 02,96 W

2042 OBH 162 2133 2140 09 07,97 N 86 00,61 W

Profil 128 HS/PS/MG

2140	Beginn Profil	09 07,97 N	86 00,61 W	
2152	Magnetometer z.W.			
2219	ä.K. auf 135 Grad	09 10,00 N	85 55,00 W	06 sml
2322	ä.K. auf 180 Grad	09 00,00 N	85 45,00 W	14 sml
17.10.1999				
0010	ä.K. auf 232 Grad	08 50,00 N	85 45,00 W	10 sml
0105	ä.K. auf 112 Grad	08 42,98 N	85 54,03 W	11 sml
0336	ä.K. auf 360 Grad	08 30,00 N	85 23,00 W	29 sml
0755	ä.K. auf 033 Grad	09 23,00 N	85 23,00 W	53 sml
0837	ä.K. auf 090 Grad	09 30,63 N	85 17,89 W	09 sml
0854	Ende Profil	09 30,60 N	85 14,10 W	04 sml
0905	Magnetometer a.D.			

Auslöseversuch OBS F/1

0916	OBS ausgelöst	LT = 181 m	09 30,60 N	85 14,10 W
0921 – 0940	Hydrofon z.W.			
0945	Ende Versuch			

Profil 129 HS/PS/MG

0952	Beginn Profil	09 30,56 N	85 14,08 W	
0955	Magnetometer z.W.			
1202	Ende Profil	09 36,97 N	84 55,33 W	23 sml
1212	Magnetometer a.D.			

Insgesamt wurden 94 OBS/OBH ausgelegt und geborgen ; 18 geborgen :
Profilmeilen Seismik / Magnetik / Hydrosweep / Parasound = 620 sml
Profilmeilen Magnetik / Hydrosweep / Parasound =1561 sml

RF Reedereigemeinschaft
Forschungsschiffahrt GmbH

Stationsprotokoll F.S. "S O N N E" Reise SO 144/2

Gebrauchtes Instrumentarium		Anzahl der Einsätze
CTD-Rosette		09
OFOS		10
TOBI-System	543 sml a 2,3 kn	04

Eingesetzte Winden :

Winde	D/M	Typ	RF-Nr	SO 144/2 Einsatz	Gesamt Einsatz	SO 144/2 S`länge	Gesamt S`länge	Zust.
W 1	18,2	LWL	816233	321 h	0740 h	38288 m	194556 m	2
W 2	18,2	LWL	865017	000	1327	00000	834249	5
W 4	11,0	NSW	817141	005	0222	03000	139383	3
W 5	11,0	NSW	817164	018	0018	016120	016120	2
W 6	18,2	DRAKO	814150	000	0501	00000	401528	3

Winde	SO 144-2 gefierte max.Länge	jemals gefierte max.Länge
W 1	6474 m	6474 m
W 2	0000	6545
W 4	3000	6100
W 5	3350	3350
W 6	0000	7900

Geräteverluste : 1 Magnetometer plus ca. 300 m Kabel

Abkürzungen im Stationsprotokoll:

z.W.	zu Wasser
a.D.	an Deck
Boko	Bodenkontakt
Bosi	Bodensicht
SL(max.)	(maximale)Seillänge
LT	Lottiefe nach Hydrosweep
W x	eingesetzte Winde
HS	Hydrosweep
PS	Parasound
XPNDR	Transponder

Zeit : UTC - 06 Stunden

20.10.1999

Station 01	*CTD W 5*		
1835	Beginn Station	LT = 3579 m	08 50,96 N 84 40,98 W
1837	CTD z.W.		
1951	Slmax = 3555 m	LT = 3575 m	08 50,97 N 84 41,02 W
2106	CTD a.D. Ende Station		
Station 02	*OFOS W 1*		
2303	Beginn Station	LT = 768 m	09 11,32 N 84 47,85 W
2304	OFOS z.W.		
2326	Bosi SL = 759 m	LT = 768 m	09 11,31 N 84 48,05 W
	Kurs = 212 Grad v = 0,8 kn		

21.10.1999

0030	Bildausfall , hieven ein
0147	OFOS a.D. Ende Station

1010 – 1028 Schiff auf Caldeira – Reede
Übernahme Lftfracht für GEOMAR
von Bord : ABB-Monteur Chagauz

FS SONNE Stationsprotokoll SO 144/2

21.10.1999 ff

Vermessung mit HS / PS

1251	Beginn Vermessung	09 30,0 N	84 45,0 W	
	Kurs = 168 Grad v = 12 kn			
1413	ä.K. auf 076 Grad	09 16,0 N	84 42,0 W	14 sml
1504	ä.K. auf 123 Grad	09 19,0 N	84 30,0 W	12 sml
1600	ä.K. auf 180 Grad	09 13,0 N	84 21,0 W	11 sml
1621	ä.K. auf 288 Grad	09 09,0 N	84 21,0 W	04 sml
1725	Ende Vermessung	09 13,0 N	84 33,0 W	07 sml

Station 03 OFOS W 1

1845	Beginn Station	LT = 778 m	09 10,81 N	84 48,37 W
1847	OFOS z.W.			
1904	Bosi SL = 775 m	LT = 786 m	09 10,75 N	84 48,42 W
	Kurs = 211 Grad v = 0,8 kn			
2400	SL = 1441 m	LT = 1502 m	09 07,57 N	84 50,38 W

22.10.1999

0430	SL = 2447 m	LT = 2433 m	09 04,64 N	84 52,27 W
	Beginn hieven			
0519	OFOS a.D.			
0520	Ende Station			

Station 04 CTD/ROS W 5

0601	Beginn Station	LT = 1922 m	09 06,91 N	84 50,85 W
0602	CTD/ROS z.W.			
0640	Slmax = 1918 m	LT = 1921 m	09 06,89 N	84 50,81 W
0752	CTD/ROS a.D.		09 06,85 N	84 50,82 W
0753	Ende Station			

Station 05 TOBI I W 1

1035	Beginn Station	LT = 1171 m	09 20,11 N	85 20,90 W
1107	TOBI z.W.			
1145	Depressor z.W.			
1148	SL = 50 m last check			
1225	SL = 1054 m			
1253	Beginn Profil TOBI I		09 19,11 N	85 19,29 W
	Kurs = 112 Grad v = 2,3 kn ü.G.			
2400	SL = 3110 m	LT = 2135 m	09 09,20 N	84 55,65 W

23.10.1999

1033	Magnetometer vorgehievt			
1041	Ende Station / Profil 01	08 59,58 N	84 32,44 W	49 sml

Station 06 Profil T 02 W 1

1242	Beginn Profil		08 57,28 N	84 34,38 W
	Kurs = 292 Grad v = 2,3 kn			
	SL = 2245 m LT = 1834 m			
1800	SL = 2428 m LT = 1914 m		09 02,02 N	84 45,66 W
2400	SL = 3310 m LT = 2306 m		09 07,41 N	84 58,43 W

24.10.1999

0600	SL = 2929 m	LT = 1717 m	09 12,71 N 85 11,30 W	
1200	SL = 1895 m	LT = 1397 m	09 18,28 N 85 24,48 W	
1800	SL = 3497 m	LT = 2463 m	09 23,55 N 85 37,00 W	
1855	Magnetometer vorgeholt			
1857	Ende Profil		09 24,50 N 85 39,09 W	68 sml

Station 06 Tobi 3 W 1l

2055	Beginn Profil		09 21,82 N 85 39,98 W	
	Kurs = 112 Grad v = 2,3 kn		SL = 3036 m LT = 2656 m	
2056	Magnetometer z.W.			
2400	SL = 4001 m	LT = 2625 m	09 19,10 N 85 33,60 W	
25.10.1999				
0600	SL = 3207 m	LT = 2299 m	09 13,73 N 85 20,83 W	
1200	SL = 3633 m	LT = 2422 m	09 08,49 N 85 08,47 W	
1800	SL = 3495 m	LT = 2178 m	09 03,25 N 84 55,60 W	
2400	SL = 2854 m	LT = 2229 m	08 57,97 N 84 42,98 W	
26.10.1999				
0500	Ende Profil			
	SL = 2679 m	LT = 2171 m	08 53,80 N 84 32,66 W	74 sml
0512	Magnetometer a.D.			
0611	Depressor a.D.			
0652	TOBI a.D.			

Station 08 CTD/ROS W 5

0814	Beginn Station	LT = 2923 m	08 55,21 N 84 40,10 W
0816	CTD z.W.		
0920	Slmax = 2910 m	LT = 2923 m	08 55,22 N 84 40,09 W
1112	CTD a.D.		08 55,20 N 84 40,09 W

Station 09 OFOS W 1

1200	Beginn Station	LT = 1381 m	09 00,13 N 84 36,28 W
1201	OFOS z.W.		
1235	Bosi SL = 1365 m	LT = 1373 m	08 59,93 N 84 36,31 W
	Kurs = 209 Grad v = 0,8 kn		
1555	ä.K. auf 221 Grad		08 57,71 N 84 37,60 W
	SL = 1102 m	LT = 1107 m	
1948	hieven ein SL = 2676 m	LT = 2766 m	08 55,40 N 84 39,55 W
2039	OFOS a.D. / Ende Station		

Station 10 CTD/ROS W 5

2104	Beginn Station	LT = 1622 m	08 57,50 N 84 39,03 W
2105	CTD z.W.		
2146	Slmax = 1597 m	LT = 1622 m	08 57,50 N 84 38,99 W
2313	CTD/ROS a.D. / Ende Station		08 57,50 N 84 38,98 W

27.10.1999

Station 11 OFOS W 1

0135	Beginn Station	LT = 213 m	08 51,54 N 84 12,70 W

FS SONNE Stationsprotokoll SO 144/2

0136	OFOS z.W.		
0149	Bosi SL = 221 m	LT = 226 m	08 51,46 N 84 12,69 W
	Kurs = 215 Grad v = 0,8 kn		
0400	SL = 576 m	LT = 581 m	08 50,00 N 8413,71W
0600	SL = 716 m	LT = 713 m	08 48,73 N 84 14,63 W
0830	hieven ein SL = 830 m	LT = 836 m	08 47,51 N 84 16,22 W
0848	OFOS a.D. / Ende Station		

Station 12 CTD/ROS W5

0924	Beginn Station	LT = 408 m	08 51,03 N 84 12,98 W
0925	CTD z.W.		
0956	Slmax = 402 m	LT = 409 m	08 51,02 N 84 12,97 W
1033	CTD a.D. / Ende Station		08 51,05 N 84 12,97 W

Station 13 OFOS W1

1719	Beginn Station	LT = 328 m	09 28,00 N 85 05,30 W
1720	OFOS z.W.		
1735	Bosi SL = 346 m	LT = 351 m	09 28,47 N 85 05,33 W
	Kurs = 205 Grad v = 0,8 kn		
2100	SL = 546 m	LT = 554 m	09 26,10 N 85 06,23 W
2400	SL = 1371 m	LT = 1389 m	09 23,94 N 85 07,13 W
28.10.1999			
0200	SL = 1718 m	LT = 1717 m	09 22,62 N 85 07,71 W
0215	hieven ein		09 22,60 N 85 07,78 W
0253	OFOS a.D. / Ende Station		

Station 14 CTD/ROS W5

0320	Beginn Station	LT = 1456 m	09 23,84 N 85 06,80 W
0321	CTD z.W.		
0358	Slmax = 1439 m	LT = 1461 m	09 23,85 N 85 06,90 W
0459	CTD a.D.		09 23,84 N 85 06,92 W
0500	Ende Station		

Station 15 OFOS W1

0755	Beginn Station	LT = 1761 m	09 00,87 N 84 44,30 W
0801	OFOS z.W.		
0828	Bosi SL = 1745 m	LT = 1751 m	09 00,73 N 84 44,12 W
	Kurs = 163 Grad v = 0,9 kn		
1000	SL = 1921 m	LT = 1936 m	08 59,53 N 84 43,75 W
	ä.K. auf 165 Grad		
1200	SL = 2281 m	LT = 2321 m	08 57,82 N 84 43,32 W
1222	ä.K. auf 163 Grad		08 57,45 N 84 43,22 W
1300	SL = 2482 m	LT = 2484 m	08 56,59 N 84 43,00 W
	hieven ein		
1419	OFOS a.D. / Ende Station		

Station 16 TOBI 4 W1 72 sml

1518	Beginn Station	LT = 2640 m	08 51,85 N 84 35,00 W
1520	TOBI z.W.		
1549	Depressor z.W.		

FS SONNE Stationsprotokoll SO 144/2

1600	Beginn Profil 4			08 51,81 N 84 35,34 W
	Kurs = 292 Grad	v = 2,3 kn		
2400	SL = 3774 m	LT = 2597 m		08 58,58 N 84 51,44 W
29.10.1999				
0600	SL = 4386 m	LT = 2728 m		09 03,73 N 85 03,73 W
1200	SL = 5205 m	LT = 3421 m		09 08,87 N 85 16,08 W
1800	SL = 4421 m	LT = 2640 m		09 14,15 N 85 28,62 W
2400	SL = 4453 m	LT = 2879 m		09 19,35 N 85 41,17 W
30.10.1999				
0057	Magnetometer vorgehievt			
0140	Ende Profil 4			09 20,78 N 85 44,60 W

Station 17 Profil 5 W 1 73 sml

0323	Beginn Profil			09 18,32 N 85 45,56 W
0401	Magnetometer z.W.			
0600	SL = 4923 m	LT = 2991 m		09 16,22 N 85 40,50 W
1200	SL = 4626 m	LT = 2865 m		09 11,01 N 85 28,05 W
1800	SL = 5940 m	LT = 3741 m		09 05,91 N 85 15,86 W
2120	Abbruch Profil, Defekt am Tobi			09 03,55 N 85 10,13 W
2151	Magnetometer a.D.			
2334	Depressor a. D. , Test			
31.10.1999				
0044	TOBI a.D.			
0100	Ende Station			

Station 18 CTD/ROS W 5

0854	Beginn Station	LT = 1850 m		09 19,31 N 85 28,86 W
0858 – 0910	verholen			
0912	CTD z.W.	LT = 2000 m		09 19,18 N 85 28,78 W
0957	Slmax = 1984 m	LT = 1994 m		09 19,18 N 85 28,79 W
1118	CTD a.D. / Ende Station			09 19,18 N 85 28,80 W

Station 19 OFOS W 1

1200	Beginn Station	LT = 1070 m		09 19,50 N 85 24,00 W
1201	OFOS z.W.			
1225	Bosi SL = 1089 m	LT = 1100 m		09 19,60 N 85 24,02 W
	Kurs = 191 Grad	v = o,7 kn		
1622	SL = 1761 m	LT = 1790 m		09 16,63 N 85 26,75 W
	ä.K. auf 210 Grad			
1846	SL = 2368 m	LT = 2382 m		09 15,24 N 85 25,43 W
	hieven ein			
1930	OFOS a.D. / Ende Station			

Station 20 TOBI 6 W 1 81 sml

2138	Beginn Station	LT = 3782 m		09 17,66 N 85 50,90 W
2142	Tobi z.W.			
2215	Depressor z.W.			
2215	Beginn Profil 6			09 17,62 N 85 51,22 W
	Kurs = 112 Grad	v = 2,3 kn		
2400	SL = 3227 m	LT = 3742 m		09 16,91 N 85 49,10 W
01.11.1999				

FS SONNE Stationsprotokoll SO 144/2

0600	SL = 5539 m	LT = 3201 m	09 11,52 N 85 36,26 W
1200	SL = 5360 m	LT = 3616 m	09 06,48 N 85 24,12 W
2400	SL = 5954 m	LT = 3544 m	08 55,53 N 84 57,81 W
02.11.1999			
0600	SL = 6172 m	LT = 3589 m	08 50,13 N 84 44,97 W
1030	SL = 5260 m	LT = 3396 m	08 46,07 N 84 35,15 W
	Ende Station und Profil ,fahren Schleife über BB		
1047	Magnetometer vorgehievt		

Station 21 Profil Tobi 7 W 1 43 sml

1300	Beginn Profil		08 49,32 N 08 36,12 W
1307	Magnetometer z.W.		
1600	SL = 5835 m	LT = 3597 m	08 51,97 N 84 42,39 W
1800	SL = 5835 m	LT = 3293 m	08 53,63 N 84 46,50 W
2400	SL = 5356 m	LT = 2937 m	08 58,92 N 84 59,20 W
03.11.1999			
0600	SL = 5739 m	LT = 3477 m	09 04,39 N 85 12,18 W
0725	Magnetometer vorgehievt		
0730	Ende Profil		09 05,67 N 85 15,41 W
	SL = 6013 m	LT = 3739 m	

Station 22 Profil Tobi 8 W 1 05 sml

0753	Beginn Profil		09 05,75 N 85 16,18 W
	SL = 6100 m	LT = 3740 m	
0845	Magnetometer z.W.		
1005	Ende Profil Magnetometer ein		09 02,78 N 85 20,37 W

Station 23 Profil Tobi 9 W 1 27 sml

1035	Beginn Profil		09 02,67 N 85 21,57 W
	SL = 6054 m	LT = 3381 m	
1050	Magnetometer z.W.		
1200	SL = 5364 m	LT = 3189 m	09 03,88 N 85 24,58 W
1800	SL = 6085 m	LT = 3660 m	09 09,13 N 85 37,24 W
2310	SL = 6300 m	LT = 3693 m	09 13,70 N 85 48,48 W
	Ende Profil	hieven ein	
2325	Magnetometer a.D.		
04.11.1999			
0229	Depressor a.D.		
0255	Tobi a.D.		
0300	Ende Station		

Station 24 Profil Tobi 10 W 1 20 sml

0850	Beginn Station	LT = 622 m	09 27,02 N 84 51,83 W
0854	Tobi z.W.		
0922	Depressor z.W.		
0930	Beginn Profil		09 26,96 N 84 51,56 W
	SL = 220 m LT = 220 m Kurs = 170 Grad v = 2,5 kn		

FS SONNE Stationsprotokoll SO 144/2

1200	SL = 1978 m	LT = 1476 m	09 21,16 N	84 50,30 W
1724	Magnetometer vorgehievt			
1725	Ende Profil Tobi 10		09 07,50 N	84 48,00 W
	SL = 831 m LT = 884 m			

Station 25 Profil Tobi 11 W1 16 sml

1908	Beginn Profil		09 08,26 N	84 50,83 W
	SL = 837 m	LT = 1259 m	v = 2,5 kn	Kurs = 349 Grad
1916	Magnetometer z.W.			
2400	SL = 2498 m	LT = 1755 m	09 20,21 N	84 53,08 W
05.11.1999				
0128	Magnetometer vorgehievt			
0129	Ende Profil SL = 1329 m	LT = 1053 m	09 24,69 N	84 54,83 W

Station 26 Profil Tobi 12 W1 15 sml

0205	Beginn Profil		09 24,69 N	84 54,83 W
	SL = 919 m LT = 1002 m	Kurs = 269 Grad	v = 2,5 kn	
0220	Magnetometer z.W.			
0600	SL = 997 m LT = 1048 m		09 24,32 N	85 04,59 W
0757	Ende Profil SL = 1404 m	LT = 1136 m	09 24,29 N	85 09,57 W
0805	Magnetometer a.D.			
0945	Depressor a.D.			
0905	TOBI a.D.			
0915	Ende Station			

Station 27 OFOS W1

1013	Beginn Station	LT = 462 m	09 19,32 N	85 16,21 W
1024	Bosi SL = 496 m	LT = 465 m	09 19,34 N	85 16,22 W
	Kurs = 303 Grad v = 1,0 kn			
1200	SL = 598 m LT = 600 m		09 20,10 N	85 17,33 W
1327	ä.K. auf 43 Grad SL = 741 m	LT = 743 m	09 20,88 N	85 18,46 W
1445	ä.K. auf 301 Grad SL = 707 m	LT = 706 m	09 21,59 N	85 17,79 W
1558	hieven SL = 854 m	LT = 862 m	09 22,41 N	85 18,85 W
1625	OFOS a,D. / Ende Station			

Station 28 CTD/ROS W5

1652	Beginn Station	LT = 589 m	09 20,00 N	85 17,20 W
1653	CTD z.W.			
1721	Simax = 580 m	LT = 586 m	09 20,01 N	85 17,20 W
1800	CTD a.D. / Ende Station		09 20,00 N	85 17,16 W

Station 29 OFOS W1

1932	Beginn Station	LT = 2370 m	09 22,05 N	85 35,09 W
1936	OFOS z.W.			
2020	Bosi SL = 2341 m	LT = 2366 m	09 22,00 N	85 25,08 W
	Kurs = 196 Grad v = 0,8 kn			
2400	SL = 2744 m	LT = 2751 m	09 19,42 N	85 35,85 W
06.11.1999				
0220	SL = 2825 m	LT = 2749 m	09 17,57 N	85 36,41 W
	ä.K. auf 191 Grad			
0644	hieven SL = 2939 m	LT = 2943 m	09 14,17 N	85 37,07 W

FS SONNE Stationsprotokoll SO 144/2

0735	OFOS a.D. / Ende Station		
Station 30	*CTD/ROS W 5*		
1045	Beginn Station	LT = 1915 m	09 39,39 N 85 52,95 W
1048	CTD z.W.		
1136	Slmax = 1735 m	LT = 1918 m	09 39,39 N 85 52,93 W
1258	CTD a.D. Ende Station		09 39,40 N 85 52,92 W
Station 31	*OFOS W 1*		
1318	Beginn Station	LT = 1864 m	09 41,28 N 85 53,02 W
1359	Bosi SL = 1837 m	LT = 1860 m	09 41,32 N 85 53,02 W
	Kurs = 177 Grad v = 0,8 kn		
1837	SL = 2104 m	LT = 2092 m	09 37,85 N 85 53,62 W
	ä.K. auf 24 Grad		
2132	SL = 1902 m	LT = 1950 m	09 39,64 N 85 52,97 W
	a.K. auf 176 Grad		
2246	hieven SL = 1939 m	LT = 1954 m	09 39,66 N 85 53,11 W
2320	OFOS a.D. / Ende Station		

PRESS

CLIPPINGS

Observatorios sísmicos en azul

Si la leyenda del Capitán Nemo fuera hoy realidad, probablemente hasta él mismo se sorprendería de que en nuestro fondo océanico existieran observatorios sísmicos. A bordo del barco alemán "Sonne", una tripulación científica en sismología, geofísica y geología, llevará a cabo una travesía en el Pacífico de setiembre a diciembre próximo, para investigar los linderos entre la corteza océánica y continental en el mar territorial de Costa Rica, Panamá, Nicaragua, Colombia y Ecuador.

En el área costarricense, este proyecto de investigación tendrá especial énfasis en la Península de Osa, Boruca y Talamanca.

Como parte de él se realizarán varios perfiles de reflexión y dos de refracción sísmica (ondas sísmicas bifurcadas entre la corteza continental y la capa o manto superior). Uno en el mar, paralelo a la costa, desde la fractura de Panamá a Caldera, y el segundo desde el mar Pacífico cerca de Osa hasta el Caribe, cruzando la cordillera de Talamanca hasta el Valle de La Estrella. Este último será de gran interés nacional, puesto que se obtendrá un modelo de corteza continental-oceánico, casualmente donde se han registrado los temblores y terremotos de mayor magnitud en Costa Rica, superiores a los siete grados en la escala Richter.

Asimismo, este perfil cruzará el sitio donde el ICE tiene planeado el mayor proyecto hidroeléctrico (Boruca), con un costo estimado en $2.000 millones.

Las estaciones sismológicas submarinas permitirán localizar por más de dos meses, temblores y terremotos con una precisión de menos de un kilómetro. Se trata de instrumentos que pueden medir los eventos en sus componentes verticales y horizontales, con el fin de conocer mejor la distribución sísmica de la corteza oceánica y del manto superior.

El ambicioso proyecto, denominado Paganini, es desarrollado por el Instituto de Investigaciones de Geociencias Marinas (GEOMAR) de Kiel, Alemania, con el apoyo de la Escuela Centroamericana de Geología de la Universidad de Costa Rica, el ICE y RECOPE.

El crucero es coordinado por el Dr. Ernst R. Flueh, de GEOMAR, quien ha participado en otros proyectos en el Pacífico costarricense, como Pacomar (1992-1993), Ticosect (1995), y Cotcor (1997).

EL CRUCERO

Según relató el geofísico German Leandro, funcionario de la UCR y del ICE, "Sonne" partirá de San Diego, California, el 14 de setiembre y arribará a Golfito el 29 de dicho mes, lapso en que se realizará un mapeo del fondo oceánico, complementario entre Nicaragua y Costa Rica. En esta etapa se lanzarán al fondo océanico las estaciones sismológicas (OBS), las cuales cubrirán toda la zona de estudio.

Luego parte de Golfito para realizar los dos perfiles de refracción sísmica en varios lugares del mar. En el perfil mar-tierra

Los geofísicos German Leandro (UCR-ICE) y Ernst Flueh (GEOMAR), observan eventos sísmicos de la Península de Osa.

de Osa, Boruca y Talamanca se pondrá instrumentación en sitios accesibles para recibir ondas sísmicas generadas desde el mar, y en tierra por medio de explosivos en perforaciones de 50 metros.

Posteriormente se estudiarán los montes marinos (Sea mount) en la margen continental de Costa Rica, frente a Quepos. Se especula que en la placa Cocos estos montes se originaron de un punto caliente, o de una erupción muy grande que ocurrió en Galápagos, hace aproximadamente unos dos o tres millones de años.

La cuarta y última etapa es con énfasis geológico, e incluye la colecta de rocas y sedimentos del fondo océanico, y también la recuperación de los sismómetros lanzados al fondo del mar.

Por otra parte, investigadores de España, Francia y Estados Unidos, instalarán entre 20 y 30 estaciones móviles en la región del sur de Costa Rica, para monitorear los sismos en una red local del ICE, junto con los instrumentos en el fondo océanico.

Entre los logros que se esperan de este proyecto, el cual sobrepasa los $4 millones, está conocer la morfología (forma y transformaciones) del fondo océanico, así como la estratigrafía o geología estructural de la corteza océanica del mar territorial de nuestro país y sus vecinos Nicaragua, Panamá, Colombia y Ecuador.

Además permitirá a los científicos costarricenses conocer nuevas técnicas para la adquisición de datos geofísicos-geológicos, participar en publicaciones internacionales con el grupo científico del proyecto, así como el intercambio de profesionales y estudiantes con GEOMAR.

INFLUENCIA DE LAS PLACAS

El Dr. Flueh manifestó que el proyecto Paganini es regional, por lo que también se estudiará la influencia de la placa Cocos con la Galápagos, la cual es muy profunda y con características de vulcanismo. Por esta razón, se analizarán los montes submarinos, pues se cree que han sido los focos de los terremotos. En el caso de Costa Rica, frente a la Península de Osa, existe una anomalía grande, producto de dicho vulcanismo.

Leandro relató que en los anteriores proyectos desarrollados en nuestro país, se trazó una línea sísmica en el norte, desde Marbella hasta Los Chiles y en la parte central, desde Dominical hasta Matina. Ésta información está disponible para los interesados.

La zona que se estudiará próximamente tiene condiciones geométricas y geomorfológicas muy especiales, ya que el espesor de la Placa Cocos es pequeña (2 km), de manera que se piensa hacer una perforación para observar las calidades y propiedades de las rocas, casualmente donde se están rozando las dos placas (Cocos-Caribe).

EXPECTATIVAS

El Dr. Flueh indicó que una de las expectativas con este proyecto, es la nucleación de terremotos, y aunque no se puede hacer una proyección para predecirlos, si es posible entender la geometría y comportamiento de las fallas sísmicas. Esto ayudará a los ingenieros a tomar en cuenta la máxima aceleración para la construcción de viviendas y otras obras civiles de mayor envergadura, como el Proyecto Hidroeléctrico Boruca.

Por su parte, el geofísico Leandro expresó que en este proyecto se conocerá un poco más de la topografía y morfología del fondo océanico, debido a que se extenderá el área de investigación, cubriendo de Nicaragua a Costa Rica.

Agregó que además se tendrán mayores conocimientos de la parte estructural o sea los espesores de la corteza océanica y de la placa Caribe sobre Cocos.

En lo que respecta a la parte científica sismológica, la importancia es que al conocer bien la corteza océánica y continental, en esa área se pueden relocalizar mejor los temblores y se va a tener un modelo de corteza más real, debido a que actualmente se trabaja con algunos modelos importados o extrapolados desde observaciones continentales.

Los científicos consideran que esta es una oportunidad para determinar con más precisión los espesores de la corteza terrestre en aproximadamente unos 30 ó 40 km de espesor, las variaciones laterales de las capas, y sus velocidades sísmicas desde la trinchera con origen en Osa. Con este modelo, los sismólogos posteriormente podrán relocalizar muchos temblores

Expedición científica alemana trabaja con el ICE en el Pacífico

Grupo trazará mapa de fallas

Investigación permitirá conocer en detalle el comportamiento sísmico del país

ERNESTO RIVERA
La República

La expedición científica internacional Geomar, en coordinación con el Instituto Costarricense de Electricidad (ICE), comenzó este martes una investigación submarina en el Océano Pacífico para investigar el comportamiento sísmico de Costa Rica.

El proyecto, realizado a bordo del barco científico alemán "Sonne", recorrerá hasta el 20 de diciembre las aguas costarricenses, para colocar sismógrafos, elaborar mapas de la topografía del fondo marino y calibrando la red sismológica de tierra.

El geofísico alemán Ernest Flueh, director de la expedición, explicó a LA REPUBLICA que la información recabada permitirá calcular los efectos que podría tener un terremoto originado por el choque de las placas Cocos y Caribe, y saber la magnitud máxima que recibiría la infraestructura, sean casas, puentes o represas hidroeléctricas, en diferentes zonas del país, durante un eventual sismo.

"No se puede prevenir los terremotos, pero podemos estudiar con detalle la dinámica entre las placas y calcular el riesgo sísmico del país. Esta información es valiosa para los ingenieros costarricenses", dijo el científico.

Abelardo Fonseca / La República

La geóloga costarricense Ivonne Arroyo colabora con el director de la expedición, Ernest Flueh, en el procesamiento de datos sismológicos que se recolecten durante el viaje.

Una tica en alta mar

Con la expectativa de aprender "todo lo posible" de la interacción con 24 científicos de distintas nacionalidades y un poco "asustada" por la perspectiva de no tocar tierra firme en todo un mes, Ivonne Arroyo definió su estado de ánimo al ingresar en el barco Sonne.

Esta geóloga, de 24 años, representará a Costa Rica en la misión internacional durante la primera etapa de 20 días, tras los cuales se incorporarán sus colegas Guillermo Alvarado y German Leandro.

"Tengo la expectativa de aprender todo lo posible. Confío en aprender sobre la vida a bordo, ya que nunca he estado en un barco", expresó Arroyo. Su función será apoyar y colaborar en la tarea de procesamiento de datos sismológicos, entre otras labores.

Arroyo, quien labora en el ICE, dijo que estarán 20 días sin tocar tierra realizando experimentos, incluso en la Isla del Coco.

LOS EXPERIMENTOS

Flueh informó que el Sonne barrerá cerca de 250 kilómetros diarios de mar tico, incluyendo la isla del Coco, para estudiar la composición y forma en que interaccionan de las placas Cocos y Caribe.

Los científicos provocarán temblores artificiales basados en explosiones de aire comprimido para calibrar la red sismológica nacional.

"Hemos trazado geotransectas (líneas de marcación sísmica) que atraviesan Costa Rica de océano a océano, que junto con las estaciones de tierra permitirán estudiar la relación entre la placas oceánicas y obtener un patrón geofísico de la zona", explicó Flueh.

No todo el trabajo estará mar adentro. El ICE dará apoyo desde tierra provocando explosiones a distintas profundidades para simular temblores, que serán medidos desde el mar.

"La idea es que tanto desde el mar como desde la tierra se pueda provocar temblores de manera controlada y cronometrada para calibrar la red sismológica de tierra y mar", explicó Luis Sáenz, geofísico del ICE.

El geólogo del ICE, Juan Ramón Chacón, informó que los estudios serán útiles para una cadena de proyectos hidroeléctricos que se planea construir sobre la cuenca del río General.

Además se beneficiará la nueva línea de transmisión eléctrica que atravesará Centroamérica por el Pacífico con un costo de $300 millones, "será útil conocer qué problemas de movimientos tendrán las torres y en qué lugares existirían amenazas sísmicas", expresó Sáenz.

Sofisticada embarcación

El Sonne es un barco equipado con sofisticados instrumentos para investigación científica. Su estadía en la plataforma continental tica se extenderá hasta el 20 de diciembre.

- Tiene 93 metros de eslora, una tripulación de 30 marinos y técnicos, 25 ingenieros, geólogos y geofísicos de Alemania, Estados Unidos, Austria, Perú, Australia, Francia y Costa Rica.
- La misión científica trabaja en turnos que cubren las 24 horas y producirá mapas topográficos de la geografía submarina, de acuerdo con los detalles obtenidos cada 48 horas.
- Posee un sistema de cámaras de vídeo sumergibles que permite observar el fondo marino, hasta 8 mil metros de profundidad, a través un cable de fibra óptica.
- Posee un sonar que interpreta el eco de la actividad sísmica marina y brazos mecánicos para sacar muestras del fondo del mar.
- El costo total del proyecto en la etapa costarricense será de $10 millones (¢2.920 millones), costeados por Alemania.

Anclado frente a la península de Osa

Barco estudia riesgo sísmico

VANESSA LOAIZA NARANJO
Redactora de La Nación

Un panel de 25 investigadores de Gran Bretaña, Alemania y otras partes del mundo analizan desde el 27 de setiembre pasado el fondo marino costarricense.

Sus estudios permitirían pronosticar la magnitud de eventuales movimientos sísmicos y el lugar en donde ocurrirían.

Una embarcación alemana capacitada para evaluar la composición del fondo marino realiza análisis en diferentes sectores del mar territorial costarricense.

Actualmente el *RV-Sonne* perteneciente a un organismo de investigación alemán denominado GEOMAR se encuentra frente a las costas de la península de Osa.

El biólogo marino Moisés Mug, del Instituto de los Recursos Costeros y Marinos (Inrecosmar), explicó que los especialistas emplearán la técnica del sonar.

Los sonares son aparatos que sirven para detectar la presencia y ubicación de objetos sumergidos mediante vibraciones inaudibles de alta frecuencia.

A través de estas ondas sonoras se puede determinar la dureza o composición del fondo marino. *(Ver infográfico adjunto).*

En Osa se realiza la primera expedición del *RV-Sonne*, otras dos se efectuarán en los próximos días frente a las costas de la península de Nicoya y en las cercanías de la isla del Coco. El costo de los estudios aún no ha sido detallado por los especialistas.

Una investigación similar se realizó entre noviembre y diciembre de 1996, cuando un barco perforó varios puntos de las placas tectónicas frente a la península de Nicoya.

En esa ocasión, los estudios pronosticaron un fuerte sismo en la zona guanacasteca.

Mug Villanueva aclaró que el objetivo de la embarcación alemana no es decir cuándo ocurrirá un sismo, sino cuan fuerte podría ser, esto tomando en cuenta el choque entre las placas y el punto exacto en donde ocurriría.

Evaluarán cordillera

Aparte de la incidencia sísmica, uno de los motivos que favorecieron la llegada de este barco de investigación fue la dinámica de las placas continentales.

Según Moisés Mug, la zona es catalogada por los investigadores como uno de los mejores sitios para evaluar los procesos de subducción.

Muy cerca de las placas también se desarrolla la cordillera sumergida de Cocos que, inclusive, tiene montes mucho más altos que el cerro Chirripó.

El experto confirmó que en algún momento estos grandes promontorios empezarían a introducirse bajo la placa Caribe.

Claro, debe entenderse que estos procesos tardarían miles de años si se toma en cuenta que la placa de Cocos avanza 10 centímetros por año bajo la Caribe.

Además, llamó la atención de los científicos la presencia de volcanes inactivos y fosas que superan los 5.000 metros de profundidad, que forman parte de lo que comúnmente se conoce como la fosa Mesoamericana.

Para Inrecosmar, si se toma en cuenta todo el terreno sumergido bajo el mar patrimonial costarricense, Costa Rica sería el país más grande de Centroamérica.

SISMOS EN EL MAR

El barco RV-Sonne *de la organización alemana GEOMAR realiza estudios en diferentes puntos del mar territorial costarricense para determinar la composición del suelo marino y la magnitud de eventuales movimientos sísmicos.*

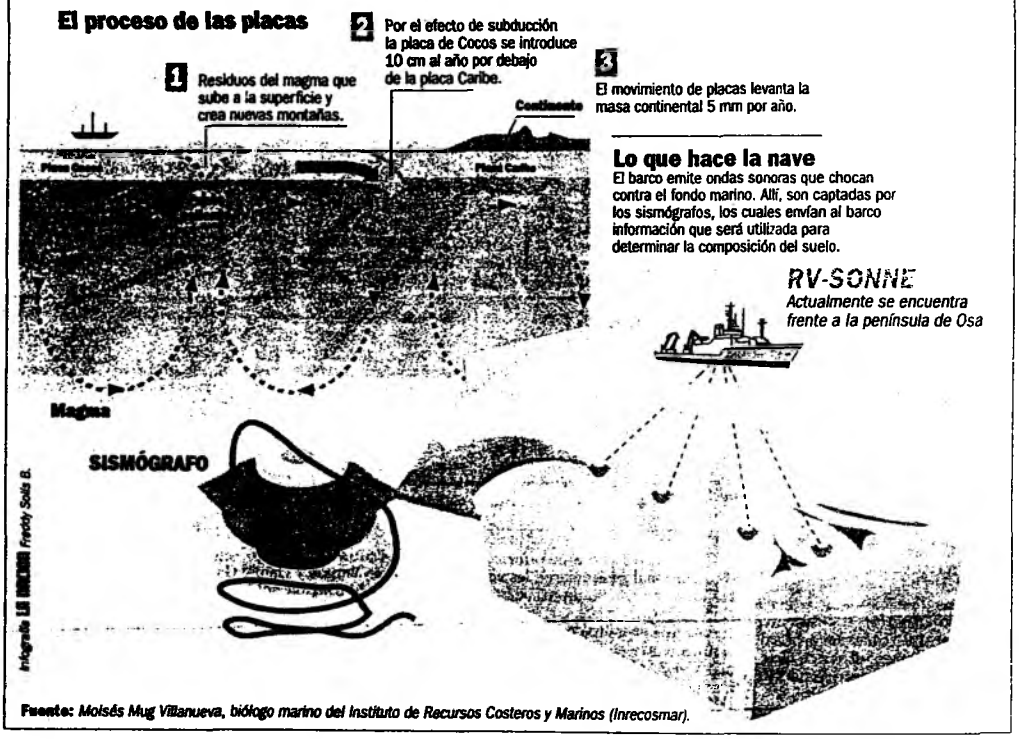

Fuente: *Moisés Mug Villanueva, biólogo marino del Instituto de Recursos Costeros y Marinos (Inrecosmar).*

● Investigación de barco alemán:

DESCUBREN 20 VOLCANES EN NUESTRA COSTA PACÍFICA

ILUSTRACIÓN GERMÁN MEZA

El descubrimiento de la presencia de 20 volcanes frente a la costa pacífica de nuestro país ha sido uno de los principales resultados de las investigaciones que realiza un grupo de científicos a bordo del barco alemán Sonne, que zarpó ayer del puerto de Caldera en la provincia de Puntarenas para continuar sus estudios en el Océano Pacífico.

Así lo dieron a conocer en una conferencia de prensa los científicos y miembros de la tripulación a bordo de esta embarcación, especialmente equipada para la realización de investigaciones geocientíficas marinas (que incluye las ramas de la Geología, Geofísica y Geoquímica) así como investigaciones de Oceanografía física, química, Planctología y Zoología Marina.

La comunidad científica ha decidido dar a conocer la existencia de estas formaciones volcánicas al público en general, no sólo con fines informativos sino con el afán de brindar detalles de nuestra evolución geológica y captar el interés educativo.

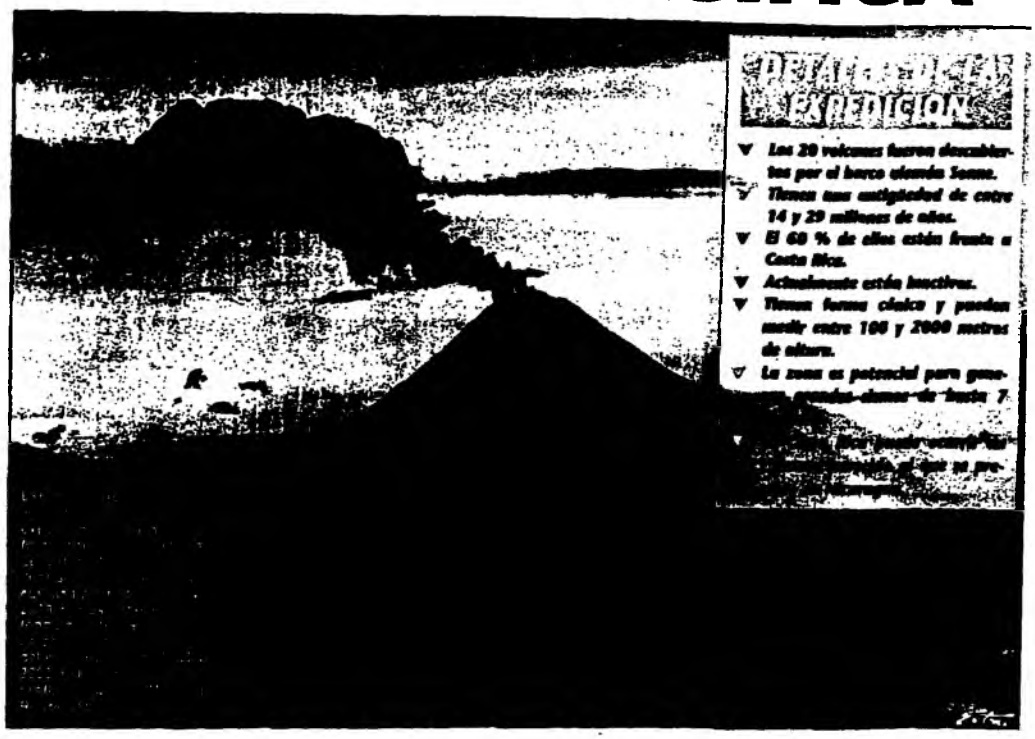

29 MILLONES DE AÑOS DE ANTIGUEDAD

Los volcanes que forman esta cadena montañosa submarina tienen una antigüedad de entre 14 y 29 millones de años y forman parte de grandes cordilleras volcánicas que se extienden entre el archipiélago de las Galápagos y los márgenes continentales de Centro y Sudamérica con una longitud de más de 1.100 kilómetros (más grande que la cordillera volcánica centroamericana). El 60% (unos 20 volcanes) de esta cordillera volcánica submarina se encuentra frente al territorio costarricense.

FORMA PARECIDA AL VOLCAN ARENAL

En la actualidad, según explicó el geólogo Guillermo Alvarado, coordinador del área de Sismología y Vulcanología del ICE y quien participa de las investigaciones desde 1991, estos volcanes están inactivos, tienen forma cónica con una altura de entre 100 y los 2000 metros sobre el fondo marino (similares al volcán Arenal) y su ubicación bajo el nivel del mar oscila entre los 1500 y 3000 metros de profundidad.

Los montes en mención están siendo sumergidos bajo el continente mediante el proceso tectónico de las placas de Coco y Caribe generando lo que se conoce como una "espera sísmica: (zonas de fricción) las cuales son zonas potenciales para la generación de grandes sismos con magnitudes más allá de los 7 grados.

Los científicos se han abocado a estudiar estos mecanismos de fricción no sólo frente a nuestras costas sino a lo largo de toda la cordillera volcánica en la que se incluye también la isla del Coco con dos millones de años de antigüedad y es de origen volcánico.

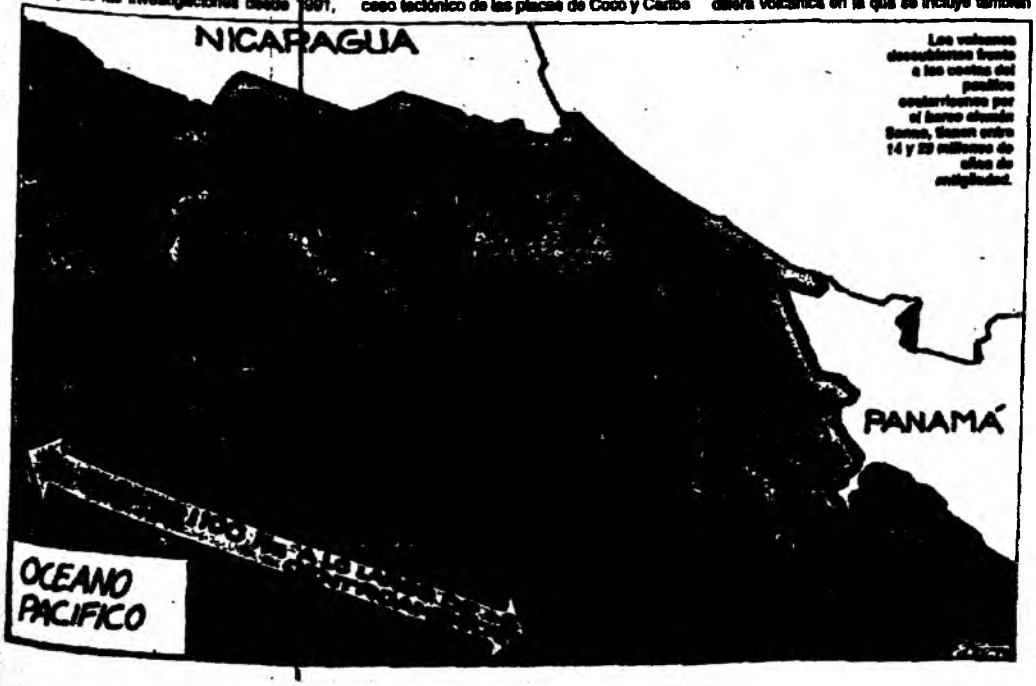

LAS EXPEDICIONES DEL SONNE

Las cinco expediciones científicas del barco Sonne forman parte del proyecto denominado PAGANINI cuyas siglas en inglés significan Panamá basin and Galápagos plume - New investigations of intraplate magmatism (Cuenca de Panamá y pluma de Galápagos - Nuevas investigaciones de Magmatismo Intraplaca). Estas exploraciones se realizan desde principios de setiembre y hasta mediados de diciembre del presente año. Pretenden efectuar un estudio multidisciplinario extensivo de la región de las cordilleras oceánicas del Coco, Carnegie, Malpelo y Colba, así como la corteza oceánica y la plataforma continental frente a Costa Rica y Nicaragua.

LOS TZUNAMIS

Otro de los objetivos que analizan los científicos, principalmente de la Universidad de Costa Rica, es la potencialidad de Tzunamis en las costas continentales frente a la cordillera en cuestión. En lo que respecta a Costa Rica, hasta la fecha, sólo han registrado olas de dos metros de altura y una de mayor magnitud en 1906 en la isla del Coco. Sin embargo, lo anterior no significa que el comportamiento de este fenómeno siempre sea igual y pueda suceder un Tzunami sorpresivo como el que ocurrió en la costa pacífica de Nicaragua.

El proyecto científico PAGANINI tiene un costo aproximado a los 40 mil dólares diarios y es financiado por el Ministerio de Educación de Alemania y aportes secundarios de otras instituciones participantes.

El análisis e interpretación de la información, que se obtenga de este proyecto requerirá de alrededor de dos años y medio de trabajo por parte del grupo de científicos y sus asistentes.

SABADO 1º MAYO. Científicos realizarán travesía por el Pacífico

Alemanes estudiarán mar costarricense

Grupo instalará estaciones sismológicas submarinas

barco alemán que partió de San Diego, Califor-

Provocan sismos

● Tres sismos artificiales tuvieron lugar ayer en la zona sur, en el marco de un proyecto realizado por el Instituto de Investigaciones de Geociencias Marinas (Geomar), de Alemania, juntamente con la Escuela Centroamericana de Geología de la Universidad de Costa Rica y el Instituto Costarricense de Electricidad (ICE).

Los expertos colocaron cargas de explosivos en tres puntos de 50 metros de profundidad cada uno, las cuales generaron movimientos en un kilómetro a la redonda, con el propósito de estudiar el fondo del océano y la-

Suficientes productos

● El ministro de Agricultura y Ganadería, Esteban Brenes, señaló que pese a las pérdidas en los cultivos en Guanacaste, debido a recientes lluvias, no será necesaria la importación de productos ni habrá aumentos en los precios del arroz y los frijoles.

Brenes realizó ayer, ante el Consejo de Gobierno, una exposición acerca de los principales logros de su cartera hasta a junio pasado. Destacó la concesión de ¢3.202 millones en crédito a los agroempresarios mediante el programa de reconversión productiva.

También aseguró que, por medio

14 oct

SABADO 1º MAYO.

Científicos realizarán travesía por el Pacífico

Alemanes estudiarán mar costarricense

Grupo instalará estaciones sismológicas submarinas

barco alemán que partirá de San Diego, Californ[illegible] el 14 de setiembre y [illegible] de ese mes.

Una travesía por el Pacífico para investigar los límites entre la corteza oceánica y continental en el mar territorial de Costa Rica realizará un grupo de científicos [illegible]

El proyecto será desarrollado por el Instituto de Investigaciones de Geociencias Marinas (GEOMAR) de Alemania y contará con el apoyo de la Escuela Centroamericana de Geología de la Universidad de Costa Rica (UCR), el Instituto Costarricense de Electricidad (ICE) y la Refinadora Costarricense de Petróleo (RECOPE).

El geofísico de la UCR, German Leandro, quien participará en el estudio, explicó que entre los aspectos más importantes estarán estacionar[illegible]

14 oct

Provocan sismos

● Tres sismos artificiales tuvieron lugar ayer en la zona sur, en el marco de un proyecto realizado por el Instituto de Investigaciones de Geociencias Marinas (Geomar), de Alemania, juntamente con la Escuela Centroamericana de Geología de la Universidad de Costa Rica y el Instituto Costarricense de Electricidad (ICE).

Los expertos colocaron cargas de explosivos en tres pozos de 50 metros de profundidad cada uno, las cuales generaron microsismos en un kilómetro a la redonda, con el propósito de estudiar el fondo del océano y ha-

Suficientes productos

● El ministro de Agricultura y Ganadería, Esteban Brenes, señaló que pese a las pérdidas en los cultivos en Guanacaste, debido a recientes lluvias, no será necesaria la importación de productos ni habrá aumentos en los precios del arroz y los frijoles.

Brenes realizó ayer, ante el Consejo de Gobierno, una exposición acerca de los principales logros de su cartera hasta a junio pasado. Destacó la concesión de ¢3.202 millones en crédito a los agroempresarios mediante el programa de reconversión productiva.

También aseguró que, por medio

Advierten sobre posible causa de sismos

Monte marino amenaza a Nicoya

●Utilizan barco alemán en estudio

VANESSA LOAIZA NARANJO
Redactora de La Nación

Un monte marino de más de 2.500 metros de altura situado frente a las costas de la península de Nicoya, en el Pacífico, podría convertirse en el causante de eventuales movimientos sísmicos de considerable magnitud en la zona.

El monte se ubica a unos 70 kilómetros de la península de Nicoya y está posado sobre la placa Cocos, que se desplaza a razón de 10 centímetros por año hacia territorio continental.

Desde el pasado 19 de octubre, científicos que ocupan un barco alemán especialmente equipado se dedican a investigar este promontorio, junto con el resto de montes y volcanes que conforman la cordillera sumergida de Cocos, ubicada frente a las costas del Pacífico Central costarricense. *(Vea infográfico adjunto.)*

El jefe científico de la expedición, Gerhard Bohrmann, explicó que el choque de esta elevación contra la placa Caribe podría causar eventuales sismos, que se sentirían con mayor intensidad en la provincia guanacasteca.

Lo anterior está relacionado directamente con el fenómeno de subducción, que en este caso consiste en que la placa Cocos se introduce a presión bajo la Caribe.

Un estudio similar se realizó entre noviembre y diciembre de 1996, cuando un barco perforó varios puntos de las placas tectónicas frente a la península de Nicoya.

La investigación es auspiciada por el grupo científico alemán Geomar y se desarrolla en cooperación con el Observatorio Vulcanológico y Sismológico de la Universidad Nacional (Ovsicori), y varias universidades estadounidenses.

Según el subdirector del Ovsicori, Carlos Montero, todos los resultados del estudio serán evaluados en conjunto con el Observatorio a fin de tomar las medidas pertinentes.

Monte viejo

Desde hace tiempo el Ovsicori tenía conocimiento de la situación, pero solo el barco cuenta con los equipos para trabajar directamente sobre la zona en la que se ubica el promontorio.

Para Moisés Mug, del Instituto de Recursos Costeros y Marinos (Inrecosmar), que también participa en la misión, un eventual terremoto en la península guanacasteca es un tema que permanece en el tapete.

Sin embargo, recalca que con este tipo de estudios no se puede predecir cuándo ocurrirá el sismo, por lo que no se debe alarmar a la población.

Precisamente, un equipo de 24 científicos alemanes y un ecólogo costarricense trabajan en estos momentos, con modernos artefactos sumergibles, en procura de determinar la composición del suelo submarino y la posible intensidad de eventuales sismos. *(Vea recuadro adjunto.)*

Aparte de las evaluaciones sísmicas, la embarcación *RV-Sonne* también trata de identificar gases congelados en el fondo marino como el metano, su vinculación con el cambio climático y el movimiento de las placas.

El ecólogo costarricense que participa en la misión, Omar Rodríguez, comunicó, a través de un correo electrónico desde el barco, que la primera exploración del suelo marino se realizó en Punta Judas, unos 100 kilómetros mar adentro al oeste de playa Hermosa, en el Pacífico Central.

Allí encontraron organismos marinos como estrellas y algunas variedades de peces luminiscentes.

La profundidad en esa zona va desde los 700 metros hasta los 2.500 metros, en lo que se llama la "Fosa Mesoamericana", que es donde se juntan las placas tectónicas mencionadas.

La misión actual es la segunda de tres que se realizarán con el barco alemán en aguas territoriales costarricenses.

La primera fue a finales de setiembre, frente a la península de Osa, donde se evaluó la composición del suelo marino y su grado de sismicidad.

La última expedición será en las cercanías de la isla del Coco, con el fin de estudiar las especies marinas y su vinculación con las islas Galápagos.

Rodríguez explicó que los informes sobre la cordillera sumergida se entregarán a 300 maestros de escuelas en la península de Nicoya, con el fin de educar a los niños sobre el territorio cercano.

LA CIENCIA VIAJA EN BARCO

El *RV Sonne* es un barco científico dedicado al estudio de los fondos marinos, la composición de los suelos y las especies marinas que se desarrollan en lo profundo del mar.

Desde finales de setiembre esta embarcación realiza diversos estudios en el mar patrimonial de Costa Rica, con un costo de operación diario superior a los $37.000 (¢10.841.000).

Un grupo de 24 científicos pasan recluidos en la nave por más de 20 días en cada una de las expediciones. Allí manipulan costosos instrumentos que permiten, entre otras cosas, sondear el fondo marino e identificar las especies que se reproducen en las zonas más profundas.

Para ello, un aparato remolcado por grúas se coloca en el fondo del mar y permite tomar fotografías en blanco y negro y vídeos inclusive a 5.000 metros de profundidad. *(Vea foto 1).*


Francisco Rodríguez / La Nación


Francisco Rodríguez / La Nación
2

Una de las principales ventajas de este artefacto es su alta resolución (gran nitidez); para ello, el barco está dotado de 10 kilómetros de cable de fibra óptica que se almacena en grandes carruchas en la parte baja de la nave. *(Vea foto 2).*

La embarcación también cuenta con el CTD, una herramienta que mide la temperatura del agua, la profundidad y la conductividad, además de que toma muestras de líquido que luego son analizadas químicamente para distinguir los elementos que lo conforman.

THE TICO TIMES

CENTRAL AMERICA'S LEADING ENGLISH-LANGUAGE NEWSPAPER

Member of the Inter-American Press Association

VOL. XLIII Nº 1547 — 40 pages San José, Costa Rica, Friday, November 12, 1999

German Research Ship Probes Underwater Range

By Jeffrey Van Fleet
Special to The Tico Times

EVERYONE knows Costa Rica is mountainous. Less known is that the ocean floor off the country's Pacific coast could be a replica of the country's topside landscape.

A team of German research scientists is in the midst of a three-and-one-half month project studying that underwater terrain, hoping to gain a better understanding of the earth's movements.

The German research vessel Sonne docked in the Central Pacific port of Caldera, its Costa Rican home port, this week between the second and third phases of the team's current expedition.

THE ship, whose name means "sun" in German, is a multipurpose research vessel. On the present expedition, its 144th, the ship carries a crew of 30 and a research team of 25

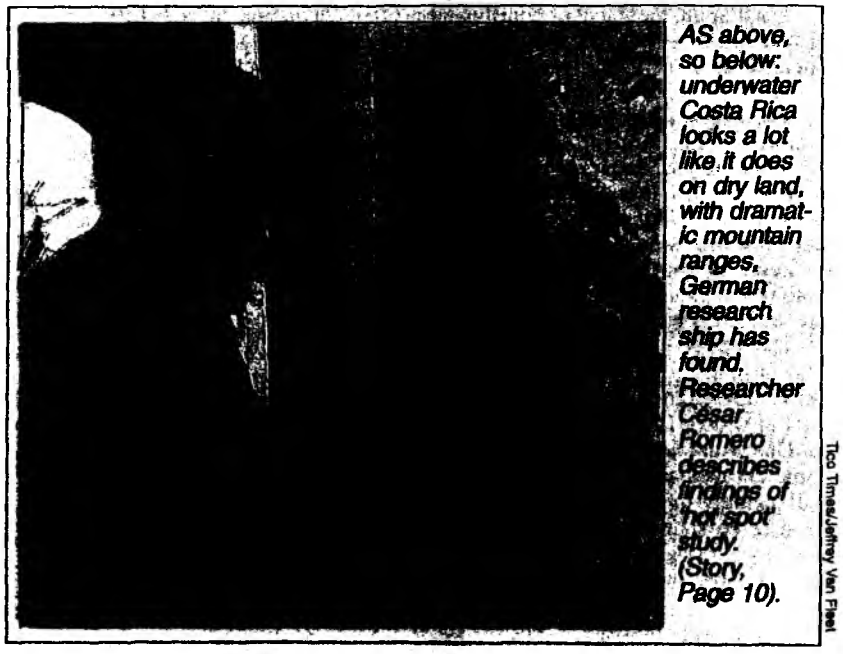

Tico Times/Jeffrey Van Fleet

AS above, so below: underwater Costa Rica looks a lot like it does on dry land, with dramatic mountain ranges. German research ship has found. Researcher César Romero describes findings of 'hot spot' study. (Story, Page 10).

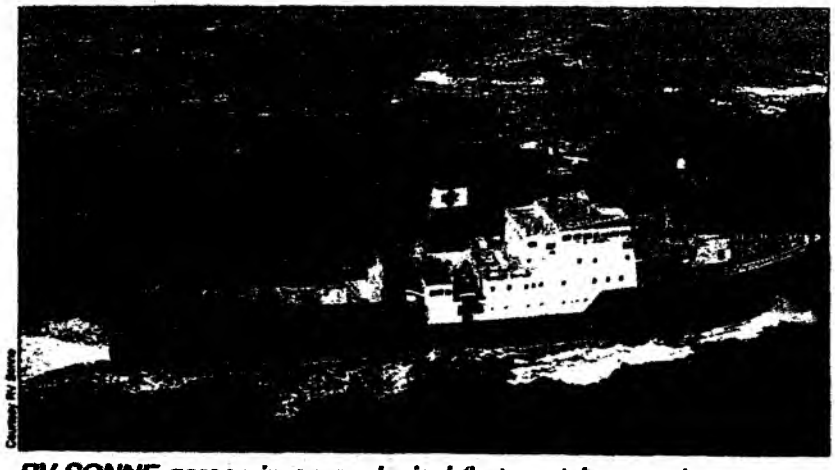

Courtesy RV Sonne

RV SONNE zeroes in on geological 'hot spots': map shows mountainous terrain in Pacific off Nicoya Peninsula and Quepos.

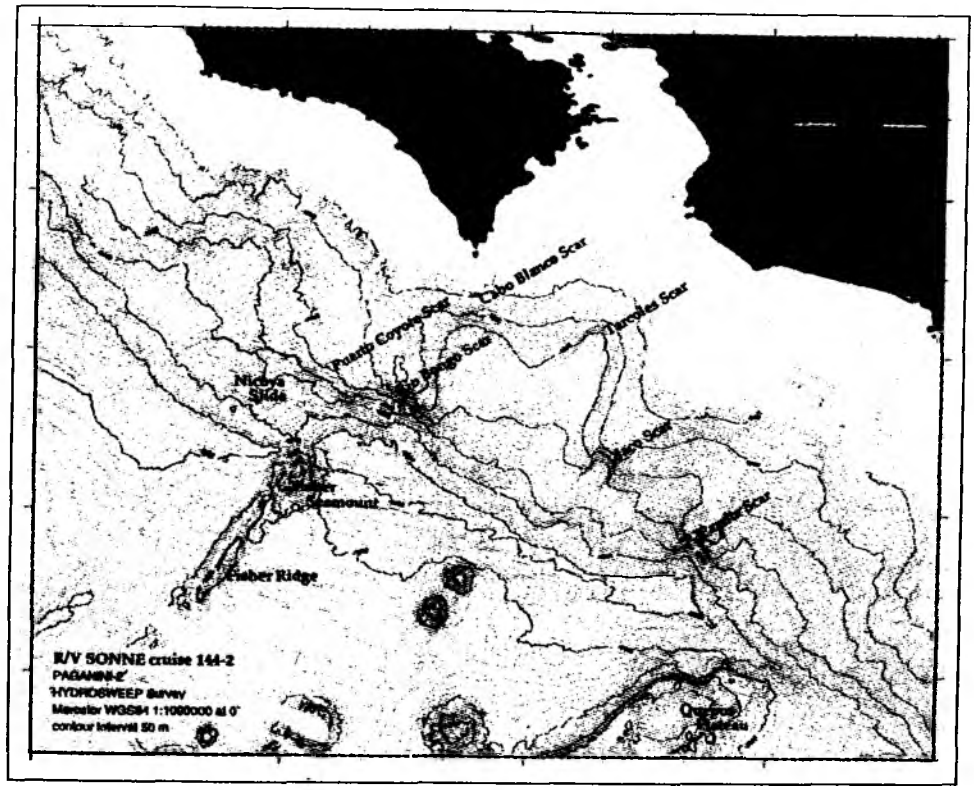

scientists from the GEOMAR Marine Research Center affiliated with Christian-Albrechts University in northern German city of Kiel.

The expedition is part of the PAGANINI Project (short for **P**anamanian Basin and **G**alapagos Plume – **N**ew **I**nvestigations of **I**ntraplate Magmatism). Researchers are studying the 1,100-km. underwater volcanic chain connecting Costa Rica's Cocos Island to the Galapagos Islands, some 1,000 km. west of Ecuador.

The study is focusing on so-called "hot spots", geologically younger sites on the earth's surface.

"The Galapagos archipelago is one of these hot spots, as is Hawaii," said researcher Gerhard Bohrmann.

THE earth's plates are thought to shift around these fixed points, moving an average of 10 cm. per year in this section of the Pacific, according to Bohrmann. Researchers have identified 20 volcanoes in this part of the "mountain chain", some 80 km. south of the coast, connecting Cocos to the Galapagos. They rise 100 to 2,000 meters from their bases 1,500 to 3,000 meters below the ocean surface.

"Normally the ocean floor is quite flat," Bohrmann said. "But Costa Rica below the sea looks much like Costa Rica above the sea."

PAGANINI phases 1 and 2 allowed the team to map the range with underwater cameras. Phase 3, which began this past Tuesday and will conclude Dec. 2, will entail actual sampling of ocean floor materials.

"THE sampling can be done less precisely with steel netting, dragged on the surface 2 to 3 km below," researcher Kay Hörnle focused fashion, with a television platform lowered to that depth. When we find an appropriate sampling site, We can then manipulate two large attached arms to collect samples."

The samples permit more precise age dating. The researchers estimate that 13-14.5 million years ago, these volcanoes were islands, or had summits at a very shallow depth beneath the water surface.

Better knowledge about long-range movements of the plate will give scientists a better understanding of tectonics and seismology of this part of the Pacific Ocean. That issue was brought home to Costa Rica with the Aug. 20 earthquake, whose epicenter was located in this part of the ocean south of the coastal community of Quepos (TT, Aug. 27).

THE $53,000-per-day PAGANINI Project is financed by German Ministry of Education. The government of that country spends some $150 million per year in oceanic research. The Costa Rican Electricity Institute and the University of Costa Rica's Coastal and Maritime Resource Institute are participating in the project.

The 30-year-old Sonne was re-outfitted in 1991 to do scientific research. Satellite-directed Global Positioning System allows the crew to navigate the 97-meter-long vessel. The ship can spend a maximum of 50 days at sea.

Why choose Costa Rica for a project such as this?

"The country offers a unique combination of everything we need," Hörnle said, describing the site as perfect for the subject of the PAGANINI Project. "It is relatively easy to work in Costa Rica. The seas are reasonably calm, and the climate is mild.